Modification of n-type and p-type metal oxide semiconductor systems for gas sensing applications

Paula Tarttelin Hernández

This thesis is submitted in partial fulfilment of the requirement of the Degree of Doctor of Philosophy

University College London
Chemistry Department

2017

I, Paula Tarttelin Hernández confirm that the work presented in this thesis is my own. Where information has been derived from other sources, I confirm that this has been indicated in the thesis.

Acknowledgements

I would like to express my deepest and most sincere gratitude to my supervisors, Professors Ivan Parkin and Steve Hailes. Thank you, from the bottom of my heart, for allowing me to work on a project that has been of utmost interest to me, for giving me great support, guidance and advice over the last few years but, also, thank you for believing in me.

I would also like to thank all those I have collaborated with and have provided me with their invaluable knowledge and expertise, time for meetings, fantastic discussions and advice. Also, thank you for granting me the opportunity to carry out two wonderful internships during the course of the PhD – they have made this a truly unforgettable and remarkable experience. Thank you to Prof. David E. Williams, Dr. Geoff Henshaw, Dr. Ayo Afonja, Dr. Russell Binions, Dr. Chris Blackman, Dr. Simon Naisbitt, Dr. Dewi Lewis, Prof. Maxim Kuznetsov, Dr. Pascal Plaza. Mrs. Alexandra Wills and Mr. James Pollard.

I would like to thank Dr. Anupriya Naik and Dr. Emma Newton profoundly for being the best possible mentors one could wish for.

Thank you to those who have assisted me and/or have trained me in using equipment during the PhD: Dr. Tom Gregory, Dr. Steve Firth, Mr. Martin Vickers, and Mr. Kevin Reeves. I would particularly like to thank Mr. Tony Bernard for being simply amazing and coming to the rescue whenever needed. Also, special thanks go to Dr. Carlos Sotelo Vázquez and to Dr. Michael Powell for running some XRD and XPS for me.

Thank you, also, to my lovely friends and colleagues both in the Chemistry Department and outside of work for always lifting me up during times of despair.

Words fall short to express how grateful I am to my wonderful family for giving me the opportunity to move to a foreign country many years ago. Thank you for giving me the freedom and encouragement to pursue a dream. Thank you, in particular, to my Mum. Thank you for your never-ending support, patience and love – this Thesis is forever dedicated to you.

List of Acronyms and Abbreviations

CNT – Carbon Nanotube

CMOS – Complementary Metal Oxide Semiconductor

C – Cost Function

CV – Cross-Validation

CVD – Chemical Vapour Deposition

EDL – Electron Depletion Layer

FAU – Faujasite

HAL – Hole Accumulation Layer

HC – Hydrocarbon

LTA – Linde Type A

MEMS – Micro-Electro-Mechanical System

MFI – Mordenite Framework Inverted

MOS – Metal Oxide Semiconductor

MOSFET – Metal Oxide Semiconductor Field Effect Transistor

QCM – Quartz Crystal Microbalance

RBF – Radial Basis Function

S – Sensitivity

SAW – Surface Acoustic Wave

SDG – Sustainable Development Goals

SI – Surface Ionisation

SOI – Silicon on Insulator

SWCNT – Single-Walled Carbon Nanotube

τ_{90} – Response Time

τ_{10} – Recovery Time

UNODC – United Nations Office on Drugs and Crime

VOC – Volatile Organic Compound

WHO – World Health Organisation

YSZ – Yttria Stabilised Zirconia

Abstract

This thesis investigates the modification of three metal oxide semiconductor gas sensors with zeolite materials for the purposes of detecting trace concentrations of gases that have an effect on health, security, safety and the environment.

SnO_2, Cr_2O_3 and Fe_2O_3 were chosen as the base materials of interest. Zeolites H-ZSM-5, Na-A and H-Y were incorporated into the sensing system either as admixtures with the base material or as coatings on top of it. The aim of introducing zeolites into the sensing system was to improve the performance of the otherwise unmodified sensors.

Twenty-two novel zeolite-modified sensor systems are presented for the detection of a range of hydrocarbons and inorganic gases. Whilst sensors based on SnO_2 systems were more responsive to gases, some sensors were also found to provide a greater degree of variability among repeat tests, particularly at lower operating temperatures i.e. 300 ˚C. Cr_2O_3 sensors modified by admixture with zeolite H-ZSM-5 were seen to be poorly sensitive to most analytes. Cr_2O_3 sensors modified by admixture with zeolite Na-A and by overlayer of zeolite H-Y provided very promising sensitive and selective results towards toluene gas. Sensors based on the zeolite modification of Fe_2O_3 were not found to be promising candidates as gas sensors at this stage.

Sensors were purposely exposed to gases that had similar molecular structures or kinetic diameters to assess the true capability of the sensors to discriminate among analytes. An array of four sensors based on n-type and p-type systems was subsequently chosen to see whether machine learning classifiers could be used to accurately discriminate among nine analytes. Using an SVM SMO classifier with a polykernel function, the model was 94.1% accurate in correctly classifying nine analytes of interest just after five seconds into the gas injection. Using an RBF kernel function, the model was 90.2% accurate in correctly classifying the data into gas type. These are very encouraging results, which highlight the importance of furthering research in this field; a sensing array based on zeolite-modified metal oxide semiconductor sensors may benefit a number of research domains by providing accurate results in a very fast and inexpensive manner.

1 TABLE OF CONTENTS

TABLE OF FIGURES

TABLE OF TABLES

Table 8-9 Summary of maximum resistive (R/R_0) and maximum conductive (R_0/R) responses attained with 'Cr_2O_3 + 40% (wt.) H-ZSM-5' and 'Cr_2O_3 + H-Y' selected to carry out SVM classification tests upon exposure to nine test gases. Note that additional information was inputted for SVM analysis such as the value of the responses after 5 secs, 10 secs, 50 secs, 100 secs, 200 secs, 300 secs, 400 secs and 500 secs. Tests that led to high variability between tests were also left out of the input dataset for SVM analysis. 302

1. Introduction

1.1 Motivation and Objectives

This thesis details the results of zeolite-modified thick-film Metal Oxide Semiconductor (MOS) gas sensors as a means to detect substances that pose a threat to health, safety, security and the environment.

The work presented here was largely motivated by the pressing need – and a gap in research – of inexpensive, portable, reliable and real-time technology able to detect illicit drugs, drug precursors, drug by-products and solvents that are either abused recreationally or involved in the process of illegal drug trafficking. To date, there is no commercial device based on MOS technology for the detection of illegally trafficked or abused substances. However, the potential of integrating this technology into a portable electronic nose to detect solvents and drugs or to distinguish among cannabis or non-cannabis consumers has been discussed in the literature.[1–3]

Detecting substances associated with illegal drug traffic is necessary not only due to their far-reaching implications affecting health and the environment, but because they also impact on some of the most pressing United Nations Sustainable Development Goals (SDG),[1] as highlighted in the 2016 World Drug Report published by the United Nations Office on Drugs and Crime (UNODC).[4] It must be noted, however, that the target analytes investigated in this thesis also find themselves relevant to air-quality, safety and medical fields.

Authorities currently face great challenges implementing resources and technology on a large-enough scale to fight against illegal drug markets. The vast volume of containers that are moved worldwide and on a daily basis means that trafficking operations may easily go undetected. Organised criminals take advantage of this by targeting vulnerable hub ports to keep illegal markets active.[5]

It is envisaged that MOS technology could complement existing technologies and benefit current drug interdiction operations. There are, in fact, a number of limitations associated with techniques presently used in drug traffic detection e.g. high cost, lack of portability and sample preparation and expertise is often required for data analysis. Sniffer dog detection is an attractive alternative to technology-based methods, given their ability to detect illegal substances at the part per trillion (ppt) level.[6]

[1] The United Nations Office on Drugs and Crime (UNODC) interlinks the drug problem to some of the 2030 Agenda Goals for Sustainable Development. These include SDG 1 – No poverty – SDG 3 – Good Health and Wellbeing – SDG 5 – Gender equality – SDG 10 Reduced Inequalities – SDG 15 Life of Land – SDG 16 Peace, Justice and Strong Institutions – SDG 17 Partnership for the Goals.

Nevertheless, dogs are also expensive to train and use; they only respond to materials they have been trained to detect and they require regular breaks. Furthermore, it remains unclear how environmental conditions may affect their performance.[6]

MOS gas sensors have been extensively studied to suit a variety of research domains and they have been commercialised for environmental, air-quality and safety purposes. This technology offers great potential to address key societal needs on a global scale, particularly due to its low cost. The technology is versatile, the sensors are sensitive and highly responsive to a variety of gases and vapours, and they are small in size, offering the added potential of portability. Furthermore, manufacture, training and large-scale production is straightforward and feasible. However, MOS gas sensors suffer from two fundamental drawbacks: (1) the inability to selectively and specifically target a gas of interest in a complex gaseous matrix and (2) the high power consumption they require for operation. As such, this thesis has investigated means of addressing these shortcomings.

Three different MOS sensors were selected as the base materials for this thesis. Namely, tin oxide (SnO_2), chromium oxide (Cr_2O_3) and iron oxide (Fe_2O_3). The suitability of these materials as gas sensors is well-established in the literature.[7–12] SnO_2 is perhaps the material that has been most widely researched for gas-sensing purposes. Further, because the base materials, as such, are unselective or lack complete specificity towards one gas, they are often strategically modified to improve their sensing performance. Common practices to improve sensing performance include the incorporation of additives and/or sieving agents,[10,13–15] the grain size reduction of the sensing material,[16,17] or the mixture of different metal oxides to form composites.[18,19]

In this thesis, base material modification was investigated by means of zeolite incorporation (H-ZSM-5, Na-A and H-Y) as admixtures and as coatings, using screen-printing as the fabrication method. Zeolites are described as microporous crystalline structures that are commonly composed of silicon, aluminium and oxygen.[20] The inclusion of zeolites in gas sensor systems is still a relatively new approach in the field. Typically, their catalytic properties, high surface areas, contrasting frameworks and pore-size characteristics are factors reported to contribute to the overall improvement in performance of conventional sensors.[15,21–24] Studies have mostly reported the works of zeolite addition in the form of cover layers, which often work as a sieve to fine-tune the diffusion and detection of molecules according to their size and/or shape.[15,22,23,25,26] Less attention has been paid to zeolite/MOS admixtures; this has been work mostly carried out by our group at UCL.[3,27–29] Aside from introducing

selectivity to sensing systems, zeolites have also been seen to improve the sensor responsiveness towards some gases, in relation to unmodified materials. This line of work has, therefore, opened new avenues to achieving selective, highly-sensitive and responsive gas sensors.

1.2 Novelty of Work

An exhaustive list of all the sensors fabricated for the purposes of this thesis has been presented at the end of Chapter 2 (Tables 2-4, 2-5 and 2-6).

The literature has reported results on the modification of SnO_2 with zeolites with Linde Type A (LTA) and Mordenite Inverted Framework (MFI) frameworks as coatings.[21,22,30] Nevertheless, these studies used different fabrication methods to the ones reported here. For instance, zeolites were grown over Pd-SnO_2 using a seeding process and dip-coating techniques to coat the Pd-SnO_2 surface with zeolites. As such, the work presented in this thesis constitutes novel data. Furthermore, to the best of our knowledge, it is the first time that the incorporation of zeolite coatings of H-Y or Na-A over SnO_2 have been investigated, except for a previous study that was carried out by the author,[3] which reported the gas sensing results of a SnO_2 sensor modified by H-Y coatings upon exposure to acetone, ethanol, nitrogen dioxide, toluene and ammonia. In addition to this, it is the first time that admixtures of all three zeolites have been investigated with SnO_2. In reference to producing some sensors the work of which has already been reported (cover layers of zeolites with MFI and LTA frameworks), they were fabricated to compare our results to that of other groups' but, most importantly, to understand how the performance of the zeolite-overlaid sensors compared to that of the admixed ones.

The effects of zeolite H-ZSM-5 as a coating over Cr_2O_3 have been described in the literature.[26,31,32] In this thesis, admixtures of Cr_2O_3 with zeolite H-ZSM-5 were investigated; to the best of our knowledge, the incorporation of zeolites H-ZSM-5 and Na-A as admixtures with this base material have not yet been reported. Further, layers of zeolite H-Y were screen-printed on top of Cr_2O_3 which, to the best of our knowledge, also constitutes novel data.

It is thought that it is also the first time that the zeolite-modification of Fe_2O_3 sensors is reported.

It follows that the exposure of these sensors to the target analytes reported in this thesis has not yet been reported. Furthermore, it is the first time that the detection of

methyl benzoate – a marker of cocaine commonly targeted by sniffer dogs [33,34] – has been investigated with MOS systems.

Finally, a collection of four zeolite-modified sensors was investigated with classification tools to evaluate whether different classifiers could accurately discriminate among a range of gases of interest. The use of classifiers to investigate the discriminating capabilities of the sensors enabled a better understanding of the real potential of this technology. As such, this thesis investigates:

- The fabrication of three MOS sensor systems based on zeolite-modified SnO_2, Cr_2O_3 and Fe_2O_3. Two different ways of incorporating zeolites into the base material were explored – as admixtures and as overlayers. This was carried out with the aim of inducing selectivity as well as investigating whether zeolite incorporation would support lower temperature operation of the sensors.

- Solvents detection e.g. acetone, toluene, ethanol, not only due to their significance in the drug trafficking world but, also, due to the fact that the detection of trace concentrations of these substances would benefit, for instance, environmental, air-quality, medical, and other security-related fields.

- Hydrocarbons (HC) detection to assess sensor behaviour when exposed to HCs with increasing chain length and to analytes with similar molecular structures. Sensors were exposed to molecules with different functional groups. It was hoped that these results could inform on the MOS/zeolite combinations best suited to detect organic gases with particular functional groups in future.

- The detection of two common illicit drug markers; methyl benzoate as a marker of cocaine and ammonia as a marker of amphetamine-based drugs. Sniffer dogs target these markers in drug interdiction efforts. Sensors were also exposed to a solution of amphetamine in methanol to mimic illegal trafficking strategies.

- The feasibility of using the fabricated sensor arrays to accurately discriminate among a range of analytes of interest. This was evaluated using Support Vector Machines and Random Forests.

1.3 Introduction to Solid State Gas Sensor Technology

The need to monitor polluting or hazardous gases as a result of industrial and domestic activities has grown extensively over the years, given that these gases are known to impact on health, safety and the environment.[35] Gas sensor technology is usually employed to detect individual gases or to selectively target a particular gas in a complex and mixed-gas environment.[36]

Gas sensor technology has found relevancy in numerous applications such as environmental monitoring for air-quality purposes e.g. CO_2, NO_2, CH_4, O_3,[37–39] automotive monitoring for the detection of polluting exhaust gases e.g. NO_x, CO, HCs, SO_x,[26,37,40,41] Volatile Organic Compounds (VOCs), offensive odours and aromas monitoring,[41–45] in medical [46–48] and food quality domains [49,50] and to improve security for explosive, drug and warfare-agent detection.[51–53] As such, the need to develop optimal and reliable sensor technology has surged in the last ~30–40 years and research has focused on designing sensors capable of sensitive, selective, stable and reliable mobile-monitoring of gases. To this end, new materials and architectures, mostly based on nanostructures, have been designed and various fabrication techniques have been studied to better control the microstructure, properties and performance of sensors. Furthermore, different metal oxide composite combinations (hetero- and homo-junctions) have been reported and MOS-material modifications with catalysts and/or filtering agents have also been explored.[13,15,23,54–56]

Gas sensor technology has evolved to what is referred to as 'new generation' gas sensors, which consist of low-powered systems, such as micro-electro-mechanical systems (MEMS).[57] Due to their reduced thermal mass, miniaturised size and low cost, they encourage multi-sensor operation and temperature programming that may also inform on the kinetics of surface processes.[58,59] They serve as great candidates for mobile systems to monitor gases, suitable both for intermittent or continuous operation.[60] Further, self-heating sensors or materials that are gas sensitive at room temperature, such as carbon nanotubes (CNTs), have also been assessed as a means to lower power consumption of sensor devices.[46,61,62]

It is worth noting that gas sensors have been commercialised by several companies e.g. Figaro Engineering *Inc.*, SGX Sensortech, Aeroqual Ltd., α-sense, and monitoring of some of the aforementioned gases is a well-established task in the field.

1.3.1 Gas Sensors Classification Scheme

Before moving on to describing different classification systems for gas sensors, it is important to note that gas sensors operate through the combination of two main functions: (1) a *receptor function*, which enables the recognition of the gas molecules being tested and (2) a *transducer function*, which transduces this said 'recognition' into a signal output. Recognition occurs as a result of the interaction between gas molecules and a suitable sensing material or electrodes – termed the receptors. The interaction between gas and receptor leads to physical or chemical processes such as reaction products, optical property changes, calorimetric effects, variation of the receptor's mass, or to changes in the surface or bulk properties of the sensing material that can be transduced into an electrical or optical signal.[63]

The extensive number of sensing materials and operating principles behind existing gas-sensing technology allows for diverse sensor classification systems. For instance, some classifications are based on the mechanism of the transducer e.g. electrochemical, electrical, mass sensitive, optical, magnetic and thermometric,[64] or on the operating principle of the receptor, resulting in physical, chemical and biochemical sensors.[65,66] Others have classified gas sensor devices into those that see a change in their electrical properties e.g. MOS, polymers, CNTs, and those that undergo a different type of change e.g. optical, acoustic, calorimetric.[67] Table 1-1 below summarises key characteristics of different sensor types based on the transducer function classification scheme.

The sections that follow provide the reader with an introduction to MOS gas sensors, as they have been the type of sensors used in this thesis. The following sections review: the operating mechanism of MOS sensors, the features commonly sought in the fabrication of novel sensors for practical applications, the factors and parameters that influence sensing performance, and the research that has been carried out in recent years to address some of the most pressing disadvantages of the devices.

1.4 Metal Oxide Semiconducting Gas Sensors

Metal Oxide Semiconductors are gas-sensitive resistors that show a reversible change in the conductivity of the sensing material when exposed to gases at temperatures that usually fall in the range of 150 – 500 °C. A typical sensor of the kind used in this thesis has been illustrated in Fig. 1-1; it is composed of an insulating alumina substrate (3 mm × 3 mm) with wide-gap pre-printed interdigitated gold electrodes (150 μm electrode spacing) on the obverse of the sensor (Fig. 1-1A) and a heater track on its

Table 1-1 Summarised comparison of electrochemical, mass sensitive, thermometric, optical and electrical sensor types. HC refers to hydrocarbons, QCM refers to Quartz Crystal Microbalance, SAW refers to Surface Acoustic Wave, YSZ refers to Yttria Stabilised Zirconia.

Sensor Type	Electrochemical	Mass Sensitive	Thermometric	Optical	Electrical
Operating Principle	Based on the reaction of a gas with an electrode, which produces an electrical signal proportional to the concentration of gas. [66]	Mass of sensor surface varies as target gas accumulates on sensitive layer. This mass change is measured by a change in the properties of the support material.	Change of an electrical signal due to a rise in temperature measured as a result of combustion reactions between gas and sensor in air.[66]	Detect change in visible light/other electromagnetic waves upon interaction with a gas, producing a measurable signal. [64]	Sensing material responds by producing a reversible change in electrical properties of the material in the presence of a gas.[67]
Advantages	**Potentiometric:** highly sensitive, selective, mechanically & chemically stable, on-board measurements of polluting gases, fast response/recovery times.[68] **Amperometric:** Good selectivity with biological components, assist in sub-ppm detection e.g. ethanol, formaldehyde.[35] Good for trace gas detection. Low power operation.[69]	Sensitivity and selectivity improved using different polymers in a sensor array.[70] Micro-cantilevers are smaller in size than SAW and QCM sensors and offer higher sensitivity and lower power consumption.[71]	Low cost, [67] stable, reliable, accurate, rugged and durable. [72]	Higher sensitivity, selectivity, stability, lifetime in relation to other gas detectors. Real-time detection possible/quick sensor response times. Not susceptible to changing environmental conditions and gas poisoning. Low drift.[67,73] Miniaturisation [73] and multi-gas detection chambers possible. [74]	Widely studied, commercialise, small size, portable, high sensitivity to gases, fast response and recovery times, low cost and real-time provision of data.[75]
Limitations	**Potentiometric:** high temperature operation, poisoning effects (e.g. HC, CO, Pb), resolution limitations, short lifetime, cost.[76] **Amperometric:** susceptible to environmental changes. Lifetime dependent on gas/experimental conditions. Sensitive to humidity.[64] Solid separator can decompose. Poor exchange may occur between phases at low partial pressures of gas. [64]	Frequency oscillating devices in SAW and QCM sensors are costly and bulky.[64]	Poorly selective and risk of catalyst poisoning or explosion. [67] Commonly used for methane detection and require high power operation (350 –850 mW) at 500 °C. [77]	Larger size and higher cost in relation to other gas sensors. Usually unsuitable for portable applications.	Poorly selective to gases, high power consumption. Surface reactions poorly understood, sensor drift, some sensors may be susceptible to environmental changes.
Examples	YSZ for on-board monitoring of car combustion processes.	SAW, microcantilever and QCM. Used for VOC monitoring.	Pellistors and catalytic bead sensors.[64]	Most common techniques: absorption, chemi-luminescence and fluorescence.[64]	MOS, carbon nanotubes and conducting polymers for reducing and oxidising gas detection.[67]

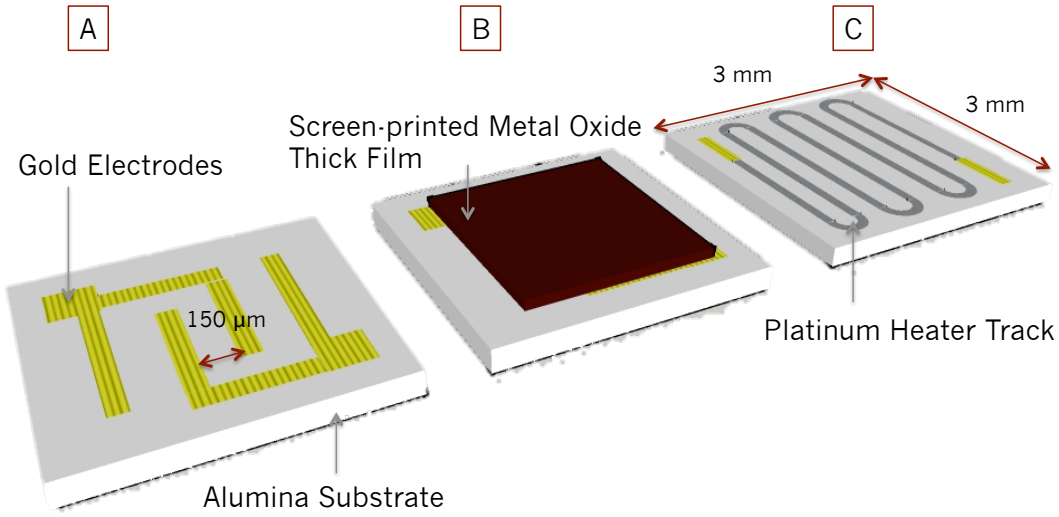

Figure 1-1 Sensor substrate schematic showing (A) obverse of sensor with interdigitated gold electrodes (B) alumina substrate with printed metal oxide semiconductor thick film and (C) reverse of sensor showing platinum heater track. Each substrate measures 3 mm × 3 mm. Figure drawn using Google SketchUp 2014.

reverse (Fig. 1-1C). Gold electrodes enable resistance measurements of the sensing material. The heater is responsible for providing the heat required for sensor operation. The sensitive layer, composed of a number of thick-film screen-printed metal oxide depositions, is illustrated in Fig. 1-1B.

The works of Brattain and Bardeen in 1952 revealed variations in the electrical properties of different germanium surfaces upon interaction with gases.[78] This research inspired further studies of semiconductor materials as gas sensors; Seiyama et al. [79] were the first to publish the gas sensing properties of a ZnO thin film towards a range of HC gases at temperatures ranging between ~200 – 490 °C. Taguchi independently patented his work on thick-film SnO_2 the same year and in 1968 he was the first to commercialise a device for the detection of reducing gases, the renowned Taguchi Gas Sensors (TGS). A year later, the first MOS-type gas sensor company, Figaro Engineering *Inc.*, was established. Since then, extensive work has been carried out on SnO_2 and ZnO, but also on a range of other MOS materials based on n-type e.g. WO_3, Fe_2O_3, TiO_2 and p-type semiconductors e.g. Cr_2O_3, NiO, CuO (see sections 1.4.2 and 1.4.3 for details on the key differences between n-type and p-type semiconductors materials and for details on the mechanism of operation).

The appeal of MOS sensors lies in their high sensitivity to ppm and ppb levels of a wide range of reducing and oxidising gases, they have rapid response and recovery times, they are small in size and they can therefore be assembled into a portable device.[67,75] Moreover, they are inexpensive, their fabrication is straightforward and large-scale production is feasible.[75] Fabrication methods are versatile and a wide range of them

are available to produce either thick or thin film sensitive layers, which include but are not limited to chemical vapour deposition (CVD), sputtering deposition methods, evaporation methods and screen-printing techniques (see section 1.4.4.3). Nevertheless, the high power required for their operation and the sensors' inability to individually respond to vapours selectively constitute major drawbacks for mobile systems.[23,77,80] Further details on the issues of power consumption and other associated drawbacks of MOS technology are provided below.

It is worth noting at this stage that when a MOS sensor is exposed to air and heated to temperatures above ambient, oxygen can ionise and chemisorb on the surface of the sensing material, establishing an initial baseline resistance of the sensor in air. In basic terms, the change in the resistance of a MOS sensor that occurs upon exposure to a gas is due to a change in the concentration of chemisorbed oxygen species, which are consumed as a result of surface reactions with gas molecules (see section 1.4.3 for further details). In fact, the reasons for using high temperatures e.g. 400 °C for sensor operation are that the reactions with oxygen are more specific, the reaction kinetics are faster and cross-sensitivity with water vapour is minimised.[81] Nevertheless, the power needed to drive the heating of the substrate and to control heat dissipation into the surroundings is generally very high (~1–5 W),[82,83] which undoubtedly hinders continuous operation with batteries. Consequently, 'new generation' sensors have been designed to control the thermal properties of these devices. As reported in the literature, novel designs aim to reduce heat dissipation, the overall size of the sensor and the distance between the external heater and the sensing component,[83] whilst ensuring high performance and low cost for mass-production.[57]

In addition to the constraints of consuming high power during operation and the inherent lack of selectivity of the sensors, there are other reported disadvantages of MOS devices. For instance, the reaction processes that occur between gas molecules and the sensor surface – often modified in some way to improve the sensing properties of the base material – are not yet fully understood.[84–86] The sensors may also be susceptible to reversible or irreversible gas poisoning, particularly when exposed to sulphur-based gases and, as a consequence, the lifetime of sensors may be compromised.[87] Further, changes in the environmental conditions may influence the stability of the sensor and lead to drift, which is the variation seen in sensor response, sensitivity, and selectivity, over time.[88] When drift occurs, sensors may require a power-cycling step to regenerate the sensor surface. Alternatively, the use of algorithms may also be employed to mitigate drift effects.[88]

1.4.1 Features and Characteristics Typically Sought in MOS Devices

An assortment of features is typically sought when designing and/or selecting a gas sensor for practical purposes; sensitivity, selectivity, and stability being vital characteristics.

It is important to note that, whilst in several studies the term sensitivity is used to describe how responsive a sensor is to a gas, a different convention has been followed in this thesis. Sensitivity (*S*) is an inherent property of the gas sensor towards a gas and it is described as the degree of reaction of a given sensitive material property (*X*), with respect to a measurand change, which may be infinitesimal, finite or total.[89] The sensor response, or responsiveness, however, represents the output of the response as a function of the measurand applied to its input.[89] It is commonly represented as R_0/R_g, which compares the resistance of the sensor in the presence of just air (R_0) to that in the presence of a target gas (R_g). Selectivity is described as the capability of a sensor to respond selectively to a group of gases or to show specificity towards one target gas.[90] The sensor response time (τ_{90}) is the time taken by the sensor to reach 90% of its saturation resistance value from the moment the gas is injected into the system. Conversely, the sensor recovery time (τ_{10}) is the time taken by the sensor to return back to 10% of its baseline resistance value upon removal of the gas from its immediate surroundings.[80] Stability describes the capability of a sensor to provide reproducible results over time, maintaining key features such as sensitivity, sensor response, selectivity and response and recovery times.[90] Linearity is defined as the relative deviation of a calibration curve from an ideal straight line.[90] Reproducibility refers to the ability of the technology to provide the same sensor responses under different operating conditions.[91] Repeatability is the ability of the device to provide the same sensor responses and performance over repeat tests. The sensor lifetime, as the word describes, represents the time during which the sensor will remain operable.

Due to the fact that the 'ideal' sensor has not yet been designed, selecting or developing a sensor will, indeed, require some form of compromise so that the most important requirements can be met depending on the application.[92] Ideally, a sensor would provide the user with reliable and real-time data, responding or alerting to the presence of an analyte gas in the environment being tested, regardless of its concentration.[64] Thus, the sensor ought to respond quickly and selectively to minimise false alarms and, equally, it should be able to reliably inform the user of the absence of the analyte gas both under intermittent or continuous operation. It should be sensitive and highly responsive to a gas showing specificity towards a single gas or displaying selectivity towards an analyte when presented with a complex gas mixture.[75] The ideal

gas sensor should be stable under harsh environments, resistant to humidity, temperature fluctuations and to gas poisoning and should display minimal drift or noise.[64] Moreover, a sensor or device should be able to withstand high temperatures without the risk of explosion or degradation.[41] Repeatable and reproducible responses should be obtained over time and sensors should respond linearly to trace gas concentrations without needing continuous recalibration steps.[64] Alternatively, sensors should be disposed of and replaced cheaply. Practical applications require small, robust, cheap, durable, easy-to-fabricate sensors producible on a large scale.[64,93] Mobile systems must be easy to use and handle, requiring simple training and maintenance.[64]

1.4.2 N-type and P-type Semiconductor Gas Sensors

Semiconductor materials exhibit conductivities that lie between those of metals and insulators and they can be classified into intrinsic or extrinsic semiconductors.[93] The energy levels in a solid are very closely spaced together such that they can be said to form an energy band. In semiconductors, there exists a valence band, which is partially filled with electrons and a conduction band that is higher in energy and is empty. The energy bands are separated by an energy band gap, E_g, where the existence of electrons is not permitted. The energy of the highest filled state in the energy band at absolute zero (T = 0 K) is called the Fermi level (E_F).[93] The Fermi function $f(E)$ corresponds to the probability that an energy level will be occupied by an electron. In order for conduction to occur in metals, electrons have to 'jump' to unoccupied levels – above the Fermi level – and this can be achieved with an external energy source such as thermal excitation above absolute zero. In an insulator (such as diamond), thermal energy is not sufficient to promote electrons from the valence band, which is completely filled with electrons, to the conduction band, thus $f(E) = 0$ in the conduction band.[93] Semiconductors have an energy gap in the region of 0.5 – 5.0 eV and, at energies below the Fermi level, conduction does not occur.[75] Conversely, at energies above the Fermi level, electrons begin to populate the conduction band, which leads to an increase in the material's conductivity.[75] In semiconductor materials, conduction electrons and holes are the charge carriers. Common MOS materials used in gas sensing have band gaps of: SnO_2 (3.6 eV),[94] ZnO (3.35 eV),[94] Cr_2O_3 (3.4 eV),[11] CuO (1.4 eV),[95] NiO (3.7 eV), Fe_2O_3 (2.1 eV).[96]

Intrinsic Semiconductors

In a semiconductor, when an electron gets promoted to the conduction band, it creates a pair of charge carriers, namely, an electron and a hole pair.[93] In a pure silicon

material, for instance, there will be an equal number of electrons and of holes. This sort of semiconductor is named intrinsic semiconductor, and it is a property of the pure material. The conductivity will increase exponentially with temperature, which is the opposite trend seen in metals.[93] Examples of intrinsic semiconductors include germanium and silicon and they have a high degree of purity.

Extrinsic Semiconductors

This thesis focuses on extrinsic semiconductors. Extrinsic semiconductors are semiconductors that contain impurities in their structure, which have been added to the pure material and are referred to as dopants.[93] Extrinsic semiconductors can be divided into n-type and p-type materials. The former has a majority of negative (n) charge carriers, or electrons, dominating conductivity. In p-type semiconductors the majority charge carriers are holes and they have a positive (p) charge. As an example, intrinsic silicon has four outer-shell electrons and the incorporation of an n-dopant such as phosphorous (P^{5+}), which has five valence electrons, would lead to an excess of negative charge in the structure.[93] The excess electrons could thus promote conductivity. Conversely, the incorporation of a p-dopant into the pure silicon structure such as aluminium (Al^{3+}) (three valence electrons) may produce an electron hole following the substitution of a Si atom for an Al atom.[93]

Note that the incorporation of an n-dopant e.g. phosphorous into the silicon structure will affect the band energy structure of a semiconductor material. The excess electron originating from phosphorous will be unstable and will create a donor level below the conduction band which, as a result, produces conduction electrons in an easy fashion.[93] For this reason, conduction electrons in extrinsic semiconductors have smaller band gaps than intrinsic ones. In essence, the Fermi level will be shifted upwards as a consequence of the excess electrons. On the other hand, an acceptor level will be formed near the valence band when incorporating a p-dopant into the silicon structure.[93] That is, a valence electron from Si can be easily promoted to this acceptor level, leaving a hole behind i.e. a positive charge carrier. Similarly to n-type semiconductors, the energy barrier to producing a positive charge carrier will be lessened, in relation to an intrinsic semiconductor material.[93] The position of E_F will be shifted downwards in this case. An illustration of this is provided in Fig. 1-2 below.

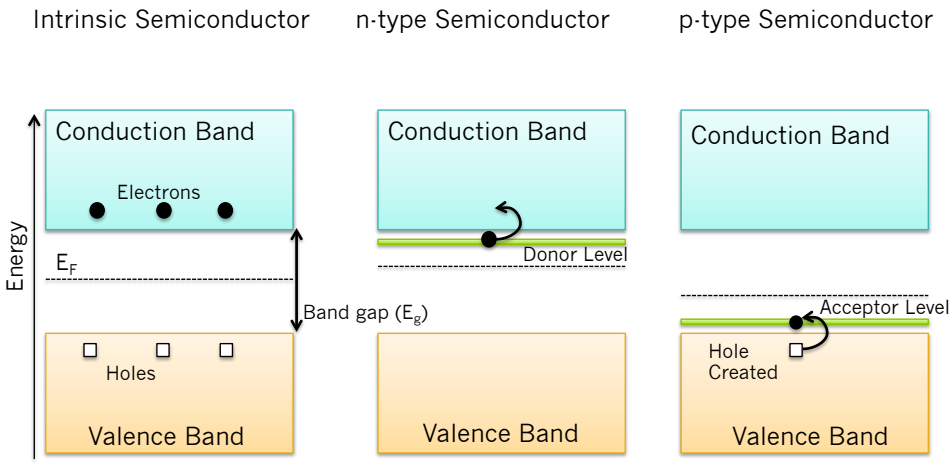

Figure 1-2 Energy band representation of an intrinsic semiconductor (left), an n-type semiconductor (middle) and a p-type semiconductor (right). Image adapted and redrawn from [29,93].

N-type and p-type semiconductors behave differently upon exposure to reducing and oxidising gases – the mechanism of operation is explained in detail in section 1.4.3 below.

1.4.3 Operating Mechanism in MOS Sensors

The operating mechanism of MOS sensors is based on a change in the resistance of the sensitive material, which is brought about by changes in the composition of the surrounding atmosphere.[97] The conduction mechanism in n-type and p-type systems is described by two models; one considers the ionosorption of gaseous species at the sensor surface and the other attributes the effects of sensing to changes in the oxygen stoichiometry, which occur because of a variation in the amount of (sub-)surface oxygen vacancies and their ionisation.[98] Nevertheless, the mechanism of gas detection with MOS systems is still a subject of debate and both models have been criticised because of a lack of spectroscopic and electrical data to back them up.[98] The former is the most widely accepted model,[99] and has been explained in further detail below.

In essence, in air and at temperatures in the range of 150 °C to 500 °C, oxygen adsorbs on the surface of the MOS material and it traps electrons from the bulk, serving to either increase the resistance of the material (n-type semiconductors) or to decrease it (p-type semiconductors).[81] The resistance change is the result of various processes that are thought to occur at the surface, at grain boundaries and in the bulk of the sensing material.[100,101] These processes include adsorption/desorption, redox reactions, catalysis, diffusion, chemical reactions and so on. In turn, these processes are largely influenced by other factors such as the type of sensing material, its microstructure, morphology, concentration of reactive surface sites and of charge

carriers, and energetic parameters of adsorption and desorption, to name of a few.[101,102]

The resistance changes and response patterns measured in a typical n-type or p-type MOS gas sensor upon exposure to a reducing gas are illustrated in Fig. 1-3 and Fig. 1-4 below, respectively. A test is performed at a temperature of choice e.g. 400 °C and it consists of (1) initial sensor exposure to air, (2) a concentration of gas is supplied for a specific amount of time and then (3) the gas is switched off and just an air atmosphere is supplied to the sensor once again, whereby the surface state density ought to be restored and the sensor should respond by reversibly returning to its initial baseline value.[103] Fig. 1-3A illustrates how the resistance of the sensor varies with the surrounding atmosphere: in an n-type semiconductor the resistance of the sensor decreases when it is exposed to a reducing gas such as carbon monoxide.[104] The sensor response in this case is calculated as a ratio of the sensor resistance in air (R_0) to that in the presence of the gas (R_g), thus $R = R_0/R_g$. When an n-type semiconductor is exposed to an oxidising gas such as nitrogen dioxide (NO_2), the response is calculated as $R = R_g/R_0$.

Conversely, in p-type semiconductors the sensor response is calculated as $R = R_g/R_0$ upon exposure to a reducing gas and as $R = R_0/R_g$ when exposed to an oxidising gas. The concepts of response and recovery times elucidated in section 1.4.1 above have also been illustrated in Figs. 1-3A and 1.4C for clarification purposes.

The behaviour of n-type and p-type materials upon exposure to reducing and oxidising gases can be summarised as follows:[104] When an n-type semiconductor is exposed to air, atmospheric oxygen will populate the surface of the material. At low temperatures, oxygen may adsorb on the surface in molecular (O_2) or atomic form (O).[105] The high electronegativity of oxygen atoms and molecules allows them to act as electron acceptors, thus extracting and trapping electrons from the bulk of the sensing material, becoming ionised to form O^-, O^{2-}, O_2^- species.[104,105] However, the type of oxygen species that dominate on the surface depends on the operating temperature and on the humidity conditions.[106] The extraction of electrons from the sensing material results in the creation of additional surface states within the band gap of the material.[104] In turn, trapped electrons form an electron depletion layer near the surface of the material, termed EDL, which creates a potential barrier (or Schottky barrier) between adjoining grains.[107] This establishes the baseline resistance of the sensor in air.

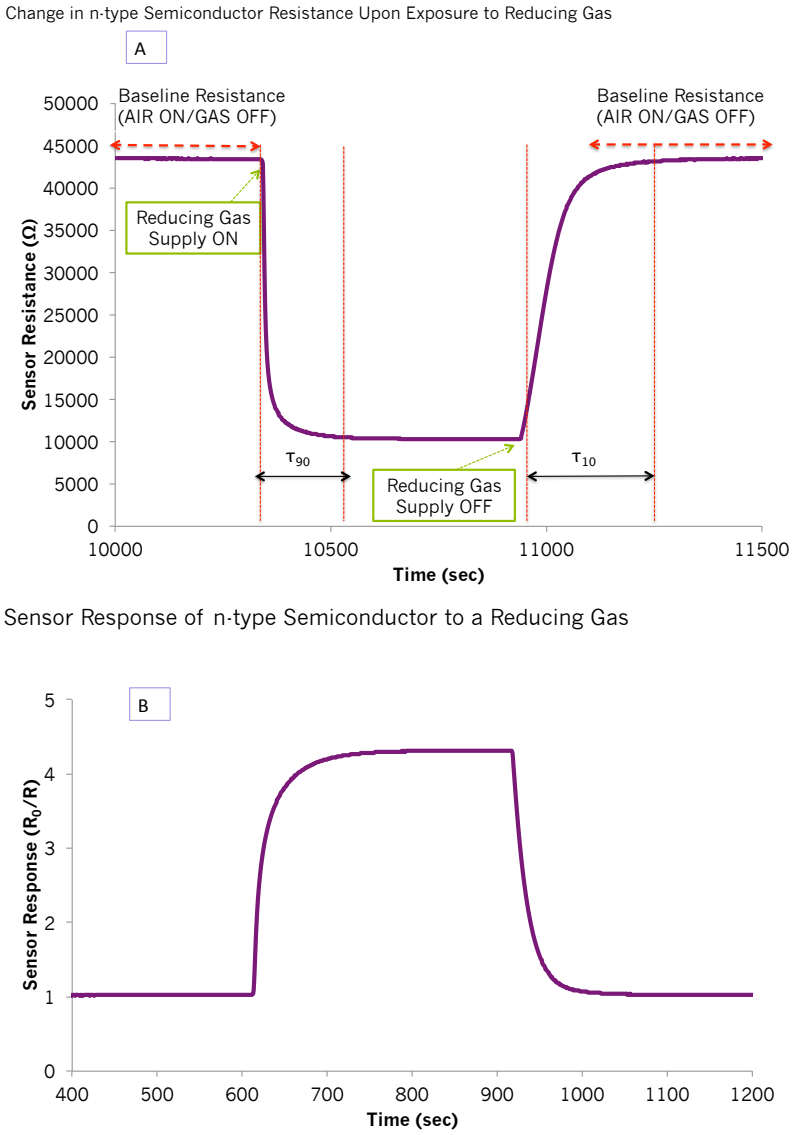

Sensor Response of n-type Semiconductor to a Reducing Gas

Figure 1-3 (A) Resistance change of an n-type semiconductor material from an air ambience to one containing a reducing gas, e.g. ethanol, at a certain temperature. (B) Sensor response of an n-type material (R_0/R_g) upon exposure to a reducing gas of choice at an operating temperature of 400 ˚C.

The supply of a reducing gas such as carbon monoxide (CO) to an n-type semiconductor e.g. SnO_2 leads to its reaction with chemisorbed oxygen species at the surface, producing carbon dioxide (CO_2), which then desorbs off the surface.[81] The occurrence of this reaction leads to a change in the concentration of oxygen species at the surface of the material. In essence, oxygen oxidises the gas and the trapped electrons are injected back into the semiconductor.[103,107] This process reduces the thickness of the EDL, lowering the height of the potential barrier between adjoining grains, and leading to an increase in the conductivity of the sensing material.[108] This is illustrated in Fig. 1-5A below.

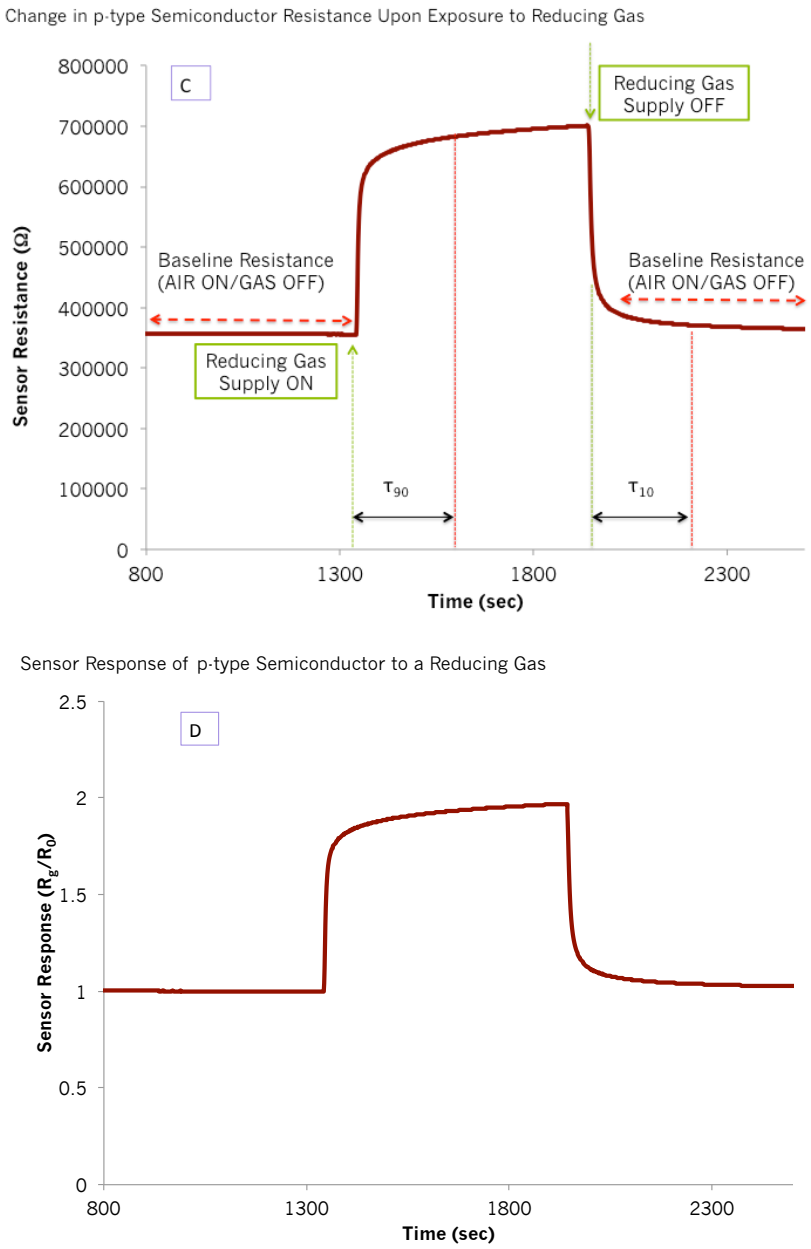

Figure 1-4 (C) Resistance change of a p-type semiconductor material from an air ambience to one containing a reducing gas e.g. ethanol at a certain temperature. (D) Sensor response of a p-type material (R_g/R_0) upon exposure to a reducing gas of choice at an operating temperature of 400 ˚C.

Conversely, when an n-type material is exposed to an oxidising gas such as NO_2, the gas will extract electrons from the metal oxide material, reducing the concentration of the majority carriers in the material. This, in turn, leads to an increase in the size of the EDL and the resistance of the sensor material increases.

P-type semiconductors such as Cr_2O_3 behave in an opposite fashion. When molecular oxygen adsorbs on the surface of a p-type semiconductor, oxygen will ionise, extracting electrons from the sensing material.[109] This, in turn, leads to the formation of a hole

accumulation layer, (HAL), at the surface of the material.[107] As a consequence, the oxidation reaction between carbon monoxide and oxygen species results in a reduction of the concentration of the majority charge carriers – holes – as the electrons are injected back into the oxide and recombine with the holes in the valence band. This leads to an increase in sensor resistance with exposure to a reducing gas (Fig. 1-5B).

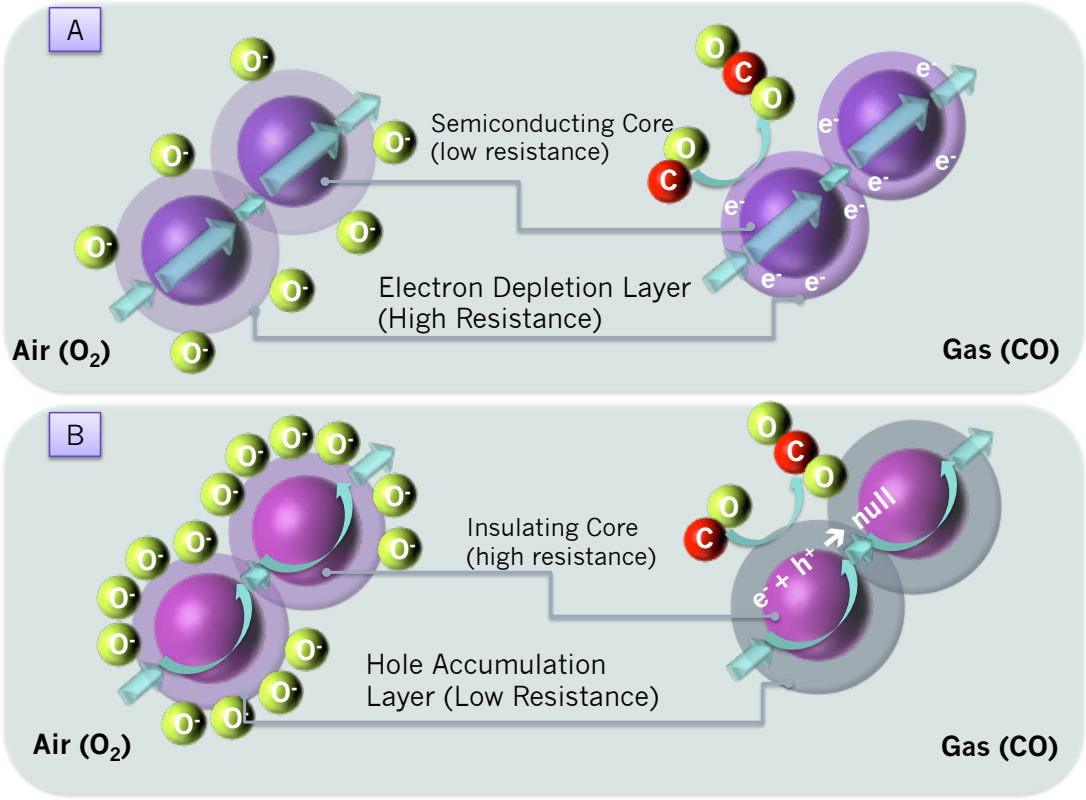

Figure 1-5 (A) Gas sensing mechanism of an n-type semiconductor when exposed to air (left image) and when carbon monoxide is supplied to the sensor (right image). (B) Gas sensing mechanism of a p-type semiconductor when exposed to air (left image) and when carbon monoxide is supplied to the sensor (right image). Figure adapted and redrawn from [110].

The opposite trend is seen when a p-type material is exposed to an oxidising gas. The oxidising gas can remove electrons from the MOS, increasing the concentration of holes and therefore the conductivity of the material.[109] The resistance change exhibited by n- and p-type materials is summarised in Table 1-2 below.[104]

Table 1-2 Type of resistance change seen in n-type and p-type semiconducting materials according to the gas atmosphere the sensors are exposed to.[104]

Semiconductor Type	Reducing Gas	Oxidising Gas	Decrease of P_{O2}
n-type	Decrease	Increase	Decrease
p-type	Increase	Decrease	Increase

1.4.4 Parameters that Affect the Sensing Performance of MOS Sensors

As alluded to in section 1.4.3 above, there are a range of factors that influence the performance and gas-sensing characteristics of MOS sensors. As detailed by Korotcenkov [101], the rate of gas response will be directly affected by diffusion and reaction processes (catalysis, redox reactions, adsorption/desorption, charge transfer between adsorbed species and bulk and chemical reactions) occurring at the sensor. These processes are also reported to be influenced by structural parameters of the sensors such as the material microstructure,[100] the grain size,[16] the size distribution of particles,[111] the incorporation of additives,[112] the film thickness,[7] and properties of the semiconducting materials such as the density of surface states and the electronic structure of metal oxides.[111] Some of these issues are considered in the following sections.

1.4.4.1 Temperature Effects on the Adsorption and Desorption of Gases

MOS commonly see a bell-shaped curve in the sensor response with increasing temperatures e.g. from 150 °C to 500 °C. This is because the adsorption/desorption of gas molecules and the rate at which gases react with the sensor will differ with temperature. In essence, when a sensor is heated, the gases may either adsorb due to the high reactivity of the MOS surface or they may react with pre-adsorbed species on the surface.[101]

As discussed in previous sections, changes in sensor resistance are introduced by the consumption of oxygen species adsorbed at the surface upon interaction with a gas. Barsan and Weimar [113] detailed the different oxygen species that populate the sensor surface as a function of temperature. Molecular (O_2^-) or atomic (O^-, O^{2-}) oxygen may chemisorb at the sensor surface. At temperatures below 150 °C, molecular chemisorption predominates and, above this temperature, atomic species prevail. From this, it can be understood that a gas may interact with different oxygen species as the temperature is progressively incremented and, as such, sensor responses to a gas will differ with temperature.[114]

Further, water vapour can adsorb on the surface of metal oxides by physisorption or hydrogen bonding.[113] Adsorption of water molecules occurs more readily at lower operating temperatures (≤ 200 °C). Further, surface hydroxyls begin to desorb at 400 °C.[115] It is suggested that for every water molecule that adsorbs, two hydroxyl ions will form through a dissociative process – a hydroxyl group adsorbs on metal cations at the surface, which has high local charge density and a strong electrostatic field. The proton then reacts with chemisorbed O^{2-} and a second hydroxyl group will form.[115] As more water vapour comes into contact with the adsorbed hydroxyl ion layer, it can dissociate

to form H_3O^+.[115] The adsorption of water is also reported to lower the responses towards gases and, also, due to hydroxyl groups populating the surface of the material, there are fewer available surface sites for oxygen to chemisorb and this results in a reduction of the baseline resistance of n-type semiconductors.[113,116]

Typically, gas-sensing tests are performed at different temperatures so as to determine the optimal operating temperature at which the sensor provides the highest response to a gas. The reasons why sensor responses are diminished in the lower and higher temperature ranges of the described bell-shaped response vs. temperature curve are explained below.

Betty et al. [117] described the effects of high temperatures on the adsorption of gaseous species at the surface of a SnO_2 sensing material; they found that gas sensitivity was higher at lower operating temperatures and this was due to a higher concentration of adsorbed gaseous species at lower operating temperatures. The sensitivity to test gases decreased as the temperature incremented, which was the result of fewer oxygen and gaseous species adsorbing at the surface, failing to produce a sizeable resistance change during gas/oxygen interaction.

The above study is in line with what is reported by Korotcenkov [64]; where it is stated that at high temperatures the rates of gas desorption increase and there are fewer adsorbed species available for gas interaction, which leads to lower sensor responses. As reported by Ahlers et al. [118], high temperatures lead to higher reactivity between gaseous species and oxygen and to a limited penetration of gas molecules into the material bulk, which consequently leads to increased rates of gas desorption. In a different report by Korotcenkov,[119] it was detailed that at high temperatures the rate of response kinetics is fast, which leads to an equilibrium being reached between the partial pressure of oxygen and the material bulk. At moderate temperatures, the gas will react with the sensitive material. However, due to the diffusion of oxygen into the material bulk being less profound, the chemical composition of the sensing material fails to reach an equilibrium state during the time of gas exposure. At moderate temperatures, redox reactions are thought to take place. At low operating temperatures chemisorption based on adsorption and desorption processes is thought to prevail.[119]

The sensitivity maximum seen at a particular temperature is dependent on the type of gas supplied and also on gas concentration. Ahlers et al. [118] describe temperature and concentration distributions via a rate equation approach. They showed that the sensitivity maximum at a certain temperature is dependent on the strength of

adsorption of the analyte gas on the material surface and on the kinetic barrier or activation energy that needs to be overcome to induce a combustion reaction at the surface. They suggested that with higher analyte concentrations the reaction threshold with oxygen and the strength of adsorption of test gas is reduced. Further, at high operating temperatures fewer combustion reactions occur due to poorer surface coverage and, as a result, sensor responses decrease.

1.4.4.2 Microstructural and Morphological Effects on Sensing Performance

The microstructure and morphology of the sensing layer has been seen to affect the properties of the surface, the bulk and particle contacts such that they lead to great differences in sensing performance.[16] Microstructural and morphological effects may refer, for instance, to the porosity of the material, the concentration of surface-reactive sites, the level of sintering between particles, as well as their size and shape and film homogeneity.

The way in which a sensing material is fabricated and the subsequent heat treatment it is subjected to will influence grain connectivity such that open necks, closed necks or grain contact intergranular boundaries will form (see Fig. 1-6 below for an illustration of this). The type of connectivity between grains inherently affects the changes in sensor resistance and their performance upon exposure to gases. Open necks are formed in well-sintered materials, where the EDL is continuous between neighbouring grains.[29] The central, bulk, region of the necks exhibits low resistance. Conductivity, in this case, is dependent on the gas and its supplied concentration, as gas adsorption and interaction with the sensing material will govern the size of the conduction path.[29] On the other hand, closed necks are formed in less well-sintered materials. In this case, the EDL between neighbouring grains overlaps, creating high-resistance paths in the central region of the necks.[29] Conductivity across the necks will be dependent on the injection of surface state electrons back into the conduction band and the subsequent interaction with a gas. Grain contact boundaries occur when grains are barely touching and they form porous films, where the trapped charge on surface states leads to high-energy barriers, also known as double Schottky barriers between neighbouring grains.[16,29] Conductivity will be dependent on the activation energy needed to overcome the formed potential barrier.[29]

The effects of grain size on sensor responses have been studied widely in the literature.[16,120–123] It has been established that lowering the size of particles from the μm to the nm scale enhances sensor responses due to the introduction of an increased porosity and surface area. Indeed, controlling the grain size and the surface area works

towards the amplification of the surface sites and accessibility for gas interaction. The EDL extends to a depth, *L*, in the presence of air. *L* is determined by the Debye length and the strength of oxygen chemisorption.[16] Xu et al. [16] detailed that reducing the diameter of a grain (*D*) to a value comparable to 2*L*, resulted in the entire grain being depleted of electrons. As such, it can be deduced that the sensitivity of a material to a gas varies with *D*. In their study, *L* was found to be 3 nm for both thin and porous films of SnO_2, making the expected critical grain size ≈6 nm. Due to the fact that at such small particle sizes the pure SnO_2 was unstable above 400 °C, the same group found a way of stabilising SnO_2 with small grain sizes by incorporation of foreign oxides so that SnO_2 could withstand the sintering temperatures needed for fabrication whilst simultaneously controlling the crystallite size.

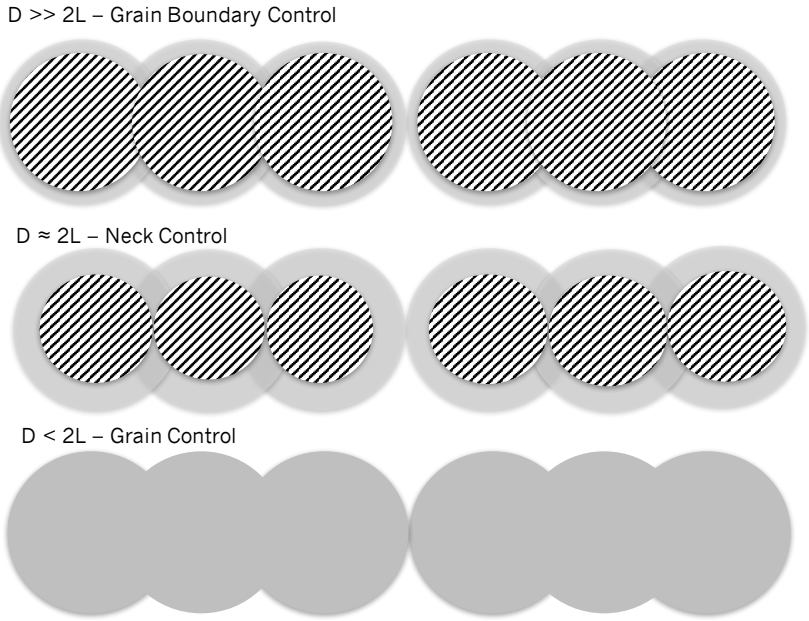

Figure 1-6 Illustration of the grain size effect model. The highlighted region marks the core region of the grain, which is low in resistance. The unmarked region illustrates the electron depletion layer which is high in resistance. Image adapted and redrawn from [16].

Similarly, *L* was also controlled by impurity incorporation into the lattice of semiconducting materials. For instance, the substitution of Sn^{4+} in the SnO_2 lattice for Al^{3+} resulted in an increase of *L*, whereas its substitution with Sb^{5+} caused it to decrease. In their paper,[16] they evaluated how the modification of *L* and *D* influenced gas sensitivity of SnO_2 sensors. They found that in pure SnO_2, *D* increased steeply with increasing sintering temperatures. Sensor sensitivity (defined as R_0/R_g in their paper) to 800 ppm H_2 was seen to increase sharply in both pure and impregnated SnO_2 sensors when the crystallite size was comparable to or lower than 2*L* and the incorporation of additives did not influence the inherent sensitivity of SnO_2 to H_2. A correlation was found between sensor sensitivity and crystallite size both in pure and impregnated

sensors upon exposure to H_2 and CO. With sensor exposure to less reactive gases such as butane, the data was scattered more widely and it was seen to depend on the catalytic properties of the additives. When the reactivity of the gases was more complex (C_2H_5OH, NO_2 and NO), no correlation was found between sensitivity and crystallite size. They developed a model to explain why sensitivity increased with increasing *L* when comparing samples with the same grain diameter; note that grains in a sensing element are connected to each other by grain boundary contacts or by necks. When *D* or the neck size, *X*, is much larger than 2*L (D >> 2L)*, the grain contacts are the most resistant points to electron conduction in the chain of crystallites. In this case, grain-boundaries control the resistance and sensitivity of the sensor. Where *D* is comparable to 2*L (D ≈ 2L),* sensitivity is governed by the necks, which are the most resistant points to electron conduction. Finally, when *D* is lower than 2*L (D < 2L)*, grains dominate the resistance as well as the sensor sensitivity. This is illustrated in Fig. 1-6.

Barsan and Weimar [113] suggest that a straightforward approach to achieving optimal sensor sensitivity is to increase the porosity of the sensing film, and they provide the following explanation as to why. In compact thin films, for example, gas interaction is restricted to the geometric surface of the sensor. As such, porous films offer an amplified area available for gas interaction, when compared to the geometric area available in dense films (see Fig. 1-7 below). Porous films exhibit a reduced area of contact between particles or a reduced width of necks. As such, using porous sensing materials with high specific surface areas may lead to great enhancements in sensor responses, whilst also assisting in the reduction of the operating temperature of sensors.[101] In the same review paper by Korotcenkov,[101] it was suggested that porous films offer a higher rate of response kinetics than those based on dense films.

Employing materials with small pore sizes may also serve to minimise the effects of sensor poisoning.[101] The importance of having a porous film to obtain enhanced sensor responses was also highlighted by Traversa [115]. In the latter study, it was also suggested that the total open porosity of the system as well as the pore size distribution play a key role in improving sensor responses.[115]

D. E. Williams' group published a number of reports on the effects of microstructure on sensor responses as well.[100,124,125] In Naisbitt et al. [100], they explained the influence of microstructure on the sensor responses of p-type chromium titanium oxide (CTO) by building a model that predicted sensor behaviour as a function of the level of inter-grain connectivity.

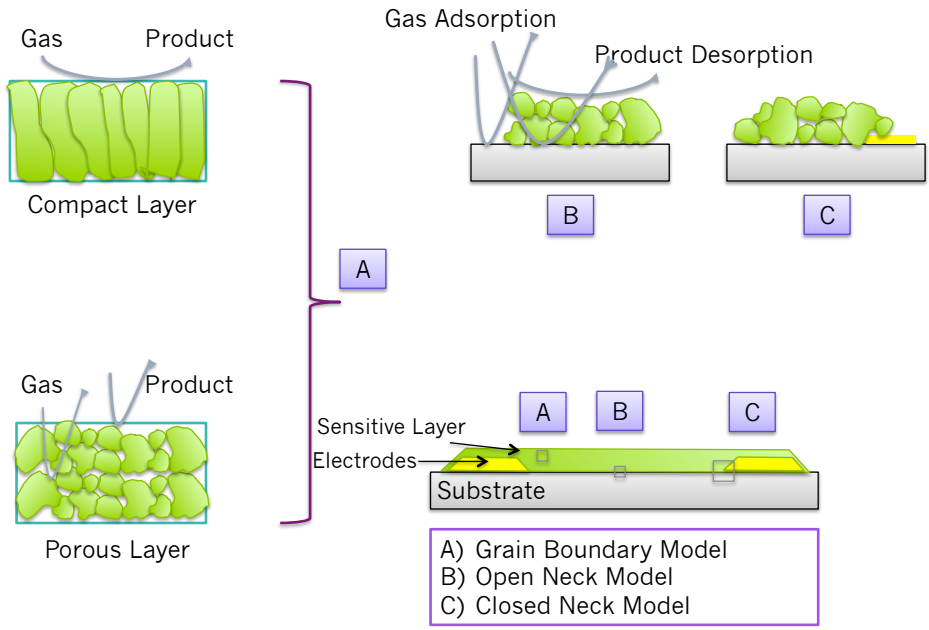

Figure 1-7 Illustration of the sensitive layer in a resistive gas sensor. Compact layers depict how the gas interaction with the sensitive layer is restricted to the sensor surface. Porous layers enable gas diffusion through the system down to the substrate. In porous layers, gas interaction may occur at the surface of individual grains, at the boundaries between adjacent grains and at the interface between the grains and the electrodes or the substrate. Image adapted and redrawn from [113].

The model was based on the assumption that only the surface of the material that is accessible to gas molecules will result in a change in sensor resistance. They modelled a porous, sintered, particulate sensing material using three key regions: the surface, the bulk and the particle boundary (Fig. 1-8). It was reported that the surface, which extends to a depth that equals the Debye length, is sensitive to gases, whereas the bulk remains unaffected by the presence of a gas and its resistance is not dependent on the concentration of the gas.[100] In well-sintered materials the inner regions of necks behave as the bulk and only the outer regions of the necks are sensitive to gases. In materials that are less well sintered, the entire region of the necks is gas sensitive and a Schottky barrier may exist between particles.

When the sintering temperature was increased, the number of necks, the regions of interaction and the particle sizes augmented. This, in turn, increased the effective area over which the particle boundaries interacted and it was predicted that the proportion of the total resistance that the particle boundaries accounted for in such situations would decrease. Further, with increasing particle size, the proportion of the total bulk volume increases and that which is surface decreases. Given that the effective area of the bulk and surface resistances change proportionally to their volume, the overall contribution of the bulk resistance would decrease i.e. a bulkier resistor has lower resistance, and that of the surface would increase with an increase in sintering

temperature.[100] This was also highlighted by Korotcenkov [101], who stated that with the purpose of reaching optimal sensor sensitivity it is necessary to increase the role of surface conductivity or the contribution of inter-crystalline contact barriers by decreasing the contact region between particles or the width of necks.[101]

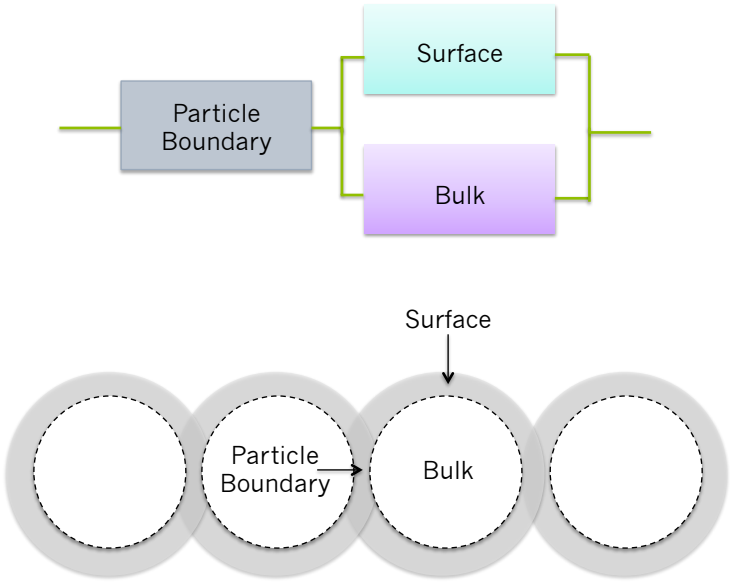

Figure 1-8 Schematic of the network of resistors representing the particle boundaries, the surface and the bulk of a sensing material and how they relate to sintered, spherical particles. The dashed line depicts the depth of the surface - the depth corresponds to the Debye length. Image adapted and redrawn from [100].

The microstructure and morphology of particles will also affect the way in which gases diffuse and percolate through the system. For instance, Shimizu et al. [126] studied the effects of diffusivity of a gas and its reactivity on the sensing properties of thick-film SnO_2 sensors by evaluating the sensitivity of the sensor in the inner regions and on the surface of sensors, which had different noble metal loading. They found that when the diffusion through a thick-film material is governed by molecular flow i.e. the size and viscosity of the sample molecules, O_2 is able to move readily through the sensing system due to its small size and larger mean free path in comparison to larger molecules such as CH_4. This therefore results in a lower concentration ratio of CH_4/O_2 in the inner region of the sensor, when compared to the surface of the material. The increased coverage of oxygen adsorbates in steady state consequently leads to lower sensitivity towards CH_4 in the inner region of the sensing material. The same behaviour was found when exposing the sensors to larger molecules i.e. ethanol. The opposite effect was found upon exposure to a smaller molecule, H_2, which was said to have higher diffusivity than O_2.[126] Similar work was performed by the same group in Shimizu et al. [127].

1.4.4.3 Film Thickness Effects on Sensor Responses

The thickness of the sensitive layer in MOS devices has been shown to greatly influence sensor responses, the temperature at which sensor sensitivity is highest, sensor response kinetics and film morphology.[7] There is a variety of methods available to deposit MOS layers but technologies are divided into those that produce either thick or thin films. The thickness of thin films ranges between 6 – 1000 nm and that of thick films usually ranges between a few μm and a few hundred μm (10–300 μm).[128]

There is a wide range of techniques available for producing thin films such as chemical vapour deposition (CVD), sol-gel deposition, sputtering and evaporation. Thick-film technology is mostly carried out via screen-printing, but there are other methods available such as drop coating, dip coating and pipetting.[129] The effects of film thickness on the sensor responses vary as reported in the literature; whilst some studies report that thinner films result in higher sensor responses and higher sensitivity to vapours, other studies report opposite trends (see below). This serves as a clear indication of the numerous variables and factors that, in fact, influence the sensing characteristics of sensors. A brief account of different deposition methods and a comparison among thin and thick-film technologies is provided below.

CVD employs one or more precursor gases that contain the metal of interest and, through an oxidation reaction or decomposition process, the metal oxide film is deposited on a heated substrate. This technique commonly produces dense films that may lead to diminished sensitivity in relation to thick-film sensors. CVD offers great reproducibility and spatial control. However, aside from affording the control of the size of the material particles, it limits any further control of the material structure.[105]

Sputtering and evaporation thin film deposition techniques are also referred to as Physical Vapour Deposition (PVD) technologies. Sputtering deposition utilises a target, which is a plate of a stoichiometric mixture containing the metal of interest, positioned such that it faces the heated substrate onto which the material will grow. A gas such as argon (Ar) will be introduced into the system and when power is connected to the target it will cause electrons to travel away from it. The collision between electrons and the ionised gas e.g. Ar^+ will create plasma that travels to and deposits on the substrate. A drawback of this technique is that the path of the ejected particles may fail to cover certain regions of the substrate and it also requires a vacuum for operation. This technique also provides compact material morphologies, which may hinder or affect gas diffusion.[105,128,130] Reactive sputtering is also employed for the fabrication on gas sensitive films. In the latter, a target of a particular composition will be sputtered in the

presence of an individual gas or a mixture of gases such as argon and oxygen. The gases then react with the target to form a coating of the desired material.

Evaporation is a high-vacuum method in which the target material is heated through electrical or beam heating and it is, in turn, turned into the gas phase. The material condenses on the substrate without colliding with energised particles and begins to form a film. This technique is straightforward; it can be used to deposit a wide range of materials and enables the accurate control of film growth rate and thickness. Furthermore, due to its operation under vacuum, sources of contamination are eliminated.[131] A key drawback of this method is that the vapour composition is dependent on the vapour pressures particular to the elements in the target and thus, the deposition of several materials with well-defined stoichiometry becomes intricate.[105]

Korotcenkov and Cho [7] provided a very detailed study of the effects of film thickness on sensor responses, optimal operating temperatures, film morphology, and sensor kinetics of SnO_2-based sensors. They reported that in thin films, the grain size of the sensing material will be influenced by the film thickness, whereas this is not observed in thick films, the grain size of which is dependent on the fabrication method and heat treatment the sensors are subjected to.[7] They reported work based on thin-film SnO_2; as the film thickness was incremented, the grain size of the SnO_2 material also increased. They found that thicker films were more porous than thinner ones, which were, in turn, more densely packed due to smaller grain sizes of the material. Thicker films were said to be more responsive to reducing vapours than thin-filmed ones, which were, conversely, more responsive to oxidising gases. They also found that with thin films, as the film was made thicker, there was a shift in the optimal operating temperature towards lower temperatures but the thickness had little effect on the magnitude of response of the sensor towards a gas. Furthermore, although it would be favourable to use sensors that worked well at lower operating temperatures, the thicker films came with an increase in response time, which is unfavourable for practical applications.[7]

Du et al. [132] reported the responses of thin-filmed SnO_2 towards CO and found that above and below a certain film thickness (26.2 Å), the responses towards the gas decreased. Conversely, Preiβ et al. [133] noticed an increase in SnO_2 sensor response with an increase in film thickness (55 nm, 110 nm, 213 nm) upon exposure to CO. Although compact films have an associated lower responsiveness to gases, they offer higher thermal and temporal stability.[101]

Thick-filmed sensors are most commonly fabricated by screen-printing [134,135] and they have been the method of choice in this thesis. This method is popular because it is inexpensive, its operation and sample preparation is straightforward, process reproducibility and large-scale production is easily achievable and it can be an automated process.[136] Additionally, it is a versatile technique that enables working with different dimensions of miniaturised sensor substrates and the patterned mesh on the screens can be designed to extrude different sensing material shapes and areas.[108,137] Because the technique allows controlled and simultaneous printing of a large number of sensors, the variability among sensors ought to be minimal and good repeatability among sensor batches should be obtained.[136] The technique works as follows: a metal oxide paste is screen-printed onto a ceramics substrate, which covers the electrodes. The paste is prepared by mixing an organic binder with the oxide powder and ground in a pestle and mortar so that a homogenous ink is obtained. The binder ensures adhesion of the paste onto the substrate upon printing. The ink is extruded through a patterned screen-printing mesh by means of a squeegee. Following the first deposition of the paste, subsequent layers can be printed on top after drying it. The film thickness commonly varies between 10 and 300 μm.[138] However, other studies have reported thicker films (500 μm).[122] Once the depositions process is completed, sensors are placed in a furnace so as to evaporate the organic vehicle and to ensure strong adherence of the material to the substrate.

The effects of film thickness on sensor response are contrasting in the literature, while some studies noted that an increase in film thickness resulted in a decrease in sensitivity,[139–141] other studies have found opposing trends.[108,142] Other groups report that an initial increase in the response of a SnO_2 sensor was attained when increasing the thickness from 5 μm to 10 μm, but subsequently the sensor responses were unaffected by film thickness.[134] Montmeat et al. [143] tested different SnO_2 film thicknesses ranging between 10 – 80 μm and found that the sensor responses decreased with film thickness upon exposure to ethanol. It must be noted that as the film thickness increases, cracks may appear in the film that may affect the sensing properties of the layer by decreasing the connectivity between films and the surface area. This is thought to deteriorate the sensing device.

Sol-gel deposition methods include spin coating and dip coating. The process makes use of a precursor that contains the metal of interest and through hydrolysis and polymerisation reactions it will form a sol.[128] In spin coating, the precursor is mixed with a volatile solvent to form the sol. The solution can then be transferred onto the substrate via spin-coating, spraying and dipping techniques, which are then followed by an evaporation process that occurs during spinning so as to remove the solvent from

the sample. In turn, a polymer forms as a thin film on the substrate. The substrate is rotated at high speed so that the fluid is extended through centrifugal force. In dip coating, the substrate will commonly be submerged in a bath containing a polymer or a particulate sol. Following extraction from the bath the substrate will keep a boundary layer and the solvent will evaporate. The rate at which evaporation occurs and the drying conditions utilised will impact on the microstructure of the material. These two techniques may lead to cracks in the material film if evaporation is not adequately controlled and the quality of the film might be compromised.[105]

The techniques described above have drawbacks – their ability to effectively control the microstructure of the material is limited, the direct-writing capabilities are poor, post-processing techniques are commonly required and the fixed pattern on meshes may hinder the versatility of some techniques.[105] Furthermore, the manual input involved in some of these fabrication methods may affect reproducibility and repeatability aspects.[136] Novel techniques have been developed to address some of these issues. They include Matrix Assisted Pulsed Vapour Deposition (MAPLE), ink-jet deposition, 3D printing, flame spray pyrolysis and thermal spray direct writing, to name a few. More detail can be found in Sahner et al. [105].

1.4.4.4 Incorporation of Additives

It has long been recognised that sensitivity and selectivity enhancements are frequently seen upon modification of the surface microstructure of the control sensing material by addition of catalytically active agents and/or porous materials with high surface area, the framework structure of which is strategically used to induce molecular filtering.[15,56,137,144]

The incorporation of catalytic agents into the base material can serve to promote chemical and physical interactions between a gas and the sensor surface.[145] Common metal sensitizers include noble metal nanoparticles such as Pt, Pd, Ag and Au. Their incorporation affects gas responses due to chemical or electronic sensitisation. In the former type of sensitisation, metal clusters favour the interaction between oxygen accumulated on the sensing material and the gas. Sensitivity enhancements are attributed to the metal's contribution to the acceleration of surface reactions, which alter the density of oxygen species in the sensor and result in a conductivity change. An example of chemical sensitisation occurs when doping SnO_2 with Pt.

Electronic sensitisation, on the other hand, affects the position of surface energy levels, due to a change in oxidation state of the metal dopant through interaction with the

surrounding atmosphere. As such, in the presence of atmospheric air the metal dopant e.g. Ag or Pd, will be oxidised to form Ag_2O or PdO. Due to the higher work function of the oxidised metal in relation to the sensing material, an electron depletion layer will form near the surface of the material, resulting in increased sensor resistance. Upon interaction with an inflammable gas, the dopant will be reduced to its metal form, reducing the work function and increasing the conductivity of the material.[63,145,146] The incorporation of noble metals has been seen to significantly enhance sensor sensitivity, gas sensing responses and, also, to lower the operating temperature of the otherwise unmodified sensing material.[14,144,145,147–149]

A major component of this thesis was to incorporate zeolite materials into the sensing layers either in the form of admixtures or in the form of cover layers. Zeolites have been shown to greatly enhance the sensor responses both towards reducing and oxidising gases and in combination with n-type and p-type materials. Section 1.5 below reviews this topic in detail.

1.4.5 Current Optimisation Approaches in MOS Gas Sensor Devices

1.4.5.1 Reducing Power Consumption

Different approaches have been proposed to reduce power consumption. An example includes the integration of MOS into Micro-Electro-Mechanical Systems (MEMS), termed micro-hotplates platforms, which consume ~3–150 mW.[82,150] The sensing layer can be that of a *thin film* deposited on a hotplate with deposition techniques such as atomic layer deposition (ALD),[150] chemical vapour deposition (CVD), plasma-enhanced chemical vapour deposition (PECVD),[77] low pressure chemical vapour deposition (LPCVD),[151] sputtering, or that of a *thick film*, using methods such as pipetting, drop coating and specially-adapted screen-printing to form layers ~5–6 μm in thickness. The reduced thermal mass of these systems allows for remote operation; the sensors can be heated very quickly and it has been suggested that, although under continuous operation sensors may consume ~25 mW, when used intermittently, power consumption may be reduced to 1 mW.[82] Nevertheless, intermittent operation is less accurate, it requires smart-measurement algorithms and occasional sensor recalibration.[82] Various approaches have been found that investigated new ways to deposit the sensing material onto a substrate, and also, a range of different sensing materials and material combinations have also been investigated. Some of these are briefly described below to highlight the great improvements attained in reducing power consumption, whilst maintaining excellent response magnitudes and discrimination among gases.

Mozalev et al. [151] suggested that forming WO_3 films through sputter-deposition on porous anodic alumina (PAA) films – used as a template for nanostructuring the WO_3 layers – resulted in 100-fold enhancements in sensor responses towards 1000 ppm H_2, in relation to conventional, smooth, unstructured WO_3 films.[151] In the latter study, the response times towards H_2 were ~500 seconds at 200 °C. While other studies have reported shorter response times (5 seconds to H_2/N_2 at 4 vol. % at room temperature) with Pt-WO_3 thin films that used optical methods to detect H_2, the equipment was costly, non-portable and required higher power operation.[82]

Other groups have investigated the deposition of different metal oxide-metal oxide (MO-MO) composites onto MEMS to obtain low-power, high-response sensors. For instance, SnO_2-WO_3 composites were deposited onto MEMS platforms for the detection of oxidising gases such as NO_2, attaining high responses (R/R_0 = 37) towards 3 ppm of the gas at 300 °C.[152]

Other groups reported the results of ZnO-CuO nanoflakes deposited onto planar MEMS, attaining responses towards a range of reducing and oxidising gases with very low response and recovery times i.e. 22 and 26 seconds at 300 °C, respectively.[153] In the latter study they also showed that under humid conditions (80% RH) the sensor's response was not significantly compromised under simultaneous exposure to 10 ppm acetone gas.

Pandya et al. [154] designed ZnO nanostructures on MEMS platforms for ethanol detection reducing the operating temperature to 100 °C, consuming ~100 mW. The sensor was also found to display selectivity towards ethanol in relation to other inflammable gases. Conversely, other groups deposited nano-sized SnO_2 (35 – 50 nm) on a micro-hotplate platform using ALD and exposed the sensors to 100 ppm ethanol and acetone and 20 ppm acrylonitrile at 300 °C. Although the sensor response times were fast (2 – 5 seconds), the sensor responses towards the test gases were very poor in comparison to the sensor responses of conventional nano-sized SnO_2 towards the same gases reported in the literature,[54,155–157] but this was potentially due to lack of catalytic dopants or modification agents in the sensing system.[150] The microstructure of SnO_2 appeared dense, potentially affecting the diffusion of the gas through the film. In the same study, the long-term stability of the sensors was compromised due to degradation of the heater. In general, the response times attained with the MEMS systems described above were comparable to those of conventional sensors, [49-52] *ca.* 8-100 seconds, upon exposure to the same gas concentrations and temperatures (200 – 300 °C).

Guha et al. [77] described the design of CMOS-compatible micro-hotplates for elevated temperature operation. The SOI CMOS MOSFET[2] micro-heaters consumed 16 mW and had a thermal mass rise of 10 ms, which are also very promising results for future gas-sensor technology.[77] Other groups have focused on assessing whether this technology also favours gas discrimination. For instance, in Vergara et al. [158] the authors used global feature extraction analysis termed 'energy vector method' to assess whether the best temperature-modulating frequencies could be identified to favour the identification and quantification of ammonia, ethylene and acetaldehyde gases using a four-sensor array based on micro-hotplate gas sensors to do so. They found that just after 1 second into the gas response the method was highly accurate in classifying all three gases.[158]

Other alternatives are also being sought that are based on self-heating systems e.g. Joule self-heating of nanowires, which can heat or cool down in microseconds.[61,83,159–161] The small dimensions of nanowires result in self-heating effects caused by dissipated power when they work as part of electrical devices.[162] Prades et al. [162] showed that self-heating SnO_2 nanowires could achieve sensor responses towards NO_2 that were almost identical to those attained with an external heater.

Other strategies to reducing power consumption include using materials that are able to operate at low or room temperature, such as CNTs, which have small size and high surface-to-volume-ratios, and have been seen to greatly improve the sensing properties of conventional MOS sensors when prepared as composites.[45,46] However, when used individually, they are seen to be poorly sensitive to gases, they are costly, they display poor recovery times [163] and exhibit sensitivity to humidity, often masking the responses towards test gases. Nevertheless, introducing silicalite zeolites into single-walled carbon nanotubes (SWCNT) has been seen to introduce resistance to humidity.[62] Methods are available to reduce CNT recovery times such as UV sources, but these increase the desired low power consumption.

1.4.5.2 Addressing Sensor Selectivity

As alluded to previously, a major constraint of MOS gas sensors is their inability to individually respond to gases selectively. As such, the usability of MOS sensors may be limited to intermittent and/or localised detection environments where there is only one target vapour with little or no interference from competing vapours.[22] For this reason,

[2] Silicon on Insulator (SOI)/Complementary Metal Oxide Semiconductor (CMOS)/metal oxide semiconductor field effect transistor (MOSFET).

research efforts have been principally aimed at improving the discriminating capabilities of either individual sensors or of sensing arrays when exposed to mixed-gas environments.

The fundamental drawback of selectivity can be overcome by using a number of approaches, one of which is to use an integrated array of different sensors, each responding to a simple or a complex mixture of gases at a different rate and to a greater or lesser degree.[164] The combined response of the array, also referred to as an electronic nose (e-nose), may then provide the necessary specificity and sensitivity for the gas detection being sought with the help of signal processing and pattern recognition tools.[36] The collection of individual signals provided by each sensor of the array can be compiled and translated into a unique fingerprint of the gas. In essence, an e-nose shifts away from the 'ideal' sensor concept described in section 1.4.1, in that the integrated sensors ought to display partial sensitivity to a broad range of gases, rather than total specificity towards one gas.[164]

E-noses have been studied for various purposes. Some examples include: to discriminate among common lung cancer organic volatile biomarkers with five room-temperature operated CNTs conducting polymer nanocomposites,[45] to discriminate among the blend and roasting level of coffees with a twelve sensor array,[165] to detect artificial fruit aromas such as apple, grape and strawberry with sensors based on polyaniline-coated tracing papers,[42] and to analyse the freshness and quality of food.[166–168]

Given that reaction processes on MOS sensors are temperature specific, the modulation of a sensor's temperature may lead to very different sensor behaviours.[169] More specifically, MOS sensors typically see a sensitivity maximum when heated over a temperature range and these maxima change with gas type. As such, temperature modulation serves as an additional means of achieving selectivity but also, by using feature extraction tools one may abstract qualitative and quantitative information particular to a gas.[169]

The case of promoting selectivity improvements through the incorporation catalysts (described above 1.4.4.4) or of zeolites as catalytic/sieving agents that modify the surface microstructure and affect the diffusion of a gas through the sensing material whilst also affecting response kinetics, is described in further detail in section 1.5. Zeolites have been shown to greatly enhance sensor responses of conventional semiconductor gas sensors towards certain gases. They are seen to either promote

sensitivity to a gas or to supress it altogether. This is due to the fact that their properties can be strategically used to fine-tune the diffusion of molecules according to their shape and/or size, inducing selectivity.[15,21–23,30,56]

Support Vector Machines (SVMs)

Gas sensor data is readily processed and interpreted with pattern recognition and classification methodologies that can be divided into linear and non-linear methods.[170] The main difference arises in how the data is processed to attain the desired result of reliably recognising test gases or accurately classifying the dataset into gas type.[170]

In essence, unsupervised and supervised machine learning methods can be distinguished.[170] Unsupervised methods focus on the analysis of response patterns and they maximise the difference in the response provided by each sensor when subjected to different stimuli [170] e.g. concentration or temperature changes. They can be employed to cluster the input data according to class. Examples of unsupervised methods include Principal Component Analysis (PCA) and Self-Organising Maps (SOM). Conversely, supervised methods identify key differences in the dataset so as to enable its correct classification, whilst ignoring data variations.[170] Common supervised methods used in gas sensing include Linear Discriminant Analysis (LDA) and Support Vector Machines (SVM).[170] The latter has been the method of choice in this thesis and is explained in further detail below.

The process of classification sets out to learn a target function or classification model, *f*, that maps each attribute set, *x*, to a particular class from a predefined set of labels, *y*.[171] This, in turn, enables the extraction of useful information from multidimensional data. Classification tools can be useful in predictive or descriptive modelling tasks, where a classification model may be able to predict the class labels from a set of unknown data or used descriptively as a tool to distinguish between objects of different classes.[171] In order to solve classification problems, one needs to use a classifier – a systematic method used as a means of building classification models from an input dataset. Common classifiers include decision trees, SVMs, naïve Bayes and neural networks.

Classifiers use learning algorithms to find the model that best fits the relationship between the attribute set and the class labels in the input dataset.[171] The learning algorithm ought to fit the input data well and, additionally, it must be able to accurately predict the class labels of unknown data.[171] It is crucial that the built models have good generalisation performance, particularly when using the classifiers for real-world

applications. Further, the performance of a classifier is assessed by the counts of data from a test set that are correctly and incorrectly classified by the model, which is usually computed into a confusion matrix.[171] In the case of classifying data into two classes, *a* and *b*, the confusion matrix enables one to visually see the number of instances from class *a*, which have been misclassified as class *b*, and vice versa. The accuracy of the model in correctly classifying the class labels is also used as a means of understanding how well a classifier performs.[171]

SVMs were first introduced by Vladimir Vapnik in the early 1990s. They constitute a set of supervised learning methods primarily used for classification and regression purposes.[172] SVMs have been demonstrated to be valuable tools in real-world applications such as facial recognition, medical diagnostics,[173] handwritten character recognition[174] and, more recently, in gas sensing applications.[27,28,167,175]

In pattern recognition tasks, SVM uses a linear separating hyperplane to create a classifier with maximal margin.[176] What this means is that SVM assumes that the variables in the data are dichotomous in nature. The dataset therefore belongs to either of two classes, the elements of which can be separated by a hyperplane.[177] As such, all elements particular to one class will fall under the same side of the plane. SVM then finds the equation of the optimal hyperplane by maximising the distance between the closest points in the dataset.[177–180]

In more realistic scenarios the classes may not be linearly separable. SVM then transforms the original input space into a higher dimensional feature space, after which the optimal linear separating hyperplane is sought.[179] Furthermore, although SVM was developed as a binary classifier, it has also been used in multiclass problems, either by building a classifier for each pair of classes, referred to as one-versus-one strategy, or by building a classifier for each class, which is trained to discern the samples in a single class from the samples in all the remaining classes, following a one-versus-all strategy.[181]

In this thesis, a Sequential Minimal Optimisation (SMO) SVM provided by the WEKA software (University of Waikato, NZ) was used as a classifier; The SMO approach used to train the SVM solves multi-class problems using a one-versus-one strategy. This algorithm was initially introduced by Platt for SVM classifier design.[172] The SMO algorithm offers advantages such as computational speed and straightforward implementation.[172] It must be noted that the SVM has a set of parameters that have an effect on the decision boundary of the SVM. These are the soft margin constant or

cost function, 'C', and any set of parameters that may affect the kernel function being used.[177] For a large value of 'C' a large penalty is assigned to errors or margin errors, causing the two points that are closest to the hyperplane to directly affect its orientation (Fig. 1-9A).[177] As such, the hyperplane lies close to other points in the dataset. For smaller values of 'C' these two points become margin errors and the orientation of the hyperplane is altered, leading to a much larger margin for the remaining data.[177] The 'C' value may thus be adjusted to maximise the margin and minimise the variables that erroneously lie within the margin or that are misclassified. Kernel parameters, such as γ, will also impact on the decision margin, essentially by directing the flexibility of the classifier (Fig. 1-9B). With small values of γ, a smooth decision boundary is obtained. Conversely, with larger values of γ the curvature of the decision boundary increases. With very large values of γ, the classifier will overfit the data.[177]

Note that when using the SMO algorithm, the cost function 'C' was subsequently modified so as to find the optimal parameters for classification. There are several model selection methods that assist in minimising the expectation of errors when the classifiers are used as diagnostic tools.[173] Two examples include the leave-one-out or the k-fold cross validation (CV) approaches. The former removes a sample from the training set and builds the decision function to infer the class type the removed sample belongs to.[173] The k-fold CV, on the other hand, randomly divides the training dataset to form 'k' subsets with approximately equal size. It then removes the 'i^{th}' subset from the training set and uses the remaining 'k–1' subsets to build the model so that the class type of the removed subset can be inferred.[173] Furthermore, the leave-one-out approach was employed as a tool to evaluate the generalisation performance of the classifier.[182]

In addition to the use of SVMs for classification, other classifiers, such as decision trees [183] or random forests,[184] which have been reported to have similar predictive accuracy and performance, may be used to assess the robustness of a method in classifying data.[182]

For clarification purposes, a decision tree will produce a set of rules that are employed in order to make a decision to recognise the classes.[185] It leads to a flow-chart type of tree structure,[186] which has three different types of nodes: a root node, internal nodes, and terminal nodes.[171] Essentially, the root and internal nodes contain attribute test conditions or rules that are used to separate data that has different features. The terminal nodes, however, are the ones that are given a class label.[171] Random forests,

on the other hand, operate as a collection of decision trees, whereby a randomly selected subset of the dataset is used to train the model. The decision tree is then built on this subset of the data.

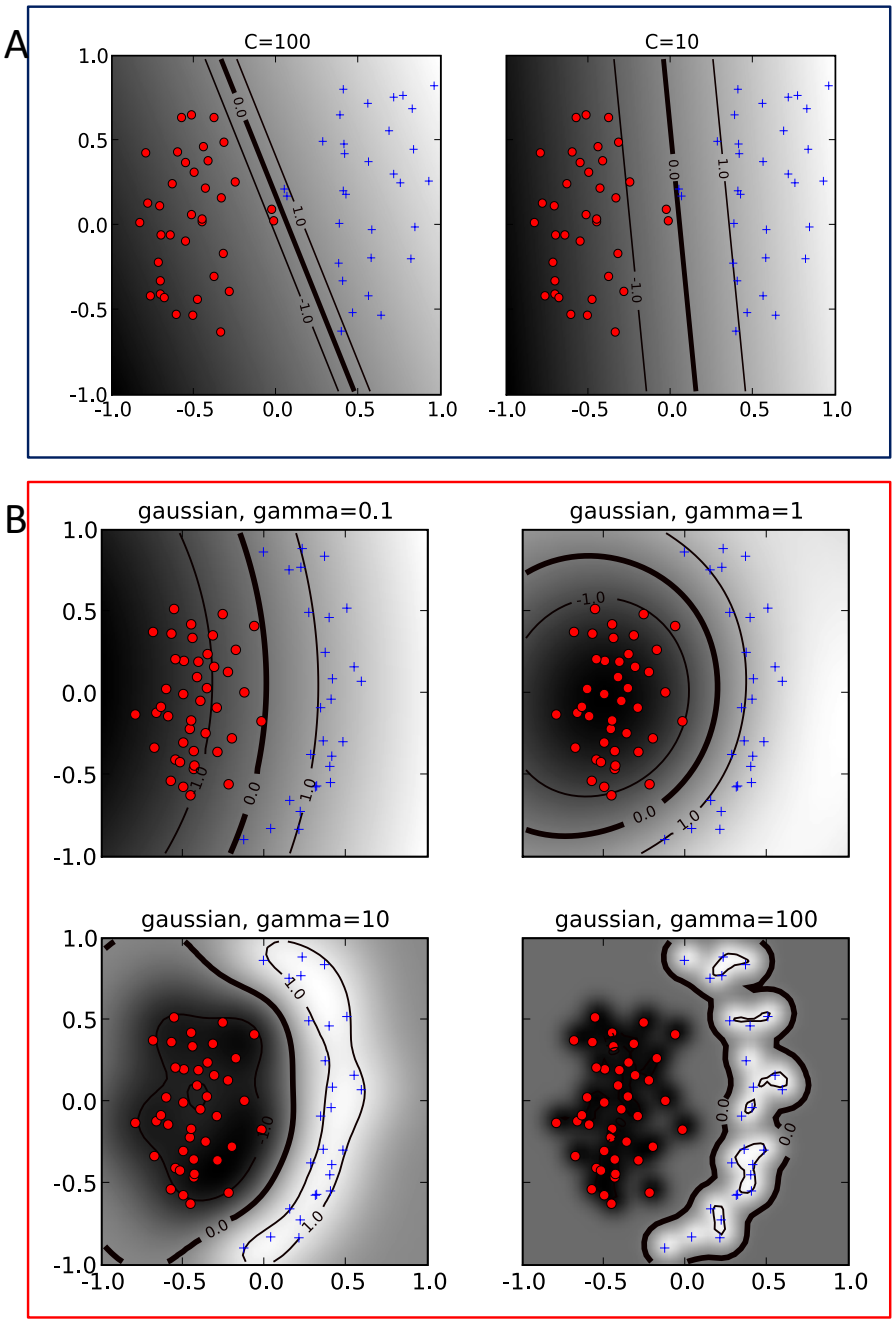

Figure 1-9 (A) Displays the influence of the soft margin classifier 'C' on the decision boundary. (B) Displays the influence of the kernel parameter gamma for a fixed value of the cost function 'C'. With higher values of γ, the flexibility of the decision boundary increases. Large values of γ can lead to overfitting. Image adapted from [177].

The classifiers described are also able to replace missing values.[187] When using classification methods, one must be aware of the problem of overfitting, which refers to the generalisation ability of the classifier being lost, producing misleading or deceptive

classification results.[173] This can occur particularly when working with datasets that are small or have a large number of attributes, the likelihood of a classifier overfitting in classification increases.[173] Overfitting may also occur due to the presence of noise in the data or due to lack of representative samples in the data.

1.4.6 Metal Oxide Semiconductors of Choice

1.4.6.1 Tin Oxide (SnO_2)

SnO_2 is one of the most widely studied materials in gas sensing applications due to the high responses it provides to a range of reducing and oxidising gases.[188] Furthermore, SnO_2 combines high conductivity with optical transparency, which makes it suitable for optoelectronic applications.[189] It is also attractive because of its low cost and low toxicity.[156] There are two main oxides of tin, stannic oxide (SnO_2) and stannous oxide (SnO). However, other intermediate and less stable phases of tin oxide such as Sn_2O_3 and Sn_3O_4 have also been reported.[190] Stannic oxide is the most common form and it crystallises with the structure of rutile, illustrated in Fig. 1-10 below. It has a tetragonal unit cell with a space group symmetry of $P4_2/mnm$. In the bulk all Sn atoms are six-fold coordinated to three-fold coordinated oxygen atoms.[94] The wide band gap of SnO_2 makes it an insulator when in stoichiometric form but in oxygen-deficient form it is an n-type semiconductor material (SnO_{2-x}) with a wide band gap of 3.6 eV. Aside from its widespread use in gas sensing, SnO_2 is readily used in lithium-ion batteries, in sensitised solar cells, catalysts,[191] and as starting materials for indium-tin oxide films used as transparent electrodes.[192]

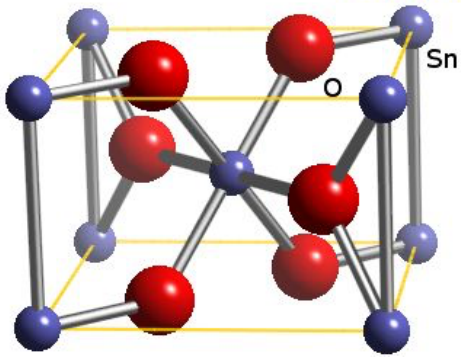

Figure 1-10 Crystal structure of stannic oxide (SnO_2). The purple spheres represent tin atoms and the red spheres represent oxygen atoms. Image from WebElements™.

SnO_2 gas sensors have been reported to provide high error margins in the sensing responses, it is reported that the grain size of SnO_2 crystallites as well as the size and dispersion of noble metals and the concentration of hydroxyl groups at the surface may all influence the sensitivity and stability of the material.[193] In the latter study, it was

found that a screen-printed large-grain SnO_2 with mixed Al_2O_3 and Pd, presented long-term stability and selectivity towards methane, however sensitivity towards the gases tested decreased over time.

Studies have investigated several different topics that include but are not limited to: the effects of grain size on sensor sensitivity,[16,122,194] the effects of diffusivity of H_2 and O_2 through porous thick films on its sensing properties,[126,127] the effects of film thickness,[7,12,129,195–199] the interactions of the surface with oxygen, water, hydrogen, and carbon monoxide [113,200] molecular shape selectivity of alkanes,[201] catalyst incorporation for sensitivity enhancements and influence of humidity [200,202] and for selectivity improvements.[203] Other studies have investigated the long-term stability of the sensors,[198] the fabrication of ordered, stable, mesoporous SnO_2 for enhanced sensitivity to gases,[204–206] amelioration of existing fabrication methods,[142] and how to better understand the interactions between SnO_2 and oxygen.[84]

1.4.6.2 Chromium Oxide (Cr_2O_3)

Cr_2O_3 is a p-type semiconducting material that has a band gap of 3.4 eV.[11] It is commonly used in catalytic reactions such as the oxidation of SO_2, alcohol dehydrogenation and dehydration and methanol synthesis [11] and is a major constituent in ceramics.[207] It is also used in solar thermal energy collectors, protective layers against corrosion, wear-resistance of stainless steel and as an adhesion promoter.[207] Further, it is an antiferromagnetic insulator and it is also utilised in spintronic devices such as non-volatile magneto-electric memories.[207] Cr_2O_3 has the corundum structure (with space group $R\bar{3}c$) with hexagonal close-packed (001) layers of O atoms and 2/3 of the octahedral holes in between filled with Cr (Fig. 1-11).

Cr_2O_3 has also found use in the gas-sensing field, although in a much lower scale when compared to SnO_2. Cr_2O_3 has been reported to exhibit lower sensing responses to gases in relation to n-type materials.[208] As such, its performance is often improved by using nanostructured materials or through the incorporation of noble metal catalysts [208] or zeolites.[26,31,32] It was suggested in Kim et al. [110] that due to the different oxygen adsorption seen in p-type semiconductors they could be employed for the design of high-performance and humidity-resistant sensors with lower recovery times.

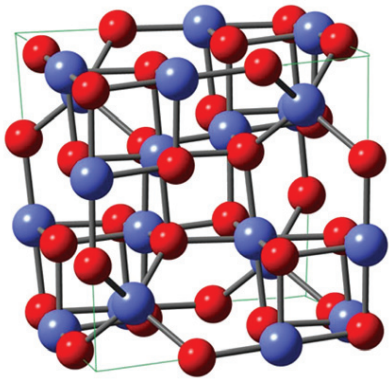

Figure 1-11 Crystal structure of Cr_2O_3. The blue spheres represent chromium and the red spheres represent oxygen. Image adapted from [209].

Reports in the literature have also investigated thin [210] and thick-film [32,211,212] Cr_2O_3 films. Different morphological designs have been investigated such as porous microspheres for toluene detection,[211] Cr_2O_3 yolk-shelled spheres for trimethylamine detection,[208] Ag/Cr_2O_3 mesoporous microspheres for triethylamine detection,[213] hollow microspheres for ethanol detection,[214] and plate-like Cr_2O_3 for nitric oxide detection.[9] Further information can be found in Chapter 4.

1.4.6.3 Iron Oxide (Fe_2O_3)

Fe_2O_3 is an n-type semiconducting material that has a band gap of 2.2 eV under ambient conditions.[215] α-hematite and γ-maghemite are two crystal phases of ferric oxide. They are both interesting candidates in the field of gas sensing due to their low cost and good chemical stability.[216] Hematite is the most thermodynamically stable of the oxides and it finds widespread use in industry.[217] For instance, it is a corrosion product of steel and is commonly employed catalytically or as a microelectrode for electrochemical and photoelectrochemical reactions. It is also valuable due to its ferromagnetic properties.[216] The basal planes of hematite consist of hexagonal closed-packed oxygen planes with layers of octahedrally coordinated Fe atoms.[217] The crystal structure of Fe_2O_3 has been presented in Fig. 1-12.

Fe_2O_3 has also been studied in gas sensing and, particularly over the last 5 – 10 years, several studies have published a range of different architectures of the material to enhance the sensing properties of conventional Fe_2O_3 sensors. For instance, mesoporous Fe_2O_3 microrods have been fabricated for triethylamine detection,[218] ultrafine nanoparticles [219] and porous monodisperse hamburger-like microparticles [220] have been fabricated for acetone detection, hollow balls,[221] porous microrods,[218] and nanoparticles [222] have been fabricated for ethanol detection, ultra-thin nanosheets

for acetone and ethanol detection,[223] and also nanoparticles for high-performance CO sensing.[224]

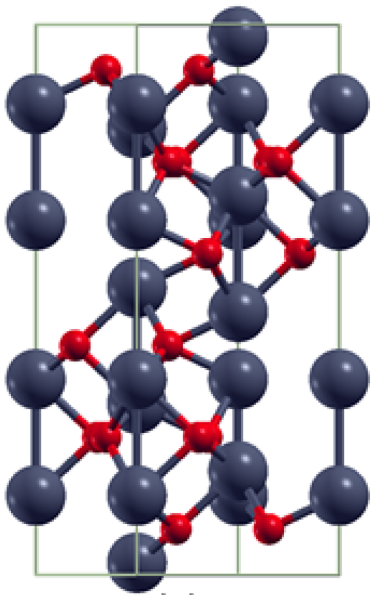

Figure 1-12 Crystal structure of α-Fe_2O_3. The dark blue spheres represent the iron atoms and the red spheres represent the oxygen atoms. Image adapted from [225].

Additionally, it has been investigated as a low-temperature sensor for H_2S [215] and for NO_2 detection.[226] Further, Au-modified Fe_2O_3 thin films have also been investigated for the detection of H_2S,[227] and nanoparticles have also been reported to detect H_2S at the ppb level.[96] Fe_2O_3 has been reported to switch from n-type behaviour to p-type behaviour or vice versa, [228] which is considered further in Chapter 5.

1.5 Zeolite Materials Applied to MOS Gas Sensor Devices

Zeolites are described as microporous crystalline structures that are commonly composed of silicon, aluminium and oxygen.[20] The atoms form tetrahedral units (TO_4) – the central T atom in the tetrahedron being T = Si or another suitable heteroatom such as Al or Ti [229,230] – making up the primary blocks in the zeolite structure.[20] The SiO_4 and AlO_4 are linked together through oxygen atoms to form 3D frameworks with pores of molecular size. TO_4 atoms will link together to form a siliceous structure (SiO_2), which is neutral. However, the incorporation of Al^{3+} ions into the silica framework leads to a negatively charged framework and thus the incorporation of extra framework cations is necessary to maintain the framework neutral.[231] These extra framework cations act as ion exchangers, making zeolites rich ion exchange materials. As such, the

incorporation of alkali metals will give the zeolite a basic character, whereas the incorporation of protons into the framework results in Brønsted acidity.[231]

The aforementioned primary blocks combine to form secondary building units and *ca.* 23 units have been identified. In turn, these secondary building units form a set of zeolite frameworks that are characterised by different unit cell dimensions and pore sizes.[20] The frameworks are identified by three-letter codes e.g. MFI, FAU, LTA, MOR, BEA.[20] Each zeolite framework has a specific structure characterised by 6, 8, 10 or 12-membered oxygen ring pores that give them particular cavities and channels within the framework. The International Zeolite Association Commission has so far assigned 232 framework type codes.

Zeolites are required in a wide range of procedures such as catalysis for hydrocarbon transformation.[231] The latter is promoted by the strong acidity of some zeolites. They are also used as adsorbents to remove polar or polarizable molecules or to separate molecules using their filtering properties. They are also employed as ion exchangers for water softening applications.[231] Examples of common zeolite frameworks and their pore openings are illustrated in Fig. 1-13 below. Although zeolites are found in nature, they may also be synthesised in the laboratory and they are made into highly porous materials. Natural zeolites have lower Si/Al ratios. Note that the number of Al^{3+} ions within a framework can vary widely, and the silicon to aluminium ratio can be adjusted so that synthesised zeolites may have Si/Al ranging between 1 to ∞. Zeolite synthesis is divided into low-silica or aluminium-rich zeolites, intermediate silica zeolites and high-silica zeolites.[231] Low-silica zeolites are excellent ion exchangers and have the highest cation content. Examples of this type of zeolite include zeolites A and X.[231] Intermediate silica zeolites include zeolite Y, which has a Si/Al ratio that ranges between 1.5 and 3.8.[231] A decrease of the aluminium content leads to much-improved thermal and acid properties of zeolites. Finally, high-silica zeolites have ratios that usually range between 10–100. This type of zeolite is readily used in catalytic processes for hydrocarbon cracking.[231]

The role of zeolites as catalytic filters has been increasingly used in recent years and their physicochemical properties make them perfectly suited to prompt selectivity and sensitivity enhancements in gas sensors. Zeolites have interconnected cages and channels in their frameworks that vary in dimension from 1D to 3D.[232]

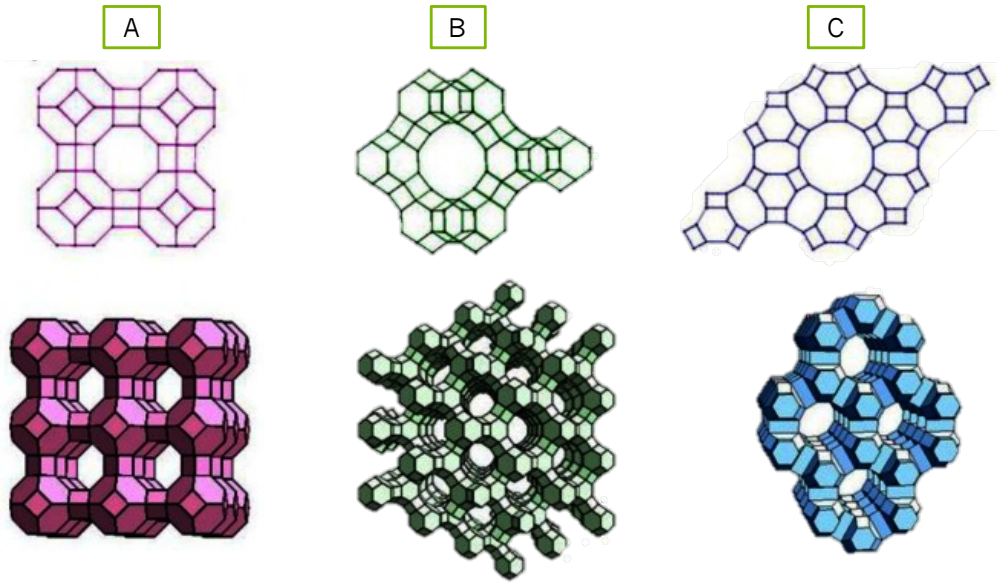

Figure 1-13 Zeolite frameworks and pore openings of (A) zeolite A (3D), (B) zeolite Y (3D), (C) zeolite ZSM-5 (2D). Image adapted and modified from [232].

Zeolites are known to be thermally stable and, as such, useful candidates for gas-sensing applications. The large band gap of zeolites (~7 eV) means that they are not electronically conductive.[24] Zeolites do, however, exhibit ionic conductivity due to the translational mobility of exchange metal cations.[24] Using a thick film of a zeolite as a functional film can serve as a gas sensing device, given that the electrical impedance of the zeolite changes in the presence of a gas.[24,40] The framework and composition of zeolites will directly affect their chemical properties such that high aluminium content (low Si/Al ratio) will result in a hydrophilic character as seen, for instance, in zeolites with an LTA framework.[21] Conversely, low aluminium content (high Si/Al ratio) will lead to a hydrophobic character as seen, for instance, in zeolites with an MFI framework.[21] Furthermore, the Si/Al ratio determines the acidic centres per unit cell and content of mobile cations, which consequently affects the ionic conductivity of the material when interacting with gas molecules.[24] Nevertheless, it is the pore dimensions and channels in zeolites that render them suitable in gas sensing applications to achieve selectivity; they can be used to fine-tune the passage of molecules according to their shape/size.[15,25] Small molecules may be able to reach the active sites inside the zeolite pores and be transformed into other products, whereas larger molecules may not.[229] Additionally, smaller reaction products may be formed, enabling their diffusion out of the pores, whereas larger molecules may diffuse out of the pores very slowly or get converted to other products prior to diffusing.[229] In combination with n- and p-type materials, zeolites are particularly efficient at selectively targeting trace concentrations of saturated and unsaturated HC gases, solvents and inorganic gases like NO_2.[22,27,28]

The internal porous structure of zeolites makes them materials with very high specific surface areas, usually in the order of 300–800 m^2/g.[229] Their uniform nanometre-sized pores and well-defined crystalline structures and pore channels allow molecules to adsorb and diffuse through like-sized pores, which results in strong interactions between the pore walls and external molecules entering the structure. Furthermore, their structural framework and high surface area offer an excellent catalytic environment favouring reactions at their surface. Inclusion of metal ions into zeolite frameworks can also result in increased catalytic activity. This directly affects the ratio of Si/Al, thus adjusting the acidic properties of zeolites.

The incorporation of zeolite materials into MOS gas-sensing systems has mostly been in the form of layers on top of the control material, referred to as overlayers or coatings.[21,22,26,30] Used as a physical barrier between the metal semiconductor and the air/gas atmosphere, they assist in filtering molecules according to shape/size. The thickness of the zeolite film influences sensor selectivity, sensitivity and response times such that the thicker the zeolite overlayers, the better the selectivity and the slower the response times.[24] Although MOS admixtures (powders mixed with zeolites in organic ink), have received less attention in the literature, recent studies carried out by our group have shown outstanding improvements in the sensing properties of the sensors, particularly by significantly enhancing the responses to gases, in comparison to an otherwise unmodified base material sensor.[3,27–29]

Below, information on the zeolites used in this thesis, namely H-ZSM-5, Na-A and H-Y, has been provided.

1.5.1 Zeolite A

Linde type zeolite A (framework LTA) is used as a molecular sieve. It is characterised by a 3D channel network. The pore diameter has an 8-membered oxygen ring of 4.1 Å in diameter. This opening is connected to a larger cavity with a minimum free diameter of 11.4 Å. This cavity is surrounded by eight sodalite cages.[233] The small pore dimensions of this type of zeolite may assist in separating small molecules, controllable through ion exchange with several cations. This zeolite commonly has a Si/Al = ~1.[233] Further, it is usually employed in the Na-A form and its use lies in the detergent manufacturing industries, as a water softener. The use of this zeolite as a coating over different base MOS materials has been reported for gas sensing applications.[22,30] See Fig. 1-14 for an illustration of its structure.

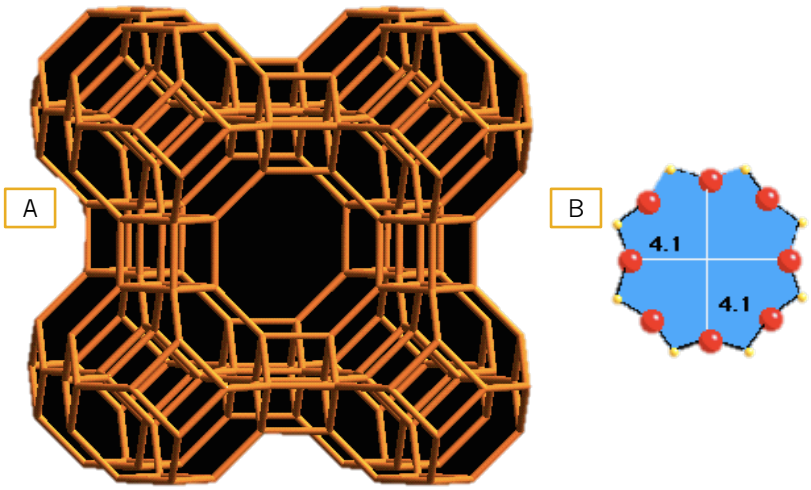

Figure 1-14 (A) 3D structure of zeolite Linden type A (LTA) viewed along the [100]. (B) 8-ring viewed along [100]. Images obtained from http://rcsr.fos.su.se/IZA-SC/. The yellow spheres refer to oxygen whereas the red spheres refer to aluminium or silicon.

1.5.2 Zeolite ZSM-5

ZSM-5 is a high-silica zeolite that has an inverted mordenite framework. It holds a two dimensional channel network of intersecting channels with 10-membered rings, which control the dimensions of the microchannels.[234] Its structure is formed from the pentasil unit (Fig. 1-15D), which link into chains to form layers. One channel system is sinusoidal and has pore sizes of 5.1 × 5.5 Å. The other channel system has openings of 5.3 × 5.6 Å and they run straight and perpendicular to the first system.[235] ZSM-5 is strongly acidic and its protonated form can be used for molecular sieving. This means that only molecules that have a smaller kinetic diameter than the channel network will be able to access the pore network.[234] Further, it also provides product selectivity, through which adsorbed molecules will react inside the zeolite pores and get converted to products that may not be able to diffuse out of the pores.

This type of zeolite is used in numerous catalytic processes such as fluid catalytic cracking, alkylation of aromatics and the conversion of oxygenates.[234] Its use as a sieve in catalytic processes served as the basis of its use in gas sensing. It is perhaps the zeolite that has been most widely employed in gas sensing. Its incorporation to sensors containing WO_3 has shown enhanced responses over that of the control sensor to test gases sought in explosive detection and in environmental detection of pollutants.[28] A summary of how it has been employed in gas sensing has been provided in the introduction of each of the results chapters.

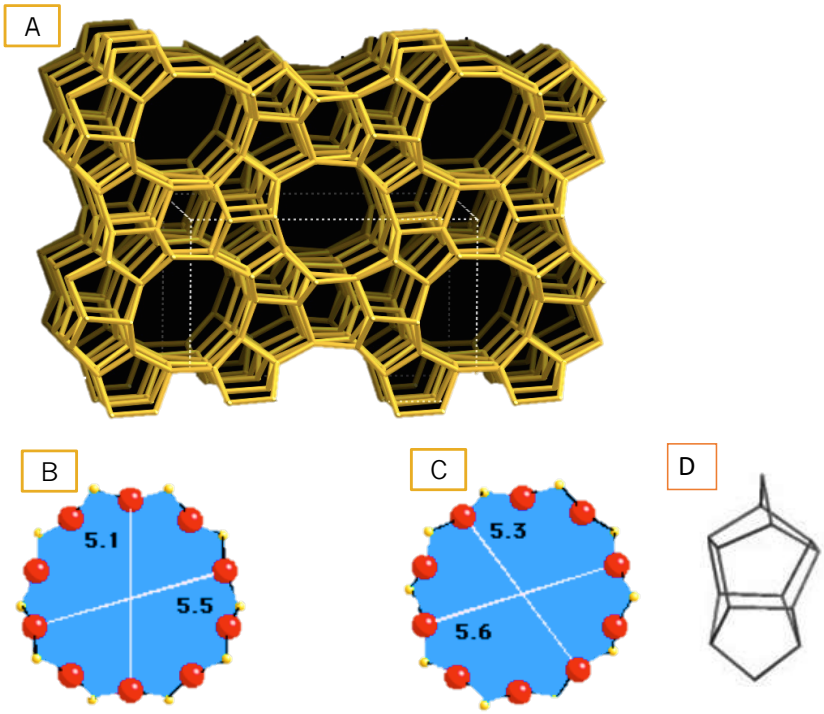

Figure 1-15 (A) ZSM-5 zeolite (MFI) viewed along [010]. (B) 10-ring viewed along [100]. (C) 10-ring viewed along [010]. (D) Pentasil unit. Images obtained from http://rcsr.fos.su.se/IZA-SC/

1.5.3 Zeolite Y

Y zeolite (FAU) holds a 3D pore structure with openings that are perpendicular to each other in the x, y and z planes.[233] Its structure is characterised by a double 6-ring, a sodalite cage and a supercage. It has pore dimensions of 7.4 Å, with an aperture that is characterised by its 12 oxygen-membered rings, which leads into a supercage of 12 Å.[233] This, in turn, enables molecules of a large size to enter their supercages. In contrast to H-ZSM-5, this zeolite has a lower Si/Al ratio of 2.5. The structure of FAU is presented in Fig. 1-16 below. This type of zeolite has been widely used as an ion exchanger, as a catalyst and as an adsorbent. It is more stable at elevated temperatures than other FAU zeolites such as X due to its higher Si/Al ratio. Ion-exchanged H-Y zeolite shows thermal stability and displays a more acidic character in comparison to its unmodified form due to the formation of acid sites brought about by H^+. Although the reported use of this zeolite in gas sensing is scarce in the literature, recent studies showed the ability of this zeolite to discriminate successfully across a series of alkanes, yielding dramatic changes in sensor response regardless of the similarity in chemical structure of the alkanes.[3,15,27]

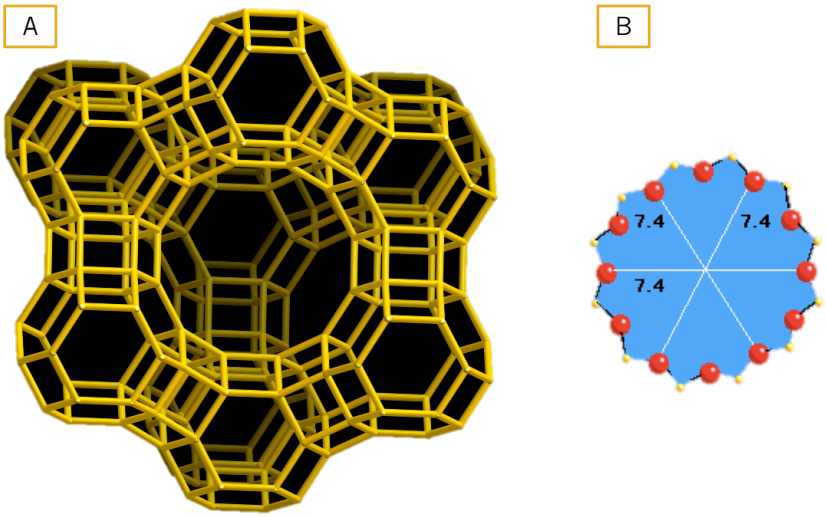

Figure 1-16 (A) Y zeolite (FAU) viewed along [111]. (B) 12-ring viewed along [111]. Images obtained from http://rcsr.fos.su.se/IZA-SC/

The following section stresses the importance of reforming current practices used to control and prevent drug trafficking. Global trends and information published by the most recent Drug World Report (2016) are summarised. Further, the severe impact that drug traffic continues to pose on health and the environment is highlighted. Finally, some major constraints found in the technology that is currently used to prevent, control and detect the illicit traffic of drugs are elucidated.

1.6 Drug Trafficking Trends: The Need of a Systematic Global Reform to Increment and Enhance Illicit Drug Detection Practices

Drug trafficking is defined as an activity involving the cultivation, importation, manufacture and/or distribution of illicit drugs.[236] The drug trafficking market is a very lucrative one, the network and profits of which interlink with other serious organised criminal activities associated, for instance, with terrorism and traffic of firearms, posing a severe global threat.[237] Traffickers employ very sophisticated methods of concealment, which makes it challenging for the authorities to successfully implement adequate detection and prevention strategies. In fact, it has been suggested that international efforts to control the trafficking market cannot compete against criminal organisations, whose financial gains enable them to penetrate, control and corrupt governments, businesses and society.[238] Boivin [239] suggested that although law enforcement agencies may disrupt or affect specific illegal drug trafficking markets on a temporary basis, they fail to redefine global markets.[239] Empirical studies on drug

traffic are scarce and one can mostly refer to the annual publications of the United Nations Office on Drugs and Crime (UNODC) reports or to briefings posted in governmental websites. It has long been recognised, however, that the trafficking network is a dynamic and continuously evolving one as market conditions and demand change over time.[240]

The National Crime Agency (NCA) reports that the UK drug market is particularly attractive to organised criminals, given that the prices charged at street level are some of the highest in Europe.[241] Drug importation to countries that depend on peripheral countries for drug supply, as in the case of cocaine, which is only produced in a limited number of countries, causes prices to rise steeply. This is because trade occurs in countries that lead in the world economy.[239] This trade provides sufficient funds to smuggle drugs into the country. The NCA reports that drug trafficking to the UK costs an estimated £10.7 billion a year and, particularly class A drugs, e.g. cocaine, heroin, 3,4-methylenedioxymethamphetamine (MDMA), are widely available throughout the country. Current global drug trafficking trends, as published in the 2016 World Drug Report,[4] show that cannabis is still the most widely used drug, followed by amphetamine. Opiates are less frequently used but may impact severely on health. A rise in heroin use is reported, particularly in North America. Cannabis intake has also risen in North America, East and Western Europe. A rise in cocaine use was also noted, attributed to an increase in consumption in South American countries. Amphetamine use was stable but this could be due to a lack of data pertaining to East and South-East Asian countries.

The effects of illegal drug consumption on health are well documented and continue to cost many lives; the latest figures worldwide estimated to be 207,400 in 2014.[4] The impact of illegal crop cultivation on the environment also needs to be acknowledged; it occurs in forested regions, which have to be later cleared of woodland, leading to deforestation. Deforestation also occurs due to the creation of ‘narco-estates’ where illegal infrastructure and roads are built.[4] Displacement following crop eradication, only serves to re-start the cycle again. The inadequate disposal of solvents used during drug production directly affects the environment, contributing to pollution and creating a hazard to human and animal health both in rural and urban settings.[4]

Technology developments to detect trafficked drugs have been researched mostly for airport applications, where individuals are constantly subjected to invasive scrutiny. This high standard of detection is not met in maritime trafficking control, where confiscations only amount to 11% of all drug seizures, yet are more likely to contain

larger drug quantities than in road or airmail traffic. As a consequence, reports have stressed the need to increment security levels in ports with, ideally, inexpensive and reliable technology that can provide results in-situ and in real-time.[242] Although drug seizures in the UK are still significant (167,059 in 2014/15),[243] it is difficult to estimate the number of undetected trafficking operations, particularly in seaports, where container shipments exceed 420 million/annum and container inspection and subsequent analysis is time consuming, expensive and complex.

Current detection technology is insufficient to accommodate global trends and far too expensive to implement in developing nations, where drug consumption is increasing, but also, where drug cultivation and exportation is more likely to go undetected. Further, there are a number of downfalls associated with current technology such as Gas Chromatography-Mass Spectrometry (GC-MS), Raman and Infrared spectroscopy or imaging tools such as X-Rays or scanners. They are costly, frequently non-portable and lab-based and require sample preparation and expertise for data analysis.[244] Sniffer dogs are frequently used to detect illegal drugs and are useful due to their very sensitive olfactory system – down to ppt levels – but they are also costly. They will only respond to what they have been trained to detect and it is unclear how environmental conditions or fatigue may affect their performance.[6]

1.7 Selection of Test Gases

This section explains the reasons behind choosing the analytes of interest in this thesis. As alluded to previously in the chapter, the gases chosen for detection have, either directly or indirectly, an effect on health, the environment and safety and their monitoring is therefore essential. Nevertheless, a particular focus on the detection of substances relevant to drug traffic has been pursued.

Ethane (C_2H_6): colourless and odourless gas. It is the second largest component of natural gas and is commonly used for the production of ethylene and other commodity chemicals. Its detection has been reported with optical carbon/silicon film [245] and with infrared tunable direct laser adsorption spectroscopy (TDLAS) sensors.[246] Its detection is reported as relevant in environmental monitoring, and in medical fields, as it can be used as a breath marker for lung cancer and asthma. Furthermore, it can serve as an indicator of electrical faults in high-voltage electrical transformers.[245,246]

Propane (C_3H_8): colourless, odourless, flammable, non-toxic gas, which is one of the main components in liquefied petroleum gas (LPG).[247] The latter is extensively used in fuels, heating appliances and vehicles. Its detection is relevant to address potential

leaks and prevent explosions in domestic and industrial settings.[10] Furthermore, propane is also used recreationally as an inhaled volatile compound that may lead to euphoria but it may also lead to loss of sensitivity and unconsciousness when prolonged inhalation is carried out.[248] Chronic exposure to the gas can lead to more severe effects with severe damage to the heart, liver and kidneys. Its abuse has led to fatal intoxication among adolescents.[248] Its detection with gas sensors has been studied and reported in the literature.[21,247,249]

Butane (C_4H_{10}): flammable, odourless and explosive gas. It is one of the major constituents in LPG.[250] As such, its detection is needed to prevent major leaks and the potential of an explosion. Its emission levels from vehicles has also been monitored.[251] Like propane, butane is also abused recreationally and it provides similar toxicological effects if inhaled. Its intake has also lead to fatal intoxication among adolescents.[248] MOS sensors have been employed to detect 250–1000 ppm,[252] 50–1000 ppm,[253] and 830–1660 ppm [250] butane. In Pati et al. [250], the following reaction is suggested for HC gases with chemisorbed oxygen at the surface of a MOS sensor:

$$C_nH_{2n+2} + O^- \longrightarrow H_2O + C_nH_{2n} : O + e^-$$
$$C_nH_{2n} : O + O^- \longrightarrow CO_2 + H_2O + e^-$$

Methanol (CH_3OH): highly toxic organic solvent that is used in the manufacture of drugs, dyes, perfumes, and in energy-related applications such as vehicle fuel. Exposure to small amounts may lead to headaches, nausea and vomiting. Consumption of 20 mL can lead to blindness and metabolic acidosis and larger amounts of 60 mL, to death.[254,255] Its detection has been explored with chemiresistive sensors in the past to evaluate its presence in alcoholic drinks [255] and to explore whether sensors could successfully differentiate between propanol and methanol gases.[254] Although not many studies have been carried out to detect methanol, it can be detected in human breath and it is suggested that elevated levels of methanol may be indicative of renal failure, pancreatic insufficiency and poor carbohydrate absorption.[256]

Ethanol (C_2H_5OH): colourless, clear, flammable, volatile solvent. It is one of the most extensively employed alcohols and finds its use in food, chemical, biomedical and transport industries. Although direct exposure to ethanol may cause headaches, drowsiness, eye irritation, and so on, its consumption leads to many road-traffic accidents, making its detection necessary for medical and social reasons.[41] Furthermore, ethanol is a common interfering gas that ought to be targeted selectively as it can affect the detection of methane from domestic appliances. As such,

interferences originating from cooking, food or other volatiles should be controlled.[144] Ethanol is also a common metabolite in bacteria and fungi and it can also serve as a marker to monitor food quality.[144] Its detection with MOS sensors has been widely reported in the literature.[54,141,144,157,222,257,258] Its adsorption on the surface of a MOS sensor has been reported to result in the following surface reaction [257,259]:

$C_2H_5OH_{(gas)} \rightarrow CH_3CH_2OH_{(ads)}$

$C_2H_5OH_{(ads)} + 6O^-_{(ads)} \rightarrow 2CO_{2\,(gas)} + 3H_2O + 6e^-$

And as published in Qiang et al. [157]:

$C_2H_5OH + 6O^{2-}_{(ads)} \rightarrow 2CO_2 + 3H_2O + 12e^-$

And in Pawar et al. [260] similar to what is suggested in Mirzaei et al. [41] they highlight the intermediate products produced as part of the reaction with oxygen:

$C_2H_5OH + O^{2-} \rightarrow CH_3CHO + H_2O + 2e^-$

$CH_3CHO + 5O^{2-} \rightarrow 2CO_2 + 2H_2O + 10e^-$

$C_2H_5OH_{(ads)} + O^-_{(ads)} \rightarrow CH_3CHO_{(ads)} + H_2O + e^-$

$CH_3CHO_{(ads)} + 5O^-_{(ads)} \rightarrow 2CO_2 + 2H_2O + 5e^-$

The dehydrogenation process of ethanol to form acetaldehyde is specified in Pandya et al. [154].

Acetone ($(CH_3)COCH_3$): colourless, flammable organic solvent with a strong pungent odour. One of the major applications of acetone detection is in the medical field; it can serve as a biomarker to detect diabetes. Acetone in healthy individuals is in the range of 0.2 – 1.8 ppm but rises to 1.25 – 2.4 ppm in people with diabetes.[261] It is used extensively in the pharmaceutical industry, to dissolve plastics and to purify paraffin. Further, it is harmful to health and exposure to ~300 – 500 ppm of the gas for five minutes may cause irritating side effects to skin and the throat and inhalation may result in headaches, fatigue, narcosis and may be harmful to the central nervous system.[41] Additionally, acetone is a common solvent used in clandestine labs for the manufacture of cocaine [262] and amphetamine-type drugs [263] and to dissolve herbal blends that contain an active ingredient.[264] Gas sensors have previously been investigated for the detection of acetone, some examples include nanostructured ZnO to detect acetone concentrations ranging between 0.25 – 100 ppm,[47] ultrafine α-Fe_2O_3 nanoparticles to detect concentrations ranging from 5 to 3000 ppm,[219] Fe_2O_3

hamburger like α-Fe_2O_3 micro-particles to detect 25 – 500 ppm acetone, SnO_2 sensors enhanced via molecular imprinting to detect concentrations ranging between 50 ppb and 100 ppm,[155] and a highly sensitive CNT-SnO_2 composite to detect concentrations in the range of 0.5 – 5 ppm.[46] The reactions reported as a result of the interaction between acetone and chemisorbed oxygen at the sensor surface are:

$CH_3COCH_3 + 2O^- \rightarrow C^+H_3 + CO_2 + CH_3O^- + 2e^-$ (47)

$CH_3COCH_3 + 8O^- \rightarrow 3CO_2 + 3H_2O + 8e^-$ (265)

$CH_3COCH_{3\,(gas)} + OH^- \rightarrow CH_3CHO + CH_3O^-$ (173)

$CH_3COCH_{3\,(gas)} + O^- \rightarrow [CH_3COCH_2]^+ + OH^- + e^-$ (173)

$CH_3CHO + O_{(bulk)} \rightarrow CH_3COOH + O_{(vacancies)}$ (173)

or

$CH_3COCH_{3\,(gas)} + O^- \rightarrow [CH_3CO]^+ + CH_3O^- + e^-$ (173)

$CH_3CO \rightarrow [CH_3]^+ + CO$ (173)

$CO + O^- \rightarrow CO_2 + e^-$ (173)

Toluene ($C_6H_5CH_3$): colourless liquid that has a characteristic aromatic odour. It is an aromatic HC that is emitted from crude oil in the process of making gasoline and other fuels and in the making of coke from coal.[41] It is used in the manufacture of paints, paint thinners, nail polish, adhesives, rubber and so on. Toluene is acutely toxic and it affects the central nervous system. The World Health Organisation (WHO) reports that indoor air should not exceed toluene concentrations of 0.07 ppm at 25 °C. Toluene is a product sniffed and abused recreationally, usually, among adolescents. Toluene detection has also been explored with gas sensors. Some studies include: C-doped WO_3 microtubes to detect concentrations ranging between 50 ppb and 500 ppb at 90 °C,[266] SnO_2 nanofibers to detect concentrations ranging between 10 and 8000 ppm of toluene, the sensors showed good selectivity towards toluene in relation to other HC gases,[267] monodispersed porous Cr_2O_3 microspheres for the selective detection of 1–200 ppm toluene in relation to benzene and chlorobenzene.[268] The reaction processes occurring at the sensor surface have been reported as:[269,270]

$C_7H_8 + 2O^- \rightarrow C_7H_6O + H_2O + 2e^-$

$C_7H_6O + O^- \rightarrow C_7H_6O_2 + e^-$

However, other studies report the direct combustion of toluene to CO_2.[271,272]

$C_7H_8 + 18O^{2-} \rightarrow 7CO_2 + 4H_2O + 36e^-$

Isopropyl Alcohol (C_3H_7OH): colourless, flammable solvent that smells like alcohol and has a bitter taste. It is employed to produce acetone and isopropyl halides and is extensively used as a solvent for paints, polishes and insecticides. If inhaled it may cause irritation to the eyes and nose and ingestion can lead to a coma.[41] Gas sensors have also been employed to detect C_3H_7OH. For instance, a silicon polymer chemical gas sensor was found exposed to a range of gases (ethanol, acetone, methanol and 2-propanol) and was found to be selective towards 2-propanol. The authors investigated gas concentrations ranging between 2 – 12 ppth. Binions et al. [15] successfully discriminated between ethanol and 2-propanol molecules using sensor arrays based on zeolite-modified WO_3 and CTO materials. Kumar et al. [273] report the sensitivity of a four-sensor array based on SnO_2 thick films that were doped with Pd and Pt and ZnO, which were able to discriminate between acetone, LPG, N_2O and Isopropyl alcohol gases.[273]

Ammonia (NH_3): colourless, reactive gas at room temperature, easily dissolved in water. It has a distinct, pungent odour and it is very toxic. Exposure to 50 ppm of the gas may cause acute poisoning or life-threating situations.[274] Its detection is of interest to environmental and automotive gas monitoring, to industry and for medical diagnostics. In environmental monitoring, ammonia detection is necessary because in farming environments the concentrations may exceed those recommended as safe. It is extensively used in the manufacture of plastics, dyes, explosives and pharmaceuticals. Its use is also relevant in the production of illegal drugs such as of methamphetamine. Its pungent smell is used as a characteristic sign of clandestine laboratory activities. During anhydrous ammonia 'cooks', ammonia levels exceed the immediately dangerous to life and health NIOSH levels.

Several studies have reported the detection of ammonia with gas sensors. Some examples include: detection with heterogeneous nickel oxide/zinc oxide sensors for room temperature operation to 50 ppm of the gas. The sensor was highly selective towards ammonia, when compared to other gases like 2-propanol, toluene, formaldehyde, chloroform, heptane and dichloromethane.[274] Cr_2O_3-activated ZnO thick films also exhibited high selectivity towards ammonia when compared to LPS, CO_2, C_2H_5OH, H_2 and Cl_2 gas exposure.[275] The concentrations of ammonia explored in the latter study ranged between 13.7 ppm and 300 ppm. Moos et al. [40] developed a selective ammonia sensor for vehicle exhaust applications, using zeolites as the sensitive elements. Mani et al. [276] also developed a highly selective ammonia sensor for room temperature operation when exposed to 25 ppm of potentially interfering

gases such as 2-propanol, methanol, ethanol, acetone, acetic acid. The surface reaction with chemisorbed oxygen has been reported as [29,136,276]:

$$2NH_3 + 5O^- \rightarrow 2NO + 3H_2O + 5e^-$$
$$2NH_3 + 3O^- \rightarrow N_2 + 3H_2O + 3e^-$$
$$2NH_3 + 4O^- \rightarrow N_2O + 3H_2O + 4e^-$$

Carbon Monoxide (CO): poisonous, colourless and odourless gas. Its harmful effects come from the displacement of oxygen in blood and the subsequent deprivation of oxygen in vital organs which, if inhaled, can lead to death. It is in fact the third most common reason for human intoxication after drugs and alcohol. Furthermore, it is an atmospheric pollutant generated from natural gas and anthropogenic sources, depending on multiple physical and chemical processes.[277] It promotes the formation of other major environmental pollutants such as ozone (O_3).[277] Sources of CO originate from cigarette smoke, gas ovens, wood stoves, incomplete combustion of fossil fuels, traffic exhaust and the mining industry and power plants.[278] The OSHA limits of exposure for this gas are 50 ppm over an eight-hour period. Its detection has been widely researched with MOS sensors, some studies reporting its detection at 30 and 50 ppm with zeolite modified WO_3 sensors,[23] 10–100 ppm with α-Fe_2O_3 nanoparticles,[224] and SnO_2 sensors coated with microporous ceramics at 10–100 ppm.[65] Surface reactions are reported as a full combustion to carbon dioxide (CO_2):[23,202]

$$CO + O^-_{(ads)} \rightarrow CO_2{}^-_{(ads)} \rightarrow CO_{2\,(gas)} + e^-$$
$$CO + 2O^-_{(ads)} \rightarrow CO_{2\,(gas)} + O^-_{(ads)} + e^-$$
$$\rightarrow CO_{2\,(gas)} + \tfrac{1}{2}\,O_2 + 2e^- + S$$

Where *S* refers to an unoccupied oxygen vacancy.

Nitrogen Dioxide (NO_2): yellow or reddish gas with a strong pungent odour. Exposure to NO_2 has been reported to cause lung damage and worsen chronic lung conditions such as bronchitis and emphysema.[23] Although nitro compounds are not typically found in narcotics, nitroethane and nitropropane are precursor molecules used to produce, for instance, phenyl-2-propanone – a precursor to methamphetamine. 'Blue nitro', a GHB analogue, has recently been introduced into the black market and has been linked to a number of deaths. MOS sensors have reactions of NO_2 on the sensor surface and have been reported as:[249]

$$NO_2 + O^- \rightarrow NO + O_2 + e^-$$

$NO_2 + O_2^- + 2e^- \rightarrow NO_2^- + 2O^-$

In Varsani et al. [23] WO_3 zeolite-modified sensors were employed to detect 50 – 400 ppb NO_2 and the interaction with the gas was suggested to be the result of NO_2 chemisorption, rather than a reaction with oxygen as follows:[23]

$NO_2 + e^- \rightarrow NO_2^-$

Methyl Benzoate ($C_6H_5CO_2CH_3$): it is a by-product of cocaine that has a sweet aroma similar to the feijoa fruit. Detection dogs target this substance as a marker in the detection of cocaine.[33] Although there is no report in the literature on its detection with sensors, studies report the detection capabilities of sniffer dogs when exposed to commercial and street drug products of cocaine.[34] No studies have been found in the literature to detect methyl benzoate with MOS technology.

Humidity ($H_2O_{(v)}$): numerous sensor types to detect humidity have been reported in the literature.[206,279–281] The need to monitor humidity is necessary in a range of fields that involve air-quality monitoring to suit human comfort and well-being, in industry for quality control and technological process control and research.[281] The basis of a lot of research in the field of gas sensing has been to better understand and control cross-sensitivity issues with humidity for practical applications of sensors.[202,274,282] It has been found that the conductivity of some MOS sensors e.g. SnO_2 is inherently affected by the presence of hydroxyl groups adsorbed at the surface which can, in turn, affect the performance of the sensor.

1.8 Summarised Thesis Aims

- To explore a range of sensing materials (based on n-type and p-type semiconductors) for the detection of trace concentrations of gases known to affect health, security, safety and the environment. This was carried out through sensor exposure to a range of HC gases of different chain length and with different functional groups. The detection of inorganic gases such as NO_2 and NH_3 was also evaluated. A range of temperatures and concentration ranges were investigated so that optimal sensing conditions could be determined. Where possible, sensors were exposed to gases in the presence of humidity to recreate more realistic scenarios.

- To explore how and if the sensing performance of the base MOS sensors could be improved by incorporating different zeolite materials. This was achieved by investigating whether zeolite incorporation meliorated aspects such as sensitivity, selectivity, response magnitudes, repeatability, reduction of the optimal operating temperature and response and recovery times.

- To explore ways in which zeolites could be better used to induce sensitivity and selectivity in sensors. This was carried out through the investigation of two different fabrication methods: zeolite admixtures and overlayers.

- To test whether sensors could detect two drug markers commonly targeted by sniffer dogs in drug trafficking interdiction efforts; methyl benzoate as a marker of cocaine and ammonia as a marker of amphetamine-based drugs.

1.9 Thesis Outline

A summary of the Chapters that have been presented in this thesis is presented below.

Chapter 2 describes the materials used and methodologies followed in this thesis. It describes the gas-sensing rigs, equipment and protocols followed in the experiments, it elucidates pertinent calculations and gives details of the list of sensing materials and fabrication approaches taken to produce the set of sensors.

Chapter 3 primarily describes the modification of a control SnO_2 sensor by incorporation of zeolites Na-A, H-ZSM-5 and H-Y in the form of admixtures and overlayers. The fabricated sensors were exposed to different HC gases with different chain lengths and to molecules with different functional groups. The sensors were exposed to gases with similar molecular structures and kinetic diameters to assess how effective the zeolites were at providing distinctive response magnitudes and patterns. A range of temperatures and gas concentrations were also explored. Additional tests were based on assessing differences in sensor responses with increasing film thickness and when testing sensors from the same batch.

Chapter 4 describes the modification of a Cr_2O_3 sensor with different amounts of admixed zeolite H-ZSM-5 to a range of HC gases. It also describes the results attained when modifying the Cr_2O_3 base material with 10% (wt.) of zeolite Na-A and it then moves on to describe the results attained when modifying the base material with overlayers of zeolite H-Y. The effects of humidity on sensor performance have also been investigated.

Chapter 5 details the results attained when modifying a Fe_2O_3 sensor with zeolites Na-A and H-ZSM-5. Another Fe_2O_3 sensor was fabricated by using a MOS powder from a different supplier and the contrasting results between the unmodified base materials are presented. The sensing performance of a Fe_2O_3 sensor modified by overlayers of zeolite H-Y has also been explored.

Chapter 6 describes the sensor responses attained upon exposure to two common drug markers, methyl benzoate and ammonia. This study was carried out due to the pressing need to develop inexpensive technology to detect illegal drugs during trafficking operations and also as a means to determine whether gas sensor technology based on MOS sensors could serve this purpose, given the benefits detailed in the introduction. Furthermore, a short study was carried out to determine whether support vector machines could be used to accurately classify the gas data into the different gas types used in this study.

Chapter 7 provides the reader with conclusive remarks about the thesis and gives an account of future work that could be performed or should have been performed if there had been more time.

2. Materials & Methods

Chapter 2 details the experimental procedure carried out in this study. It includes:

- A description of the different approaches taken to fabricate what we have referred to as 'control sensors' and 'modified sensors'. The former correspond to the unmodified sensors containing only the base material as the sensing element. Modified sensors are those which have been modified in some way e.g. by incorporating zeolites in the form of admixtures with the base material or as additional film coatings on top of it.
- The protocols followed when performing gas-sensing experiments and the specifications of the gas-sensing rigs, with examples of a test programme and of the calculations needed to translate the output data into meaningful information i.e. sensor resistance and sensor responses.
- An account of the physicochemical characterisation techniques performed on the sensing materials to measure any potential changes in the crystallinity and microstructure of the materials in the process of manufacture and testing.

2.1 Base Material Selection, Target Analytes and Sourcing

Three different metal oxide semiconductor (MOS) materials were selected to investigate their capabilities as detectors of substances that pose a severe effect on health, safety, the environment and air quality when modified with different zeolite materials. However, as indicated in Chapter 1, it was of particular interest to detect gases and vapours in the context of drug trafficking and drug abuse. An exhaustive list of the analytes tested in this thesis was provided in section 1.7 (Chapter 1). The motivations for detecting these analytes with MOS sensors were also elucidated in this section.

The MOS materials of choice were tin oxide (SnO_2), chromium oxide (Cr_2O_3) and iron oxide (Fe_2O_3). Fe_2O_3 gas sensors were fabricated from two different suppliers (Sigma Aldrich and BDH) to consider any variability in the gas-sensing characteristics of the materials (Table 2-1).

Table 2-1 Base sensor materials investigated, supplier information and zeolite agents used.

Control Sensing Materials	Supplier	Modifying Agents
SnO_2	Sigma Aldrich	Na-A, H-Y, H-ZSM-5
Cr_2O_3	BDH	Na-A, H-Y, H-ZSM-5, Fe_2O_3
Fe_2O_3 (1)	Sigma Aldrich	Na-A, H-ZSM-5, H-Y
Fe_2O_3 (2)	BDH	None

Note that the base sensing materials were selected due to their well-established suitability in the gas-sensing field, particularly in the case of SnO_2. Novel sensors were fabricated and explored by combination of the base material with zeolites. Although zeolite incorporation to enhance sensor performance has, indeed, been reported in the literature, the topic is still a relatively new one. As such, studies on the zeolite modification of the sensing materials of choice are scarce (in the case of Cr_2O_3 and SnO_2) and, to the best of our knowledge, have not yet been reported with Fe_2O_3.

Table 2-2 – List of analytes investigated in this thesis, source concentrations and supplier information. The concentration of methyl benzoate is based on its vapour pressure at 25 °C. Under 'Test Vapour' the phase of the analyte has been indicated in brackets, (l) refers to liquid and (g) to gas.

Test Vapour	Source Concentration	Supplier
Ethanol (g)	100 ppm	BOC Gases
Isopropyl Alcohol (g)	500 ppm	BOC Gases
Acetone (g)	10 ppm	BOC Gases
Toluene (g)	50 ppm	BOC Gases
Ammonia (g)	50 ppm	BOC Gases
Ethane (g)	100 ppm	BOC Gases
Propane (g)	100 ppm	BOC Gases
Butane (g)	100 ppm	BOC Gases
Methanol (g)	100 ppm	BOC Gases
Nitrogen Dioxide (g)	1 ppm	BOC Gases
Carbon Monoxide (g)	1000 ppm	BOC Gases
Methyl Benzoate (l)	368 ppm	Sigma Aldrich
Amphetamine in Methanol (l)	1g/ml	Sigma Aldrich

2.2 Thick-Film Metal Oxide Semiconductor Gas Sensor Fabrication

This section describes the steps required to fabricate a thick-film gas sensor using screen-printing as the method to deposit the sensing material onto the sensor substrate. An illustration of what the end product looks like has been presented in Fig. 2-1 below to assist in visually anticipating how the items were assembled during fabrication and to get acquainted with terms used in forthcoming sections.

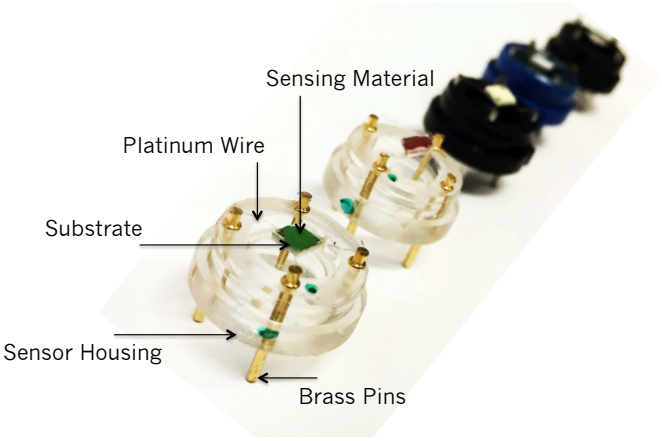

Figure 2-1 Illustration of a gas sensor array showing 3 mm × 3 mm alumina substrates with different sensing materials screen-printed on top. As appreciated in the image, each sensor has four terminals that are connected to brass pins on the polycarbonate sensor housing by means of platinum wire.

2.2.1 Sensor Substrates

The sensor tiles used in this study (Capteur Sensors Ltd.) were composed of an insulating alumina substrate measuring 3 mm × 3 mm that was later connected to a sensor housing (Aeroqual, NZ) with four brass terminals that protruded from a polycarbonate or polyphenylene base. Two of the terminals were connected to the electrodes on the obverse of the sensor, which had pre-printed interdigitated gold electrode geometries with wide gap (150 μm) electrode spacing. The other two terminals were connected to the heater track on the reverse of the sensor to enable its heating during gas-sensing tests. This has been illustrated in two SEM micrographs of a sensor chip of the kind used in this study (Fig. 2-2).

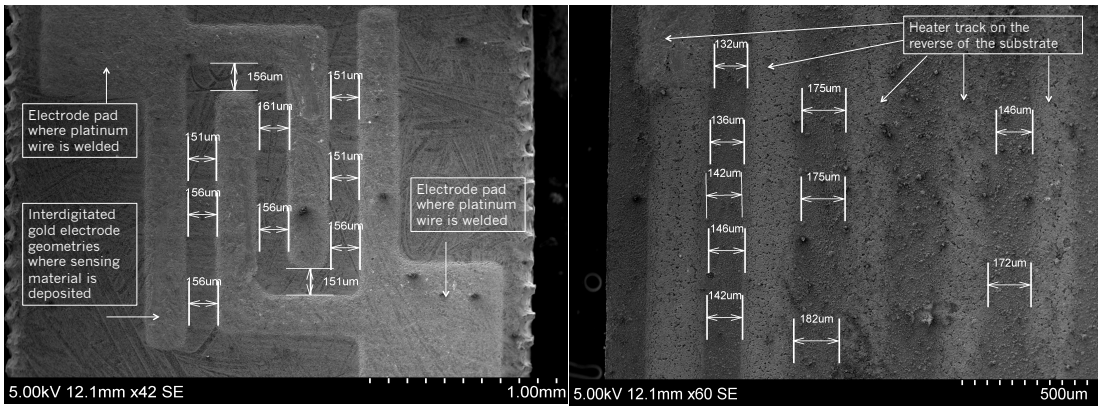

Figure 2-2 Sensor substrate showing interdigitated gold electrodes where the sensing material is deposited (top) and integrated heater track on the reverse of the substrate (bottom). The electrode spacing has also been marked, as well as the pads where the platinum wire is spot-welded.

2.2.2 Preparation of the Powder/Vehicle Mixture for Screen-Printing

A printable paste or ink is required to screen-print a semiconducting material onto a given set of sensor chips, in this case onto 13 sensor chips, as shown in Fig. 2-3 below. The paste was prepared by mixing a metal oxide powder with an organic binder (ESL 400) in an agate mortar and pestle for a specific time (i.e. 30 minutes), so as to obtain a homogeneous paste with a consistency similar to that of toothpaste. Although various ideal ratios (powder material (wt.)/binder (wt.)) have been reported in other studies, the optimal amount of binder required to achieve good paste consistency is directly dependent on the particle size of the material and its surface area. Achieving the right consistency is essential; too liquid a paste may lead to thinner films due to transference of the paste to adjacent sensor chips and too thick a paste may prevent the paste from spreading across the full length of the strip during a print, leading to unequal film thicknesses across it. Table 2-3 shows the powder (wt.)/binder (wt.) ratios utilised in this study.

Table 2-3 Fabrication characteristics of the metal oxide semiconductor powders employed.

Control Materials	Powder Weight (g)	Vehicle Weight (g)	Ratio (Powder/Vehicle)
SnO_2	2.00	1.24	1.61
Cr_2O_3	1.72	1.18	1.46
Fe_2O_3 (BDH)	1.01	0.73	1.38
Fe_2O_3 (Sigma)	1.38	1.04	1.32

2.2.3 Screen-Printing and Spot-Welding

A DEK 1202 screen printer was employed in combination with a MCI 3 × 3 precision screen with a patterned mesh that enabled the paste to be deposited between the two gold electrode pads and onto individual sensors on the strip (Fig. 2-3). Pressure was inflicted with a squeegee, set to automatically move and transfer the paste through the mesh, covering the full length of the strip. After each film deposition, the paste was allowed to dry under an IR lamp. Following completion of the printing process, the sensors would then be sintered in a furnace (Elite Thermal Systems Limited) at 600 °C for an hour, increasing the temperature at a rate of 25 °C/min. The sensor strip would then be broken down to individual chips and, typically, a sensor with a specific location on the strip (i.e. position 2 out of 13) would be selected for testing to minimise any potential variability caused during the fabrication process.

The effects of film thickness on sensor performance were explored by printing three, four and five layers of SnO_2 on the substrate (Chapter 3) and by printing three, five and seven layers of Cr_2O_3 (Chapter 4) and Fe_2O_3 (Chapter 5) on the sensor substrates. The

results on film thickness were used as guidance to later fabricate zeolite-modified sensors.

A Macgregor DC601 spot welder was used to connect the platinum wire to the four pads on each sensor i.e. the two pads on the obverse of the sensor and the two on the reverse. Then, the sensor was connected to the housing by spot welding the platinum wire to each of the four protruding terminals, as shown in Fig. 2-1 above.

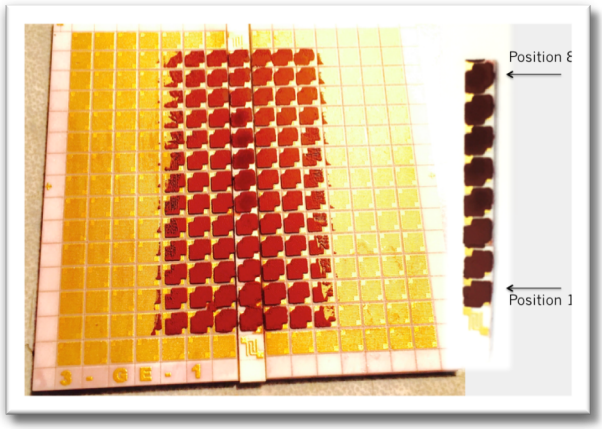

Figure 2-3 Iron Oxide (Fe_2O_3) printed onto a strip of 13 sensors. A strip of 8 sensors is shown with details on how the sensor position numbers were chosen in this study.

As was described in Chapter 1, zeolite incorporation was approached in two ways: by mixing the metal oxide powder with a zeolite material of choice and by screen-printing additional coatings of a zeolite over the base material. This process has been described in further detail below.

2.2.4 Fabrication of Zeolite-Modified MOS Gas Sensors

The modification of base sensor materials to enhance sensing performance is well established in the field. The modification of the base material through zeolite incorporation has been investigated by a number of research groups and very promising results have been attained to date. Whilst most groups have reported the works of zeolite coatings over a base material of choice, the UCL Chemistry department has recently been focussing on the admixture of the base material with zeolites. This work has been continued in this thesis, where new combinations of zeolites have been explored with SnO_2, Cr_2O_3 and Fe_2O_3 for gas-sensing purposes. The concept of overlaid and admixed sensors has been illustrated in Fig. 2-4 below. Zeolites H-ZSM-5 and H-Y were obtained from Zeolyst International USA (H-ZSM-5 CBV 8014 and Y-zeolite CBV 600) and zeolite Na-A from Advera PQ-Corporation.

In **zeolite overlayers** the zeolite powder is mixed with the ESL 400 organic vehicle and then printed on top of the base material. The effect of increasing the number of zeolite layers on top of the control sensor was investigated by printing one or three additional film depositions on top of the base material. The sensors were generally fabricated with five layers of the control. Variations of this fabrication process have been specified individually in each chapter.

Zeolite admixtures were prepared by mixing the metal oxide and zeolite powders together with the organic vehicle. A control material was typically mixed with 10% (wt.) and 30% (wt.) of zeolites H-ZSM-5, H-Y and Na-A. Variations of this have been disclosed individually in each chapter. For instance, Cr_2O_3 sensors were mixed with a broader range of H-ZSM-5 loadings (10% to 40% (wt.)). At the end of this chapter one can find a detailed compilation of all the sensors fabricated and described in this thesis (Tables 2-4, 2-5 and 2-6).

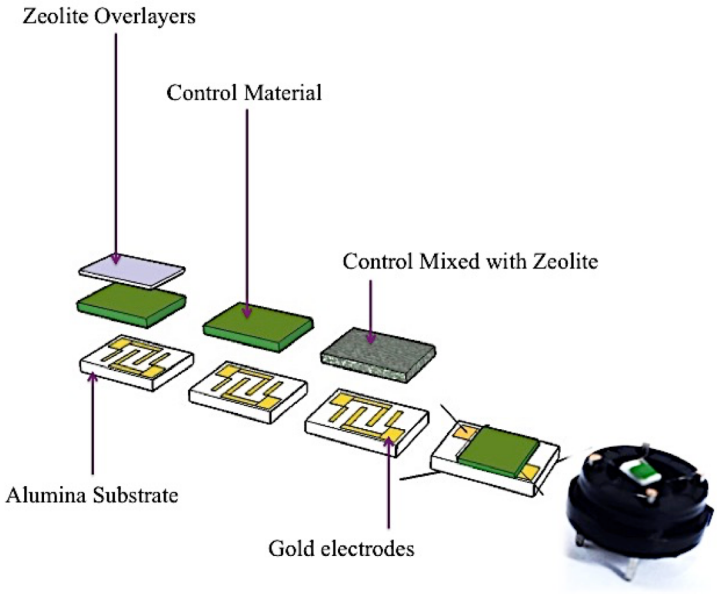

Figure 2-4 Schematic of the sensor fabrication process followed in this thesis. The differences between the fabrication of a control sensor and of sensors modified through zeolite incorporation in the form of overlayers or admixtures have been illustrated. A sensor with spot-welded platinum wires and a sensor welded onto a sensor housing have also been included for clarification purposes.

2.3 Gas Sensing Rigs and Test Programmes

The gas-sensing rigs employed during the course of the thesis were custom built by previous researchers at UCL. Although two different rigs were employed to carry out gas-sensing tests, the majority of the work was performed on 'AA rig'. As such, the specifications and protocols followed on this rig are explained in detail in this section. Relevant information pertaining to the other rig can be found in Peveler et al. [28].

2.3.1 AA Rig

AA rig was designed and fabricated by Dr Afonja at UCL (Fig. 2-5). It was deliberately designed to address issues previously encountered with other gas-sensing rigs available in the lab. A schematic of its key constituents is presented in Fig. 2-6. In essence, it shows how the rig was configured to supply air and gas into the sensing chamber and indicates what is needed, electronically, for sensor operation and data acquisition.

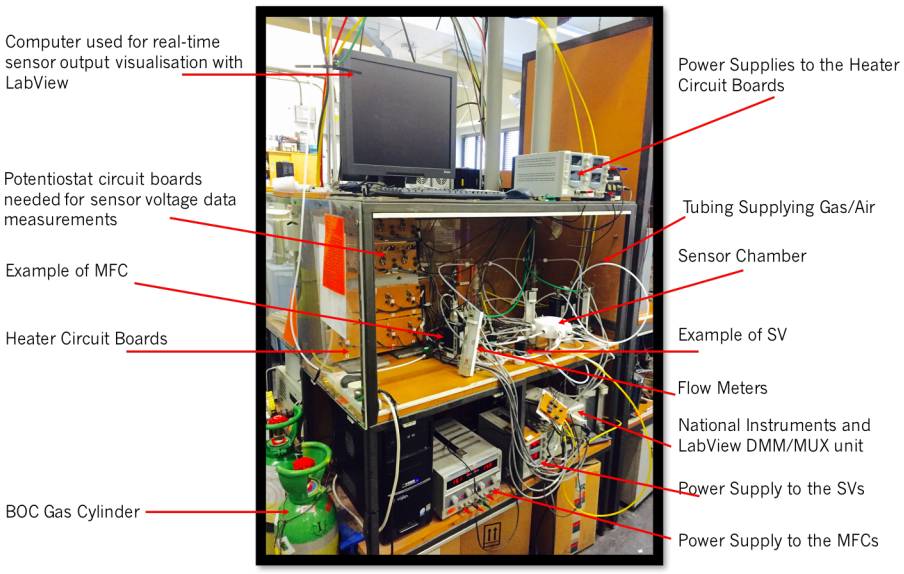

Figure 2-5 Picture of AA rig. The components that were involved in its design and operation have been explained in coming sections.

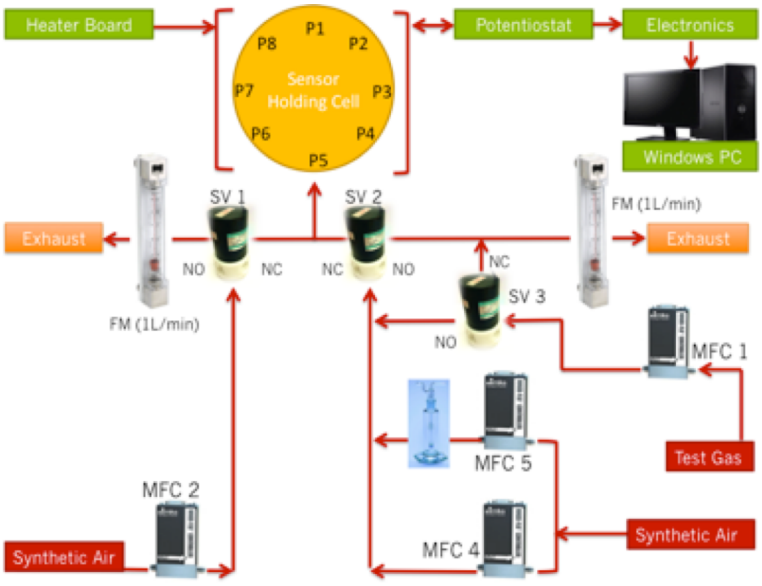

Figure 2-6 AA rig configuration. P1-P8 refer to the port numbers housing the sensors in the sensing chamber. MFC refers to Mass Flow Controllers. SV refers to solenoid valves. FM refers to flow meters. A Dreschel flask was placed after MFC-5 so that tests could be performed under humid conditions and to test liquids relevant for detection. Image adapted and redrawn from [29], accommodating modifications made since its original design.

2.3.2 Gas Sensing Chamber

The gas-sensing chamber was made of solid PTFE due to its inertness towards a wide range of compounds. It was cylindrical in shape and able to house eight sensors.

Fig. 2-7 shows the configuration of the sensing chamber. The air/gas was supplied through an inlet at the base of it, which was then radially subdivided into eight separate airtight compartments, one for each sensor, simultaneously supplying airflow in a uniform and equal fashion.[29] The internal volume of the compartments was purposely small so as to achieve fast response times during testing. The four pins protruding downwards from the sensor housings were inserted onto a support that would screw into the chamber, making the system air-tight. This was necessary to prevent fumes or toxic vapours from leaking into the lab during the course of experiments.

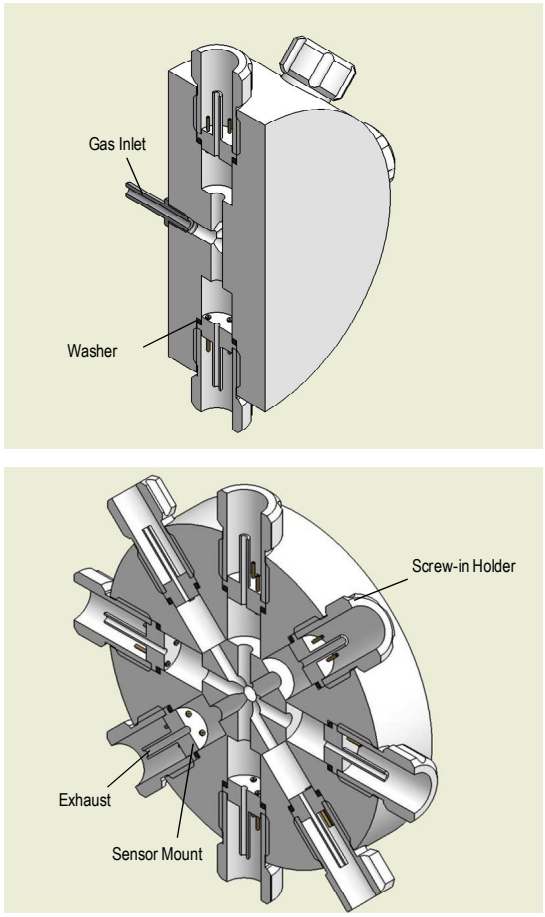

Figure 2-7 Cross-sectional view of the gas-sensing chamber. The location of the air/gas inlet is depicted, showing how the supply of air or gas was distributed radially and individually into each of the eight sensor compartments. The way in which each sensor mount would screw into its allocated position in the sensing chamber can also be appreciated in the image. Image from [29].

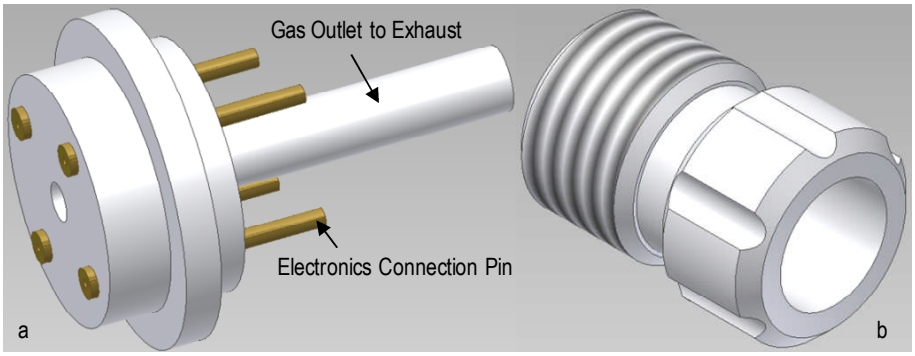

Figure 2-8 Design of the support to which the four pins protruding downwards from the sensor housing were inserted (left). The design of the support used to tightly screw the sensor mount onto the sensing chamber has also been illustrated (right). Image from [29].

Each sensor compartment had an independent air/gas outlet connection to exhaust and independent electrical connections to the heater circuit boards and to the potentiostat circuits required for sensor operation and data acquisition.[29]

Dr Afonja designed and fabricated the sensor heater boards used to heat the sensing devices (Fig. 2-9). The design was inspired by that of Capteur's heater boards, which have been shown to maintain the sensors' platinum heater track at a stable temperature over long periods of time, with shifts (±3 °C) attributable to ambient temperature changes.

The obsolete transistor in this novel heater board design was a SUD19P06-60 p-channel MOSFET (2SJ182L p-channel MOSFET in Capteur designs). The new design had a low-temperature coefficient potentiometer (±20-50 ppm/°C) and high precision metal film transistors (±15 ppm/°C) to minimise damaging effects to the temperature sensitivity of the Wheatstone bridge.[29]

The unit that enabled all eight sensors to be heated was divided into two single-sided strip-boards (368 mm × 117 mm × 1.6 mm), each of which was powered by a PSD30-3B DC power supply (Fig. 2-10). This setup was in place to avoid overload.[29] Each board had four separate heater driver units. When heating the sensors to temperatures ranging between 250 °C and 500 °C, they would typically draw between 0.25 – 0.30 A.

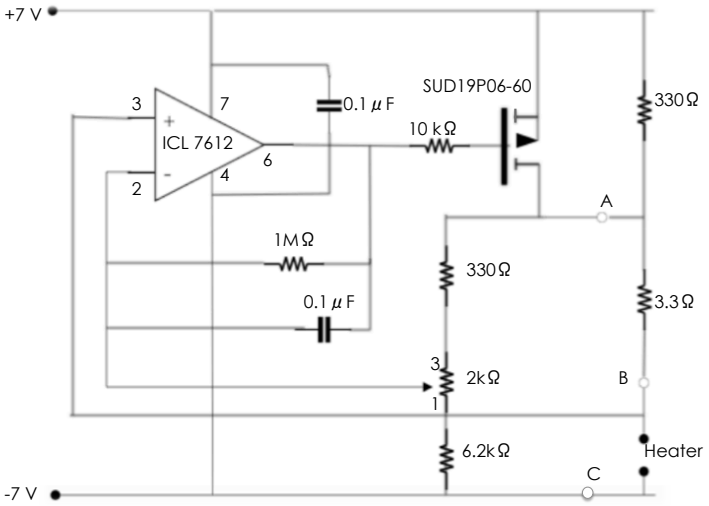

Figure 2-9 Sensor heater diagram, adapted and redrawn from [29].

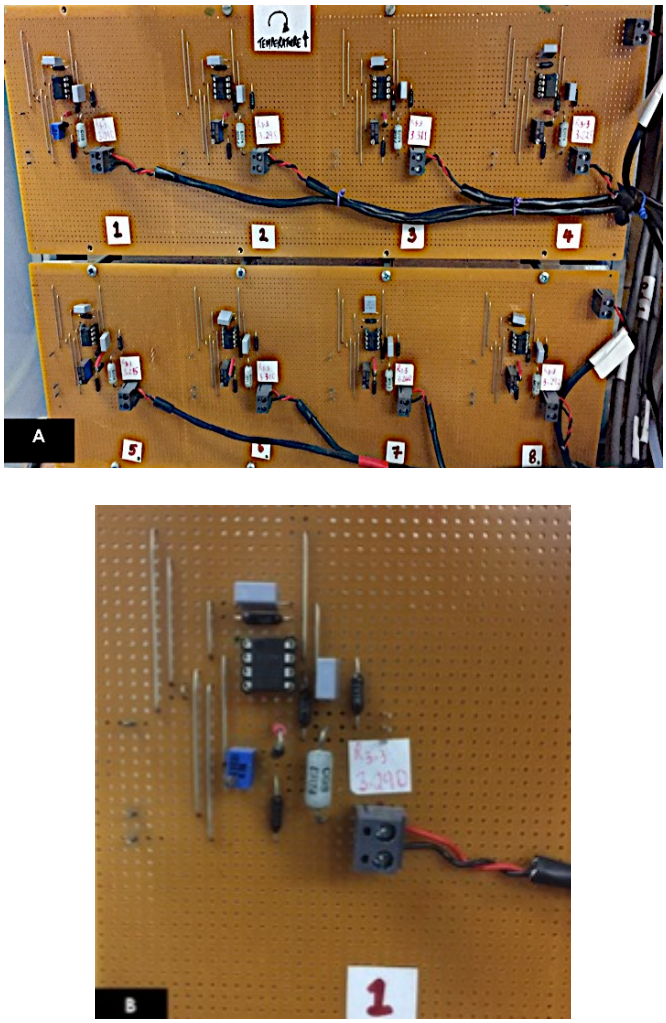

Figure 2-10 (A) Sensor heating unit for the eight sensors used in this system. (B) Close up of an individual heating board responsible for heating the sensor in port 1.

2.3.3 Control of Air and Gas Supplies to the Sensing Chamber

The rig was built to enable different configurations of air and test gas supplies into the sensing chamber. This can be visually appreciated in Fig. 2-6 above. It was possible to enable the supply of:

- Just synthetic dry air
- Just a test gas
- Just humid air
- Mixtures of dry air and a test gas
- Mixtures of dry and humid air with a test gas.
- Dry air with a vapour originating from a liquid sample placed in a Dreschel flask. A specific flow of air was passed through it and then delivered in to the sensing chamber.

The supply of air/gas to the sensing chamber was controlled by the following components:

1) Mass Flow Controllers (MFCs) - Four different analog MKS mass flow controllers (MFCs) were used, which could deliver a flow of up to 1 L/min to the chamber. They were powered by a digimess HY 3003-3 PSU with dual outputs that supplied the ±15 V and 200 mA needed for each of the MFC's operation.[29] They had Kalrez seals and valve seat made of an inert perfluoroelastomer. They had eleven-core shielded cables responsible for the supply of power and signal transmission to and from the MFCs via a 15-pin D-type connector.[29] Their operation was controlled via a Windows computer using LabVIEW software, which enabled the desired flow of air/gas to be delivered into the sensing chamber through an analog output card (NI PXI6722). The latter generated the necessary input (0 – 5 V) to operate the MFCs and also controlled their internal valves such that when they were not in use, the valves would shut.[29] In essence, while 5 V were necessary to supply 100% of the flow, 2.5 V would be required to supply 50 % of the flow. An analog input card (NI USB-6008) would ensure that the correct voltage was received by the MFCs. Further information on the technical details of the rig can be found in Afonja [29]. As displayed in Fig. 2-6 above, MFC 2 was responsible for the supply of dry air into the system. MFC 1 supplied the flow of test gas. MFC 4 was responsible for the supply of dry air when needed in a mixture with the test gas. MFC 5 was in place to carry out tests under humid conditions. The necessary air/gas concentrations were written manually by the user, creating a CSV file that was later uploaded to LabVIEW, prior to commencing a test.

2) *Solenoid Valves (SV):* Three Takasago 3-way SV (NRV-4E2N) were used to control the sections of the system one wished to use to supply air and/or gas into the sensing chamber. In turn, the part of the system that was at the time idle, i.e. not supplying a flow into the chamber, would direct the air, test gas or mixture of both to exhaust, as displayed in Fig. 2-6 above. The SVs had PTFE supports and seals to prevent chemical reactivity with test gases. A PSD30/3B DC PSU provided 24 V to operate the SVs, with a 200 mA draw per valve. The open or closed states of the SVs were monitored by a PXI 6722 analog output and a high voltage Darlington array (ULN2803).[29] As was the case for the MFCs, the CSV file also contained details of the direction of flow provided by the SV into the sensing chamber or to exhaust, via a normally closed (NC) or normally open (NO) system, respectively, as shown in Fig. 2-6.

3) *Flow meters:* Several flow meters were placed around the rig to be able to identify any potential issues with the flow in a straightforward way. Although not displayed in Fig. 2-6, two additional flow meters were incorporated prior to the synthetic air and air/gas mixtures entering the chamber.

4) *Input and Output cards:* National instrument input and output cards were employed to control the MFCs and SVs remotely through a LabVIEW graphical programming software.[29]

5) ¼ inch PTFE tubing connected with Swagelok tube fittings to carry the air and gas from the air/gas cylinders into the sensing chamber and to exhaust.[29]

Typically, test gases were introduced into a stream of dry air using different airflow dilutions to obtain a desired concentration of a target gas that would range between 5% – 100% of the gas cylinder concentration (Fig. 2-11). In the example provided in the screenshot below, when using a cylinder with a source gas concentration of 100 ppm, the concentrations that were investigated were: 10 ppm, 20 ppm, 50 ppm, 80 ppm and 100 ppm.

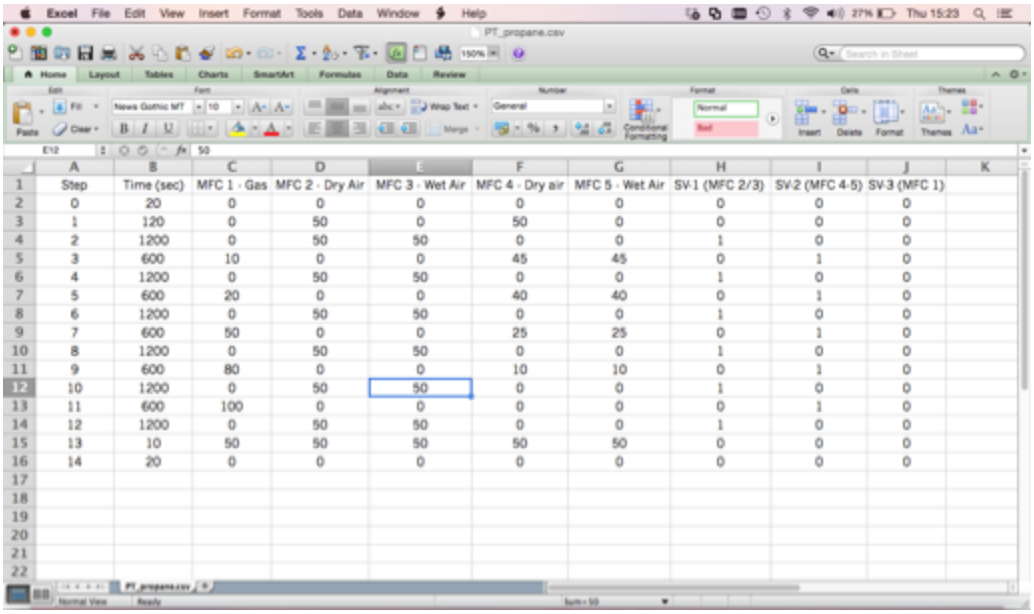

	A	B	C	D	E	F	G	H	I	J	K
1	Step	Time (sec)	MFC 1 - Gas	MFC 2 - Dry Air	MFC 3 - Wet Air	MFC 4 - Dry air	MFC 5 - Wet Air	SV-1 (MFC 2/3)	SV-2 (MFC 4-5)	SV-3 (MFC 1)	
2	0	20	0	0	0	0	0	0	0	0	
3	1	120	0	50	0	50	0	0	0	0	
4	2	1200	0	50	50	0	0	1	0	0	
5	3	600	10	0	0	45	45	0	1	0	
6	4	1200	0	50	50	0	0	1	0	0	
7	5	600	20	0	0	40	40	0	1	0	
8	6	1200	0	50	50	0	0	1	0	0	
9	7	600	50	0	0	25	25	0	1	0	
10	8	1200	0	50	50	0	0	1	0	0	
11	9	600	80	0	0	10	10	0	1	0	
12	10	1200	0	50	50	0	0	1	0	0	
13	11	600	100	0	0	0	0	0	1	0	
14	12	1200	0	50	50	0	0	1	0	0	
15	13	10	50	50	50	50	50	0	0	0	
16	14	20	0	0	0	0	0	0	0	0	

Figure 2-11 Screenshot of an Excel CSV file corresponding to a test programme typically used during gas-sensing experiments on AA rig. This file would be uploaded to LabVIEW before running a test and enabled one to write the concentrations of test gas to be supplied to the sensing chamber, the time interval for each gas pulse and purging steps with air, and the MFCs and SV that one wished to utilise during a test.

2.3.4 Sensor Resistance Measurements and Data Acquisition

The change in resistance undergone by a sensor when exposed to a target gas was determined by measuring the potential difference across the interdigitated gold electrodes in the sensor using a potentiostat circuit.

The sensors' operation could be monitored by means of eight different potentiostats, a digital multimeter (NI 7½-digit DMM with model PXI-4701), a multiplexer PXI (NI PXI-2503 Switch) and a Windows computer which, by means of the LabVIEW software, allowed real-time monitoring and visualisation of the sensors' behaviour.[29]

A schematic of the potentiostat circuit diagram devised by Dr Afonja has been presented in Fig. 2-12 below. The circuit diagram has been subdivided into three separate schematics for clarification purposes. Fig. 2-12B represents the supply of a small steady voltage that was kept at 100 mV (referred to as Vp in the diagram) needed for the sensors' operation. Schematic 2-12C displays the conductivity measurement of the DMM. Schematic 2-12A represents the circuits drawing power to operate this system. As can be seen in 2-12A, two PSUs were used to power the system, delivering ±15 V, 200 mA.

Similarly to the boards employed in the heater driver circuit, they were also configured in single-sided strip-board with dimensions 368 mm × 117 mm × 1.6 mm. An image of the 8-potentiostat boards used in AA rig can be found in Fig. 2-13. Note that the potentiostat circuit design was adapted from a triple potentiostat used in another gas-sensing rig in our lab, designed and fabricated by Dr Pratt.

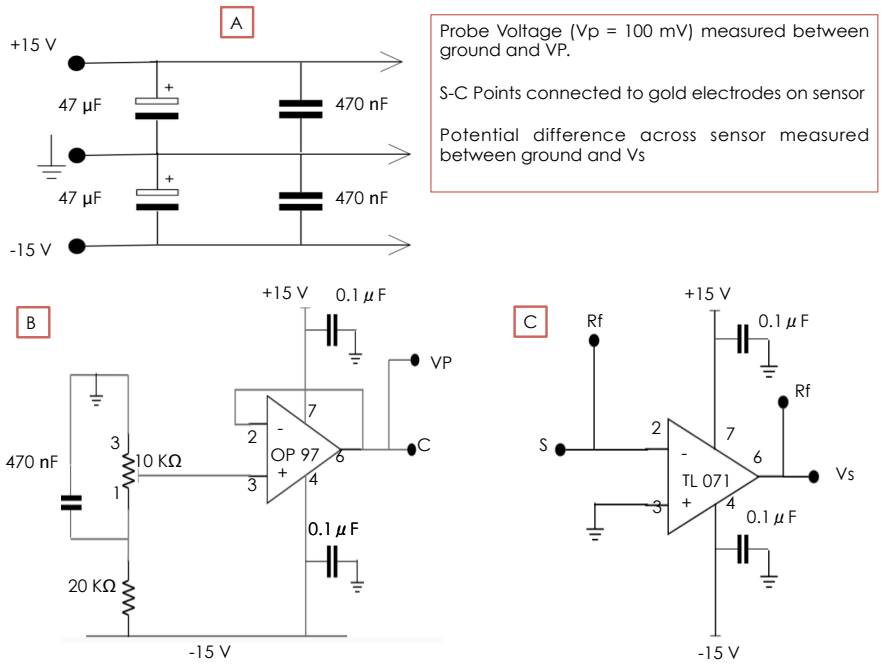

Figure 2-12 (A) Circuit diagram of the potentiostat supplying power to the system. (B) Control circuit responsible for supplying power to the probe voltage (Vp). (C) Circuit of the sensor measurement. The gold electrodes of the sensor are connected to points C and S in the diagram, the probe voltage is fixed and measured between ground and Vp and the potential difference across the sensor is measured across ground and Vs. This schematic was adapted and redrawn from [29].

The voltage output data produced by the potentiostats during a test is measured by the NI DMM and Switch cards which, when combined, provide a high-voltage data acquisition system that enables data to be viewed on the computer via the LabVIEW software.[29] The DMM card is able to deliver fast and accurate voltage measurements in the range of ±10 nV – 1000 V, resistance measurements in the range of 10 µΩ – 5 GΩ and current measurements in the range of ±1 pA – 3 A.[29]

In order to translate the voltage output data into useful information i.e. into resistance values, an inverting operational amplifier was incorporated into the sensing rig design.

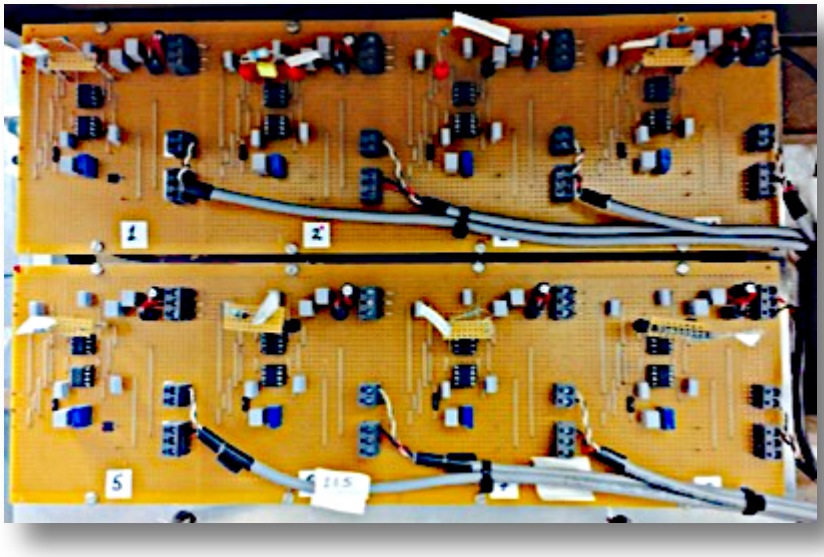

Figure 2-13 Picture of the 8 potentiostat circuits used to operate the sensors.

The inverting operational amplifier equation is expressed as follows:

$$V_{out} = -V_{in}\, R_{fb} / R_{in} \qquad \text{(Equation 1)}$$

In fact, when we relate this to our specific measurement system, we know that the input voltage corresponds to the 100 mV probe voltage, the output voltage is given by the LabVIEW software, which can be seen in real time on a computer, and the feedback resistor is manually changed by the user to ensure that the output voltage of the sensors remains within a specific measurement scale of 0 – 10 V.

By rearranging Equation 1, one can then calculate the resistance value of the sensor, R_s, as a function of time when it is exposed to a changing air/gas ambient.

$$R_s = V_p * R_{fb} / V_{out} \qquad \text{(Equation 2)}$$

For instance, at the start of a test the unknown resistance of the sensor (R_s) would be calculated as follows if a 1 MΩ feedback resistor was being used and the output voltage was given as 2.6 V at the time:

$$R_s = 0.1\ V * 1\ M\Omega / 2.6\ V;\ R_s = 38.5\ k\Omega.$$

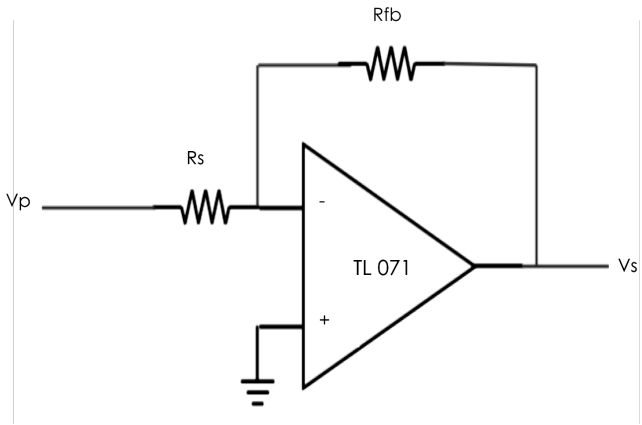

Figure 2-14 Schematic of an inverting operational amplifier.

Note that when exposing an n-type material to a reducing gas, the resistance of the material is expected to decrease as the voltage signal on the screen increases. As a result, a value of the feedback resistor should be chosen such that the output voltage when the sensors are exposed to air is closer 0 V. This is to allow the voltage signal associated to a sensor to increase upon exposure to a reducing gas. Conversely, when investigating the exposure of a p-type material to a reducing gas, one would expect the resistance of the sensing material to increase and, therefore, the output voltage in the presence of clean air should be closer to 10 V.

2.3.5 Experimental Setup and Examples of Gas Sensing Tests

The integrated heater track of the sensors is part of a Wheatstone bridge circuit; by means of an iterative excel programme designed by Dr Pratt, one was able to achieve a desired temperature by modifying voltage ratios between points A and B and B and C (Fig. 2-9) by gradually changing the resistance of the blue potentiostat shown in Fig. 2-10B. Additional information had to be inputted manually such as the desired temperature the sensor ought to be heated to, the room temperature, the heater track resistance at room temperature (in ohms) and the resistance of the 3R3 resistors. The programme would provide information regarding the temperature of a sensor as the voltage ratios were progressively modified.

Prior to commencing new tests the sensors would be heated to 500 °C and would be exposed to synthetic air for a minimum of two hours to desorb any residual gas from the sensor surface and to clean the PTFE tubes used to carry gases. Sensors would typically be heated to a range of temperatures in order to determine the optimal operating temperature at which the sensors were most responsive to gases. The integrated heater tracks on the sensors were usually heated to temperatures ranging between 250 °C and 500 °C.

A typical experiment consisted of an initial 20-minute pulse of dry air to determine the baseline resistance of the sensors (R_0) in air. Although different gas pulse durations were explored to see how the sensors would respond to gases over time, commonly, five 10-minute pulses of test gas were supplied to the sensing chamber, progressively increasing the gas concentration. The sensors were allowed to return to baseline in-between gas pulses with a 20-minute pulse of dry air.

The sensor response was calculated by comparing the resistance of the sensor in air (R_0) to that in the presence of a test gas (R). With an n-type semiconducting material, an observed increase in resistance (resistive response) is calculated as R/R_0, whereas a decrease in resistance (conductive response) is calculated as R_0/R. The opposite is true for p-type materials. The maximum response achieved upon exposure to a test gas has been reported as R_{max}. The sensitivity (S) of a sensor to a gas is equal to the derivative of the response (r) as a function of the concentration (c).

$$S = \frac{d(r)}{d(c)} \qquad \text{(Equation 3)}$$

Where this relationship was not linear, a polynomial equation of second or third order was fitted to the response curve. By taking the derivative of the polynomial equation, one may then obtain a sensitivity curve for a particular sensor to a gas as a function of concentration. This was also tried by manually taking $S = \Delta r/\Delta c$ between each concentration point. To calculate the delta for the first point, it was assumed that at a concentration of 0 ppm of gas, there would be a response of $R_0/R = 1$. The selectivity of a sensor to a test gas *i*, considering a set of *n* gases assuming 1 ppm of a contaminant gas is calculated as:[144]

$$\text{Selectivity(i)} = \frac{{}^{Ra}/_{R1i}-1}{\sum_{j=1}^{n}\left({}^{Ra}/_{R1j}-1\right)} \qquad \text{(Equation 4)}$$

Where R_a refers to the resistance of the sensor in air and R_{1i} refers to the resistance of the sensor in the presence of 1 ppm of contaminant. The selectivity will then be defined by a value between 0 and 1, with higher values indicating higher selectivity of a sensor towards a gas.[144]

The sensor response time was the time taken by the sensor to reach 90% of its maximum saturation value once the gas was introduced into the chamber (termed τ_{90}). The sensor's recovery time was the time taken by the sensor to return to within 10% of its initial baseline value once the gas was switched off and removed from the sensing chamber (termed τ_{10}).

Support vector machines (SVM) were used to assess whether a model could be built to accurately classify the dataset obtained after exposing a five and a four-sensor array to a range of gases. To do this, a CSV file was compiled that contained the maximum conductive and resistive sensor responses attained when exposed to each target sample. Data was inputted after 5 secs, 10 secs, 50 secs, 100 secs, 200 secs, 300 secs, 400 secs and 500 secs, following gas injection at an operating temperature of 400 °C. The file was then uploaded to the WEKA software (University of Waikato, NZ) and a model was built using different classifiers e.g. SMO algorithms with polykernel and RBF kernel functions e.g. C = 10 and γ = 0.01. The cost function 'C' was subsequently modified to find the optimal parameters for classification. Eventually, the performance of the final classifier was tested using the leave-one-out approach. Further, the robustness of the method was also assessed by classifying the data with Random Forests.

2.4 Materials Physicochemical Characterisation Techniques

Sensor characterisation was performed on all sensing materials before analysis to ensure that the crystallinity of the material remained unaltered after fabrication. Some sensors were also tested after having been exposed to test gases and after being used on and off for 6-12 months. Some of the characterisation techniques, such as Scanning Electron Microscopy (SEM) and Brunauner-Emmet-Teller (BET) were used to get a better understanding of how the test gases might interact with the different surface microstructures of the sensors.

2.4.1 X-Ray Diffraction (XRD)

XRD was carried out on a Bruker D8 discover diffractometer with Cu Kα1/Kα2 radiation (λ = 1.5418 Å) operating at 30 W with a Vantec 500 detector. XRD patterns were collected over the 2θ range 15 - 70°, with a time step of 100 s/step x 3 steps, using a 1 mm collimator. XRD in this instance was performed on the sensor chips before being exposed to test gases.

2.4.2 Scanning Electron Microscopy (SEM)

SEM was carried out on a Phillips XL30 environmental scanning electron microscope. The micrographs were collected at a magnification of ×10,000 but additional micrographs were collected at magnifications of ×20, ×1000, ×3000, ×5000, ×20000, and ×40000. The film thickness of the sensors was assessed with a Hitachi S-3400N microscope operated at 5 kV using a working distance of approximately 16 mm.

2.4.3 Energy Dispersive X-Ray Spectroscopy (EDS)

Energy dispersive X-ray spectroscopy (EDS) was carried out for elemental analysis with an Oxford Instruments INCA energy system in conjunction with a Phillips XL30 environmental scanning electron microscope (SEM).

2.4.4 Raman Spectroscopy

Raman Spectroscopy was executed on a Renishaw inVia microscope using a 514 nm excitation laser. Raman spectroscopy was carried out on the powdered materials and the control sensors prior to and after gas and heat exposure to assess any differences caused in the process of testing. Sensors containing zeolites were tested using a 325 nm excitation laser but fluorescence masked the spectra of the samples. For this reason, this data has not been included in this Thesis.

2.4.5 Brunauner-Emmet-Teller (BET)

BET measurements were used in this study to determine the surface area of the materials using a micromeritics ASAP 2420 analyzer. This information was later related to the gas-sensing results. Degassing was performed at 150 °C for 12 h and the volume of gas adsorbed to the surface of the particles was determined at the boiling point of nitrogen (N_2) i.e. at -196 ˚C.

2.4.6 X-Ray Photoelectron Spectroscopy (XPS)

XPS was conducted on a Thermo Scientific K-alpha spectrometer with monochromated Al-Kα radiation, a dual beam charge compensation system and constant pass energy of 50 eV (spot size 400 µm). Survey scans were collected in the binding energy range 0–1200 eV. High-resolution peaks were used for the principal peaks of Fe (2p), O (1s) and C (1s). Data was calibrated against C1s (285.0 eV). Data was fitted using CASA XPS software.

2.5 Nomenclature of Sensors

Tables 2-4, 2-5 and 2-6 include a compilation of all the sensors that have been fabricated for the purpose of this thesis.

Table 2-4 Fabrication details of the control sensors developed in this study.

Fabrication Method	Sensor Material	Printed Layers	Powder/Vehicle Ratio	Name
Controls	SnO_2	3, 5, 6	1.61	SnO_2 CTL
	Cr_2O_3	3, 5, 7	1.46	Cr_2O_3 CTL
	Fe_2O_3 (BDH)	3, 5, 7	1.38	Fe_2O_3 CTL old
	Fe_2O_3 (Sigma)	5	1.32	Fe_2O_3 CTL new

Table 2-5 Fabrication details of zeolite-overlaid sensors. The powder to vehicle ratio of the control has been included first and then the powder to vehicle ratio of the zeolite.

Fabrication Method	Sensor Materials	Printed Layers	Powder/Vehicle Ratios	Nomenclature
Overlayers	SnO_2 + Na-A	5 + 1	1.6 / 1.1	SnO_2 + 1 L Na-A
	SnO_2 + Na-A	5 + 3	1.6 /1.1	SnO_2 + 3 L Na-A
	SnO_2+ HZSM5	5 + 1	1.6 / 0.9	SnO_2 + 1 L HZSM5
	SnO_2+HZSM5	5 + 3	1.6 / 0.9	SnO_2 + 3 L HZSM5
	SnO_2+ H-Y	5 + 1	1.6 / 0.6	SnO_2 + 1 L HY
	SnO_2+ H-Y	5 + 3	1.6 / 0.6	SnO_2 + 1 L HY
	Cr_2O_3+ H-Y	5 + 3	1.6 / 0.6	Cr_2O_3+ 3 L H-Y
	Fe_2O_3+ H-Y	5 + 3	1.3 / 0.6	Fe_2O_3+ 3L H-Y

Table 2-6 Fabrication details of zeolite admixed sensors developed in this thesis.

Fabrication Method	Sensor Materials	Printed Layers	Powder/Vehicle Ratio	Nomenclature
Admixtures	SnO_2 +10% (wt.) Na-A	5	0.9	SnO_2 + 10% Na-A
	SnO_2 + 30% (wt.) Na-A	5	0.9	SnO_2 + 30% Na-A
	SnO_2 + 10% (wt.) HZSM5	5	1.2	SnO_2 + 10% H-ZSM-5
	SnO_2 + 30% (wt.) HZSM5	5	1.2	SnO_2 + 30% H-ZSM-5
	SnO_2 + 50% (wt.) HZSM5	5	1.2	SnO_2 + 50% H-ZSM-5
	SnO_2 + 10% (wt.) H-Y	5	1.2	SnO_2 + 10% H-Y
	SnO_2 + 30% (wt.) H-Y	5	0.9	SnO_2 + 30% H-Y
	Cr_2O_3 +10% (wt.) H-ZSM-5	5	1.1	Cr_2O_3 + 10% H-ZSM-5
	Cr_2O_3+ 20% (wt.) H-ZSM-5	5	1.4	Cr_2O_3 + 20% H-ZSM-5
	Cr_2O_3 +30% (wt.) H-ZSM-5	5	1.5	Cr_2O_3+30% H-ZSM-5
	Cr_2O_3 +40% (wt.) H-ZSM-5	5	1.4	Cr_2O_3 + 40% H-ZSM-5
	Cr_2O_3 + 10% (wt.) Na-A	5	1.9	Cr_2O_3 +10% Na-A
	Fe_2O + 10% (wt.) H-ZSM-5	5	2.3	Fe_2O_3 + 10% HZSM5
	Fe_2O_3 + 10% (wt.) Na-A	5	2.1	Fe_2O_3 + 10% Na-A

Summary tables of the sensor responses attained towards most test gases have been provided in Tables 8-1 to 8-9 in the Appendix.

Chapter 3 details the results attained upon modification of a control SnO_2 gas sensor with zeolite materials that had different properties, contrasting frameworks and pore size dimensions. The aim of the study was to modify the SnO_2 sensor with agents that could potentially improve the overall performance of the unmodified sensor. The zeolites were chosen strategically, some had bigger pore sizes than others and they were also more or less hydrophobic in nature and are renowned in catalysis for hydrocarbon cracking. Zeolites were incorporated into the sensing system in the form of admixtures and overlayers to get a better idea of how the sensor microstructure and particle morphology influenced sensing performance. The developed sensors were exposed to a range of HC gases that had similar molecular structures and kinetic diameters to assess whether the presence of zeolites better enabled gas discrimination.

3. N-Type Zeolite-Modified MOS Gas Sensors

Chapter 3 details the results obtained when modifying a control thick-film SnO_2 gas sensor with zeolites holding Linde Type A (LTA), Faujasite (FAU) and Mordenite Framework Inverted (MFI) frameworks. Two different approaches were used to integrate them into the gas-sensing interface – zeolite coatings over the metal oxide semiconductor (MOS) and mixtures of the zeolite with the MOS (refer to Fig. 2-4 for a schematic of zeolite-overlaid and admixed sensors).

Preliminary tests were performed with the unmodified SnO_2 sensor to establish the film thickness and the operating temperature that led to optimal sensor performance in the presence of gases of interest. This exercise was later carried out with other base materials, namely Cr_2O_3 (Chapter 4) and Fe_2O_3 (Chapter 5) to evaluate how the film thickness in different systems impacted on the performance of the sensors.

Using the SnO_2 control sensor as a single entity meant that it could not resolve gases that had similar molecular structures or contained the same functional groups. As discussed in section 1.4.4.2 (Chapter 1), the response of a sensor to a gas may be affected by the *diffusion* of the gas through the sensing material, the *rate of the reaction processes* and the *type of reactions or interactions occurring in the sensor*. This chapter evaluates:

- How the introduction of zeolites to the SnO_2 sensing system influenced sensor responses to test gases.

- How the effects of diffusion, sensor response kinetics, and gas/sensor interactions may assist in the selection of a sensing array with high discriminatory power.

3.1 Introduction

SnO_2 is one of the most widely studied and commercialised gas sensor materials. Its first use as a gas sensor was reported by Taguchi in 1962.[97,112] It is an n-type material that has been reported to exhibit great sensitivity to a wide range of reducing and oxidising gases.[3,204,267,283] Different material architectures have recently been explored,[13,258,267] as well as the effects of grain size [16,204] and film thickness on the sensor responses.[7,197] For instance, in thin film SnO_2 sensors, the optimal film thickness is said to lie within 40 – 350 nm and the selection of the optimal thickness is said to be dependent on three factors; the needed rate of response, the nature of the

target gas the sensor is designed to detect and the operating temperature.[7] Furthermore, different studies have investigated the incorporation of metal additives and filtering agents such as zeolites to meliorate the sensing performance of conventional sensors.[14,21,22,30,249,284,285]

Conductivity models have been reported by Barsan et al. [121], where they explain conduction from the point of view of the receptor and transducer functions, described in Chapter 1. Although the general convention states that in order for conduction to occur, the presence of pre-adsorbed oxygen species is a requirement, it has been shown that gases may still be detected in the presence of small concentrations of oxygen (20 ppm) and also in its absence, where the sensing responses of SnO_2 sensors towards H_2, CO and C_3H_8 were found to be more prominent.[286] Hübner et al. [286] concluded that because water was not formed in the absence of atmospheric oxygen, it could be deduced that the sensor signal was not attributable to the reduction of the surface. As such, the change in conductance as a result of the formation of oxygen vacancies was ruled out. Instead, they attributed the change in conductance upon exposure to H_2 to the formation of rooted hydroxyl groups, the appearance of surface donors and their ionisation. This, in turn, led to an increase in the density of electrons and a subsequent decrease of the sensor resistance.[286] Where atmospheric oxygen was present, water was formed as part of reaction processes between the gas an pre-adsorbed oxygen, which led to the observed decrease in sensor conductance.[286]

3.2 Preliminary Tests on the Unmodified SnO_2 Gas Sensor

Sensors were fabricated by printing 3 – 5 layers of SnO_2 on a strip of alumina substrates with pre-printed interdigitated gold electrodes. At this stage, it was of interest to understand whether the fabrication process had an effect on the materials' crystallinity and, also, to assess any potential changes in the surface morphology and microstructure with increasing film thickness. This data was then evaluated to determine if a particular sensor configuration provided optimal gas sensing results. That is, higher response magnitudes to a selected gas (ethanol) over a range of temperatures (300 °C – 450 °C), shorter response and recovery times and higher repeatability between two pulses of the same concentration of the gas. As alluded to in previous Chapters, the sensor response of an n-type material upon exposure to a reducing gas is typically calculated as the ratio of the sensor's resistance in air (R_0) to that in the presence of a gas (R), termed conductive response. Note that in the tests presented in this Chapter, the resistance of SnO_2 was occasionally seen to increase upon exposure to a reducing gas and, in this case, the response was calculated as R/R_0 and termed resistive response.

3.2.1 Effects of Film Thickness on Material Crystallinity, Morphology and Microstructure

The XRD patterns provided in Fig. 3-1 display sharp SnO_2 peaks, which indicate high film crystallinity. Identical XRD data collection positions were sought when analysing both sensors. The XRD pattern of the sensor with three film depositions of SnO_2 displayed 2θ peaks that could be attributed to alumina and a gold in the substrate, which have also been marked in the figure for clarification purposes. This is likely due to the X-ray beam penetrating down to the substrate more readily due to the thinner film. Both sensors displayed comparable peak widths.

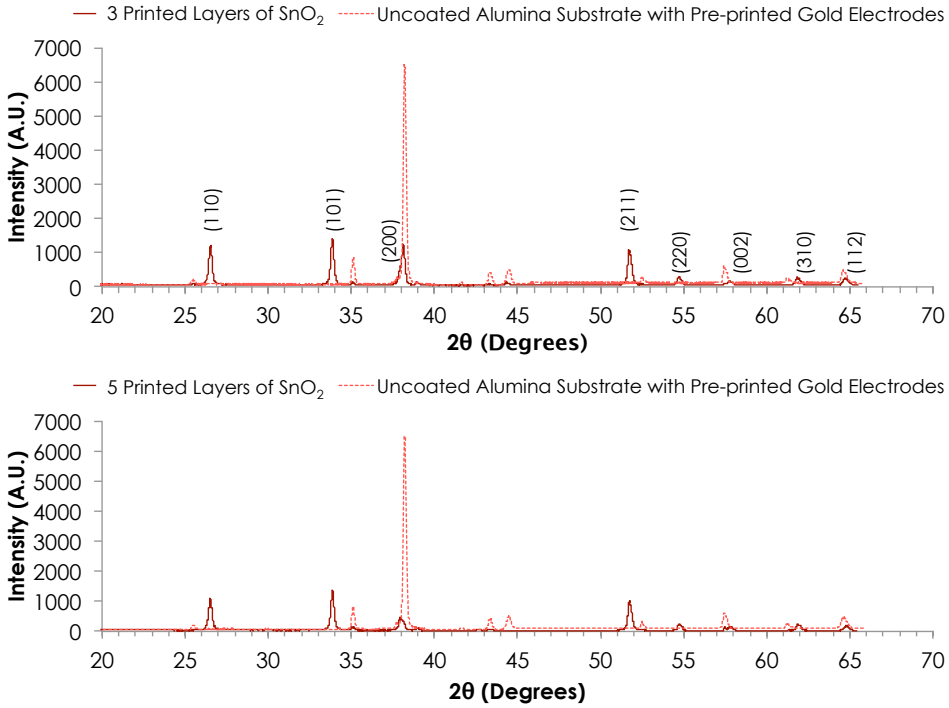

Figure 3-1 XRD patterns of two SnO_2 sensors made with three (top) and five (bottom) film depositions. XRD patterns are in accordance with those provided in the literature and they have been indexed according to the SnO_2 standard provided in JCPDS 041-1445.[287] XRD pattern of an uncoated alumina substrate with gold electrodes also included for reference.

The microstructures of the sensors were investigated with SEM imaging (Fig. 3-2): no major differences were identified in the surface microstructures and particle morphologies of sensors with different film thicknesses, except for moderate flattening of the outermost layer in sensors with five depositions. This could potentially be the result of more intense friction between the squeegee and the material surface during screen-printing.

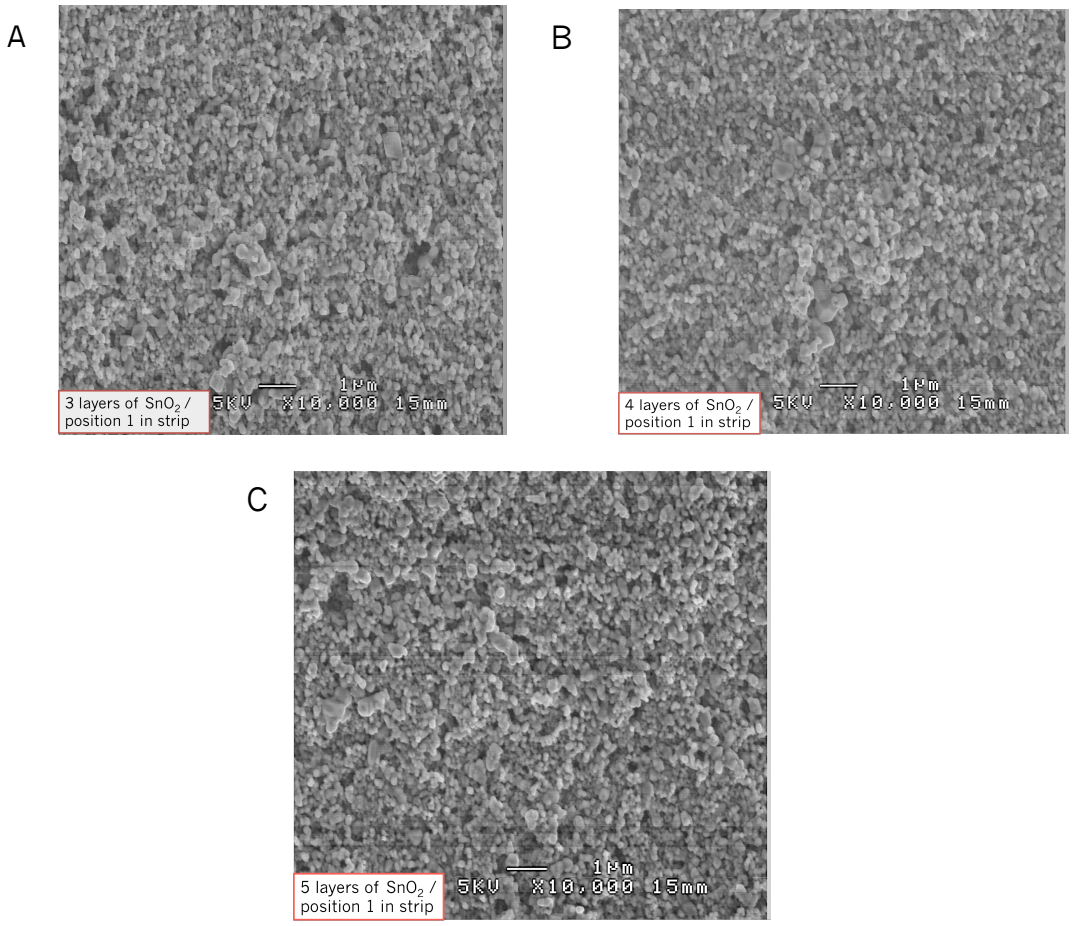

Figure 3-2 SEM micrographs of SnO_2 sensors taken at a magnification of ×10,000. A) Sensor fabricated with three SnO_2 depositions. B) Sensor fabricated with four SnO_2 depositions. C) Sensor fabricated with five SnO_2 depositions. Sensors were taken from position one in the sensor strip.

3.2.2 Effects of Film Thickness on Sensor Responses as a Function of Temperature

It was found that a thicker film resulted in lower sensor responses to ethanol gas (Fig. 3-3). Other studies have also reported this behaviour when exposing thick-film SnO_2 sensors to ethanol.[143,193] However, the effects of film thickness on sensor responses are reported as ambiguous in the literature; a review paper on the effects of film thickness on SnO_2-based sensors details that whilst some groups report an increase in sensor response with film thickness, others report a decrease.[7]

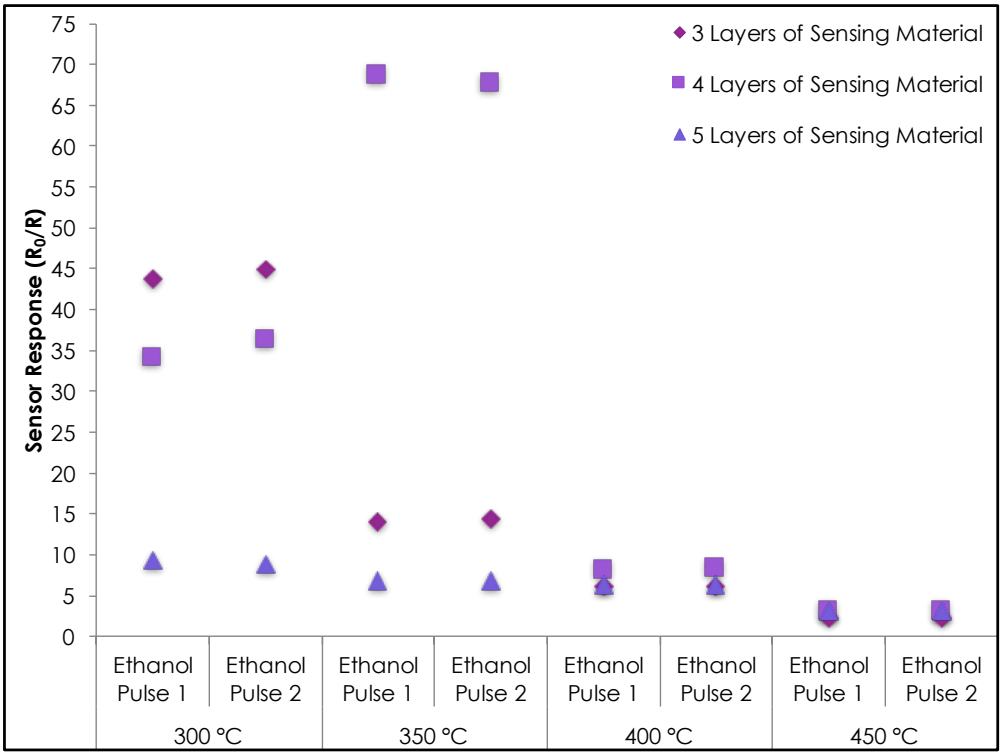

Figure 3-3 SnO_2 sensor responses to 50 ppm ethanol gas. Sensors had different number of screen-printed depositions of SnO_2 and were heated to temperatures ranging from 300 °C to 450 °C.

Angelis et al. [193] reported that the sensitivity of SnO_2 sensors to ethanol decreased as the film thickness increased, whereas the sensitivity towards other gases such as methane remained more or less unaffected by changes in film thickness. This effect was attributed to ethanol's easy oxidation on a very hot sensor surface.[193] Conversely, more stable gases such as methane are only oxidised due to the interaction with SnO_2 and a catalyst. Thus, while oxidation of gases such as methane involves the whole depth of the film, only the outer layer is involved in the oxidation of ethanol and, as such, thicker films have less of an effect on sensitivity to ethanol.[193]

It is well known that the response of an n-type MOS sensor to a reducing gas depends on the operating temperature and it results in a bell-shaped 'response vs. temperature' curve. The bell-shaped correlation can be deduced by looking at the graph in Fig. 3-3. Had the gas-sensing rig permitted the investigation of lower temperatures such as 150 °C it is thought that the complete bell-shaped curve would have been attained. As described by Yamazoe et al. [81] in Chapter 1 of 'Semiconductor Gas Sensors', sensor response and recovery rates are faster with increasing temperature and the sensor response will typically provide contrasting response types upon exposure to reducing and oxidising gases i.e. conductive and resistive responses, respectively.

It is acknowledged here that the response maximum will be influenced by factors such as the type of semiconductor material (n-type or p-type), the sensing material itself and its microstructural characteristics, the film thickness, operating temperature and the test gas. However, it has been established that the bell-shaped curve occurs because the rate constant of the surface reaction between a gas and oxygen species, κ_R, increases exponentially as the temperature increases, whereas the Knudsen diffusion coefficient of the gas, (D_K), increases in a sub-linear fashion with temperature increments.[81] At lower temperatures, the rates of reaction are slower, such that $\kappa_R < D_K$. It follows that the poorer sensor responses observed at lower temperatures are the result of the gas not being able to react with the chemisorbed oxygen at a fast-enough rate to produce a sizeable response to a gas. At higher temperatures, however, the sensor responses will be attenuated due to faster reaction kinetics, which affect gas diffusion by shortening the penetration depth of the gas into the sensing layer.[81] Nevertheless, it is also possible that the lower concentration of oxygen species populating the sensor surface at higher operating temperatures causes a diminution in sensor responses due to less oxygen being available to interact with the gas.[81]

The temperature at which the response maximum to ethanol gas was obtained appeared to be influenced by film thickness. That is, the sensor made with four SnO_2 depositions expressed behaviour that differed from the other two sensors; it was most responsive towards ethanol at 350 °C – rather than 300 °C – and showed excellent responsiveness (R_0/R = ~70). Be that as it may, it is the sensor that struggled most to return back to baseline following gas exposure (see section 3.2.3 below). Furthermore, it was anticipated that zeolite incorporation could later add to this retardation effect, at least when incorporated as overlayers.[24] Therefore, this sensor was not regarded as a good candidate for future tests.

Other studies reported that with thin-film SnO_2 sensors, the maximum response shifted to lower operating temperatures as the thickness of the film was incremented.[7] This was not found here as both sensors with three and five film depositions provided enhanced sensor responses at 300 °C. The increase in response magnitude seen in the 5-layered sensor as the operating temperature was lowered was moderate in relation to the other two sensors. It was expected, however, that zeolite incorporation would serve to significantly enhance the response magnitudes towards gases of interest.

As far as repeatability is concerned, the responses of the 5-layered sensor differed by <1% in the temperature range of 350 – 450 °C. At 300 °C all sensors showed a

moderate increase in variability between sensor responses (within ~6% for the 4- and 5-layered sensors and <3% for the 3-layered sensor).

3.2.3 Effects of Film Thickness on the Kinetics of Sensor Response

The response and recovery times became significantly slower in all sensors as the temperature was lowered. For instance, at 300 °C, τ_{90} in the 3-layered and 4-layered sensors was ~ 3 and 5 minutes, respectively.

The 3-layered sensor took ~11 minutes to return to baseline once the gas was switched off and the 4-layered sensor failed to recover. The 5-layered sensor, however, responded in ~2 minutes and recovered in <7 minutes, which was more promising.

It is acknowledged that these results were in no way ideal and, although the 5-layered sensor exhibited longer τ_{90} and τ_{10} than the 3-layered one at 400 °C and 450 °C due to its thickness, it was hoped that the incorporation of catalytic agents would improve these effects considerably. Furthermore, the 5-layered sensor consistently achieved steady state at all the temperatures tested (see Fig. 3-4 below).

Table 3-1 Response and recovery times of SnO_2 sensors towards ethanol gas with three, four and five film depositions investigated at temperatures ranging between 300 – 450 °C. τ_{90} refers to the sensor response time (sec) and τ_{10} to the sensor recovery time (sec).

Temperature	τ_{90}/ τ_{10}	Response & Recovery Times (sec)		
		3 SnO_2 Film Depositions	4 SnO_2 Film Depositions	5 SnO_2 Film Depositions
450 °C	τ_{90}	2	19	14
	τ_{10}	6	73	51
400 °C	τ_{90}	4	68	66
	τ_{10}	22	92	200
350 °C	τ_{90}	71	341	49
	τ_{10}	73	737	182
300 °C	τ_{90}	200	324	147
	τ_{10}	661	1198	392

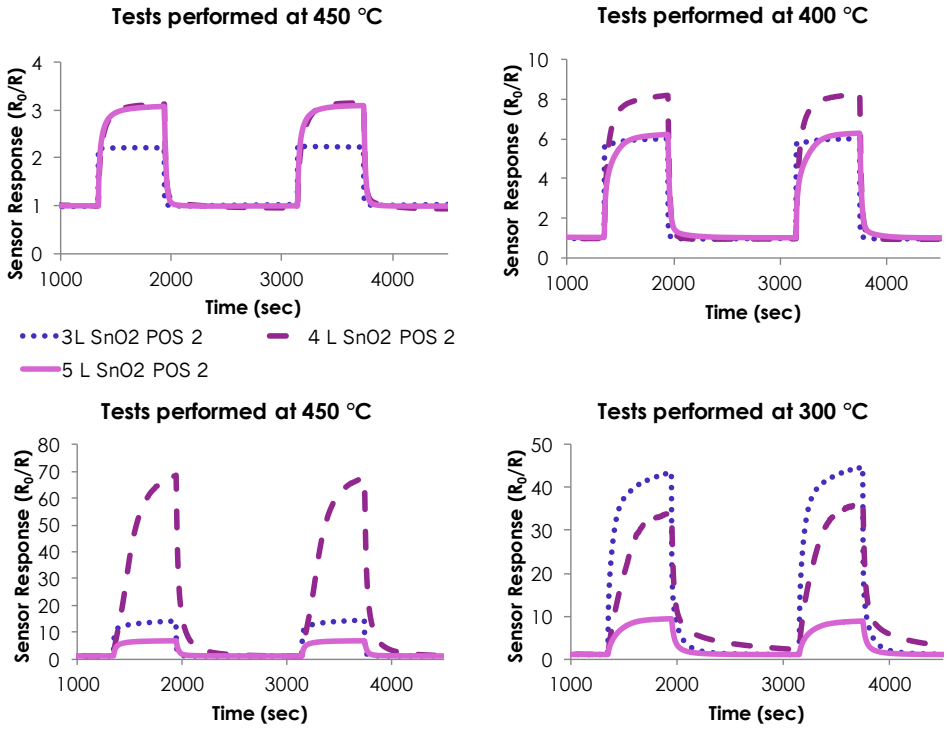

Figure 3-4 SnO_2 Sensor responses to 50 ppm ethanol gas at different temperatures (300 - 450 °C). 3L, 4L and 5L refer to the number of SnO_2 layers printed on the substrate.

Other papers, for instance, report shorter sensor response and recovery times of conventional SnO_2 sensors upon exposure to 50 ppm ethanol at 300 °C and for a film thickness of 20 µm (τ_{90} = 33.6 seconds and τ_{10} = 85.2 seconds).[30]

3.2.4 Selection of a Specific Position on the Sensor Strip for Testing

As described in Chapter 2, the process of screen-printing resulted in 13 sensors coated with the material of interest. Position 1 was assigned to the sensor covered firstly with the metal oxide paste during the course of a print and position 13 was that which was lastly covered by it (refer to Fig. 2-3). A selection of four sensors (positions 2 – 5 in the strip) was chosen to evaluate variability across the strip when exposed to 50 ppm of ethanol gas.

Firstly, SEM images were taken to understand whether the surface microstructure was different among sensors after fabrication. No major differences could be observed across the sensor batch. Nevertheless, it must be noted that the way in which the material paste spread across the gold electrodes looked different across the strip. This could be appreciated in the images taken at a magnification of x20, which have been included as an inset in Fig. 3-5 below.

Ideally, all sensors taken from the strip should provide similar results when exposed to a gas. However, as can be seen in Fig. 3-6 below this was not the case here. At 300 °C, the variability among sensor responses was significant, with Relative Standard Deviation (RSD) ~61%. At higher temperatures (400 °C and 450 °C) the variability in sensor responses across the strip was minimised with $RSD_{400°C}$ = 13% and $RSD_{450°C}$ = 26%. This could be attributed to different coverage of the electrodes with the paste across the strip, potentially due to wear and tear of the screen-printing mesh and the squeegee. The variability in sensor responses across a strip of sensors and that associated with screen-printing methods has been reported by other researchers.[29,59] Another explanation could be that the materials sintered differently according to their location in the furnace, leading to slight microstructural differences that affected the gas-sensing results.

The results found here were later used as guidance when fabricating other sensors. The sensor containing five film depositions of SnO_2 was selected as the control due to the relevant and suitable features it presented i.e. faster response and recovery times at lower operating temperatures in relation to the other fabricated sensors and repeatable responses following two pulses of the same concentration of a gas were obtained. Note that in order to minimise any potential variability across batches, the same position in the sensor strip was always selected for testing.

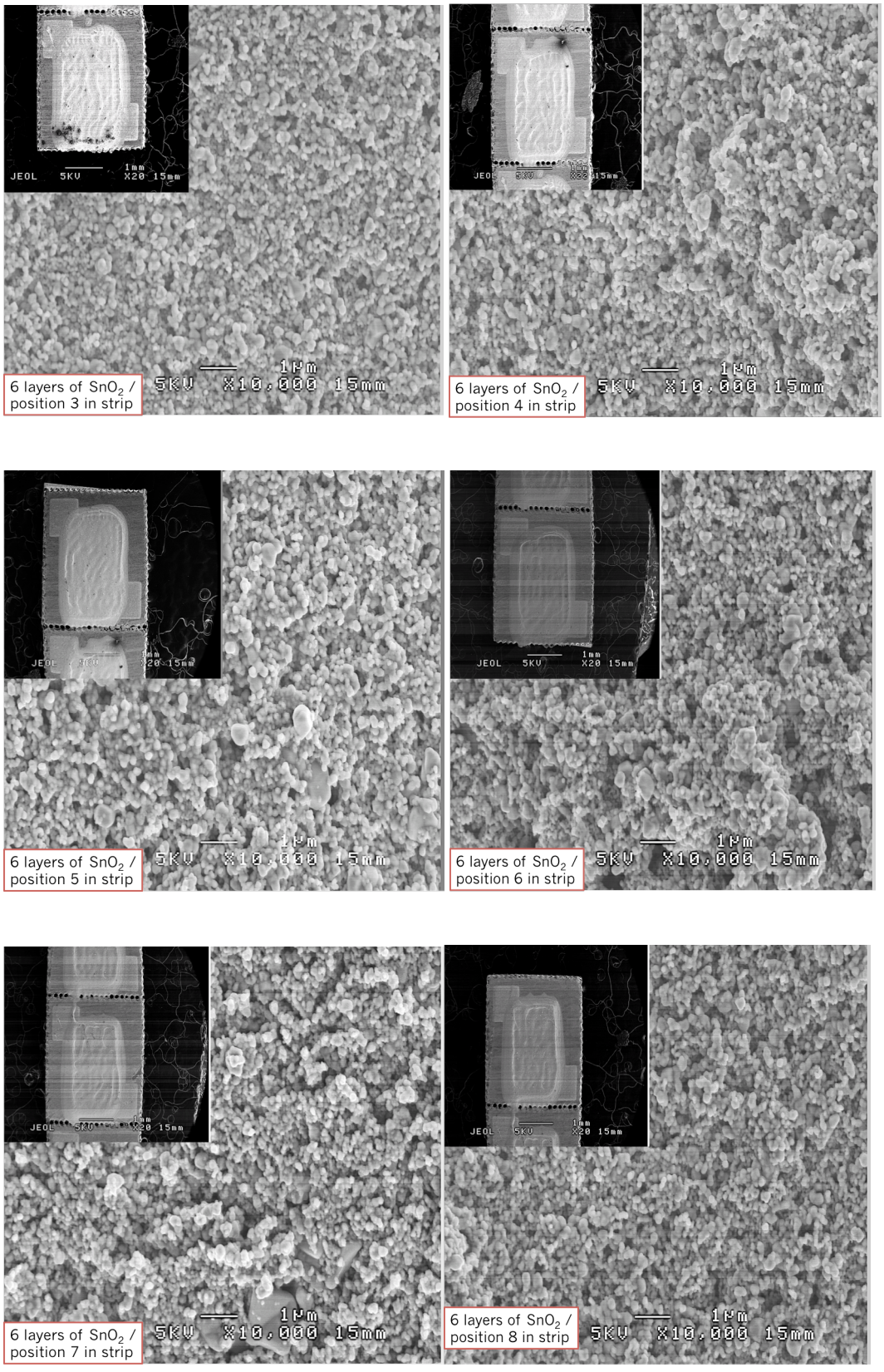

Figure 3-5 SEM images of SnO_2 sensors from positions 3-8 in a strip at magnifications of x20 and x10,000. The inset image corresponds to magnifications of x20 and the larger images correspond to magnifications of x10,000.

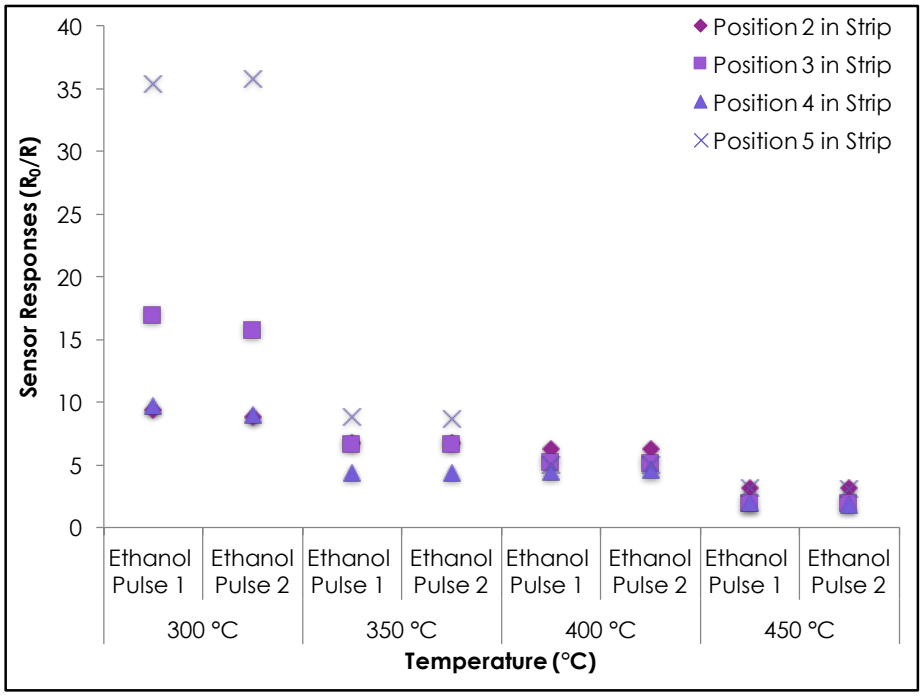

Figure 3-6 Sensor responses towards 50 ppm ethanol according to their relative position in the sensor strip used in the process of screen-printing. Position 2 corresponded to the sensor firstly covered with the material paste and position 5 corresponded to the one that was lastly covered with the material during the course of a print. Sensor in position 1 was excluded from testing due to poor coverage of the substrate with the material.

3.3 Exposure of the Control SnO_2 Material to Test Gases

The following sections describe the results attained after exposing a control SnO_2 sensor to a range of reducing gases at different operating temperatures. It was of interest to assess whether the sensor was able to provide different response magnitudes and patterns to a range of gases.

3.3.1 Test Details and Range of Gases Tested

Test gases were introduced into a stream of dry baseline air (R_0) in five 10-minute pulses. The source cylinder concentration was diluted in a stream of air to investigate a range of concentrations as follows: 5%, 10%, 25%, 50%, 80% and 100% of the original cylinder concentration, which has been specified in brackets below. This allowed the sensor resistance in the presence of a test gas to be determined. Gases were obtained from and certified by BOC gases: isopropyl alcohol (500 ppm), ethanol (100 ppm), acetone (10 ppm), toluene (50 ppm), ethane (100 ppm), propane (100 ppm), butane (100 ppm), and carbon monoxide (1000 ppm).

Trace gas concentrations were evaluated to get a better idea of the suitability of the sensors for practical applications. These often require gas/vapour detection and discrimination at ppm or sub-ppm levels, such as in the case of detecting hazardous gases, pollutants and Volatile Organic Compound (VOC) for air-quality and environmental monitoring.[39,288] Further, the detection of trace gas concentrations is also required in safety alarms, for security purposes and for medical diagnostics.[28,46]

The detection temperature and the supplied gas concentrations were progressively modified to establish the temperature at which the sensor responses to test gases were optimal. It was also noteworthy to understand whether the sensors responded linearly to increased concentrations of a gas, whilst providing repeatable and stable results over time. Tests were also performed in humid conditions. An additional test was performed by mixing ethane with humid air at 10% and 25% relative humidity (RH) to better explore the selective potential of the sensors. Gas-sensing tests were performed at temperatures that ranged between 250 °C and 500 °C. Most tests were repeated three times. When possible, tests were also repeated at a later date to ensure sensor stability. Because sensors were utilised on and off for a period of ~4 – 5 months, it was important to ensure that, over time, the sensing results were consistent with previous data.

3.3.2 Concentration and Temperature Effects Seen in the Control SnO_2 Sensor

The control SnO_2 sensor was initially exposed to six different concentrations of ethanol gas (5 – 100 ppm) and was heated to temperatures in the range of 250 °C to 500 °C (Fig. 3-7). The sensor behaved as expected, increasing in conductivity with exposure to ethanol gas. Raising the concentration of ethanol resulted in an increase in sensor response. The sensor's optimal temperature upon exposure to 100 ppm of ethanol at 300 °C was R_0/R ~12 (SD ± 0.4).

It was noticed that when performing repeat tests, the sensor responses varied more markedly at lower operating temperatures and when the gas concentration exceeded 50 ppm. For instance, at 250 °C and upon exposure to 100 ppm ethanol, R_0/R was ~10 (SD ± 1.6), providing a 15% difference in sensor responses from three repeats. This is not uncommon; sensor response variability has long been reported in SnO_2 sensors.[59,67,129,289]

The control SnO_2 sensor was then supplied with IPA gas concentrations in the range of 25 – 125 ppm and at temperatures between 300 °C – 450 °C. Once again, the variability among repeat tests upon exposure to 100 ppm IPA was more prominent at 300 °C e.g. R_0/R = 12.3 (SD ± 1.0), when compared to higher temperatures such as 450 °C, where R_0/R = 5.3 (SD ± 0.1)

The unmodified SnO_2 sensor was unable to differentiate between ethanol and IPA gases across the range of temperatures investigated. Given the higher error margins seen at lower operating temperatures, forthcoming tests were performed at 350 °C, 400 °C and 450 °C. In general, at 450 °C, τ_{90} and τ_{10} were faster and, at this temperature, the sensor often reached steady state more quickly.

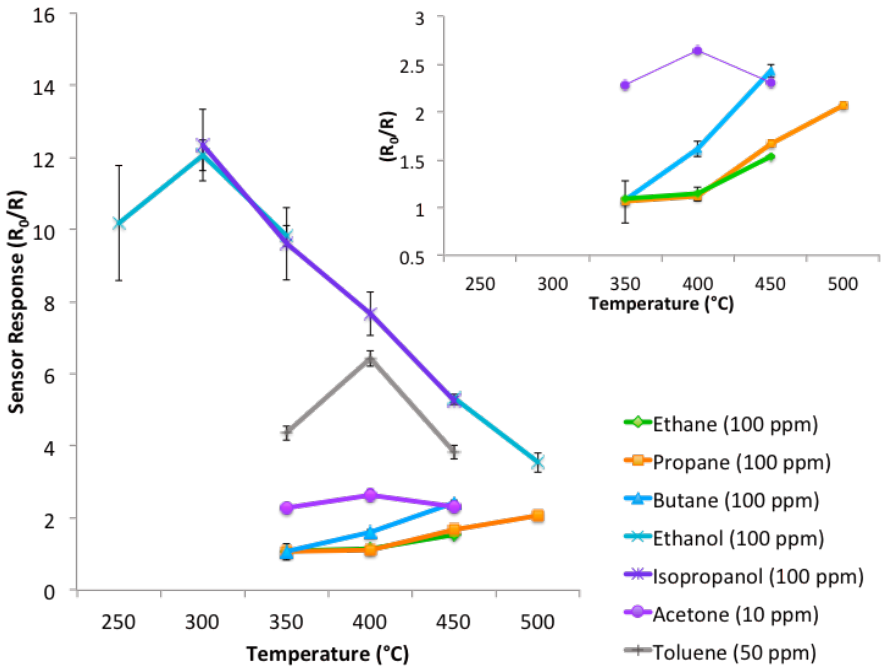

Figure 3-7 SnO_2 sensor exposure to 100 ppm ethane, propane, butane, ethanol and isopropanol, 10 ppm acetone and 50 ppm toluene gases at temperatures ranging between 250 °C and 500 °C. Error bars correspond to the Standard Deviation (SD) from three repeat tests. The inset on the right hand side corner corresponds to facilitate the visualisation of sensor responses towards acetone, butane, ethane and propane gases.

The control sensor failed to distinguish between acetone (10 ppm) and butane (100 ppm) gases at 450 °C and also between ethane and propane across the range of temperatures investigated. Exposure to ethane, propane and butane led to a moderate increase in sensor response when incrementing the gas concentrations and the operating temperature (Fig. 3-7).

3.4 Zeolite Modification of the Control SnO_2 Material

The SnO_2 sensor was modified by admixture and overlayer using zeolites H-ZSM-5, H-Y and Na-A. Table 3-2 below provides summarised details of the zeolite-modified sensors fabricated for the purposes of this chapter.

Zeolite overlayers were prepared as explained in Chapter 2 (refer to Fig. 2-4). The effect of increasing the number of zeolite layers was evaluated by screen-printing either one or three additional film depositions on top of the SnO_2 material.

Zeolite admixtures were prepared as described in Chapter 2 (Fig. 2-4). The SnO_2 powder was mixed with 10% (wt.) or 30% (wt.) of zeolites H-ZSM-5, H-Y and Na-A and with an organic vehicle to create the screen-printing paste.

Table 3-2 Fabrication details of zeolite-modified sensors with corresponding sensor nomenclature. Under 'Zeolite Type' the zeolite used has been specified, followed by the zeolite framework in brackets. *CTL refers to control sensor.

	Modification Agent	Admixtures		Overlayers	
Control Sensor	Zeolite Name & Framework	Admixture Sensor Names	Zeolite percentage weight (%)	Overlayer Sensor Names	Zeolite Coatings
SnO_2 (CTL)*	H-ZSM-5 (MFI)	SnO_2 + 10% (wt.) H-ZSM-5	10	SnO_2 + 1 L H-ZSM-5	1
		SnO_2 + 30% (wt.) H-ZSM-5	30	SnO_2 + 3L H-ZSM-5	3
	Na-A (LTA)	SnO_2 + 10% (wt.) Na-A	10	SnO_2 + 1 L Na-A	1
		SnO_2 + 30% (wt.) Na-A	30	SnO_2 + 3 L Na-A	3
	H-Y (FAU)	SnO_2 + 10% (wt.) H-Y	10	SnO_2 + 1 L H-Y	1
		SnO_2 + 30% H-Y	30	SnO_2 + 3 L H-Y	3

3.4.1 Physicochemical Characterisation of Zeolite-modified SnO_2 Sensors

SnO_2 powders were mixed with an organic vehicle, to form a paste suitable for screen-printing onto 3 mm × 3 mm alumina substrates. Pastes were fired in a furnace at 600 °C for an hour to sinter the material and to evaporate the organic vehicle. Physicochemical characterisation of the sensor materials revealed that their crystalline structure was unaffected by the fabrication procedure.

3.4.1.1 X-Ray Diffraction (XRD)

The crystalline structure of the sensing materials remained unaffected following heat treatment, which was used during sensor fabrication. The XRD pattern of

SnO_2 was identified in all the zeolite-modified sensors, regardless of the fabrication method (Fig. 3-8). SnO_2 was tetragonal in structure with characteristic 2θ peaks at 26.5 (110), 33.8 (101), 38.1 (200), 38.9 (111), 51.7 (211), 54.7 (220), 57.7 (002) and 61.8 (310). As expected, the peaks corresponding to the zeolite-overlaid sensors were more intense than those of the admixed sensors.

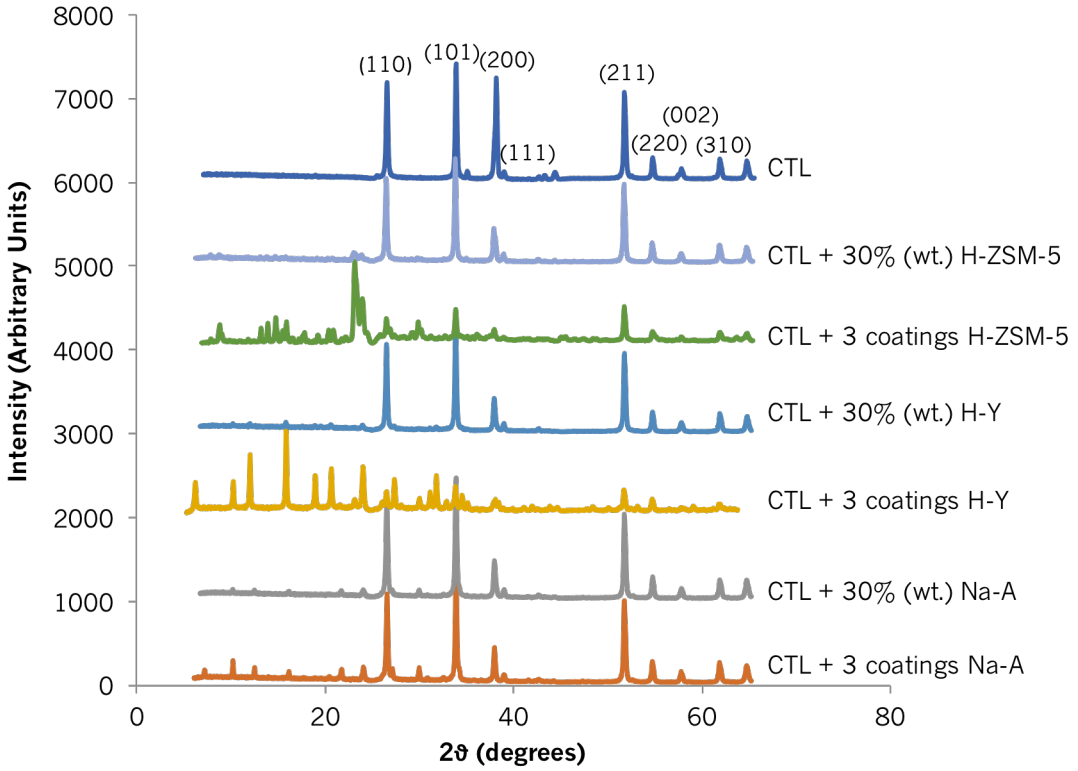

Figure 3-8 XRD patterns of a control SnO_2 sensor and of SnO_2 admixed and overlaid and with zeolites H-ZSM-5, H-Y and Na-A. SnO_2 has been indexed in accordance with literature references.[287] The indexed peaks correspond only to the control material. The XRD patterns of H-ZSM-5,[234] H-Y,[290] and Na-A [291] were also in accordance with the literature. CTL refers to control sensor.

3.4.1.2 Scanning Electron Microscopy (SEM)

The SnO_2 particles were round in shape and interconnected (Fig. 3-9). Lower magnifications of the control sensor's microstructure revealed a pattern on the surface of the sensing material left during the screen-printing process (not shown). The surface was modestly uniform and clear voids and ridges could be identified throughout. The particles were ~100 – 200 nm in size.

Zeolite-overlaid sensors: The presence of SnO_2 could not be visually appreciated in the zeolite-overlaid sensors. The particles of sensors overlaid with zeolite H-Y showed sharp edges and appeared to be ~500 nm in size (Fig. 3-9). The surface

microstructure of this material was porous and it had visible voids. The surface of the sensor containing three layers of zeolite H-Y was somewhat different to that containing one layer; the particle shapes were less well defined and appeared flatter. It is thought that this could be the result of pressure inflicted by the screen-printing mesh and squeegee as more layers were deposited onto the sensor chips. The H-Y zeolite coatings were mechanically unstable and would easily detach from the chip when handled. This could be due to poor adherence of the material to the substrate during the sintering process. The sensors containing zeolite Na-A coatings had cubic-shaped particles with round edges, which differed in size. Although most particles displayed an average size of ~2 µm, some of them were as small as ~400 nm. The sensors overlaid with zeolite H-ZSM-5 presented a wide size distribution, with particles that were somewhat oval in shape with smooth edges. As observed with other sensors, there were clear cavities in the structure, which is promising for gas access during testing.

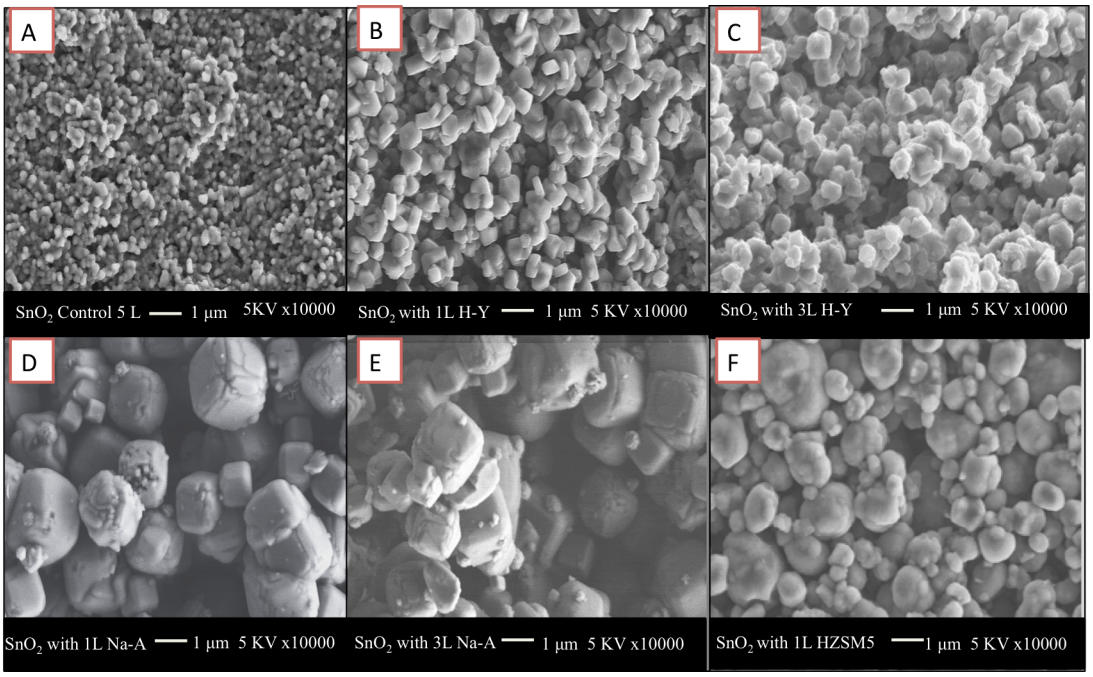

Figure 3-9 SEM micrographs of SnO_2 sensors overlaid with zeolites. A) SnO_2 control sensor. B) SnO_2 sensor with 1 layer of zeolite H-Y. C) SnO_2 sensor with 3 layers of zeolite H-Y. D) SnO_2 sensor with 1 layer of zeolite Na-A. E) SnO_2 sensor with 3 layers of zeolite Na-A. F) SnO_2 sensor with 1 layer of zeolite H-ZSM-5. Images taken at a magnification of ×10,000.

Zeolite-Admixed Sensors: The SnO_2 material could be visually identified in all the zeolite-admixed sensors (refer to Fig. 3-9A and Fig. 3-10). The increase in zeolite loading could also be appreciated in the SEM images. The sensors modified by zeolite admixture exhibited a microstructural appearance resembling, mostly, that of SnO_2.

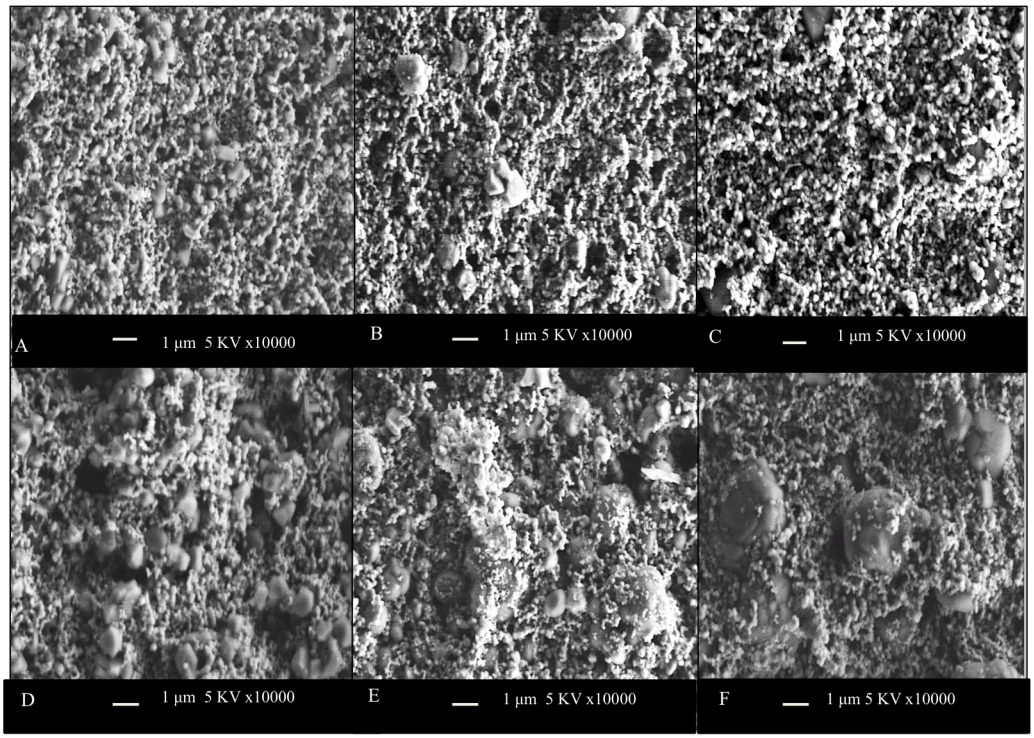

Figure 3-10 SEM images of SnO_2 sensors admixed with zeolites. (A) SnO_2 with 10% (wt.) H-Y. (B) SnO_2 with 10% (wt.) H-ZSM-5. (C) SnO_2 with 10% (wt.) Na-A. (D) SnO_2 with 30% (wt.) H-Y. (E) SnO_2 with 30% (wt.) H-ZSM-5. (F) SnO_2 with 30% (wt.) Na-A. Images taken at a magnification of ×10,000.

The film thickness of SnO_2 was ~130 µm and that of the layer of zeolite H-ZSM-5 corresponded to ~26 µm (Fig. 3-11). This was only used for guidance.

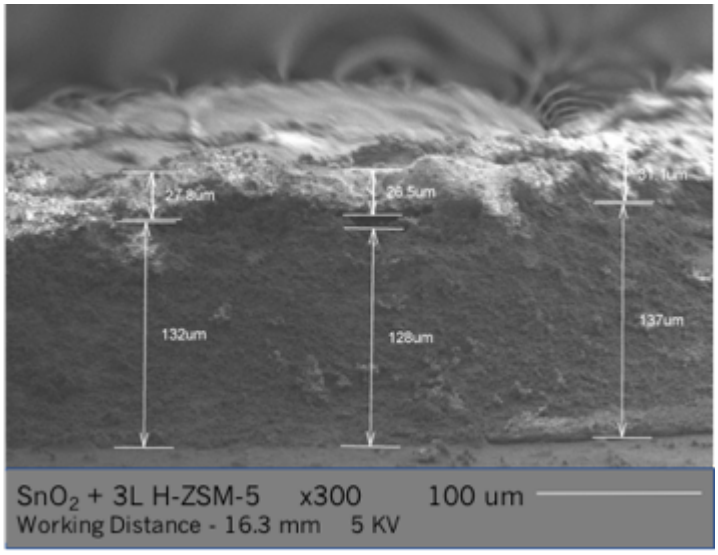

Figure 3-11 Cross-sectional SEM image of a SnO_2 sensor coated with three depositions of zeolite H-ZSM-5. The image shows the five SnO_2 film depositions (~130 µm) and the three zeolite coatings on top (~28 µm). Image taken on a Hitachi S-3400N microscope operated at 5 kV using a working distance of 16.3 mm.

Raman spectroscopy was performed on the control SnO_2 powder and on the material printed on the chip after gas exposure to ensure the material remained intact after fabrication and analysis. Results are presented in Fig. 3-12 below.

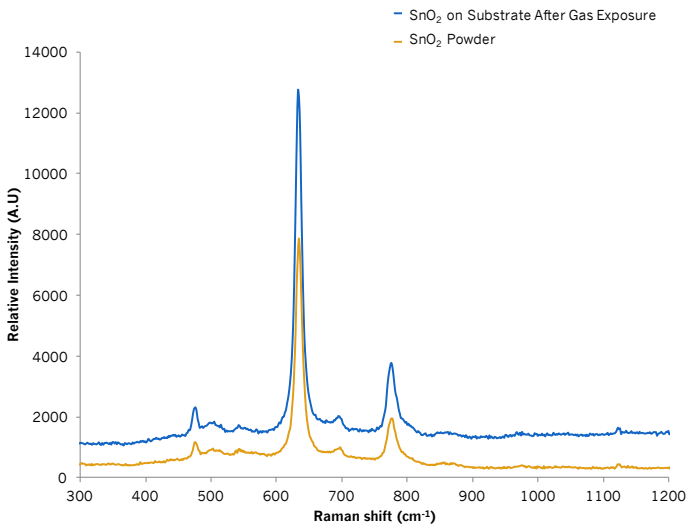

Figure 3-12 Raman spectra of SnO_2 powder and SnO_2 on a chip after it had been exposed to gases of interest for several months.

3.5 Parameters Affecting the Sensing Performance of Zeolite-Modified SnO_2 Gas Sensors

3.5.1 Temperature Effects

The optimal temperature of the zeolite-modified sensors did not always match the optimal temperature of the control SnO_2 sensor (Fig. 3-7, Fig. 3-13, Fig. 3-14, Fig. 3-15). Changing the number of zeolite coatings provided different sensor responses to test gases. However, the temperature at which the maximum response values were attained was generally maintained for each zeolite group, irrespective of the zeolite film thickness. This was not the case for the zeolite-admixed sensors. Typically, the zeolite loading (wt.) present in the sensing systems was seen to directly affect the optimal operating temperature of the sensors (Fig 3-13 to 3-15). This behaviour has also been observed in other studies based on zeolite-admixed n-type and p-type MOS.[27,28] It therefore follows that the way in which a sensing material is combined with zeolites may result in contrasting effects on sensor responsiveness and selectivity to gases as a function of temperature e.g. sensor 'SnO_2 + 1 Layer Na-A' provided different responses to IPA and ethanol gases only at 300 °C, whereas that mixed with 10% (wt.) Na-A provided significantly different responses to the gases across most of the temperatures investigated.

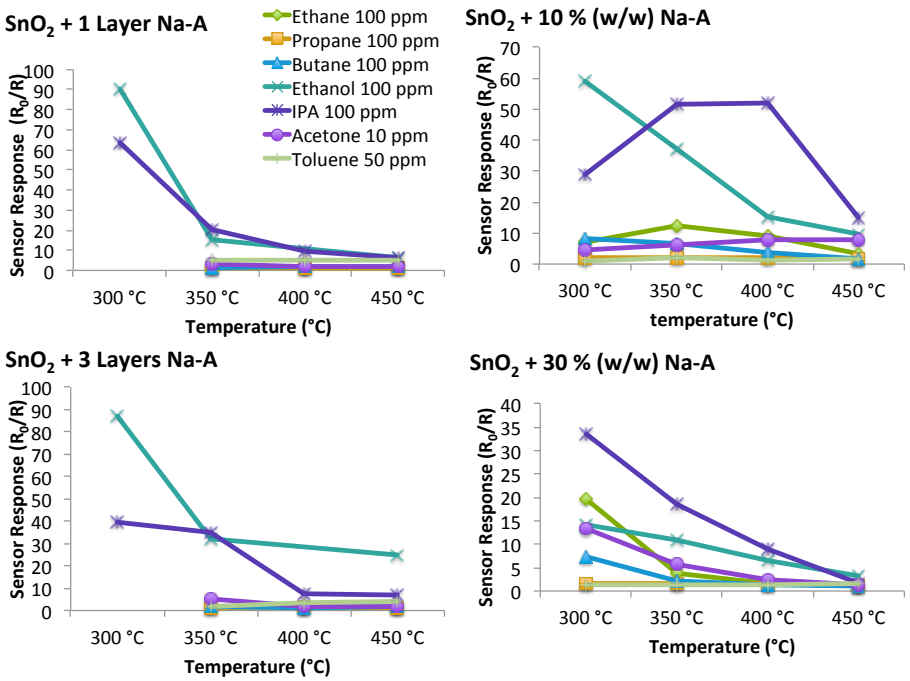

Figure 3-13 Sensor responses of SnO_2 sensor modified by admixture and overlayer of zeolite Na-A to a range of gases as a function of temperature. This figure illustrates how the inclusion of zeolite into the sensing system affected sensor behaviour as the temperature was progressively lowered.

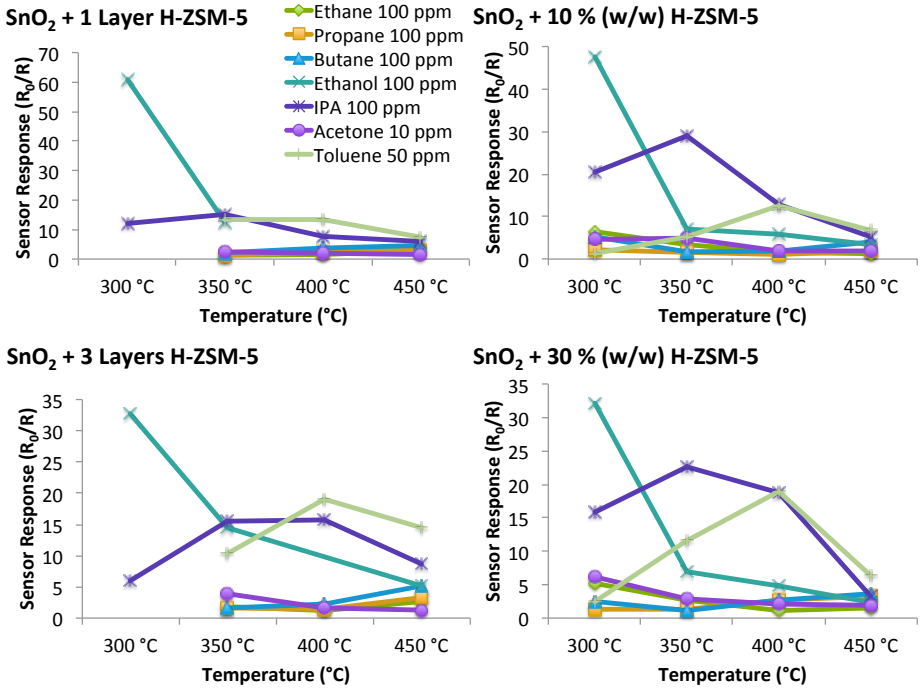

Figure 3-14 Sensor responses of SnO_2 sensor modified by admixture and overlayer of zeolite H-ZSM-5 to a range of gases as a function of temperature. This figure illustrates how the inclusion of zeolite into the sensing system affected sensor behaviour as the temperature was progressively lowered.

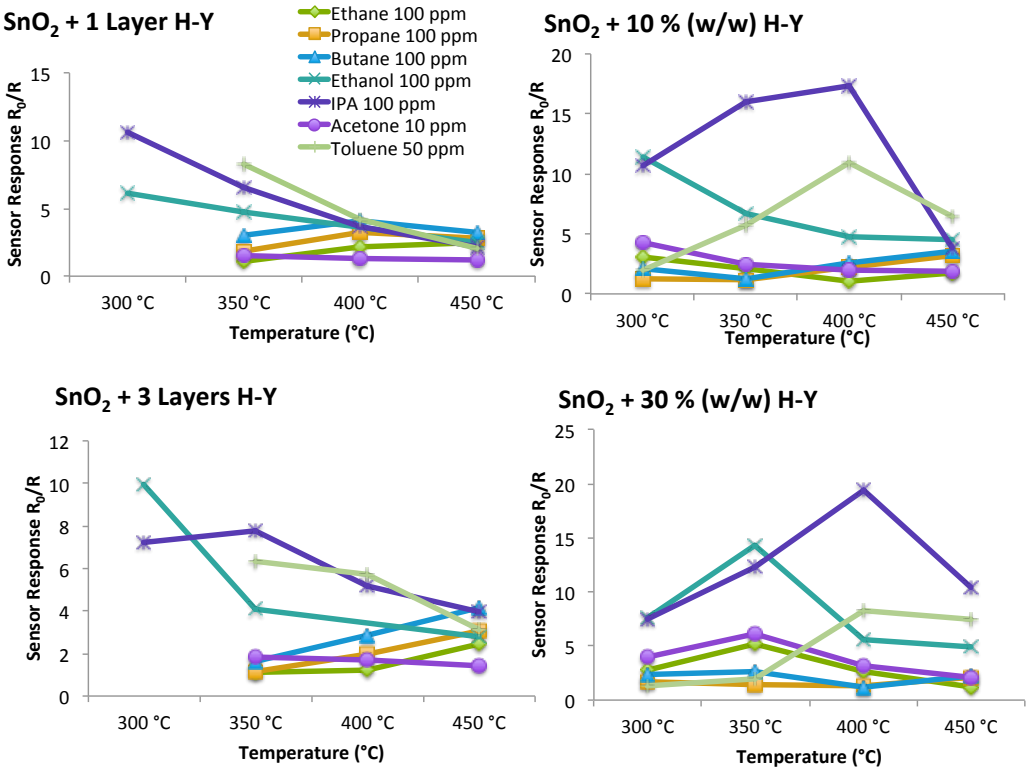

Figure 3-15 Sensor responses of SnO_2 modified by zeolite admixture and overlayer of H-Y to a range of gases as a function of temperature. This figure illustrates how the inclusion of zeolite into the sensing system affected sensor behaviour as the temperature was progressively lowered.

To be more specific, the control SnO_2 sensor (Fig. 3-7) could not discern between 100 ppm IPA and ethanol gases whereas some zeolite modified sensors could (Figs. 3-12 through to 3-15). When incorporating one layer of zeolite Na-A, the sensor could discriminate among gases at 300 °C and 350 °C. When three layers of zeolite Na-A were incorporated, the sensors were able to discriminate between IPA and ethanol at every temperature except 350 °C. With zeolite Na-A incorporation as an admixture, a loading of 10% (wt.) Na-A provided different responses to IPA and ethanol at every temperature and with a loading of 30% (wt.) Na-A the sensor discriminated between both gases at every temperature except 450 °C.

In regards to sensor exposure to 50 ppm toluene gas, the SnO_2 sensor modified by overlayers and admixtures of zeolite Na-A provided lower sensor responses in relation to the control sensor. Having more zeolite Na-A layers led to lower sensor responses at all temperatures with exposure to the gas.

With exposure to 10 ppm acetone gas, the control sensor provided relatively low sensor responses at the temperatures tested i.e. $R_0/R \sim 2.5$. The gas was safely discerned from others at 350 °C and 400 °C but not at 450 °C, where it was confounded with butane

gas. When incorporating zeolite Na-A, the sensor response was improved over that of the control with three depositions of the zeolite, especially at 350 ˚C. It also improved considerably (by a factor of 3) when incorporating 10% (wt.) of zeolite Na-A at 400 ˚C. With incorporation of 30% (wt.) Na-A and at 300 ˚C the sensor response towards 10 ppm acetone improved by a factor of ~6 over the control SnO_2 sensor.

The control SnO_2 sensor was unable to discriminate between ethane and propane gases across the range of temperatures tested. Incorporation of Na-A as an admixture provided discrimination with 10% (wt.) Na-A at temperatures in the range of 300 ˚C to 400 ˚C. When the sensor contained 30% (wt.) Na-A, discrimination between propane and ethane was attained at 300 ˚C and 350 ˚C. Further, the control sensor could not differentiate between butane and propane gases at 350 ˚C and between butane and acetone gases at 450 ˚C. This issue was resolved by testing at 300 ˚C, when zeolite Na-A was incorporated as an admixture e.g. 10% (wt.) Na-A, the sensor was able to discern between propane and butane at 300 ˚C and 350 ˚C and between acetone and butane at 450 ˚C. The sensor containing a zeolite loading of 30% (wt.) Na-A was able to discern between butane, propane and acetone gases at 300 ˚C.

Incorporation of zeolite H-ZSM-5 provided discrimination between ethanol and IPA gases at 300 ˚C both when incorporated as an admixture and when incorporated as an overlayer, which was not seen with the control SnO_2 sensor. This discrimination between ethanol and IPA gases was also possible when the sensor was modified by three layers of zeolite H-ZSM-5 at 400 ˚C and 450 ˚C.

The control sensor was able to provide different response magnitudes towards toluene gas, in relation to other gases. However, when zeolite H-ZSM-5 was incorporated as an overlayer, discrimination was attained with three layers of the zeolite at all temperatures and with 30% (wt.) H-ZSM-5 at 350 ˚C and 450 ˚C. At other operating temperatures the responses of the sensors were similar to the responses attained towards other gases.

The similarity in response magnitudes attained with exposure to acetone and butane gases at 450 ˚C with the control sensor, was overcome with the incorporation of zeolite H-ZSM-5 both as an admixture and as an overlayer (better observed in Figs. 3-18 and 3-19). The lack of discrimination between ethane and propane gases seen with the control sensor, was also overcome when incorporating zeolite H-ZSM-5 as an admixture at 300 ˚C.

Incorporation of three zeolite H-Y film depositions resulted in discrimination between ethanol and IPA gases at all the temperatures tested, which was unattained with the control sensor. When one deposition of zeolite H-Y was used, the sensor was able to discriminate between ethanol and IPA at 300 ˚C and 350 ˚C. When 10% (wt.) H-Y was incorporated to the sensor as an admixture, it could discern between both gases at 350 ˚C and 400 ˚C. When 30% (wt.) was employed, discrimination was possible in the temperature range of 350 – 450 ˚C.

Toluene could be safely discerned from other gases with the control sensor at all temperatures. With zeolite H-Y overlayers, it could be distinguished from other gases at 350 ˚C. This was also true when the sensor contained three depositions of zeolite H-Y at 400 ˚C. With the sensor containing 10% (wt.) H-Y and at temperatures ranging between 350 ˚C and 450 ˚C, notably different sensor response magnitudes were attained in relation to those attained towards other gases. With the 30% (wt.) H-Y sensor, notably different response magnitudes were attained at 400 ˚C and 450 ˚C.

Whilst the control sensor could not discriminate between butane and acetone gases at 450 ˚C, this was addressed with one and three film depositions of zeolite H-Y and with 10% (wt.) H-Y. Further, ethane and propane gases could not be discriminated with the control. Nevertheless, using zeolite H-Y solved the issue at 400 ˚C with three depositions of zeolite over the control sensor and with 30% (wt.) H-Y at 350 ˚C. Sensors containing 10% (wt.) and 30% (wt.) H-Y also provided different magnitudes of response upon exposure to ethane and propane gases at 300 ˚C. Discrimination was also possible at other temperatures but it was less evident.

3.5.2 Microstructural Effects

The response of a sensor to a gas may be influenced by its diffusion through the sensing material, the sensor response kinetics and the reactions or interactions that occur at the sensor.[15,22] This section looks at how zeolite incorporation into the sensing system altered the sensor responses that were otherwise obtained with the unmodified SnO_2 sensor. Diffusion, sensor response kinetics and reaction factors have been discussed. The effects of zeolite incorporation on gas discrimination have also been addressed.

3.5.2.1 Diffusion, Sensor Response Kinetics and Reaction Processes

As described by Binions et al. [15] the microstructure of a sensor plays a key role in the kinetics of reactions that take place at the sensor surface; porous microstructures

introduce a high area-to-volume ratio to the sensing element, which consequently amplify the concentration of surface-reactive sites. In turn, this promotes the overall conductivity of the sensing system. In the presence of a test gas, the sensing material may react with it such that an enhancement or diminution of the sensor response is attained. This is a direct result of the sensitivity of the sensing system to the reaction products.[15] That is, where the sensing layers are highly sensitive to the reaction product(s), the sensor response will increase. In the case where the sensor is less sensitive to the reaction product(s), its response will decrease.[15]

The effects of zeolite coatings on top of a sensing material to promote an enhancement in the response of conventional MOS gas sensors as well as to favour the exclusion of interfering molecules has already been reported in the literature.[21,22,25,26,30] The diffusion of gas molecules through the zeolite layers will be largely dependent on the size and/or shape of the molecules, the zeolite pores and their channels. Incorporating zeolite layers may delay the response times of sensors due to the diffusion resistance imposed by the layers.[21,24] The longer response times occur because the zeolite layers hinder the direct interaction between the gas molecules and the sensing material underneath it. Gas molecules that have similar sizes or are larger than the zeolite pores may still diffuse through the cracks or voids in the system.[22] Nevertheless, the rate of diffusion will be slow enough that diffusion can be deemed negligible. The effects of admixed zeolite incorporation on the response times of sensors have not yet been discussed in the literature.

As described in section 1.5 (Chapter 1), the catalytic properties of zeolites may lead to the formation of reaction products that are different to those obtained solely with the unmodified material. Some zeolites may be used as cracking agents, serving to break molecules down into other products.[231] This can result in the aforementioned increase or decrease of the sensor response, according to the inherent sensitivity of the sensor to the reaction products.

The inability of the unmodified sensor to discriminate between some test gases which had similar molecular structures and/or the same functional groups was illustrated in section 3.3.2 above. Binions et al. [15] reported similar results with an unmodified Chromium Titanium Oxide (CTO) gas sensor upon exposure to IPA and ethanol gases. They explained the results by assuming that similar molecules would lead to similar reactions with the sensor surface of an unmodified material. As shown in Fig. 3-7 above, the response magnitude of the control SnO_2 sensor towards ethanol and IPA gases was identical and the peak shapes (not shown) were as well. It was expected that,

by altering the surface microstructure of the control SnO_2 material with zeolites that had different properties, different response patterns would be obtained.

Tests performed in the lower temperature range (i.e. 300 °C or 350 °C) led to larger error margins among repeat tests, especially when a sensor was particularly sensitive to a gas. This behaviour was also more prominent as the test gas concentrations were raised. It is possible that the gas becomes trapped in the material and/or zeolite pores which, in turn, leads to poor desorption of the gas itself or of the reaction products.[136,229] An example of this is presented in Fig. 3-16 below with sensors modified with Na-A zeolite. This zeolite is hydrophilic in nature and SnO_2 has also been reported to show an affinity for water vapour.[21,22]

It may be the case that water molecules produced during the reaction processes that take place at the sensor could interfere with the detection of the test gas.[22] Furthermore, the thick physical barrier imposed by the zeolite could also be more effective at retaining water vapour and not desorbing it effectively after removal of the test gas, thus preventing the sensor's resistance from recovering and returning to baseline.

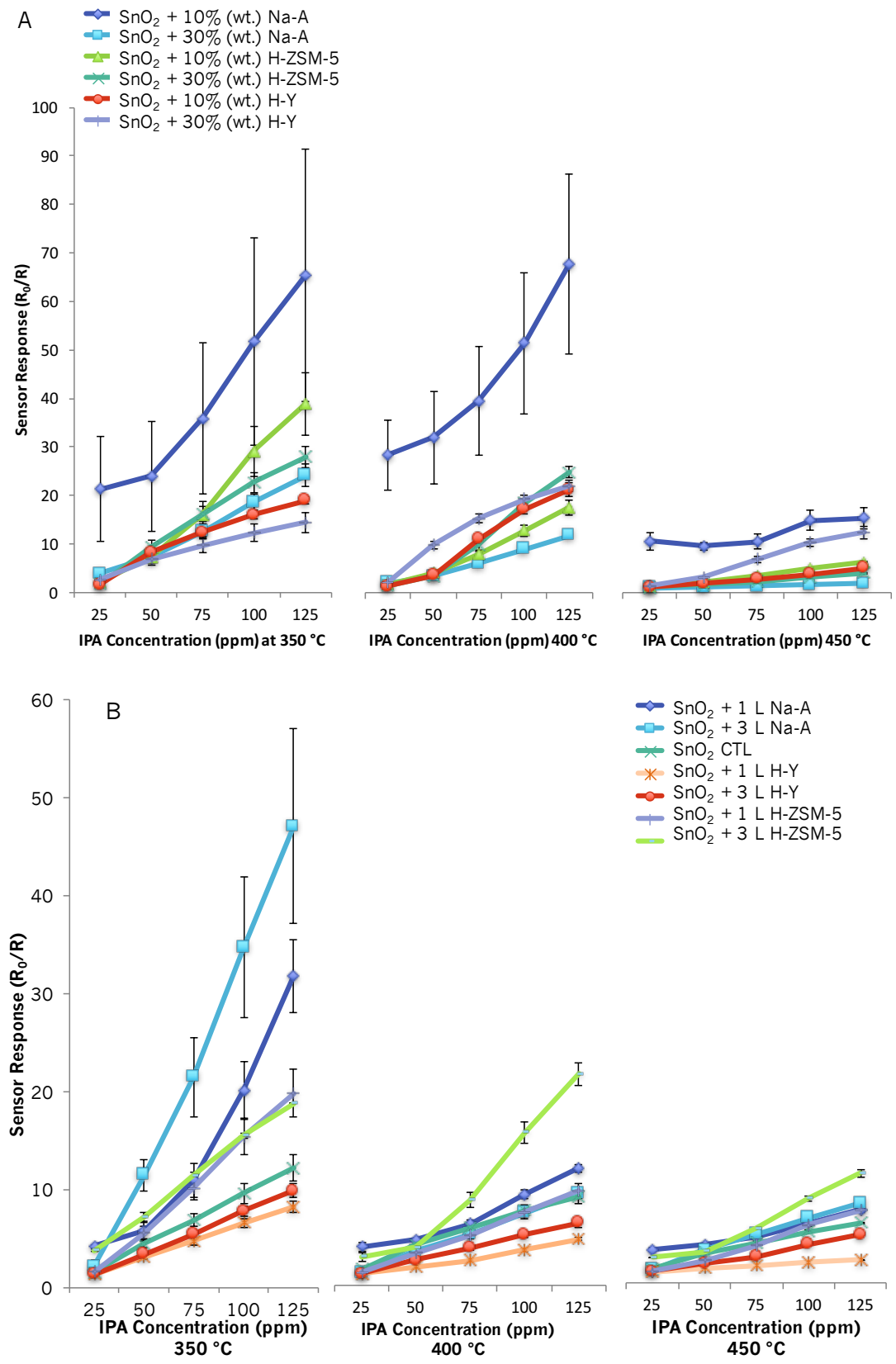

Figure 3-16 SnO_2-based sensor responses of (A) zeolite-admixed and (B) zeolite-overlaid sensors towards IPA at 350 °C, 400 °C and 450 °C. The image illustrates how at lower temperatures the variability in sensor responses is more prominent, particularly with the incorporation of zeolite Na-A.

It is noteworthy that at higher operating temperatures the pore sizes of zeolites may distend and, as such, they may enable the diffusion of molecules that may be more effectively hindered from diffusion at lower temperatures.[292] It therefore follows that the selective capabilities of zeolite-modified sensors may be less effective at higher operating temperatures. The high sensitivity of H-ZSM-5 in both overlaid and admixed sensors towards toluene in the higher temperature range may be an example of this (Fig. 3-17). The pores of H-ZSM-5 are essentially too small for toluene to pass through them (kinetic diameter: 5.8 Å).[293] If at higher temperatures the gas molecules become more flexible and the zeolite pores become slightly larger than reported as part of crystallographic calculations, it would explain the more similar response magnitudes obtained when the sensors are heated to 400 °C.[292] Sensor responsiveness towards toluene was highest at 400 °C. This enhancement in sensor response could potentially be attributed to a lesser effect of water vapour cross-sensitivity at this temperature. As such, the hydrophobic nature of zeolite H-ZSM-5 may lead to better affinity and interaction with toluene gas at this temperature.

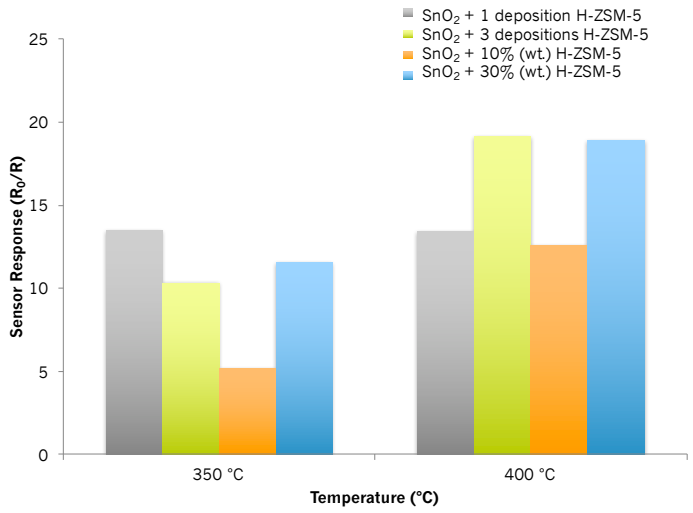

Figure 3-17 Sensor responses of SnO_2 sensors overlaid and admixed with zeolite H-ZSM-5 towards 50 ppm toluene gas at 350 °C and 400 °C. This figure illustrates how more distinct sensor patterns are obtained at 350 °C. At 400 °C it is thought that discrimination was compromised due to the zeolite pores distending slightly and allowing the diffusion of toluene molecules more readily.

3.5.2.2 Response/Recovery Times and Peak Shapes

Inspection of the peak shapes upon sensor exposure to hydrocarbon (HC) gases revealed that at higher temperatures (450 °C) sensors typically responded more quickly, as expected. The peak shapes resembled that of an ideal sensor response, which was consistent with reaching steady state (see, for instance, Fig. 3-22).[15] The fast responses seen with sensor exposure to HCs at 450 °C could potentially be the

result of complete combustion reactions leading to the production of CO_2 and $H_2O_{(v)}$.[15] It is therefore possible that at higher operating temperatures the reactions are principally surface-driven.[118] However, sensor exposure to toluene gas led to peak shapes that resembled shark-fins (further detail in section 3.5.4.4 below).

In general, gas discrimination was more effective with zeolite-modified sensors as the temperature was lowered, often resulting in large enhancements in sensor responsiveness. It must be noted, however, that diffusion through the zeolite-containing sensors at lower operating temperatures was thought to lead to longer response times, characterised by the aforementioned shark-fin peak shapes. As alluded to previously, because at lower operating temperatures the gas may be able to penetrate deeper into the sensing layer, it is able to react inside the zeolite pores as it passes through the system, potentially producing reaction products that have higher affinity towards the sensing material than the originally supplied gas. Examples of the shark-fin shapes can be seen in Fig. 3-22 with sensor exposure to ethane and butane at 350 °C.

Figs. 3-18 and 3-19 show the relationship between the types of zeolite utilised and their interaction with ethanol, IPA, toluene and acetone gases. The response times (τ_{90}) and recovery times (τ_{10}) have also been included in Figs. 3-20 and 3-21. It can be seen, for instance, that more layers of zeolite Na-A could result in longer response times upon exposure to test gases. Although the incorporation of one layer of zeolite Na-A led to a mild enhancement in sensor response to ethanol and IPA gases in relation to the control sensor, the response towards ethanol gas was considerably improved (by a factor of 4) when incorporating three film depositions of zeolite Na-A into the sensing system. The smaller kinetic diameter of ethanol (4.3 Å) favours its diffusion into the inner layers of the sensing material, whereas the branched and slightly larger IPA molecule (4.7 Å) may experience more resistance in diffusing through the system. Another study also found that while a control CTO sensor could not discriminate between ethanol and IPA, the incorporation of zeolite H-ZSM-5 led to contrasting sensor responses, which was attributed to the branched configuration of the IPA molecule.[15] It was generally observed that zeolite-admixed sensors led to faster response times than the zeolite-overlaid sensors. This is potentially due to the added resistance of the zeolite film attained with zeolite overlayers.[22,24] Sensor responses towards toluene gas were typically slower than for other gases and this trend was seen in both zeolite-admixed and overlaid sensors. Further, the zeolite-admixed sensors displayed slower recovery times upon exposure to toluene gas than the overlaid sensors. The zeolite-modified sensors responded very similarly to IPA gas, irrespective of the number of zeolite Na-A layers. The modest enhancement seen in sensor

responses in relation to the control SnO_2 sensor could potentially be the result of the hydrophilic character of the zeolite and the polarity of the IPA (polarity index = 3.9)[294] molecule. The sensor response towards acetone gas was worsened with the incorporation of zeolite Na-A coatings, when compared to the unmodified sensor. Despite the similar kinetic diameters of IPA, ethanol and acetone, the underlying sensing material was not particularly sensitive to acetone. Nevertheless, it must be noted that the concentration of acetone was much lower (8 ppm) than that of ethanol and IPA gases (100 ppm). At 450 °C, the fabricated sensors were generally more responsive to gases when covered with three film depositions of a zeolite.

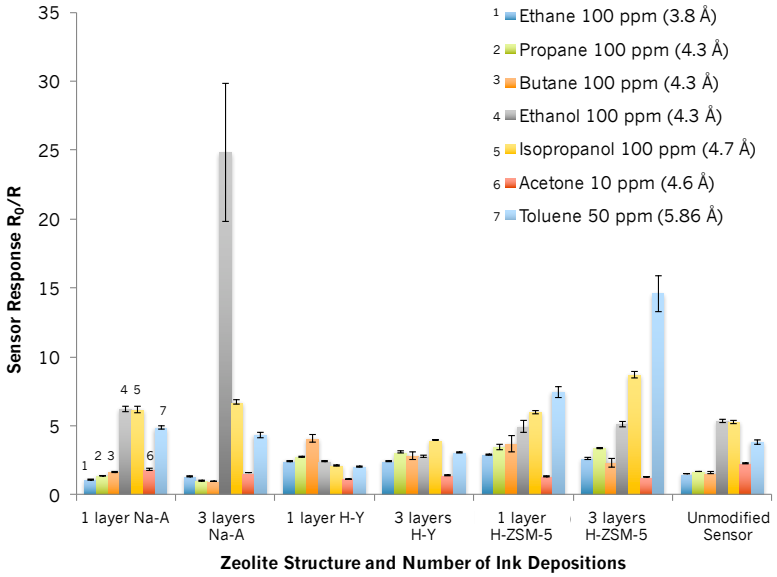

Figure 3-18 Responses of zeolite-overlaid sensors at 450 °C when supplied with the maximum concentration of test gas. The kinetic diameters (Å) of the molecules used have been included in brackets.

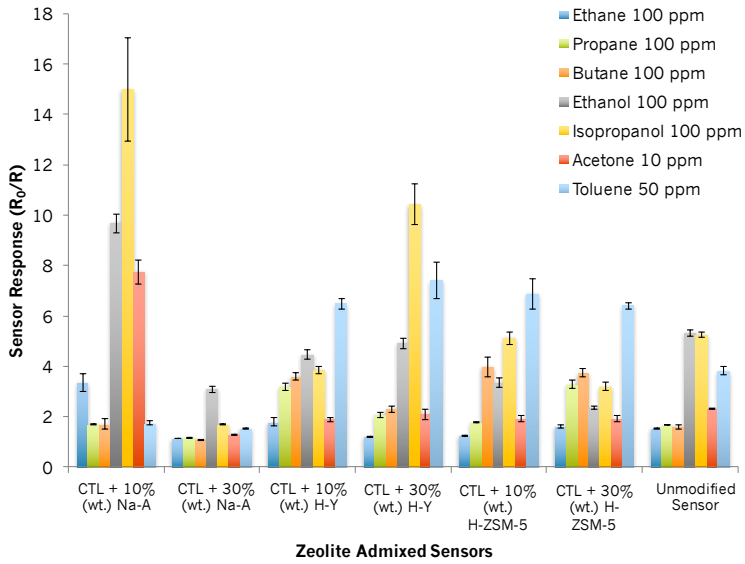

Figure 3-19 Sensor responses of zeolite-admixed sensors at 450 °C when supplied with the maximum concentration of test gas.

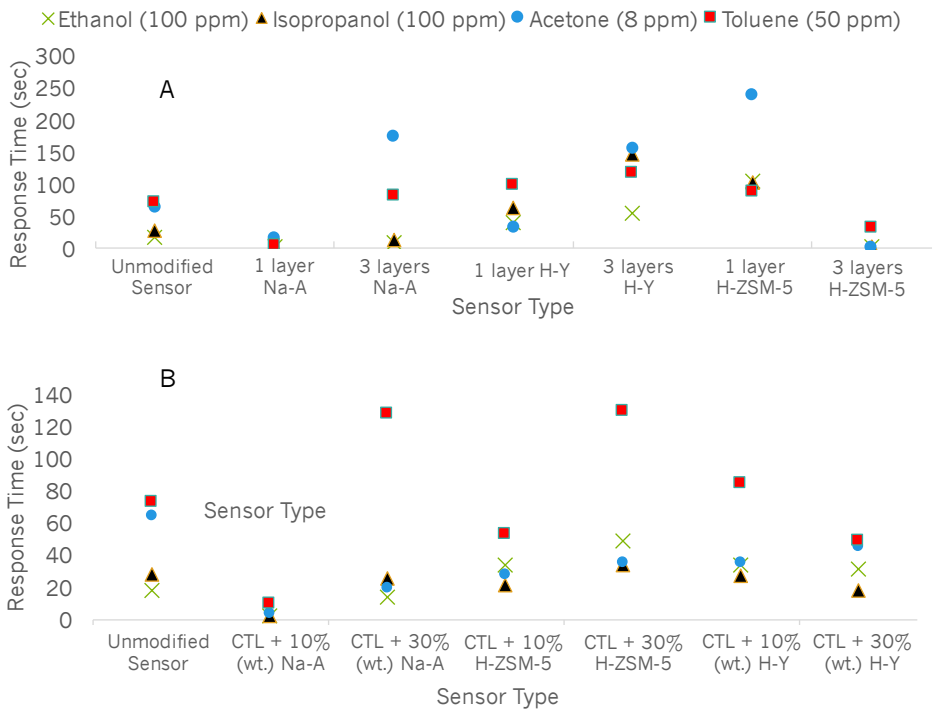

Figure 3-20 Response times (τ_{90}) of a control SnO_2 sensor and of those modified by zeolite (A) overlayers and (B) admixtures.

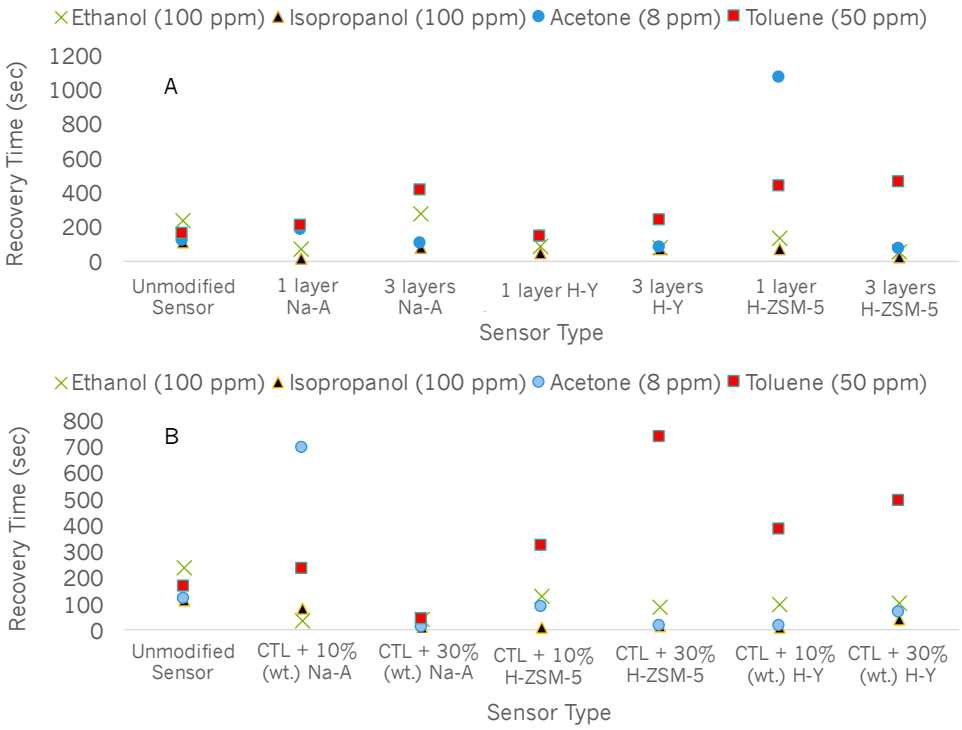

Figure 3-21 Recovery times (τ_{10}) of a control SnO_2 sensor and of those modified by zeolite (A) overlayers and (B) admixtures.

3.5.3 Zeolite Film Thickness/Loading Effects on Sensor Responses

As elucidated in Chapter 1, the thickness of the sensitive layers play a key role in sensor sensitivity and responsiveness. A summary of the sensor responses attained for

all sensors discussed in this section at 450 °C and 400 °C have been provided in the Appendix for reference.

The zeolite-admixed SnO_2 sensors often provided contrasting sensor responses when they had the same zeolite in the system but a different zeolite loading. In general, the sensors that had a 10% (wt.) loading of zeolite Na-A in the system were more responsive to gases than those with a 30% (wt.) zeolite loading. Upon exposure to toluene and carbon monoxide gases, the sensors provided similar responses, irrespective of the zeolite loading. Sensors admixed with 10% (wt.) zeolite H-ZSM-5 provided more responsive outputs than those mixed with 30% (wt.) H-ZSM-5 upon exposure to ethanol and IPA gases (providing a 1.5-fold enhancement in both instances) and to NO_2 (providing a 1.3-fold enhancement – refer to images in the Appendix for NO_2 sensor responses). Upon exposure to acetone, toluene, ethane and butane, both sensors admixed with zeolite H-ZSM-5 provided comparable sensor responses. The SnO_2 sensors admixed with zeolite H-Y led to comparable results upon exposure to ethanol and acetone gases. The SnO_2 sensor loaded with 10% (wt.) zeolite H-Y was more responsive than the 30% (wt.) counterpart towards butane, propane and carbon monoxide gases. Note that CO results have been provided in section 3.5.4.5 below. 'SnO_2 + 30% (wt.) H-Y' was very responsive to IPA and NO_2 gases, but provided more prominent sensor variability in relation to the 10% (wt.) counterpart.

The 'SnO_2 + 10% (wt.) Na-A' resulted in a remarkable enhancement in sensor response to ethanol, IPA and acetone, when compared to 'SnO_2 + 30% (wt.) Na-A' and to the control sensor. Although the improvement in sensor responsiveness was more conservative, sensors admixed with 30% (wt.) H-Y also showed an enhancement in response over the unmodified sensor when exposed to gases such as propane, butane, toluene and IPA. However, 'SnO_2 + 10% (wt.) H-Y' was slightly more responsive towards ethane, propane and butane gases than its counterpart, with 30% (wt.) zeolite H-Y. SnO_2 sensors admixed with zeolite H-ZSM-5 responded in a similar fashion when exposed to toluene and acetone gases, irrespective of the zeolite loading. It is noteworthy that although it did so discreetly, the 30% (wt.) H-ZSM-5 sensor improved the responses to butane and propane gases, in relation to the control.

The most promising aspect of the zeolite-admixed sensors was that, for instance, sensors containing zeolites Na-A and H-ZSM-5 often displayed opposing behaviours to some gases such as acetone, toluene, ethane, butane. Upon exposure to ethanol, IPA, CO and NO_2 gases (refer to graphs in the Appendix), both zeolite-modified systems were very responsive to the gases and the magnitudes of response were different

enough that gas discrimination seemed, indeed, like a plausible option with classification tools at this stage.

Zeolite-overlaid sensors perhaps provided more comparable sensor responses to gases, irrespective of the thickness of the zeolite film. There were exceptions to this such as 'SnO_2 + 1L Na-A' and 'SnO_2 + 3L Na-A': they provided very different responses towards ethanol gas, the latter displaying high variability between repeat tests. 'SnO_2 + 1L H-ZSM-5' and 'SnO_2 + 3L H-ZSM-5' provided different responses towards IPA gas, the latter providing a 1.5-fold enhancement over the 1-layered sensor. 'SnO_2 + 1L H-ZSM-5' and 'SnO_2 + 3L H-ZSM-5' provided different responses towards toluene gas, the latter providing a 2-fold enhancement in the sensor response. Nevertheless, the 3-layered H-ZSM-5 sensor provided higher variability among repeat tests than the 1-layered one. Furthermore, it was noteworthy that whilst the sensors admixed with zeolites were responsive towards NO_2 gas, the overlaid ones were not (refer to the Appendix).

At first glance, if the sensors were used as arrays, the zeolite-overlaid sensors did not seem as suitable as the admixed sensors for practical applications as the responses were lower and discrimination among gas types was not as evident as it was with the zeolite-admixed sensors. Although the sensor responses of the zeolite-overlaid sensors were much-improved for some gases at 400 ˚C, sensor variability among repeat tests increased slightly at this temperature. The same was found with the zeolite-admixed sensors.

3.5.4 Effects of Zeolite Incorporation on Sensor Sensitivity, Selectivity and Responsiveness to Test Gases

It is noteworthy that sensors did not always follow the behaviour of an n-type material. This behaviour occurred specifically with exposure to alkanes and it was seen to vary with operating temperature. The unmodified SnO_2 sensor behaved as a p-type semiconductor when exposed to ethane and propane gases both at 350 °C and 400 °C and the presence of zeolites only served to further promote this behaviour (Fig. 3-22). For instance, whilst sensors overlaid with zeolites H-Y and H-ZSM-5 showed an increase in conductivity upon exposure to ethane gas at 450 °C, sensors that were overlaid with zeolite Na-A were unresponsive to the gas. As the temperature was gradually dropped to 350 °C, all the zeolite-overlaid sensors (H-ZSM-5, H-Y and Na-A) displayed sensor responses that were consistent with p-type behaviour upon exposure to ethane.

Sensors fabricated with zeolite admixtures behaved differently to the overlaid ones and often provided remarkable enhancements in sensor responsiveness. For instance, at 450 °C, only certain sensors displayed an increase in sensor resistance with exposure to ethane, propane and butane, but as the temperature was dropped to 300 °C, all sensors consistently showed an increase in sensor resistance. This could potentially be due to the production of new reaction products (see section 3.5.4.1 below for a more in-depth discussion on this topic). It must be noted here that in order to confirm that the sensors did, indeed, display p-type behaviour upon exposure to an oxidising gas, they were also exposed to NO_2, the responses of which have been provided in the Appendix.

As an example of how great the differences in sensitivity were among the zeolite-overlaid and the zeolite-admixed sensors, at 400 °C the resistive response to 100 ppm ethane gas with 'SnO_2 + 10% (wt.) Na-A' was R/R_0 = ~9 (SD ± 0.5), compared to R/R_0 = ~1.3 (SD ± 0.01) and ~1.4 (SD ± 0.02) with the sensors overlaid with one and three depositions of zeolite Na-A, respectively. At 350 °C, the response R/R_0 to 100 ppm ethane with 'SnO_2 + 10% (wt.) Na-A' was ~12 (SD ± 0.3), yet sensors coated with zeolite Na-A were virtually unresponsive to it.

With the exception of sensor exposure to toluene, which led to poor sensor recovery in some sensors, sensor performance was generally fit for purpose. That is, the sensors were sensitive to trace concentrations of test gases and providing response and peak shape differentiations when exposed to a range of test gases. Further, sensors generally provided fast response and recovery times and reached steady state. This makes some of the fabricated sensors particularly strong candidates for selective MOS sensing arrays. The incorporation of zeolites resulted in great sensitivity enhancements over the control sensor at first glance. It seemed that some zeolite-modified sensors encouraged gas discrimination that was previously unattained with the unmodified sensor. The sensors typically provided repeatable responses, particularly at higher temperatures i.e. 400 °C and 450 °C.

The sensitivity of three zeolite-overlaid and zeolite-admixed SnO_2 sensors was evaluated by fitting second order polynomial equations to their response vs. concentration curves and by later taking the derivative of the equations. This was done for ethanol, IPA, acetone, toluene gases and the results have been presented in each of the pertinent sections presented below.

3.5.4.1 Sensor Exposure to Alkanes

Given that p-type behaviour was affected by the fabrication procedure and by the operating temperature (e.g. Fig. 3-22), the following conclusions have been drawn. It is possible that p-type behaviour occurred as a result of the formation of an oxidising gas such as acetic acid. Yin et al [295] exposed Ag/Ag_2SnO_3 nanoparticles to acetic acid, reporting an increase in resistance upon exposure to the gas. As such, the production of acetic acid due to the interaction of ethane with oxygen species at the sensor surface may have led to this result. P-type behaviour in zeolite-overlaid sensors was less common but it was observed occasionally in some sensors when heated to 350 °C. This suggests that in the zeolite-admixed and zeolite-overlaid sensor systems different reaction products were formed. Conversely, some zeolite-admixed sensors began to provide a p-type response at 450 °C and, by the time the temperature had been dropped to 350 °C, they all consistently displayed p-type behaviour.

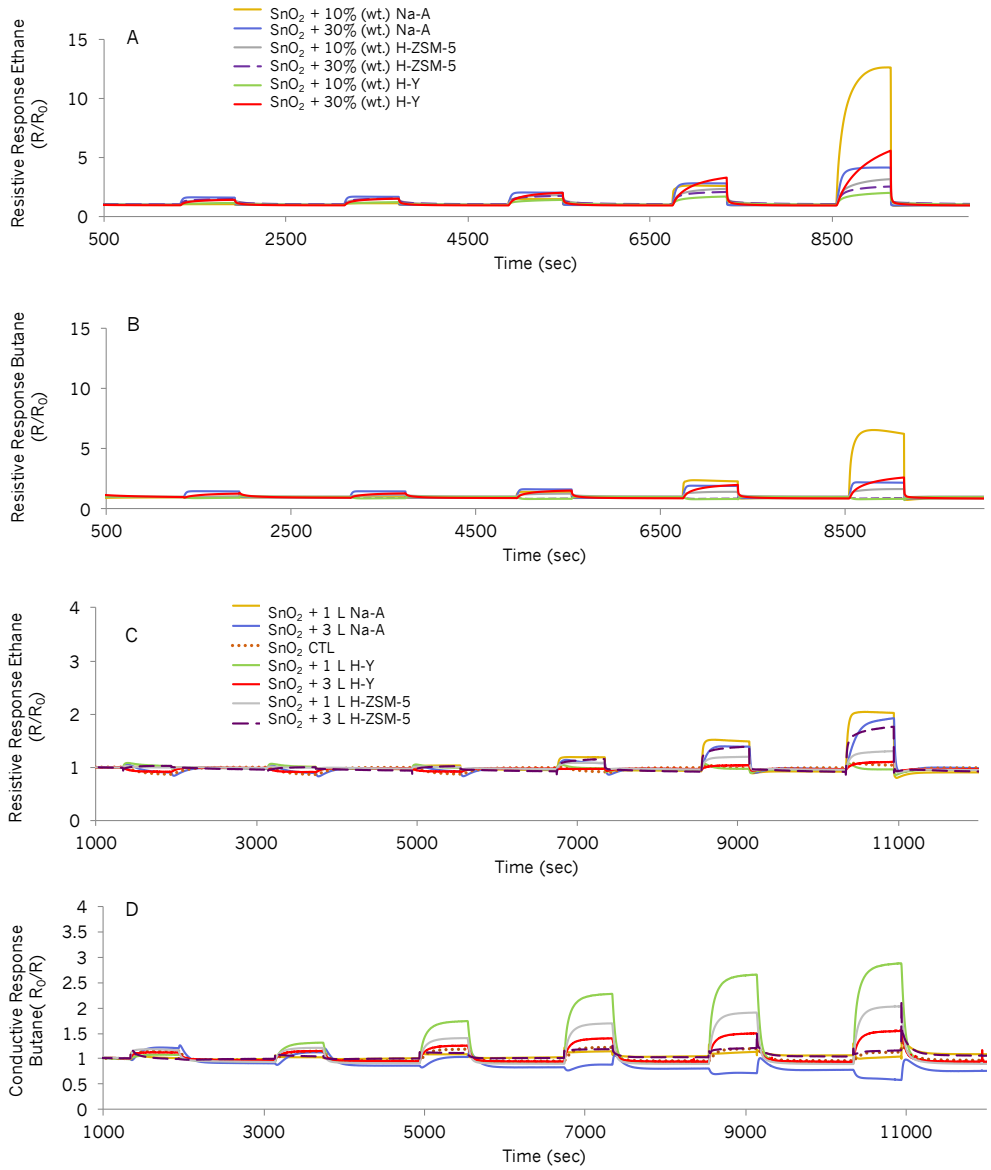

Figure 3-22 (A) Admixed resistive sensor responses to ethane gas when exposed to 10 ppm, 20 ppm, 50 ppm, 80 ppm and 100 ppm. (B) Admixed resistive sensor responses to butane gas when exposed to the same gas concentrations. (C) Overlaid resistive sensor responses to ethane gas concentrations ranging between 5 ppm, 10 ppm, 20 ppm, 50 ppm, 80 ppm and 100 ppm. (D) Overlaid conductive sensor responses to butane gas at the same gas concentrations. Tests performed at 350 °C.

The kinetic diameters of propane and butane are reported as 4.3 Å in the literature [296] and it is interesting to see how, despite the similarity in size, their interaction with zeolite-overlaid sensors differed potentially as a result of their shape; at 450 °C all sensors were more responsive to butane gas than to propane and, although sensors coated with zeolite Na-A were slightly more responsive to butane gas, they were essentially unresponsive to propane. However, sensors were not very responsive to both gases.

The poor response obtained in sensors containing zeolite Na-A can potentially be explained by the hydrophilic character of the zeolite and the non-polar character of the alkane chains. In addition to this, butane and propane are too large to diffuse through the 4.1 Å sized pores of zeolite Na-A, which may be another contributing factor to the poor responses attained. At 450 °C, the sensors overlaid with zeolites provided very similar sensor responses to ethane and propane gases, providing the same order of magnitude (Fig. 3-18). Although the size of the ethane molecule should enable its diffusion through the pores of zeolite Na-A, the poor responsiveness is potentially attributable to its poor affinity with the hydrophilic surface of the zeolite. This behaviour changed, leading to enhanced sensor responses, when the molecule contained a hydroxyl group, for instance. When sensors were heated to 450 °C and overlaid with one film deposition of a zeolite, sensor responsiveness increased with chain length.

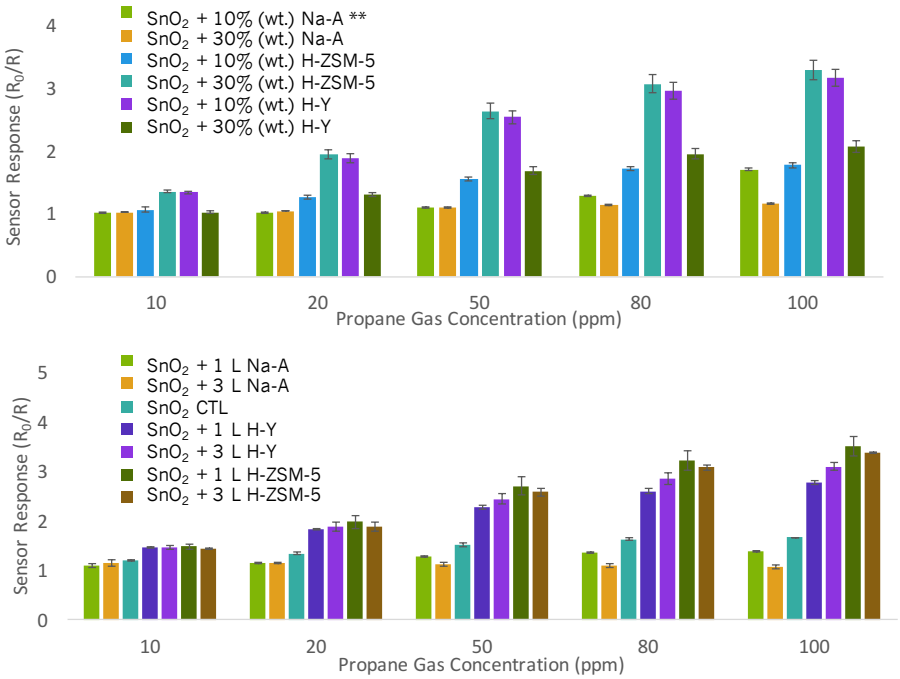

Figure 3-23 Conductive sensor responses towards propane gas at 450 °C. The top image corresponds to responses of SnO_2 zeolite-admixed sensors and the bottom image corresponds to zeolite-overlaid sensor responses. The symbol ** refers to a resistive behaviour of the sensor and the sensor response was thus calculated as R/R_0 instead.

The zeolite-admixed sensors behaved similarly upon exposure to butane and propane gases at 450 °C and they only behaved considerably differently at 350 °C. The predominance of p-type behaviour seen in the admixed sensors could potentially be due to a microstructural effect; it is possible that the admixed sensor microstructures favour the cracking of hydrocarbons to more polar and oxidising compounds with functional groups which exhibit greater affinity towards zeolite Na-A, leading to enhanced responses towards the gases.

Note that at 350 °C sensor exposure to ethane and butane displayed the same order of sensor responses (10% Na-A > 30% HY > 30% Na-A > 10% H-ZSM-5 > 30% H-ZSM-5), with quasi-identical peak shapes, though showing higher responsiveness to ethane than to butane (Fig. 3-22). This could suggest that these hydrocarbons break down to similar reaction products on these sensing materials. Generally, the zeolite-admixed sensors proved to be more successful in enhancing responses to gases at lower temperatures, particularly when exposing the sensors to ethane and butane gases.

Other groups have investigated SnO_2 as a gas sensor for HC detection, using coatings of zeolites with MFI and LTA frameworks. Vilaseca et al. [30] used a Pd-SnO_2 sensor coated with an LTA zeolite and, despite heating the sensors across 250 – 400 °C and exposing them to propane, they did not find the increase in sensor resistance reported in this thesis. In a different study, [22] the same group exposed the Pd-SnO_2 sensors with coatings of zeolites with MFI and LTA frameworks to a range of gases at different temperatures and, once again, their sensors displayed the expected n-type behaviour when exposed to HC. This may be due to a number of reasons, such as the Pd dopant they used, the microstructure of their sensors, the fabrication method, which consisted of zeolite films grown on top of the SnO_2 material, or due to the much higher gas concentrations they investigated.

3.5.4.2 Sensor Exposure to Alcohols

The sensor responses to ethanol and IPA gases previously unresolved by the control SnO_2 sensor were successfully discriminated with zeolite-containing sensors. With the exception of sensors 'SnO_2 + 1L Na-A' and 'SnO_2 + 1L H-Y', which were unable to discriminate between 100 ppm of both alcohols at 450 °C, the remaining sensors produced sensor responses that differed to those provided by the control sensor, also displaying selectivity towards either gas, as shown in Figs. 3-18 and 3-19. More specifically, 'SnO_2 + 3 L Na-A' displayed selectivity towards ethanol, suggesting that the branched conformation of the IPA molecule was most likely hindered from diffusing to the sensitive layer of the sensor. On the other hand, sensors 'SnO_2 + 3 L H-ZSM-5', 'SnO_2 + 10% (wt.) Na-A', 'SnO_2 + 30% (wt.) H-Y' displayed selectivity towards IPA, either due to the formation of reaction products to which SnO_2 was more sensitive or due to a more open microstructure, enabling the access of IPA into inner layers more readily and enabling its reaction with the zeolites.

The zeolite-overlaid sensors were remarkably responsive to ethanol gas, particularly at 300 °C with 'SnO_2 + 1 L Na-A' providing a response of R_0/R = 90.4 (SD ± 4.5) and 'SnO_2 + 1 L H-ZSM-5' R_0/R = 60.9 (SD ± 3.9) but, as alluded to previously, there were

associated downsides to performing tests at lower operating temperatures. At 450 °C the sensors showed very fast response and recovery times, reaching steady state in <18 seconds with sensors 'SnO_2 + 1 L and 3 L Na-A' and 'SnO_2 + 3 L H-ZSM-5'. In the case of zeolite-overlaid sensor exposure to ethanol gas, τ_{90} was always below 50 seconds, and sensor 'SnO_2 + 10% (wt.) Na-A' saturated in ~2 seconds. Although τ_{90} was generally faster upon exposure to ethanol gas than to IPA, this trend was often reversed in the zeolite-admixed sensors (Fig. 3-20).

At 450 °C the sensor that was most responsive to ethanol was 'SnO_2 + 3 L Na-A' with R_0/R ~24 (Fig. 3-18). Although the kinetic diameter of ethanol is larger than the pores of zeolite Na-A, this result may be attributable to the hydrophilic character of the zeolite and the polar character of the ethanol molecule.[22] It can be seen how big an effect the functional group has on the sensor response in sensors containing hydrophilic zeolites and how it can benefit the detection of specific gases (compare to the sensor responses obtained with exposure to ethane). Despite ethanol's ability to diffuse through the pores of zeolite H-ZSM-5 it can be seen that, when used as a coating, the response of sensors containing zeolite H-ZSM-5 towards this polar molecule were very similar to those obtained with the unmodified SnO_2 sensor.

Sensor responses towards ethanol obtained with sensors modified by overlayers of zeolite H-Y decreased in relation to those obtained with the control sensor. When zeolite H-Y was incorporated as an admixture with the base material, sensor responses were very similar to the control. At 450 °C, the number of zeolite layers in sensors containing zeolites H-ZSM-5 and H-Y made little difference to the sensor responses.

The most prominent difference in sensor response among zeolite groups was that obtained by the sensors with three depositions of zeolite Na-A, when compared to one layer of zeolite Na-A over the control SnO_2 base material. The number of zeolite depositions directly affected response and recovery times and they did not always slow down the response and recovery times with increasing thickness of the zeolite film (Fig. 3-20). For instance, three layers of zeolite H-ZSM-5 provided very fast responses to the alcohols, with steady state achieved, whereas the 1-layered sensor responded in a slow fashion. This feature could be used to assist discrimination when using data mining tools such as Support Vector Machines (SVM). At temperatures in the range of 250 – 350 °C sensor 'SnO_2 + 3 L Na-A' failed to return to baseline when ethanol was removed from the sensing atmosphere.

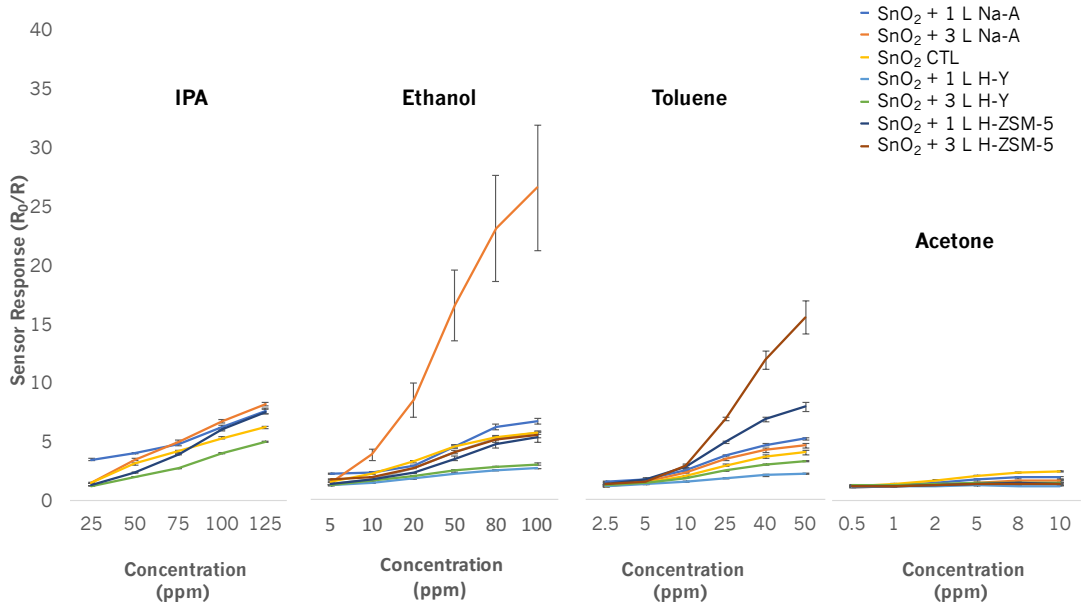

Figure 3-24 Zeolite-overlaid SnO_2 sensor responses to increased concentrations (ppm) of IPA, ethanol, toluene and acetone vapours at 450 °C.

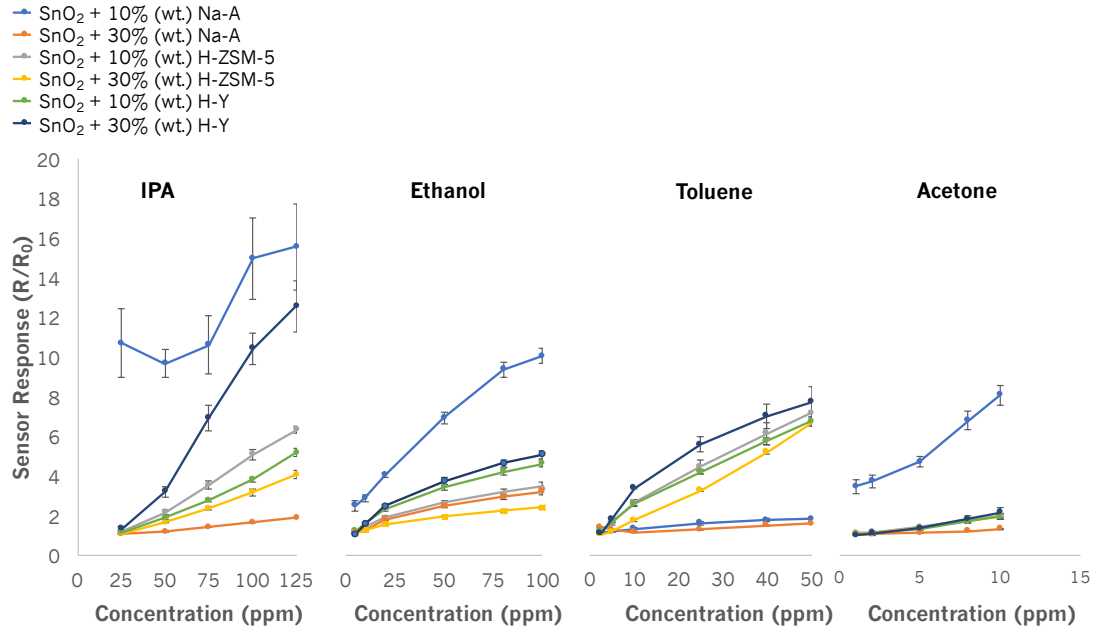

Figure 3-25 Zeolite-admixed SnO_2 sensor responses to increased concentrations (ppm) of IPA, ethanol, toluene and acetone vapours at 450 °C.

At 450 °C the zeolite-overlaid sensor most responsive to 100 ppm IPA was that containing three layers of zeolite H-ZSM-5, providing a response R_0/R = ~9, compared to R_0/R = ~5 attained upon exposure to ethanol gas. The responses of sensors overlaid with three layers of zeolite H-Y were smaller in magnitude than those of the control sensor, as with ethanol exposure. However, sensing differences upon exposure to both gases were still evident. Sensors containing 'SnO_2 10% (wt.) Na-A' and 'SnO_2 10% (wt.)

+ H-ZSM-5' were more responsive to alcohols than the ones containing 30% (wt.) of the relevant zeolite. Generally, the zeolite-admixed sensors were more responsive to IPA than those coated with zeolites.

The sensors were remarkably responsive to IPA at lower temperatures such as 300 °C. For instance, sensor 'SnO_2 + 1 L Na-A' provided R_0/R = ~10 (SD ± 0.5) to 25 ppm and ~87 (SD ± 4.8) to 125 ppm of IPA gas. Responses obtained with 'SnO_2 + 1 L H-Y' and 'SnO_2 + 1 L H-ZSM-5' were comparatively lower i.e. 12.9 (SD ± 0.7) and 16 (SD ± 3.3), respectively but, nevertheless, significant (not shown).

Second order polynomial equations were fitted to the response curves shown in Figs. 3-24 and 3-25 for seven out of the thirteen sensors fabricated. The polynomial equations for ethanol gas exposure have been tabulated in Tables 3-3 and 3-4 and those for IPA gas in Tables 3-5 and 3-6. Figs. 3-26 and 3-27 provide the sensitivity curves of the zeolite-overlaid and admixed sensors against ethanol and IPA gases, respectively. As can be seen in the graphs displaying the sensitivity curves, both zeolite-overlaid and admixed sensors' sensitivity decreased upon exposure to higher concentrations of ethanol (Fig. 3-26). Sensors coated with one layer of zeolites Na-A and H-ZSM-5 showed that the sensitivity curve remained almost constant as the concentration of ethanol increased, which is promising if the sensors were to be used in practical applications, as they display a high dynamic range. The remaining sensors would be better suited to work with the purpose of detecting lower gas concentrations.

Table 3-3 Second order polynomial equations fitted to ethanol's response curves (see Fig. 3-24) attained for overlaid SnO_2 sensors coated with one layer of zeolites Na-A (LTA), H-Y (FAU) and H-ZSM-5 (MFI). The R^2 values attained for each fit have also been provided.

Overlayers	Sensor Type	2nd Order Polynomial Equation	R-Squared Value
Ethanol	SnO_2 CTL	$y = -0.0004x^2 + 0.0824x + 1.1866$	0.98
	SnO_2 1L LTA	$y = -0.0001x^2 + 0.06x + 1.5997$	0.99
	SnO_2 + 1L FAU	$y = -0.0002x^2 + 0.0292x + 1.0053$	0.98
	SnO_2 + 1L MFI	$y = -0.0001x^2 + 0.0535x + 0.9829$	0.99

Table 3-4 Second order polynomial equations fitted to ethanol's response curves (see Fig. 3-25) attained for SnO_2 sensors admixed with 10% (wt.) of zeolites Na-A (LTA), H-Y (FAU) and H-ZSM-5 (MFI). The R^2 values attained for each fit have also been provided.

Admixtures	Sensor Type	2nd Order Polynomial Equation	R-Squared Value
Ethanol	SnO_2 + 10% (wt.) LTA	$y = -0.0004x^2 + 0.1219x + 1.6963$	0.99
	SnO_2 + 10% (wt.) MFI	$y = -0.0002x^2 + 0.0413x + 0.9842$	0.99
	SnO_2 + 10% (wt.) FAU	$y = -0.0003x^2 + 0.0605x + 0.9988$	0.99

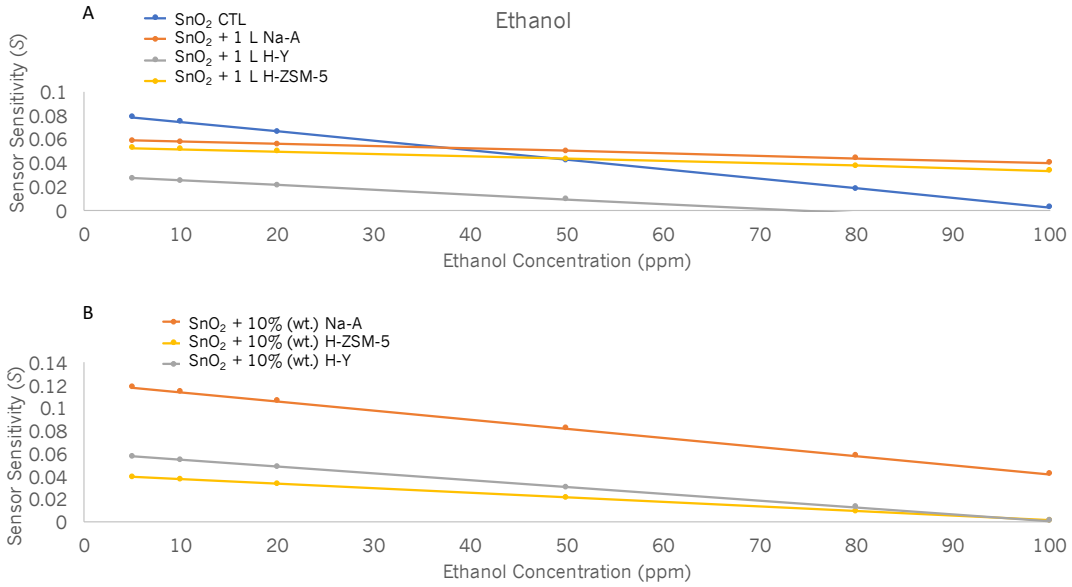

Figure 3-26 Sensor sensitivity curves to ethanol gas for (A) SnO_2 sensors overlaid with one layer of zeolites Na-A, H-Y and H-ZSM-5 and (B) SnO_2 sensors admixed with 10% (wt.) of zeolites Na-A, H-ZSM-5 and H-Y.

Table 3-5 Second order polynomial equations fitted to IPA's response curves (see Fig. 3-24) attained for overlaid SnO_2 sensors coated with one layer of zeolites Na-A (LTA), H-Y (FAU) and H-ZSM-5 (MFI). The R^2 values attained for each fit have also been provided.

Overlayers	Sensor Type	2nd Order Polynomial Equation	R-Squared Value
IPA	SnO_2 CTL	$y = -0.0002x^2 + 0.0696x - 0.13$	0.99
	SnO_2 1L LTA	$y = 0.0003x^2 + 0.0001x + 3.2417$	0.99
	SnO_2 + 1L FAU	$y = -4E\text{-}05x^2 + 0.0183x + 0.7102$	0.99
	SnO_2 + 1L MFI	$y = 0.0002x^2 + 0.0416x - 0.0064$	0.99

Table 3-6 Second order polynomial equations fitted to IPA's response curves (see Fig. 3-25) attained for SnO_2 sensors admixed with 10% (wt.) of zeolites H-ZSM-5 (MFI) and H-Y (FAU). The R^2 values attained for each fit have also been provided. Sensor Na-A was not included as the polynomial equation did not fit the curve well.

Admixtures	Sensor Type	2nd Order Polynomial Equation	R-Squared Value
IPA	SnO_2 + 10% (wt.) MFI	$y = 9E\text{-}05x^2 + 0.0387x + 0.1531$	0.99
	SnO_2 + 10% (wt.) FAU	$y = 0.0002x^2 + 0.015x + 0.726$	0.99

The zeolite-modified sensors' sensitivity to IPA gas generally increased with concentration. Lower gas concentrations should be investigated in the future. The sensitivity of the sensor coated with one layer of zeolite H-Y decreased slightly with concentration.

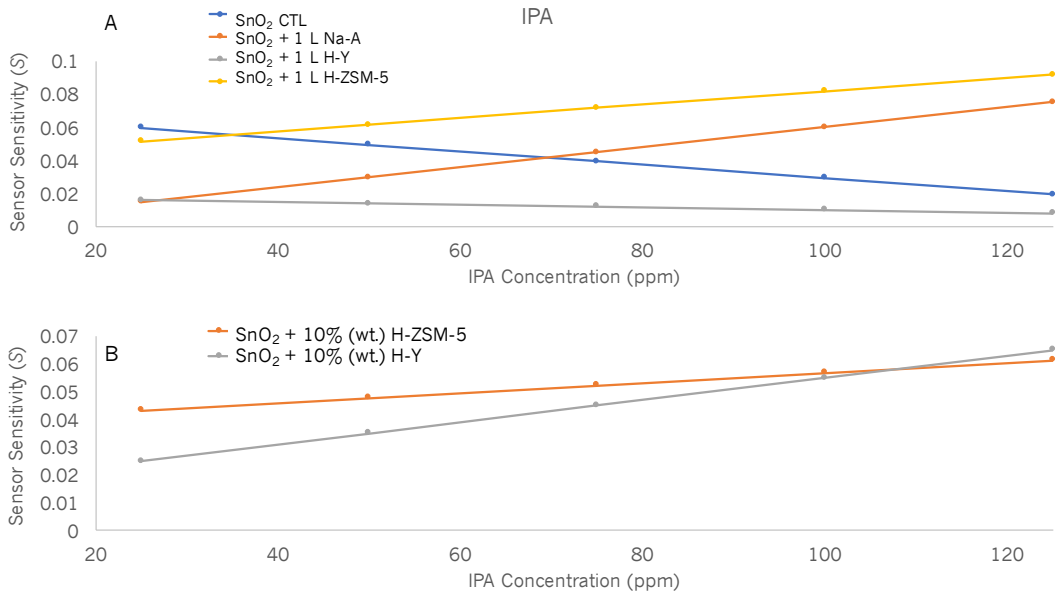

Figure 3-27 Sensor sensitivity curves to IPA gas for (A) SnO_2 sensors overlaid with one layer of zeolites Na-A, H-Y and H-ZSM-5 and (B) SnO_2 sensors admixed with 10% (wt.) of zeolites Na-A, H-ZSM-5 and H-Y.

Sensors modified by zeolite Na-A were more sensitive to ethanol than to IPA. Sensors modified with overlayers of zeolite H-ZSM-5 were more sensitive to IPA than to ethanol. Exposure of the Na-A zeolite admixed sensor to IPA resulted in high variability among repeat tests and these results have not been included. The zeolite admixed sensors were more sensitive towards ethanol gas than to IPA.

3.5.4.3 Sensor Exposure to Acetone

Zeolite-overlaid sensor exposure to acetone gas resulted in sensor responses lower than those obtained with the control sensor at 400 °C and 450 °C (refer to Tables in the Appendix). Sensor responsiveness was almost unaffected by increments in gas concentration at these temperatures (Fig. 3-24). At 350 °C, sensor 'SnO_2 + 3 L Na-A' responded to 10 ppm of acetone gas with R_0/R = ~5, providing a 2.4-fold increase in sensor response over the control sensor. Nevertheless, this sensor's response was slow and did not reach steady state. Although the kinetic diameter of acetone (4.6 Å) is smaller than the pore diameters of zeolites H-ZSM-5 and H-Y, they were moderately responsive to the gas with responses $R_0/R < 3$.

When exposing the zeolite-admixed sensors to acetone gas, the responses were enhanced considerably in relation to the zeolite-overlaid sensors and to the unmodified sensor (Fig. 3-25). It is possible that at 450 °C, the higher sensor responses (R_0/R ~8) seen with 'SnO_2 + 10% (wt.) Na-A' were due to water formation as part of surface

reactions and subsequent adsorption of water vapour into the sensing material. This was supported by the peak shapes, which were distinct and specifically seen when testing against humid air (section 3.5.4.6 below). The microstructure of the zeolite-admixed sensors could act in favour of acetone's combustion to CO_2 and $H_2O_{(v)}$, to which the sensors are more or less sensitive. This was supported by the peak shapes, which indicated fast reactions, reaching steady state quickly (not shown).

Note that at certain temperatures, some sensors overlaid with the same zeolite could respond very similarly to a gas irrespective of the number of zeolite film depositions over the SnO_2 base material. For instance, sensors coated with one and three layers of zeolite H-ZSM-5 upon exposure to acetone at 400 °C and 450 °C. These sensors worsened the response towards acetone in relation to the unmodified SnO_2 sensor. This similarity in response output seen among sensors containing the same zeolite was common when the incorporation of zeolite worsened the response to a gas relative to the control and resulted in little or no sensitivity to a gas. At 450 °C, it was often the case that the responses of sensors containing coatings of the same zeolite would be grouped together, i.e. zeolite H-ZSM-5 coatings produced a markedly different response to those covered with zeolite H-Y and those were, in turn, different to those coated with zeolite Na-A (Fig. 3-24). Despite this, differences in sensitivity attributed to the number of zeolite layers could typically be observed.

Sensor sensitivity was evaluated by fitting third order polynomial equations to the response curves in Figs. 3-24 and 3-25. The polynomial equations have been tabulated in Table 3-7 and Table 3-8 below. The corresponding sensitivity curves have been presented in Fig. 3-28 below.

Table 3-7 Third order polynomial equations fitted to acetone's response curves (see Fig. 3-24) attained for overlaid SnO_2 sensors coated with one layer of zeolites Na-A (LTA), H-Y (FAU) and H-ZSM-5 (MFI). The R^2 values attained for each fit have also been provided.

Overlayers	Sensor Type	3rd Order Polynomial Equation	R-Squared Value
Acetone	SnO_2 CTL	$y = 0.0021x^3 - 0.0461x^2 + 0.3815x + 0.9607$	0.99
	SnO_2 + 1L LTA	$y = 0.0004x^3 - 0.0137x^2 + 0.1791x + 1.048$	0.99
	SnO_2 + 1L FAU	$y = 0.0007x^3 - 0.0142x^2 + 0.0842x + 1.0083$	0.99
	SnO_2 + 1L MFI	$y = 0.0002x^3 - 0.0063x^2 + 0.0706x + 1.0849$	0.99

Table 3-8 Second order polynomial equations fitted to acetone's response curves (see Fig. 3-25) attained for SnO_2 sensors admixed with 10% (wt.) of zeolites Na-A (LTA), H-Y (FAU) and H-ZSM-5 (MFI). The R^2 values attained for each fit have also been provided.

Admixtures	Sensor Type	2nd Order Polynomial Equation	R-Squared Value
Acetone	SnO_2 + 10% (wt.) LTA	$y = 0.0334x^2 + 0.1327x + 3.163$	0.99
	SnO_2 + 10% (wt.) MFI	$y = 0.0038x^2 + 0.0513x + 1.0293$	0.99
	SnO_2 + 10% (wt.) FAU	$y = 0.0045x^2 + 0.0473x + 0.9659$	0.99

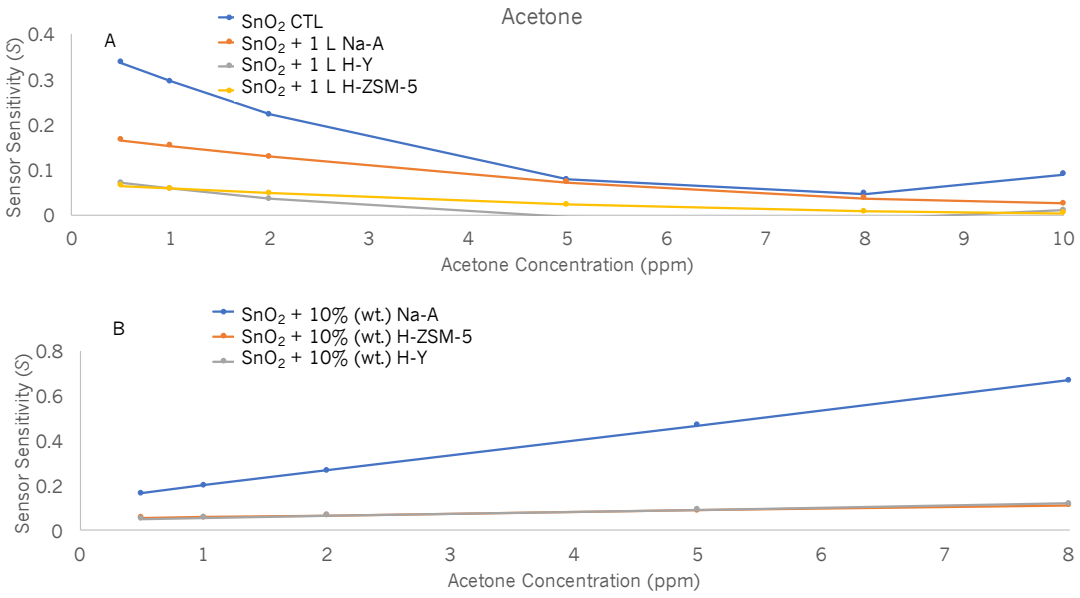

Figure 3-28 Sensor sensitivity curves to acetone gas for (A) SnO_2 sensors overlaid with one layer of zeolites Na-A, H-Y and H-ZSM-5 and (B) SnO_2 sensors admixed with 10% (wt.) of zeolites Na-A, H-ZSM-5 and H-Y.

As can be seen in Fig. 3-28 above, the sensitivity of the zeolite-overlaid sensors decreased with increasing concentration of acetone gas. In regard to the zeolite-admixed sensors, those mixed with 10% (wt.) of zeolites H-ZSM-5 and H-Y displayed approximately a constant sensitivity value toward acetone, irrespective of increments in concentration. The sensitivity of the sensor admixed with 10% (wt.) Na-A increased with concentration of acetone. As such, the latter sensors would be more promising if they were to be used in practical applications as the sensor responses increased linearly with concentration when admixed with zeolites H-ZSM-5 and H-Y and sensor sensitivity increased progressively upon exposure to higher concentrations of acetone with sensor 'SnO_2 + 10% Na-A', showing a higher dynamic range.

3.5.4.4 Sensor Exposure to Toluene

Sensors that contained zeolite H-ZSM-5 were especially responsive to toluene gas irrespective of whether it was incorporated as an admixture or an overlayer.

Given that the larger kinetic diameter of toluene would affect its diffusion through this zeolite's pores, it is likely that sensor sensitivity is the result of hydrophobic affinity between zeolite H-ZSM-5 and toluene gas.[22] This was supported by these sensors' inability to fully return to baseline following each pulse of toluene. This could mean that the gas failed to fully desorb off the sensing material. This effect was less pronounced at 450 °C (Fig. 3-29). The sensors provided a response to low gas concentrations i.e. 2.5 ppm at all temperatures. When supplied with 10 ppm of toluene gas at 400 °C, the sensor overlaid with three depositions of zeolite H-ZSM-5 gave a response R_0/R = ~5, providing a 1.8-fold enhancement in response over the unmodified SnO_2 sensor. When supplied with 50 ppm of toluene gas, the same sensor provided a 2.9-fold enhancement in sensor response over the control SnO_2 sensor. At 450 °C, the response of 'SnO_2 + 3 L H-ZSM-5' sensor towards 50 ppm of gas was enhanced 3.8-fold over that of the control. These sensors did not reach steady state, potentially due to toluene's lagged diffusion into the sensitive layer and because the molecule may not be as easily catalysed to CO_2 and water vapour. 'SnO_2 + 1 L Na-A' and 'SnO_2 + 10% (wt.) Na-A' sensors, however, responded in less than 4 seconds and reached steady state (Fig. 3-29). The enhancements obtained when compared to the control sensor were, nevertheless, moderate. For instance, sensor 'SnO_2 + 1 L Na-A' provided a 1.3-fold enhancement in response over the control sensor.

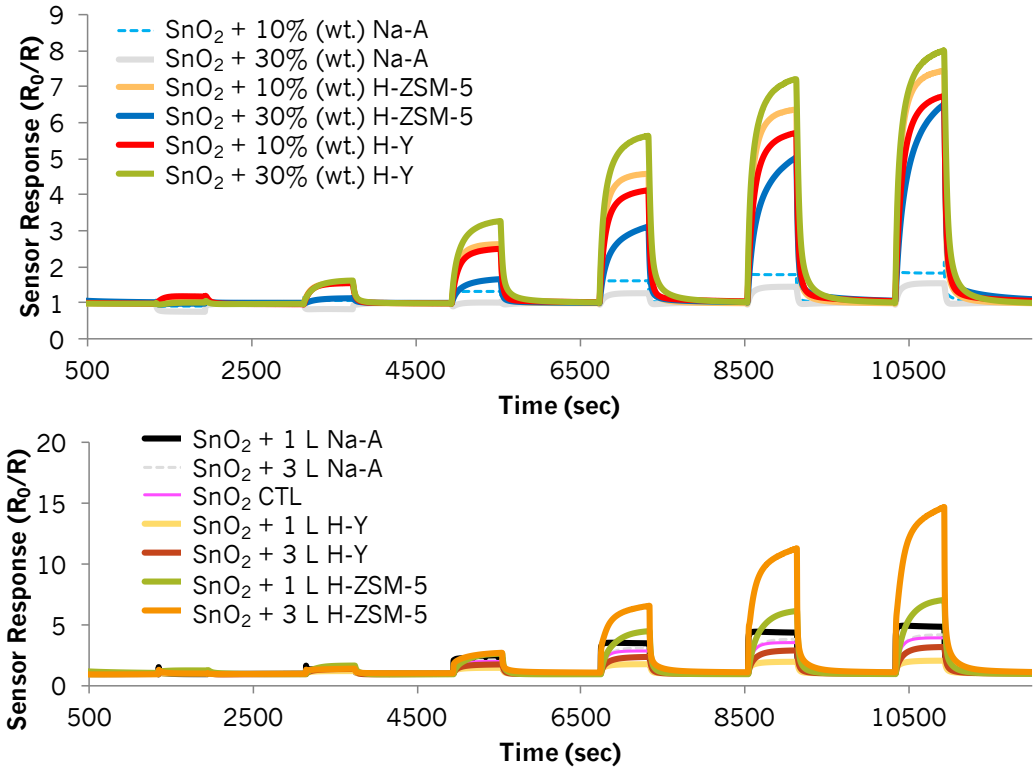

Figure 3-29 Zeolite-overlaid and zeolite-admixed SnO_2 sensor exposure to 2.5 ppm, 5 ppm, 10 ppm, 25 ppm, 40 ppm and 50 ppm toluene gas at 450 °C.

Sensors coated with zeolite H-Y were less responsive to toluene gas than the control sensor. Sensor 'SnO_2 + 1 L H-Y' showed faster sensor responses than that containing three layers of zeolite H-Y. This could be directly related to the thickness of the zeolite film, delaying its access to the underlying SnO_2 material. It is possible that catalytic reactions at the sensor surface led to reaction products to which SnO_2 was less responsive.

The admixed sensors were also very responsive to toluene gas, with each sensor providing a distinctive response. At 400 °C, the response trends did not match those seen in the zeolite-overlaid sensors. Sensors modified with zeolite H-ZSM-5 were, once again, consistently responsive to toluene gas. 'SnO_2 + 30% (wt.) H-ZSM-5' was more responsive to toluene than its 10% (wt.) counterpart at concentrations above 25 ppm. The sensor that contained 10% (wt.) zeolite H-Y was consistently more responsive to toluene gas than the sensor modified by 30% (wt.) zeolite H-Y. The latter failed to return to baseline following each gas pulse. Sensors containing Na-A zeolite were unresponsive to toluene at this temperature. At 450 °C, sensors modified with zeolite Na-A were sensitive to the gas, leading to very fast response times, reaching steady state. The remaining sensors continued to show shark-fin shapes.

When the sensors modified with Na-A zeolite were exposed to toluene, their responses were very moderately improved when compared to those obtained with the control sensor. The response of the sensor containing one film deposition of zeolite Na-A improved by a factor of ~1.3 and the one with three depositions by a factor of 1.1. The hydrophilicity of zeolite Na-A resulted in poor affinity towards toluene and the larger kinetic diameter of toluene prevented its straightforward access to the underlying sensing material. Having only one film deposition of zeolite mildly improved the sensor responses towards toluene, the response time of which was much faster than that obtained with a thicker filtering layer, as expected.

Second order polynomial equations were fitted to the response curves for toluene (Fig. 3-24 and Fig. 3-25 above). The polynomial equations have been tabulated in Tables 3-9 (zeolite-overlaid sensors) and 3-10 (zeolite-admixed sensors). Sensitivity curves of the sensors towards toluene are presented in Fig. 3-30 below.

Table 3-9 Second order polynomial equations fitted to toluene's response curves (see Fig. 3-24) attained for overlaid SnO_2 sensors coated with one layer of zeolites Na-A (LTA), H-Y (FAU) and H-ZSM-5 (MFI). The R^2 values attained for each fit have also been provided.

Overlayers	Sensor Type	2nd Order Polynomial Equation	R-Squared Value
Toluene	SnO_2 CTL	$y = -0.0007x^2 + 0.0913x + 0.9616$	0.99
	SnO_2 + 1L LTA	$y = -0.0009x^2 + 0.1165x + 1.1623$	0.99
	SnO_2 + 1L FAU	$y = -0.0004x^2 + 0.0419x + 1.0167$	0.98
	SnO_2 + 1L MFI	$y = -0.0008x^2 + 0.1707x + 0.8845$	0.99

Table 3-10 Second order polynomial equations fitted to toluene's response curves (see Fig. 3-25) attained for SnO_2 sensors admixed with 10% (wt.) of zeolites Na-A (LTA), H-Y (FAU) and H-ZSM-5 (MFI). The R^2 values attained for each fit have also been provided.

Admixture	Sensor Type	2nd Order Polynomial Equation	R-Squared Value
Toluene	SnO_2 + 10% (wt.) LTA	$y = -0.0003x^2 + 0.0273x + 1.0219$	0.99
	SnO_2 + 10% (wt.) MFI	$y = -0.0008x^2 + 0.1624x + 0.7945$	0.99
	SnO_2 + 10% (wt.) FAU	$y = -0.0007x^2 + 0.1443x + 0.9105$	0.99

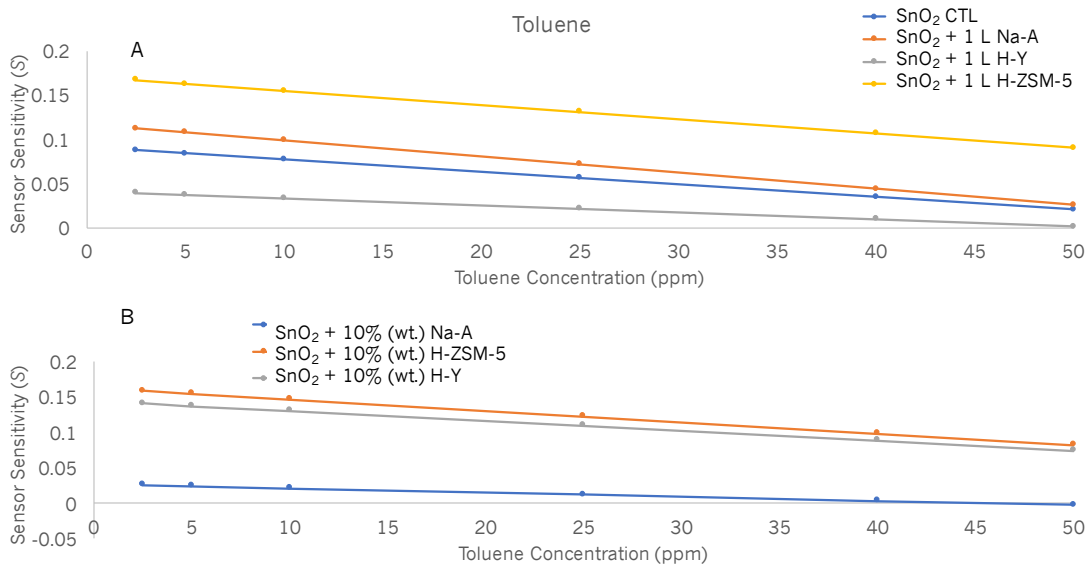

Figure 3-30 Sensor sensitivity curves to toluene gas for (A) SnO_2 sensors overlaid with one layer of zeolites Na-A, H-Y and H-ZSM-5 and (B) SnO_2 sensors admixed with 10% (wt.) of zeolites Na-A, H-ZSM-5 and H-Y.

As can be observed in Fig. 3-30, the sensitivity of all the zeolite-modified sensors decreased with increasing concentrations of the gas. The sensors containing zeolite H-ZSM-5 were more sensitive to toluene than those containing Na-A, which are promising results if these sensors had to be used as part of an e-nose to identify different gases. For instance, in previous tests, sensors containing zeolite Na-A were found to be more sensitive to ethanol and acetone than those containing zeolite H-ZSM-5.

3.5.4.5 Sensor Exposure to Carbon Monoxide

Zeolite-modified sensors were essentially unresponsive to CO gas (kinetic diameter 3.76 Å) from 50 ppm to 250 ppm. When exposing both zeolite-admixed and overlaid sensors to 400 ppm and 500 ppm of CO, the sensors began to show a response (Fig. 3-31). Zeolite-admixed sensors provided fast responses upon exposure to the gas, suggesting that CO gas was converted to CO_2. Sensors overlaid with zeolites were slightly more responsive to the gas than the admixed ones. It is possible that this was due to a greater catalytic effect of the zeolites when they were coated over the base material. As can be seen in Figure 3-31 the relative response of the control sensor towards 400 ppm and 500 ppm of CO gas was considerably low (R_0/R = ~1.3).

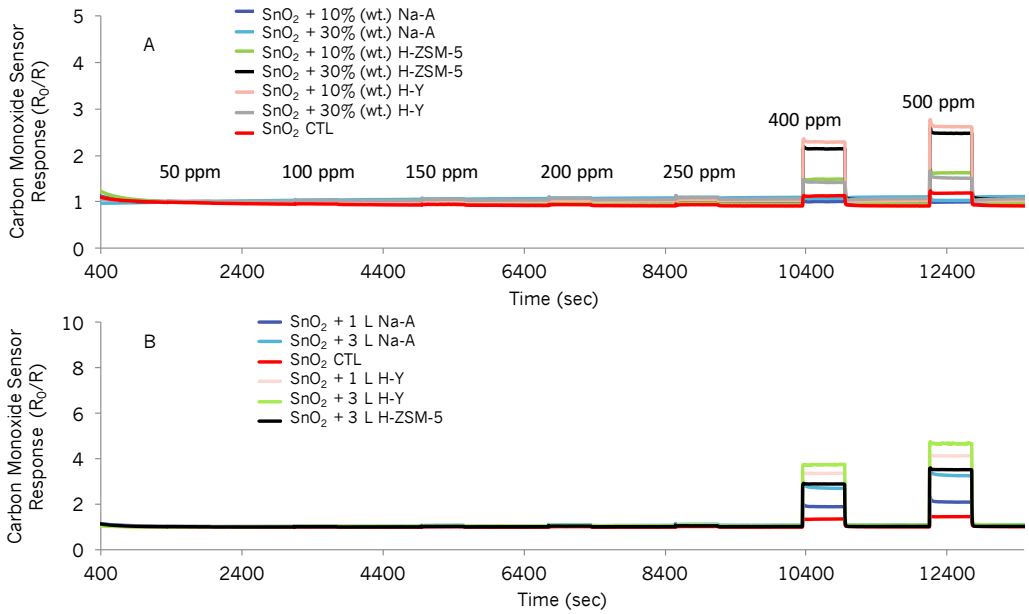

Figure 3-31 Sensor responses to different concentrations of carbon monoxide gas at 450 °C. The top figure illustrates the zeolite-admixed sensor responses to the gas and the bottom figure that of the zeolite-overlaid sensor responses to CO gas.

Once again, it was interesting to see that the microstructure of the sensors affected gas responses and sensitivity greatly: while the sensors coated with zeolite Na-A responded to the gas, those admixed with the same zeolite did not.

Ghosh et al. [80] provided a thorough account of the detection of CO with SnO_2-based sensors. Other studies have detected lower concentrations of the gas at levels of, for instance, 30 ppm. Nevertheless, achieving recovery times in the order of seconds has previously been reported as a challenge. The results presented here are promising as very fast response and recovery times were attained. Having said this, further tests ought to be carried out in order to improve CO gas detection at lower gas concentrations.

3.5.4.6 Sensor Exposure to Water Vapour

The sensors were exposed to water vapour from 250 – 500 °C. The relative humidity RH (%) was progressively increased from 5 – 50% (Fig. 3-32). All zeolite-overlaid sensors saturated quickly and presented an increase in resistance for the duration of the water vapour pulse. Although the reason why the sensors appeared to undergo multistep reactions is unclear, it is thought it could be the result of water vapour preventing any further adsorption of molecular oxygen on the sensor surface; a progressive decrease of electron transfer back to the SnO_2 material could potentially lead to this behaviour.

It is also possible that the different chemisorbed species at the sensor surface, affect the interaction with water molecules and consequently the conduction of the system.[67] The strange peak shapes were noticeable at all the RHs investigated. For the majority of the sensors there was a conservative increment in sensor responses with higher RH, but this enhancement was more prominent in the sensor containing three coatings of zeolite Na-A, due to its hydrophilic nature. All the zeolite-containing sensors were more responsive to water vapour than the unmodified sensor.

Zeolite-admixed sensors also provided higher sensing responses to water vapour than the unmodified SnO_2 sensor, which exhibited similar responses to water vapour at 400 °C and 450 °C. The zeolite-admixed sensors that contained higher zeolite concentrations were less responsive to water vapour than their counterparts. Once again, there was a slight increase in responsiveness towards water vapour as the RH (%) was incremented. Water sensitivity was almost suppressed with 'SnO_2 + 30% (wt.) H-Y' between 250 – 350 °C. The most responsive sensor to 25 % RH at 450 °C was that admixed with 10% (wt.) H-ZSM-5. SEM images revealed that zeolite Na-A was poorly visible in the mixtures and it is possible that the microstructure and smaller particle size of zeolite H-ZSM-5, when compared to those of zeolite Na-A, led to more surface-reactive sites for water to interact with and to pass through the pores and inter-crystalline cavities, displacing the chemisorbed oxygen and leading to the specified decrease in resistance.[20] With the exception of sensors mixed with 30% (wt.) H-Y and 10% (wt.) H-ZSM-5, which gave distinct sensor responses, the rest behaved very similarly.

3.5.4.7 Ethane Detection in the Presence of Humid Air

All the sensors investigated behaved as n-type upon exposure to a mixture of ethane and humid air. Exposing the zeolite-overlaid sensors to a mixture of 50 ppm ethane and 10% RH, followed by a pulse of 50 ppm ethane with humid air corresponding to 25% RH illustrated the sensors' selectivity towards water vapour and suppression towards the detection of ethane gas (Fig. 3-33). The resistive behaviour initially encountered upon exposure to just ethane in dry air was no longer visible and the sensors exhibited n-type behaviour, with peak shapes resembling those attained with exposure to just humid air.

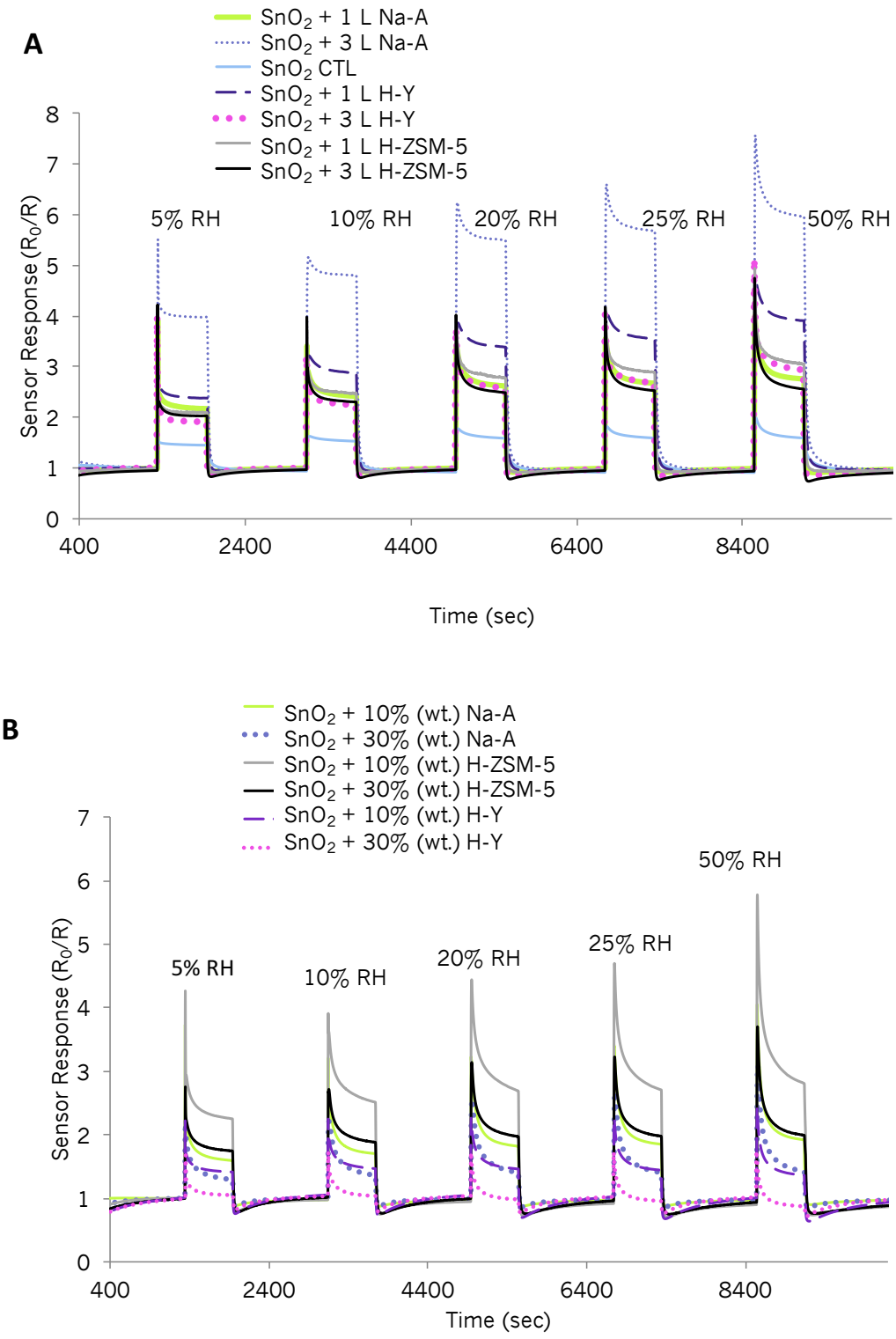

Figure 3-32 (A) Overlaid sensor exposure to humid air corresponding to 5% - 50% RH. (B) Admixed sensor exposure to humid air corresponding to 5% - 50% RH. All tests were performed at 350 °C.

Although at 350 °C the zeolite-overlaid sensors' responses to 50 ppm ethane gas were practically nullified ($R/R_0 < 1.5$ as displayed in Fig. 3-22), the resistance of

the sensors increased when they were supplied with ethane gas. In a humidity/ethane environment, however, water vapour molecules compete with ethane molecules, preventing ethane from accessing the sensitive layer of the sensor. This was potentially the reason why all sensors tended to display an increase in conductivity when exposed to the ethane/water vapour mixture. Nevertheless, the interference introduced by ethane caused the response towards humid air to be partially diminished. This is in line with what other studies have reported in the literature when investigating water interference in MOS sensor systems.[30]

Similarly, when admixed sensors were exposed to ethane gas in the presence of water vapour at 350 °C, the sensor responses could mostly be attributed to water vapour as, once again, conductive responses were attained. It is thought that the peak shapes decreased during the duration of the gas pulse due to quick saturation of the sensor surface and thus limited electron transfer back into the metal oxide system. The responses given by sensors containing 10% (wt.) and 30% (wt.) of zeolite Na-A, however, provided different peak shapes and sensor responsiveness was slightly enhanced, when compared to the results obtained with the supply of just water vapour. This could mean that new reaction products were formed, to which sensor 'SnO_2 + 10% (wt.) Na-A' was particularly responsive (R_0/R ~5.6) when mixed with 50 ppm ethane and 10% RH.

Sensor 'SnO_2 + 10% (wt.) H-ZSM-5' was particularly responsive to just water vapour (Fig. 3-32), but its response decreased upon exposure to a mixture of ethane and humid air (Fig. 3-33). It is possible that the pores of zeolite H-ZSM-5 saturate quicker in the presence of water and a larger molecule like ethane. SnO_2 admixed with zeolite H-Y suppressed the response to just water vapour but the conductive response of the sensor was seen to increase slightly with the introduction of ethane gas. Given that as part of the combustion process of ethane, water is produced, it is possible that this enhancement in sensor response is a result of more water molecules being adsorbed into the pores of the zeolite which may, in turn, block the direct interaction of ethane with the zeolite, supressing the resistive response attained when exposed to just ethane. However, this is unlikely as when supplied with 50% RH the response of the SnO_2 sensor admixed with 30% zeolite H-Y diminished further. Therefore, an alternative explanation is that a different reaction product may be formed, leading to the observed enhancement in sensor response.

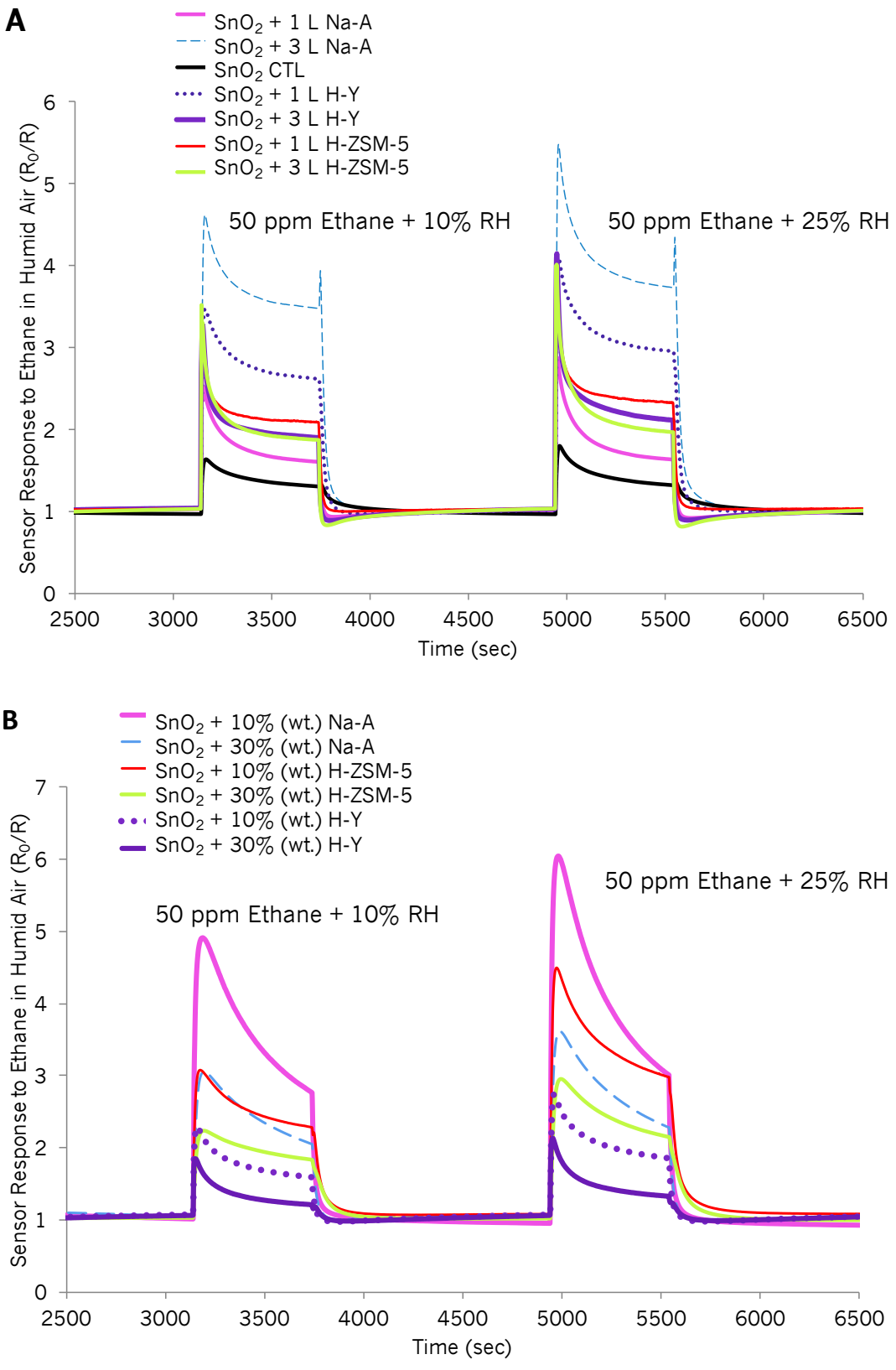

Figure 3-33 (A) zeolite-overlaid sensor exposure to 50 ppm ethane in 10% RH (first gas pulse) and 25% RH (second gas pulse). (B) Zeolite-admixed sensor exposure to 50 ppm ethane in 10% RH (first gas pulse) and 25%RH (second gas pulse). All tests were performed at 350 °C.

It must be acknowledged that at first glance it could seem that the strange peak shapes could be the result of issues with the flow system. That is, the MFCs and SVs, could lead to pressure build up in the system and consequently affect the sensor responses. Nevertheless, this option was discarded as tests with other liquids were tested in the rig and this behaviour was not observed. In order to evaluate this further, tests were carried out using only MFCs 1, 4 and 5 and SV 2 (refer to Fig. 2-6 in Chapter 2) to see whether this behaviour was also observed. The results supported the convention that multistep reactions were taking place on the sensor and were therefore the explanation for the odd peak shapes observed.

Note that summary tables including the sensor responses towards most gases are presented in Tables 8-1 to 8-4 in the Appendix.

3.6 Summary of Results

The modification of an SnO_2 control sensor by zeolite incorporation generally induced great improvements in the performance characteristics of the sensors.

SnO_2 sensors admixed with zeolites were found to be great candidates for the detection of ethane and butane, providing enhanced sensor responses over those seen in zeolite-overlaid sensors. Sensor 'SnO_2 10% (wt.) Na-A' provided particularly promising results towards ethane across the whole range of temperatures tested. The same sensor was very responsive to butane at 350 °C ($R/R_{0\ (100\ ppm\ ethane)}$ = 6.5) and those mixed with zeolite H-ZSM-5 were more responsive to the gas at higher operating temperatures i.e. 450 °C. Sensors overlaid with zeolite H-ZSM-5 were responsive to butane but displayed variability among repeat tests at 450 °C. The sensor coated with three layers of zeolite H-Y showed promise for butane detection at the same temperature ($R_0/R_{(100\ ppm\ butane)}$ = ~5.2). Sensors modified with zeolite H-ZSM-5 were responsive to propane gas at 450 °C – but the responses of sensors worsened at lower operating temperatures.

Sensor exposure to straight-chain alkanes potentially led to reaction processes that converted the source gas into an oxidising one, resulting in an n- to p-type switch. This behaviour was more commonly seen in the zeolite-admixed sensors.

The set of sensors fabricated was successful in discriminating among gases that were very similar in molecular structure. It is thought that gas discrimination was achieved as a result of the different frameworks and pore structures of the zeolites chosen, as well as their different hydrophobic/hydrophilic characters and microstructure, which is in line with what other groups have reported in the literature.

The sensors displayed other features sought in gas sensing such as stability and relatively fast response and recovery times, on occasion improved over the response and recovery times of the control sensing material. Some sensors responded linearly as the gas concentrations of some gases were raised e.g. 'SnO_2 + 10% (wt.) H-ZSM-5' and 'SnO_2 + 10% (wt.) H-Y' upon exposure to acetone. The sensitivity of some sensors was seen to increase upon exposure to some gases e.g. 'SnO_2 + 10% (wt.) H-ZSM-5' and 'SnO_2 + 10% (wt.) H-Y' upon exposure to IPA. Some sensors' sensitivity was also found to decrease when exposed to some gases as the concentrations were raised e.g. zeolite-admixed and overlaid sensors upon exposure to ethanol. Sensor sensitivity decreased slightly upon exposure to increased concentrations of toluene gas. When the sensitivity was constant with gas concentration increments or when it increased with gas concentration increments it means that sensors could potentially be used in practical applications both qualitatively and quantitatively.

Temperature modulation of sensors could prove useful to assist gas discrimination in future. Nevertheless, sensor variability should be better controlled in the lower temperature range. It was observed that when a sensor was highly responsive to a gas, particularly at higher supplied concentrations and at lower operating temperatures i.e. 300 °C and 350 °C, great variability among repeat tests was observed.

It is also noteworthy that the sensors were responsive to trace concentrations of test gases, showing great promise for practical applications. Toluene, for instance, was detected well below its threatening-to-life level of 200 ppm specified by the CDC. Acetone and ethanol were detected at concentrations as low as 5 ppm in the case of ethanol and <1 ppm in the case of acetone. Nevertheless, for practical applications they ought to be reliably detected beyond these concentration levels. This enabled a better understanding of how the sensors can be strategically designed to respond to some molecules and less so to others.

Chapter 4 details the effects of incorporating zeolites Na-A and H-ZSM-5 in the form of admixtures to Cr_2O_3, a p-type semiconductor. This was carried out with the aim of providing new data as it was found that these combinations have not yet been reported in the literature. Also, it was of interest to the author to find out whether p-type systems would later introduce a new platform to provide gas discrimination when combined with other n-type materials, which is further discussed in Chapter 6 of this thesis.

4. P-type Zeolite Modified MOS Gas Sensors

This chapter details the results obtained when modifying a p-type semiconducting material, namely Cr_2O_3, with different zeolite combinations. Several of the zeolite–oxide systems developed showed little promise for gas sensing applications. Thus, only the most noteworthy results have been reported, such as those obtained from the modification of Cr_2O_3 sensors with zeolites H-ZSM-5 and Na-A as admixtures and from the modification of Cr_2O_3 with zeolite H-Y as overlayers. The Cr_2O_3-based sensors were exposed to target gases in dry air and, where possible, they were later exposed to the same gases in humid conditions. This chapter evaluates:

- Different zeolite combinations with a p-type metal oxide semiconductor material for gas sensing applications.
- The effects that zeolite incorporation imparts on the sensor responses, sensitivity and selectivity, relative to the control sensor.
- The influence of humidity on sensor performance.

The Chapter has been organised such that: **(1)** Preliminary gas-sensing tests that were performed on unmodified Cr_2O_3 sensors are presented first. These tests helped in selecting the optimal fabrication conditions for future zeolite-modified Cr_2O_3 sensors. This is followed by the gas-sensing results obtained with exposure of the unmodified Cr_2O_3 sensor towards five gases, explored to evaluate whether the sensor was, indeed, responsive to a range of gases of interest. **(2)** The chapter then moves on to describe physicochemical characterisation techniques performed on the control sensor and those modified by admixture of zeolite H-ZSM-5, followed by the pertinent gas-sensing results. **(3)** Then, the physicochemical characterisation techniques of the sensor modified by admixture of zeolite Na-A are described, followed by the gas-sensing results. **(4)** Finally, the physicochemical characterisation techniques of the sensor modified by overlayer of zeolite H-Y are described, followed by the gas-sensing results.

4.1 Introduction

P-type metal oxide semiconductors display different surface characteristics to n-type systems. First of all, the adsorption of oxygen on multi-valent transition metals has been reported to be larger than in n-type systems; the low stability and the multiple oxidation states of p-type transition metal oxides leads to redox reactions that favour oxygen adsorption.[107] Further, as elucidated in Chapter 1, conduction changes that occur as a result of reactions between a gas and adsorbed oxygen species and/or water vapour are also different in n-type and p-type systems. In essence, oxygen adsorption on p-type semiconductors leads to the formation of a hole accumulation layer (HAL)

that results in a decrease in sensor resistance, due to the concentration of majority free charge carriers – holes – increasing as electrons are extracted from the bulk of the material. Conversely, oxygen adsorption in n-type systems leads to the formation of an electron depletion layer (EDL) that serves to increase the resistance of the sensor. It therefore follows that these differences will lead to distinctive interactions with test gases.

P-type systems are reported to exhibit little sensitivity to humid atmospheres, which is a sought attribute, particularly in the pursuit of gas-detection systems that operate reliably in real-world applications. Nevertheless, p-type MOS are known to be poorly sensitive to inflammable gases when compared to n-type semiconductors.[107] Hübner et al. [282] suggested that the signal of a p-type MOS to a gas equates to the square root of the signal of an n-type MOS towards the same gas when the morphologies of the materials are identical. For this reason, and as highlighted by Kim et al. [107], trace gas detection with p-type semiconductors requires finding means of optimising sensor responses. In the same review by Kim et al. [107] it was suggested that p-type systems are, in fact, excellent candidates for gas sensing and that great sensitivity and selectivity can be achieved using approaches such as morphological design of nanostructures, chemical and electronic sensitisation methods with catalyst incorporation and dopant control, and by fabricating p-n junction oxide sensors. Furthermore, the loading of p-type semiconductors such as NiO onto SnO_2 nanostructures was found to provide humidity resistant sensors. In addition to this, other research groups have explored the incorporation of zeolites to enhance the performance of p-type semiconductors as gas sensors.[25–27,31,32,139,297]

Cr_2O_3 has been chosen as the test p-type material in this Chapter. It offers attractive features for gas sensing due to its catalytic properties.[298,299] It has previously been used in catalysis for the dehydrogenation and dehydration of alcohol, methanol synthesis and oxidation of SO_2.[11] It has also been used in the field of gas sensing by different research groups, as follows below.

Ma et al. [211] synthesised mono-dispersed Cr_2O_3 nanoparticle microspheres for toluene detection with a detection limit of 1 ppm at 170 °C. In the latter study, the sensor did not show cross-sensitivity to benzene and a chlorobenzene. Nevertheless, the tests were not performed in mixed-gas environments and thus the study only highlighted the sensor's potential application as a toluene detector.

Hagen et al. [32] developed screen-printed thick-film Cr_2O_3 on top of a Pt-ZSM-5 layer as a novel arrangement for the detection of hydrocarbon (HC) gases. They showed that when using just an unmodified Cr_2O_3 sensor it displayed sensitivity towards a range of reducing gases. The incorporation of a zeolite layer on top of Cr_2O_3 led to a filtering effect of propene, but the sensor still responded to propane and other reducing gases. However, when the configuration was altered such that the zeolite layer was printed first and then the metal oxide on top, it resulted in selectivity towards HCs and no cross-sensitivity towards other reducing gases like H_2 and CO. Although no clear explanation was provided as to why this behaviour was observed, it was attributed to the interface created between the Cr_2O_3 and the zeolite layers. To the same effect, the group used platinum-doped Na-ZSM-5 thick films over Cr_2O_3 to create sensors that were selective towards HCs (methane, propane and propene) and limited cross-sensitivity towards other gases (H_2, CO, NO and CO_2).[26] In the latter study it was suggested that an interaction occurring between zeolite cations and the oxide directly at the interface of Cr_2O_3/zeolite led to the observed effect.[26]

Our group has previously doped Cr_2O_3 with titanium to form Chromium Titanium Oxide (CTO) gas sensors and later added zeolite modification layers or mixtures to test the ability of sensors to discriminate between molecules holding similar structures.[15,25] Binions et al. [15] incorporated zeolite coatings over CTO to discriminate between ethanol and isopropyl alcohol (IPA) gases. It is known that zeolite incorporation often leads to enhancements in sensor responses in relation to unmodified sensor materials. The contribution to the overall conductivity of the system was assigned to a higher surface area of the sensor microstructure, which was introduced by the zeolites. In turn, this leads to the provision of more surface-reactive sites for gas molecules to interact with, promoting further reaction processes between the gaseous molecules and the sensor systems.[15]

H-Y zeolite cover layers on top of CTO have also been used to promote great enhancements in sensor responses towards a range of HC gases.[297,300] Furthermore, the admixture of CTO with zeolites Beta, Mordenite, H-ZSM-5 and H-Y has also been reported with zeolites.[27] The latter study found that zeolite modification of CTO resulted in great response enhancements, when compared to the conventional CTO sensor upon exposure to ammonia, toluene and ethanol gases.

To the best of our knowledge, no work has been reported that investigates the zeolite modification of Cr_2O_3 with admixtures of zeolites H-ZSM-5 and Na-A or the

incorporation of H-Y filter layers over Cr_2O_3. The following section details initial tests that were carried out on the unmodified Cr_2O_3 sensor.

4.2 Preliminary Gas-Sensing Tests on the Unmodified Cr_2O_3 Sensor

The effects of film thickness on the response of a control Cr_2O_3 sensor were investigated by printing three, five and seven depositions of the material on a sensor substrate of the type described in Chapters 1 and 2. This was carried out to determine if any particular configuration provided enhanced sensor performance.

Although initial tests were performed at 300 °C (section 4.2.1 and 4.2.2), the effects of temperature on sensor responses were also investigated so that the best operating parameters could be chosen for future testing (section 4.2.3). The tests carried out in those three sections were performed on a different rig, 'Sparky', the details of which can be found in Peveler et al. [28].

4.2.1 Effects of Film Thickness on Cr_2O_3 Sensor Responses

Sensors with progressively increased film thicknesses were exposed to two pulses of the same concentration of IPA and toluene gases, (Fig. 4-1 and 4-2, respectively). This test was carried out to understand if sensors were responsive to gases, whether sensor responses were dependent on film thickness and, also, whether a particular sensor was consistently more responsive to test gases. Initial tests were carried out at 300 °C given the beneficial implications of exercising gas detection in the lower temperature range. This was the lowest temperature that could be reached on Sparky rig.

Cr_2O_3 sensors behaved as expected, displaying an increase in resistance upon exposure to reducing gases. Although the surface reactivity of Cr_2O_3 has been poorly investigated in the literature, the general convention is that oxygen will adsorb on the material and act as a surface acceptor.[11] Sensitivity to gases occurs as a result of a variation in the oxygen concentration as it interacts with gaseous molecules.[11]

As can be seen in Fig. 4-1, the sensor printed with five Cr_2O_3 depositions was slightly more responsive to IPA gas than the sensors fabricated with three or seven film depositions. Nevertheless, the responsiveness of the sensors to this gas was conservative ($R/R_0 < \sim 2.5$).

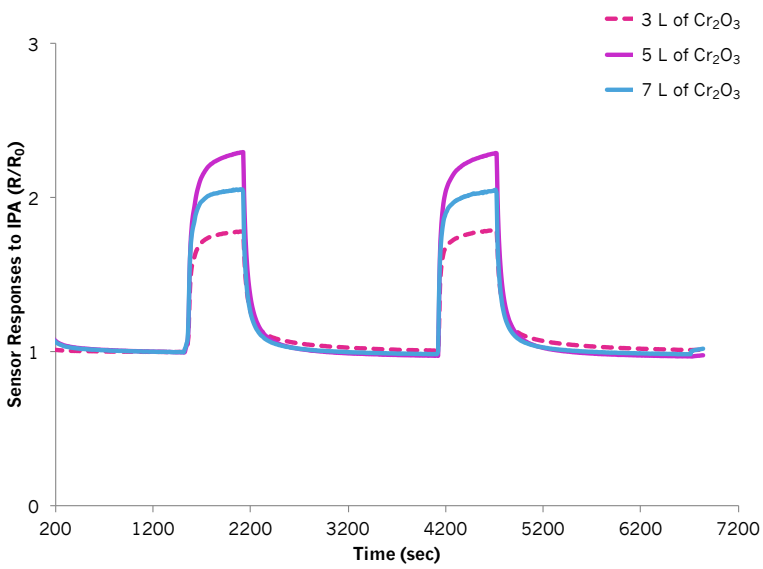

Figure 4-1 Cr_2O_3 sensor responses to two pulses of 50 ppm IPA gas when printed with three, five or seven film depositions at 300 °C.

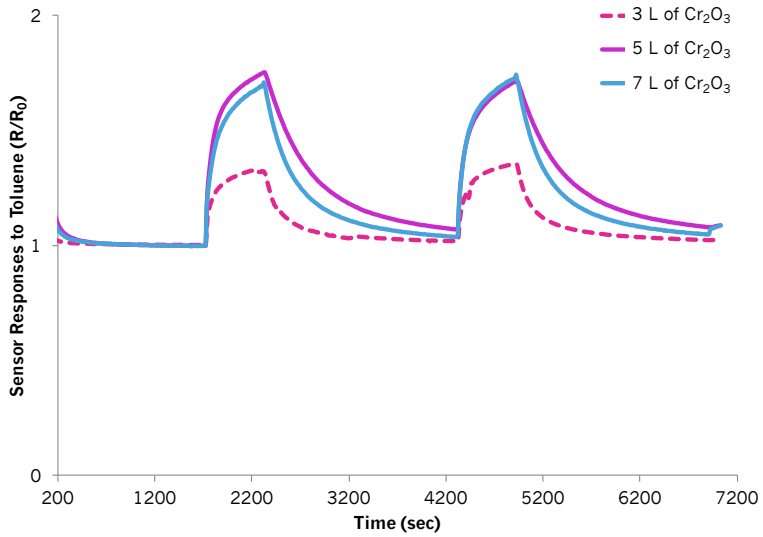

Figure 4-2 Cr_2O_3 sensor responses to two pulses of 45 ppm toluene gas when printed with three, five or seven film depositions at 300 °C.

Similarly, sensor exposure to toluene gas provided sensor responses that were R/R_0 = <2. The sensors printed with five and seven film depositions responded very similarly to toluene. Sensors failed to reach steady state and displayed long sensor recovery times upon exposure to toluene gas. It can be seen that supplying two pulses of the same concentration of a gas provided repeatable results. Further repeat tests were not carried out at this stage.

Similarities in the response magnitudes of sensors with different film thicknesses have been reported in the literature, although mostly with thin SnO_2 films.[7] Du et al. [132] reported that a SnO_2 sensor's response to carbon monoxide (CO) saw a sensitivity maximum at a film thickness of 25 Å and the sensor response values corresponding to film thicknesses immediately above or below 25 Å were very similar. They reported that the response versus film thickness relationship provided a bell-shaped curve. Further film thicknesses should be investigated here to better understand the relationship with the sensor responses.

It was noticed that during the screen-printing process it became difficult to get full coverage of the sensor surface with the material ink beyond five film depositions. This could suggest that the actual thickness of the sensors was not that dissimilar, leading to comparable response patterns between sensors. This was investigated further with cross-section SEM imaging (Fig. 4.3).

As can be seen in the SEM micrographs (Fig. 4-3), the sensing layers looked very different in that the sensors containing three and five depositions had a crumbly appearance, whereas the one with seven layers exhibited a very defined and solid structure and thickness. It was evident that more depositions did, indeed, lead to an increase in film thickness. Every layer corresponded to ~10 μm.

For the purposes of this study, it was noteworthy at this stage that unmodified Cr_2O_3 sensors displayed sensitivity to both test gases. With IPA gas exposure, it seemed that above and below a certain thickness i.e. ~50 μm, the sensor responsiveness decreased slightly. This is in line with what other studies have reported in the literature.[7] In the case of toluene exposure, the results suggest that above a certain thickness, sensor responsiveness was unaffected by the thickness of the sensitive layer. Work reported by Montmeat et al. [143] showed that the effect of film thickness on sensor responses was also gas specific.

While the results reported in this thesis suggest that the sensor responses were, indeed, gas-dependent, batch to batch variation ought to be studied, as well as additional film thicknesses and sensor exposure to other gases. This would perhaps enable one to draw more informed conclusions on the effects of film thickness on the sensor responses of Cr_2O_3 sensors.

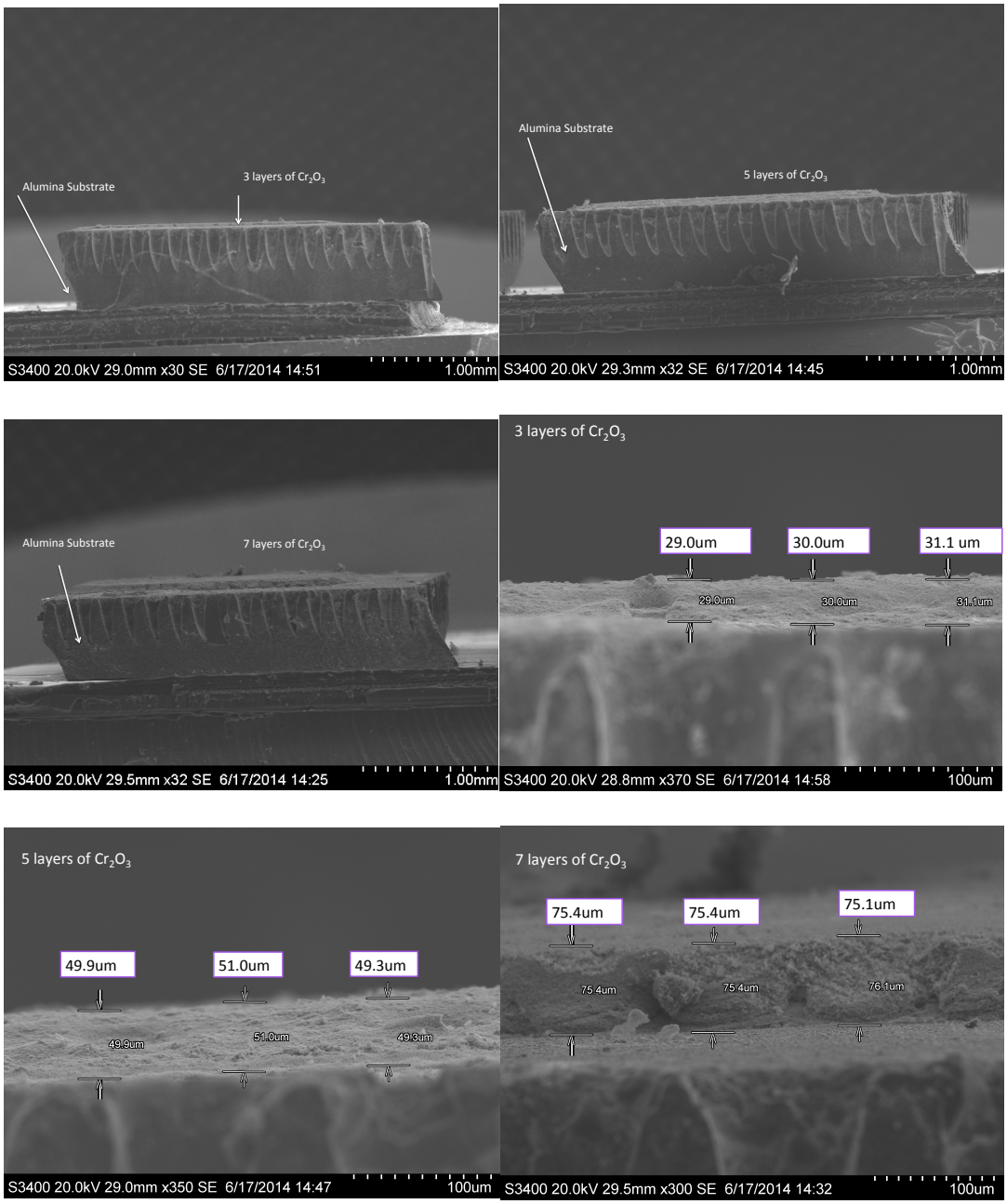

Figure 4-3 Cross-section SEM imaging of Cr_2O_3 sensors with three, five and seven film depositions.

4.2.2 Effects of Film Thickness on the Kinetics of Cr_2O_3 Sensor Responses

Exposure to toluene gas resulted in shorter sensor response times in the sensor with five depositions of Cr_2O_3 (Table 4-1). This was also the sensor that took a longer time to recover upon exposure to the gas. Long response and recovery times were also noted with toluene exposure in the n-type systems studied in Chapter 3. The sensor fabricated with seven depositions of Cr_2O_3 exhibited longer response times upon exposure to toluene, yet it was the sensor that responded more quickly upon exposure to IPA gas. The recovery times were generally very long when exposed to toluene (~ 11

minutes for the 3-layered sensor and >19 minutes in the 5-layered and 7-layered sensors) and much longer than other values reported in the literature, which are ~15 seconds to 1 ppm of toluene,[272] 39 seconds to 50 ppm,[301] and 3 minutes upon exposure to 500 ppm.[247] The sensor with a thinner film had the smallest sensor response magnitude towards toluene (refer to Fig. 4-2) and was the one to recover more quickly.

Table 4-1 Response and recovery times of Cr_2O_3 sensors made with different film thicknesses upon exposure to toluene and isopropyl alcohol (IPA) gases.

		Response & Recovery Times (sec) According to Sensor Film Thickness		
Gas Type		3 Layers Cr_2O_3	5 Layers Cr_2O_3	7 Layers Cr_2O_3
45 ppm Toluene	T_{90}	349	289	389
	T_{10}	719	1799	1169
50 ppm IPA	T_{90}	169	199	149
	T_{10}	379	99	189

Conversely, sensor exposure to IPA resulted in faster response times, in relation to toluene exposure. Sensors with three and five Cr_2O_3 film depositions took longer times to respond than the sensor with seven film depositions. The sensor with five film depositions took less time to recover (<2 minutes) upon exposure to IPA, in relation to the other two sensors.

It was expected that with thicker films the response times would increase due to a longer time taken by the gas molecules to diffuse down the sensitive layers. Having said this, it was suggested by Korotcenkov [101] that with thicker films it is often possible to get cracking in the structure, which leads to shorter response times as a result of improved gas permeability. Further, because the length and depth of the cracks is complex to control, it may directly affect the response magnitudes. Whilst cracking in the sensing layer would explain the faster response times seen in the system with seven film depositions when exposed to IPA, it would be expected that desorption in such a system would also be faster, but it was not. In this study, no trends or conclusions could be identified as the sensors' thickness was increased.

To summarise, sensors with different Cr_2O_3 thicknesses showed different behaviours upon exposure to IPA and toluene gases and it became difficult to identify any clear trends both in sensor responses or response kinetics as a function of film thickness. It follows that additional film thicknesses ought to be explored as well as exposure to more gases. Note that the effect of slow sensor recovery at low operating temperatures

was also seen in the n-type systems discussed in Chapter 3. For this reason, it was investigated whether these factors could be minimised at higher operating temperatures. Furthermore, it was expected that zeolite incorporation would enhance sensor responses in relation to the control sensor and would potentially fasten the response and recovery times, as was the case for some zeolite-modified sensors fabricated and discussed in Chapter 3 and in other systems reported in the literature.[30]

The sensor with five film depositions of Cr_2O_3 was chosen to carry out further tests as it was considered that, although it displayed unfavourable sensor response kinetics, they would be improved by the incorporation of zeolite materials. Furthermore, it was more responsive to IPA gas than the other two sensors and it was equally as responsive to toluene than the sensor with seven depositions. Despite the sensor showing long recovery times upon exposure to toluene, some studies indicate that gas discrimination is possible just after a few seconds of gas exposure, so an alarm could be given in practical applications.[167] A quick step could be introduced to desorb any remaining gas from the sensor surface by heating the sensor to higher temperatures.[39] The sensor with seven depositions was discarded as an option due to poorer sensor responsiveness to IPA and due to very long response times attained with toluene exposure. In regards to the sensor with three film depositions, it provided lower sensor responses to both gases with very long response times towards toluene gas. Furthermore, given that the sensors in Chapter 3 were also fabricated with five film depositions of the base material it was considered it would be better for comparison purposes.

4.2.3 Evaluating the Effects of Temperature on Cr_2O_3 Sensor Responses

In order to study the effects of temperature on sensor responses, the sensor fabricated with five Cr_2O_3 depositions was exposed to 90 ppm ethanol and to 45 ppm toluene (Fig. 4-4) at temperatures in the range of 300 – 400 °C. As can be seen in the figure, the sensor responses increased only slightly with ethanol exposure as the temperatures were lowered. Nevertheless, the sensor responses seemed generally unaffected by temperature with toluene exposure. The results correspond to two repeat pulses for each gas at each temperature.

The response magnitude of p-type materials typically decreases with increasing temperature.[81] Nevertheless, bell-shaped response vs. temperature curves have been reported in some studies.[31,139,208,211,302] Other studies such as Suryawanshi et al. [212]

looked at the modification of Cr_2O_3 with activated Fe_2O_3, which saw different sensitivity maxima with exposure to different gases over temperatures in the 200 – 500 °C range.

The effects on response and recovery times were also assessed as a function of temperature. As shown in Table 4-2 below, response and recovery times were shortened when raising the sensor's temperature, as expected. Heating the sensor temperature will increase the thermal energy of the system, accelerating the transport of charge carriers and leading to increased reactivity. The gas molecules' penetration depth will be shorter and this, in turn, will lead to straightforward gas desorption.[128,303] Furthermore, and as described by Betty and Choudhury [117], the surface adsorption of oxygen is influenced by the operating temperature. The lower responses seen at higher temperatures, i.e. 400 °C, are the result of fewer oxygen species adsorbing at and desorbing off the surface. As such, fewer oxygen species are available to interact with gaseous molecules and the reactions occur at a fast-enough rate that they do not produce a sizeable resistance change with the introduction of a gas. The sensitivity maximum seen at a particular temperature is dependent on the type of gas supplied and also on concentration.[118] The latter study describes temperature and concentration distributions via a rate equation approach. They showed that the sensitivity maximum at a certain temperature is dependent on the strength of adsorption of the analyte gas on the material surface and on the kinetic barrier or activation energy that needs to be overcome to induce a combustion reaction at the surface. They suggested that with higher analyte concentrations the reaction threshold with oxygen and the strength of adsorption of test gas is reduced.

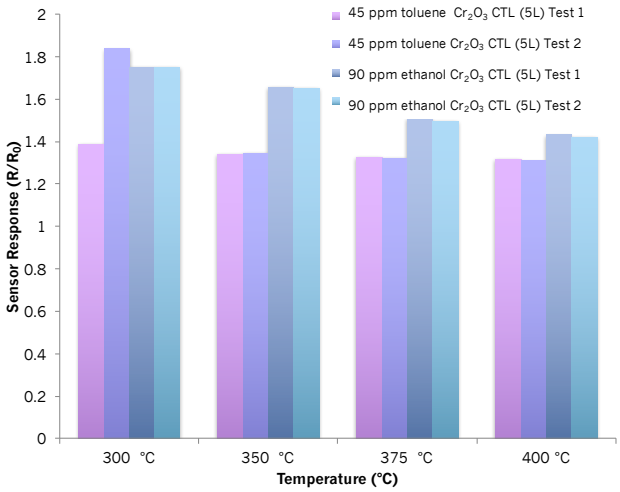

Figure 4-4 Sensor responses of five-layered Cr_2O_3 sensors to 45 ppm toluene and to 90 ppm ethanol as a function of temperature. Two pulses of the same concentration of ethanol were supplied to the sensors during a test.

Table 4-2 Sensor response and recovery times of Cr_2O_3 5-layered sensor when exposed to 45-ppm toluene gas over a range of temperatures. τ_{90} refers to the response time of the sensor (in sec) and τ_{10} and refers to the sensor recovery time (in sec).

Temperature	Sensor Response and Recovery Times (sec) /Toluene	
	τ_{90}	τ_{10}
300 °C	289	1799
350 °C	289	1049
375 °C	219	889
400 °C	209	499

Due to sensor variability being more apparent at lower temperatures and response and recovery times being longer, other tests were performed at 400 °C. It was anticipated that zeolite incorporation would enhance the responsiveness towards test gases.

4.3 Cr_2O_3 Control Material Exposure to Solvents

4.3.1 Test Details and Range of Gases Tested

Tests followed the structure described in section 3.2 described in Chapter 3. However, the operating temperature here was 400 °C. The tests described below were all performed on AA rig. The gases investigated were: ethane (100 ppm), methanol (100 ppm), ethanol (100 ppm), acetone (100 ppm) and toluene (50 ppm). Tests were then repeated in environments with different relative humidity (25% RH, 50% RH and 75% RH) to understand how humid air affected sensor responses and to better understand how the sensors would behave in real-life environments. Tests were generally repeated twice to ensure consistency among repeats.

4.3.2 Gas-sensing Results of a Control Cr_2O_3 Sensor to Solvent Gases

The control sensor was exposed to the five gases (Fig. 4-5 below). It was responsive to all the gases tested. However, it provided very similar response patterns to test gases, particularly when it was supplied with the lowest concentration of a gas. As the concentrations of each gas were subsequently increased, the sensor was unable to differentiate between molecules that had very similar kinetic diameters such as ethanol (4.5 Å) and acetone (4.6 Å).[304] The response patterns towards ethane were quite different: as the concentration supplied was increased to 80 and 100 ppm, the sensor began to show n-type behaviour. This switch was also noted with the n-type systems discussed in Chapter 3. It is thought that it could be due to the production of an oxidising gas when the gas reacts with the sensor surface, forming acetic acid as follows:

$$C_2H_6 + 3O^- \rightarrow CH_3COOH + H_2O + 3e^- \quad \text{(Scheme 4.1)}$$

It must be noted that no work has been found in the literature that supports that ethane may get converted to acetic acid on a MOS surface. However, Mann et al. [335] detected trace amounts of acetic acid when connecting a GC-MS to the exhaust of a zeolite bed which had alkane gases pass through it.

Although the concentration ranges of each gas supplied were different: (10–100 ppm for ethanol, acetone, methanol and ethane, and 2.5–50 ppm for toluene), the sensor was still unable to discriminate between them and the response curves obtained were quasi-identical for acetone, ethanol and methanol gases (see bottom image in Fig. 4-5). The control Cr_2O_3 sensor responded very quickly to all gases, reaching steady state. The flat peak shapes seen are generally associated with fast and full combustion reactions that lead to the production of CO_2 and $H_2O_{(v)}$ when zeolites are incorporated into a sensing system.[15] It can be inferred that ethanol, acetone and methanol adsorb, diffuse and desorb very similarly in the unmodified Cr_2O_3 system. The results of the control sensor imply that when used individually it would not be favourable for the detection of a specific gas in a mixed-gas environment, which is needed in practical applications.

The baseline resistance remained unchanged upon exposure to all gases, despite having exposed the sensor to different gases and having experienced temperature cycling at 500 °C prior to exposing the sensor to a new gas. It was interesting to see that the exposure to some gases (ethanol, methanol), resulted in an odd peak shape with the initial concentration pulse supplied, potentially due to multi-step reactions taking place within the sensor and/or to the production and subsequent interference of water vapour as part of reaction processes occurring between the gas and the sensor surface.[22]

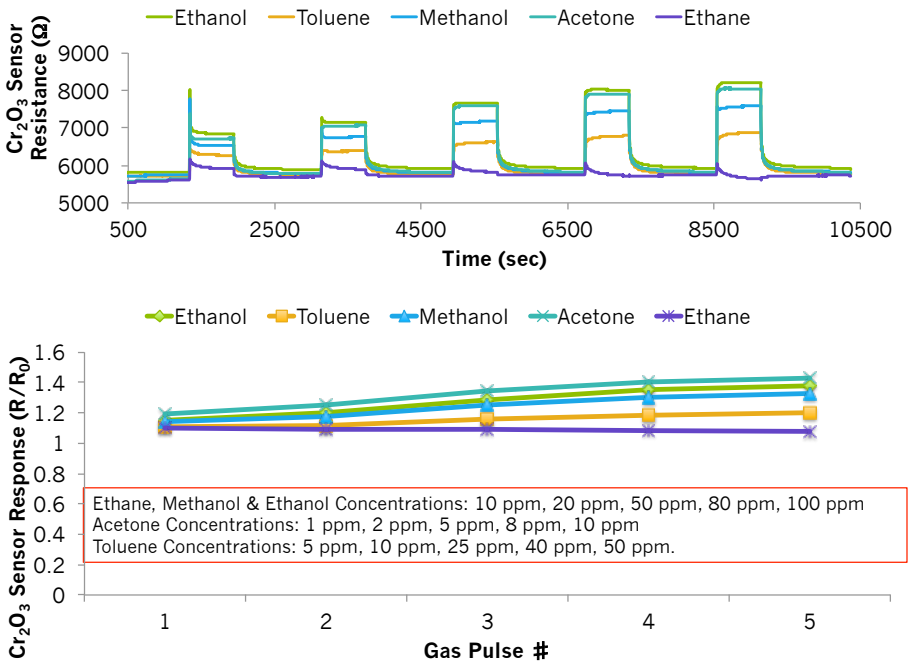

Figure 4-5 (Top image) Cr_2O_3 control sensor resistance change upon exposure to increasing concentrations of ethanol, toluene, methanol, acetone and ethane gases. (Bottom image) Sensor responses to gases as a function of the number of concentration pulses supplied to the sensor. It can be seen that although different concentrations were tested for each gas, the response curves looked similar. The unmodified sensor was unable to differentiate between gas types.

4.4 Zeolite Modification of the Control Cr_2O_3 Sensor

The control sensor was modified by progressively increasing the amount of zeolite H-ZSM-5 that was mixed with the metal oxide from 10 – 40% (wt.), with 10% (wt.) increments. XRD spectra and SEM images were collected for all samples. EDS was carried out to confirm the elemental and atomic percentage composition in the sensor materials and the uniformity of elemental dispersion around the sensor surface. BET was carried out to characterise the surface area of the zeolite materials used, relative to the control material. The sensors were then exposed to a range of HCs at 400 °C both in dry and humid air conditions.

4.4.1 Physicochemical Characterisation of Zeolite-Modified Sensors

The sensors were kept in a furnace at 600 °C for an hour to sinter the materials and to evaporate the organic vehicle prior to analysis. Physicochemical characterisation techniques were carried out to assess whether the fabrication process had affected the crystalline structure and/or morphology and microstructure of the materials. The Raman spectra of a control Cr_2O_3 sensor and that of the powder have been included for reference in the Appendix. No differences were encountered in the spectral fingerprints before and after fabrication.

4.4.1.1 X-Ray Diffraction (XRD)

The XRD pattern showed Cr_2O_3 was hexagonal in structure and had characteristic 2θ peaks at 24.4°, 33.6° 36.2°, 39.6°, 41.4°, 50.1° (Fig. 4-6 below). The sensors that contained zeolite H-ZSM-5 as an admixture also displayed the characteristic peaks of Cr_2O_3 and as the amount of the zeolite in the sensing system was incremented, a few peaks attributed to it could be appreciated at 2θ of 22.9° and 23.9° [234] seen, for instance, in the sensor containing 40% (wt.) zeolite H-ZSM-5.

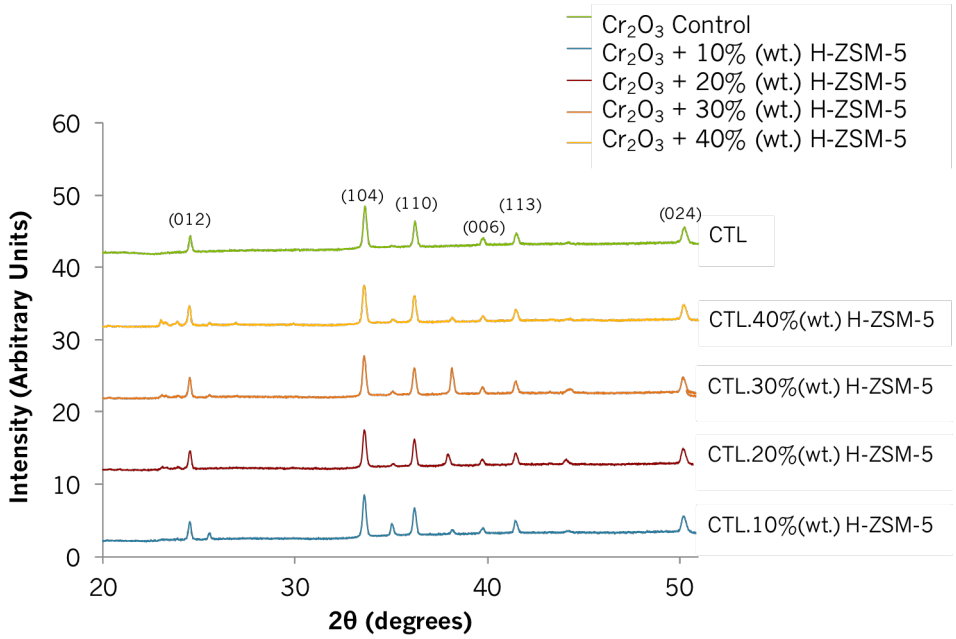

Figure 4-6 XRD patterns of a control Cr_2O_3 sensor and those modified with 10% (wt.) zeolite H-ZSM-5, 20% (wt.) zeolite H-ZSM-5, 30% (wt.) zeolite H-ZSM-5 and 40% (wt.) zeolite H-ZSM-5. Peaks have been indexed according to the literature. [299]

4.4.1.2 Scanning Electron Microscopy (SEM)

SEM images of the Cr_2O_3 sensors modified with different amounts of H-ZSM-5 were taken at a magnification of x10,000 (Fig. 4-7). As can be seen in the image corresponding to the control sensor the particles were loosely stacked together and displayed a porous microstructure with clear voids. The particles exhibited a broad size distribution, ranging from ~100 nm to 400 nm and their shape was not uniform throughout the structure. The progressive increase in loading of zeolite H-ZSM-5 was clearly appreciated in the images. The zeolite particles were generally oval in shape and ~1 μm in size. The structure continued to appear porous but seemed to become more compact as the amount of zeolite was incremented. Compact or denser films are usually considered to result in poorer sensitivity to test gases in relation to more porous films.[7,305] This is because the gas has access, primarily, to the surface of the sensor. There was no evidence of fusion between the oxide and zeolite particles. Nevertheless, the sensor with 10% (wt.) H-ZSM-5 displayed slightly different shapes of

the zeolite particles, some of which had sharp edges. Upon closer inspection of the SEM micrographs at higher magnifications (not shown), there was evidence of some particle agglomeration. As the percentage weight was increased, all zeolite particles showed signs of agglomeration, the particle shapes were oval and they also displayed a rough outer appearance.

4.4.1.3 Energy Dispersive X-Ray Spectroscopy (EDS)

EDS analysis was carried out by taking five spectra from different areas in the sensor and taking an average of the values obtained. These results have been provided in Table 4-3 below. As expected, the atomic percentage of silica detected increased with the increase of zeolite loading in the sensors.

The Cr/O ratio was slightly off, which may be attributed to the electron beam not being able to knock electrons off inner shells in the chromium atoms. The Si/Al ratio of zeolite H-ZSM-5 as reported by Zeolyst is 80 and other researchers found the Si/Al to be 44.4 when used as coatings over WO_3 sensor materials.[29] In the fabricated admixed films, aluminium was not detected. Previous tests carried out and presented in Chapter 3, did reveal the presence of aluminium when zeolites were incorporated as coatings. Given that the zeolite coatings were subjected to the same treatment as the admixtures, it is thought that the composition of the zeolites was not affected by fabrication and that aluminium was not detected due to trace amounts of it in the mixture, due to an uneven dispersion of the zeolite in the system and due to the limited penetration depth of the electron beam.[306]

Table 4-3 EDS analysis providing the atomic percentage of a Cr_2O_3 control sensor and those modified by admixture of zeolite H-ZSM-5.

Sensor	Atomic Percentage (%)		
	Cr	O	Si
Cr_2O_3 Control	35.7	64.3	n/a
Cr_2O_3 with 10 % (wt.) HZSM5	34.1	61.5	4.3
Cr_2O_3 with 20 % (wt.) HZSM5	27.5	63.4	9.1
Cr_2O_3 with 30 % (wt.) HZSM5	25.9	63.0	11.1
Cr_2O_3 with 40 % (wt.) HZSM5	23.5	63.9	12.6

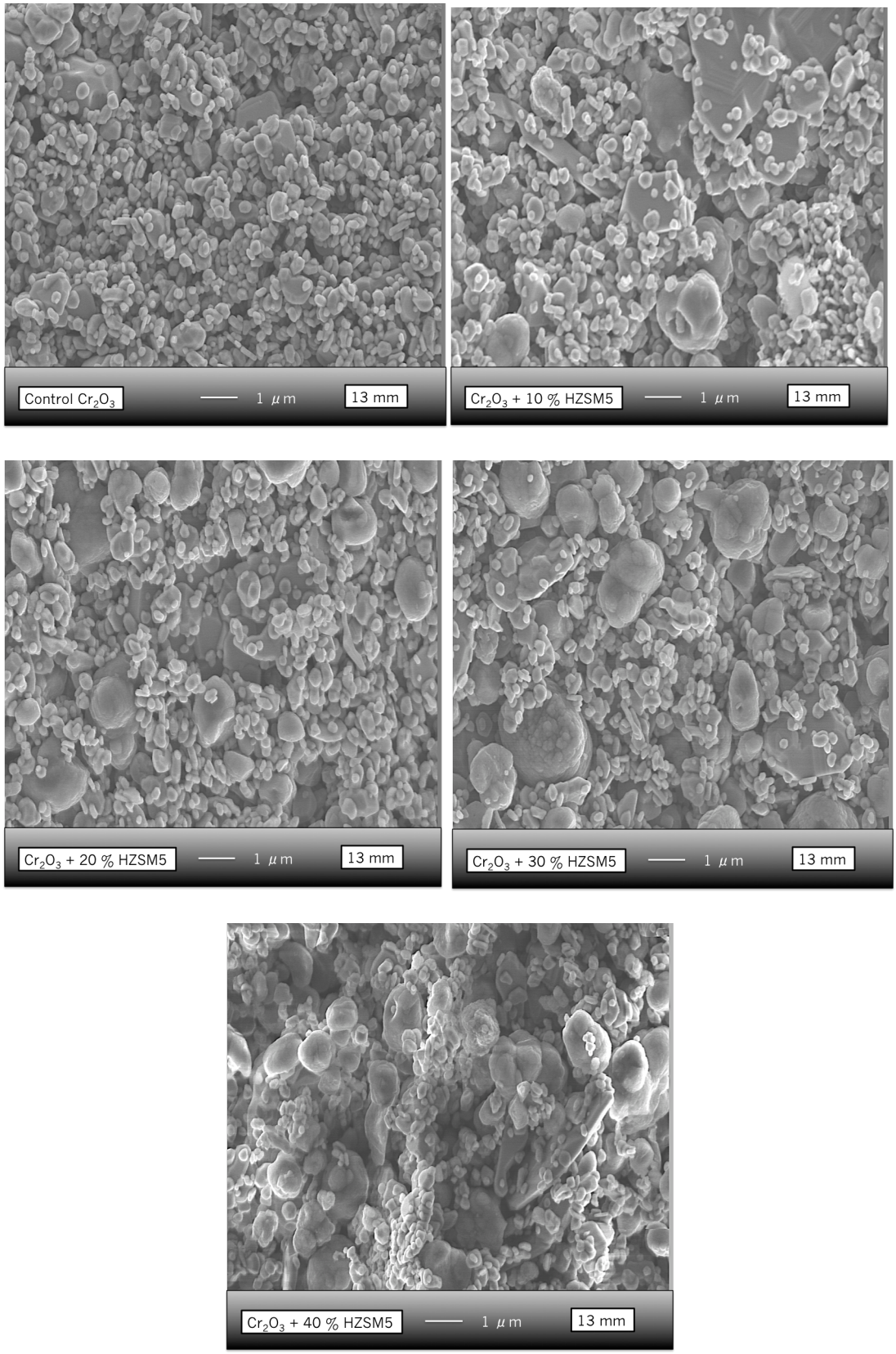

Figure 4-7 SEM images of Cr_2O_3 sensors modified with different amounts of zeolite H-ZSM-5 (10–40% (wt.)). The progressive increase of zeolite can be visually appreciated in the images as more particles of ~1 µm are seen in the sensor microstructure.

4.4.1.4 Brunauer-Emmett-Teller

BET analysis of the Cr_2O_3 and H-ZSM-5 powders revealed that the surface area of the control was 2.3 m^2/g and that of H-ZSM-5 was 382.6 m^2/g. This corresponds to a 166-fold increase in surface area in relation to the control material. The incorporation of zeolite materials was therefore expected to alter the microstructure of the sensors by raising the surface area and the number of surface-reactive sites available for gas interaction. It was expected that by incrementing the amount of zeolite in the sensor structure, a trend might be observed in the sensor responses to gases. This is discussed further in the following sections.

4.4.2 Parameters Affecting the Sensing Performance of Zeolite-modified Cr_2O_3

The following section investigates the effects that zeolite H-ZSM-5 imparted on sensor performance when exposed to gases at 400 °C. The same tests were also repeated in environments with humid air (25% RH, 50% RH and 75% RH).

4.4.2.1 Microstructural Effects

As described in section 3.5.2, the kinetics of surface reactions are affected by the microstructure of a sensor. It is understood that the introduction of a porous zeolite with high surface area provides a higher concentration of surface reactive sites for gaseous molecules to interact with which, in turn, contributes to the overall conductivity of the system.[15] Obtaining a higher or a lower sensor response is dependent on the inherent sensitivity of the sensing material to the reaction products.[15]

It has been suggested that sensors fabricated with cover layers will exhibit a retardation in the sensor response and recovery times.[15,24] Nevertheless, this retardation effect may be dependent on the microstructural configuration of the sensing system as, if the diffusion of gaseous species is favoured, response times can be faster.[307] With n-type semiconductor admixed sensors it was found that the retardation effect was more pronounced at lower temperatures such as 300 °C (Chapter 3). It was of interest to see how p-type systems compared to the n-type system test results carried out at 400 °C. In addition to this, it was important to assess whether incorporating more zeolite into the oxide-zeolite mixture would result in enhanced or diminished responses to gases and to quicker or longer response and recovery times. As shown in section 4.3, the control sensor responded poorly to most gases and provided similar magnitudes of response and peak shape patterns to gases such as ethanol, methanol and acetone. Thus, it was worth determining whether the fabricated sensors would respond differently when exposed to the same gas and if each individual sensor provided

different response patterns and response magnitudes when exposed to other gases with similar molecular structures and kinetic diameters. As such, the discriminating capabilities of the fabricated sensors have also been investigated.

Due to the dispersed presence of the zeolite within the sensing element, the effects of diffusion are dissimilar to those attained with a zeolite coating, which acts as a physical barrier between the gas molecules and the sensitive layer in the sensor. Whereas gas molecules do not come across the sensitive layer until they pass through the zeolite membrane, in an admixture the gas 'sees' or is able to react with a combination of zeolite and oxide particles simultaneously. It was expected that in such configuration, molecules would diffuse through available cavities or voids in the sensing structure as well as through the zeolite pores. This configuration also interrupts connectivity between oxide particles.[29] Toluene gas, however, has a kinetic diameter of 5.8 Å [308], which is larger than the zeolite pores in H-ZSM-5 (5.1 × 5.5 and 5.3 × 5.6) and it was anticipated that it may experience more difficulty in diffusing through the sensitive layers of the system. The rest of the gas molecules tested were small enough to also diffuse through the zeolite pores.

4.4.2.2 Response/Recovery Times & Peak Shapes in Zeolite-modified Sensors

Table 4-4 below provides a compilation of the response and recovery times seen for each sensor when exposed to the highest concentration of each gas. In addition to this, τ_{90} and τ_{10} can be related to the responses patterns shown in Figs. 4-8 to 4-12 below.

Note that an odd peak shape was seen in some sensors when supplied with the lowest concentration of a gas. This effect was not seen at higher concentrations. Although an explanation of why the sensors respond as such only at lower concentrations is not known, it is thought to be associated with different chemical reactions occurring at the sensor. It was initially thought that it could be an electronic issue or the result of pressure build-up in the system. Nevertheless, it does not consistently occur for the same sensor port when exposed to different gases and it only occurs in the first pulse of gas supplied. It was investigated whether a high dilution of gas in air i.e. 10% of a cylinder concentration could lead to a 'jump' in the flow of air as a result of a switch in the SVs in the rig, that would lead to a sharp increase in sensor resistance. However, no 'jump' was observed. Furthermore, if that was the case it ought to be seen consistently in tests that used the same CSV file, and it was not. It is therefore plausible that the reaction products differ with gas concentration. Other studies have presented similar peak shapes but have not commented on the basis of the behaviour.[26,31,32,96]

As seen in Table 4-4, the response times attained in the zeolite-modified sensors were generally longer than those of the control sensor. Note that 'Cr_2O_3 + 20% (wt.) H-ZSM-5' displayed unreliable behaviour e.g. Fig. 4-12 and thus its results ought to be analysed with caution; it did not follow the trends seen in other sensors and consistently provided the lowest sensor resistance after that of the control. It is possible that if the sensor, for some reason, was not being heated in a stable fashion it could have led to those results. However, this is unlikely as it was not observed when other sensors were heated in this port.

Some sensors such as 'Cr_2O_3 + 30% (wt.) H-ZSM-5' provided the same response time to acetone as the control sensor and also provided faster recovery times than the control. The 'Cr_2O_3 + 10% (wt.) H-ZSM-5' sensor provided the highest responsiveness to acetone and took a longer time to respond in relation to other sensors (1.6 minutes) but recovered in under a minute. Similar sensor kinetics were seen with exposure to ethanol gas. In fact, the response patterns to both gases were quasi-identical. Sensors responded more quickly to methanol gas: once again, the sensor that provided the highest response, 'Cr_2O_3 + 10% (wt.) H-ZSM-5', was the one to take longer to respond (~12 seconds). The remaining zeolite-modified sensors responded similarly to the control but they all took longer times to recover.

Response and recovery times were much slower with toluene exposure than with other gases. The peak shapes towards this gas were shark-finned and sensors such as 'Cr_2O_3 + 10% (wt.) H-ZSM-5' struggled to return to baseline following gas removal. Once again, less amount of zeolite in the sensor resulted in longer response/recovery times and increased magnitudes of response. It is noteworthy that the SEM micrograph of sensor 'Cr_2O_3 + 10% (wt.) H-ZSM-5' in the system presented different zeolite particle shapes to the other zeolite-modified sensors. It is also the sensor that provided the highest sensor responses to gases and that which provided the slowest sensor kinetics.

Table 4-4 Response times (T_{90}) and recovery times (T_{10}) seen in the sensors when exposed to 100 ppm acetone, 100 ppm ethanol, 100 ppm methanol and 50 ppm toluene. Sensor 'Cr_2O_3 + 20% (wt.) H-ZSM-5' provided unreliable data (Fig. 4-12) and results should be analysed with caution.

Response & Recovery Times (sec) to	**Acetone**		**Ethanol**		**Methanol**		**Toluene**	
Gas Type	T_{90}	T_{10}	T_{90}	T_{10}	T_{90}	T_{10}	T_{90}	T_{10}
Cr_2O_3 Control	4	74	2	65	2	45	59	159
Cr_2O_3 + 10% (wt.) H-ZSM-5	98	45	86	27	12	53	208	286
Cr_2O_3 + 20% (wt.) H-ZSM-5	55	8	178	14	2	55	327	69
Cr_2O_3 + 30% (wt.) H-ZSM-5	4	55	4	63	4	104	151	127
Cr_2O_3 + 40% (wt.) H-ZSM-5	4	102	2	106	2	204	163	112

It was typical to see that with increasing zeolite concentration, the sensor devices responded more quickly and recovered more slowly, except for toluene exposure; a higher loading of zeolite led to faster response and recovery times. Sensors with increased zeolite loadings presented flat peak shapes, whereas less zeolite (10% (wt.) H-ZSM-5) resulted in shark-fin shapes with ethanol, acetone and toluene exposure. It is thought that this is a result of the zeolite catalysing surface reactions more efficiently when there is more of it and providing a higher concentration of surface-reactive sites for gas interaction. However, its presence subsequently delays the rate of gas desorption from the structure potentially due to the reaction products being effectively trapped in the zeolite pores or displaying an affinity for the sensing system.[229]

Therefore, it was found that:

- Having less zeolite in the sensing system assisted in fastening desorption times with exposure to ethanol, acetone and methanol gases, in relation to the control.
- The response times to methanol, acetone and ethanol gases were comparable in the control and the 30% (wt.) and 40% (wt.) sensors.
- In regard to the sensor with 10% (wt.) H-ZSM-5, the response times were consistently longer towards all test gases and they were found to be longer with increasing kinetic diameter of the molecules (methanol < ethanol < acetone < toluene). Recovery times were generally longer with smaller kinetic diameter of molecules and with more zeolite in the sensing system. However, sensor exposure to toluene gas led to an opposite effect.
- Interestingly, the sensor loaded with 40% (wt.) of the zeolite rarely saw response improvements with increasing gas concentration and the response magnitudes were generally worsened over those of the control sensor. It is thought that due to the higher concentration of zeolite H-ZSM-5 in this system, the sensing layers were able to combust test gases such as ethanol and acetone to CO_2 and water vapour more readily. This combustion process led to flat peak shapes and small response magnitudes, due to poor sensitivity of the sensing system to CO_2 and potentially to water as well. In the case of exposure to more complex molecules i.e. toluene, the source molecule may break down to intermediate products which may, in turn, react further with the sensing system. The sensing system may exhibit higher sensitivity to the reaction products of toluene and it is not as efficient at fully combusting it to CO_2 and $H_2O_{(v)}$. It is therefore possible that the sensitivity of the sensing system to different reaction products could result in resistance increments upon exposure to molecules of a larger size and with a non-polar character.

It is possible that methanol fully combusts to CO_2 and $H_2O_{(v)}$, which is supported by the flat peak shapes seen in all sensors when exposed to this gas i.e. sensors reached steady state quickly (<12 seconds). At an operating temperature of 400 °C it is reasonable to believe that water vapour or hydroxyl groups could affect sensor responses.[113] Further, as seen in scheme 4.2 below, for every methanol molecule, two water molecules are produced. In the systems that contain more zeolite, it is possible that surface reactions are catalysed more readily and water molecules cause more of an interference with the source gas.[22] Although H-ZSM-5 is a hydrophobic zeolite, it is suggested in the literature that water will still be adsorbed in its pores due to the presence of silanol defects.[22] This was also supported by the results presented in Chapter 3. As such, its desorption may somewhat be affected by this, leading to the reported longer recovery times in sensors containing more zeolite. In addition to this, the slightly different shapes of the H-ZSM-5 zeolite particles seen in the sensor with 10% (wt.) zeolite loading, may have opened up the microstructure of the system, resulting in an easier pathway of diffusion for gas molecules in this sensor and thus resulting in enhanced sensor responses towards test gases.

$$CH_3OH + 3O^- \rightarrow CO_2 + 2H_2O + 3e^- \quad \text{(Scheme 4.2)}$$

It is thought that with more zeolite in the system, ethanol potentially combusts to CO_2 and $H_2O_{(v)}$. However, a smaller zeolite loading favours further reactions inside the system due to the more open microstructure, enabling further reactions of the gas inside the sensing layers and potentially to products such as acetaldehyde, as detailed in Chapter 1. This is supported by the shark-fin shapes seen in the sensor 'Cr_2O_3 + 10 % H-ZSM-5'. It is possible that the enhancements in sensor response over the control seen in this sensor upon exposure to ethanol and acetone (~2.4-fold and ~2.2, respectively) were the result of intermediate reaction products to which the sensing material was more sensitive. The quasi-identical profiles obtained with exposure to acetone and ethanol suggest similar reaction products formed during interaction with the sensors (Fig. 4-8 and 4-12).

All sensors except the control exhibited shark-fin shapes upon exposure to toluene gas. This behaviour suggests that the diffusion of toluene through the sensing layers was potentially hindered by its size, leading to longer response times. The sensors containing 20% (wt.), 30% (wt.) and 40% (wt.) of zeolite H-ZSM-5 provided similar response magnitudes to toluene. Having more zeolite in the system resulted in an

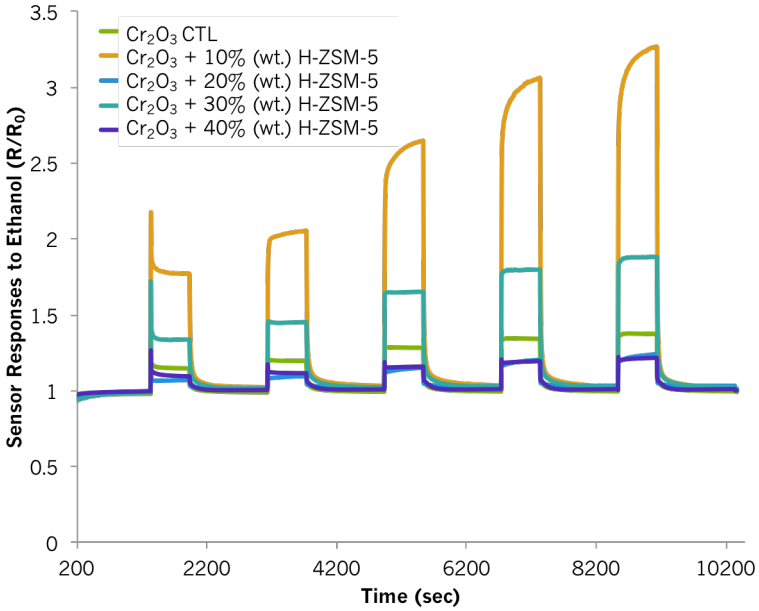

Figure 4-8 Zeolite-admixed sensor responses to ethanol gas at 400 °C. The concentrations correspond to 10 ppm, 20 ppm, 50 ppm, 80 ppm and 100 ppm. The sensors used as shown in the legend from top to bottom correspond to the control Cr_2O_3, to Cr_2O_3 mixed with 10% (wt.) H-ZSM-5, to Cr_2O_3 mixed with 20% (wt.) H-ZSM-5, to Cr_2O_3 mixed with 30% (wt.) zeolite H-ZSM-5 and to Cr_2O_3 mixed with 40% (wt.) H-ZSM-5.

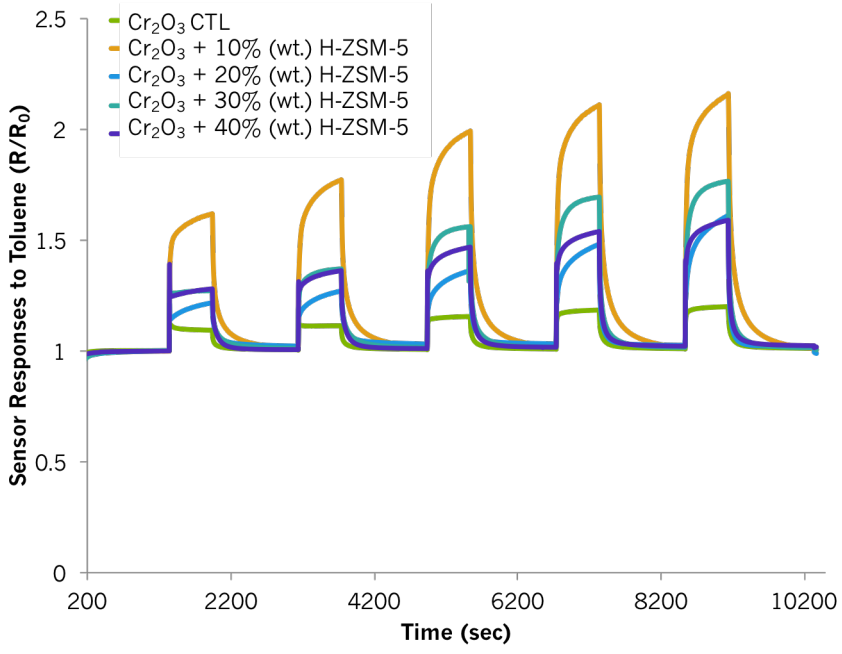

Figure 4-9 Admixed sensor responses to toluene gas at 400 °C. The concentrations correspond to 5 ppm, 10 ppm, 25 ppm, 40 ppm and 50 ppm. The sensors used as shown in the legend from top to bottom correspond to the control Cr_2O_3, to Cr_2O_3 mixed with 10 % (wt.) H-ZSM-5, to Cr_2O_3 mixed with 20 % (wt.) H-ZSM-5, to Cr_2O_3 mixed with 30 % (wt.) zeolite H-ZSM-5 and to Cr_2O_3 mixed with 40 % (wt.) H-ZSM-5.

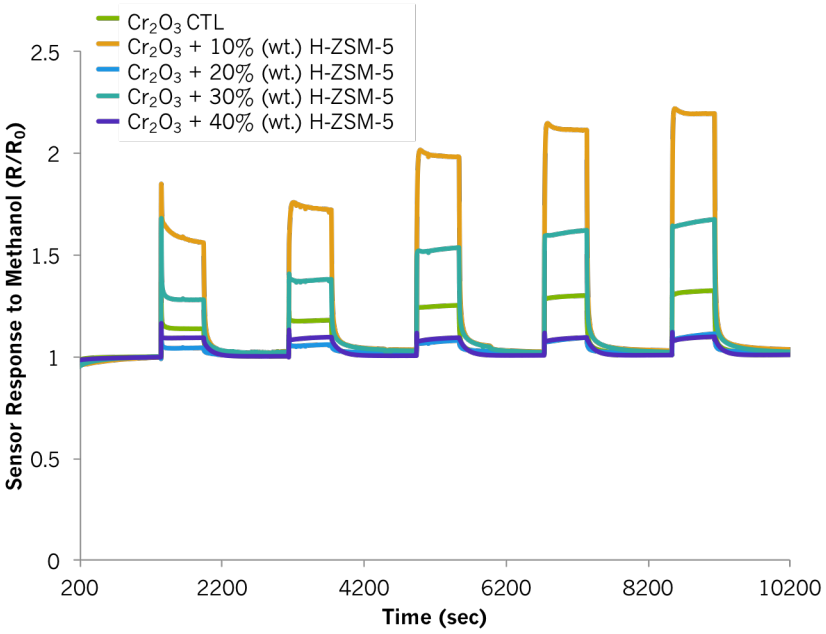

Figure 4-10 Admixed sensor responses to methanol gas at 400 °C. The concentrations correspond to 10 ppm, 20 ppm, 50 ppm, 80 ppm and 100 ppm. The sensors used as shown in the legend from top to bottom correspond to the control Cr_2O_3, to Cr_2O_3 mixed with 10 % (wt.) H-ZSM-5, to Cr_2O_3 mixed with 20 % (wt.) H-ZSM-5, to Cr_2O_3 mixed with 30 % (wt.) zeolite H-ZSM-5 and to Cr_2O_3 mixed with 40 % (wt.) H-ZSM-5.

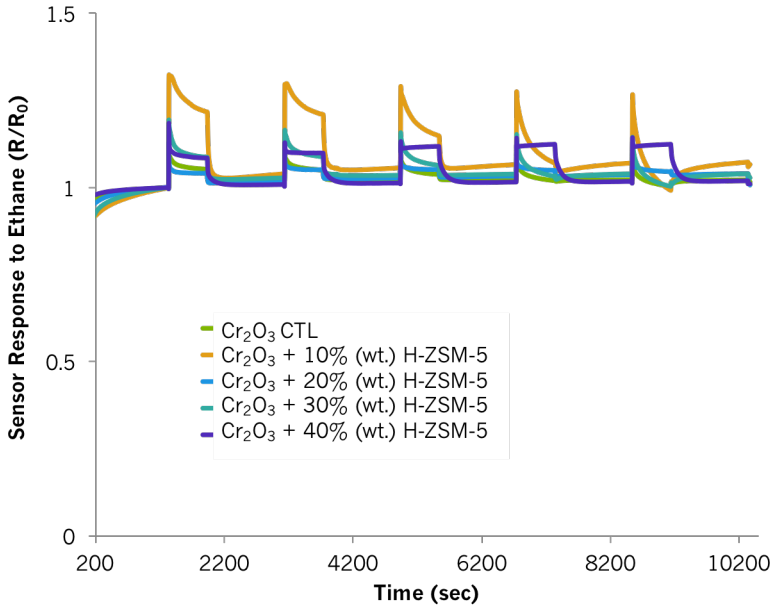

Figure 4-11 Admixed sensor responses to ethane gas at 400 °C. The concentrations correspond to 10 ppm, 20 ppm, 50 ppm, 80 ppm and 100 ppm. The sensors used as shown in the legend from top to bottom correspond to the control Cr_2O_3, to Cr_2O_3 mixed with 10 % (wt.) H-ZSM-5, to Cr_2O_3 mixed with 20 % (wt.) H-ZSM-5, to Cr_2O_3 mixed with 30 % (wt.) zeolite H-ZSM-5 and to Cr_2O_3 mixed with 40 % (wt.) H-ZSM-5.

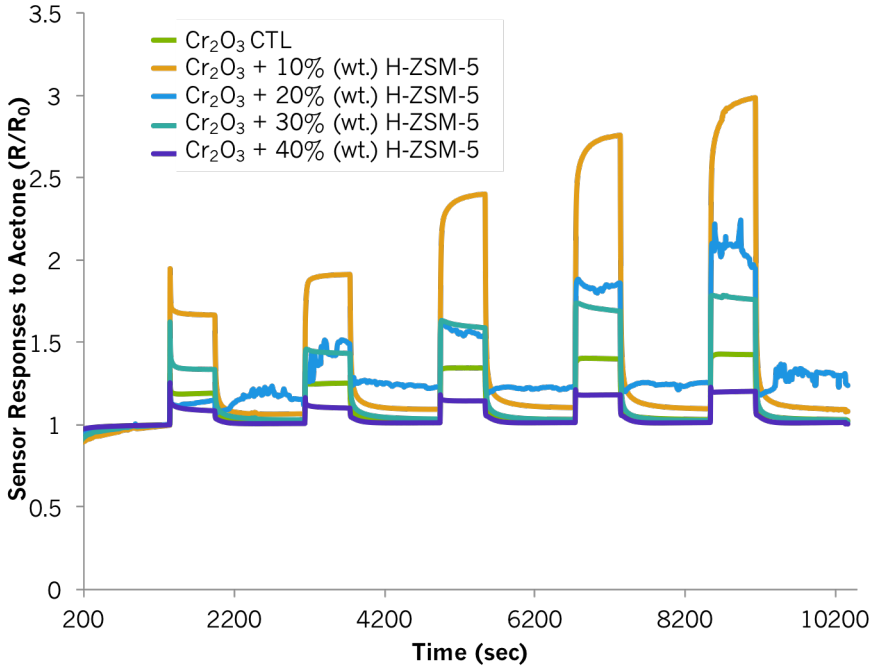

Figure 4-12 Admixed sensor responses to acetone gas at 400 °C. The concentrations correspond to 10 ppm, 20 ppm, 50 ppm, 80 ppm and 100 ppm. The sensors used as shown in the legend from top to bottom correspond to the control Cr_2O_3, to Cr_2O_3 mixed with 10 % (wt.) H-ZSM-5, to Cr_2O_3 mixed with 20 % (wt.) H-ZSM-5, to Cr_2O_3 mixed with 30 % (wt.) zeolite H-ZSM-5 and to Cr_2O_3 mixed with 40 % (wt.) H-ZSM-5.

enhancement in response over the control sensor, which was not obtained with exposure to other gases. This is likely due to the more hydrophobic nature of the surface and the affinity of zeolite H-ZSM-5 towards toluene and its reaction products.

Exposure to ethane led to odd peak shapes; the response magnitudes decreased with concentration increments in all sensors except 'Cr_2O_3 + 40% H-ZSM-5', which provided the same response magnitude towards all ethane concentrations. With higher ethane concentrations, the responses began to switch towards n-type behaviour. The peak shapes were indicative of multi-step reactions occurring at the sensor. This could be due to the production of an oxidising gas such as acetic acid and water. This switch in semiconductor behaviour with ethane exposure was also noted in the n-type systems described in Chapter 3.

4.4.3 Zeolite Influence on Sensor Sensitivity and Selectivity

This section discusses the sensitivity of the sensors towards the gases of interest and it assesses the selective capabilities of the sensors.

The sensitivity, *S*, of each sensor towards the gases under consideration was investigated. This was done as follows: response vs. sensitivity curves were initially

plotted to understand if the sensors responded linearly to increased gas concentrations. Note that when an initial sharp peak was attained towards the first concentration pulse, the value used to plot the curve was that obtained at steady state. Because sensor responses did not increase linearly with concentration, the curves were fitted to second or third order polynomial equations, which best modelled sensor behaviour. This sub-linear increase in concentration is not uncommon in metal oxide semiconductors.[118] Third order polynomial equations generally represented the trends observed well. The derivative of the polynomial equations displayed in the figures was taken to find out the sensitivity of each sensor towards each gas. The results are shown in Fig. 4-13 to 4-20. A numerical approach was also tried to find sensor sensitivity and the results of both methods have been presented below. The first point in the numerical calculation of sensitivity was found by assuming that at a concentration of zero gas, the sensor response was 1.

As displayed in Fig. 4-14 below, both sensor sensitivity curves towards ethanol provided similar results. Generally, sensor sensitivity to ethanol decreased with concentration. Further to this, sensors 'control Cr_2O_3', 'Cr_2O_3 + 20% (wt.) H-ZSM-5' and 'Cr_2O_3 + 40% (wt.) H-ZSM-5' exhibited poor sensitivities throughout the tested concentration range. Sensor sensitivity was highest with ethanol and acetone exposure and it was lowest with exposure to ethane. Comparison between Fig. 4-14 and 4-16 revealed that sensor sensitivity was very similar between ethanol and acetone and that sensors modified by 10% (wt.) and 30% (wt.) H-ZSM-5 were the most sensitive to both gases. Like the control sensor, this collection of sensors was not successful at discriminating between ethanol and acetone. Note that the results attained with sensor 'Cr_2O_3 + 20% H-ZSM-5' in Figure 4-16 ought to be ignored, given that the sensor did not provide reliable results – seen more clearly in Fig. 4-12.

Table 4-5 Polynomial equations fitted to the response curves in Fig. 4-13 for each sensor upon exposure to ethanol gas.

	Ethanol	
Sensor Type	**Polynomial Equation**	**R-squared Value**
Cr_2O_3 CTL	$y = 2E\text{-}07x^3 - 5E\text{-}05x^2 + 0.0061x + 1.0978$	$R^2 = 0.99$
Cr_2O_3 + 10% (wt.) HZSM5	$y = 6E\text{-}07x^3 - 0.0002x^2 + 0.0312x + 1.4976$	$R^2 = 0.99$
Cr_2O_3 20% (wt.) HZSM5	$y = 7E\text{-}07x^3 - 0.0001x^2 + 0.0078x + 1.0481$	$R^2 = 0.93$
Cr_2O_3 + 30% (wt.) HZSM5	$y = 5E\text{-}07x^3 - 0.0001x^2 + 0.0138x + 1.2182$	$R^2 = 0.99$
Cr_2O_3 + 40% (wt.) HZSM5	$y = 5E\text{-}07x^3 - 9E\text{-}05x^2 + 0.0057x + 1.0324$	$R^2 = 0.96$

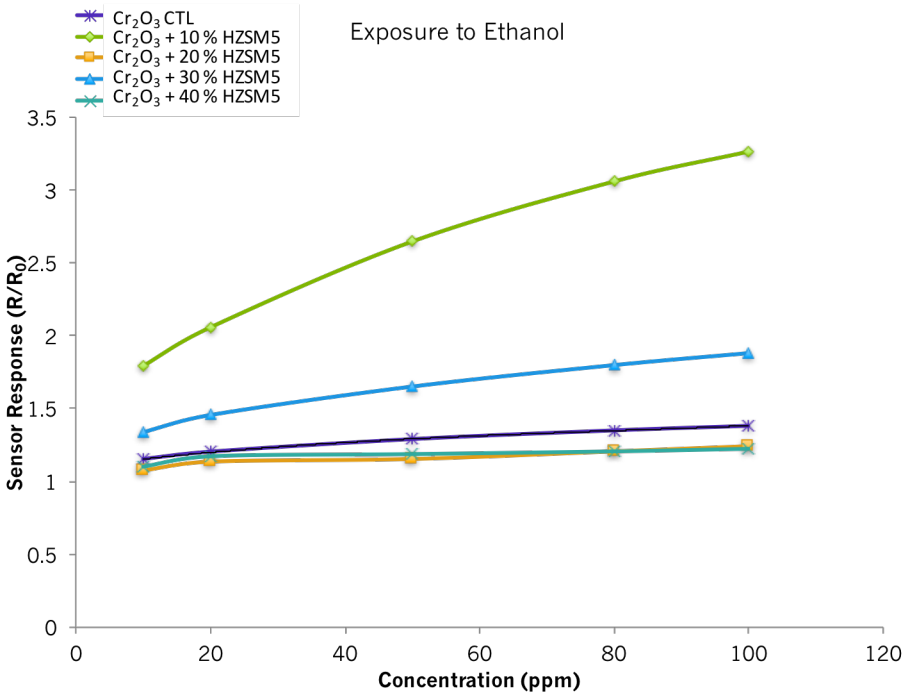

Figure 4-13 Sensor responses towards ethanol gas at 400 °C. The response vs. concentration curve was fitted to a third order equation, which has been displayed individually for each sensor in Table 4-5.

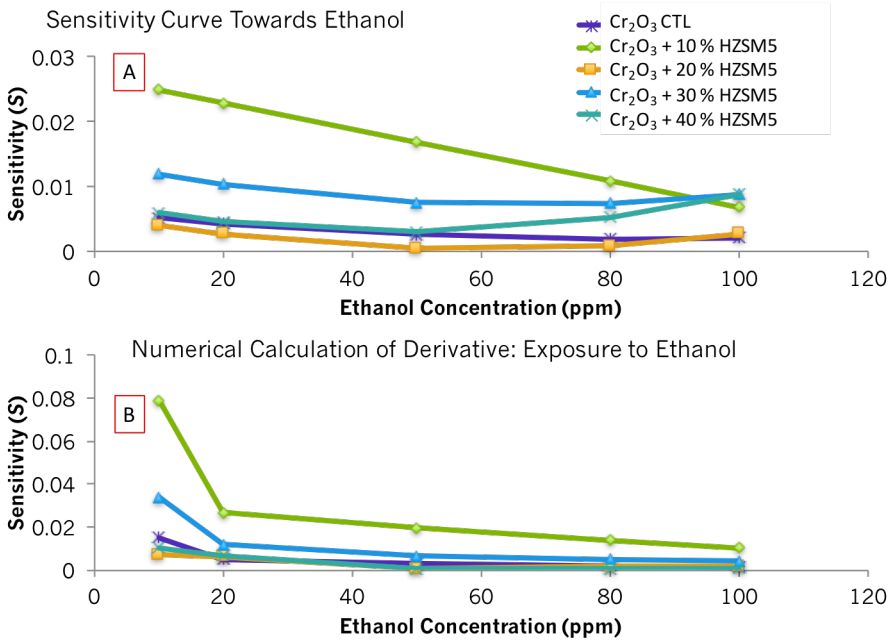

Figure 4-14 Sensitivity curve of Cr_2O_3 modified sensors towards ethanol gas at 400 °C. (A) Sensitivity curve obtained from fitting the response vs. concentration curves to third order polynomial equations. (B) Sensitivity curve obtained numerically.

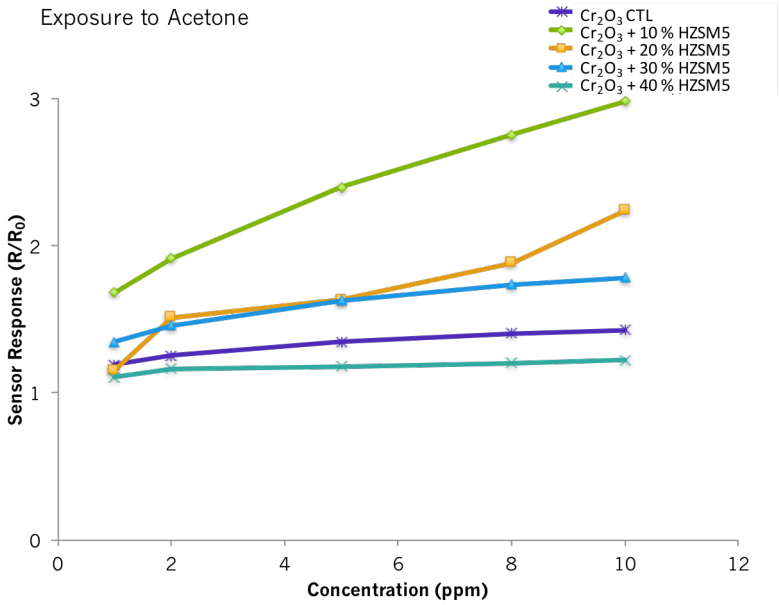

Figure 4-15 Sensor responses towards acetone gas at 400 °C. The response vs. concentration curve was fitted to a third order equation, which has been displayed individually for each sensor in Table 4-6 below.

Table 4-6 Polynomial equations fitted to the response curves in Fig. 4-15 for each sensor upon exposure to acetone gas.

	Acetone	
Sensor Type	**Polynomial Equation**	**R-squared Value**
Cr_2O_3 CTL	$y = 3E\text{-}07x^3 - 7E\text{-}05x^2 + 0.0072x + 1.1298$	$R^2 = 0.99$
Cr_2O_3 + 10% (wt.) HZSM5	$y = 1E\text{-}06x^3 - 0.0002x^2 + 0.0284x + 1.4234$	$R^2 = 0.99$
Cr_2O_3 20% (wt.) HZSM5	$y = 5E\text{-}06x^3 - 0.0008x^2 + 0.0439x + 0.8293$	$R^2 = 0.98$
Cr_2O_3 + 30% (wt.) HZSM5	$y = 5E\text{-}07x^3 - 0.0001x^2 + 0.0132x + 1.2323$	$R^2 = 0.99$
Cr_2O_3 + 40% (wt.) HZSM5	$y = 5E\text{-}07x^3 - 1E\text{-}04x^2 + 0.0062x + 1.0608$	$R^2 = 0.95$

Sensor sensitivity towards methanol was poorer than towards acetone and ethanol. Once again, sensor sensitivity generally decreased with concentration increments. In the plot attained by taking the derivative of the polynomial equation, it can be seen that the sensitivity of the control Cr_2O_3 sensor and the sensor with 20% (wt.) H-ZSM-5 initially decreased with concentration but increased again after 50 ppm.

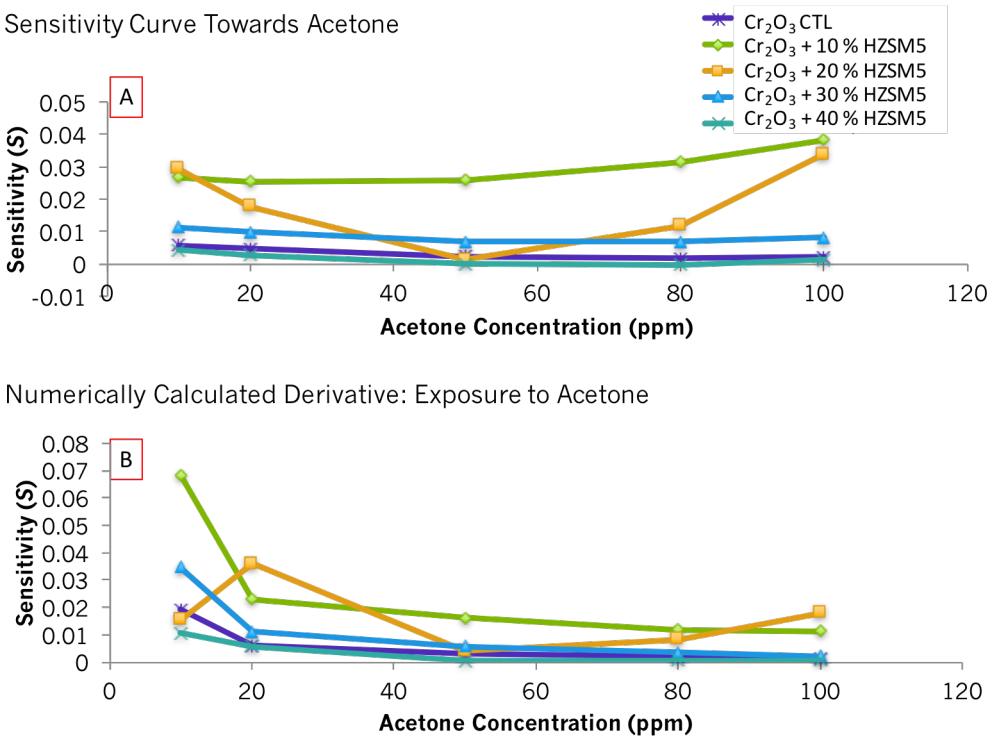

Figure 4-16 Sensitivity curve of Cr_2O_3 modified sensors towards acetone gas at 400 °C. (A) Sensitivity curve obtained from fitting the response vs. concentration curves to third order polynomial equations. (B) Sensitivity curve obtained numerically.

Nevertheless, by looking at the response patterns and concentration plots in Fig. 4-10 and 4-17 it can be appreciated that the increase in response was not visible. In this instance, the numerical calculation might approximate the sensors' behaviour more accurately. Both sensitivity curves were comparable for the remaining sensors after the second concentration pulse (20 ppm). Sensors modified by mixing 10% (wt.) and 30% (wt.) H-ZSM-5 were also the most sensitive to methanol. The sensitivity of the sensor mixed with 40% (wt.) H-ZSM-5 was very poor across the concentration range tested.

Table 4-7 Polynomial equations fitted to the response curves in Fig. 4-17 for each sensor upon exposure to methanol gas.

	Methanol	
Sensor Type	**Polynomial Equation**	**R-squared Value**
Cr_2O_3 CTL	$y = 6E\text{-}07x^3 - 0.0001x^2 + 0.0079x + 1.0853$	$R^2 = 0.96$
Cr_2O_3 + 10% (wt.) HZSM5	$y = 7E\text{-}07x^3 - 0.0002x^2 + 0.018x + 1.4652$	$R^2 = 1$
Cr_2O_3 20% (wt.) HZSM5	$y = 8E\text{-}07x^3 - 0.0001x^2 + 0.0079x + 0.9908$	$R^2 = 0.86$
Cr_2O_3 + 30% (wt.) HZSM5	$y = 9E\text{-}07x^3 - 0.0002x^2 + 0.0144x + 1.1726$	$R^2 = 0.99$
Cr_2O_3 + 40% (wt.) HZSM5	$y = 4E\text{-}07x^3 - 8E\text{-}05x^2 + 0.0038x + 1.0701$	$R^2 = 0.59$

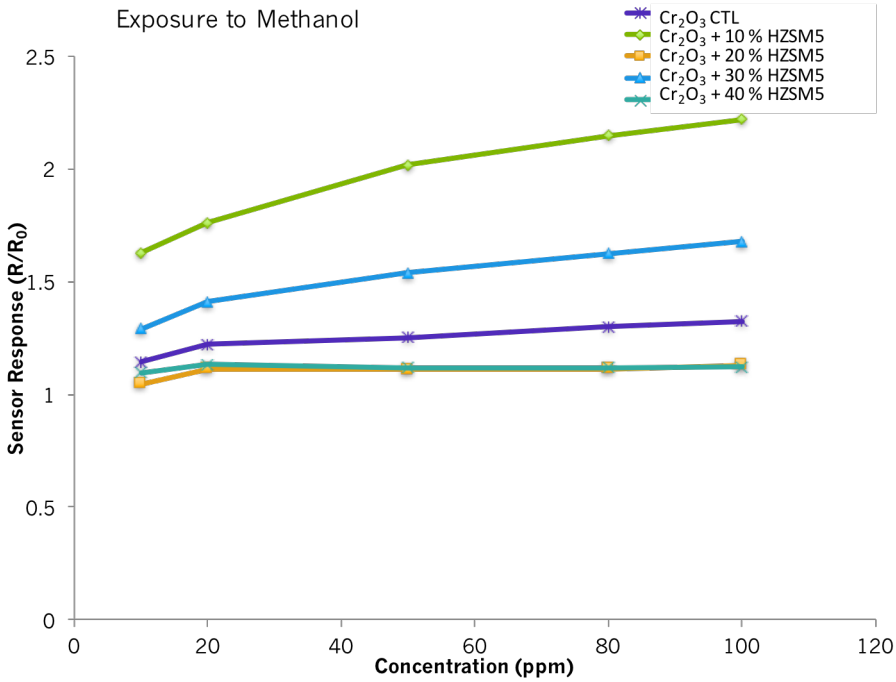

Figure 4-17 Sensor responses towards methanol gas at 400 °C. The response vs. concentration curve was fitted to a third order equation, which has been displayed individually for each sensor in Table 4-7.

Sensor sensitivity towards toluene also decreased with concentration (Fig. 4-19 and 4-20). The sensor sensitivity values were also comparable to the results obtained with ethanol and acetone exposure.

Table 4-8 Polynomial equations fitted to the response curves in Fig. 4-19 for each sensor upon exposure to toluene gas.

	Toluene	
Sensor Type	**Polynomial Equation**	**R-squared Value**
Cr_2O_3 CTL	$y = -2E\text{-}06x^3 + 0.0002x^2 - 0.0015x + 1.124$	$R^2 = 0.98$
Cr_2O_3 + 10% (wt.) HZSM5	$y = 7E\text{-}06x^3 - 0.0008x^2 + 0.0381x + 1.4551$	$R^2 = 0.99$
Cr_2O_3 20% (wt.) HZSM5	$y = 5E\text{-}06x^3 - 0.0003x^2 + 0.0137x + 1.1589$	$R^2 = 0.99$
Cr_2O_3 + 30% (wt.) HZSM5	$y = 3E\text{-}06x^3 - 0.0004x^2 + 0.0232x + 1.1669$	$R^2 = 0.99$
Cr_2O_3 + 40% (wt.) HZSM5	$y = 5E\text{-}06x^3 - 0.0005x^2 + 0.0206x + 1.1922$	$R^2 = 0.99$

Although the concentration ranges of gases tested were different (10 – 100 ppm for ethanol and acetone and 5 – 50 ppm toluene). The sensors that were most sensitive to the gas were also those modified with 10% (wt.) and 30% (wt.) H-ZSM-5.

In general, it is important to note that the methods used to find out sensor sensitivity provided comparable results, after the second concentration pulse. Nevertheless, it is acknowledged that this procedure ought to be carried out by modelling a curve based

on the physical interactions occurring between a gas and a sensor. Typically, sensors were sensitive to trace concentrations of gases but saturated at higher concentrations. This leads to higher uncertainty for the detection of these gases with Cr_2O_3-based sensors in practical applications. Furthermore, although sensor responsiveness and sensitivity were not improved drastically with zeolite incorporation, newly designed sensors provided different response magnitudes and patterns to gases, which were not seen with the unmodified sensor.

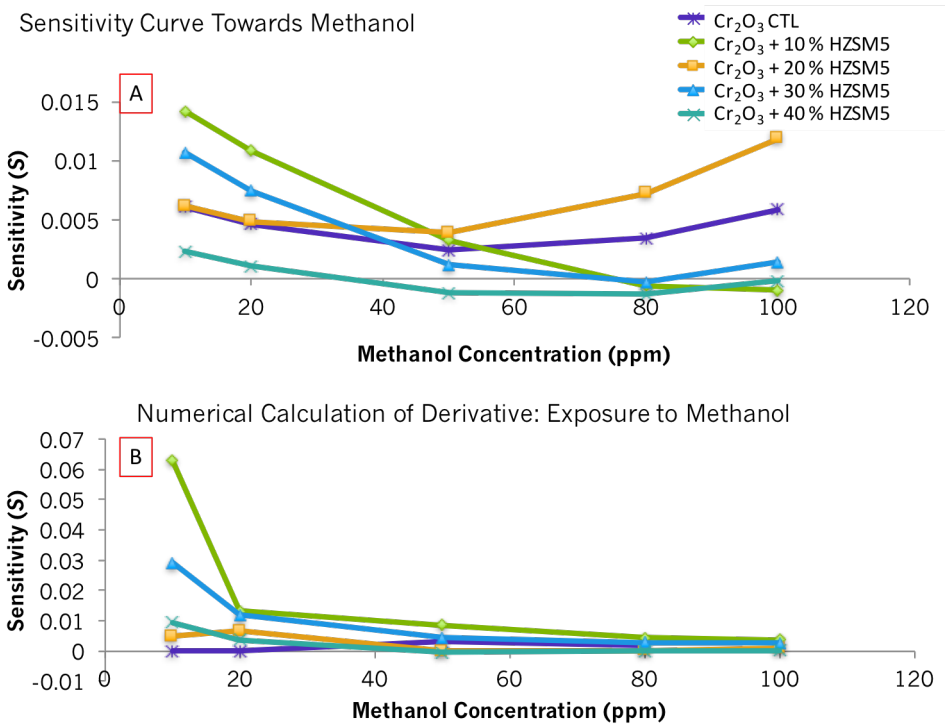

Figure 4-18 Sensitivity curve of Cr_2O_3 modified sensors towards methanol gas at 400 °C. (A) Sensitivity curve obtained from fitting the response vs. concentration curves to third order polynomial equations. (B) Sensitivity curve obtained numerically.

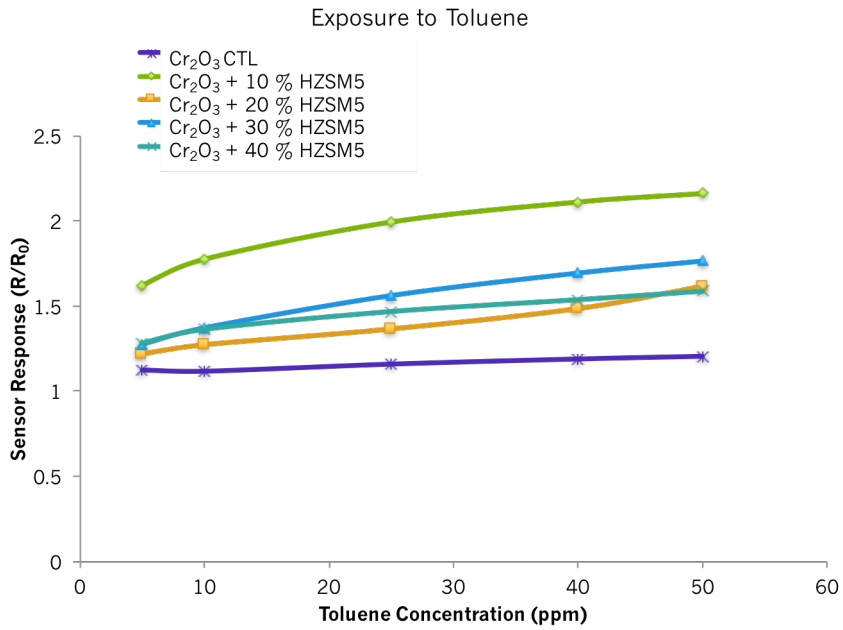

Figure 4-19 Sensor responses towards toluene gas at 400 °C. The response vs. concentration curve was fitted to a third order equation, which has been displayed individually for each sensor.

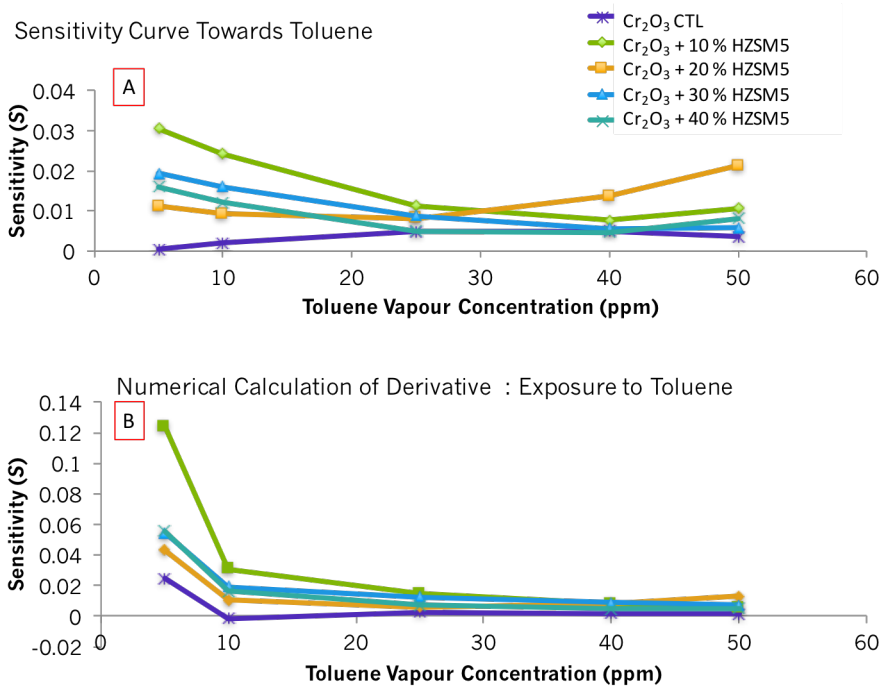

Figure 4-20 Sensitivity curve of Cr_2O_3 modified sensors towards toluene gas at 400 °C. (A) Sensitivity curve obtained from fitting the response vs. concentration curves to third order polynomial equations. (B) Sensitivity curve obtained numerically.

Thus, as previously mentioned we wanted to find out:

1) **Whether sensors modified by the same zeolite provided different response magnitudes and patterns to a particular gas due to the amount of zeolite in**

the sensor mixture. The amount of zeolite did tend to result in different response magnitudes and patterns to individual gases. If the results provided by sensor with 20% (wt.) zeolite were ignored, there was a trend where sensors with less zeolite were progressively more responsive to gases.

2) **Whether the sensor set provided different responses to different gases.** Sensors responded equally to ethanol and acetone and provided smaller response magnitudes to methanol. With higher concentrations of ethane gas, they were almost unresponsive to the gas, with some indication of n-type behaviour. The response magnitudes and peak shapes were different when exposed to toluene. However, the control sensor provided very similar response magnitudes and patterns to all gases.
3) **Whether an individual sensor would provide discrimination to the range of gases tested.** No individual sensor provided sensor responses to gases that were different enough to be able to claim selectivity (Fig. 4-21).
4) **Which sensors showed most promise for future testing.** Sensors modified with 10% and 30% (wt.) H-ZSM-5 were consistently more sensitive and responsive to gases. The former provided shorter recovery times than the control upon exposure to ethanol and acetone and the latter generally provided response times of ~4 seconds (except with toluene exposure), and shorter recovery times than the control sensor upon exposure to ethanol, acetone and toluene.

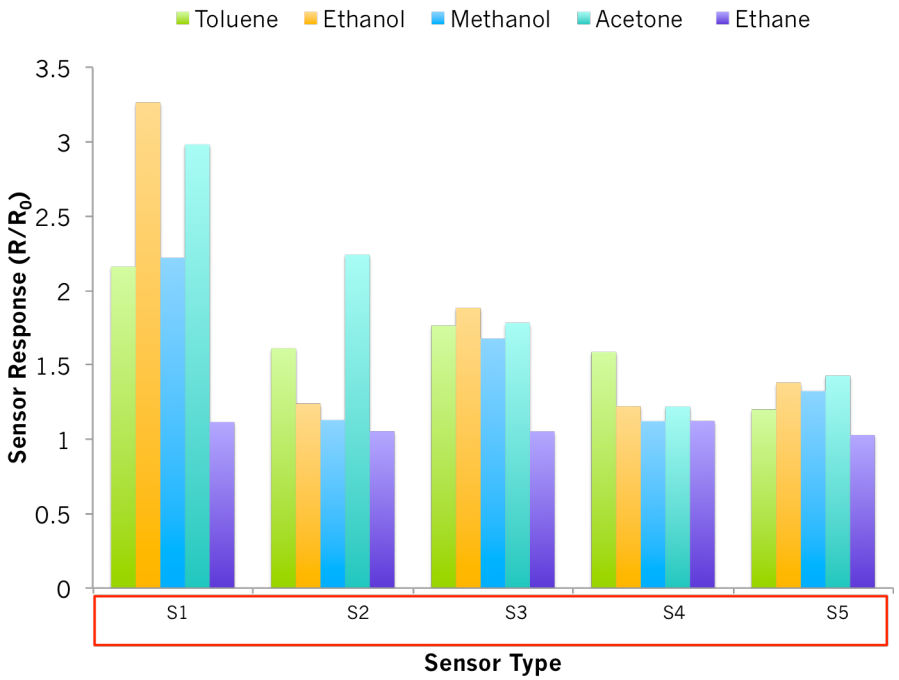

Figure 4-21 Sensor responses attained for each individual sensor towards 50 ppm toluene, 100 ppm ethanol, 100 ppm methanol, 100 ppm acetone and 100 ppm ethane. S1 corresponds to 'Cr_2O_3 + 10 % (wt.) H-ZSM-5', S2 corresponds to 'Cr_2O_3 + 20 % (wt.) H-ZSM-5', S3 corresponds to 'Cr_2O_3 + 30 % (wt.) H-ZSM-5', S4 corresponds to 'Cr_2O_3 + 40 % (wt.) H-ZSM-5' and S5 to 'Cr_2O_3 Control'. Tests were carried out at 400 °C.

4.4.4 Humidity Effects

Sensors were exposed to gases in dry air and then in the presence of 25%, 50% and 75% RH to understand whether humidity posed an effect on sensor performance (Fig. 4-22 and 4-23). Previous studies have reported that p-type semiconductors could serve as good candidates for humidity-resistant detection of gases.[107] It was expected that the incorporation of a hydrophobic zeolite such as H-ZSM-5 may serve to assist such behaviour.

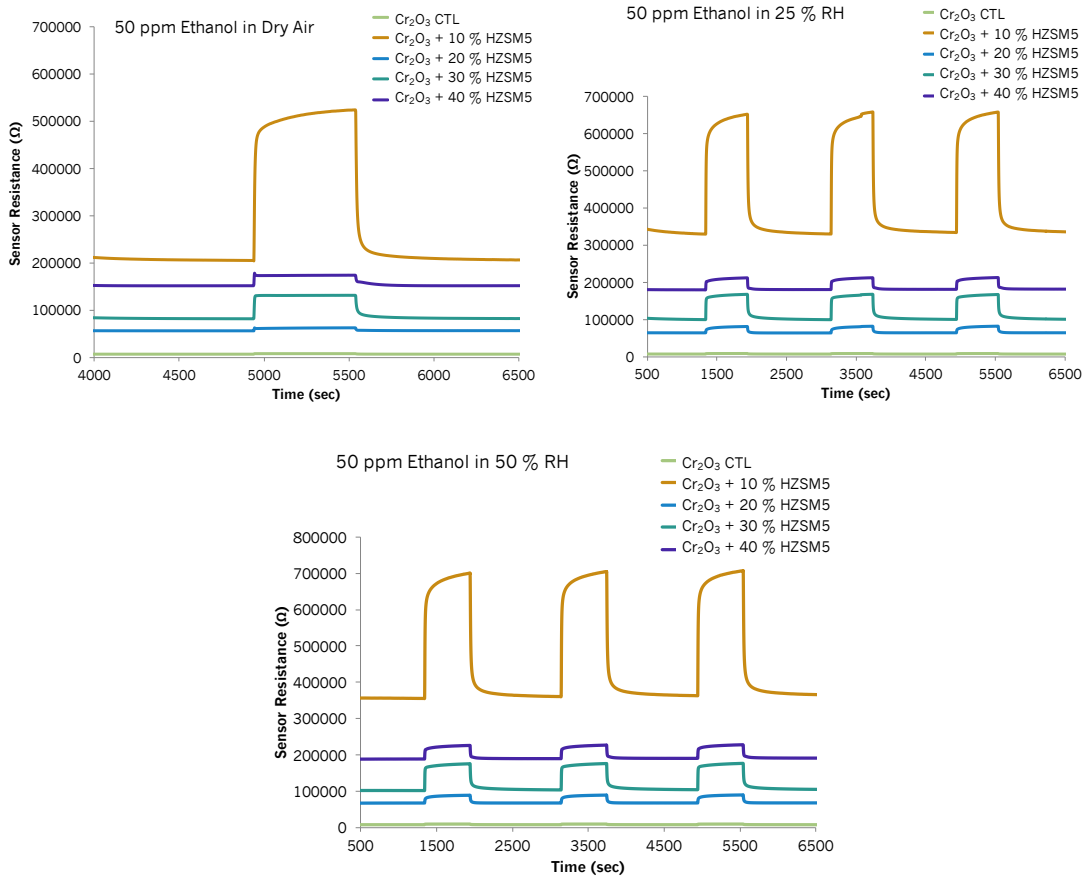

Figure 4-22 Sensor resistance to 50 ppm ethanol in dry air (top image), 25% RH (middle image) and 50% RH (bottom image). Refer to table 2-6 for sensor nomenclature.

Sensor responses to 50 ppm ethanol decreased in the presence of humid air from R/R_0 ~2.5 in dry air to R/R_0 ~2 in 25% and 50% RH. The baseline resistance of sensors increased with humidity when going from a dry air ambience to one in 25% RH, as expected. This is due to less oxygen being able to adsorb on the sensor surface due to water vapour interference. This hindrance results in a reduction of holes in the p-type system that causes an increase in the baseline resistance. Nevertheless, as the RH was progressively increased to 50% and 75% RH the baseline resistance of sensors did not change significantly. Sensors that contained more zeolite in the mixture were less

affected by humid environments. This is attributed to the hydrophobicity of zeolite H-ZSM-5.

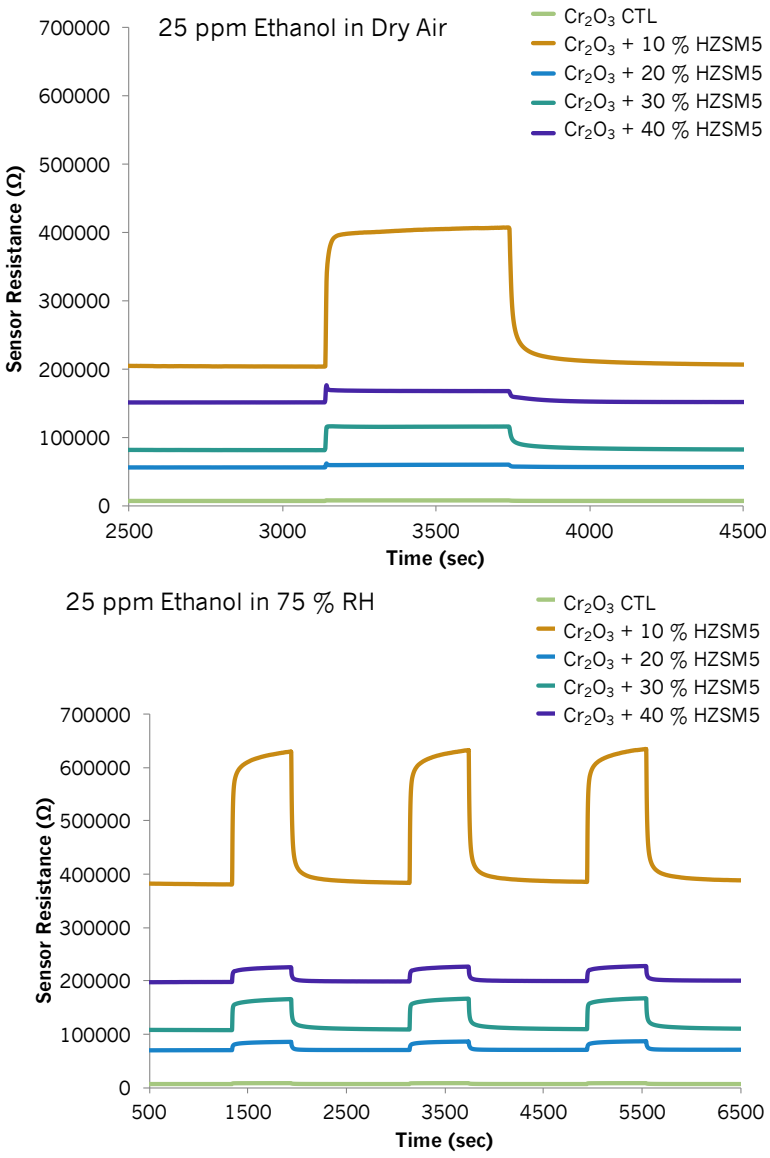

Figure 4-23 Sensor resistance to 25 ppm ethanol in dry air (top image) and in 75% RH (bottom image). Refer to table 2-6 for sensor nomenclature.

Figures 4-24 to 4-27 show how the baseline resistance changed from a dry air ambience to one with 25% RH and 50% RH with exposure to ethanol, acetone, toluene and methanol and have been provided to also illustrate the drift in baseline resistance following several gas tests and power cycles. The order followed for the tests was: toluene, ethanol, acetone and methanol. Thus, as can be seen, over time, the baseline resistance of the sensors increased. Baseline resistance drifts and instability are common with semiconductor gas sensors and have been long reported in the literature.[138,165,309] Interestingly, the control sensor was less susceptible to humidity changes overall, showing a change of ~9% in baseline resistance when switching from

an ambience of dry air to one with 50% RH. The sensor that experienced a more pronounced change in baseline resistance under humid conditions was that with 10% (wt.) H-ZSM-5, but as the RH was increased, the change was less intense (38% change from 0% RH to 25% RH and 7% change from 25% RH to 50% RH). The sensor containing 40% (wt.) H-ZSM-5, changed by ~19% when going from a test in dry air to one with 50% RH. Thus, having more zeolite in the structure did indeed assist in controlling humidity-based effects on the resistance of the sensor.

It is not well understood why the sensor containing more zeolite had a lower resistance than the one with less zeolite, given the insulating properties of zeolites. Nevertheless, the following hypothesis is put forward. Given that it is known 1) in the presence of water vapour there will be a competition between oxygen and water to reach the surface-active sites of the sensing material and that 2) the sensor with more zeolite will have a higher surface area and its surface will be more hydrophobic in nature, it could be possible that the sensor with 10% (wt.) HZSM5 will favour the surface adsorption of hydroxyl groups more readily than the one containing 40% (wt.) H-ZSM-5. As a result, the density of oxygen species populating the surface will be lowered, in relation to the sensor with less affinity for water and it will result in a higher baseline resistance given that the concentration of holes will be reduced (fewer electrons being extracted from the material bulk). Conversely, the sensor with 40% (wt.) H-ZSM-5 will potentially favour the adsorption of oxygen over water, abstracting electrons from the material bulk more easily and resulting in an increased concentration of holes, hence, lowering the sensor resistance. As the humidity in the chamber is increased further, the resistance increases due to even fewer oxygen species reaching the sensor surface due to the population of hydroxyl groups masking its straightforward access.

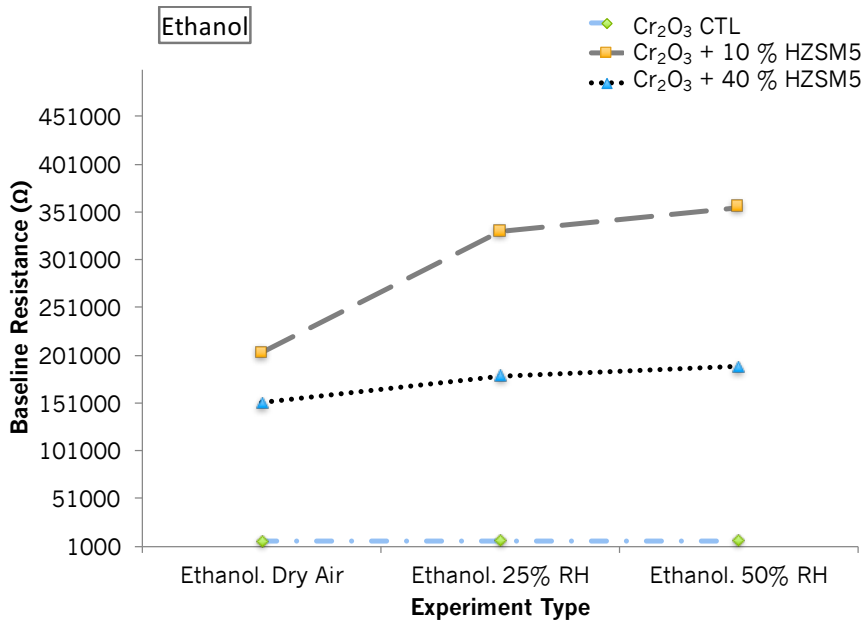

Figure 4-24 Baseline resistance values attained under dry ambient conditions, 25% RH conditions and 50% RH conditions. The values were taken as an average 60 seconds before the gas was injected into the sensing chamber with ethanol. Tests performed at 400 °C.

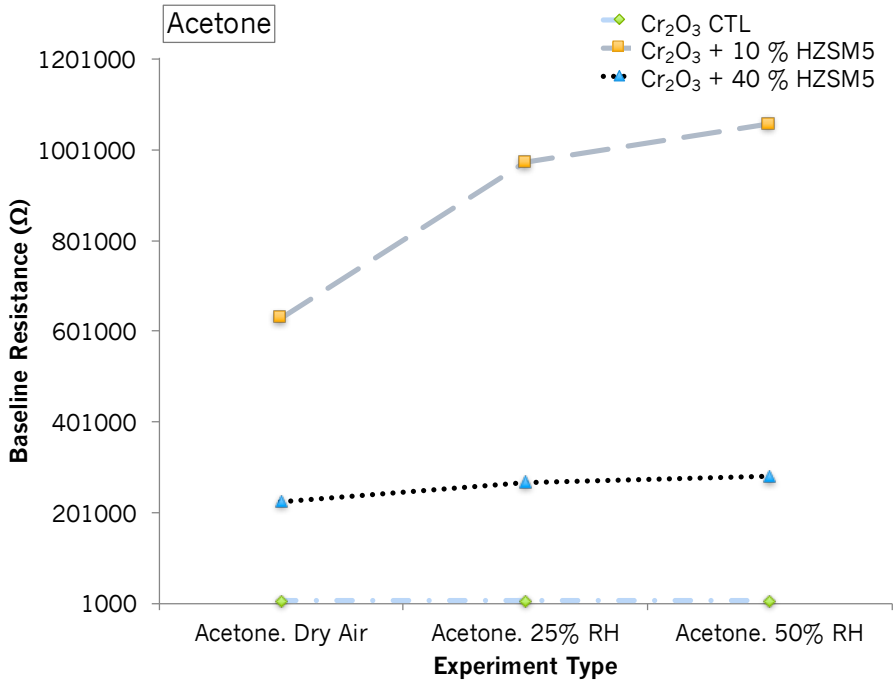

Figure 4-25 Baseline resistance values attained under dry ambient conditions, 25% RH conditions and 50% RH conditions. The values were taken as an average 60 seconds before the gas was injected into the sensing chamber with acetone. Tests performed at 400 °C.

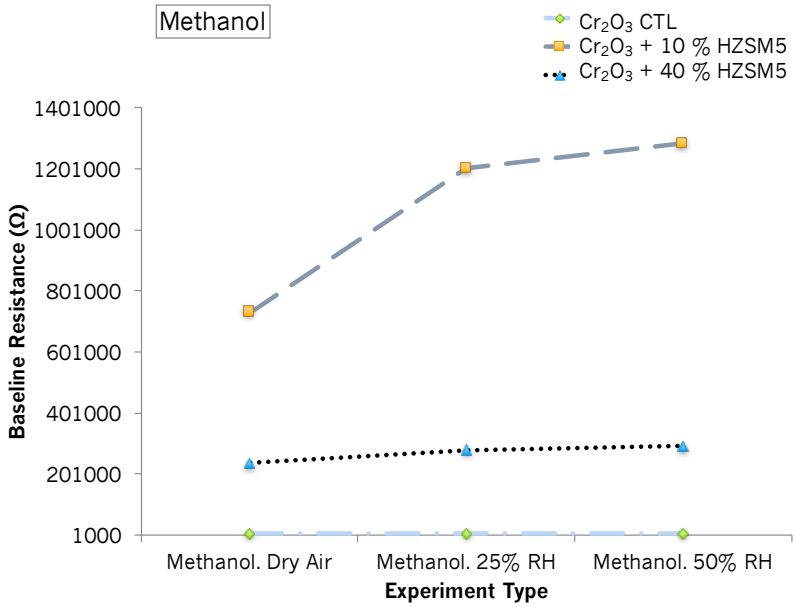

Figure 4-26 Baseline resistance values attained under dry ambient conditions, 25% RH conditions and 50% RH conditions. The values were taken as an average 60 seconds before the gas was injected into the sensing chamber with methanol. Tests performed at 400 °C.

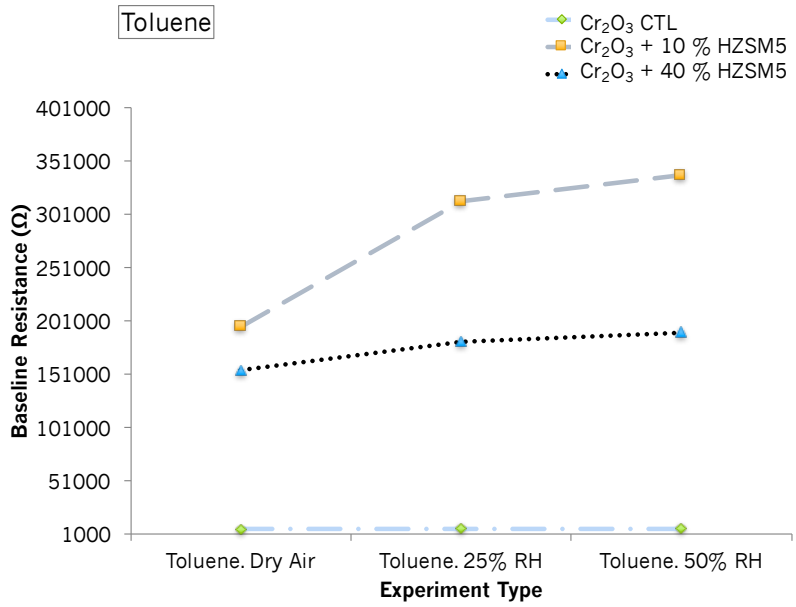

Figure 4-27 Baseline resistance values attained under dry ambient conditions, 25% RH conditions and 50% RH conditions. The values were taken as an average 60 seconds before the gas was injected into the sensing chamber with toluene. Tests performed at 400 °C.

Given the poor responses attained to these gases both in dry and humid air, this sensor array was deemed unsuitable for detection of trace gas concentrations of gases of interest for practical applications. The modification of Cr_2O_3 with mixtures of zeolite Na-A was explored next.

4.4.5 Modification of the Cr_2O_3 Sensor with 10% (wt.) Zeolite Na-A

The results with the H-ZSM-5 admixtures were not as promising as originally hoped. For this reason, Cr_2O_3 was further modified by incorporation of zeolite Na-A to understand how a zeolite with contrasting properties would influence sensor behaviour.

4.4.5.1 Physicochemical Characterisation Techniques

The XRD patterns of the control Cr_2O_3 material, together with those corresponding to that modified with an admixture with zeolite Na-A have been provided in Fig. 4-28 below. As can be seen in the figure, the incorporation of the zeolite did not alter the crystal structure of Cr_2O_3 and, in fact, the presence of the zeolite could not be appreciated in the XRD pattern. SEM images and EDS analysis confirmed the presence of the zeolite.

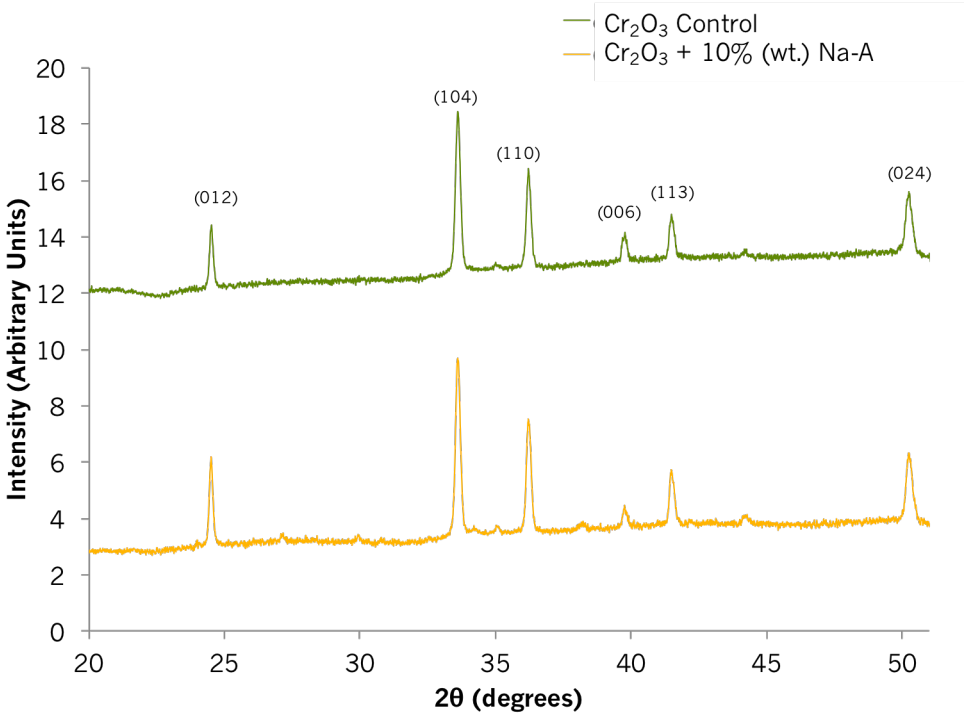

Figure 4-28 XRD pattern of a control Cr_2O_3 sensor and a Cr_2O_3 sensor modified by admixture with 10% (wt.) zeolite Na-A. XRD peaks have been indexed according to the literature.[299]

SEM images of the control and modified sensor have been provided in Fig. 4-29 below. Similarly to what was found with previous zeolite-admixed sensors, some zeolite Na-A particles that appeared cubic in shape and just over 1 μm in size could be identified and scattered throughout the surface. Inspecting the sensors at lower magnifications (×3,000) revealed that the zeolite-modified sensor had a slightly more compact appearance with less visible voids in the structure (Fig. 4-29D), when compared to the control sensor. There was no sign of particle fusion or agglomeration in the sensors and the presence of Cr_2O_3 was still very clearly seen and dominant throughout the sensor.

EDS analysis (Table 4-9) revealed the presence of Cr, O, Si, Al and Na, as expected. Advera reports the Si/Al ratio in the zeolite to be ~1.1 and here it was found to be 0.95. The ratio between Cr and O is slightly off but this could be due to the presence of oxygen in the zeolite structure.

Table 4-9 EDS analysis providing the atomic percentage of a Cr_2O_3 sensor mixed with 10% (wt.) zeolite Na-A. Atomic % of the unmodified sensor presented in Table 4-3 above.

	Atomic Percentage (%)				
Cr_2O_3 admixed with 10% (wt.) Na-A	O	Cr	Si	Al	Na
	60.3 (±0.9)	32.7 (±0.5)	2.1 (±0.3)	2.2 (±0.4)	2.7 (±0.7)

BET revealed that the surface area of Na-A was 0.9065 m^2/g in relation to 2.30 m^2/g of the control sensor. It was found to be 2.5 times smaller in surface area than the base material. N_2 is 3.64 Å and thus should not affect the adsorption inside the pores of zeolite Na-A, which are 4.1 × 4.1 Å. Nevertheless, the surface area of this zeolite was much lower than expected.

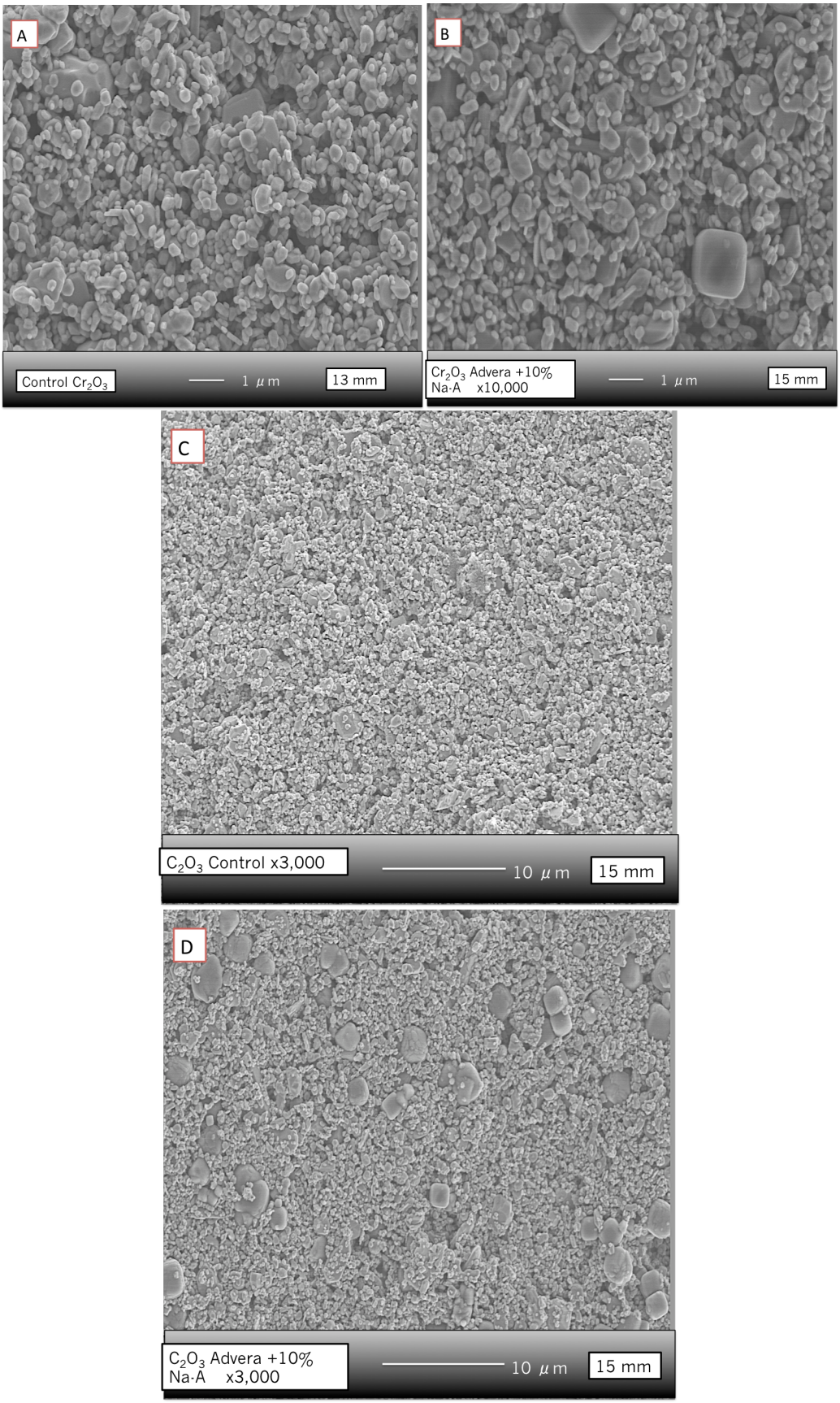

Figure 4-29 SEM images of control (A) Cr_2O_3 sensor and (B) Cr_2O_3 modified by incorporation of 10% (wt.) zeolite Na-A both at a magnification of ×10,000. (C) Cr_2O_3 control sensor at ×3,000 (D) Cr_2O_3 sensor modified with 10% (wt.) zeolite Na-A at a magnification of ×3,000.

4.4.6 Gas-Sensing Results of the Cr_2O_3 Sensor Modified by Mixtures of Zeolite Na-A

Initial tests were performed at 400 °C and test gases investigated included acetone, ethanol, toluene and water vapour. Tests were performed at this temperature so that results could somewhat be compared to those provided by the modification of Cr_2O_3 with H-ZSM-5 zeolite. Nevertheless, the zeolite-modified sensor was found to be poorly responsive to several gases (ethanol, acetone and water vapour) and, for this reason, other operating temperatures were investigated, ranging between 300 °C and 450 °C.

As per previous tests, Na-A zeolite was incorporated because it has much smaller pore dimensions and a high Al content, making it hydrophilic in nature, which would contrast well with the hydrophobic nature of H-ZSM-5 and its larger pores.[21,22,30] Thus, in essence, this zeolite should result in higher affinity towards water vapour and more polar molecules such as ethanol and acetone but should exhibit less affinity towards a non-polar molecule such as toluene. It was expected that this would be observed in the gas sensing results.

Very interestingly, the sensor containing Na-A zeolite showed incredibly poor sensitivity towards ethanol, acetone and water vapour over temperatures ranging from 300 °C to 450 °C and its presence did not meliorate the responses attained with the control Cr_2O_3 sensor (refer to graphs in the Appendix). In fact, it seemed to worsen the responses upon exposure to ethanol and acetone. The responses towards water vapour were almost identical to those seen in the control sensor. The baseline was seen to drift within tests and responses did not exceed $R/R_0 = 1.1$. The zeolite-modified sensor was non-responsive to acetone across the range of temperatures investigated.

In contrast, the exposure of the zeolite-modified sensor to toluene resulted in a vast improvement in its detection. At 400 °C and 450 °C the responses of the control and the zeolite-modified sensor were comparable. When the temperature was lowered to 350 °C, the modified sensor provided a 2.7-fold increase in sensor response over the control when supplied with a concentration of 50 ppm of toluene gas. When supplied with 5 ppm and 10 ppm both control and zeolite-modified sensors were sensitive to toluene but it was not until 25 ppm of the gas was supplied that the zeolite-modified sensor began to show a difference in the response pattern towards toluene. Cr_2O_3 has previously been reported to show excellent catalytic activity towards toluene at 350 °C [211] and other studies have found that toluene can be completely oxidised to CO_2 and H_2O over Cr_2O_3 catalysts.[310] Ma et al. [211] developed mono-dispersed porous Cr_2O_3

microspheres that exhibited great sensitivity and selectivity towards toluene. The responsiveness towards the gas was attributed to the chemisorbed oxygen being able to accept electrons from the active benzene ring in the aromatic molecule, which are then transferred back to the oxide bulk, cancelling out holes and increasing the sensor resistance.

It is observed that the diffusion of toluene through the structure is slow-paced and this is attributed to its large size. Although the molecule would not be able to pass through the pores in the zeolite, it may still diffuse through the cavities in the sensor structure. Na-A is a hydrophilic zeolite and so the affinity towards toluene is not regarded as favourable. Although Sahner et al. [24] suggests that the ionic conductivity introduced by the Na^+ cations in zeolite frameworks contributes to a measurable change in the conductivity of the system upon interaction with a gas,[302] Na-A is not a zeolite used in HC cracking and it is not thought that toluene may break down into smaller reaction products in this system. It is possible that the incorporation of zeolite Na-A, which displayed particle sizes that were considerably larger than those of Cr_2O_3, may have opened up the microstructure of the sensing system such that toluene was able to diffuse more readily through it. The shark-fin shape of the sensor transient was indicative that there were sufficient reactive sites available for the molecule to interact with at the concentrations supplied and that the oxygen was not replenished at a fast-enough rate for the sensor to saturate and reach steady state.[136]

The optimal operating temperature for toluene detection was thus 350 °C (Fig. 4-30). When supplied with 50 ppm of the gas, the sensor took ~eight minutes to reach 90% of the maximum resistance value and it took 82 seconds to recover. The control took ~6 minutes to reach 90% of its maximum resistance value and took just over five minutes to recover. Therefore, the zeolite-modified sensor provided a great enhancement in response at trace concentration of the gas, the presence of zeolite served to increase the response time but shorten the recovery time, facilitating the desorption of the gas. At 300 °C, there was clear baseline drift and the sensors did not recover in the given 20 minutes of air supplied between gas pulses (Fig. 4-31).

In the zeolite-modified sensor, the sensor responses increased linearly when supplied with 5 to 25 ppm of toluene. A third order polynomial equation (Table 4-10) was fitted to the 'response vs. concentration' plot to find the sensitivity of the sensor towards toluene (Fig. 4-32 and 4-33). It was found that as the concentration of toluene increased, the sensor sensitivity also increased.

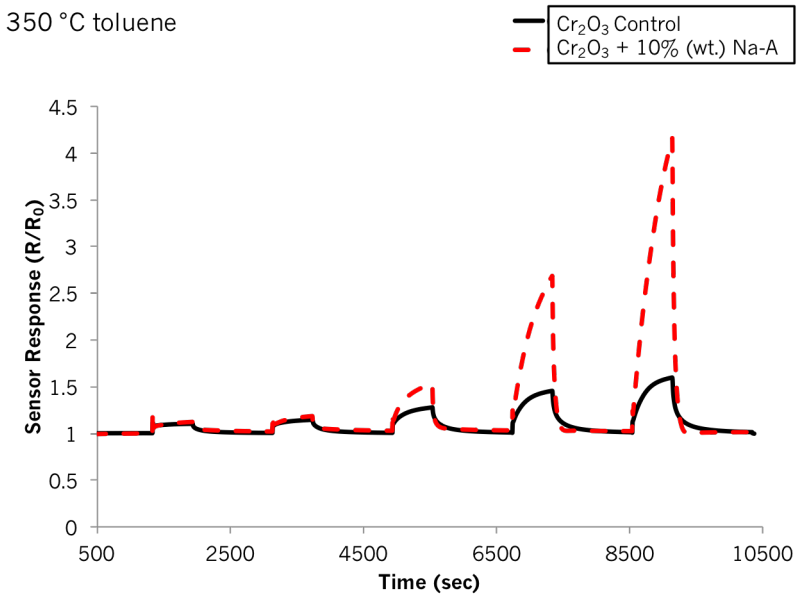

Figure 4-30 Sensor responses of a control Cr_2O_3 and Cr_2O_3 + 10% (wt.) Na-A to 5 ppm, 10 ppm, 25 ppm, 40 ppm and 50 ppm toluene vapour at 350 °C.

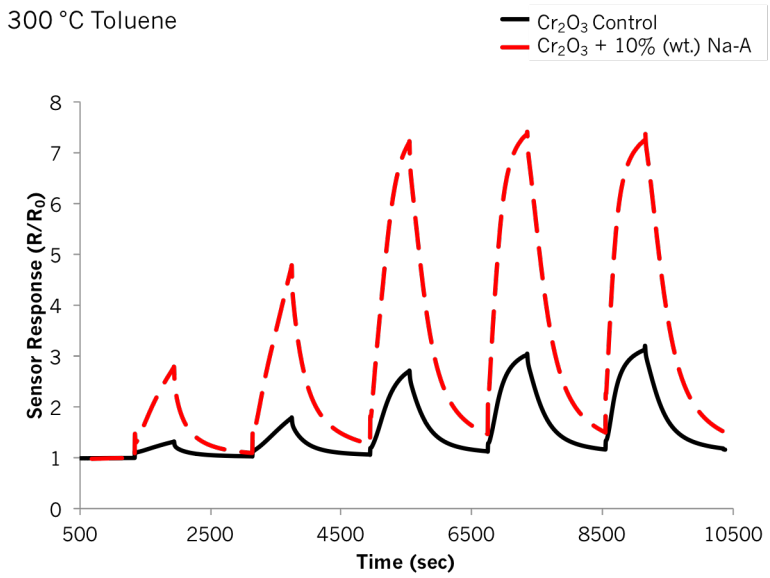

Figure 4-31 Sensor responses of a control Cr_2O_3 and Cr_2O_3 + 10% (wt.) Na-A to 5 ppm, 10 ppm, 25 ppm, 40 ppm and 50 ppm toluene vapour at 300 °C.

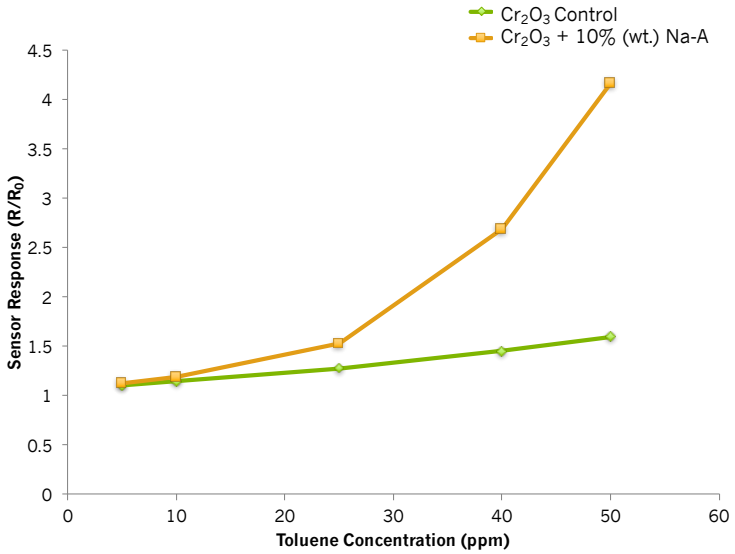

Figure 4-32 Sensor responses to toluene at 400 °C. The response vs. concentration curve was fitted to a third order equation, which has been displayed individually for each sensor in Table 4-10.

Table 4-10 Polynomial equations fitted to the response curves in Fig. 4-32 for each the Cr_2O_3 sensor modified by 10% (wt.) admixture with zeolite Na-A upon exposure to toluene gas.

Sensor Type	Polynomial Equation	R-Squared Value
Cr_2O_3 + 10% (wt.) Na-A	$y = 3E\text{-}05x^3 - 0.0004x^2 + 0.0102x + 1.0848$	0.99

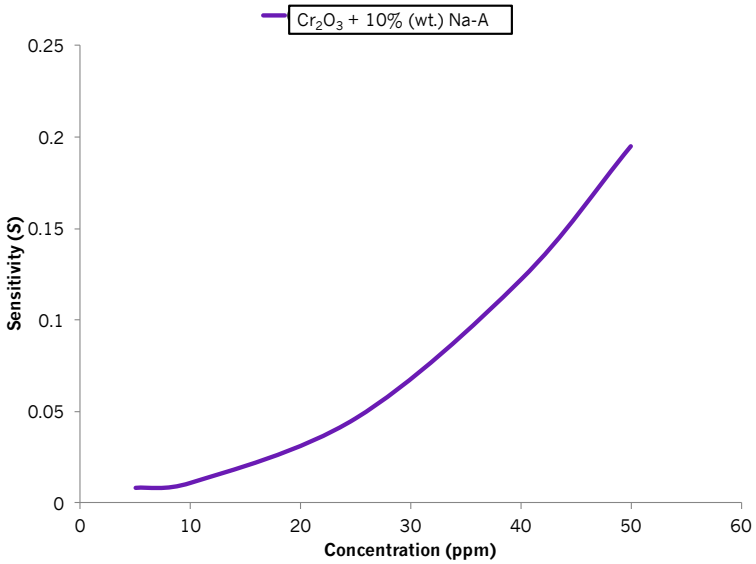

Figure 4-33 Sensitivity curve of Cr_2O_3 modified sensors towards toluene gas at 400 °C. Sensitivity curve obtained from fitting the response vs. concentration curves to third order polynomial equations.

Because at 350 ˚C the sensor was not sensitive to other gases it can be said that it was selective towards toluene. Its detection is important in indoor environments due to its noxious effect on health and it is also abused recreationally.[211,269] The results found here are very promising for the selective detection of toluene. Because the sensor did not show sensitivity towards water vapour it is thought that in humid environments the sensor would still be able to respond well to toluene.

4.4.7 Modification of the Cr_2O_3 Sensor with Coatings of Zeolite H-Y

Zeolite H-Y has been reported to facilitate toluene adsorption in its super-cages and it is also a well-known zeolite used in catalysis to crack HCs. The aim of this study was to understand whether a zeolite with higher surface area and with pores and channels of larger dimension would provide an improvement to sensor responses due to more direct access of the material to a catalytic surface. Further, promising results were attained with this configuration and at an operating temperature of 400 °C, as shown in the tabulated results provided at the end of Chapter 3.

4.4.7.1 Physicochemical Characterisation Techniques

The XRD patterns of the control Cr_2O_3 sensor and that modified with overlayers of zeolite H-Y are provided in Fig. 4-34 below. The zeolite coating on top of the Cr_2O_3 base material resulted in a higher intensity of the peaks corresponding to H-Y in comparison to the control sensor material, as expected. XRD peaks corresponding to zeolite H-Y could be identified at 2θ of 10.2°, 12.02°, 15.8°, 18.9°, 20.6°, 23.9°, as displayed in the figure and are in accordance with the literature.[290]

SEM images of the control and the zeolite-modified sensor have been provided in Fig. 4-35 below. Cr_2O_3 could not be appreciated in the sensor coated with zeolite H-Y, shown in the image on the right. Instead, one could observe the zeolite particles of H-Y, which were ~300 – 500 nm in size and had a rhomboidal shape. The particles appeared to be interconnected, whereas in the control sensor they appeared loosely packed. At a magnification of ×1,000, the porosity of the zeolite-modified sensor could be easily appreciated and, although the surface of the control had a much smoother appearance, indicating hindrance to gas diffusion, the zeolite-modified sensor displayed particle agglomerations that protruded from the surface, creating access for gas molecules to diffuse and interact with.

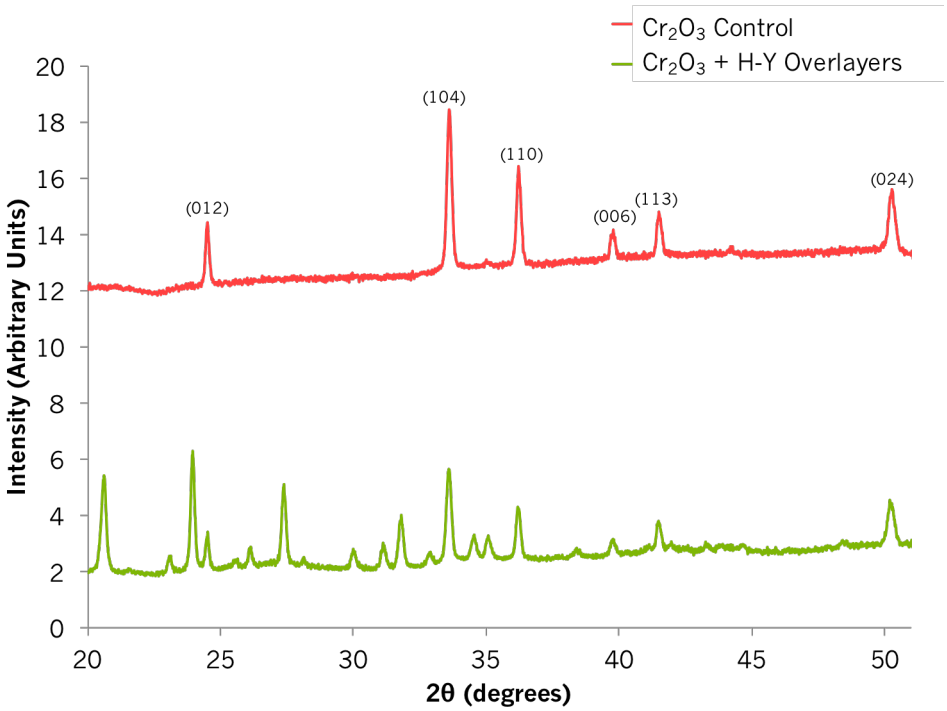

Figure 4-34 XRD patterns of a control Cr_2O_3 sensor and a Cr_2O_3 sensor modified by screen-printed layers of zeolite H-Y on top of it. Peaks have been indexed according to the literature.[299]

In essence, the gas would be able to interact not only with the surface of the system but also within the pores in zeolite structure and further down into the sensitive layer. As disclosed previously, the size distribution of the control sensor particles was ~ 100 – 400 nm.

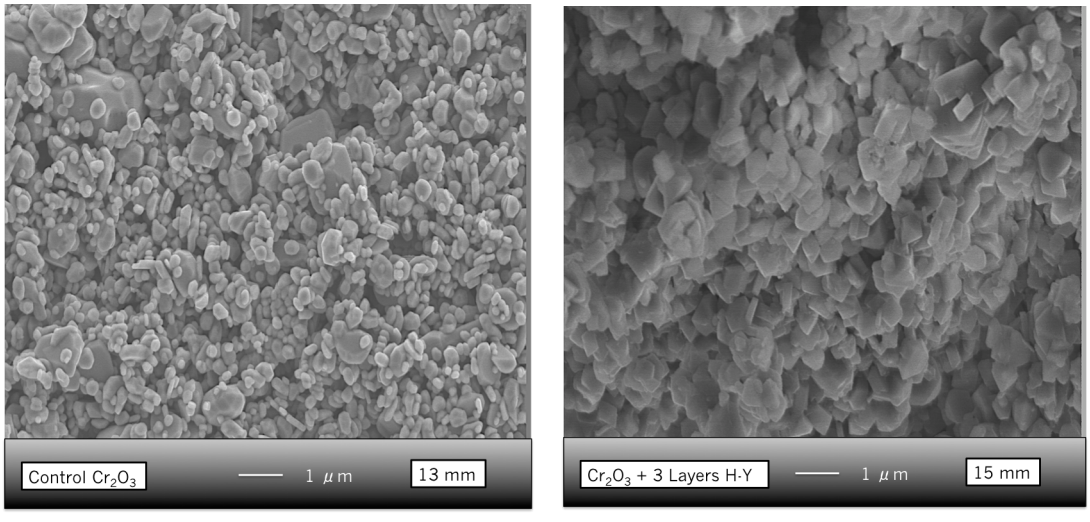

Figure 4-35 SEM images of a control Cr_2O_3 sensor (left) and a Cr_2O_3 sensor coated with three layers of zeolite H-Y (right).

BET analysis revealed that the surface area of the zeolite powder was 429.13 m^2/g, in relation to 2.30 m^2/g of the control sensor. It was expected that the much-increased

surface area of the zeolite would result in a higher concentration of surface-reactive sites for gas molecules to interact with. In turn, it was anticipated that the sensor responses towards the gases would be enhanced. The sensors were exposed to: ethane (3.8 Å), methanol (3.6 Å), ethanol (4.3 Å), acetone (4.6 Å) and toluene (5.8 Å), all of which had smaller kinetic diameters than the pore sizes of the zeolite (7.4 × 7.4 Å). It was therefore expected that these molecules would not experience hindrance when diffusing down to the sensitive layer of the sensor.

EDS analysis revealed the presence of aluminium, silica and oxygen in the system, but it did not detect chromium (Table 4-11). The Si/Al ratio of the zeolite was found to be 3, which is lower than the reported Si/Al = 5.2 by Zeolyst.

Table 4-11 EDS analysis corresponding to the atomic percentage of a Cr_2O_3 sensor coated with three layers of zeolite H-Y. The atomic ratio for the unmodified material was presented in Table 4-3 above.

	Atomic Percentage (%)		
	O	Al	Si
EDS of Cr_2O_3 sensor with H-Y Coatings	63.4 (±1.2)	8.9 (±0.6)	27.7 (±0.9)

4.4.8 Gas-Sensing Results of the Cr_2O_3 Sensor Modified by Zeolite H-Y Coatings

Modification of the control sensor with zeolite H-Y resulted in different sensor responses when exposed to test gases, in relation to the unmodified sensor. When the sensor modified by zeolite H-Y was exposed to ethane, the responses (R/R_0) were unaffected by concentration increments and they were consistently lower than 1.2. It is noteworthy that the zeolite-modified sensor did not respond by shifting its behaviour to n-type with higher concentrations of ethane, which was noticed in previous experiments reported in Chapter 3 and in previous sections of Chapter 4. This could be indicative that upon interaction with this zeolite it avoided the production of an oxidising gas and it led to the complete combustion of the gas to CO_2 and $H_2O_{(v)}$. This was also supported by the flat shape of the peaks during gas pulses, which indicate the occurrence of fast reactions at the sensor surface.[15]

With methanol exposure, the 'Cr_2O_3 + 3L H-Y' sensor began to behave differently to the control after 50 ppm (Fig. 4-36). This was also the case with ethanol and acetone exposure. The responses towards acetone and ethanol were once again very similar. However, the sensor responded more slowly with ethanol exposure. Sensor responses to toluene saw a great enhancement with the incorporation of layers of zeolite H-Y,

relative to the unmodified Cr_2O_3 sensor. The zeolite-modified sensor responded to all gas concentrations and provided a ~4-fold increase in sensor response upon exposure to 40 ppm of toluene over the control, and a 5.6-fold increase in response when exposed to 50 ppm of toluene gas.

Zeolite H-Y has been reported to be able to adsorb toluene well in its super-cages and it is said that it interacts weakly with the pore walls and thus is able to diffuse rather quickly through them when there is a low loading of gas molecules.(311) In the temperature range of 200–400 °C, cracking of toluene is likely to occur when in contact with the zeolite due to the occurrence of –OH groups with Brönsted acid character.(311) The same paper suggests that transalkylation may result in the production of light alkenes and those may react further with the acid sites in the zeolites.

Response vs. concentration curves were plotted to understand whether the zeolite-overlaid sensor responded linearly to increased gas concentrations (Fig. 4-37). Sensitivity curves were fitted to second order polynomial equations to model the behaviour of the H-Y sensor (Fig. 4-38). As can be seen in the figures, the sensitivity of the zeolite-modified sensor was seen to increase with gas concentration increments. This is promising for practical applications as it means that the sensor could be employed to cover a wide dynamic range of gas concentrations. Nevertheless, it is acknowledged that additional concentrations should be evaluated to understand its behaviour and capability in further detail.

The selectivity of the 'Cr_2O_3 + 3L H-Y' sensor towards gases was assessed by using Equation 4 introduced in Chapter 2. Sensor responses were compared with exposure to 50 ppm of the gases tested. It was found that selectivity towards toluene was 0.79, in relation to 0.08 towards both ethanol and acetone and 0.04 towards methanol. The sensor was therefore much more sensitive and selective towards toluene than it was to other gases. It is thought that toluene was able to interact well with the zeolite layers, potentially being oxidised to produce reaction products such as phenol, CO_2 and $H_2O_{(v)}$ or intermediates such as benzaldehyde and benzoic acid. These results suggest that the sensing material exhibited greater affinity towards the reaction products, which resulted in an enhancement in sensor response. Nevertheless, toluene gas has been found to take very long times to respond and recover in the sensor systems investigated in this thesis, in relation to other toluene gas sensor devices described in the literature.(301,312) This, in turn, makes this sensor potentially impractical for real-life detector systems that need to be used continuously. The sensor took 1.5 minutes to

reach τ_{90} at 50 ppm toluene and >7 minutes to recover. Future work ought to explore the option of reducing the number of zeolite layers to try and shorten these.

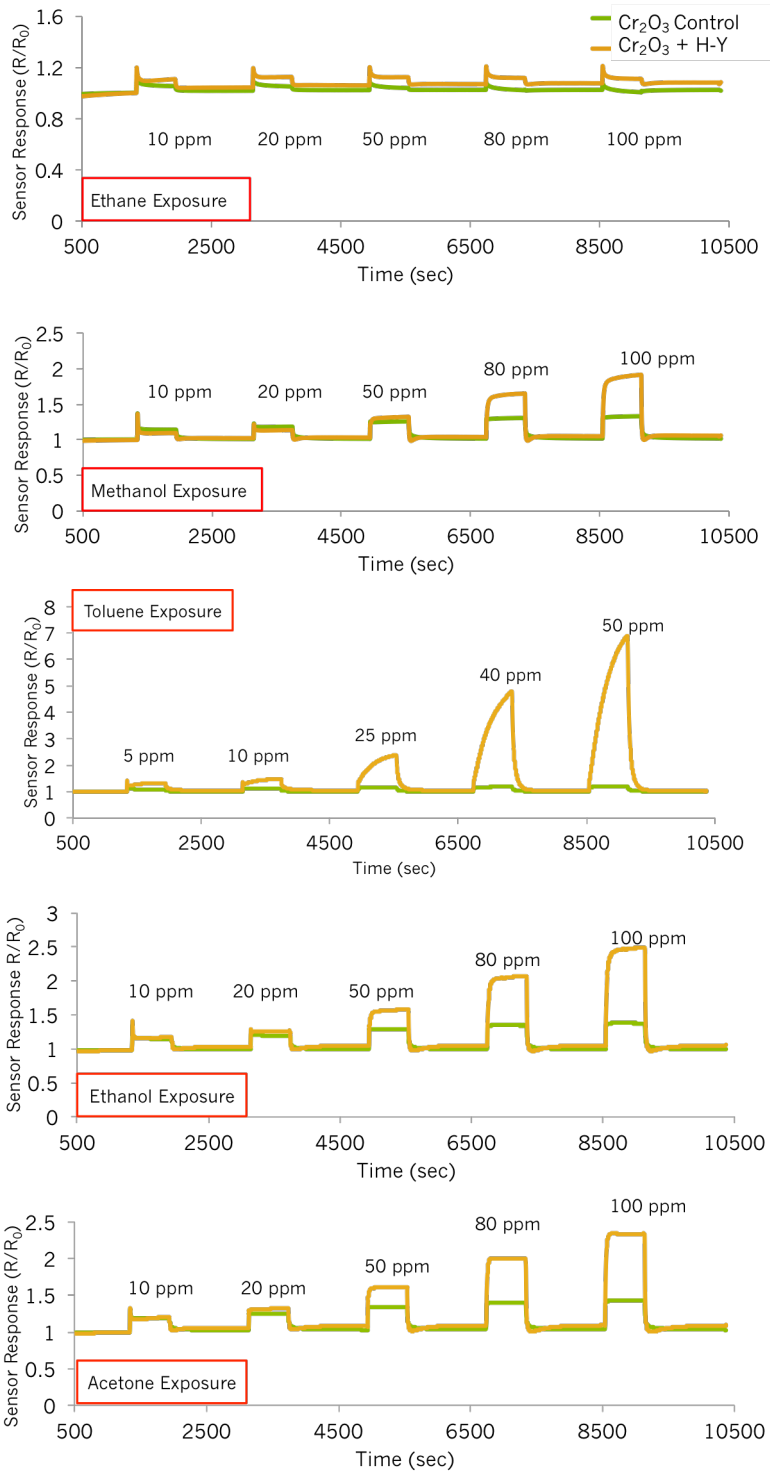

Figure 4-36 Sensor responses to ethane, methanol, ethanol, acetone and toluene gases of the Cr_2O_3 control sensor and Cr_2O_3 modified with three layers of zeolite H-Y at 400 °C.

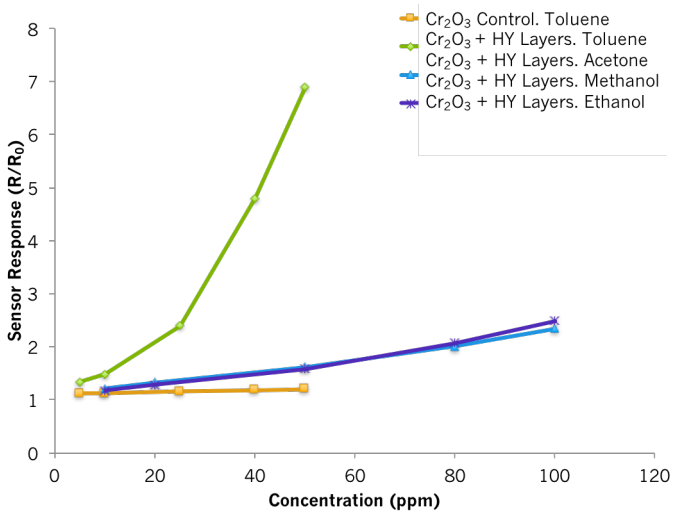

Figure 4-37 Sensor responses to toluene, acetone, ethanol and methanol gases at 400 °C. The sensor response of the control Cr_2O_3 to 5 – 50 ppm of toluene has also been included for comparison purposes.

Table 4-12 Polynomial equations fitted to the response curves in Fig. 4-37 for each sensor upon exposure to toluene, ethanol, acetone and methanol gases.

		Polynomial Equation	R-squared Value
Toluene	Cr_2O_3 CTL	$y = -3E\text{-}06x^2 + 0.0022x + 1.1031$	0.98
	Cr_2O_3 + H-Y	$y = 0.0027x^2 - 0.0268x + 1.4257$	0.99
Ethanol	Cr_2O_3 + H-Y	$y = 9E\text{-}05x^2 + 0.0047x + 1.1314$	0.99
Acetone	Cr_2O_3 + H-Y	$y = 5E\text{-}05x^2 + 0.0067x + 1.1514$	0.99
Methanol	Cr_2O_3 + H-Y	$y = 6E\text{-}05x^2 + 0.0015x + 1.1086$	0.99

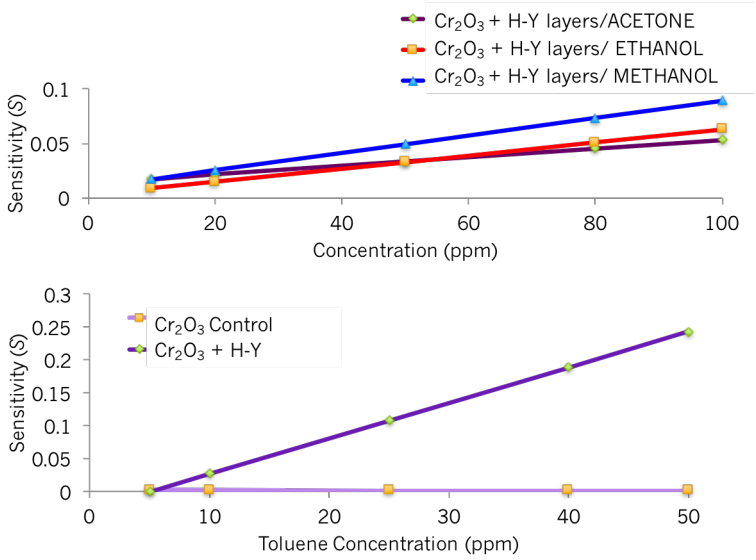

Figure 4-38 Sensitivity curves of H-Y sensor to acetone, ethanol, methanol and toluene. Sensitivity curves were attained by fitting a second order polynomial equation to the curves shown in Fig. 4-37.

4.4.9 Humidity Effects

Humidity effects were investigated upon exposure to toluene gas, given the modified sensor's sensitivity towards toluene. The effects were tried when supplying the sensor with three pulses of 25 ppm of toluene at 400 °C under 25% RH and under 50% RH (Fig. 4-39 and 4-40).

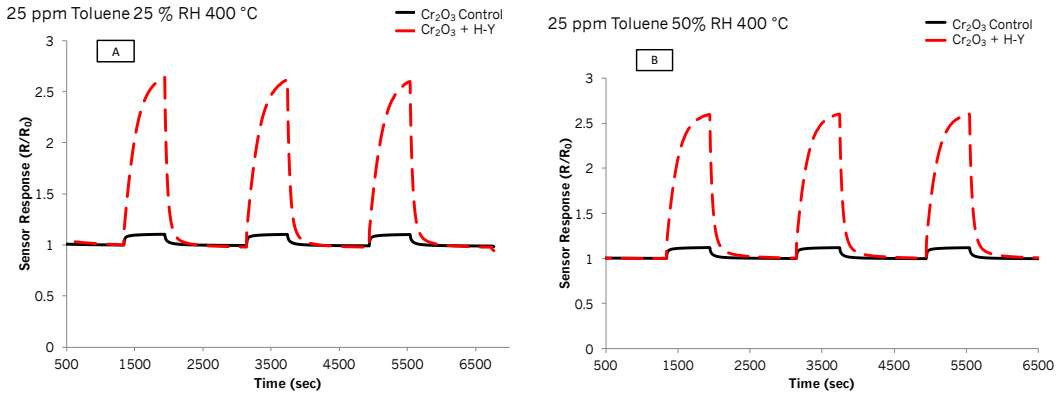

Figure 4-39 Sensor responses of a control Cr_2O_3 sensor and a Cr_2O_3 sensor modified with 3L of zeolite H-Y towards 25 ppm toluene gas at 400 ˚C under (A) 25% RH and (B) 50% RH.

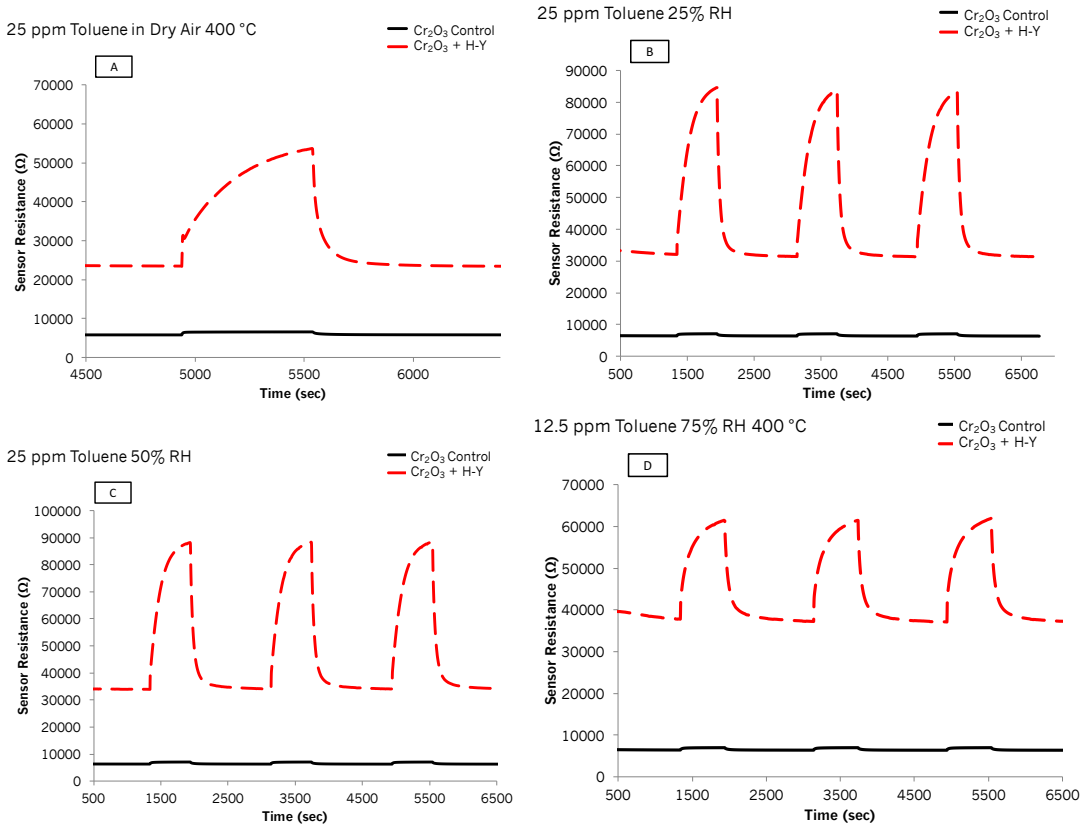

Figure 4-40 Sensor resistances of a control Cr_2O_3 sensor and a Cr_2O_3 sensor modified with layers of zeolite H-Y towards (A) 25 ppm toluene in dry air, (B) 25 ppm toluene under 25% RH, (C) 25 ppm toluene under 50% RH and (D) 12.5 ppm toluene under 75% RH. All tests were carried out at 400 °C.

As shown in Fig. 4-39 and when compared to the sensor responses seen under a dry air ambience, it can be seen that the sensor modified with layers of zeolite H-Y was resistant to humidity, the sensor provided the same response magnitude and response pattern towards the gas. This was the case both under 25% RH and under 50% RH. The baseline resistance of the sensor increased, as expected, when going from a dry air environment to one in humid air. Nevertheless, when going from 25% RH to 50% RH the baseline resistance remained mostly unaffected. When increasing the RH to 75% there was another noticeable increase in the baseline resistance.

Note that a summary of the sensor responses obtained in this chapter have been presented in Tables 8-5 to 8-7 in the Appendix.

4.5 Summary of Results

This chapter has presented the results of a modified Cr_2O_3 sensor with different zeolite combinations. Although p-type systems are known to be less responsive to reducing gases than n-type ones, recent research in the field of gas sensing had shown promise for the detection of HCs and solvent vapours. This study reports that although the different H-ZSM-5-modified sensors provided different responses and patterns to a particular gas they often provided similar responses and patterns towards molecules that were similar in size and shape.

The incorporation of zeolite H-ZSM-5 did enhance the responses when compared to the unmodified Cr_2O_3 material and sensors that contained 10% (wt.) and 30% (wt.) of the zeolite were the most promising for gas detection. The modification of the Cr_2O_3 control with 10% (wt.) Na-A showed poor responses towards ethanol, acetone and water vapour over a range of temperatures (300 – 450 °C). However, its response towards toluene gas was highly promising, as were the gas sensing responses attained with the modification of Cr_2O_3 with layers of zeolite H-Y. Both sensors were selective towards toluene. In the Cr_2O_3 sensor modified by H-Y layers, the sensor response was kept the same in the presence of water vapour and this can be potentially attributed to little interference for the active sites from water vapour.

The following Chapter focuses on the gas-sensing results attained when modifying Fe_2O_3 through admixtures with zeolites H-ZSM-5 and Na-A and overlayers with zeolite H-Y. Initial tests were carried out with a control Fe_2O_3 sensor, the powdered material of which was commercially sourced from BDH Laboratories and it was used to assess its potential as a gas sensor. Although typically n-type, the sensor displayed p-type semiconducting behaviour towards a range of reducing gases. Due to the powder

material being unavailable when it was later needed to fabricate the zeolite-modified sensors, another commercial Fe_2O_3 was used from Sigma Aldrich. The new sensor displayed n-type behaviour towards the gases tested.

5. Zeolite-Modified Iron Oxide Based Gas Sensors

Chapter 5 details the results attained when modifying a control n-type Fe_2O_3 material with admixtures of zeolites H-ZSM-5 and Na-A and overlayers of zeolite H-Y. Modifying the base material with zeolites did not improve the results towards gases of interest. However, testing another unmodified Fe_2O_3 base material that was sourced from a different company provided much-enhanced sensor responses to gases, as well as p-type behaviour, which were noteworthy results. This Chapter thus investigates:

- Sensor responses of two base Fe_2O_3 sensors fabricated with powders obtained from different commercial sources.
- The effects of humidity on the base materials.
- The effects of incorporating zeolites Na-A and H-ZSM-5 in the form of admixtures and H-Y in the form of overlayers to enhance the performance of the basic sensor.

5.1 Introduction

Fe_2O_3 is an n-type material that has gained great attraction in the gas-sensing field, particularly over the last 5-10 years. It has been widely used in several applications due to its chemical stability,[313] narrow band gap (Eg ≈2.2 eV),[314] low toxicity, environmentally friendly properties and low cost.[224] The high mobility of oxygen ions on its surface makes this material suitable for catalytic oxidative reactions and this extends to its suitability as a gas sensor.[224] The morphology of the particles in Fe_2O_3 has been found to be a determinant factor for high sensitivity in gas sensors. As such, much of the research published in the last 2-5 years has focussed on the fabrication of different architectures of the material, such as hollow spheres for methanol[313] and ethanol detection,[221] mono-dispersed porous microparticles for acetone detection,[220] porous microrods for ethanol detection,[314] mesoporous microrods for triethylamine detection,[218] and ultrathin nanosheets for ethanol and acetone detection,[223] to name a few. Other groups have decorated Fe_2O_3 with metal Au nanoparticles for H_2S detection,[227] and others have decorated n-type materials such as SnO_2 nanowires with Fe_2O_3 nanoparticles for ethanol detection.[258]

To the best of our knowledge zeolite modification of Fe_2O_3 has not been reported in the literature and it was one of the motivations behind this study.

5.2 Preliminary Tests on the Unmodified Fe_2O_3 Sensor

Sensors with different number of Fe_2O_3 layers were fabricated to assess sensor responses as a function of film thickness against toluene and isopropyl alcohol (IPA)

gases (5.2.1 and 5.2.2). The optimal operating temperature was then found using the most responsive sensor against two gases of interest, ethanol and toluene (5.2.3). Preliminary tests in the aforementioned sections were all performed on Sparky rig (details in Peveler et al. [28]). Initial tests were carried out with a sensor fabricated with the Fe_2O_3 powder attained from BDH.

5.2.1 Effects of Film Thickness on Fe_2O_3 BDH Sensor Responses

Initial tests were carried out at 300 °C. As mentioned previously, this is a temperature of interest in practical gas sensing applications and it was the lowest temperature that could be reached on Sparky rig.

It must firstly be noted that this sensor displayed p-type behaviour upon exposure to reducing gases. Fe_2O_3 has been reported to behave as n-type or p-type in several studies in the literature.[221,228,315,316] The reasons behind this behaviour are still a subject of debate and they are explained in further detail in coming sections. Nevertheless, Gurlo et al. [317] describe that the three types of defects in the Fe_2O_3 structure, namely oxygen vacancies, Fe^{3+} interstitials and Fe^{2+} interstitials, give rise to semiconductor behaviour in this system.[228] As such, where additional oxygen enters the lattice as O^{2-}, it leads to a shortage of electrons (holes are introduced) that results in p-type behaviour. Conversely, the loss of oxygen will leave electrons in the lattice that will result in n-type behaviour.[228]

As shown in Fig. 5-1 and 5-2 below, the sensor that was most responsive to the gases was that fabricated with five Fe_2O_3 depositions. With exposure to IPA gas, the sensors with three and seven film depositions responded almost identically to it. With exposure to toluene, the sensor with three film depositions was the one that was least responsive to the gas, followed by the one with seven film depositions and then the one with five film depositions.

As observed with the Cr_2O_3 sensors in Chapter 4, above and below a certain film thickness, i.e. five film depositions, the responses towards test gases decreased. The baseline resistance of the sensors ranged between 4 – 10 MΩ, which is in line with other studies found in the literature that investigated this sensing material.[223,314]

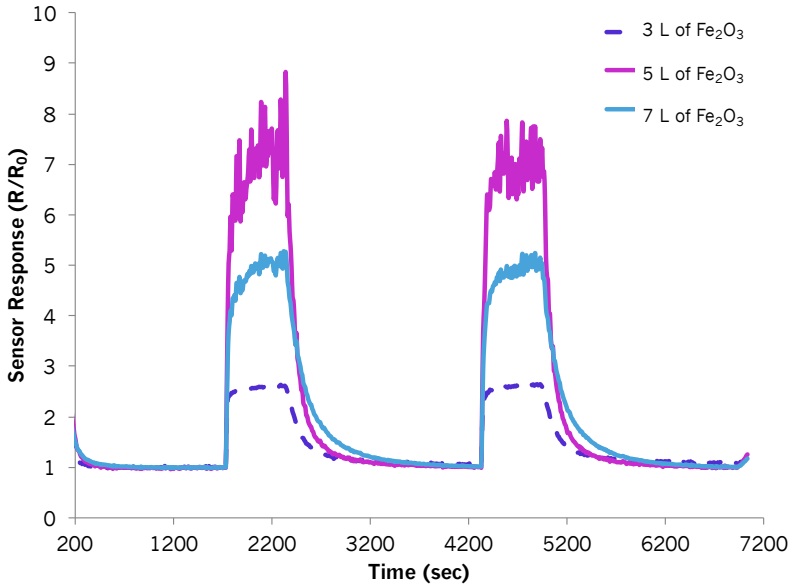

Figure 5-1 Fe_2O_3 sensor responses to two pulses of 45 ppm toluene vapour when printed with three, five or seven film depositions at 300 °C.

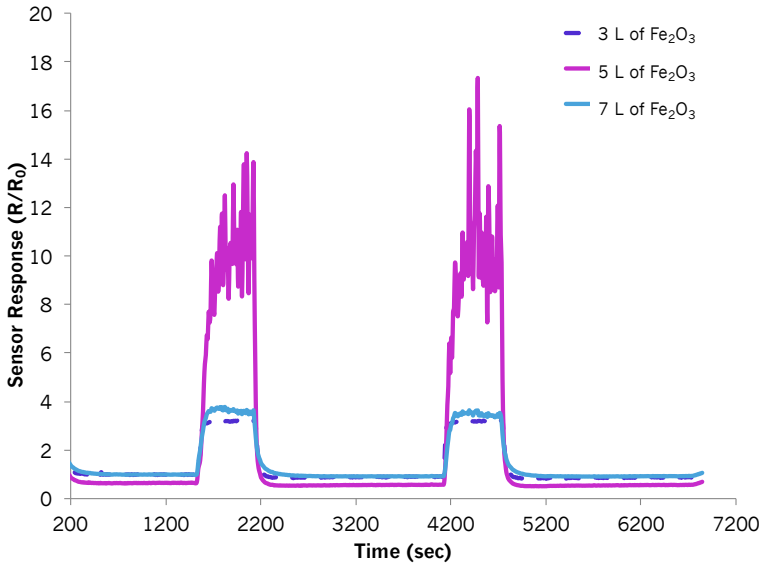

Figure 5-2 Fe_2O_3 sensor responses to two pulses of 50 ppm IPA vapour when printed with three, five or seven film depositions at 300 °C.

5.2.2 Effects of Film Thickness on the Sensor Response Kinetics of the BDH Fe_2O_3 Sensor

The sensor with five film depositions was the most responsive to toluene and IPA gases. Although it was the sensor that took a longer time to respond to both gases it showed promise due to shorter recovery times, ~5 minutes, in relation to the 8 and 10 minutes seen in the other sensors (Table 5-1).

It is acknowledged that particularly the sensor with five film depositions provided very noisy responses, which could potentially be due to poor particle connectivity within the

structure. This could, in turn, affect the straightforward transport of charge carriers in the system.[29] Although it was evident that the sensors were very responsive to both gases, the response times were difficult to calculate and the results provided in Table 5-1 should only be taken as an approximation. It must be noted, however, that this behaviour was occasionally found with newly fabricated sensors and it was attributed to them needing a longer period of stabilisation in air prior to gas testing. Furthermore, it must be noted that the material was not mechanically stable and would detach from the sensor substrate very easily. Although different powder/vehicle ratios were tried, together with different sintering rates in the furnace, the same issues were encountered.

Table 5-1 Response and recovery times of Fe_2O_3 sensors made with different film thicknesses upon exposure to toluene and isopropyl alcohol (IPA).

300 °C		Response & Recovery Times (sec)		
Vapour Type		3 Layers Fe_2O_3	5 Layers Fe_2O_3	7 Layers Fe_2O_3
45 ppm Toluene	τ_{90}	59	259	239
	τ_{10}	499	279	599
50 ppm IPA	τ_{90}	69	389	119
	τ_{10}	79	39	119

5.2.3 Evaluating the Effects of Temperature on Fe_2O_3 Sensor Responses

The control Fe_2O_3 sensor with five film depositions was exposed to toluene and ethanol gases at temperatures ranging between 300 °C and 400 °C (Fig. 5-3). The results of two repeat gas pulses have been provided in Fig. 5-3.

With toluene exposure, sensor responses were seen to increase gradually as the temperature was lowered from 400 °C to 300 °C. Although with ethanol exposure the response magnitudes also increased with lower operating temperatures, the sensor responded in a similar fashion at 300 °C and 350 °C. In these tests the noisy peak shapes were not apparent anymore (not shown).

As noted with other sensing systems, lower operating temperatures led to sensor variability. In the tests discussed in this section, the sensor provided responses that differed by 4.5% at 350 °C and by 1.5% at 300 °C with ethanol exposure and by 28% with toluene exposure at 300 °C. Because sensors responded and recovered more quickly and variability was reduced at 400 °C, this was the selected temperature for future tests.

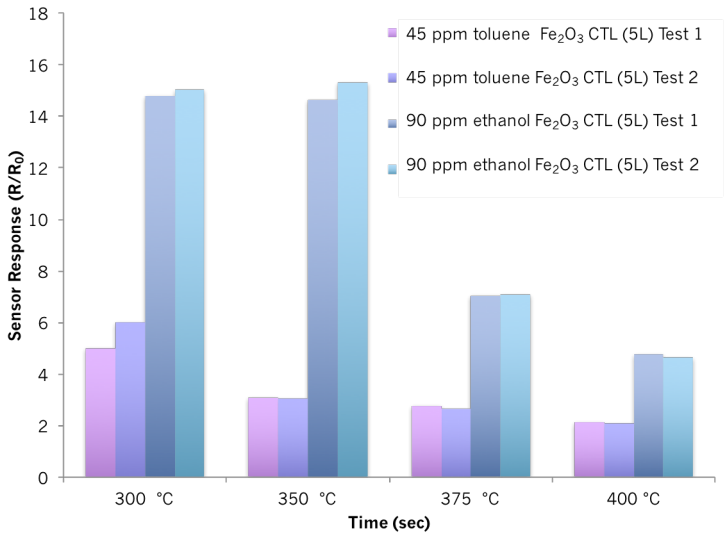

Figure 5-3 Sensor responses of Fe_2O_3 control sensors to 45 ppm toluene gas and to 90 ppm ethanol gas as a function of temperature. Two pulses of the same concentration of gas were supplied to the sensors during a test. '5L' refers to five film depositions.

5.3 Test Details and Range of Gases Tested

The tests followed the same structure as described in section 4.2 and were exposed to the same test gases. Nevertheless, it must be noted that the initial tests shown above were carried out with a sensor fabricated with a powder attained from BDH suppliers to understand its behaviour towards gases. However, when new sensors were going to be fabricated with zeolites, it was noticed that the BDH powder was no longer available and had been replaced by a Sigma Aldrich one. As such, a new control sensor was then fabricated with the Sigma Aldrich powder and subsequent zeolite-modified sensors were fabricated with it as the base material. The modified sensors had 10% (wt.) Na-A and 10% (wt.) H-ZSM-5. After sintering the materials and trying to break the strip of sensors into individual chips the materials were mechanically unstable. Although zeolite overlayers were initially fabricated with the same zeolites as well, the zeolite would consistently detach off the surface and thus this line of work was discontinued. Only one sensor, Fe_2O_3 modified with layers of zeolite H-Y, did not break and, for this reason, it was the only zeolite overlayer tested in this study. Both Fe_2O_3 base materials were tested to understand how they compared to each other. Gas sensing experiments in the following sections (5.3 to 5.10) were all performed on AA rig (see section 2.3.1 in Chapter 2). To summarise:

Sections 5-4 to 5-8: Tests carried out at 400 °C. The gas sensing performance of two different base materials fabricated with powders attained from different companies, namely BDH and Sigma Aldrich were investigated. Gases tested included ethanol,

methanol, acetone, ethane and toluene. Tests were later performed under humid conditions.

Section 5-8 and 5-9: Tests based on the modification of the Sigma-based Fe_2O_3 sensor with admixtures of zeolite Na-A and H-ZSM-5 (5-8) and overlayers of zeolite H-Y (5-9). Tests were carried out at different temperatures ranging between 300 °C and 450 °C. Gases tested included ethanol, acetone, toluene and water vapour. Physicochemical characterisation results have been included in each of the pertinent sections described.

5.4 Physicochemical Characterisation of Fe_2O_3 based Sensors

Sensor materials were characterised using XRD, SEM, EDS and XPS following fabrication and heat treatment processes. BET was carried out on the powdered samples to determine the surface area of the materials. These results have been discussed in the following sections. The sensors were also investigated with Raman Spectroscopy before and after carrying out gas-sensing experiments.

5.4.1.1 X-Ray Diffraction

The Sigma and BDH Fe_2O_3 sensors showed XRD patterns corresponding to hematite, which has a rhombohedral crystal lattice with 2θ peaks at 24.1°, 33.2°, 35.7°, 41°, 49.5° (Fig. 5-4). Both sensors displayed the same XRD patterns. Note that the baseline of the Fe_2O_3 based sensors presented some drift. This behaviour is not uncommon in iron-based samples due to fluorescence.

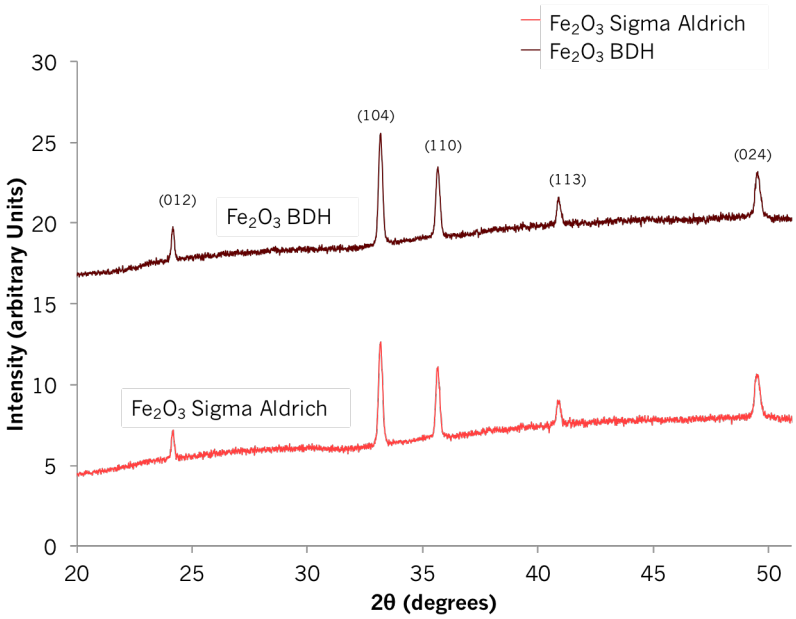

Figure 5-4 XRD patterns of two sensors fabricated with powders from different commercial sources: BDH and Sigma Aldrich. Both sensor materials displayed the same crystal structure of hematite. The patterns have been indexed according to the literature.[8]

5.4.1.2 Raman Spectroscopy

Raman spectra were taken from the powders used to fabricate the sensors and once the material had been deposited on the sensors to see if there were any differences in the Raman shifts after fabrication, heat exposure and gas sensing. The Raman spectra revealed the spectral features of hematite and did not have peaks associated with magnetite or maghemite. The bands corresponding to hematite had the following Raman shifts: 224 cm^{-1}, 245 cm^{-1}, 290 cm^{-1}, 407 cm^{-1}, 503 cm^{-1}, 608 cm^{-1}. The Raman spectra were also taken on the material printed – and used – on the sensor chips (Fig. 5-5). The spectral fingerprint matched all samples, despite them being attained from different commercial sources.

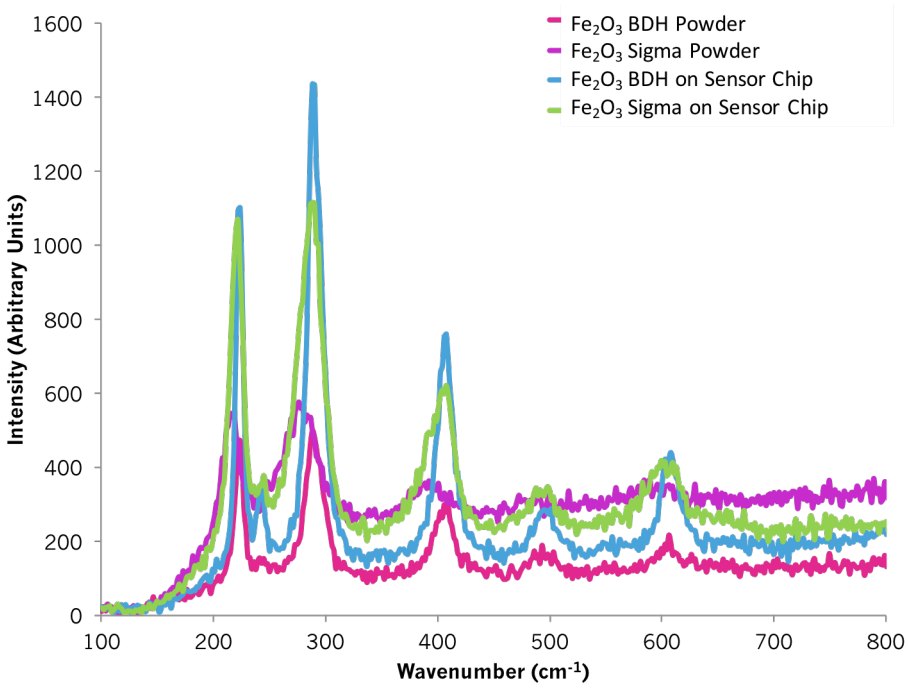

Figure 5-5 Raman spectra of Fe_2O_3 films attained from the BDH powder, the Sigma powder and the sensors containing both powders once they were deposited on the chip and subjected to firing in a furnace at 600 °C for one hour.

5.4.1.3 Scanning Electron Microscope

SEM images of the BDH and Sigma Aldrich Fe_2O_3 sensors have been provided below. Different magnifications (×1,000, ×10,000 and ×30,000) of the microstructures are presented given the very clear differences in connectivity between the particles in both sensors. While the BDH sensor (Fig. 5-6A) displayed a very rough surface with obvious cavities throughout its structure, that of Sigma Aldrich did not at first glance (Fig. 5-6D). The particles in the BDH sensor fused together during sintering to form a very connected network, although some individual particles of ~100 nm in size could be identified. Particle agglomeration is commonly regarded as disadvantageous in gas

sensing as it is thought to be unfavourable for the passage of molecules to the sensitive layer.[318] However, in this system the porosity and potential access for gas molecule diffusion was still evident. In contrast, the morphology of the Fe_2O_3 particles pertaining to the Sigma-based sensor was very different. Particles were between ~50 – 200 nm in size. Evidence of some particle fusion could be observed at magnifications of ×80,000 (not shown). For the most part, the particles appeared to be loosely stacked together and voids could be appreciated in-between them, suggesting possible access for gas molecules to diffuse through.

5.4.1.4 Energy Dispersive X-Ray Spectroscopy

EDS confirmed the presence of the elements expected in the sensors (Table 5-2). The variability among the atomic percentages was high; EDS is a poor energy resolution technique and trace elements may lead to poor counting statistics. One of its limitations is identifying emissions that are close to each other in energy and it is possible that peak broadening in the Fe and O emissions lead to higher errors among measurements. Furthermore, the analysis of rough surfaces may also lead to poor counting statistics.

Table 5-2 EDS analysis corresponding to the atomic percentages of Fe_2O_3 based sensors fabricated from powders attained from Sigma Aldrich and BDH.

	Atomic Percentage (%)	
EDS Analysis	Fe	O
Fe_2O_3 BDH	42.6 (±0.4)	57.4 (±0.4)
Fe_2O_3 Sigma	38.1 (±2.9)	61.9 (±2.9)

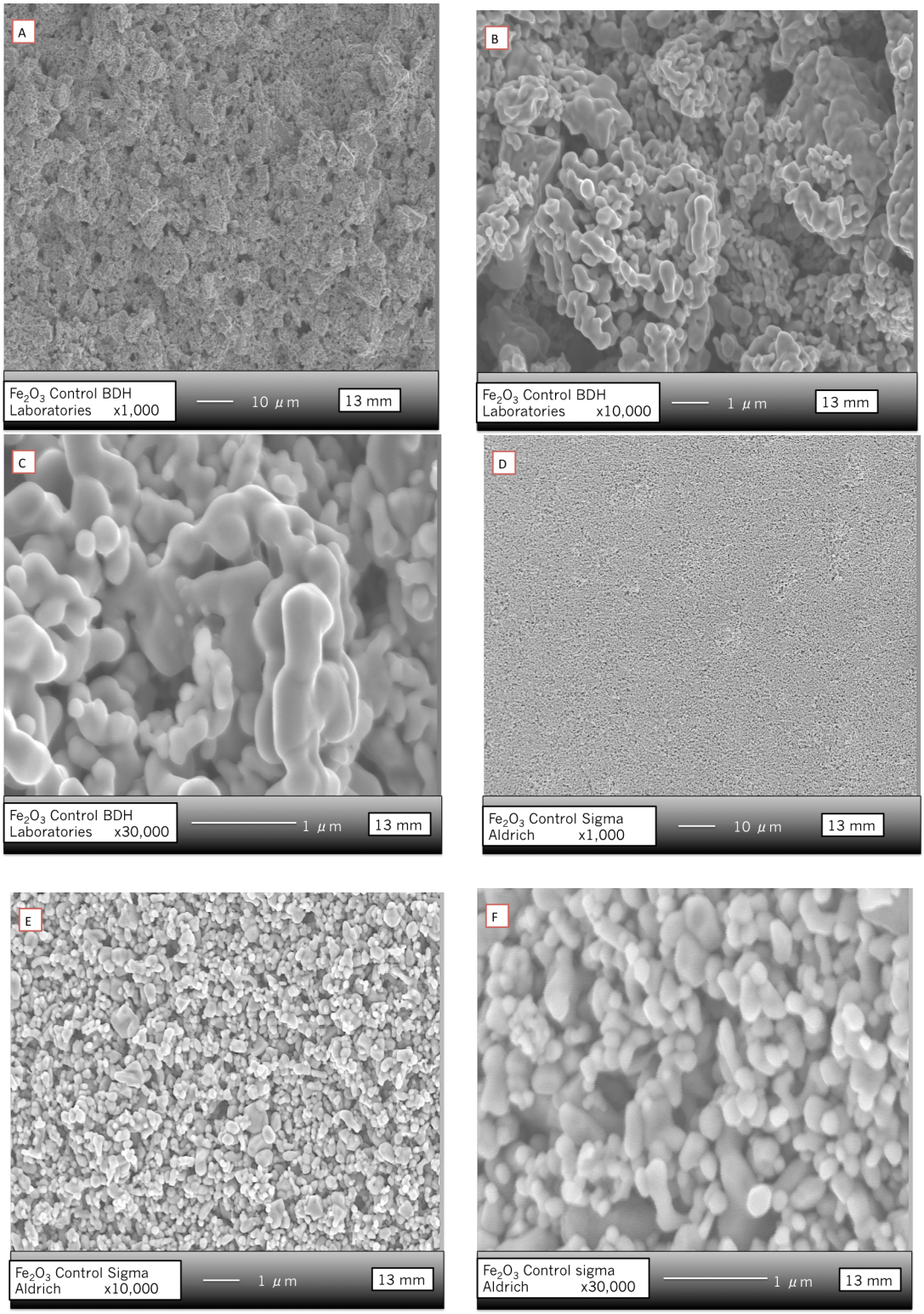

Figure 5-6 SEM images of controls Fe_2O_3 sensors from BDH laboratories (A, B and C) at magnifications x1,000, x10,000 and x30,000, respectively and Fe_2O_3 control from Sigma Aldrich (D, E, F) at magnifications of x1,000, x10,000 and x30,000.

5.4.1.5 X-Ray Photoelectron Spectroscopy (XPS)

XPS was carried out on both powdered samples and on the materials on the sensor chips. No major differences were found in the XPS spectra of all four samples. An example of the Fe 2p spectrum and of the modelled XPS spectrum of the O 1s environments of the Sigma powdered sample have been provided in Figs. 5-7 and 5-8, respectively. The spectra were in accordance with the Fe2p and O1s spectra presented in the literature.[319–321] They revealed that the binding energies of the Fe $2p_{3/2}$ and the Fe $2p_{1/2}$ were at approximately 710.8 eV and 724.5 eV, respectively. Iron oxide was found to be present in the Fe^{3+} state in all the samples tested. There were three main environments found in the XPS spectrum of the O 1s peak, the main peak corresponding to oxidic O^{2-} had a binding energy of 530 eV, which had a weaker shoulder with higher binding energy, attributed to OH^- that may be caused by moisture in the air or non-stoichiometric surface oxygen.[320]

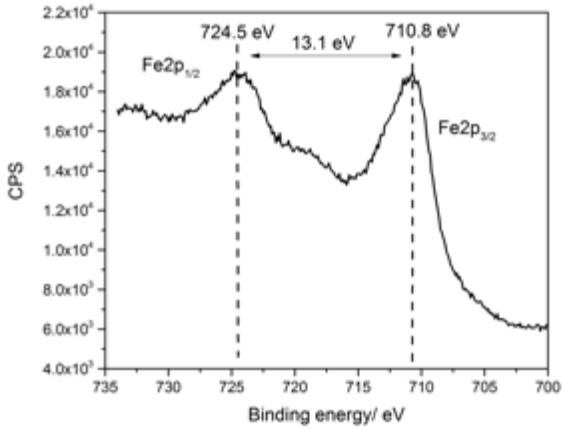

Figure 5-7 Example of XPS spectrum of the Fe 2p Sigma Fe_2O_3 powdered sample.

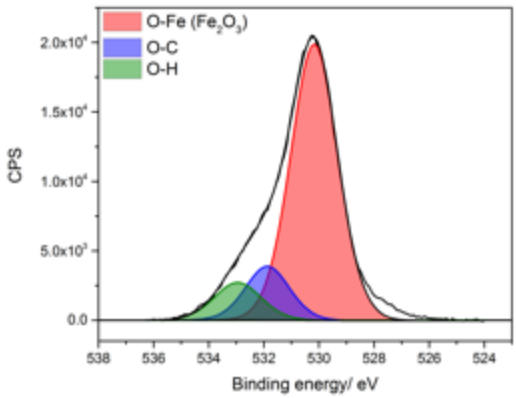

Figure 5-8 Modelled X-ray photoelectron spectrum of the O 1s environments in the Fe_2O_3 Sigma powdered material indicating the presence of iron in the Fe^{3+} state.

5.4.1.6 Brunauner-Emmet-Teller (BET)

BET analysis of the base materials revealed that the surface area of the BDH-based sensor was 1.5 m^2/g and that of the Sigma Aldrich sensor was 3.9 m^2/g. This suggests that the latter would provide more surface reactive sites for interaction with gas molecules during the course of a test.

5.5 Fe_2O_3 Sensor Exposure to Solvent Vapours

When investigating the response behaviour towards gases of both control Fe_2O_3 sensors, one fabricated with a BDH powder and the other fabricated with a Sigma Aldrich powder, it was found that while the Sigma-based sensor behaved as expected, displaying n-type behaviour, the BDH sensor behaved as a p-type semiconductor. Whilst the BDH-based sensor displayed high sensitivity and responsiveness to test gases, the Sigma Aldrich one did not. As mentioned above, tests were performed at an operating temperature of 400 °C and test gases were ethane, methanol, ethanol, acetone and toluene. Results have been presented from Fig. 5-9 to 5-13 below.

Fe_2O_3 conductivity works under the following principle; typically, α-Fe_2O_3 will become oxygen deficient with oxygen vacancies, displaying n-type behaviour [228] and, in the presence of a target gas, non-stoichiometry defects at the surface in the form of oxygen vacancies lead to a change in the conductivity of the material. However, Fe_2O_3 sensors have been reported to show n- to p-type behaviour with increasing concentrations of gas and with increasing temperatures.[317] In the latter study, they report that Fe_2O_3 will typically behave as an n-type semiconductor if it is pure and when operated at low temperatures and, conversely, it will behave as a p-type semiconductor if impure and operated at high temperatures. In the same paper, they describe that when oxygen adsorption leads to the generation of a surface inversion layer, the conduction at the surface will result in an n-to-p switch. In this case, p-type conduction occurs because the density of holes – which are often the minority carriers in α-Fe_2O_3 – increases over that of electrons.[228] Santilli et al. [322] indicated that point defects or impurities were the result of the n-to-p type switch and that microstructural effects seen in grains that displayed different size distributions may also affect this, as they can influence the band-gap and also limit charge carrier mobility. The different polymorphs of Fe_2O_3, α-Fe_2O_3 (hematite) and γ-Fe_2O_3 (maghemite) have been reported to exhibit opposing semiconducting behaviour by Flak et al. [216]. However, Arulsamy et al. [323] reported n-type behaviour of both polymorphs.

As can be seen in the images below, the Sigma-based sensor provided sensor responses (R_0/R) ≤1.2 to test gases and was unresponsive to ethane gas. With respect

to other gases, the response of the Sigma-based sensor increased slightly as the test gas concentrations were increased and the sensor quickly reached steady state. With ethanol exposure, the peak shapes showed that the response decreased progressively during the duration of the gas pulse. This could be the result of water vapour being produced as part of reaction processes occurring at the sensor and blocking further adsorption of oxygen species at the surface,[22] resulting in the observed increase in resistance during the gas pulse. The sigma-based Fe_2O_3 sensor only provided different response patterns towards ethanol and ethane gases and could not distinguish between toluene, acetone and methanol.

In contrast, the BDH-based sensor provided enhanced sensor responses to test gases. The response patterns or peak shapes were very similar towards acetone, ethanol and methanol and the sensor provided conservative enhancements in response magnitude with concentration increments. The sensor responded quickly and reached steady state. Nevertheless, the response patterns displayed odd peak shapes, particularly against toluene and ethane gases, which showed a decrease in the response magnitude during the duration of the gas pulse. Exposure to other gases showed this odd peak shape was more apparent in the first concentration pulse e.g. ethanol, acetone and methanol. The sensor's resistance thus decreased (this sensor displayed p-type behaviour) in this time.

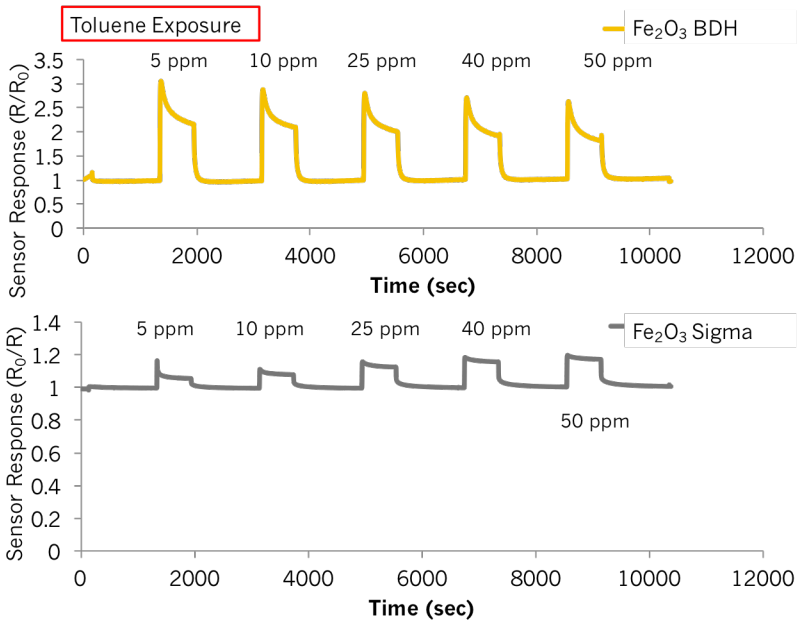

Figure 5-9 Sensor responses to toluene gas of Fe_2O_3 sensors fabricated with powders attained from BDH (top image) and Sigma Aldrich (bottom image) at 400 °C. Gas concentrations supplied were 5 ppm, 10 ppm, 25 ppm, 40 ppm and 50 ppm. The BDH sensor displayed p-type behaviour and the bottom sensor n-type behaviour.

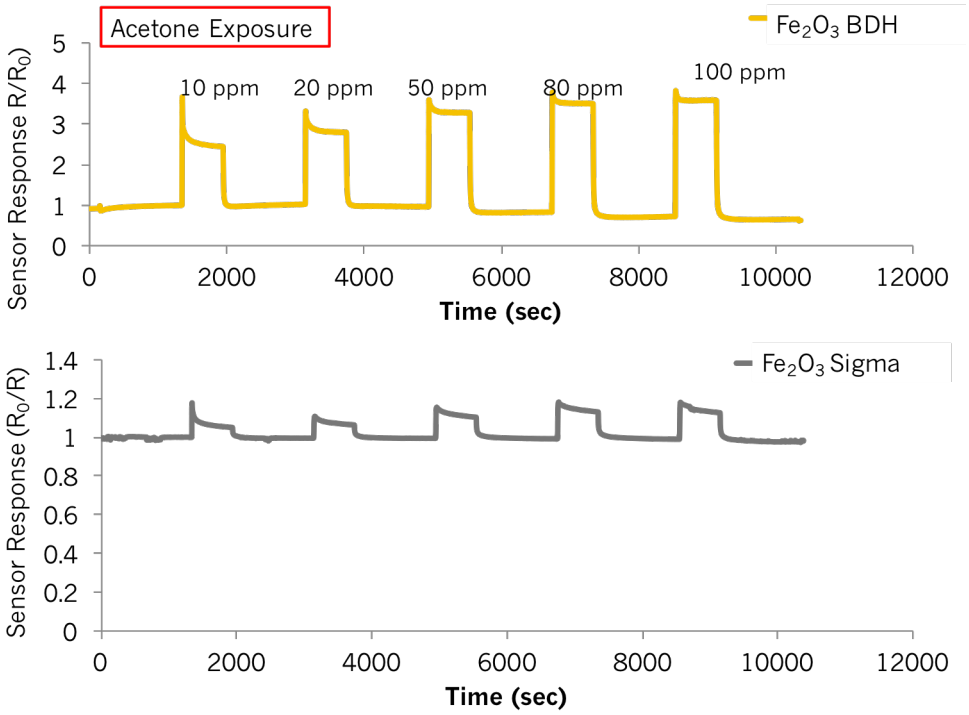

Figure 5-10 Sensor responses to acetone gas of Fe_2O_3 sensors fabricated with powders attained from BDH (top image) and Sigma Aldrich (bottom image) at 400 °C. Gas concentrations supplied were 10 ppm, 20 ppm, 50 ppm, 80 ppm and 100 ppm. The BDH sensor displayed p-type behaviour and the bottom sensor n-type behaviour.

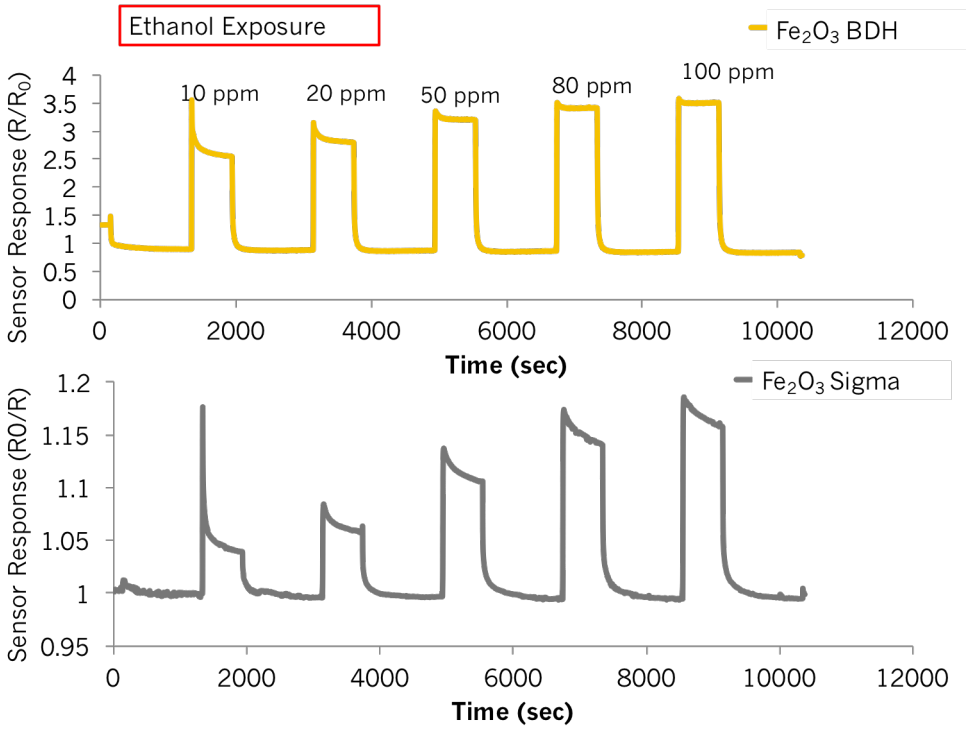

Figure 5-11 Sensor responses to ethanol gas of Fe_2O_3 sensors fabricated with powders attained from BDH (top image) and Sigma Aldrich (bottom image) at 400 °C. Gas concentrations supplied were 10 ppm, 20 ppm, 50 ppm, 80 ppm and 100 ppm. The BDH sensor displayed p-type behaviour and the bottom sensor n-type behaviour.

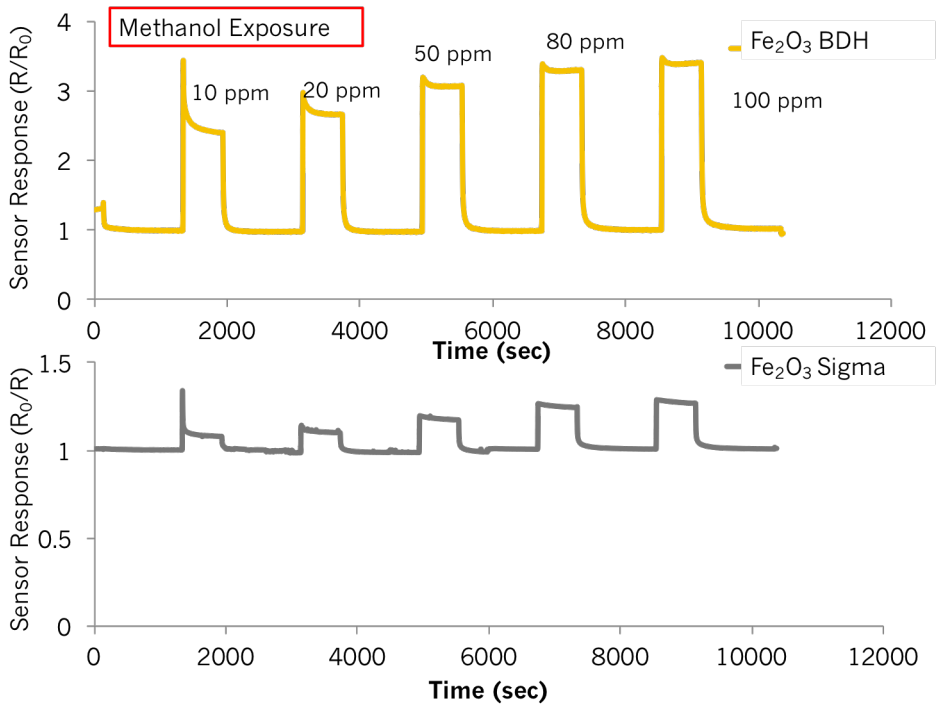

Figure 5-12 Sensor responses to methanol gas of Fe_2O_3 sensors fabricated with powders attained from BDH (top image) and Sigma Aldrich (bottom image) at 400 °C. Gas concentrations supplied were 10 ppm, 20 ppm, 50 ppm, 80 ppm and 100 ppm. The BDH sensor displayed p-type behaviour and the bottom sensor n-type behaviour.

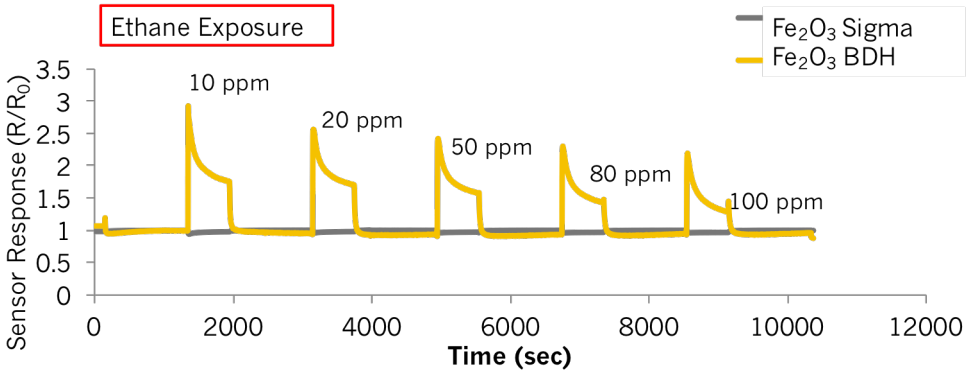

Figure 5-13 Sensor responses to ethane gas of Fe_2O_3 sensors fabricated with powders attained from BDH (top image) and Sigma Aldrich (bottom image) at 400 °C. Gas concentrations supplied were 10 ppm, 20 ppm, 50 ppm, 80 ppm and 100 ppm. The BDH sensor displayed p-type behaviour and the bottom sensor n-type behaviour.

Again, this could be due to the production of reaction products that the sensor becomes less sensitive to. Alternatively, it could also be due to the formation of reaction products blocking any further access of oxygen or the source gas, affecting the conductivity of the system. Although this type of peak shape has been identified in other papers published in the literature, no explanation was given for its occurrence.[26,31,32,96]

Interestingly, the BDH sensor's response decreased with concentration when exposed to toluene and ethane, indicating its slow transition towards a p-n switch. Gurlo et al. [228] suggest that the p-n switch is not the result of a chemical reaction that leads to a change in conduction. They suggest the effect is an electronic one, such that in the presence of oxygen the surface band bending is high and determines p-type conductivity at the surface of the material. With the introduction of a reducing gas, the band bending will decrease, as well as the concentration of holes, whilst the concentration of electrons will increase, leading to the switch to n-type conductivity.

It is noteworthy that this was the first type of sensor fabricated that led to quick response and recovery times towards toluene. As shown in Chapters 3 and 4, the sensor response times towards toluene were commonly long and the sensors often struggled to return back to their original baseline value. The baseline resistance of the Sigma-based sensor was higher, namely ~3.5 MΩ, when compared to the ~0.1 MΩ resistance seen in the BDH sensor.

5.6 Humidity Effects on the Control Fe_2O_3 Sensors

The sensors were exposed to the same gas environments under 25% RH, 50% RH and 75% RH to assess the effect of water vapour on sensor behaviour and performance. The sensor baseline resistance of the Sigma-based sensor decreased slightly with humidity increments (Fig. 5-14). More specifically, it went from ~3.4 MΩ in dry air during a test to toluene, to ~3.2 MΩ under 25% RH and 50% RH, and 3.1 MΩ under 75% RH, which indicates this sensor's relative insensitivity to humid environments. The magnitude of the sensor response towards toluene remained unaltered by the presence of humidity.

Conversely, the BDH-based sensor behaved rather differently. Whereas under a dry air ambience the sensor responded to 25 ppm toluene providing a response that initially gave a value of R/R_0 = 2.7 and progressively decreased to provide a value of R/R_0 = 2 during the gas pulse, under humid conditions the response towards toluene was practically suppressed. Careful inspection of the transient revealed that there was slight evidence of conversion to n-type behaviour (Fig. 5-15). There was also clear baseline drift. The change in conductivity behaviour when exposing the sensors to a gas as a result of humidity interferences in Fe_2O_3-based sensors was also reported by Gurlo et al. [228]. The baseline resistance in the BDH-based sensor went from ~0.21 MΩ in a dry air ambience, to ~0.73 MΩ under 25% RH and to ~0.65 MΩ under 50% RH. During the test performed under 75% RH, the baseline resistance drifted from ~0.64 MΩ down to

~0.57 MΩ during the course of the test. Nevertheless, the switch from p- to n-type was already noticeable under 25% RH.

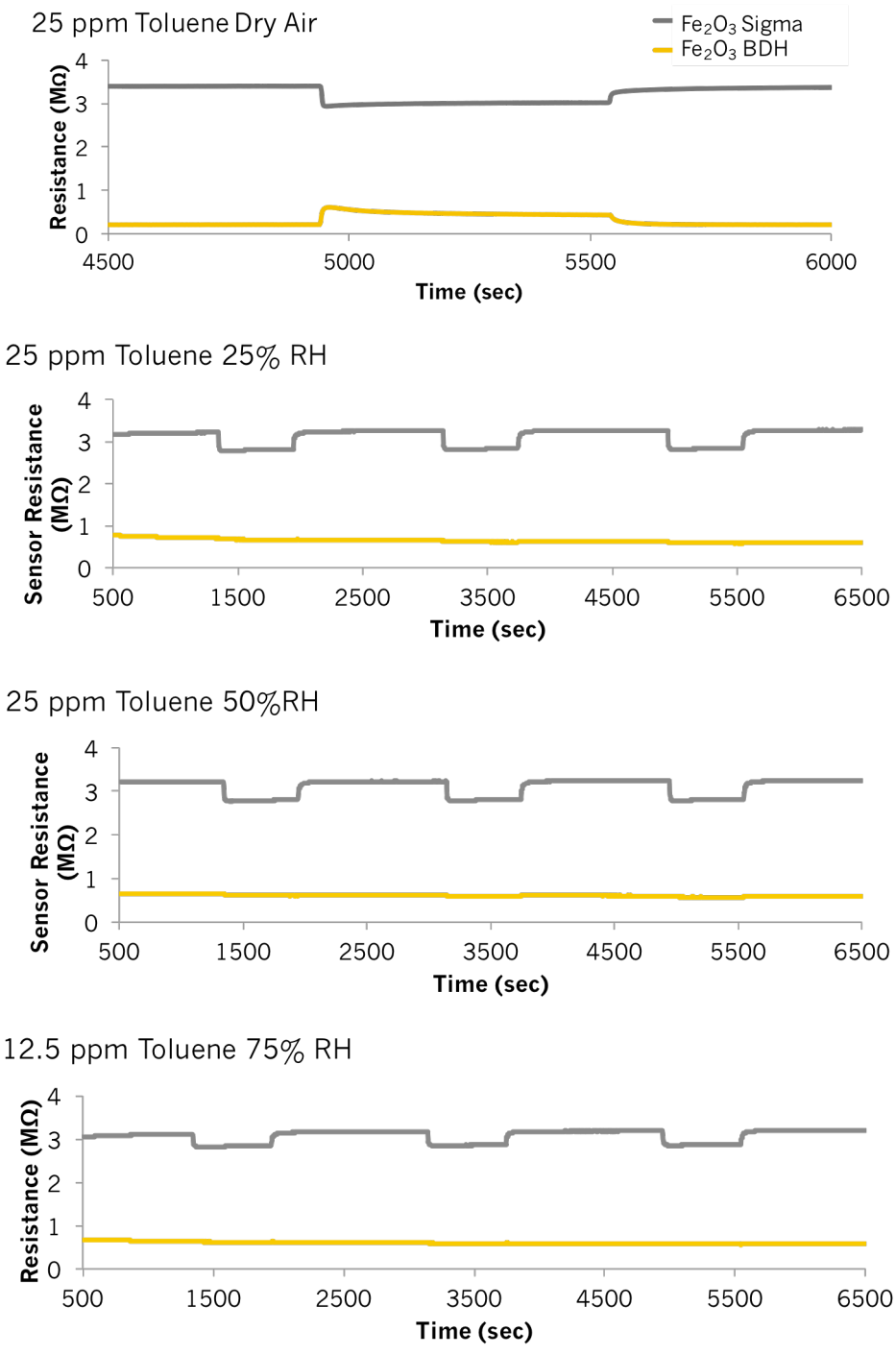

Figure 5-14 Sensor resistance change upon exposure to toluene gas under different relative humidity conditions ranging from dry air conditions to tests in 25% RH, 50% RH and 75% RH.

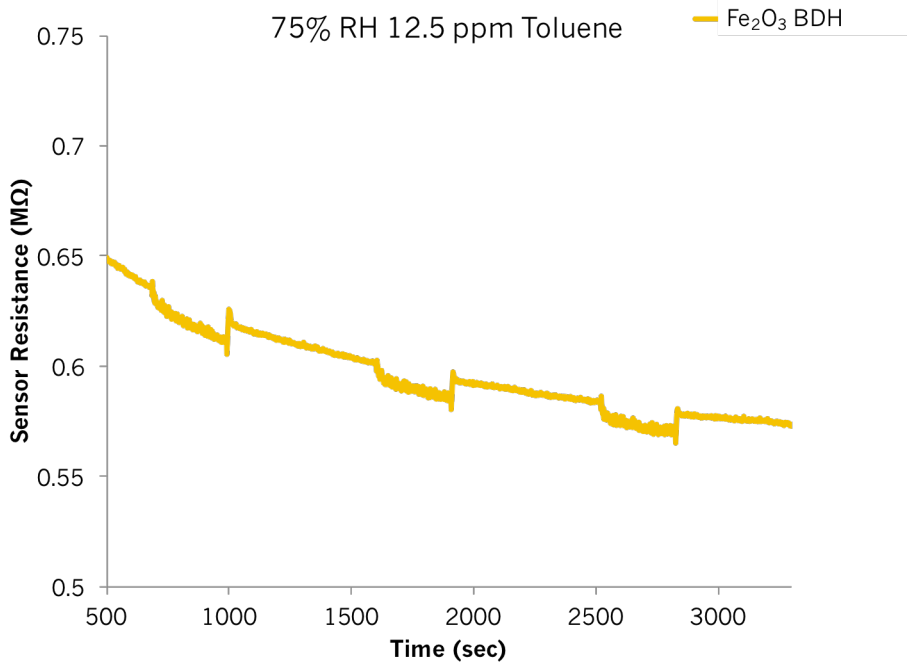

Figure 5-15 Sensor resistance change of the BDH-based Fe_2O_3 sensor upon exposure to 12.5 ppm toluene gas at 400 °C.

With exposure to ethane gas under 25% RH, the Sigma-based sensor continued to be unresponsive to it and displayed the same baseline resistance of ~13 MΩ (Fig. 5-16) as it did under dry air. The BDH sensor, however, switched to n-type behaviour. While before it had shown a response towards 50 ppm of ethane of R/R_0 = 2.3, which progressively decreased to 1.6 during the gas pulse, the R_0/R was <1.1 in 25% RH, it reached steady state quickly and showed baseline drift. Under 50% RH the presence of drift reduced, the sensor conductivity was still n-type and the response magnitude remained the same as under 25% RH. The baseline resistance in dry air was 1.4 MΩ, it increased to ~3.8 MΩ under 25% RH and ~3.6 MΩ under 50% RH.

In dry air the Sigma-based sensor provided a response of R_0/R = 1.8 to 50 ppm methanol (Fig. 5-17). With humidity increments the response magnitude remained unaltered. The baseline resistance decreased slightly when going from a dry air ambience to one in the presence of humid air. That is, from ~14.6 MΩ in dry air, to ~13.4 MΩ in 25% humid air, to ~13.2 MΩ in 50% RH to ~13 MΩ in 75% RH. The BDH sensor's response magnitude to 50 ppm of methanol decreased in humid environments from an initial value of R/R_0 = 3 to that of R/R_0 = ~1.7 in 25% and 50 % RH. Interestingly, upon exposure to methanol in humid air this sensor continued to display p-type behaviour. The resistance of this sensor in dry air was ~2 MΩ, which increased to 5.2 MΩ in 25% RH, and was ~4.7 MΩ in 50% RH. This sensor was clearly

more susceptible to humidity changes than the Sigma-based one. Both sensors reached steady state quickly under dry and humid air conditions.

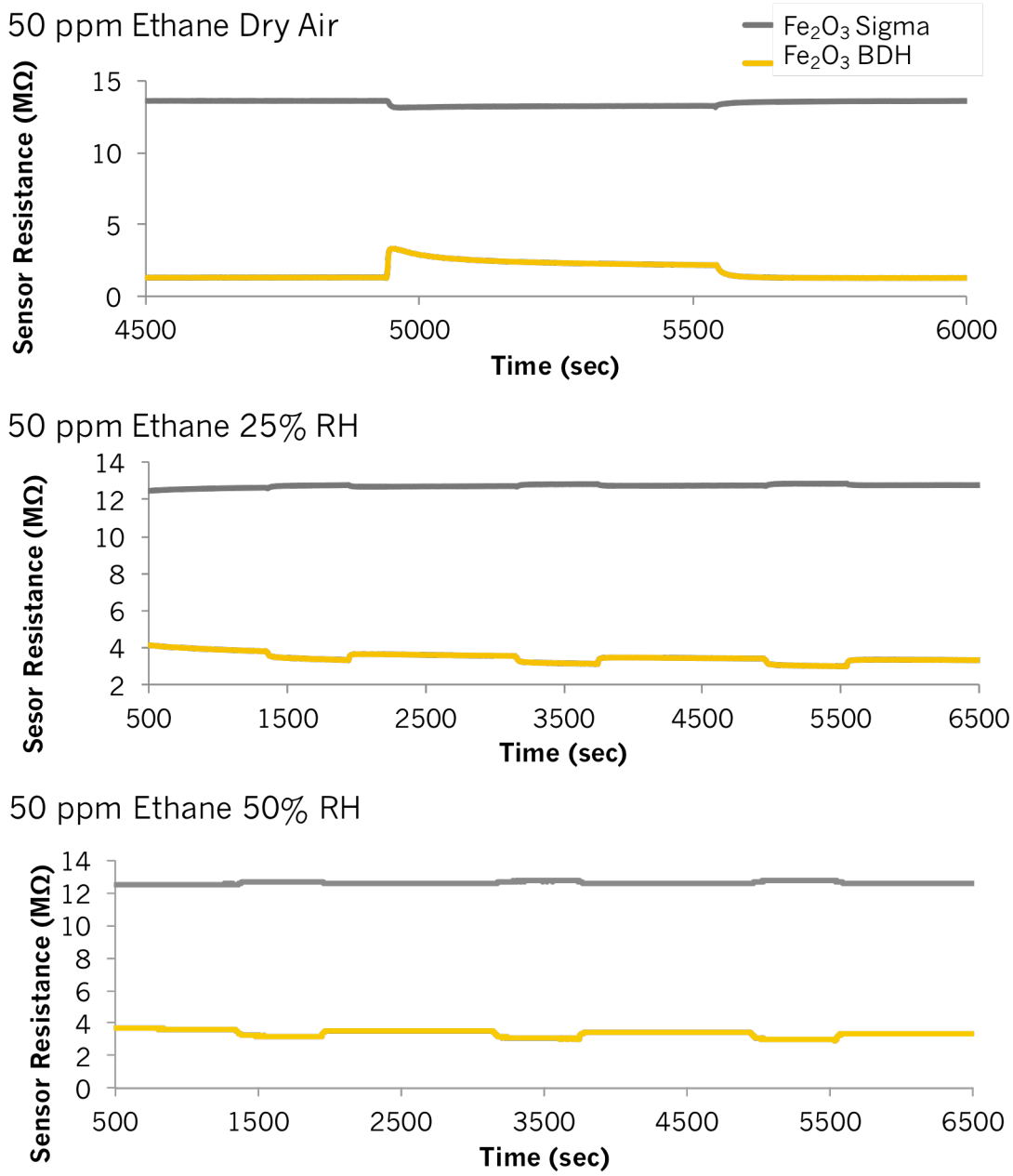

Figure 5-16 Sensor resistance change of a Fe_2O_3 sensor fabricated from a powder supplied by BDH and one supplied by Sigma Aldrich upon exposure to 50 ppm ethane at 400 °C in dry air, 25% RH and 50% RH.

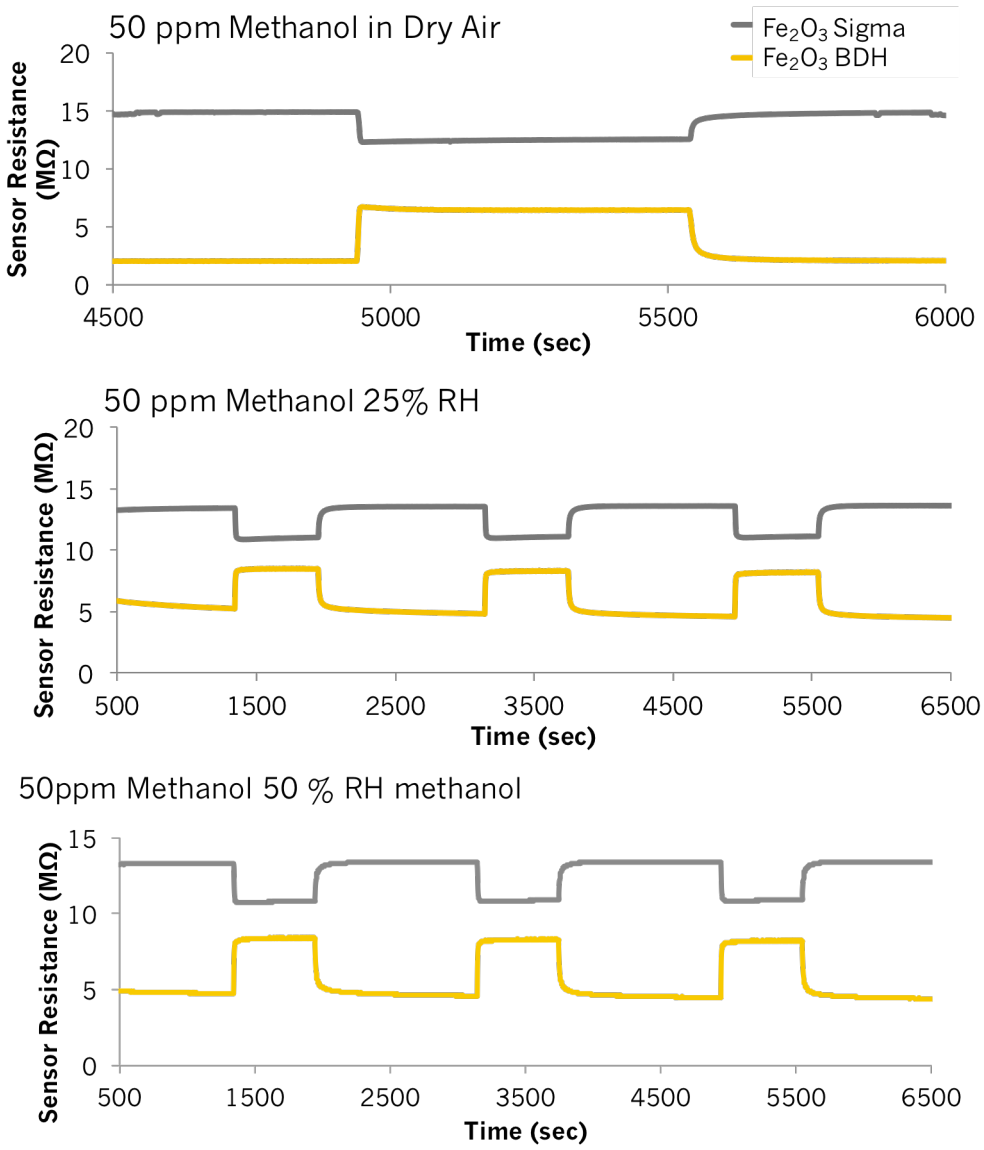

Figure 5-17 Sensor resistance change of two Fe_2O_3 sensors fabricated from powders attained from BDH and Sigma Aldrich upon exposure to 50 ppm methanol under different conditions of humidity, under dry air, 25% RH and 50% RH. Tests performed at 400 °C.

With ethanol exposure, the Sigma-based sensor continued to be unaffected by humid conditions and provided the same response magnitudes to the gas and the same baseline resistance, behaving as an n-type semiconductor (Fig. 5-18). However, the slightly odd peak shape that was observed under dry air conditions was not seen in the presence of humid air. The sensors reached steady state quickly. The BDH sensor displayed p-type behaviour and also reached steady state under humid air conditions. The response magnitude of the BDH sensor was lower in the presence of humid air towards 50 ppm ethanol vapour from an initial R/R_0 = ~3.2 in dry air to R/R_0 = 1.8 in humid air. The baseline resistance was once again seen to increase in the presence of humidity, as expected in a p-type semiconductor gas sensor. Baseline drift was also

apparent under 25% RH but was less evident with increasing humidity. The sensors displayed the same behaviour with exposure to acetone (not shown).

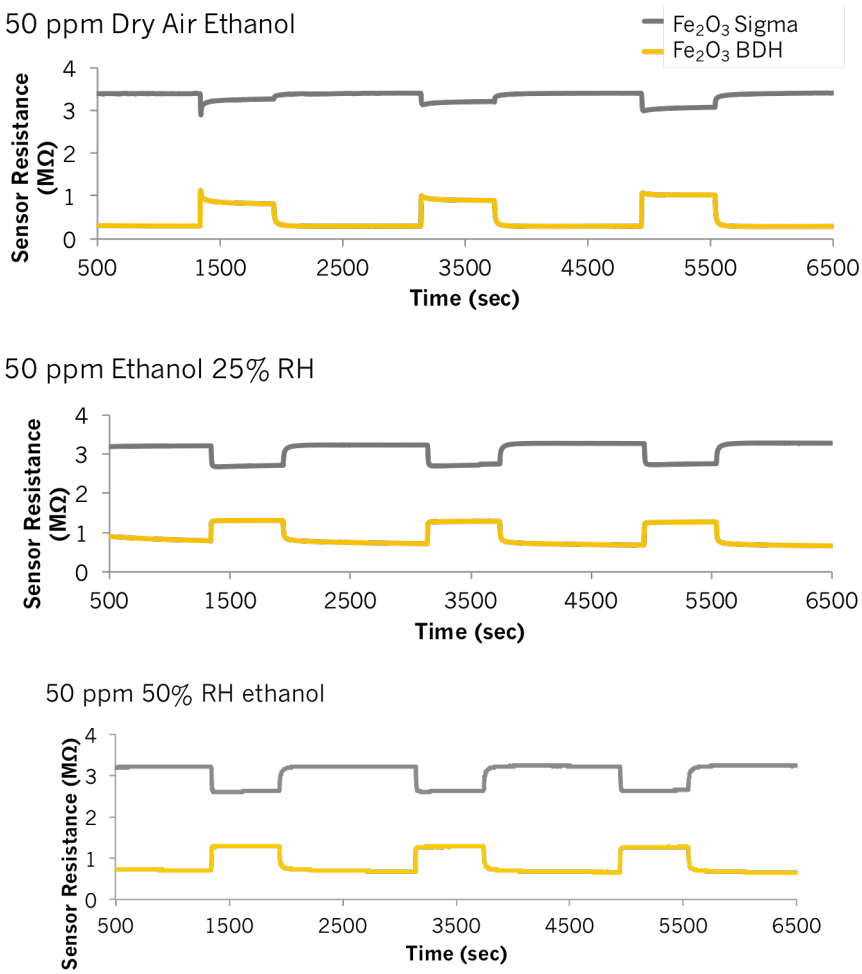

Figure 5-18 Sensor resistance change of two Fe_2O_3 sensors fabricated from powders attained from BDH and Sigma Aldrich upon exposure to 50 ppm ethanol, under dry air, 25% RH and 50% RH. Tests performed at 400 °C.

5.7 Concentration Effects Seen in the Control Fe_2O_3 Sensor

The graphs presented from Fig. 5-19 to Fig. 5-22 illustrate how both Fe_2O_3-based sensors responded with concentration and how sensitivity was affected by progressive concentration increments of a gas. Sensor sensitivity was determined as per Chapters 3 and 4. Tests were performed at 400 °C.

Sensor responses generally did not increase linearly with concentration in the BDH-based sensor. Typically, second order polynomial equations could be fitted to the response vs. concentration curve to later understand sensor sensitivity by taking the derivative of the equation defining the curve. It is reported here that sensitivity of the BDH sensor decreased with concentration when exposed to ethanol, acetone, methanol

and toluene gases. The Sigma-based sensor typically showed linear increases in concentration when the gas concentration was kept <50 ppm or in the case of methanol exposure, throughout the whole concentration range tested (10 – 100 ppm). Nevertheless, as reported in previous sections, the responses were much lower in relation to the BDH-based sensor. Both sensors only provided markedly different responses towards ethane and toluene gases. Responses towards acetone, ethanol and methanol were very similar and difficult to discriminate.

It is interesting to note that preliminary tests performed on a different rig, Sparky, provided different responses of the BDH sensor to ethanol and toluene (compare to Sparky rig results in Fig. 5-3 above). It is acknowledged that the rigs work under different operating principles, Sparky uses a potential divider and AA rig uses a potentiostat. Furthermore, the testing cell in Sparky rig does not supply the gas into individual compartments like AA rig does. As such, other sensors in the test cell in Sparky rig might somehow affect each other. In Sparky rig the BDH sensor gave a response of R/R_0 = ~4.5 to 90 ppm ethanol and R/R_0 ~2 to 45 ppm toluene and the responses provided by AA rig were lower (Figs. 5-19 and 5-22 show the responses attained towards ethanol and toluene gases on AA rig).

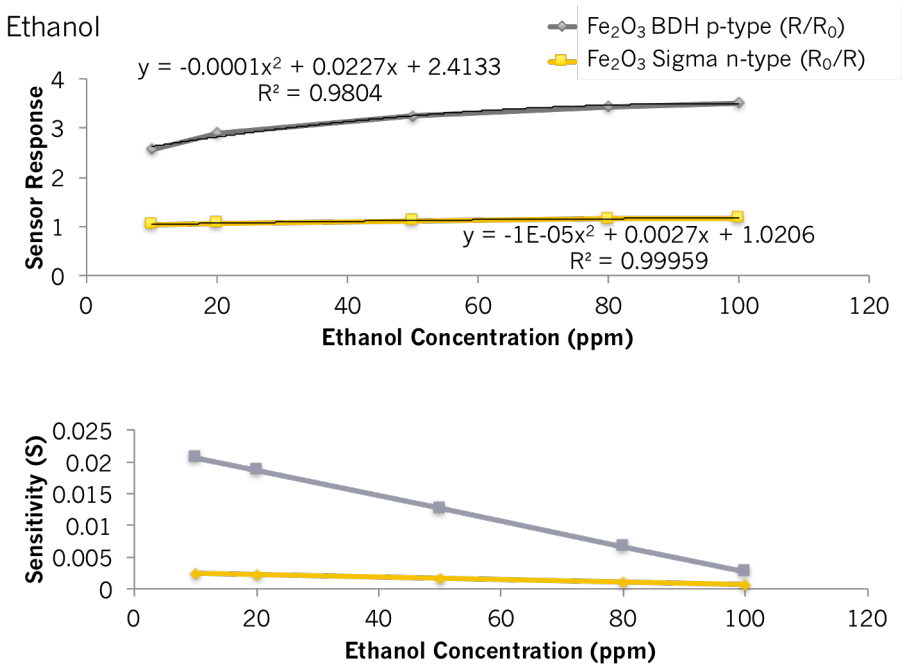

Figure 5-19 Fe_2O_3 sensor responses of two controls fabricated with powders from BDH and Sigma Aldrich towards ethanol gas at 400 °C (top image). Sensor sensitivity towards ethanol at the same temperature (bottom image).

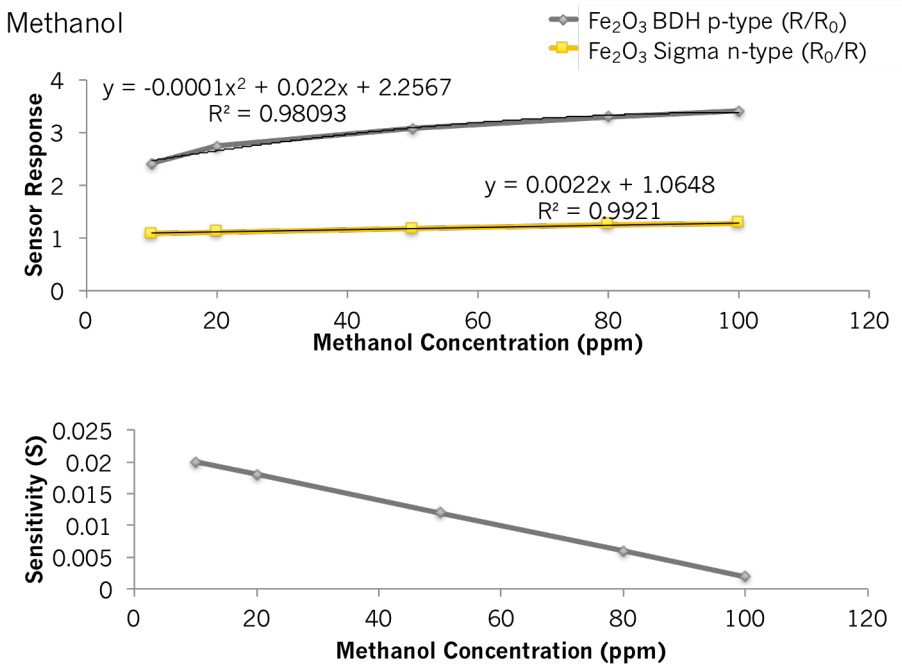

Figure 5-20 Fe_2O_3 sensor responses of two controls fabricated with powders from BDH and Sigma Aldrich towards methanol gas at 400 °C (top image). Sensor sensitivity to methanol at 400 °C (bottom image). The sensitivity of the Sigma sensor increased linearly with concentration.

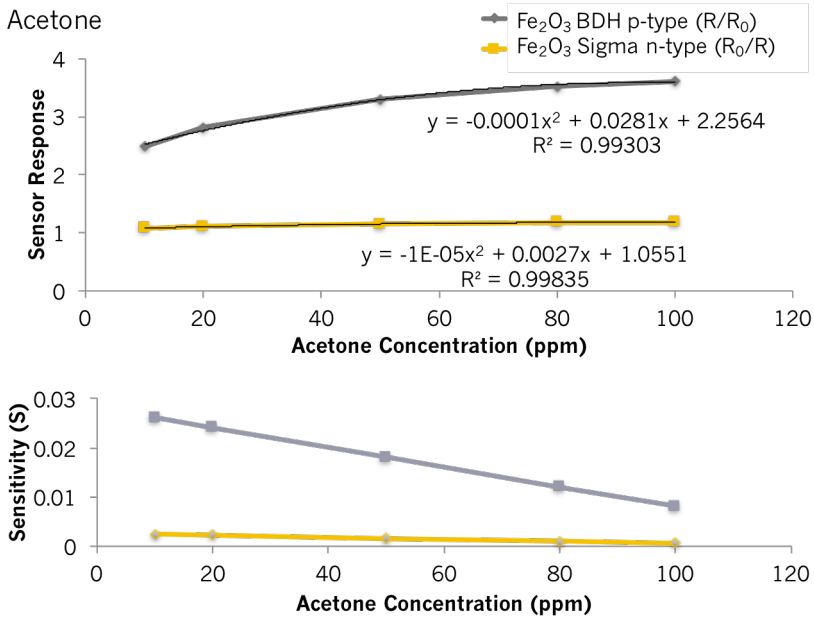

Figure 5-21 Fe_2O_3 sensor responses of two controls fabricated with powders from BDH and Sigma Aldrich towards acetone gas at 400 °C (top image). Sensor sensitivity to acetone gas at 400 °C (bottom image).

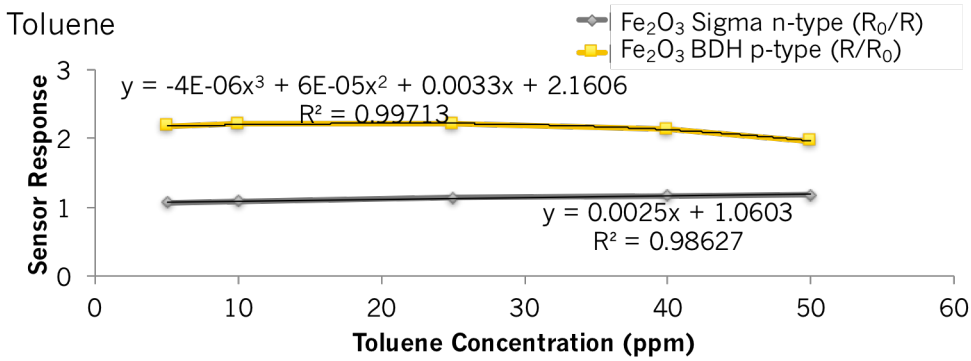

Figure 5-22 Fe_2O_3 sensor responses of two controls fabricated with powders from BDH and Sigma Aldrich towards toluene gas at 400 °C (top image). Sensor sensitivity to toluene gas at 400 °C (bottom image). Sensitivity of the BDH sensor decreased with concentration and that of Sigma Aldrich increased linearly.

5.8 Zeolite Modification of a Fe_2O_3 Sensor: Assessing the Influence of Zeolite Incorporation on Sensor Sensitivity, Selectivity and Responsiveness to Test Gases

The following sections (5.8.1 through to 5.8.3) investigate how the Sigma-based sensor's performance was influenced by the incorporation of 10% (wt.) zeolite Na-A and 10% (wt.) zeolite H-ZSM-5 and by overlayers of zeolite H-Y, respectively. The importance of using these zeolites has been highlighted in Chapters 1, 3 and 4.

5.8.1 Physicochemical Characterisation of Zeolite-Modified Sensors

Physicochemical characterisation techniques were performed on the control sensor and on the zeolite-modified sensors after fabrication to understand if the fabrication process had affected the crystal structure of the materials and to better understand how the incorporation of zeolites influenced the microstructure of the modified sensors.

Fig. 5-23 below shows the XRD patterns of the Sigma based Fe_2O_3 sensor and that of the sensor modified by 10% (wt.) H-ZSM-5 and 10% (wt.) Na-A. The zeolite-modified sensors showed little evidence of the presence of the zeolite and displayed the XRD pattern of hematite. Peaks of very low intensity corresponding to zeolite H-ZSM-5 could be slightly appreciated around 2θ of 23 – 24°. The XRD peak seen at 2θ degree of 38° can be attributed to gold.

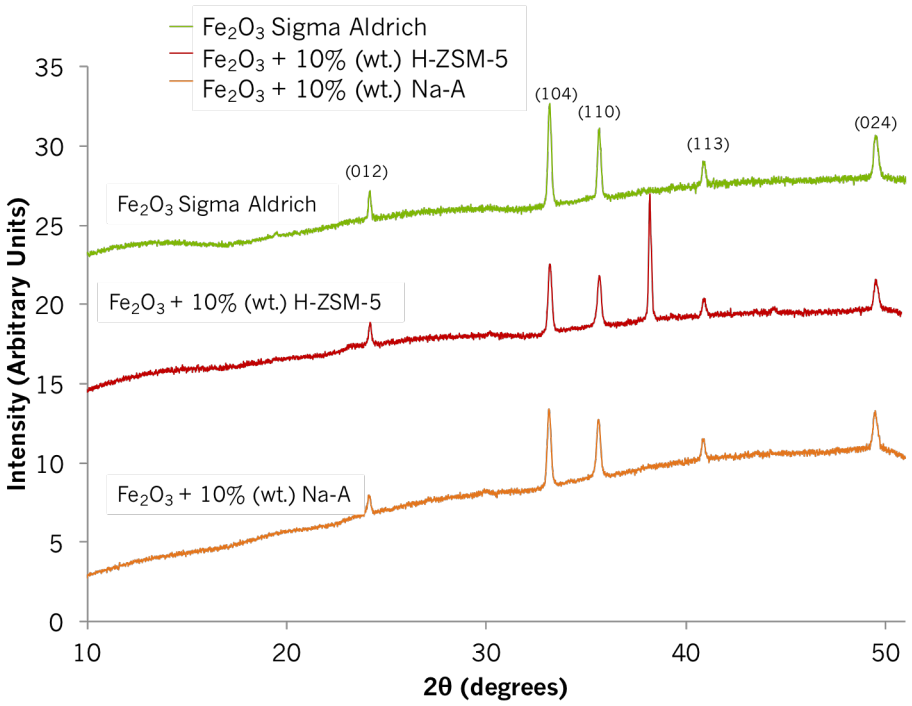

Figure 5-23 XRD patterns of a control Fe_2O_3 sensor, a Fe_2O_3 sensor modified by 10% (wt.) H-ZSM-5 and Fe_2O_3 modified by 10% (wt.) zeolite Na-A. The control Fe_2O_3 sensor has been indexed according to the literature.[8]

In the SEM images shown in Fig. 5-24 the microstructures of two admixed Fe_2O_3 zeolite-modified sensors are presented. Fig. 5-24A shows the modification with 10% (wt.) zeolite Na-A and image B, the modification with 10% (wt.) zeolite H-ZSM-5. The images display a scarce presence of zeolite particles scattered around the sensor surface.

The sensor modified with H-ZSM-5 zeolite displayed particles that were oval in shape and around ~1 μm in size. The sensor modified with zeolite Na-A displayed zeolite particles that were ~2 μm in size and cubic in shape. A lower magnification micrograph (×3,000) has been included in Fig. 5-24C, with arrows highlighting the presence of zeolite Na-A throughout the structure as in other micrographs it was complex to see it clearly. In both zeolite-modified sensors, the microstructure mostly resembled that of the unmodified Fe_2O_3 sensor (Fig. 5-5E).

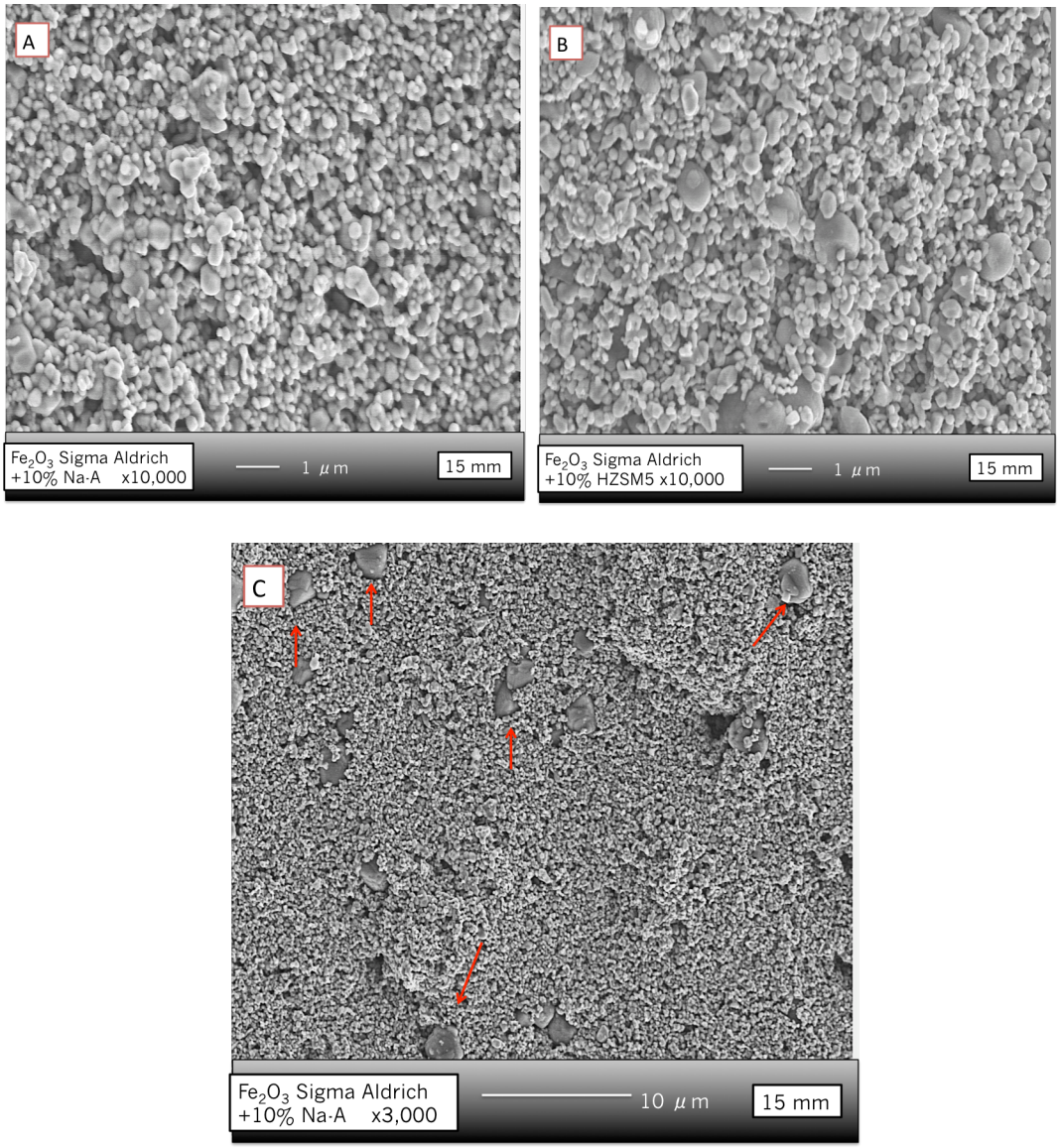

Figure 5-24 SEM images of (A) a Sigma-Fe_2O_3 sensor mixed with 10% wt. Na-A and (B) a Sigma Fe_2O_3 sensor mixed with 10% (wt.) H-ZSM-5. (C) Sigma-Fe_2O_3 sensor mixed with 10% (wt.) Na-A at a magnification of x3,000 indicating the presence of zeolite in the structure, highlighted with red arrows.

EDS analysis showing the atomic percentage of the zeolite-modified sensors is presented in Table 5-3 below. In the case of the sensor modified with zeolite H-ZSM-5, aluminium was once again not detected. The variability in the zeolite-modified sensors could be attributed to the inhomogeneous dispersion of the zeolite particles in the structure.

Table 5-3 EDS analysis showing the atomic percentage of the Fe_2O_3 zeolite-modified sensors.

	Atomic Percentage (%)				
EDS Analysis	Fe	O	Na	Al	Si
Fe_2O_3 Sigma	38.1 (±2.9)	61.9 (±2.9)			
Fe_2O_3 +10% (wt.) Na-A	33.9 (±5.8)	55.9 (±4.6)	4.3 (±1.2)	2.9 (±0.6)	2.9 (±0.4)
Fe_2O_3 + 10% (wt.) HZSM5	32.6 (±1.7)	61.5 (±1.6)			5.9 (±0.4)

5.8.2 Gas-Sensing Results of Fe_2O_3-Sigma Based Sensor with Zeolites Na-A and H-ZSM-5

This section describes the exposure of Fe_2O_3 modified sensors towards ethanol, acetone, toluene gases and water vapour. Initially, tests were performed at 400 °C.

As illustrated in Fig. 5-25, exposure to ethanol and acetone resulted in noisy sensor responses. With ethanol exposure, while the sensor modified with zeolite H-ZSM-5 displayed n-type behaviour, as expected, the Na-A modified sensor displayed what looked like p-type behaviour. However, the latter's response to ethanol was negligible. Both the H-ZSM-5-modified sensor and the control sensor increased in response magnitude with progressive increments in gas concentration. In the case of acetone exposure, the Na-A sensor did not respond to the gas and the H-ZSM-5 modified sensor provided a response that was almost identical to that of the control material.

Exposure to toluene resulted in the sensor modified with zeolite H-ZSM-5 providing responses that were comparable to those of the control of ~R_0/R <1.1 (Fig. 5-26). The Fe_2O_3 modified with zeolite Na-A switched from n-type to p-type conductivity but also provided responses R/R_0 that were below 1.1.

In relation to water vapour exposure, humid air was introduced to a stream of dry air, creating environments ranging between 5 – 75% RH (Fig. 5-26). As expected, the sensor that contained zeolite Na-A responded more intensely to water vapour than the control. The sensor modified with zeolite H-ZSM-5 provided a lower response than that seen with the control. However, it was interesting to see that the sensors provided the same response magnitudes both in dry and humid air conditions.

In order to assess how the sensors responded to toluene and water vapour at other temperatures, additional tests were performed at 300 °C, 350 °C and 450 °C (Fig. 5-27, Fig. 5-28). At 350 °C, the Fe_2O_3 sensor modified with zeolite H-ZSM-5 provided a 1.2-

fold increase in sensor response over that of the control Fe_2O_3 sensor and showed clear increments in response magnitude with concentration. The Fe_2O_3 sensor modified with zeolite Na-A provided a maximum response of R/R_0= 1.1 to 50 ppm of toluene gas, as it did at 400 °C.

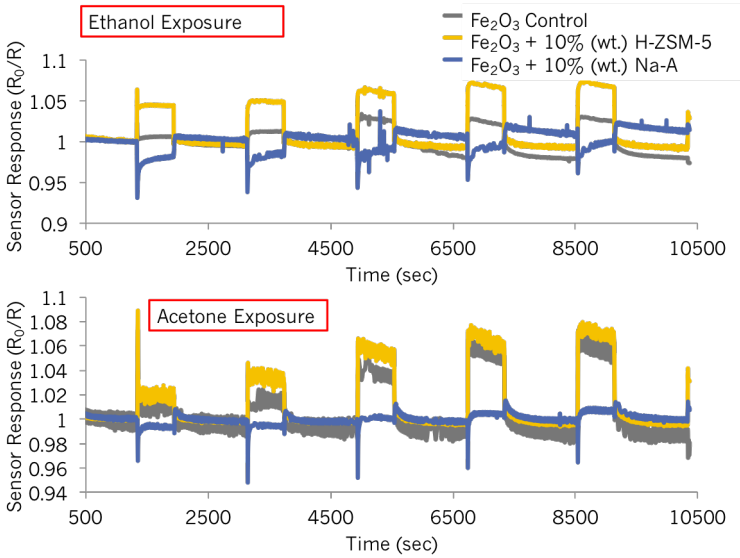

Figure 5-25 Sensor responses towards ethanol and acetone gases attained with a control Fe_2O_3 and two modified sensors through admixture with 10% (wt.) zeolite Na-A and H-ZSM-5 at 400 °C. The concentrations tested correspond to 10 ppm, 20 ppm, 50 ppm, 80 ppm and 100 ppm.

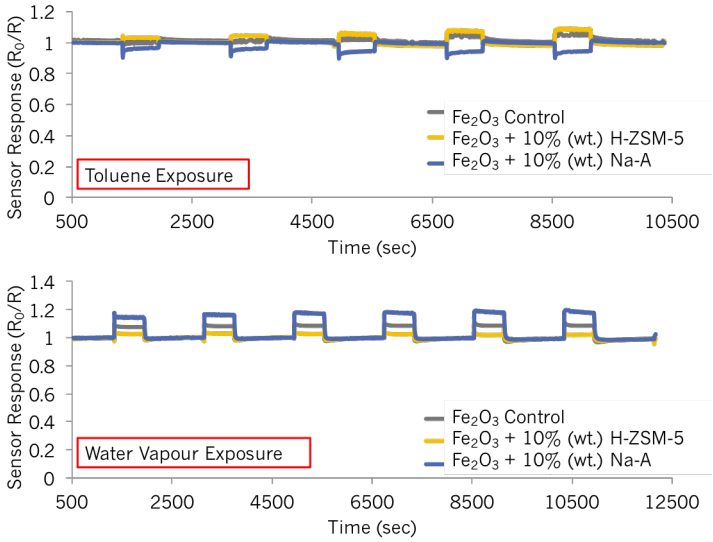

Figure 5-26 Sensor responses towards toluene and water vapours attained with a control Fe_2O_3 and two modified sensors through admixture with 10% (wt.) zeolite Na-A and H-ZSM-5. Tests performed at 400 °C. Toluene concentrations correspond to 5 ppm, 10 ppm, 25 ppm, 40 ppm and 50 ppm. Water vapour tested at 5% RH, 10% RH, 20% RH, 25% RH, 50% RH and 75% RH.

The response magnitudes of the Fe_2O_3 sensor modified with zeolite Na-A towards water vapour diminished moderately at 350 °C, providing the same pattern seen with the control sensor. When carrying out tests at higher and lower operating temperatures the

sensor responses were worsened: at higher temperatures sensitivity was essentially negligible and at lower temperatures the noisy responses prevented correct analysis of the results, as they were not computed properly. An example of this has been provided in Fig. 5-28 below for toluene exposure at 450 °C and 300 °C.

It is unclear why the responses towards some gases were so noisy. It is possible that they were due to poor particle connectivity in the structures and poor adhesion of the sensing materials to the substrates. The poor responses attained with most of the Fe_2O_3 sensors were attributed to the inherently poor sensitivity of this configuration of the base material to the gases. Although at 300 °C the sensor modified with zeolite H-ZSM-5 initially appeared to show an improvement to trace concentrations of toluene, it provided very noisy responses and the sensor eventually capped out. Further, it is clear that the microstructural differences among the BDH sensor and those seen in the Sigma-based sensors played a major role in sensor responsiveness and sensitivity to gases. Given that most of the studies published in the literature on the gas sensing properties of Fe_2O_3 sensors are based on nanostructures and different architectures of Fe_2O_3,[96,218,220–222,271] it may be the way forward in future studies, as zeolite incorporation failed to enhance the responses of the conventional sensor.

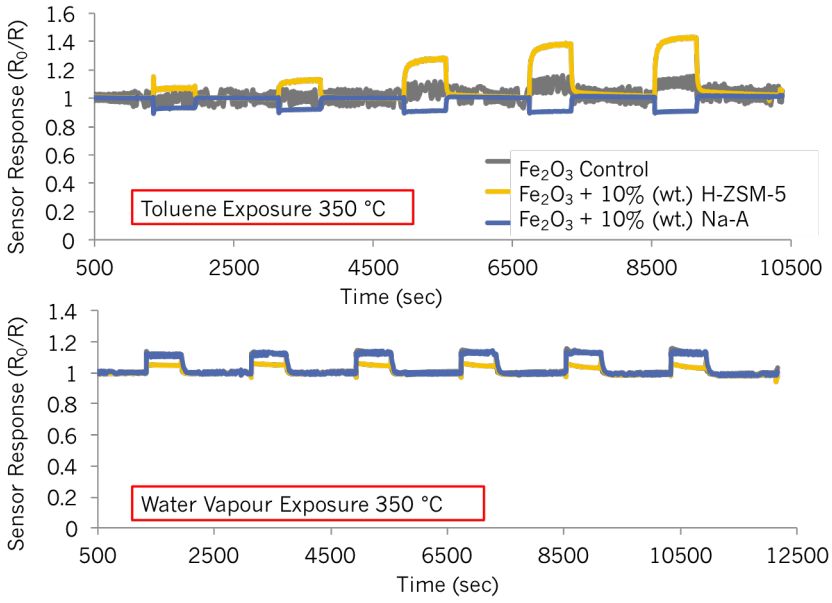

Figure 5-27 Sensor responses towards toluene and water vapour attained with a control Fe_2O_3 and two modified sensors through admixture with 10% (wt.) zeolite Na-A and H-ZSM-5. Tests were performed at 350 °C. The concentrations of toluene correspond to 5 ppm, 10 ppm, 25 ppm, 40 ppm and 50 ppm. Water vapour was tested at 5% RH, 10% RH, 20% RH, 25% RH, 50% RH and 75% RH.

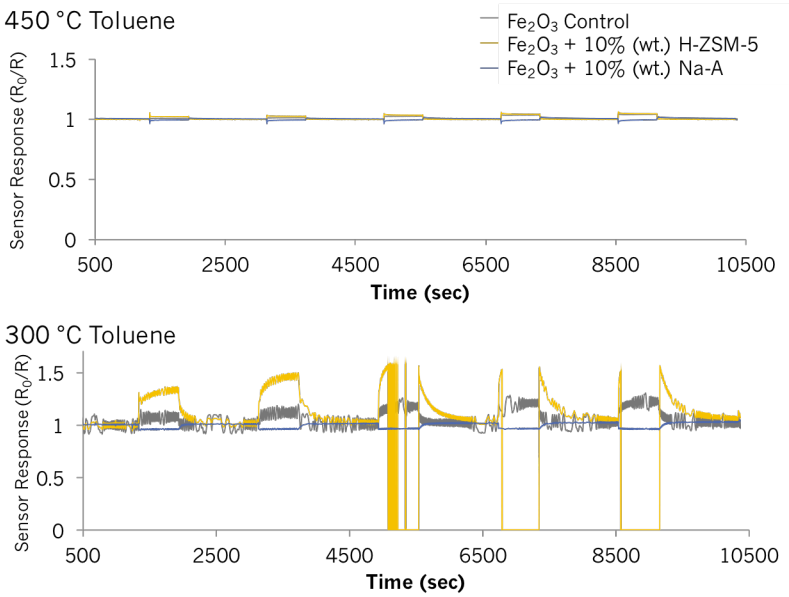

Figure 5-28 Sensor responses towards toluene attained with a control Fe_2O_3 and two modified sensors through admixture with 10% (wt.) zeolite Na-A and H-ZSM-5. Tests were performed at 300 °C and 400 °C. The concentrations of toluene correspond to 5 ppm, 10 ppm, 25 ppm, 40 ppm and 50 ppm.

5.8.3 Modification of the Sigma-based Fe_2O_3 Sensor with Zeolite H-Y Overlayers

The XRD patterns of the control Fe_2O_3 sensor and that modified with overlayers of zeolite H-Y are provided in Fig. 5-29 below. Due to the coating of zeolite on top of the Fe_2O_3 base material the intensity of the peaks corresponding to Fe_2O_3 was much lower in the modified sensor, as expected. XRD peaks corresponding to zeolite H-Y could be identified at 2θ of 10.2°, 12.02°, 15.8°, 18.9°, 20.6°, 23.9°.

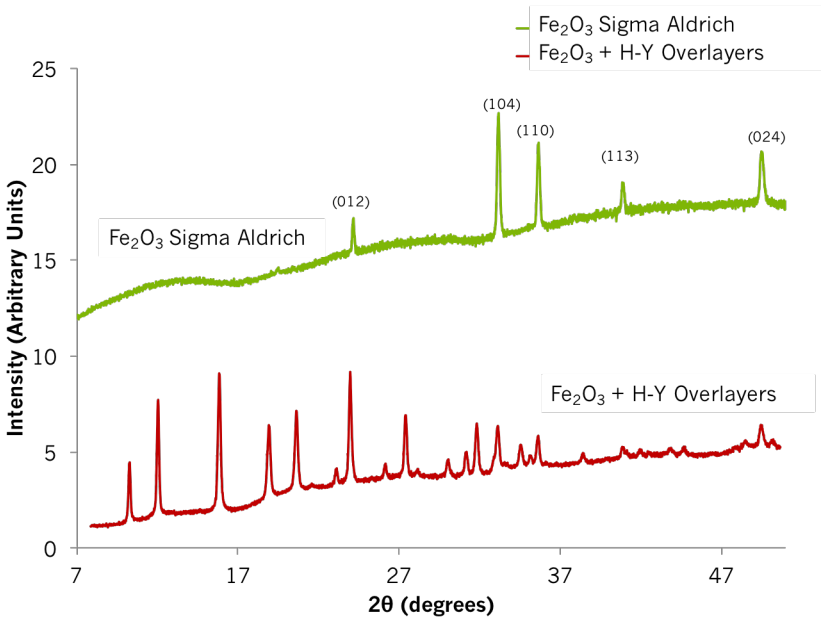

Figure 5-29 XRD patterns of a control Fe_2O_3 sensor and one modified by the incorporation of layers of zeolite H-Y. XRD peaks have been indexed according to the literature.[8]

SEM images of the zeolite-modified sensor have been provided in Fig. 5-30. Two different magnifications (×3,000 and ×10,000) are provided so as to get a better appreciation of the microstructure of the sensor. Although voids in the structure can be observed, the microstructure appears much denser than in previously fabricated sensors. This could potentially be due to the pressure inflicted by the squeegee during screen-printing. Zeolite particles appeared interconnected and were flat in appearance.

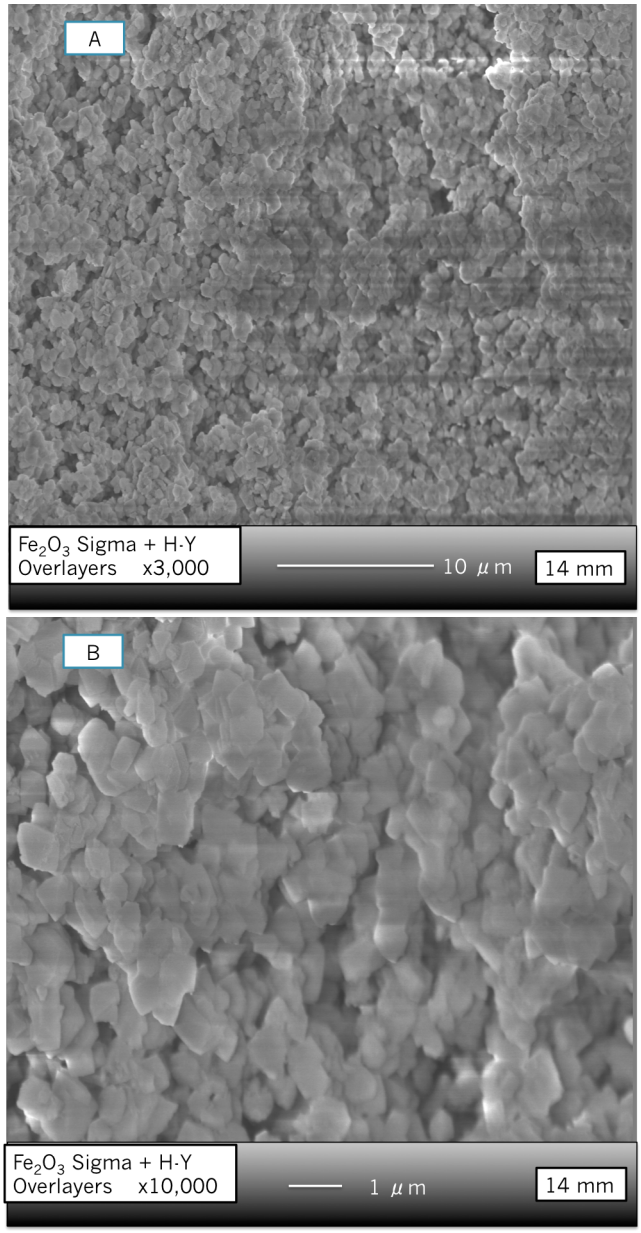

Figure 5-30 SEM images of a Fe_2O_3 sensor overlaid with coatings of zeolite H-Y at a magnification of (A) ×3,000 and (B) ×10,000. The images display uneven lighting due to charging of the zeolite. The sensor was carbon and gold-coated to try and minimise charging.

Table 5-4 EDS analysis providing atomic percentage of a Sigma-Fe_2O_3 sensor coated with layers of zeolite H-Y.

	Atomic Percentage (%)			
EDS Analysis	Fe	O	Si	Al
Fe_2O_3 + H-Y Overlayers	0.2 (±0.1)	66.0 (±0.7)	24.9 (±0.4)	8.9 (±0.2)

The Sigma-based sensor was modified with coatings of zeolite H-Y. This zeolite was previously found to host and enhance responses to gases such as toluene and thus it

seemed like a good candidate to improve sensor responses and performance of the conventional Fe_2O_3 Sigma sensor.

As per previous tests, the initial operating temperature was 400 °C but given the poor sensitivity to gases seen in the zeolite-modified sensor, other temperatures were explored (300 – 450 °C). The Fe_2O_3 sensor modified by zeolite H-Y did not work at 300 °C against toluene gas and at ≤350 °C against acetone and ethanol. The results presented in Figs. 5-31 through to 5-34 comprise the results where the zeolite-modified sensor did function.

Sensor responses towards toluene were improved over those seen in the control sensor (Fig. 5-31). The optimal operating temperature for toluene detection was 350 °C. The sensor was sensitive to concentrations as low as 5 ppm and showed sensor response increments with increasing concentration. When supplied with 5 ppm of toluene gas at 350 °C, the control sensor did not respond and it provided a very noisy pattern, particularly at 350 °C and 400 °C. This was minimised at 450 °C but, at this temperature, the sensor response towards toluene decreased. The zeolite-modified sensor reached steady state at all temperatures and provided fast response and recovery times, which were not seen in the systems described in previous chapters upon exposure to toluene gas.

The response patterns differed in shape when heating the sensors to different temperatures, which may be the result of different products being produced as part of reaction processes occurring between the gas and the sensor. At 350 °C, toluene may be able to diffuse into the inner layers of the sensor more readily and react with more active sites in the zeolite pores, resulting in the slightly longer response times seen in Fig. 5-31. It is possible that at this temperature the enhancement in response is attributed to reaction products to which Fe_2O_3 is more sensitive. As a result of thermal energy at higher temperatures, reaction rates of gas adsorption and desorption increase and due to oxygen adsorption at the surface being reduced, the response magnitudes are also minimised. The incorporation of zeolite H-Y to Fe_2O_3 resulted in a 1.1-fold increase in sensor response when exposed to 50 ppm of toluene gas, in relation to the unmodified sensor.

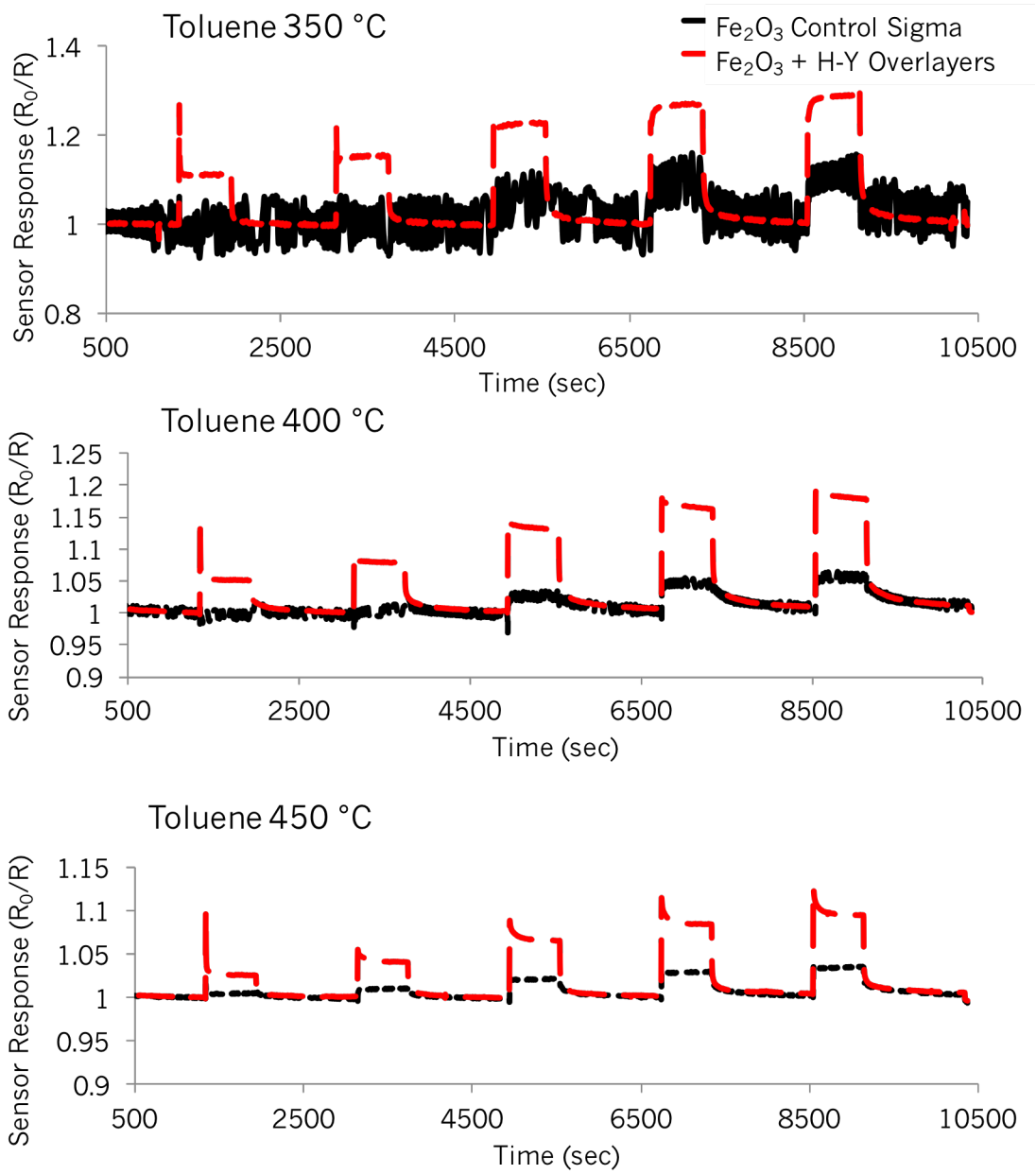

Figure 5-31 Sensor responses of control Fe_2O_3 sensor fabricated with Sigma Aldrich Powder and sensor modified with H-Y coatings upon exposure to toluene at 350 °C, 400 °C and 450 °C. Gas concentrations correspond to 5 ppm, 10 ppm, 25 ppm, 40 ppm and 50 ppm.

Exposure to water vapour also resulted in interesting results (Fig. 5-32). The responses attained were very similar at 400 °C and 450 °C. The zeolite-modified sensor provided a lower response to water vapour than the control sensor. At 350 °C, the response to humidity was even lower (R_0/R = <1.05) and as the humidity was raised from 5% RH to 75% RH, the response of the zeolite-modified sensor decreased. In fact, at 50% RH and at 75% RH, the response to water vapour was supressed. This could suggest that this sensor would be suitable to detect certain substances in real life applications, minimising cross-sensitivity to humid air. These results suggest that as humidity increases the competition for active sites between oxygen and water vapour is greater

and water vapour manages to supress the adsorption of oxygen onto the sensor surface.

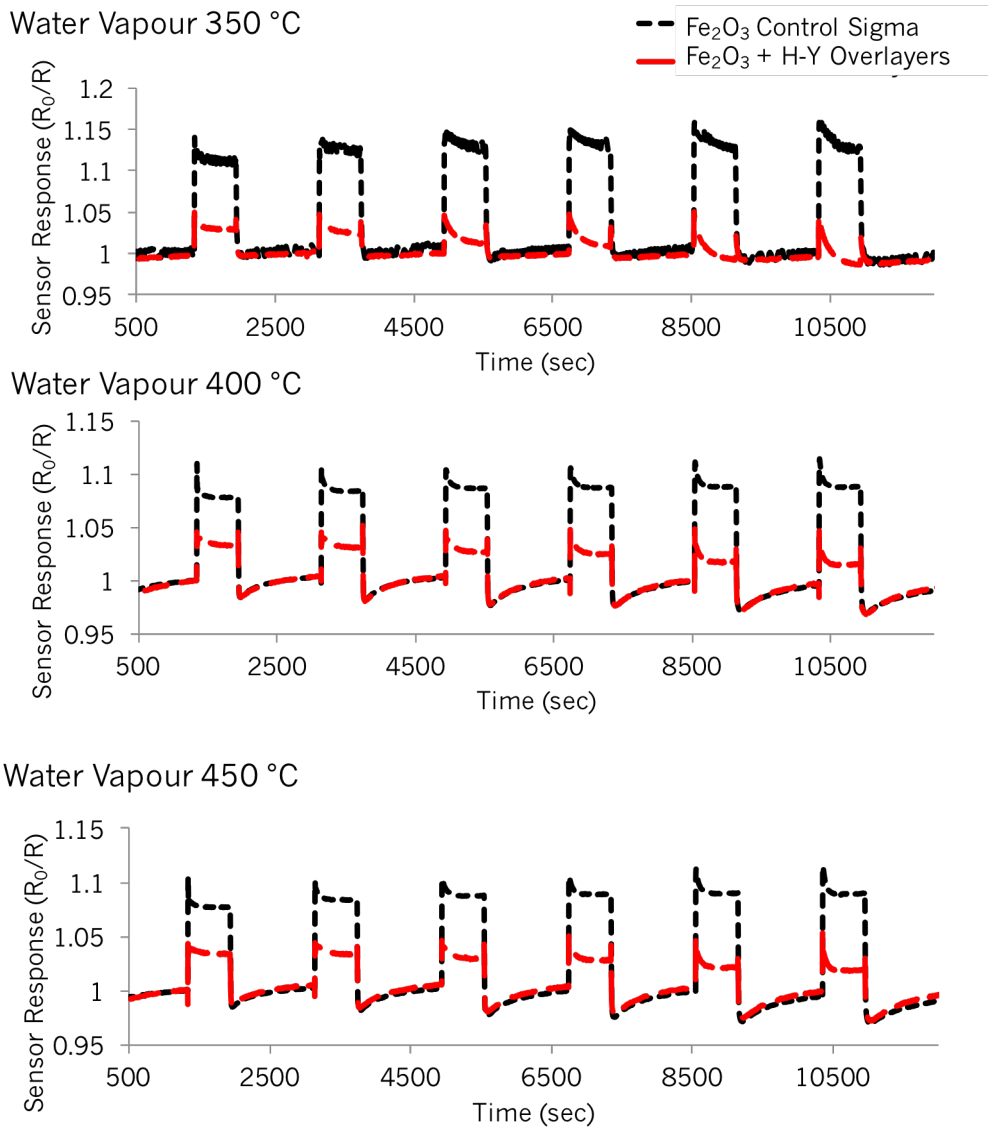

Figure 5-32 Sensor responses of control Fe_2O_3 sensor fabricated with Sigma Aldrich Powder and sensor modified with H-Y coatings upon exposure to water vapour at 350 °C, 400 °C and 450 °C. Water vapour was tested at 5% RH, 10% RH, 20% RH, 25% RH, 50% RH and 75% RH.

The results of exposure to acetone and ethanol vapours at 400 °C and 450 °C have been presented in Figs. 5-33 and 5-34 below. The Fe_2O_3 sensor modified with H-Y zeolite provided conservative enhancements in sensor response over the control. For instance, when looking at the enhancements in response towards 100 ppm upon exposure to both gases, the zeolite-modified sensor only provided a 1.1-fold improvement in response in relation to the control. Responses were seen to increase slightly with incremental gas concentration. The optimal operating temperature for

detection of these gases was 400 °C. Below this temperature, the zeolite-modified sensor stopped providing results. Unfortunately, this novel sensor configuration did not provide the results that were initially expected. However, it was found that the sensor could supress the response to water vapour above 50% RH and the response patterns seen upon exposure to toluene were different to those attained with exposure to acetone and ethanol.

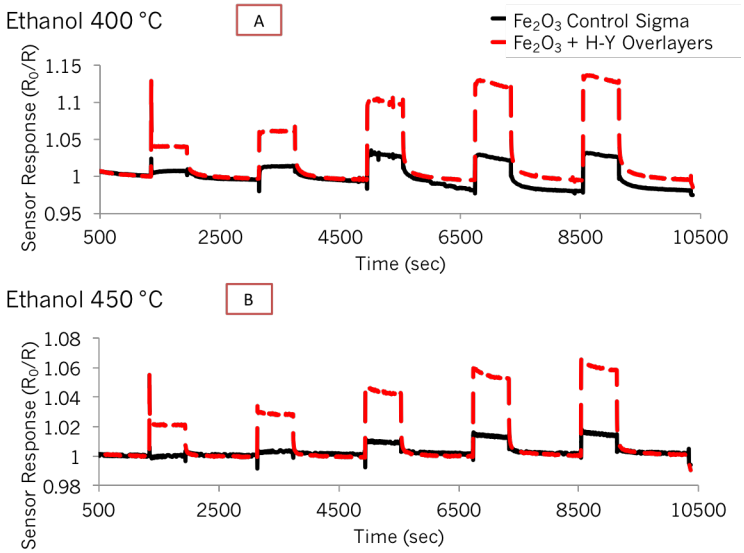

Figure 5-33 Sensor responses of a control Fe_2O_3 sensor and a Fe_2O_3 sensor modified by coatings of zeolite H-Y to (A) ethanol at 400 °C, (B) ethanol at 450 °C. Concentration for each pulse correspond to 10 ppm, 20 ppm, 50 ppm, 80 ppm and 100 ppm.

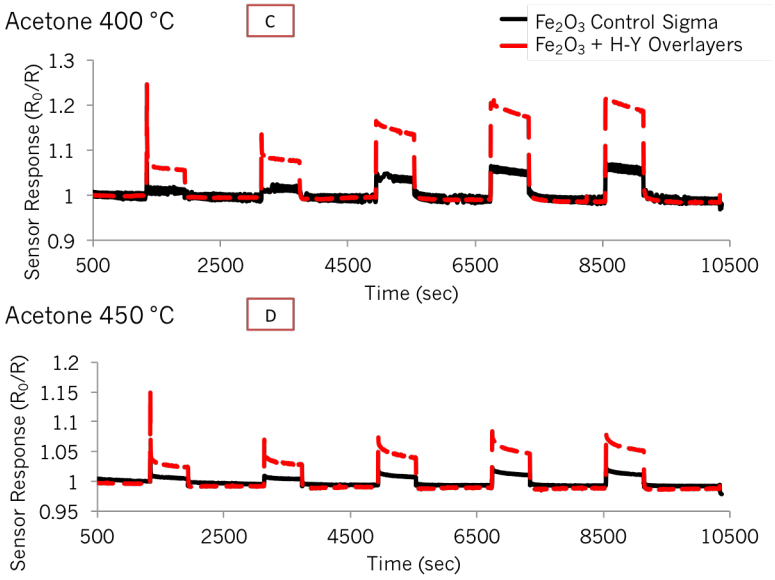

Figure 5-34 Sensor responses of a control Fe_2O_3 sensor and a Fe_2O_3 sensor modified by coatings of zeolite H-Y to (C) acetone at 400 °C and (D) acetone at 450 °C. Concentration for each pulse correspond to 10 ppm, 20 ppm, 50 ppm, 80 ppm and 100 ppm.

5.9 Summary of Results

This chapter investigated the potential of two Fe_2O_3 base materials for gas sensing applications sourced from two different commercial companies. Whilst one of the sensors fabricated from BDH powders provided promising results for gas sensing applications, the other – based on a powder attained from Sigma Aldrich – did not. The latter was later modified by admixture with 10% (wt.) of zeolites Na-A and H-ZSM-5.

Whereas with other systems described in Chapters 3 and 4 zeolite incorporation was seen to greatly improve the results towards some test gases in relation to the unmodified sensors, in this instance it did not. This was potentially due to an unfavourable microstructure of the base sensing material, which inherently resulted in poor sensitivity to gases. Although other operating temperatures were tried to prompt enhancements in sensor responses, the sensor's performance was seen to worsen, providing noisy data outputs. This could be indicative of poor network connectivity between the particles in the material or the formation of a dense/compact surface with limited access for gas molecules to diffuse through.

Although the surface area of the Sigma Aldrich sensor was found to be 2.6-fold higher than that of the BDH-based sensor, it did not result in a favourable outcome for detection. However, the Sigma-based sensor was seen to maintain the same baseline resistance under humid environments and it did not provide increments in sensor responses as the RH was incremented. Conversely, the baseline resistance of the BDH-based sensor did change when exposed to humid environments. Future tests ought to include the modification with zeolites of the BDH material as its microstructure was seen to be much more favourable for the purposes of gas detection. Further, as very clearly relayed in the literature, nanostructures are key in Fe_2O_3 gas detection sensors. For this reason, investigating the manufacture of nanoparticle materials may also serve as the best alteration pathway for successful detection of trace gas concentrations with the material.

Chapter 6 focuses on the gas-sensing results obtained with a collection of sensors based on n-type and p-type materials towards vapours relevant to the detection of illicit drugs, the so-called 'markers' or proxies of illicit drugs often targeted by sniffer dogs in interdiction strategies. These include methyl benzoate, as a marker of cocaine, ammonia as a marker of amphetamines and a solution of amphetamine in methanol. Machine learning classifiers were explored to better understand the selective capabilities of a four-sensor array.

6. Testing MOS Sensors for Drug Marker Detection

This chapter details the results attained when exposing a selected number of sensors based on the zeolite-modified n-type and p-type semiconducting systems – described in Chapters 3 and 4 – to what we have referred to here as 'drug markers' or 'proxies' of illicit drugs. We report:

- The detection of methyl benzoate, which is a by-product of cocaine and is usually targeted by sniffer dogs in interdiction efforts due to its sweet aroma and higher vapour pressure than cocaine.
- The detection of ammonia, which is a marker of amphetamine-type drugs and is used in the detection of clandestine laboratories.
- We also investigate the detection of a solution of amphetamine in methanol, as it is commonly transported as such in illegal trafficking operations.
- A short study carried out with four selected sensors to understand whether different machine learning classifiers could be employed to accurately classify the data into class labels i.e. into gas type. This exercise provides one with a better idea of the selective capabilities of the selected sensors.

6.1 Introduction

It has been established that many metal oxide semiconductor (MOS) gas sensors are very successful at detecting hazardous, toxic and explosive vapours.[28,39,40,52,288] The potential detection of illicit drugs with MOS devices has been highlighted in the literature but actual testing with MOS technology has only been found in one study.[1] In the latter, they devised an electronic nose composed of an array of Figaro-based sensors to detect cannabis-based products. They later used data-mining tools to discriminate between the samples investigated. Using support vector machines (SVMs) they attained an accuracy of 98.5% in discriminating among the vapours of interest. More recently, Voss et al. [2] showed that an array of MOS sensors could also be employed to detect odours emanating from human skin that would inform on whether an individual consumed cannabis or whether they did not. Using SVMs, they attained a classification accuracy of 92.5% in correctly classifying the data into cannabis-consuming individuals and non-consumers. On the other hand, Hackner et al. [324] fabricated surface ionisation (SI) sensors – which operate similarly to MOS sensors – and combined the SI detector to a chromatographic column so as to add selective capabilities to the system. They looked at the detection of amine-containing compounds due to the prevalence of this functional group in illegal drugs. This research group fabricated sensors that attained high sensitivity and selectivity towards amine-containing compounds.[244,324] However, whilst sensors provided discrimination

to the different agents commonly added to street drugs, they were not successful at differentiating between legal pharmaceutical drugs and illegal ones.[324]

Due to the low vapour pressure associated with most drugs, sniffer dogs are trained to detect substances that have a detectable odour, one that will favour detection due to a higher vapour pressure of the material.[33,34] An example is the detection of methyl benzoate, a by-product of cocaine, which has a sweet aroma and is targeted in canine detection as an indicator of cocaine.[33,34] The illegal manufacture of drugs can be a clumsy process carried out by inexperienced individuals that may not take the necessary precautions to ensure a product is safe.[325] Bearing in mind that drug production requires the use of organic solvents, the lack of quality control and assurance processes can mean that residual solvents may still be detectable both in the drug sample and in the environment or laboratory where they have been produced.[326] In legal pharmaceutical products there are specified limits that ought to be followed by law, to guarantee that the presence of residual solvents is below a certain threshold. This information can be found, for instance, in the British Pharmacopeia. Further, some of the solvents that are monitored in pharmaceutical drug samples include toluene, methanol, ethanol, acetone and isopropyl alcohol, all of which have been tested in this thesis with different semiconductor gas sensor systems as they are used in the illegal manufacture of drugs as well.[325,326] It has been highlighted in the literature that mobile gas sensors are needed to detect clandestine laboratories, not only due to the effect on health and the environment, but because of the risk of explosions as well.[4,326]

Through communication with experts that work in the field of drug trafficking prevention and detection, it was established that they could identify certain drug groups, themselves, by the type of odour associated with a sample. Thus, it is acknowledged that a particular compound in a drug e.g. a solvent used in manufacture, is unlikely to be identified and selectively detected by MOS technology. However, it is envisioned that the drug as a whole would have a particular odour, which would be the result of a combination of products present in the drug sample. This odour could then be translated into a unique ‘fingerprint’ when detected with a sensing array.

It must also be born in mind that trafficked drugs are kept in closed containers that may reach elevated temperatures during transit. The smell in the containers can be very strong and thus facilitate detection with vapour-based detection systems. Further, drugs are often dissolved in solvents to conceal them during traffic and, more and more, the movement of solvents and drug precursors is receiving more governmental

attention and control. All of the associated detrimental effects of illegal drug trafficking served as the main motivation of this study.

6.2 Drug-marker Detection with MOS Gas Sensors

The following section reports the detection of methyl benzoate (MB) and ammonia with n-type and p-type systems at different operating temperatures. This is followed by a short test on the detection of a 1mg/mL solution of amphetamine in methanol. Results attained with n-type and p-type systems have been presented in different graphs for clarification purposes. All tests were performed on AA rig (section 2.3.1).

Sensor selection was informed by the results attained in previous chapters. That is, SnO_2 sensors admixed with zeolites Na-A and H-ZSM-5 tended to provide contrasting responses to test gases, generally providing high repeatability among repeat tests across the temperatures investigated. Conversely, the sensing responses towards test gases provided by the Cr_2O_3 systems modified by admixture of zeolite H-ZSM-5 were not very promising. Nevertheless, with the exception of the Cr_2O_3 sensor modified by 20% (wt.) H-ZSM-5, which was found to provide inconsistent data in Chapter 4, the rest of the sensors were also exposed to MB. The Cr_2O_3 sensor modified by layers of zeolite H-Y was also investigated. It provided promising results when exposing it to toluene, a molecule of larger size (5.8 Å), and provided poor responsiveness when exposed to other test gases. Furthermore, large-sized molecules are reported to be adsorbed well in the supercages of the zeolite.[308] The same convention was followed with sensor exposure to ammonia gas and to the solution of amphetamine in methanol. When possible, tests were carried out at operating temperatures ranging between 350 °C and 450 °C.

Note that the vapour pressure of methyl benzoate at 20 °C is reported as 0.28 mmHg in the Sigma Aldrich product sheet, which corresponds to a theoretical headspace saturation of 368.4 ppm, in relation to the vapour concentration of cocaine which is reported as 0.25 ppb at room temperature.[6] Ammonia is a colourless, flammable gas that has a very pungent odour with a reported threshold of 5 ppm.[327]

Test Details:

Methyl benzoate: Liquid purchased from Sigma-Aldrich. It was placed in a Dreschel flask and progressively diluted with dry air passing through the flask, which was, in turn, connected to the sensor cell (refer to Fig. 2-6 in Chapter 2).

Ammonia: Gas purchased and certified by BOC gases with a source concentration of 50 ppm. Gas supplied to the sensing cell at different concentrations. Gas also detected in the presence of humid air.

Solution of amphetamine in methanol: the solution was placed in a small flask and a percentage of the total flow of air was passed through the flask and supplied through to the gas-sensing cell. The flow of air was also progressively increased during a test with the aim of attaining a higher response of the sensors to the vapour.

6.2.1 Methyl Benzoate Detection

SnO_2-based sensors detection of MB

The results of the SnO_2 based sensors towards MB were very interesting. Including the control SnO_2 sensor, all sensors proved to be incredibly responsive to MB both when supplied with low (*ca*. 37 ppm) and higher concentrations of the vapour (*ca.* 276 ppm) (Fig. 6-1). Further, excellent response magnitudes were attained at all the operating temperatures. It is noteworthy that the incorporation of zeolite materials was seen to greatly enhance the responses in relation to the unmodified control sensor.

As seen in Chapter 3, zeolite-modified sensors displayed their highest responsiveness at different operating temperatures. With exposure to MB, for instance, sensor 'SnO_2 + 30% (wt.) H-ZSM-5' was most responsive to the vapour at 350 °C and sensor 'SnO_2 + 10% (wt.) Na-A' was most responsive to the vapour at 450 °C (Fig. 6-1). This is information that could potentially be used commercially to identify MB.

Particularly when supplied with *ca.* 37 ppm of MB and at operating temperatures of 400 °C and 450 °C, the sensors displayed a strange peak shape. This behaviour was also observed with sensor 'SnO_2 + 10% (wt.) H-ZSM-5' at 350 °C. The sensors displayed an arch-like shape that had not been observed before with exposure to other test gases.

It was also noticed that higher response magnitudes were attained with the first concentration pulse (~37 ppm) than with the second concentration pulse (~74 ppm). With the exception of sensor 'SnO_2 + 30% (wt.) H-ZSM-5' at 350 °C, all other sensors seemed to reach steady state with the second concentration pulse. The peak shapes changed, once again, with the third and fourth concentration pulses (184 ppm and 276 ppm of MB, respectively), displaying more of a steep increase in sensor response during the gas pulse (exception: SnO_2 control sensor). Further, while some sensors increased in response with higher concentrations of MB, particularly after the second

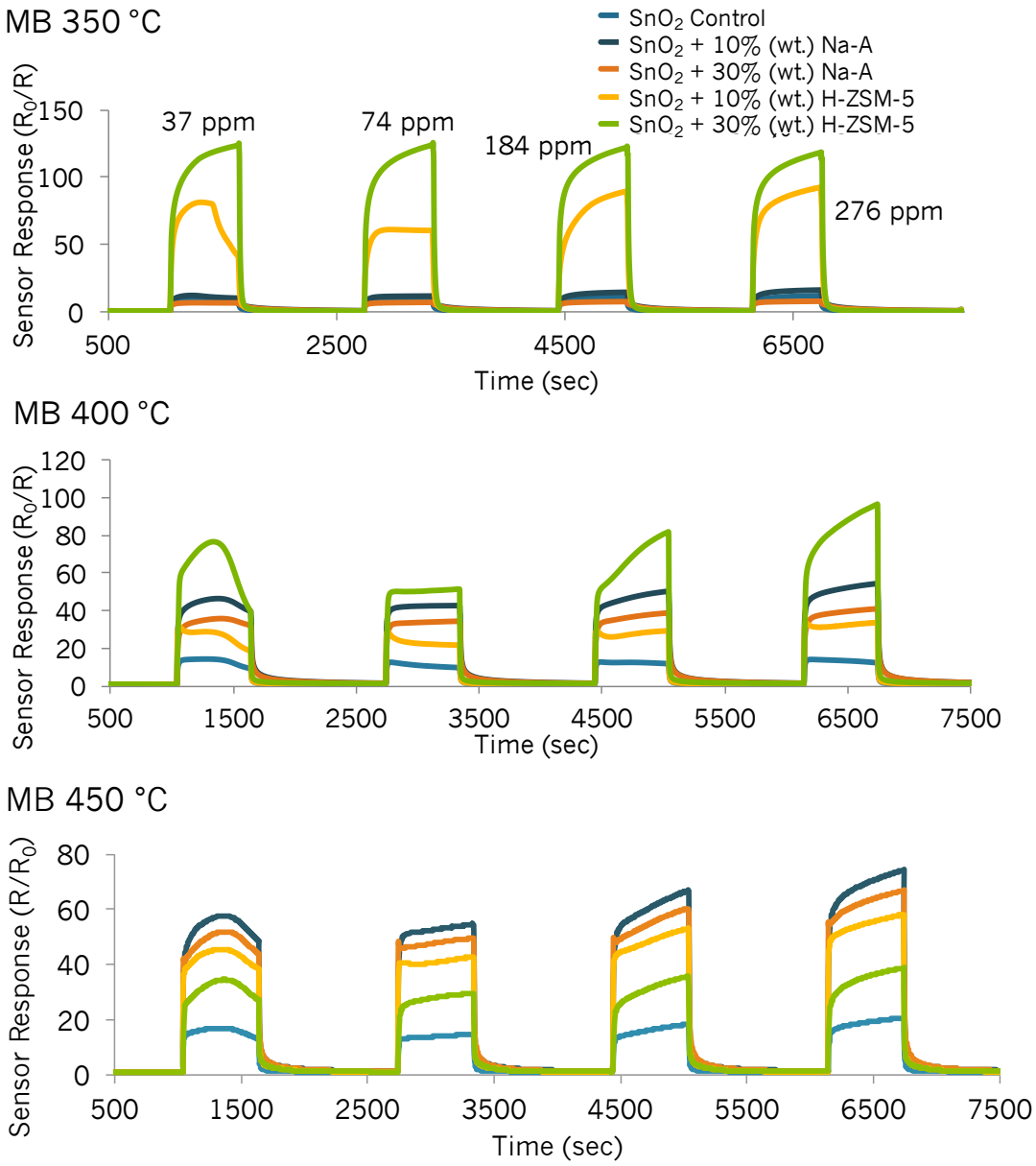

Figure 6-1 Sensor responses to methyl benzoate at 350 °C, 400 °C and 450 °C attained with a sensing array based on SnO_2 zeolite-modified materials by admixture with Na-A and H-ZSM-5. The methyl benzoate liquid was placed in a Dreschel flask and a flow of dry air was passed through it, supplying the vapour to the sensing cell.

concentration pulse of ~74 ppm, other sensors' responses were only mildly affected by concentration increments e.g. 'SnO_2 + 30% (wt.) H-ZSM-5' at 400 °C.

The shark-fin shapes seen in some sensor responses indicate slow reaction kinetics in the sensors. This could be due to the larger size of the molecule (kinetic diameter estimated as ≥ 5.8 Å). As such, it could struggle to diffuse through the microstructure of the sensors. Nevertheless, what was striking was that almost every concentration pulse led to different response shapes, potentially indicating the production of a range

of reaction products, the formation of which was strongly dependent on the concentration of MB. Although no precedent has been encountered in the literature detailing how MB may react on a metal oxide surface, some reactions that could potentially occur upon interaction with oxygen species or hydroxyl groups are suggested below:

$C_6H_5CO_2CH_3 + OH^- \rightarrow C_6H_6O + [COOCH_3]^+$

$C_6H_5CO_2CH_3 + O^- \rightarrow [C_6H_5CO_2CH_2]^+ + OH^- + e^-$

$C_6H_5CO_2CH_3 + OH^- \rightarrow C_6H_5COOH + [CH_3O]^-$

$C_6H_5CO_2CH_3 + O^{2-} \rightarrow [C_6H_5COO]^- + [CH_3O]^-$

$C_6H_5CO_2CH_3 + 18O^- \rightarrow 8CO_2 + 4H_2O + 18e^-$

These reaction products may then react further to provide newly formed products.

At 350 °C the aforementioned change in peak shape seen as the MB concentration was raised was only observed with the sensor containing 10% (wt.) zeolite H-ZSM-5. A remarkable increase in sensor response (16-fold enhancement) was obtained with the sensor containing 30% (wt.) H-ZSM-5 over that of the control, when supplied with ~37 ppm of MB. Furthermore, obtaining a response of R_0/R = 123 at low concentrations suggests that, with this sensor, much lower concentrations could be targeted in future. It must be noted, however, that with this sensor, concentrations exceeding 37 ppm resulted in the same response magnitudes; this is not too concerning if the sensors were to be used in practical applications for cocaine detection, as the concentrations sought would be considerably lower (ppb level) and the responses would potentially increase linearly with concentration. SnO_2-based sensors have, in the past, been successful at detecting gases at sub-ppm concentration levels.[3,328] As such, it is thought that SnO_2 modified with H-ZSM-5 would be a very good sensor candidate to detect this drug marker for security applications in the future.

SnO_2 sensors containing zeolite Na-A provided lower responses at 350 °C in relation to the other zeolite-modified sensors. The sensor containing more zeolite in the structure, 'SnO_2 + 30% (wt.) Na-A', provided a lower response (R_0/R = 6.5) when supplied with ~37 ppm of gas than the control SnO_2 sensor (R_0/R = ~7.7). The sensor response of 'SnO_2 + 10% (wt.) Na-A' was ~12 at this concentration. The peak shapes on the first

concentration pulse were strange in the sense that they saw an increase in resistance during the gas pulse. Furthermore, these two sensors had peak tailing, which was not present in the control sensor. It follows that, at this point, they would be unsuitable for practical applications seeking to detect MB at lower operating temperatures i.e. 350 °C. As the operating temperature was raised, the sensor responses of the SnO_2 sensors modified with zeolite Na-A increased, and provided an improvement in response over the control material. At 450 °C, both sensors modified with zeolite Na-A provided higher responses than those modified with zeolite H-ZSM-5 sensors. At 450 °C, the sensors modified by zeolite Na-A only reached steady state with the second concentration pulse (~74 ppm) and later displayed a similar steep increase in sensor response with higher concentrations of MB.

Due to the very interesting results attained with the sensor modified with 30% (wt.) zeolite H-ZSM-5 across the temperatures investigated, a new SnO_2 sensor with 50% (wt.) H-ZSM-5 was fabricated and tried for MB detection. The results have been presented in Fig. 6-2 below. As shown in the figure, the SnO_2 sensor mixed with 50% (wt.) H-ZSM-5 provided an outstanding enhancement in sensor response. The response was improved over that of the sensor modified with 30% (wt.) H-ZSM-5 at all the temperatures investigated. The optimal operating temperature to detect MB with 'SnO_2 + 50% (wt.) H-ZSM-5' was 400 °C as the responsiveness of the sensor was highest. Note that when supplied with ~37 ppm of MB the zeolite-modified sensor provided a response R_0/R = ~230 at 400 °C and, at higher concentrations such as ~184 ppm, the response was R_0/R = ~251.

The great enhancements seen in sensor response when incorporating zeolite H-ZSM-5 could be the result of catalytic reactions occurring due to the presence of the zeolite. It follows that it could break the source molecule down into intermediate products to which the sensing system, as a whole, was very sensitive. Additionally, it is also possible that introducing more zeolite into the sensing framework results in a higher surface area and, also, a more open microstructure that favours the diffusion of MB further down into the sensor bulk. This would allow the MB molecules to react with an amplified number of reactive sites as the molecules travel through the sensing layers, promoting an increase in the overall conductivity of the system.[15] The hydrophobic nature of zeolite H-ZSM-5 may also have an affinity for MB, retaining it or its reaction products well inside its pores.[22] As can be observed in Fig. 6-2 below, the zeolite-modified sensor was able to desorb the molecules successfully when MB was no longer supplied to the sensor at 400 °C. At other operating temperatures, there was evidence of peak tailing, which is unfavourable for practical applications. Nevertheless,

commercial products offer temperature cycling steps to clean the surface of the sensors.[39]

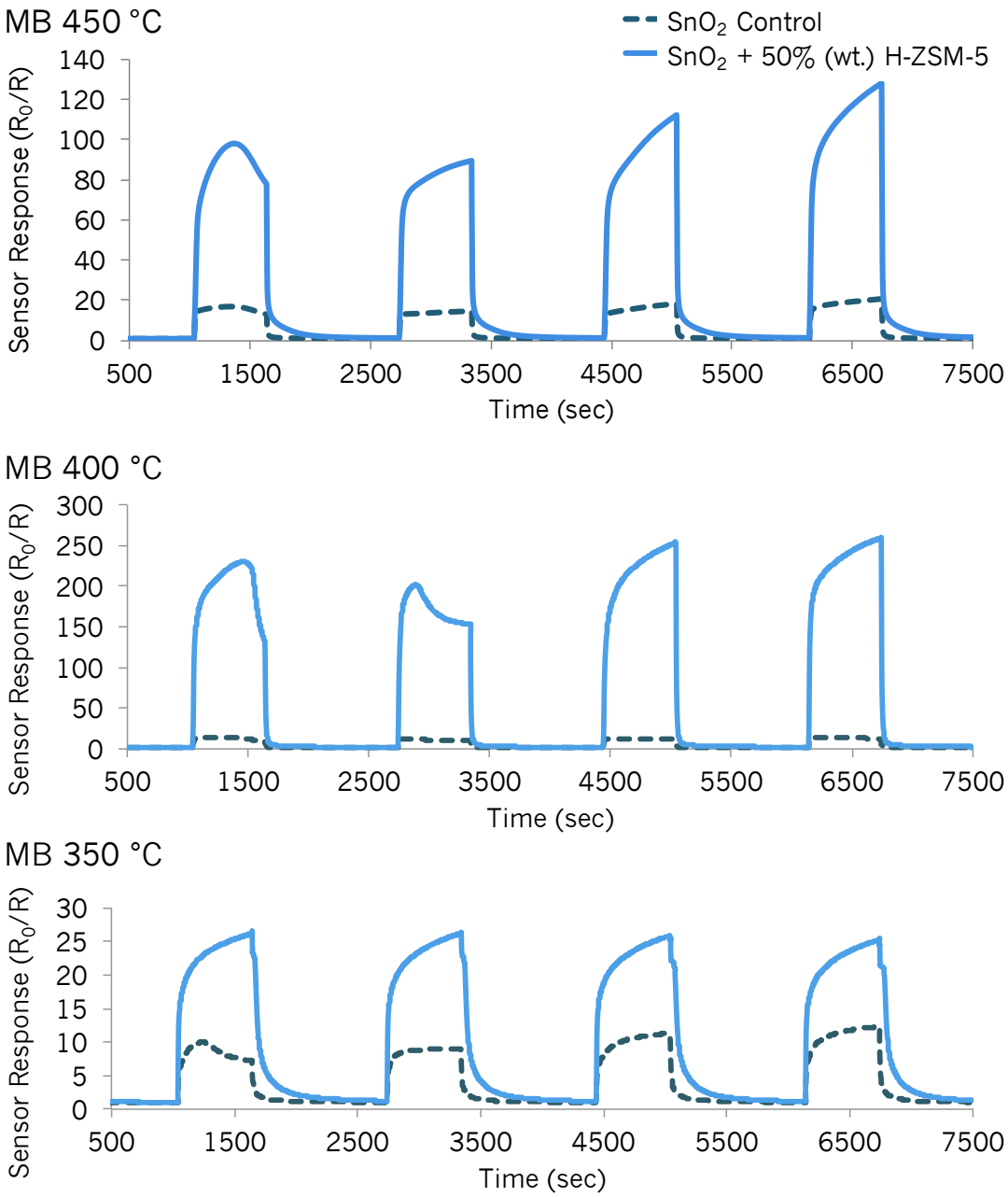

Figure 6-2 Sensor responses to MB at 350 °C, 400 °C, 450 °C of a control SnO_2 sensor (dark blue dotted line) and a SnO_2 sensor modified with 50% (wt.) zeolite H-ZSM-5 (light blue line). The concentrations of each gas pulse correspond to *ca.* 37 ppm, 74 ppm, 186 ppm and 276 ppm.

Response vs. concentration plots have been provided in Figs. 6-3 and 6-4 at 350 °C and 400 °C, respectively. It must be noted that whilst three repeat tests were performed on the SnO_2-based sensors at 350 °C, only two repeat tests were performed on the Cr_2O_3-based sensors at that temperature discussed later in the chapter. Nevertheless, the last concentration pulse corresponding to ~276 ppm was supplied to the sensors a

total of four times. As such, an indication of sensor repeatability can also be appreciated in Fig. 6-8 and 6-9 below, where n-type and p-type systems were compared at 350 °C.

As can be seen in Figs. 6-3 and 6-4 and as was the case in the other studies described in Chapters 3, 4 and 5, at lower temperatures the variability between tests was more pronounced. It can also be seen that as the concentration of MB was raised, some sensors did not provide a clear increase in response. Incorporating zeolites into the sensing system worsened the repeatability in the SnO_2-based sensors. The degree of variability changed individually for each sensor as the operating temperature was changed (Figs. 6-3 and 6-4). The results provided in the figures below correspond to an average of the maximum response attained after three repeat tests. Each test (1, 2 and 3) was studied individually to see how the sensors' behaviour varied from test to test. When focussing, for instance, on the sensor that was most responsive to MB at 350 °C, 'SnO_2 + 30% (wt.) H-ZSM-5', test 1 showed that the sensor increased in response as the vapour concentration was raised. In test 2, increasing the concentration of the vapour did not provide different response magnitudes and each pulse reached a response magnitude similar to the last pulse supplied in test 1 (276 ppm). Test 3 also failed to produce enhancements in sensor response with concentration. However, the response magnitude did increase considerably in relation to tests 1 and 2.

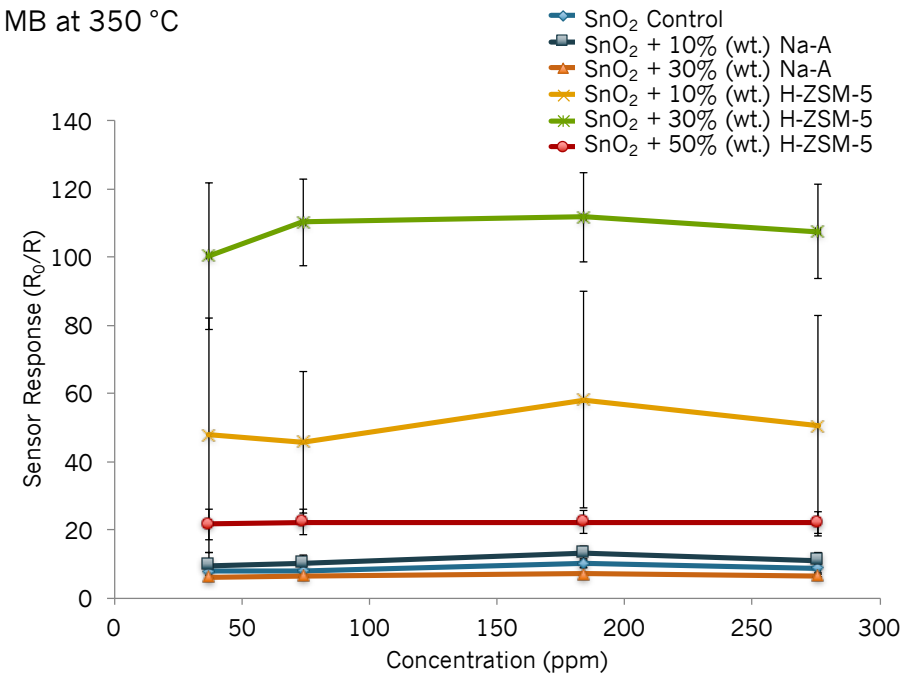

Figure 6-3 Sensor responses to different concentrations of methyl benzoate at 350 °C of a control SnO_2 sensor, a SnO_2 sensor modified by 10% (wt.) Na-A zeolite, another modified by 30% (wt.) Na-A, another by 10% (wt.) H-ZSM-5 and one modified by 30% (wt.) H-ZSM-5. Error bars corresponding to three repeat tests included.

It is possible that the zeolite was able to retain the test molecule or its reaction products inside its pores or cracks due to the very open microstructure of the SnO_2-based systems, which did not fully desorb when the vapour supply was switched off. As further tests were carried out, the molecules retained inside the structure continued to react with reactive sites and were subsequently able to penetrate deeper into the sensing layer of the material, eventually resulting in higher sensor responses than attained in test 1. Because the sensor did not reach steady state during the duration of the gas pulse this suggests that there were enough reactive sites available for the molecules to interact with.[136] In addition to this, the molecule's larger size and its reaction products may have experienced difficulty in diffusing through the sensing system.[22] Further, it must be noted that the heterogeneity of the microstructure in the sensors admixed with zeolite could also lead to the observed variability among tests; as the gas interacts differently with different areas of the system and charge transfer may have been affected by this.[116]

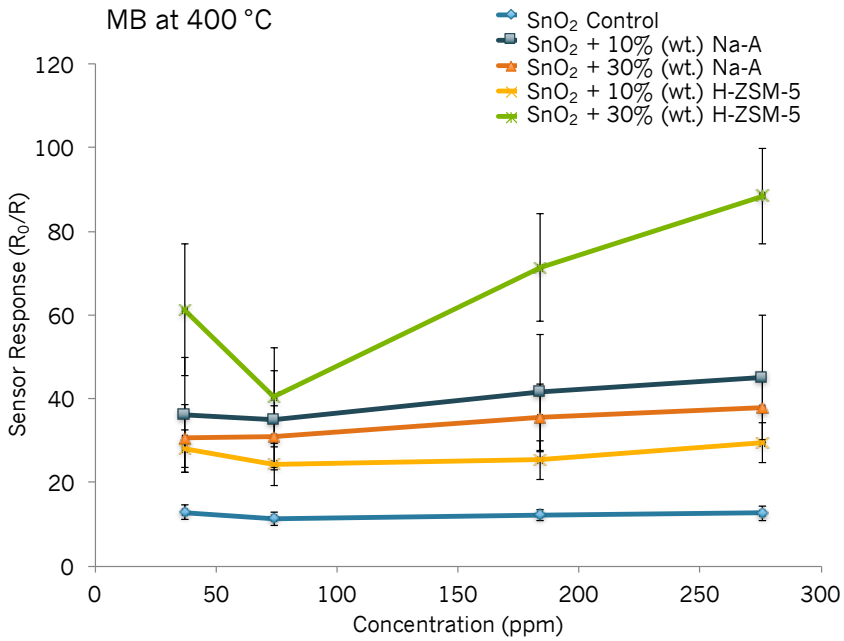

Figure 6-4 Sensor responses to different concentrations of methyl benzoate at 400 °C of a control SnO_2 sensor, a SnO_2 sensor modified by 10% (wt.) Na-A zeolite, another modified by 30% (wt.) Na-A, another by 10% (wt.) H-ZSM-5 and one modified by 30% (wt.) H-ZSM-5. Error bars corresponding to three repeat tests included.

Better insight into what might be occurring could potentially be reflected in the sensor resistance change from test to test. As such, this was investigated further. From test 1 to 3, the sensor resistance increased progressively.

It is acknowledged that the high concentrations of MB investigated here are irrelevant for the detection of cocaine but they highlight that the successful detection of trace concentrations of MB is indeed possible and worth investigating further in the future.

Cr_2O_3-based sensors detection of MB

Similar tests were carried out with Cr_2O_3-based sensors, modified by mixing zeolite H-ZSM-5 with the base material. To summarise, the detection of solvents with these sensors was certainly possible but the response magnitudes attained previously were moderate (Chapter 4), when compared to the n-type systems investigated in Chapter 3. The sensors also struggled to differentiate between ethanol and acetone gases. Nevertheless, they were still tested against MB and the results have been provided in Fig. 6-5 A, B and C corresponding to tests carried out at 350 °C, 400 °C and 450 °C.

As seen in the graphs displayed below, the Cr_2O_3 zeolite-modified sensor that was most responsive to MB was 'Cr_2O_3 + 40% (wt.) H-ZSM-5' both at 350 °C and 400 °C. At an operating temperature of 450 °C, sensor responses were all rather similar and R/R_0 = <2 for all sensors. The magnitude of response of 'Cr_2O_3 + 40% (wt.) H-ZSM-5' was practically unaffected by MB concentration increments. Further, the latter sensor failed to reach steady state during the gas pulse. At 400 °C, the same sensor seemed poorly responsive to the vapour until it was supplied with 276 ppm, and saw a 12-fold increase in sensor response in relation to the control sensor.

The odd peak shape that was observed with the first concentration pulse in the SnO_2-based sensors was also observed in some of the Cr_2O_3-based sensors at 450 °C and 400 °C. The first concentration pulse also resulted in higher magnitudes of sensor response than the second concentration pulse that followed in some sensors.

Response vs. concentration plots have been presented in Fig. 6-6 and 6-7 at 350 °C and 400 °C, respectively. The tests at 350 °C were carried out twice and the results have been presented in Fig. 6-6 to show how the responses showed little variability between tests. An inset figure has been provided for clarification purposes, corresponding to the sensor responses that were smaller in magnitude. As can be seen in these two figures, the response magnitudes towards MB were, indeed, smaller than with the SnO_2-based sensors. However, the variability between repeat tests was also reduced. The sensor most attractive for the detection of trace concentrations of MB in the future would be that containing 40% (wt.) H-ZSM-5 and at an operating temperature of 350 °C, since it was much more responsive at this temperature and the variability was low, with the exception of the first MB pulse.

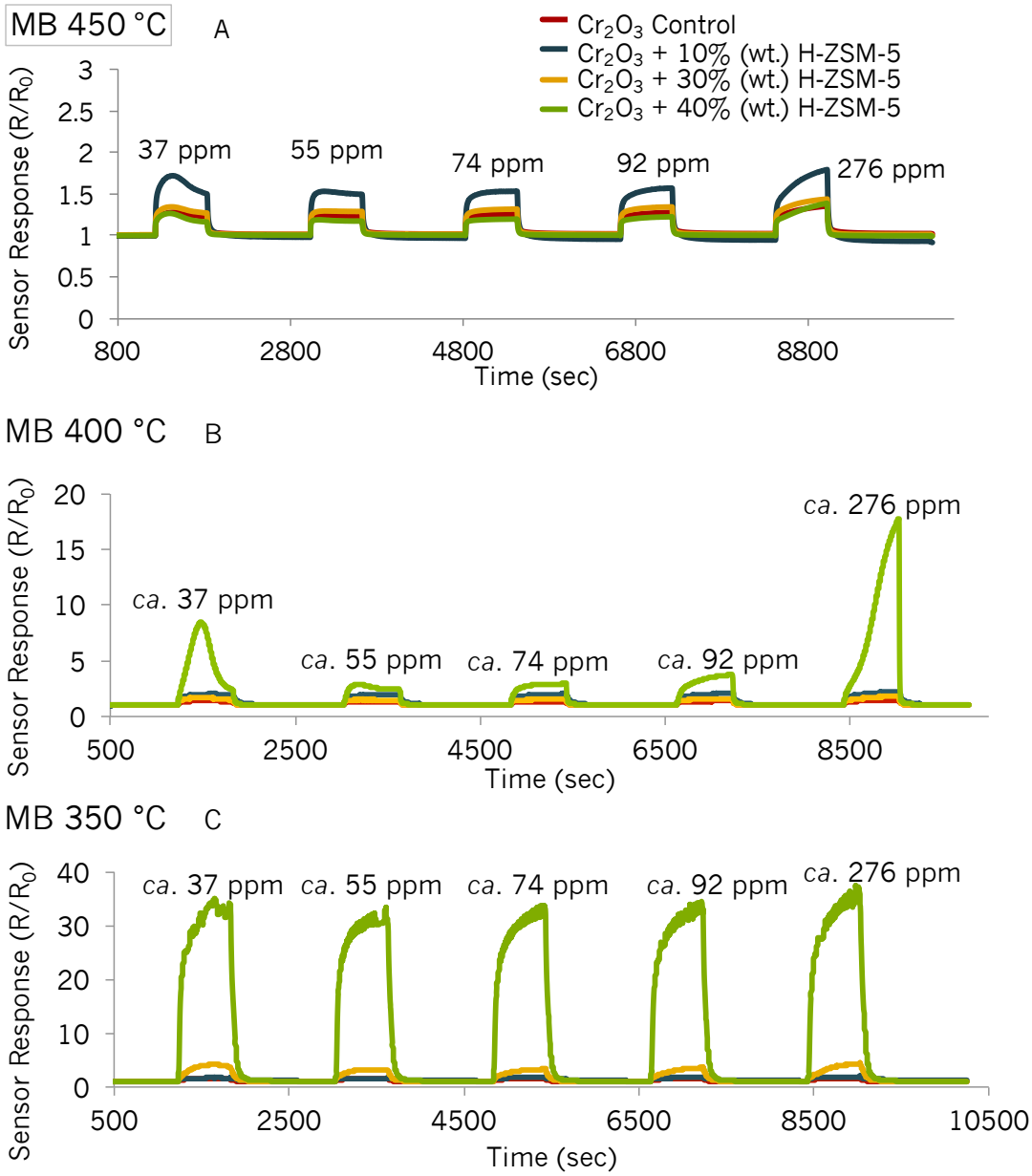

Figure 6-5 Sensor responses of Cr_2O_3 control sensor and Cr_2O_3 modified by 10% (wt.), 30% (wt.) and 40% (wt.) zeolite H-ZSM-5 to MB at 350 °C, 400 °C and 450 °C.

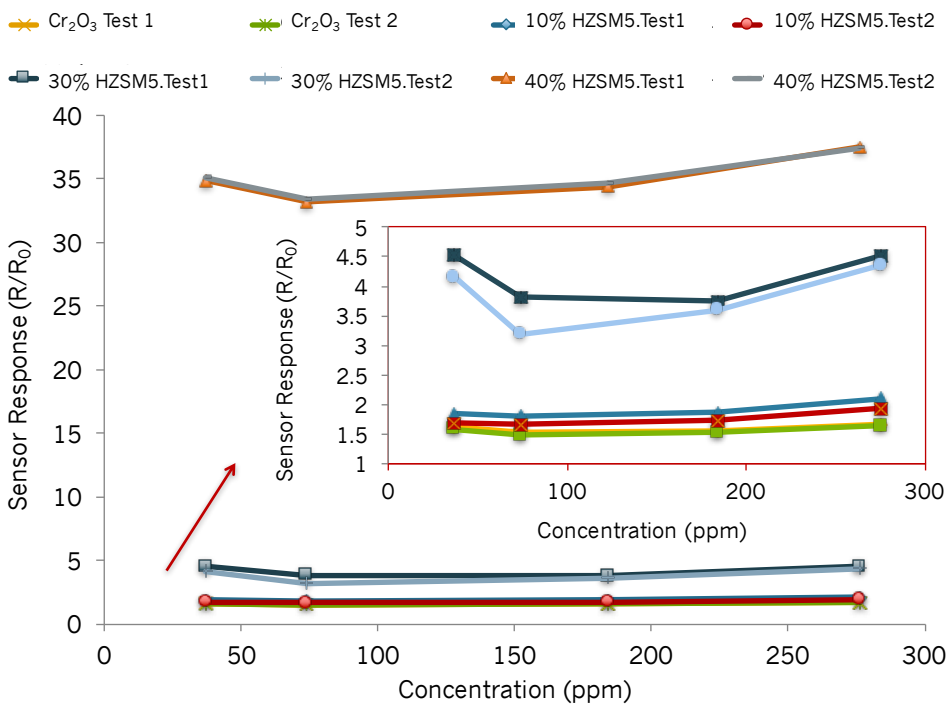

Figure 6-6 Sensor responses to different concentrations of MB at 350 °C of a Cr_2O_3 control sensor and those modified by 10% (wt.), 30 % (wt.) and 40% (wt.) zeolite H-ZSM-5. The inset corresponds to the lower sensor responses, which were difficult to see. The graph includes results of two repeat tests for each sensor.

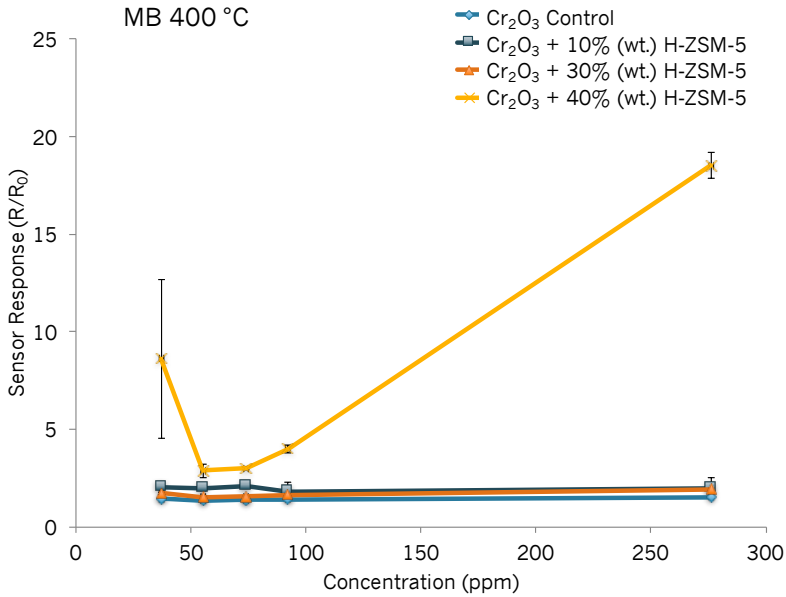

Figure 6-7 Sensor responses to different concentrations of MB at 400 °C of a Cr_2O_3 control sensor and those modified by 10% (wt.), 30 % (wt.) and 40% (wt.) of zeolite H-ZSM-5. The results correspond to the average of 3 repeat tests.

Figs. 6-8 and 6-9 provide an example of how differently the n-type and p-type sensors responded to MB at two different temperatures and how sensor variability among repeat tests could be a key determinant factor in selecting which sensors would be good candidates for further testing in the future.

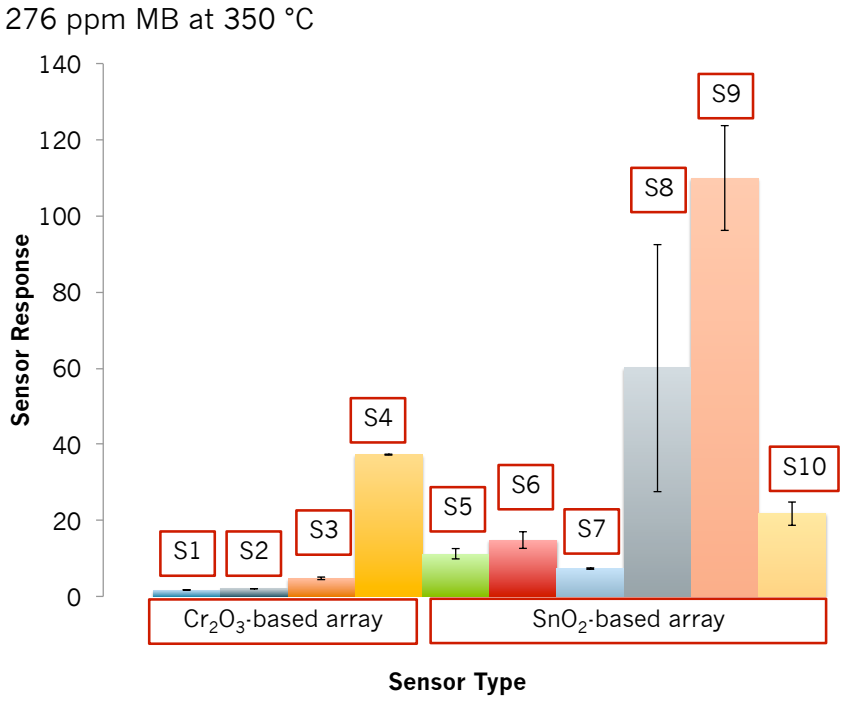

Figure 6-8 Sensor responses to *ca.* 276 ppm methyl benzoate at 350 °C. S1 = Control Cr_2O_3, S2 = Cr_2O_3 + 10% (wt.) H-ZSM-5, S3 = Cr_2O_3 + 30 % (wt.) H-ZSM-5, S4 = Cr_2O_3 + 40 % (wt.) H-ZSM-5, S5 = control SnO_2, S6 = SnO_2 + 10% (wt.) Na-A, S7 = SnO_2 + 30% (wt.) Na-A, S8 = SnO_2 + 10% (wt.) H-ZSM-5, S9 = SnO_2 + 30 % (wt.) H-ZSM-5, S10 = SnO_2 + 50 % (wt.) H-ZSM-5. Sensor response for p-type systems was calculated as R/R_0 and as R_0/R in n-type systems. As mentioned in the text, with the p-type systems the last concentration pulse was repeated four times to get an idea of variability between tests. N-type tests were repeated 3 times.

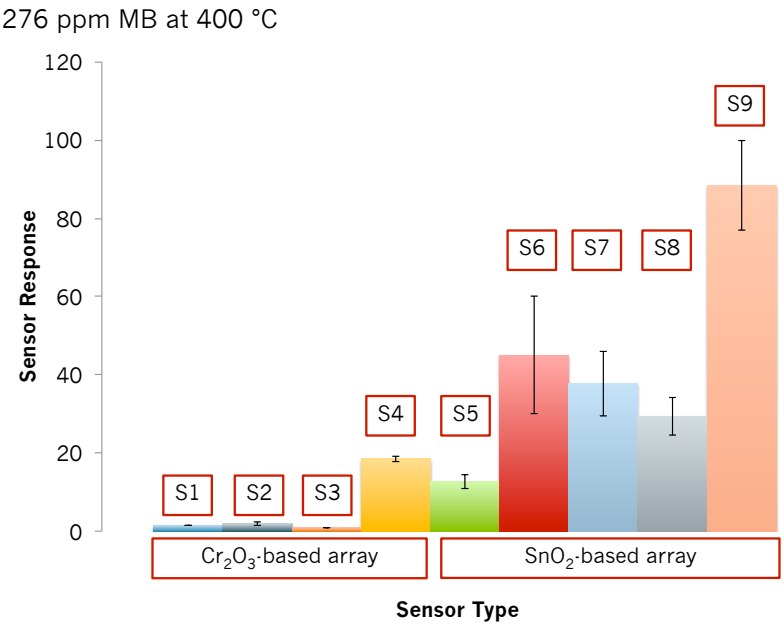

Figure 6-9 Sensor responses to *ca.* 276 ppm methyl benzoate at 400 °C. S1 = Control Cr_2O_3, S2 = Cr_2O_3 + 10% (wt.) H-ZSM-5, S3 = Cr_2O_3 + 30 % (wt.) H-ZSM-5, S4 = Cr_2O_3 + 40 % (wt.) H-ZSM-5, S5 = control SnO_2, S6 = SnO_2 + 10% (wt.) Na-A, S7 = SnO_2 + 30% (wt.) Na-A, S8 = SnO_2 + 10% (wt.) H-ZSM-5, S9 = SnO_2 + 30 % (wt.) H-ZSM-5. Sensor response for p-type systems was calculated as R/R_0 and as R_0/R in n-type systems. Tests were repeated three times in both systems.

In p-type systems the sensor that provided markedly different responses was that with 40% (wt.) zeolite H-ZSM-5 at operating temperatures of 350 °C. At 400 °C, sensors 'SnO_2 + 50% (wt.) H-ZSM-5' and 'Cr_2O_3 + 40% (wt.) H-ZSM-5' were the most responsive to MB. Lower concentrations of MB ought to be tried with sensors modified by zeolite H-ZSM-5 in future as it certainly seems like a good modification agent for the detection of this vapour both with n-type and p-type systems. As was observed in previous chapters, variability was generally reduced when lower vapour concentrations were supplied to the sensors. Given that in practical settings MB detection would be needed at much lower concentrations, it is expected that sensor variability would be less of an issue. In addition to this, it would be worth fabricating more homogenous microstructures in future, with the aim of determining whether repeatability could be better controlled. Alternatively, rather than using zeolites as modification agents, it would also be interesting to evaluate how the sensing performance of SnO_2 and Cr_2O_3-based sensors was affected by the incorporation of noble metal catalysts.

One of the concentrations tested, 276 ppm, was used as an example to investigate the sensors' response and recovery times at 350 °C and 400 °C in n-type and p-type systems. Results have been presented in Tables 6-1 (n-type) and 6-2 (p-type) below and the results are based on the last repeat test performed. In general, the incorporation of zeolites in n-type systems led to either faster or comparable sensor response times when compared to those obtained with the control sensor and they served to increase the recovery times in relation to the control SnO_2 sensor. Conversely, zeolite incorporation led to comparable or longer response times in zeolite-modified p-type systems in relation to the control Cr_2O_3 sensor and the recovery times were considerably improved over those seen with the control, particularly with higher zeolite loadings in the sensing system.

More specifically, the SnO_2 based sensors generally responded and recovered more quickly (in ~2 seconds) at 400 °C than at 350 °C, as expected. At 350 °C, the sensors modified with zeolite H-ZSM-5 responded slightly more quickly than the control SnO_2 sensor or those containing zeolite Na-A. Furthermore, at this temperature, the response times were slightly longer as the zeolite loading increased. At 400 °C, the sensor recovery times increased with higher loading of zeolites in the sensing system. Sensors containing zeolite Na-A displayed longer recovery times than those containing zeolite H-ZSM-5. The latter can potentially be the result of zeolite H-ZSM-5 catalysing reactions and breaking the MB molecule down to products whose diffusion through the system was more straightforward. Zeolite Na-A is not known as a cracking agent and it also possible that the MB molecule or its reaction products experienced more difficulty in

desorbing off a sensor microstructure that was perhaps more compact in nature (refer to Fig. 3-10E and F).

In comparison to the n-type systems, the Cr_2O_3-based sensors took a much longer time to respond and less time to recover. The zeolite-modified sensors took longer times to respond than the control at 400 °C but τ_{90} was very similar to the control sensor at 350 °C.

Table 6-1 SnO_2 based sensor response and recovery times in seconds to 276 ppm methyl benzoate vapour at 350° C and 400 °C. CTL refers to control, LTA refers to zeolite Na-A and MFI refers to zeolite H-ZSM-5. The results are based on the third repeat test performed.

	Response & Recovery Times (sec)					
276 ppm MB 400 °C	SnO_2 CTL	SnO_2 + 10% LTA	SnO_2 + 30% LTA	SnO_2 + 10% MFI	SnO_2 + 30% MFI	SnO_2 + 50% MFI
τ_{90}	2	2	2	2	2	2
τ_{10}	282	892	937	361	716	861
276 ppm MB 350 °C	SnO_2 CTL	SnO_2 + 10% LTA	SnO_2 + 30% LTA	SnO_2 + 10% MFI	SnO_2 + 30% MFI	SnO_2 + 50% MFI
τ_{90}	10	8	14	2	2	4
τ_{10}	516	910	945	653	535	806

Table 6-2 Cr_2O_3 based sensor response and recovery times in seconds to 276 ppm methyl benzoate vapour at 350° C and 400 °C. CTL refers to control, LTA refers to zeolite Na-A and MFI refers to zeolite H-ZSM-5. The results are based on the third repeat test performed.

	Response & Recovery Times (sec)			
276 ppm MB 400 °C	Cr_2O_3 CTL	Cr_2O_3 +10% MFI	Cr_2O_3 +30% MFI	Cr_2O_3 +40% MFI
τ_{90}	357	361	410	512
τ_{10}	112	190	59	10
276 ppm MB 350 °C	Cr_2O_3 CTL	Cr_2O_3 +10% MFI	Cr_2O_3 +30% MFI	Cr_2O_3 +40% MFI
τ_{90}	347	343	396	345
τ_{10}	200	875	135	84

It seemed to be the case that with p-type systems, having more zeolite in the structure assisted in vapour desorption both at 400 °C and at 350 °C, which was also appreciated upon exposure to toluene gas in Chapter 4, a molecule that was also larger in size in relation to other test analytes. The Cr_2O_3 sensor with 10% (wt.) H-ZSM-5 responded very similarly to the control sensor (~360 seconds at 400 °C and ~343 seconds at 350 °C) but recovered much more slowly at both temperatures. Although it was expected that at higher temperatures the sensors would respond more quickly due to the thermal energy accelerating the rate of the reaction processes occurring at the sensor, it was found that they were rather comparable to the 350 °C response times,

only longer. It must be noted that the Cr_2O_3 sensor that contained 40% (wt.) H-ZSM-5 exhibited a great increase in sensor response at 276 ppm (Fig. 6-5B), in relation to lower concentrations and it displayed an odd peak shape at 400 °C. This could, potentially, be indicative of different reaction products progressively interacting with the sensor as the vapour was being supplied, which could have led to the much longer response times seen in this sensor at this temperature.

It is possible that certain sensor microstructures, which appeared to be more open in nature, could favour the diffusion of larger molecules and enable the subsequent reaction of the molecules in the inner layers of the bulk.[229] In turn, some reaction products may be retained as a result of higher affinity with the system or due to their size and/or shape and may continue to interact with the zeolite particles and the pores within.[229] The issues of long response and recovery times were particularly evident with toluene exposure, another aromatic molecule of larger size.

It is thought that the n-type systems responded more quickly and the conductivity of the system was more prominent upon exposure to gases because the microstructure was more porous and the particle size of the base material was much smaller and provided a higher surface area for gas interaction than the p-type systems. If this was true, and some of the sensing microstructures used here limited the interaction between the gas and the sensing system to only the outer layers of the sensor due to their compactness, they could offer less variability between tests. The longer response times in such case would be due to the inefficiency of the molecule to pass through the cavities in the system and the shorter recovery times due to a shorter desorption pathway. It is recalled here that that the reason why the Cr_2O_3 sensor modified with 40% (wt.) H-ZSM-5 provided fast response and recovery times when exposed to molecules such as ethanol and acetone in Chapter 4 was thought to be the result of gases fully combusting to CO_2 and water vapour, due to the higher concentration of zeolite in the sensing system. As the kinetic diameter and complexity of the test molecule supplied increased i.e. toluene, the response patterns differed and the Cr_2O_3 sensor modified with 40% (wt.) H-ZSM-5 increased in responsiveness. It was thought that the higher concentration of zeolite in the system broke the toluene molecule down more efficiently into intermediate products to which Cr_2O_3 was more sensitive or which were smaller in size and had easier access to the inner layers of the sensor. It is thought that something similar occurs with exposure to MB. The system containing more zeolite is able to catalyse reactions more efficiently than those that have less zeolite. In turn, enabling the diffusion of smaller molecules into the system. P-type systems have been reported to be less responsive to inflammable gases than n-type

ones.[107] The more compact microstructure of the Cr_2O_3 based sensors may limit the access of the molecules further down inside the bulk, leading to smaller response magnitudes but, also, to fewer issues with repeatability.

Exposure to MB of the Cr_2O_3 Sensor Modified by Overlayers of Zeolite H-Y

The Cr_2O_3 sensor modified with overlayers of zeolite H-Y was previously found to provide great improvements in sensor responses to toluene (Chapter 4). Due to the larger kinetic diameter of MB, the potential of the sensor for its detection was also evaluated, expecting to obtain high responsiveness to the vapour as well. The results of this have been presented in Fig. 6-10 below.

The best operating temperature of the zeolite-modified sensor for the detection of MB was 400 °C: it provided the highest response magnitudes to the supplied vapour concentrations and the sensors recovered faster than in the test carried out at 350 °C. The first concentration pulse also led to higher response magnitudes than the pulse that followed. When supplied with *ca.* 37 ppm of MB, the zeolite-modified sensor provided a ~9-fold increase in sensor response over the control sensor at 400 °C.

Response vs. concentration plots of the control Cr_2O_3 sensor and the sensor modified with cover layers of zeolite H-Y have been presented in Fig. 6-11 at 400 °C. It can be seen that the sensors provided repeatable results. However, the sensors did not respond linearly to concentration increments. Once again, it would be useful to investigate lower concentrations of this vapour in the future.

The sensor response and recovery times were also investigated in this system (Table 6-3), using the 276 ppm MB concentration as an example of how the sensors performed. As was observed with other Cr_2O_3-modified sensors, the response times (τ_{90}) were longer than the recovery times. Nevertheless, the response times of the zeolite-modified sensor were shorter in relation to those seen in the control sensor and in previously-reported Cr_2O_3 zeolite-modified systems at 400 °C. However, they were still considered to be too long for practical applications. Having thinner printed layers of the base material could perhaps circumvent this issue.[24] The lower response magnitudes that may be attained in such a case, could be addressed by reducing the particle size of the base material, for instance, and/or by doping with noble metal catalysts.[30] This could favour the detection of trace concentrations of MB with Cr_2O_3-based materials in future.

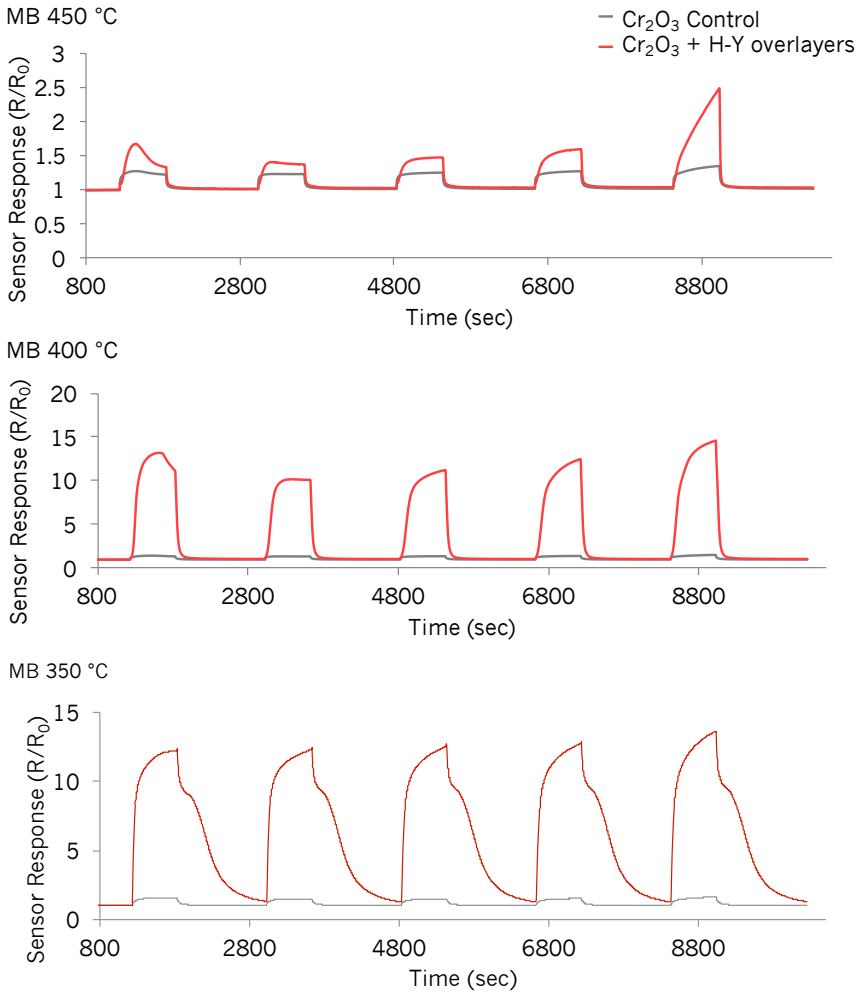

Figure 6-10 Sensor responses to methyl benzoate of a control Cr_2O_3 sensor and one modified by coatings of zeolite H-Y at three different temperatures. The concentrations tested correspond to those in Fig. 6-5, 37 ppm, 55 ppm, 74 ppm, 94 ppm and 276 ppm.

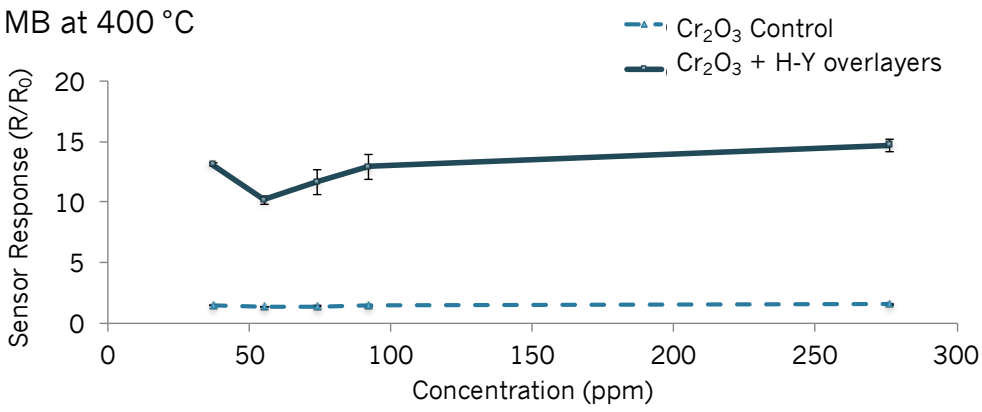

Figure 6-11 Sensor response of a control Cr_2O_3 sensor and a Cr_2O_3 sensor modified by overlayers of zeolite H-Y at 400 °C upon exposure to different concentrations of methyl benzoate.

Table 6-3 Control Cr_2O_e and Cr_2O_3 modified by coatings of zeolite H-Y sensor response and recovery times in seconds to 276 ppm methyl benzoate vapour at 400 °C. CTL refers to control. The results are based on the third repeat test performed.

	Response & Recovery Times (sec)	
276 ppm MB 400 °C	Cr_2O_3 CTL	Cr_2O_3 + H-Y overlayers
Seconds τ_{90}	356.875	311.781
Second τ_{10}	111.766	70.594

The next section evaluates the detection of ammonia as a marker of amphetamine-based drugs. The same sensor arrays have been utilised for its detection.

6.2.2 Ammonia Detection

Tests against ammonia with n-type and p-type systems were carried out at 350 °C, 400 °C and 450 °C to understand sensor behaviour and the optimal operating temperature for its detection. It must be noted that, as it occurred with many other gases tested in the lab, demand was high and thus some of the tests could only be repeated twice. When this was the case, both plots have been provided to give an indication of variability between tests. The Cr_2O_3-based sensors were also exposed to ammonia in humid conditions (25% RH, 50% RH and 75% RH). The reason why this was not done with the SnO_2-based sensors was, once again, because a lot of users needed the gas. It is acknowledged that, ideally, this ought to have been carried out with these systems as well.

SnO_2-based Sensor Exposure to Ammonia

Sensor responses of SnO_2-based sensors modified by zeolites were improved at 450 °C, over tests carried out at 400 °C and 350 °C. Examples of what the response patterns looked like at each temperature have been provided in Fig. 6-12 below.

As can be seen in the figure, the responses increased with concentration at the highest temperature tested, 450 °C. The sensors containing zeolite H-ZSM-5 responded more slowly than those containing zeolite Na-A but they reached steady state. Those containing zeolite H-ZSM-5 at 10% (wt.) and 30% (wt.) provided identical response magnitudes and patterns towards ammonia. The sensor containing more zeolite in the structure, 'SnO_2 + 50% (wt.) H-ZSM-5' provided the highest sensor response (R_0/R ~2.8) to the gas at this temperature.

The SnO_2 sensor containing 30% (wt.) zeolite Na-A, provided a p-type response at all the temperatures tested and the p-type response increased in magnitude as the

temperature was lowered to 350 °C. As alluded to in previous chapters, the reasons why n- to p-type switches occur are not fully understood. Some groups attribute this behaviour to the conversion of chemisorbed oxygen from molecular oxygen to an atomic form during interaction with reducing gases at low operating temperatures.[329] This would, in turn, result in an increase of the surface charge of the oxide leading to the observed decrease in conductivity. Korotcenkov et al. [330] detailed that water accumulation in the form of hydroxyl groups may have contributed to the n-to-p switch in In_2O_3 gas sensor materials. Nevertheless, tests were carried out in dry conditions and thus it is not thought to be the result of hydroxyl group accumulation at the surface. Furthermore, previous tests carried out against water vapour in Chapter 3 revealed that sensors modified with zeolite Na-A provided an n-type response to water vapour, thus this explanation can be ignored.

It could be possible that an n-to-p switch occurred as a result of the production of an oxidising gas such as nitrous oxide.[29] This could be possible, as it was previously tested how the SnO_2-based sensors behaved upon exposure to an oxidising gas (Appendix) and resistive responses were attained, as expected. Finally, other groups suggest that this occurs when the majority of charge carriers, in this case electrons, are reduced and the density of majority carriers switches to holes, causing an inversion layer that results in such behaviour.[250] This model was based on band-bending and as the authors themselves report, more work needs to be carried out to understand this behaviour further. It did appear that, as the temperature was progressively lowered, the responses of the sensors were slowly moving towards an n-to-p switch and, as a result of this, their magnitude of response was smaller.

Response vs. concentration plots of the sensors at 450 °C have been provided in Fig. 6-13 below. Note that the response of the 'SnO_2 + 30% (wt.) Na-A' sensor was thus calculated as R/R_0 and the rest as R_0/R. It can be observed that the majority of sensors increased linearly in response from a concentration of 2.5 ppm to 20 ppm and then saturated, which is not uncommon in MOS gas sensors, as detailed in previous chapters. Having said this, the fact that the response magnitudes to ammonia are lower than upon exposure to other gases of interest and that a sensor such as 'SnO_2 + 30 % (wt.) Na-A' provides a p-type response in its presence is actually considered a good thing for the purposes of this project. If this sensor behaves as n-type and provides very different response magnitudes and patterns to other reducing gases, the fact that it behaves so differently towards ammonia could serve as the perfect means to induce selectivity between different drug types. This would work, for instance, with a sensing array if the number of target gases was very specific and they could be tested in an

environment with minimal interference from other vapours. Nevertheless, a sensor that showed specificity towards ammonia would also be desirable. The literature suggests that CTO-based sensors could be good candidates for this purpose.[103]

Cr_2O_3-based Sensor Exposure to Ammonia

Similar tests were carried out with the Cr_2O_3 modified sensors at 400 °C and 350 °C (Figs. 6-14 and 6-15). It can be observed in the figures that at lower operating temperatures there was clear baseline drift and thus this was not deemed a suitable operating temperature for ammonia detection.

At 400 °C, it can be observed that a lower loading of zeolite H-ZSM-5 in the sensing system i.e. 'Cr_2O_3 + 10% (wt.) H-ZSM-5' provided higher response magnitudes, followed by the sensor with 30% (wt.) H-ZSM-5 and then by the one containing 40% (wt.) H-ZSM-5, which provided almost identical results to the control sensor.

The sensor responses were all $R/R_0 < 1.4$, similar to those encountered upon exposure to the gases explored in Chapter 4. The peak shapes once again looked odd, the reason why this occurred is not known, but it translates to some mechanism decreasing the sensor resistance during the gas pulse. This is thought to be because at such low concentrations of ammonia (e.g. 2.5 ppm), the gas supplied is able to react with the oxygen species that are available on the sensor surface, leading to a sharp initial increase in resistance. When the gas continues to interact with oxygen, the much higher concentration of oxygen in the surrounding atmosphere results in a quick repopulation of surface oxygen and continuous reintroduction of electrons back to the material bulk, which reduces the concentration of holes during the gas pulse and, as such, the resistance of the sensor decreases. This behaviour was observed more frequently at lower gas concentrations and with the sensor that had a lower percentage weight of zeolite. The sensors began to show a peak shape resembling that of an ideal sensor and reached steady-state with increased concentrations of ammonia gas.

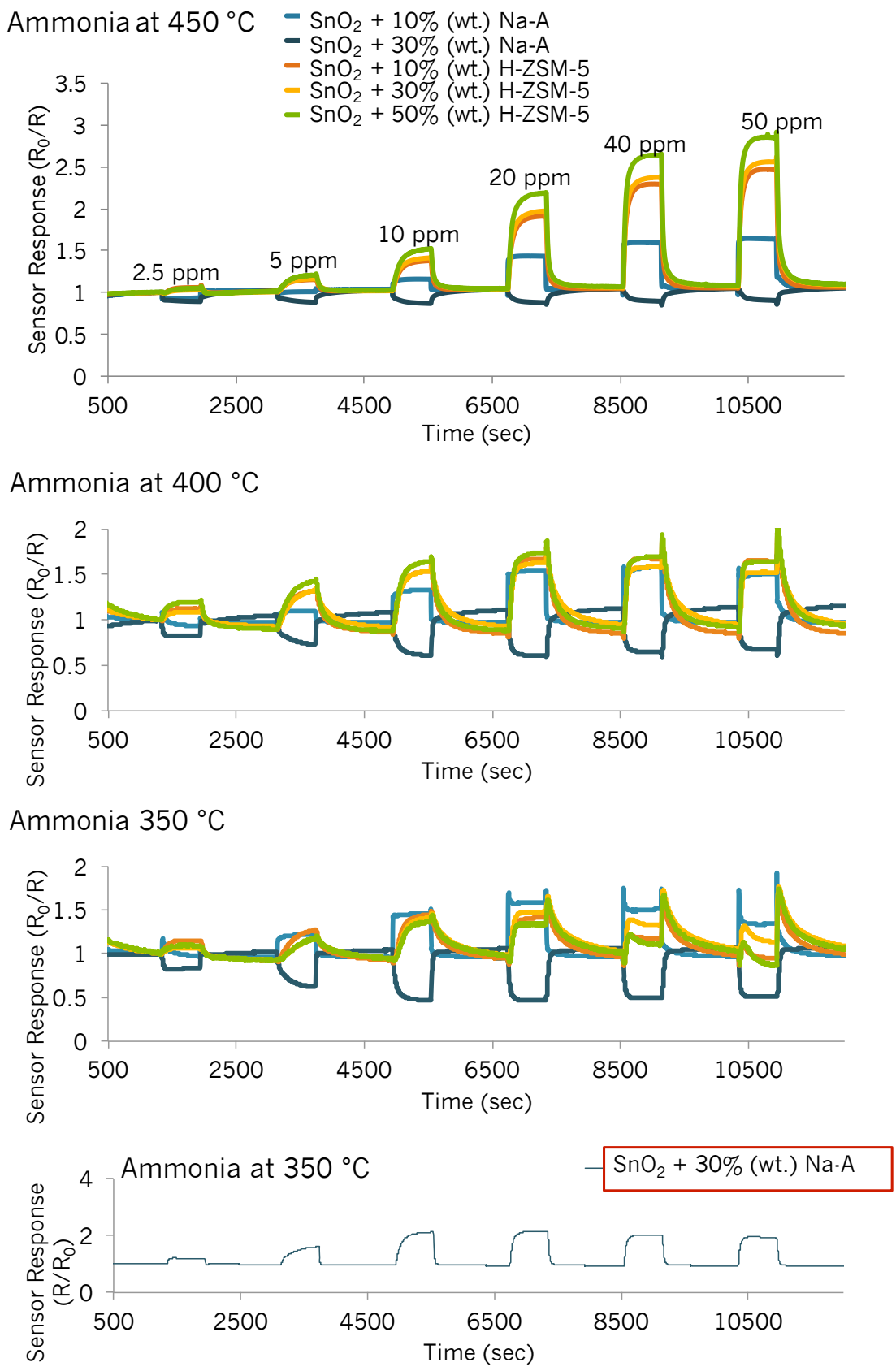

Figure 6-12 Sensor responses of SnO_2-modified sensors with zeolite H-ZSM-5 and Na-A to ammonia gas at different concentrations and temperatures, ranging between 350 °C and 450 °C. As can be seen the sensor modified with 30% (wt.) Na-A provided a p-type response, which has been provided in the bottom graph (R/R_0) to better visualise its response.

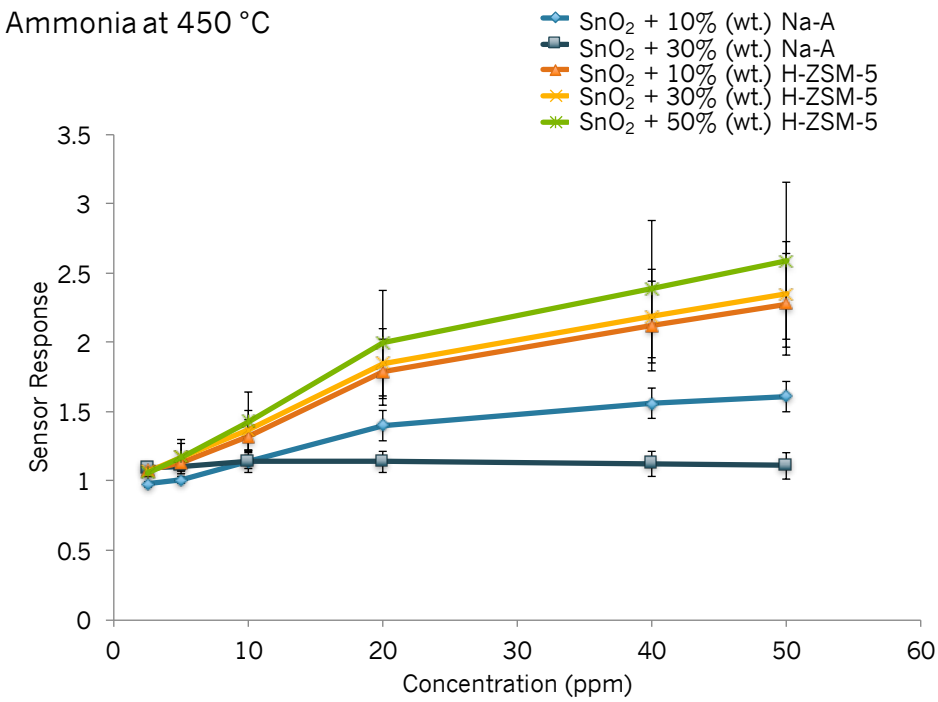

Figure 6-13 Sensor responses of SnO_2-based sensors modified by different weight percentages of zeolites Na-A and H-ZSM-5 towards ammonia gas at different concentrations. The results correspond to the average of three repeat tests.

A plot of the Cr_2O_3-based sensor responses vs. concentration towards ammonia has been presented in Fig. 6-16 below. As mentioned previously, this test was repeated twice and the results for both tests are presented together in this figure. It can be seen that 1) the response magnitudes were indeed very similar and 2) that the sensor with 10% (wt.) H-ZSM-5 provided a 10% difference in sensor response among repeat tests. However, they all showed similar patterns, some displaying a higher response magnitude with the first concentration pulse than with the second one.

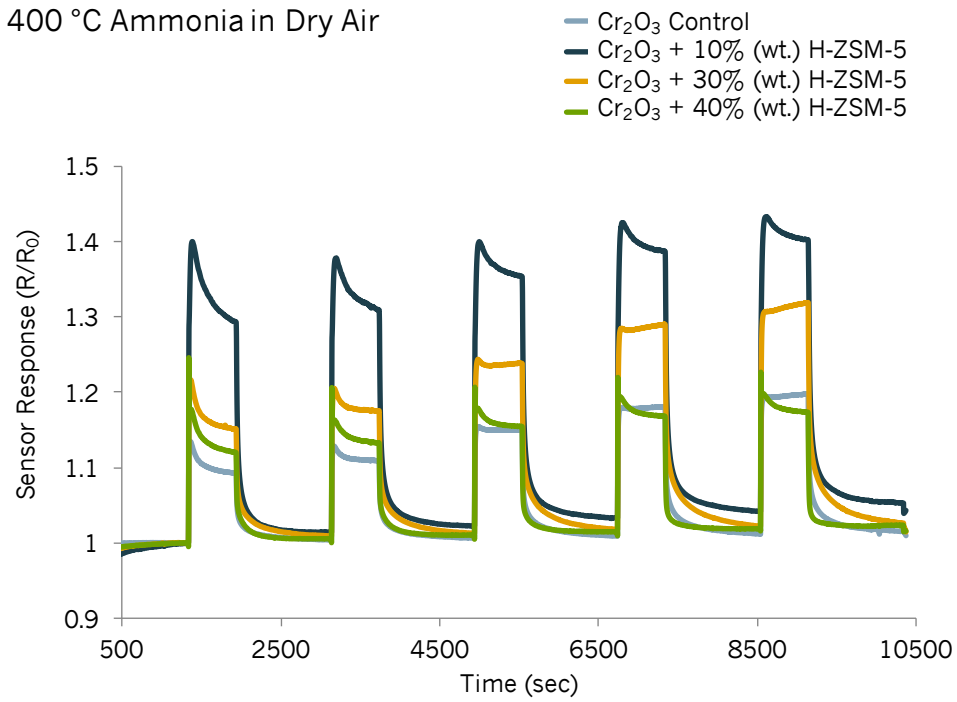

Figure 6-14 Sensor responses to different concentrations of ammonia gas of a control Cr_2O_3 sensor and to Cr_2O_3 modified sensors with different percentage weights of zeolite H-ZSM-5 at 400 °C. The concentrations correspond to 5 ppm, 10 ppm, 25 ppm, 40 ppm and 50 ppm.

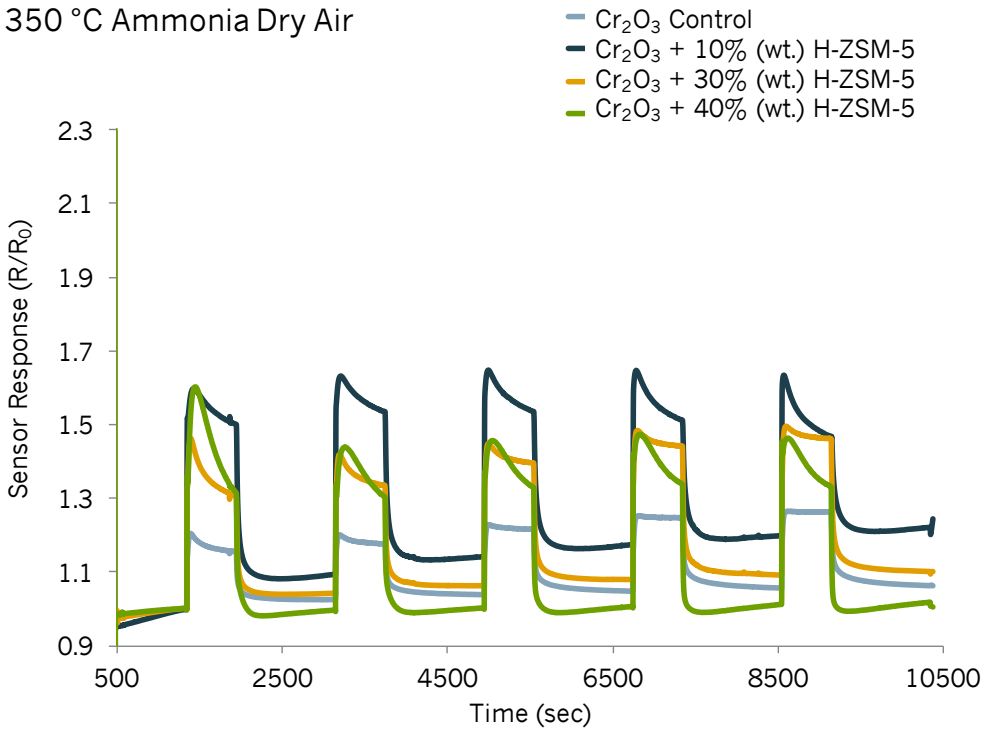

Figure 6-15 Sensor responses to different concentrations of ammonia gas of a control Cr_2O_3 sensor and to Cr_2O_3 modified sensors with different percentage weights of zeolite H-ZSM-5 at 350 °C. The concentrations correspond to 5 ppm, 10 ppm, 25 ppm, 40 ppm and 50 ppm.

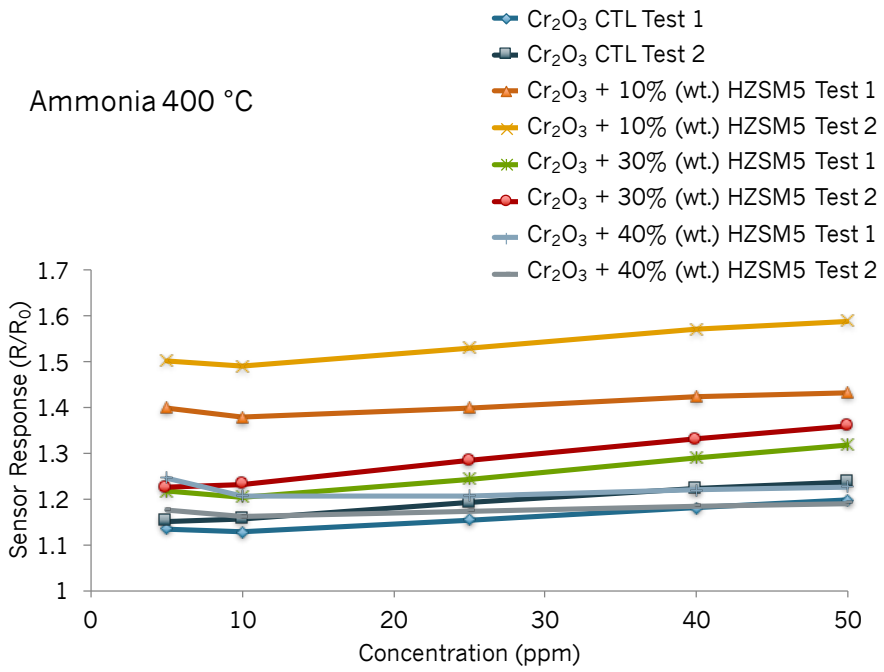

Figure 6-16 Sensor responses towards different concentrations of ammonia gas of Cr_2O_3 based sensors modified by different percentage weights of zeolite H-ZSM-5. Tests were performed at 400 °C. The results of two repeat tests have been included in the figure named as Test 1 and 2 in the legend.

The Cr_2O_3-based sensors were then exposed to 25 ppm ammonia gas in the presence of 25% RH and 50 % RH to understand sensor behaviour in the presence of humid air. The results of this have been presented in Fig. 6-17 below.

As can be observed, the response magnitudes of the sensors decreased slightly in humid air, when compared to what was attained under dry air conditions (Fig. 6-16). However, when going from an environment with 25% RH to one with 50% RH the sensor responses remained unaltered. There was also more peak tailing observed in the sensor responses in the presence of humid air, particularly with 'Cr_2O_3 + 40% (wt.) H-ZSM-5'. This could potentially be due to poorer desorption of gas occurring in the presence of humid air. Water vapour is likely to also interfere and compete for the active sites in the sensor, despite the hydrophobic character of zeolite H-ZSM-5.[22]

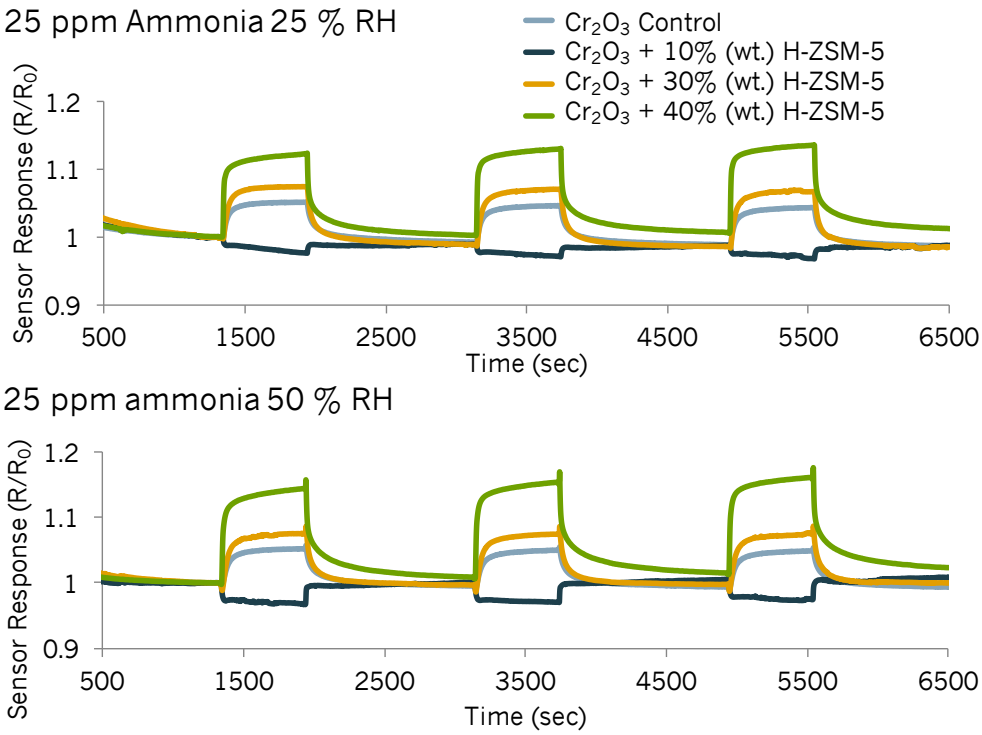

Figure 6-17 Sensor responses to 25 ppm ammonia gas under 25% RH and under 50% RH at 400 °C. The tests were performed with a control Cr_2O_3 sensor and those modified with 10% (wt.) H-ZSM-5, 30% (wt.) H-ZSM-5 and 40% (wt.) H-ZSM-5. The three pulses of gas correspond to the same concentration.

The sensor resistance in the Cr_2O_3 systems was also investigated under humid conditions (Fig. 6-18). The control Cr_2O_3 sensor did not change in baseline resistance from a dry air environment to one in 25% RH but its baseline resistance increased when in the presence of 50% RH from 6.7 KΩ to 0.8 MΩ. The increase in resistance is due to water preventing further oxygen from adsorbing on the surface of the sensor and thus resulting in a decrease of the density of charge carriers (holes). The resistance of the zeolite modified sensors changed slightly when going from a dry air ambience to one in 25% RH and then remained stable when increasing the humidity further to 50% RH. Thus, the incorporation of a hydrophobic zeolite in this instance served to minimise fluctuations seen in the otherwise unmodified sensor.

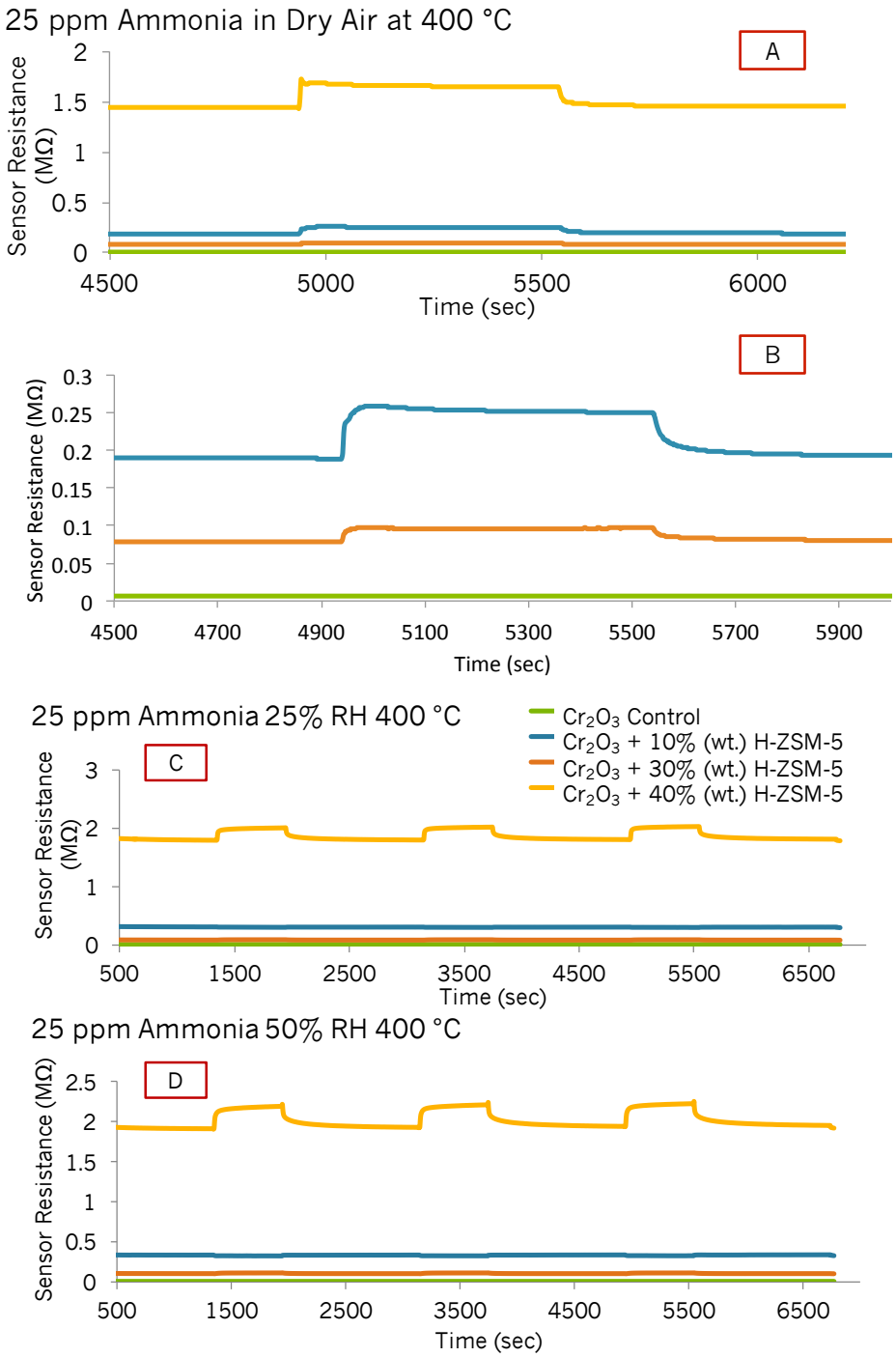

Figure 6-18 Sensor resistance change of Cr_2O_3 based sensors upon exposure to 25 ppm ammonia gas at 400 °C under different humid conditions; dry air, 25 % RH and 50 % RH.

6.2.3 Pilot Study on Amphetamine in Methanol Detection

As alluded to in the introduction of this chapter, a new tactic used by traffickers is to dissolve drugs in a legal solvent to conceal them during transit. As such, a test was carried out with amphetamine dissolved in methanol.

The test was carried out as follows: a stream of dry air was supplied to the sensors (100% of full flow at 1 L/min) and then a percentage of the total flow of air was passed

through a flask containing the target sample, which was then supplied to the sensor cell. A 1 mg/ml solution of amphetamine in methanol was placed in a small flask and 10% and 20% of the total flow of air was passed through the flask containing the solution, the vapour of which was then introduced to the sensor cell for detection. Although higher vapour concentrations were supplied to the sensor cell, the sensors capped out and the computer was not able to process the data as the voltage values were out of range. Further, the solution was smelly and the ventilation system in the lab was not considered good enough to continue doing tests with this solution due to the associated toxicity of methanol. For this reason, the test was only tried once and not all sensors that ought to have been tested were, due to lack of space in the test cell. The results obtained to date with the SnO_2-based sensors and those with two Cr_2O_3-based sensors have been provided in Figs. 6-19 and 6-20 below.

As can be seen in Fig. 6-19, the sensor responses attained when passing 10% of the full flow of air through the flask with the sample were remarkably high and, except for the most sensitive sensor 'SnO_2 + 30% (wt.) H-ZSM-5' and the control SnO_2 sensor, the responses of which were out of range for processing, the rest of the sensors saw an increase in sensor response when a higher percentage of airflow was passed through the flask.

Most sensors provided an enhanced response in relation to the control SnO_2 sensor. Further, the sensors returned to baseline and reached steady state. The SnO_2 sensor mixed with 30% (wt.) Na-A provided a sensor response that was smaller in magnitude than the control, so it could mean that it produced a reaction product to which SnO_2 was less sensitive. It is thought that the great responses attained here were due to the fact that the analyte was in liquid form, rather than trace concentrations supplied in gas form.

Ideally, it is acknowledged that a solution of just methanol without amphetamine ought to have been tested but due to the toxicity of the compound and poor ventilation in the lab it was decided not to for safety reasons. SnO_2 based sensors were exposed to trace concentrations of methanol gas to assess whether the order of the responses matched those seen here, and thus, whether the sensors were mostly responding to methanol, rather than amphetamine (Fig. 6-20). Nevertheless, the order of sensor responsiveness has been seen to change with concentration increases in previous tests. However, one can get an indication of how the sensors behaved when supplied with different concentrations of just methanol vapour. As can be observed in Figs. 6-19 and 6-20 the order of sensor response towards just methanol gas was very similar to that attained

when exposing the sensors to the amphetamine in methanol solution e.g. 30% H-ZSM-5> CTL > 30% Na-A. Slight differences may have occurred due to a higher concentration of methanol in liquid form and also due to the presence of another compound in the solution.

The polarity of methanol (polarity index 5.1)[294] would suggest a higher affinity of the molecule with a sensor that was more hydrophilic in nature, such as that admixed with zeolite Na-A, as it occurred with ethanol exposure in Chapter 3. However, the sensor responses were much improved with the sensor that contained a higher weight percentage of zeolite H-ZSM-5. It is possible that the microstructure of this sensor favoured the diffusion and interaction with methanol into the inner layers of the sensor, given its smaller kinetic diameter, in relation to other molecules such as ethanol (Fig. 6-20).

One of the most promising things of the test carried out below was that every sensor provided a very different response magnitude to the amphetamine/methanol solution and they were all very responsive as well. This is encouraging for several reasons 1) Solvent detection when sampled as a liquid may provide much-increased sensor responses, obtaining very different response patterns when using a range of modifying agents. 2) Solvent detection may be needed in the near future, for instance, in maritime ports or airports, as more controls are being put in place; it is recognised that traffickers may transport legal solvents to later manufacture drugs illegally once they have reached the end destination. 3) If such a small quantity of a solvent can provide large sensor responses it means that a small sample – extracted using a needle to minimise the potential of intoxication of the investigator handling the sample – might be possible in future with MOS devices. This is said bearing in mind that people have been intoxicated opening and coming into contact with bottles of liquid nicotine in the past, which were labelled as something else to conceal its illegal traffic. Unfortunately, at this stage it cannot be specified whether a different response pattern would have been attained if the amphetamine had not been present in the solution but it is certainly worth investigating further in future.

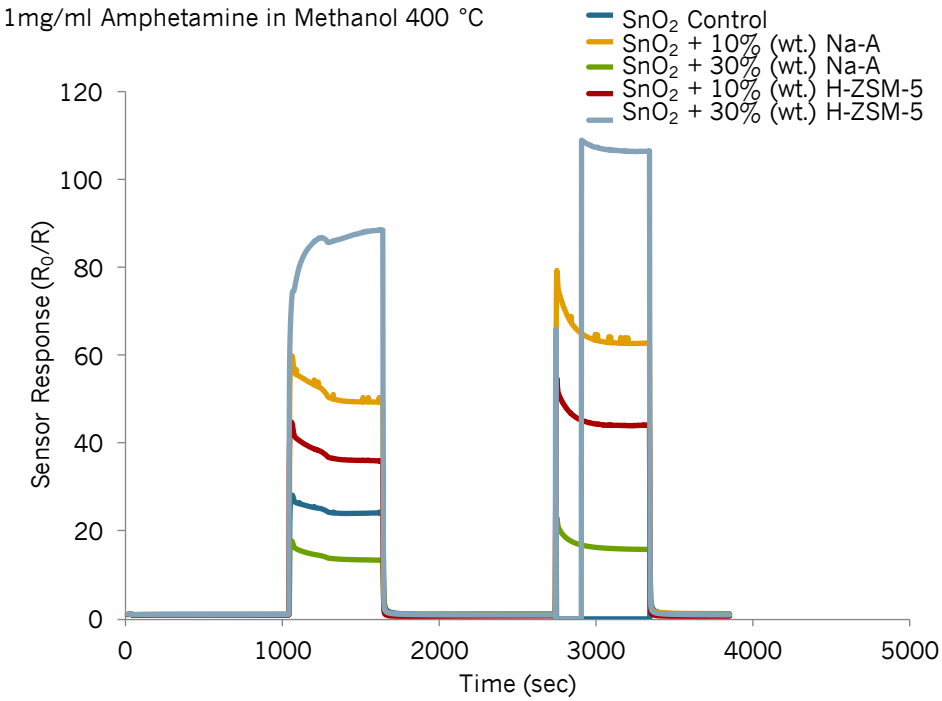

Figure 6-19 SnO_2-based sensor responses to 1mg/mL solution of amphetamine in methanol at 400 °C. The first vapour pulse was the result of passing 10% of the total flow of dry air through a flask containing the sample and the second vapour pulse, the result of passing 20% of the total flow of dry air through the flask. Two of the sensors capped out during the test and could not be processed by the program, that is why on the second vapour pulse SnO_2 control and SnO_2 + 30% (wt.) H-ZSM-5 look odd.

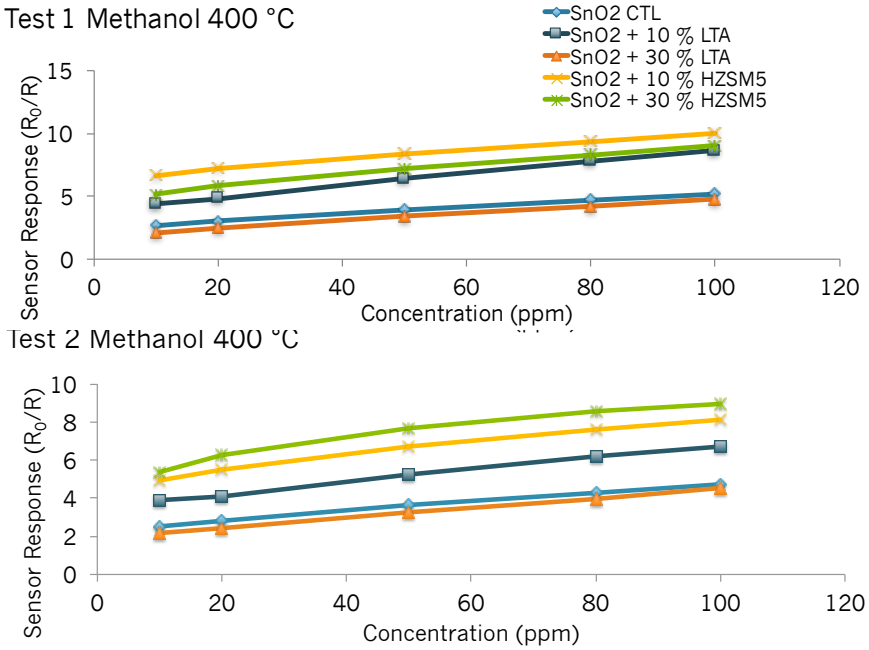

Figure 6-20 Sensor response curves upon exposure to methanol of a control SnO_2 sensor and those modified by zeolite admixture with 10% (wt.) Na-A, 30 % (wt.) Na-A, 10% (wt.) H-ZSM-5 and 30% (wt.) H-ZSM-5 at 400 °C. The results of two repeat tests have been provided for comparison purposes.

In regard to the Cr_2O_3-based sensors, it must be born in mind that in Chapter 4 it was found that the sensitivity of both the control and the Cr_2O_3 sensor modified with 10% (wt.) H-ZSM-5 decreased with methanol concentration (Fig. 4-18). When the sensors were then exposed to 100 ppm of just methanol gas, the 'Cr_2O_3 + 10% (wt.) H-ZSM-5' sensor provided a 1.65-fold enhancement in sensor response (R/R_0 = ~2) over the control sensor and, in the present study, with exposure to amphetamine in methanol it provided a 3.65-fold enhancement in sensor response over the control. The response maximum of the 10% (wt.) zeolite-modified sensor obtained reached R/R_0 = ~20 with the first gas pulse and it increased further with a higher percentage of flow passing through the flask (Fig. 6-21).

The remarkable enhancement could be due to supplying a higher concentration of methanol and higher responses being attained when bubbling a liquid, despite earlier findings that sensor sensitivity to methanol decreased with concentration increments. Alternatively, it could be due to the addition of amphetamine into the solution, which may interact well with a sensor surface containing zeolite H-ZSM-5. As mentioned previously, this is just an initial study and more tests need to be performed to understand this behaviour further. More solvents ought to be tested in a bubbler as well to see if such different response patterns are also attained.

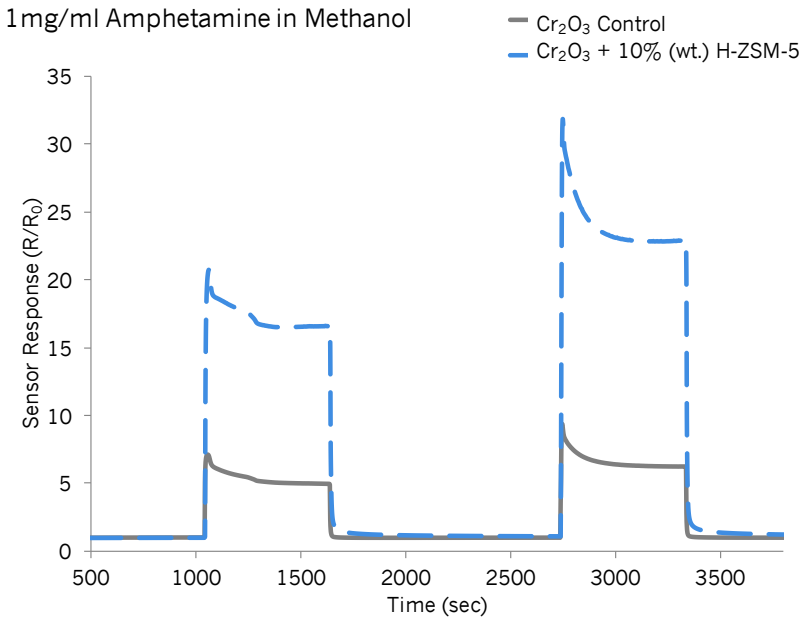

Figure 6-21 Cr_2O_3-based sensor responses to 1mg/mL solution of amphetamine in methanol at 400 °C. The first vapour pulse was the result of passing 10% of the total flow of dry air through a flask containing the sample and the second vapour pulse, the result of passing 20% of the total flow of dry air through the flask.

6.3 Support Vector Machines

Five sensors based on n-type (SnO_2) and p-type (Cr_2O_3) MOS were selected to test whether different WEKA classifiers were successful in building a model able to accurately discriminate among test gases. Five sensors were initially chosen for analysis because it would be a reasonable number of sensors for integration into a portable device. Further, the number of sensors is also in line with other sensing arrays reported in the literature.[2,27,49,167,331] The sensors chosen for analysis were 'SnO_2 + 10% (wt.) Na-A', 'SnO_2 + 10% (wt.) H-ZSM-5', 'Cr_2O_3 + 40% (wt.) H-ZSM-5, 'Cr_2O_3 + HY' and 'SnO_2 CTL' (refer to Table 2-4 and 2-5 in Chapter 2 for further information on these sensors).

These sensors were selected because they displayed selective characteristics, they also provided distinct response patterns when the response magnitudes towards some gases were similar and because variability between repeat tests was generally found to be minimal. The dataset corresponded to tests carried out at 400 °C. The input data corresponds to that attained upon sensor exposure to 9 analytes: ethanol, ethane, acetone, toluene, propane, butane, methyl benzoate, ammonia and nitrogen dioxide. Note that nitrogen dioxide was only used to compare whether the model was able to discriminate between ethane and an oxidising gas, given some sensors provided resistive responses upon exposure to ethane.

The dataset contained information regarding the maximum conductive and maximum resistive responses of each sensor (see summary Tables 8-8 and 8-9 in the Appendix) at different intervals following gas injection into the system. For instance, the response values after 5 seconds, 10 seconds, 50 seconds, 100 seconds, 200 seconds, 300 seconds, 400 seconds, 500 seconds were included initially to see how the models performed. Note that when a sensor was seen to provide high variability among repeat tests, the data was left out of the dataset.

As alluded to in section 1.4.5.2. in Chapter 1, an SVM SMO algorithm (with RBF Kernel and PolyKernel functions) was used to train the dataset. The SMO algorithm offers computational speed, using a one-against-one approach. As suggested in the literature, the one-against-one approach is suitable for practical applications aimed at solving multi-class problems with a large number of training samples, as it speeds up the decision-making process and it would therefore be useful in the future as well with further data collection.[181] Kernels are used to solve multi-class problems and whilst some groups suggest that both polynomial and RBF kernel functions provide similar classification performance,[332] other studies suggest that the performance of the

polynomial kernel is consistently better when dealing with a large number of attributes.[333,334] As alluded to in Chapter 1, the classification performance of random forests has previously been reported as comparable to that of SVMs.[184] For this reason, the classification performance of random forests was also evaluated to understand the robustness of the SVMs in accurately classifying the data into gas type.

An SMO algorithm with polynomial kernel was used to train the model using a 10-fold cross validation (CV). It was found that the cost function 'C' provided optimal classification accuracies when C = 50. The model was built in 0.11 seconds and provided a classification accuracy of 92.2%. The confusion matrix provided by the WEKA software has been presented in Table 6-4. It can be seen that 1/6 times MB was confused with NO_2, 1/10 times acetone was confused with propane and 1/5 times butane was confused with propane. Using the leave-one-out approach to test the performance of the final classifier, it was 92.2% accurate in classifying the data into gas type.

Table 6-4 Confusion matrix provided by the Weka software, using an SMO algorithm and a Polykernel function to build the model with a cost function of C = 50, providing a 94.1% accuracy in correctly classifying the data according to gas type. A five-sensor array was used for classification: 'SnO_2 + 10% (wt.) Na-A', 'SnO_2 + 10% (wt.) H-ZSM-5', 'Cr_2O_3 + 40% (wt.) H-ZSM-5, 'Cr_2O_3 + HY' and 'SnO_2 CTL'

Classified as ➔	**A**	**B**	**C**	**D**	**E**	**F**	**G**	**H**	**I**
A = Ethane	5	0	0	0	0	0	0	0	0
B = Ethanol	0	5	0	0	0	0	0	0	0
C = Nitrogen Dioxide	0	0	5	0	0	0	0	0	0
D = Ammonia	0	0	0	5	0	0	0	0	0
E = MB	0	0	1	0	5	0	0	0	0
F = Acetone	0	0	0	0	0	9	0	1	0
G = Butane	0	0	0	0	0	0	4	1	0
H = Propane	0	0	0	0	0	0	0	5	0
I = Toluene	0	0	0	0	0	0	0	0	5

When using the SMO algorithm with the RBF kernel function with $\gamma = 0.01$ and a cost function of C = 50, as in the previous case, the accuracy of the model in classifying the

data was 84.3%. As the cost function was increased to C = 250, the classification accuracy increased to 90.2%. The confusion matrix provided by the model has been presented in Table 6-5 below. Note that by increasing the cost function one must be aware of the increasing likelihood of overfitting and losing the generalisation capability of the model, particularly when using small datasets. The likelihood of overfitting could be reduced by carrying out more tests in the lab and thus including additional experimental data, which would be more representative of the gas types, into the SVM input data.

Table 6-5 Confusion matrix provided by the Weka software, using an SMO algorithm and a RBF kernel function to build the model with default values of ϒ = 0.01. A cost function of C = 250, providing a 90.2% accuracy in correctly classifying the data according to gas type. A five-sensor array was used for classification: 'SnO_2 + 10% (wt.) Na-A', 'SnO_2 + 10% (wt.) H-ZSM-5', 'Cr_2O_3 + 40% (wt.) H-ZSM-5, 'Cr_2O_3 + H-Y' and 'SnO_2 CTL'

Classified as ➔	A	B	C	D	E	F	G	H	I
A = Ethane	5	0	0	0	0	0	0	0	0
B = Ethanol	0	5	0	0	0	0	0	0	0
C = Nitrogen Dioxide	0	0	5	0	0	0	0	0	0
D = Ammonia	0	0	0	5	0	0	0	0	0
E = MB	0	0	1	0	5	0	0	0	0
F = Acetone	0	0	0	0	0	9	0	1	0
G = Butane	0	0	0	0	0	0	3	2	0
H = Propane	0	0	0	0	0	0	0	5	0
I = Toluene	0	0	0	1	0	0	0	0	4

As can be seen in Table 6-5 above, the same gases were confused as when using the Polykernel function. However, in this instance 1/5 times toluene was confused with ammonia and 2/5 times butane was confused with propane. However, similar classification accuracies were obtained with both models.

It must be noted that when classifying the data with random forests to better assess the robustness of the SMO algorithm, the classifier was 78.4% accurate in doing so (Table 6-6 below). Although the classification accuracy was lower when using this classifier, these are still very promising results; the false positive (FP) rate attained for

the drug markers of interest was zero and that of other abused substances such as toluene and butane was also zero. Ethanol and acetone had a FP rate of 0.043 and 0.098, respectively, and propane had a FP rate of 0.065. NO_2 also had a FP rate of 0.043, but it is less relevant if the array was to be used for the purposes of drug detection. Furthermore, there are sensors based on WO_3 inks that have been shown to be very selective and commercialised to identify NO_2.[23] As such, a sensor known to be selective towards NO_2 could be incorporated into the final array to potentially improve these results for practical applications.

Table 6-6 Confusion matrix provided by the Weka software using a Random Forest decision tree, providing a 78.4% accuracy in correctly classifying the data according to gas type. A five-sensor array was used for classification: 'SnO_2 + 10% (wt.) Na-A', 'SnO_2 + 10% (wt.) H-ZSM-5', 'Cr_2O_3 + 40% (wt.) H-ZSM-5, 'Cr_2O_3 + H-Y' and 'SnO_2 CTL'

Classified as ➔	A	B	C	D	E	F	G	H	I
A = Ethane	2	0	2	0	0	0	0	1	0
B = Ethanol	0	2	0	0	0	3	0	0	0
C = Nitrogen Dioxide	0	0	5	0	0	0	0	0	0
D = Ammonia	0	0	0	5	0	0	0	0	0
E = MB	0	0	0	0	6	0	0	0	0
F = Acetone	0	2	0	0	0	7	0	1	0
G = Butane	0	0	0	0	0	0	4	1	0
H = Propane	0	0	0	0	0	0	1	4	0
I = Toluene	0	0	0	0	0	0	0	0	5

It was deemed interesting to assess whether the SMO algorithm maintained the classification accuracy after 5 seconds into the gas injection. When the same parameters were used with the SVM SMO polykernel function, the model provided the same classification accuracy in discriminating between gases (92.2%). When the cost function was increased to C = 100, the classification accuracy of the model increased to 94.1%, where 1/6 times MB was confused with NO_2, 1/10 times acetone was confused with propane and 1/5 times butane was confused with propane as well.

With the SMO RBF kernel, the cost function had to be increased to C = 1500 in order to get a classification accuracy of 90.2%. The accuracy of the model was maintained

when using the leave-one-out approach, which generalises the performance of the classifier. In this instance, 1/5 times ethanol was confused acetone, 1/6 times MB was confused with NO_2, 1/10 times acetone was confused with propane and 2/3 times butane was confused with propane. As alluded to previously, increasing the value of the cost function may lead to data overfitting.

The classification accuracy of the SVM classifier was also assessed when using only four sensors. 'SnO_2 + 10% (wt.) Na-A', 'SnO_2 + 10% (wt.) H-ZSM-5', 'Cr_2O_3 + 40% (wt.) H-ZSM-5, 'Cr_2O_3 + HY', using a cost function C = 1600. The classification accuracy was 90.2%, where 2/5 times NO_2 was confused with propane, 1/10 times acetone was confused with propane and 1/5 times butane was confused with propane. The rest of the gases were classified accurately. Once again, increasing the value of the cost function may lead to overfitting.

Using the polykernel function, 94.1% classification accuracy was attained when using C = 200 (Table 6-7 below) and using the whole dataset i.e. measurements ranging between 5 seconds and 600 seconds after gas injection. The gas that was confused more was propane. Gases such as ethanol, ethane, toluene and acetone, which are markers needed in medical applications to identify diseases such as diabetes, lung cancer and alcoholism were all discriminated successfully. Other gases relevant to environmental and air-quality monitoring were also accurately classified. Those include ammonia, nitrogen dioxide, ethane and toluene. Ethanol, a common interfering gas, that needs to be accurately identified for practical reasons, was also classified correctly.

When investigating the classification accuracy of the SVM classifier after 5 seconds into the gas injection the model was also 94.1% accurate in correctly classifying the labels according to the type of gas (these results were attained with the polykernel function and C = 200).

The polykernel function generally appeared to perform better than the RBF kernel function. It must be noted, however, that the classification accuracy of the random forest was also lower (70.6%) than that of the polykernel. This indicates that the SMO model with polykernel function is perhaps not yet as robust as it ought to be for practical applications.

Table 6-7 Confusion matrix provided by the Weka software, using an SMO algorithm and a Polykernel function to build the model with a cost function of C = 200, providing a 94.1% accuracy in correctly classifying the data according to gas type using the following four sensors as an array: 'SnO_2 + 10% (wt.) Na-A', 'SnO_2 + 10% (wt.) H-ZSM-5', 'Cr_2O_3 + 40% (wt.) H-ZSM-5, 'Cr_2O_3 + H-Y'.

Classified as ➔	A	B	C	D	E	F	G	H	I
A = Ethane	5	0	0	0	0	0	0	0	0
B = Ethanol	0	5	0	0	0	0	0	0	0
C = Nitrogen Dioxide	0	0	5	0	0	0	0	0	0
D = Ammonia	0	0	0	5	0	0	0	0	0
E = MB	0	0	0	0	5	0	0	0	1
F = Acetone	0	0	0	0	0	9	0	1	0
G = Butane	0	0	0	0	0	0	4	1	0
H = Propane	0	0	0	0	0	0	0	5	0
I = Toluene	0	0	0	0	0	0	0	0	5

In general, it can be concluded that accurate results could be attained very quickly (in the order of seconds) and in a very inexpensive manner. Ultimately, this methodology could provide users with an idea of whether something needed to be investigated further with other techniques. It follows that these results are, indeed, encouraging: they support carrying out further research with zeolite-modified sensors for environmental, air-quality monitoring and for medical applications. Furthermore, they highlight the importance of advancing research in the context of illicit drug marker detection.

6.4 Summary of Results

It has been found that targeting vapours emanating from liquid samples may provide great enhancements in sensor responses. These are very promising results given that a lot of drugs that are abused, such as GBL, and solvents are liquids and a lot of other drugs are concealed or disguised in solvents as part of trafficking strategies, which have been proven to be easily and successfully detectable with MOS technology both in the literature and in this thesis.

Although it is still early days, it is considered that being able to detect methyl benzoate, a by-product of cocaine, and having attained such promising enhancements in sensor responses when compared to the control sensors, SnO_2 and Cr_2O_3, is very encouraging. As such, this line of work should be pursued further in future. Much lower concentrations of the vapours ought to be targeted, similar to those detected by sniffer dogs in the field. Although zeolite incorporation introduced huge improvements in sensor responses, it is acknowledged that they may also introduce great variability in sensor responses between repeat tests, which would be problematic in real life applications. Attaining a more homogenous microstructure using thin-film deposition methods or by triple roll milling the inks and by also reducing the particle sizes might improve the results further. It would be very interesting to incorporate metal catalysts to n-type and p-type materials to understand if the variability in sensor response would somewhat be minimised when compared to zeolite-modified sensors and whether repeatability could also be improved at lower operating temperatures.

Ammonia detection was unfortunately not as promising, as it provided very low responses with both semiconductor systems. However, it is deemed important that the sensors would thus potentially enable discrimination between two important drug groups such as cocaine and amphetamine. Introducing humidity to the Cr_2O_3 based sensors served to reduce the sensor responses further which, in a way, would work to the advantage of those using the systems in security applications if both drugs ought to be differentiated.

Detecting a solvent – methanol – which contained amphetamine was also successfully achieved and great responses were attained both with n-type and p-type systems. In Chapters 3 and 4 the sensors had previously been exposed to trace concentrations of methanol gas (up to 100 ppm) and although the sensor responses were lower in magnitude to those found when exposing the sensors to the amphetamine in methanol solution, they followed a similar order of sensor responsiveness seen with exposure to just methanol gas. This could indicate that the sensors were not sensitive to the presence of amphetamine in the solution. However, it is difficult to draw sound conclusions at this stage. Further tests ought to be performed in the future with just a methanol solution and, if possible, with real drug samples. Therefore, as of now, it cannot be concluded whether MOS sensors would be able to provide different response patterns if a drug was dissolved in a solvent. The results are promising simply because the control and movement of drug precursors and solvents is becoming more and more rigorous. It is possible that MOS technology might be useful for this sort of

application as it is inexpensive and could potentially provide reliable information as to whether solvents were being mislabelled during transit, for instance.

Classification tools were employed to understand whether different classifiers could be used to build models that would fit the input data, such that they could classify it correctly into gas type. Using an SVM classifier an accuracy of 94.1% was attained in classifying the data according to gas type with only four sensors and just five seconds into the gas injection. Whilst other classifiers such as random forests provided lower classification accuracies i.e. 70.6%, these results are still encouraging. Essentially, it was of interest to find out whether a collection of sensors could, with a certain level of accuracy, discriminate among the gases that were tested and this was achieved successfully.

MOS technology could very well improve current practices in security applications; they could indicate whether something required further investigation with alternative equipment. The results presented here reinforce the need to explore and further this line of research and have shown the potential suitability of the devices fabricated for a wide range of purposes, including environmental, air-quality, medical and security-based applications.

7. Conclusions and Future Directions

7.1 Overview of Results

This thesis set out to explore a range of zeolite-modified metal oxide semiconductor materials for the detection and discrimination of a range of analytes known to pose a risk to health, the environment, security and safety. An overview of the aims of the thesis is provided below, together with the main conclusions that can be drawn from the work carried out:

The fabrication of a wide range of semiconducting metal oxide materials modified by zeolites to investigate their capabilities as gas sensors.

Three different systems have been fabricated and studied to assess their potential capabilities as gas sensors. These were based on the modification of SnO_2, Cr_2O_3 and Fe_2O_3 metal oxide semiconductors with zeolite materials. Results on twenty-two new sensors have been presented, which included the integration of three different zeolites, namely, Na-A, H-ZSM-5 and H-Y as either admixtures with the base material or as additional film coatings over the base material.

Although SnO_2, Cr_2O_3 and Fe_2O_3 are materials the gas sensing properties of which are already established and reported in the literature, to the best of our knowledge, it is the first time that admixtures of these semiconducting materials have been investigated with the aforementioned zeolites. Although the investigation of zeolite coatings over metal oxide semiconductors is more widely reported in the literature, no reports were found on the screen-printed incorporation of H-Y coatings over SnO_2, Cr_2O_3 and Fe_2O_3 materials.

In general, the fabricated sensors were responsive to the analytes investigated. By far, the SnO_2 zeolite-modified sensors provided the most responsive results to test gases. Conversely, the zeolite-modified Fe_2O_3 modified sensors were, globally, poorly sensitive to gases, often leading to very noisy response outputs. The Cr_2O_3-based sensors modified by admixture with zeolite H-ZSM-5 generally provided very similar response patterns to gases such as acetone, ethanol and methanol. The peak shapes attained with the Cr_2O_3 sensors modified with zeolite H-ZSM-5 only provided contrasting responses upon exposure to toluene and ethane gases. However, the sensor responses were very conservative towards all test gases. Cr_2O_3 sensors modified by H-ZSM-5 displayed lower responses to gases in the presence of humid air (25% RH) but as the humidity in the system was raised to 50% RH or 75% RH, the resistance of the sensors

and response magnitudes remained mostly unaltered. Modification of the Cr_2O_3 sensor with admixtures of zeolite Na-A and overlayers of zeolite H-Y resulted in great response enhancements towards toluene, whilst the sensors were poorly responsive towards other gases such as ethanol, acetone and methanol. It must be noted that the SnO_2-based sensors were sensitive to water vapour and, although the sensors gave a p-type response towards ethane gas, in an environment of ethane and water vapour, the sensors gave responses that could be attributed to water vapour as they were conductive in nature and displayed similar peak shapes.

Incorporate zeolites as mixtures with the base metal oxide material and as coatings on top of the base material to assess any potential improvements in the sensing performance of otherwise unmodified gas-sensing materials.

It was explored how and if the sensing performance of the base materials in MOS sensors was improved by the incorporation of different zeolites. This was achieved by investigating whether zeolite incorporation meliorated aspects such as sensitivity, selectivity, response magnitudes, repeatability and response and recovery times.

The sensitivity of the SnO_2 sensors was assessed among those admixed with 10% (wt.) zeolite. The sensitivity of sensors overlaid and admixed with zeolites was seen to decrease with concentration upon exposure to ethanol gas. Whilst the SnO_2 sensors overlaid with zeolites Na-A and H-ZSM-5 provided similar sensitivities towards ethanol, the admixed sensors provided contrasting sensitivities to the gas; the sensor containing 10% (wt.) of zeolite Na-A being much more sensitive to ethanol than that containing 10% (wt.) zeolite H-ZSM-5.

SnO_2-based sensor exposure to IPA gas led to the sensitivity of the admixed zeolite sensors to increase with concentration. That of sensors overlaid with zeolites saw a linear increase in response with concentration. The sensors containing zeolite H-Y as an admixture were more sensitive to IPA than those overlaid with the zeolite. Sensors containing 10% (wt.) zeolite Na-A were the most sensitive to IPA but they provided highly variable results. Once again, sensors admixed with different zeolites provided more contrasting response magnitudes and patterns than those overlaid with zeolites.

With SnO_2-based sensor exposure to acetone, the zeolite-overlaid sensors' sensitivity decreased with concentration, whereas that of the admixed sensors increased with concentration. Further, sensors containing zeolite Na-A were more responsive to

acetone than those containing zeolites H-Y and H-ZSM-5 in the zeolite-admixed sensors.

With SnO_2-based sensor exposure to toluene, the sensitivity of the zeolite-modified sensors decreased with concentration. In both fabrication methods, the sensors containing zeolite H-ZSM-5 were more sensitive to toluene than those containing zeolites H-Y and Na-A. With the admixed sensors, there was a very pronounced difference in sensitivity between sensors containing zeolite Na-A and those containing H-ZSM-5. Sensors containing zeolite H-Y were more sensitive to toluene when admixed with the zeolite than when coated with it.

With the Cr_2O_3 sensors modified by admixture with zeolite H-ZSM-5 the sensitivities of the sensors tended to decrease with concentration upon exposure to gases. Nevertheless, sensor sensitivity was seen to increase with concentration upon exposure to toluene gas with the Cr_2O_3 sensor admixed with zeolite Na-A. Sensor sensitivity also increased with toluene concentration when Cr_2O_3 was coated with zeolite H-Y. In both instances, the sensors were also selective towards toluene, creating great improvements over the unselective character of the unmodified Cr_2O_3 sensor. To be more specific, the Cr_2O_3 sensor modified by 10% (wt.) Na-A provided a 2.6-fold increase in sensor response over the unmodified sensor and that modified by H-Y overlayers provided a 6.4-fold enhancement in sensor response over the unmodified Cr_2O_3 sensor when exposed to 50 ppm of toluene gas.

As alluded to previously, zeolite incorporation was not considered to improve the sensing performance of the Sigma Fe_2O_3-based sensors. Typically, the response magnitudes were $\sim R_0/R < 1.2$ towards most gases and they provided noisy response outputs. This could be due to an unfavourable microstructure for gas sensing in these sensors.

Different operating temperatures were evaluated to determine the optimal operating conditions for gas detection. In general, it was found that at lower temperatures i.e. 300 °C and 350 °C the sensors were considerably more responsive to gases than at 400 °C or 450 °C. However, when a sensor was particularly responsive to a gas and heated to low temperatures, the variability between repeat tests would increase as the concentration of the gas was raised. This sensor behaviour has been reported in other studies and it could be due to the production of different reaction products forming as the gas concentration increases, creating different affinities between the newly formed

products and the sensing material. This, in turn, may affect the effective desorption of the reaction products from the zeolite material and may have led to variability among repeat tests. Response and recovery times of the zeolite-modified sensors were generally faster at higher temperatures, as expected. The incorporation of zeolites into the sensing system sometimes shortened the response and recovery times but upon exposure to some gases such as toluene, they often made these times longer. Sensor drift was not noticeable with SnO_2 and Cr_2O_3 sensors but with the zeolite-modified Fe_2O_3 sensors noisy responses were attained. Exposure to toluene gas led to poor gas desorption in SnO_2 and Cr_2O_3-based sensors, particularly at lower temperatures, where peak tailing was evident.

It is recalled here that with the SnO_2 sensors different zeolite loadings were explored, as well as progressively increased screen-printed zeolite film depositions over the base material. In reference to the results carried out at 450 °C: with exposure to ethane and propane gases having one or three film depositions of a zeolite led to similar response magnitudes. With exposure to butane gas, having one film deposition of a zeolite led to enhanced sensor responses when compared to three zeolite film depositions. With ethanol exposure having three film depositions of zeolite Na-A resulted in enhanced sensor responses, over one film deposition of zeolite Na-A but the remaining sensors responded similarly to ethanol, irrespective of the number of zeolite film depositions. With IPA exposure, having one or three film depositions of zeolite Na-A did not influence the response magnitudes towards the gas, but sensors with three coatings of zeolites H-ZSM-5 and H-Y provided enhanced responses over those with one zeolite deposition. The sensor responses towards acetone were similar for all the zeolite groups, irrespective of the number of zeolite depositions. With toluene exposure, the sensor with three zeolite depositions of H-ZSM-5 and H-Y provided enhanced responses over those with one zeolite coating. Sensors with one and three depositions of zeolite Na-A responded similarly to toluene.

In regards to the admixed sensors, having 10% (wt.) zeolite Na-A in the SnO_2 sensors generally provided enhanced sensor responses to gases in relation to the sensor with 30% (wt.) Na-A. Sensors containing 10% (wt.) H-Y provided enhanced sensor responses to ethane, propane and butane gases in relation to the sensors with 30% (wt.) H-Y sensor which, in turn, provided enhanced responses to ethanol, acetone and IPA. Responses towards toluene gas were similar in the 10% (wt.) and 30% (wt.) H-Y sensors. Sensors with 10% (wt.) H-ZSM-5 and 30% (wt.) H-ZSM-5 provided comparable sensor response magnitudes to ethane and butane. Having 10% (wt.) H-ZSM-5 resulted in enhanced sensor responses to ethanol and IPA gases and having 30% (wt.) H-ZSM-5

resulted in enhanced sensor responses to propane. Toluene detection was unaffected by the weight percentage of zeolite in the sensing system.

Na-A zeolite overlayers on SnO_2 were found to be very responsive towards ethanol gas and those coated with H-ZSM-5 were very responsive towards toluene. This is thought to be the result of the hydrophilic character of zeolite Na-A, leading to increased affinity towards a polar molecule and, conversely, to the hydrophobic character of zeolite H-ZSM-5, which led to higher affinity towards less polar molecules like toluene. Admixtures were found to be more responsive to gases in relation to overlayers in the lower temperature range. Typically, the incorporation of zeolites led to response patterns and response magnitudes that differed to those provided by the control sensors. The issue of high variability was better controlled at higher operating temperatures and the peak shapes often resembled that of an ideal sensor response, indicating fast response and recovery times and that sensors reached steady state.

It was found that increasing the zeolite loading of H-ZSM-5 in the Cr_2O_3 sensors made little difference in either improving or worsening the response magnitudes to gases. However, we report that a lower zeolite loading e.g. 'Cr_2O_3 10% (wt.) H-ZSM-5', consistently provided higher response magnitudes in relation to the control sensor. Having higher concentrations of zeolite H-ZSM-5 in the structure i.e. 40% (wt.) H-ZSM-5 was thought to assist in catalysing reactions upon exposure to ethanol, acetone and methanol to CO_2 and $H_2O_{(v)}$, leading to poor response magnitudes that were worsened over those attained with the unmodified Cr_2O_3 material.

Better understanding how the incorporation of zeolites with contrasting properties influenced the detection and discrimination of different organic and inorganic gases.

It was expected that the incorporation of zeolite materials that had distinct properties, pore-sizes, channels and frameworks would introduce sufficient variability in the response magnitudes, response patterns, sensitivity and selectivity of the sensors so that a range of test gases could be accurately discriminated. This was carried out through sensor exposure to a range of relevant organic and inorganic gases of different chain length and with different functional groups. Sensors containing zeolite Na-A typically displayed an affinity towards molecules containing hydroxyl groups (ethanol and IPA). Despite other molecules having a kinetic diameter small enough for them to diffuse through the zeolite pores of Na-A, the sensors provided lower responses to gases such as ethane, propane, butane and acetone at 450 °C. Despite the similarity in molecular structure between IPA and ethanol, Na-A incorporation into SnO_2 sensors provided discrimination between both gases. This is potentially attributed to shape

selectivity, i.e. the branched structure of the IPA molecule, affected its diffusion into the sensing layer of the material in the case of the overlaid sensors. In the case of the admixtures, as more Na-A zeolite was present in the sensing system, the sensor was more responsive to IPA than to ethanol, despite the higher polarity of the ethanol molecule. This could be due to the microstructure of the material being more open as more zeolite was incorporated into the system, thus allowing the diffusion of the IPA molecule more readily. Further, it is possible that both molecules produced different reaction products to which the system was more or less sensitive. The SnO_2 sensors containing zeolite H-ZSM-5 were more responsive to molecules with a reduced polar character such as toluene. Nevertheless, both H-ZSM-5 zeolite-overlaid and admixed sensors displayed high sensitivity and responsiveness to ethanol and IPA gases, particularly in the lower temperature range.

Further, it was of interest to assess how the incorporation of zeolites into the sensing system affected the optimal operating temperature of the sensors and variability aspects among repeat tests. This was investigated with the SnO_2 based sensors and although some sensors did maintain the optimal operating temperature of the unmodified sensor, other zeolite modified sensors displayed different optimal operating temperatures, depending on the gas they were exposed to. Variability among repeat tests was reduced at higher operating temperatures. As such, using zeolites as a means to reduce the operating temperatures of sensors may not be possible unless variability among repeat tests could be better controlled at lower operating temperatures.

Putting the work in the context of illicit drug trafficking and attempting the detection of two drug markers commonly targeted by sniffer dogs.

Most of the test gases investigated in this thesis were relevant to health, environmental monitoring or to safety monitoring. However, due to a clear gap in research to investigate substances relevant to illegal drug traffic with MOS technology, it was deemed key to investigate the potential applicability of these sensors for illegal drug detection and relevant solvent detection. Thus, it was fundamental to detect solvents used in drug manufacture, solvents that are trafficked to disguise drugs and also solvents that are abused recreationally. Furthermore, it was particularly interesting to assess whether the sensors could detect two drug markers that are commonly targeted by sniffer dogs in drug trafficking interdiction efforts; methyl benzoate as a marker of cocaine and ammonia as a marker of amphetamine-based drugs.

Although, in general, the response magnitudes of the SnO_2 and Cr_2O_3 sensor systems used were quite poor upon exposure to ammonia, they provided very promising results when exposed to methyl benzoate. However, it is acknowledged that much lower concentrations of the vapour ought to be investigated in future and this study only serves as an indication that its detection is possible. At 350 °C, the response magnitudes towards MB were highest but the sensors failed to provide repeatable results. This drawback was better controlled at higher temperatures i.e. 400 °C and 450 °C but the response magnitudes decreased. The odd peak shapes of the sensors upon exposure to the vapour indicated that secondary reactions were taking place in the sensor systems. Lower concentrations of the vapour could lead to linear response outputs. What is most important finding, however, is that whilst the sensors were very responsive towards a cocaine marker, they were not as responsive to an amphetamine-type marker. These are very promising results if one needed to distinguish between both drug groups. Nevertheless, a sensor that was sensitive towards ammonia and less so towards MB ought to be found as well. CTO sensors were suggested as an option due to their reported sensitivity towards ammonia.

The selection of promising sensor candidates for analyte discrimination and subsequent testing and evaluation of the discrimination capability of the sensors with support vector machines.

Four sensors were selected to see whether they could discriminate between 9 analytes targeted during this study. The sensors were 'SnO_2 + 10% (wt.) H-ZSM-5', 'SnO_2 + 10% (wt.) Na-A', 'Cr_2O_3 + 40% (wt.) H-ZSM-5' and 'Cr_2O_3 + H-Y'. These sensors were selected because they were found to provide distinct responses to test gases and they typically provided minimal variability among repeat tests. When high variability was attained among repeat tests, the data was not used for analysis and was not included in the SVM dataset. Different classifiers were tested to understand how accurately they could classify the data into class labels i.e. gas type. The results were found to be very promising as an SMO algorithm (using a polykernel function) was able to discriminate gases with a classification accuracy of 94%. Other SMO functions based on RBF kernels provided a classification accuracy of 90%. It was found that just after 5 seconds into the gas injection, the models maintained the same level of accuracy. This highlights the promising potential of these sensors for real life applications as accurate gas discrimination could be attained very quickly. It must be noted, however, that random forests were also tested to assess the robustness of the SMO classifier. Although some variability was found in the classification accuracies of the SVM and the random forests (70.6% accuracy), they were still successful in classifying the data according to gas type.

These results are very promising, given that with only four sensors 9 key analytes relevant to different applications could be accurately classified in a very fast way. Nevertheless, it is acknowledged here that more data is needed to make the models more robust and to reduce the likelihood of overfitting. The sensors would need to be analysed against a much wider range of gases and test repeats to ensure the data was representative of what would be encountered in more realistic scenarios. It is envisioned that this inexpensive technology may provide an early-warning system that could inform as to any further analysis that may be required for a particular application.

7.2 Future Directions

Future work ought to include sensor exposure to a much wider range of gases and exposure to gas-mixtures with more in depth profiling of sensor behaviour under different environmental conditions. It follows that studies on the long-term stability of the sensors ought to be carried out to better understand how they would perform in real-life scenarios and how the sensor lifetime might affect their potential for practical applications. Although the n-type systems used in this study displayed much greater sensor responses to the test gases used, some tests suggest that p-type materials may be more stable, albeit leading to much lower sensor responses. It is something worth exploring further with sensing materials such as chromium titanium oxide (CTO), which has already been shown to be an excellent gas sensor. In order to move towards mobile systems for solvent and illegal drug detection it would be interesting to explore whether sensor performance could be maintained when miniaturised further and with the transference of the sensing materials to MEMS platforms, for instance. The use of other deposition techniques that may enable better control of the sensor microstructure ought to be explored, as well as smaller particle sizes to evaluate any further improvements in sensor performance and minimisation of variability among repeat tests in the lower temperature range. The incorporation of zeolite materials was thought to pose an important effect on variability at lower temperatures so other base material modification options could be explored further. As discussed in Chapter 1, MEMS platforms would enable further miniaturisation and lower power consumption. As such, a greater number of sensors could be used to further strengthen the classification accuracy of data classification tools such as the SVMs used in this work. A better study on the best sensor candidates should also be carried out rather than mere visual inspection. For instance, feature selection analysis might be a good means to identify an ideal set of sensors to accurately identify and discriminate among gases or vapours of interest.

Ideally, much lower concentrations of test gases should be explored with new designs so that the detection performance of sensors would be on par with other existing technologies or detection methods. Further, a sensor able to provide much higher responses towards ammonia should be fabricated and incorporated into the final sensing array to be able to discriminate and identify amphetamine-based drugs. As suggested in the literature, CTO based sensors seem like good candidates for this purpose. Sensors based on tungsten oxide could also be incorporated due to their reported selectivity towards nitrogen dioxide, which was occasionally confused in the confusion matrix provided by the WEKA classifiers.

Other markers that may assist in the detection of synthetic drugs such as substances that give the product an appealing aroma, e.g. vanillin, ought to be explored. The literature has already shown the capability of sensors to accurately identify and discern among different cannabis-based substances but further work ought to be carried out to identify other drugs such as opiates, which are said to have a distinguishing fish odour. It is hoped that given the great challenges currently faced by authorities to control and prevent drug trafficking on a global scale, MOS sensor technology advancements will assist security applications in future.

8. *Appendix*

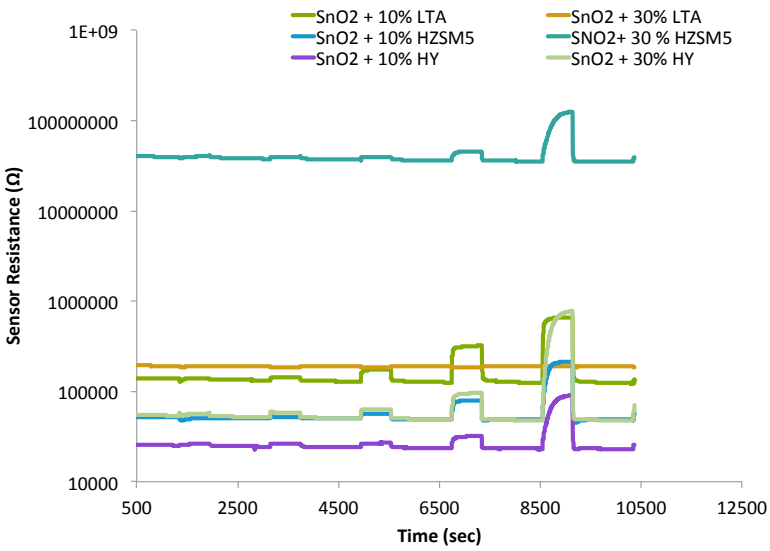

Figure 8-1 SnO_2 zeolite-admixed sensors resistance when exposed to 50 ppb, 100 ppb, 200 ppb, 500 ppb and 800 ppb of NO_2 gas at 450 °C. This test was carried out to ensure that the materials responded with an increase in resistance when exposed to an oxidising gas.

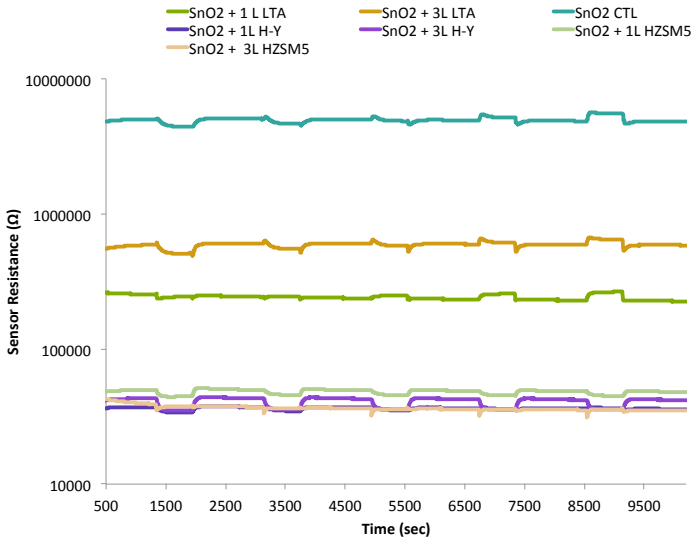

Figure 8-2 SnO_2 overlaid sensor exposure to 50 ppb, 100 ppb, 200 ppb, 500 ppb and 800 ppb of NO_2 gas at 450 °C. Test carried out to ensure resistive behaviour upon exposure to an oxidising gas.

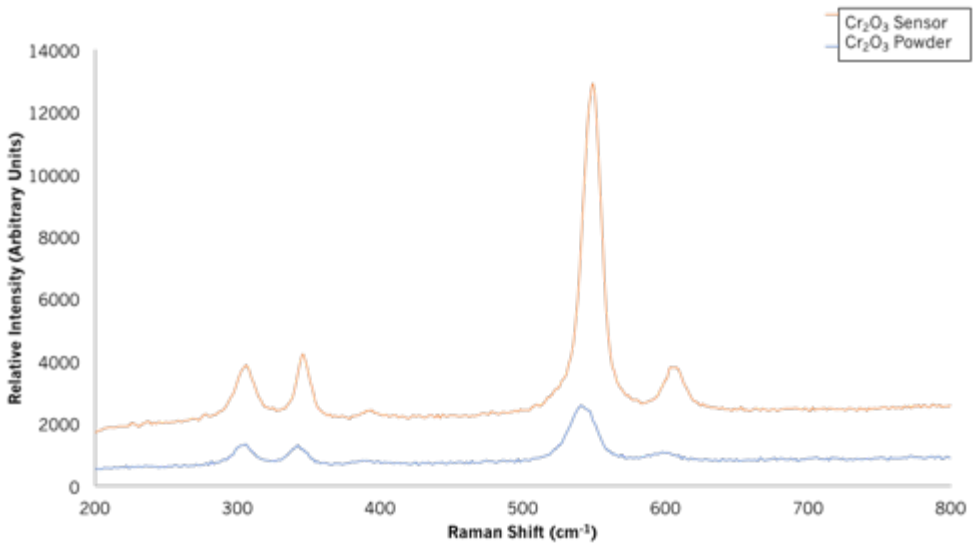

Figure 8-3 Raman spectra of Cr_2O_3 powder and Cr_2O_3 on a chip after it had been exposed to gases of interest for several months.

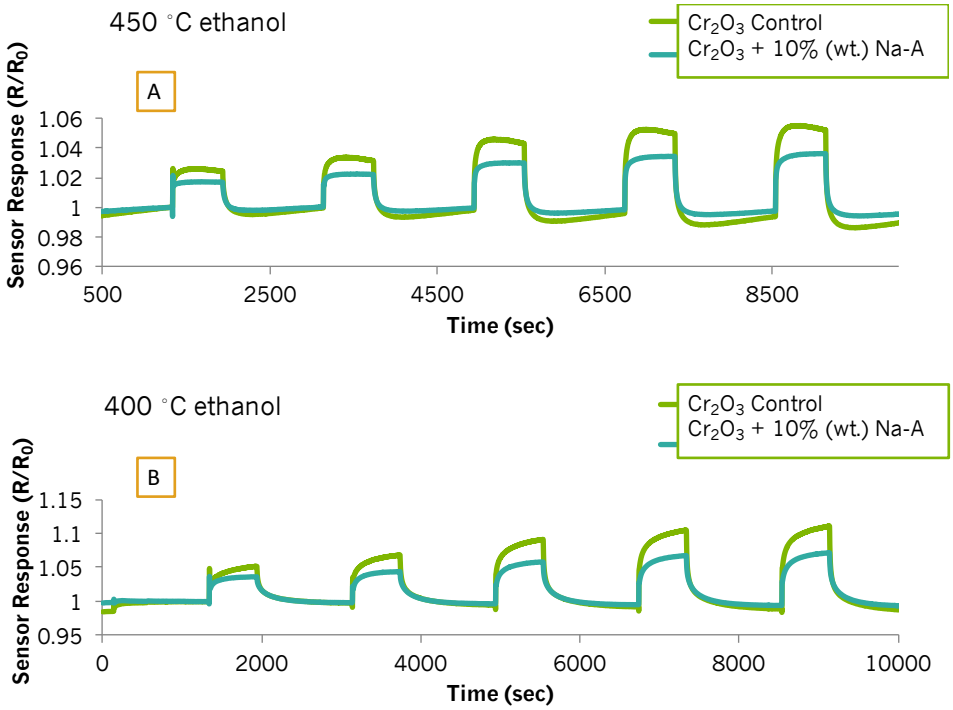

Figure 8-4 Control Cr_2O_3 and Cr_2O_3 + 10% (wt.) Na-A sensor exposure to ethanol gas at (A) 450 ˚C and (B) 400 ˚C.

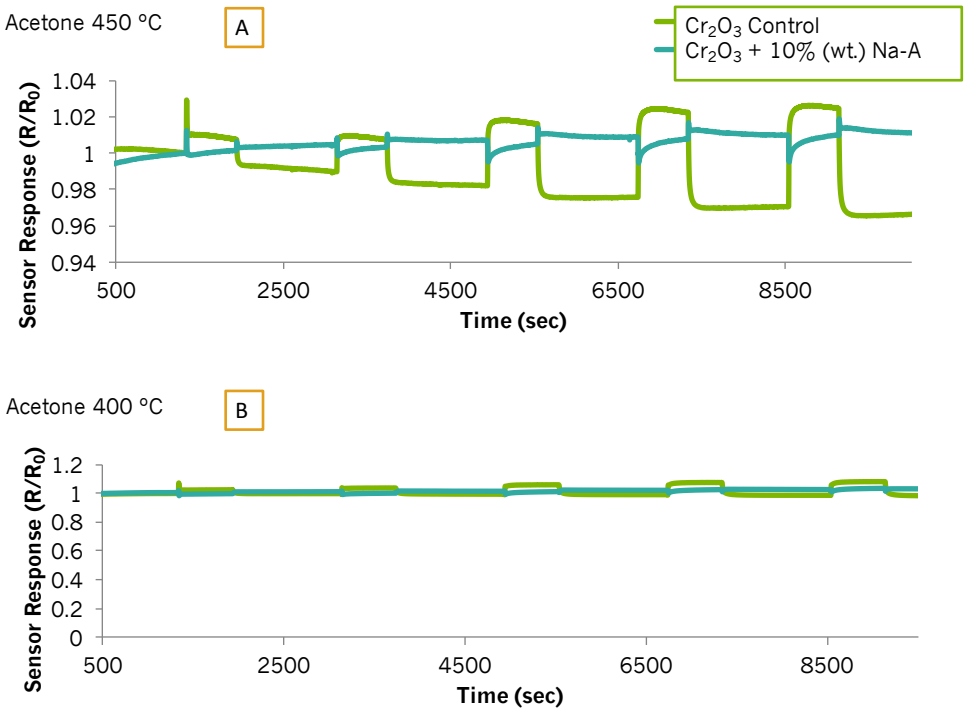

Figure 8-5 Control Cr_2O_3 and Cr_2O_3 + 10% (wt.) Na-A sensor exposure to acetone gas at (A) 450 ˚C and (B) 400 ˚C.

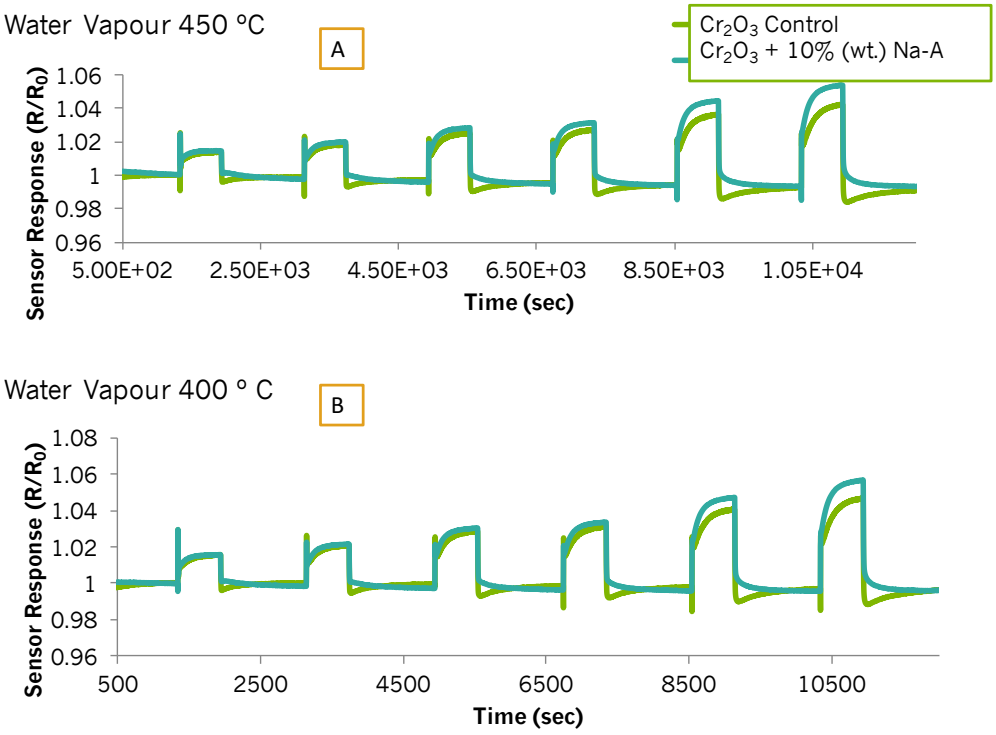

Figure 8-6 Control Cr_2O_3 and Cr_2O_3 + 10% (wt.) Na-A sensor exposure to water vapour at (A) 450 ˚C and (B) 400 ˚C.

Table 8-1 Zeolite-admixed SnO_2 sensor responses to gases at 450 ˚C. Only the percentage weight has been included with the three-letter coding for each zeolite (LTA = Na-A, MFI = H-ZSM-5 and FAU = H-Y). The standard deviation (SD) of three repeat tests (when SD <0.1 it was computed as zero). The red numbering indicates p-type behaviour. EtOH refers to ethanol, IPA to isopropyl alcohol, acet to acetone, tol to toluene, eth to ethane, prop to propane, but to butane, NO_2 to Nitrogen dioxide and CO to carbon monoxide.

Sensor Responses According to Sensor Type													
Gas Type	Conc. (ppm)	10% LTA	SD	30% LTA	SD	10% MFI	SD	30% MFI	SD	10% FAU	SD	30% FAU	SD
EtOH	5	2.4	0.3	1.1	0.0	1.1	0.0	1.1	0.0	1.2	0.0	1.1	0.0
	10	2.8	0.2	1.2	0.0	1.4	0.1	1.2	0.0	1.6	0.1	1.5	0.1
	20	3.9	0.1	1.7	0.0	1.9	0.1	1.5	0.0	2.3	0.1	2.4	0.1
	50	6.7	0.3	2.4	0.1	2.6	0.1	1.9	0.0	3.3	0.1	3.6	0.1
	80	9.0	0.4	2.9	0.1	3.1	0.2	2.2	0.1	4.1	0.2	4.5	0.2
	100	9.7	0.4	3.1	0.1	3.4	0.2	2.3	0.1	4.5	0.2	4.9	0.2
IPA	25	10.7	1.7	1.1	0.0	1.3	0.1	1.1	0.0	1.2	0.1	1.4	0.1
	50	9.7	0.7	1.2	0.0	2.2	0.1	1.7	0.1	1.9	0.1	3.3	0.3
	75	10.6	1.5	1.5	0.0	3.6	0.2	2.4	0.1	2.8	0.1	7.0	0.7
	100	15.0	2.1	1.7	0.0	5.1	0.3	3.2	0.2	3.8	0.1	10.4	0.8
	125	15.6	2.2	1.9	0.0	6.4	0.2	4.1	0.2	5.2	0.2	12.6	1.3
Acet	1	3.3	0.3	1.0	0.0	1.1	0.0	1.0	0.0	1.0	0.0	1.0	0.0
	2	3.6	0.3	1.0	0.0	1.1	0.1	1.1	0.1	1.1	0.0	1.1	0.1
	5	4.5	0.2	1.1	0.0	1.4	0.1	1.3	0.1	1.3	0.0	1.3	0.1
	8	6.5	0.5	1.2	0.0	1.7	0.1	1.7	0.1	1.6	0.1	1.8	0.2
	10	7.8	0.5	1.3	0.0	1.9	0.1	1.9	0.1	1.9	0.1	2.1	0.2
Tol	2.5	1.1	0.0	1.4	0.0	1.1	0.0	1.0	0.0	1.2	0.0	1.0	0.0
	5	1.1	0.0	1.2	0.0	1.5	0.1	1.1	0.0	1.6	0.0	1.7	0.1
	10	1.3	0.0	1.1	0.0	2.5	0.1	1.7	0.0	2.5	0.1	3.3	0.1
	25	1.5	0.1	1.2	0.0	4.3	0.3	3.1	0.0	4.0	0.1	5.4	0.3
	40	1.7	0.1	1.4	0.0	5.9	0.5	5.0	0.1	5.5	0.2	6.7	0.6
	50	1.8	0.1	1.5	0.0	6.9	0.6	6.4	0.1	6.5	0.2	7.4	0.7
Eth	10	1.1	0.0	1.1	0.0	1.0	0.0	1.0	0.0	1.0	0.0	1.2	0.0
	20	1.1	0.0	1.1	0.0	1.0	0.0	1.1	0.0	1.2	0.0	1.2	0.0
	50	1.4	0.1	1.1	0.0	1.2	0.0	1.4	0.0	1.4	0.0	1.2	0.0
	80	2.2	0.2	1.1	0.0	1.2	0.0	1.5	0.0	1.6	0.0	1.2	0.0
	100	3.3	0.3	1.1	0.0	1.3	0.0	1.6	0.0	1.8	0.2	1.2	0.0
Prop	10	1.0	0.0	1.0	0.0	1.1	0.0	1.4	0.0	1.3	0.0	1.0	0.0
	20	1.0	0.0	1.0	0.0	1.3	0.0	1.9	0.1	1.9	0.1	1.3	0.0
	50	1.1	0.0	1.1	0.0	1.6	0.0	2.6	0.1	2.5	0.1	1.7	0.1
	80	1.3	0.0	1.1	0.0	1.7	0.0	3.1	0.1	3.0	0.1	1.9	0.1
	100	1.7	0.0	1.2	0.0	1.8	0.0	3.3	0.2	3.2	0.1	2.1	0.1
But	10	1.1	0.0	1.1	0.0	1.5	0.1	1.4	0.0	1.4	0.0	1.2	0.0
	20	1.2	0.0	1.1	0.0	2.1	0.2	2.1	0.1	2.0	0.1	1.5	0.1
	50	1.2	0.1	1.1	0.0	3.0	0.3	2.9	0.1	2.8	0.1	1.9	0.1
	80	1.4	0.2	1.1	0.0	3.6	0.4	3.5	0.1	3.3	0.1	2.2	0.1
	100	1.7	0.2	1.1	0.0	4.0	0.4	3.7	0.2	3.6	0.2	2.3	0.1
NO_2	10	1.0		1.0		1.0		1.0		1.0		1.1	
	20	1.0		1.0		1.0		1.0		1.0		1.1	
	50	1.3		1.0		1.1		1.0		1.1		1.2	
	80	2.3		1.0		1.5		1.2		1.3		1.8	
	100	4.8		1.0		4.1		3.2		3.6		14.4	
CO	50	1.0		1.0		1.0		1.0		1.0		1.0	
	100	1.0		1.1		1.0		1.0		1.0		1.0	
	150	1.0		1.1		1.0		1.0		1.0		1.1	
	200	1.0		1.1		1.0		1.1		1.1		1.1	
	250	1.0		1.1		1.0		1.1		1.1		1.1	
	400	1.1		1.2		1.5		2.2		2.4		1.5	
	500	1.1		1.2		1.7		2.6		2.8		1.7	

Table 8-2 Zeolite-overlaid SnO_2 sensor responses to gases at 450 ˚C. 'L' refers to layer and the number to the depositions. The three-letter coding for each zeolite (LTA = Na-A, MFI = H-ZSM-5 and FAU = H-Y) has been used for labelling. The standard deviation (SD) of three repeat tests (when SD <0.1 it was computed as zero) has been included. The red numbering indicates p-type behaviour. EtOH refers to ethanol, IPA to isopropyl alcohol, acet to acetone, tol to toluene, eth to ethane, prop to propane, but to butane, NO_2 to Nitrogen dioxide and CO to carbon monoxide.

Sensor Responses According to Sensor Type															
Gas Type	Conc. (ppm)	SnO_2 CTL	SD	1L LTA	SD	3L LTA	SD	1L FAU	SD	3L FAU	SD	1L MFI	SD	3L MFI	SD
EtOH	5	1.3	0.0	2.0	0.1	1.3	0.1	1.1	0.0	1.1	0.0	1.2	0.0	1.6	0.0
	10	2.0	0.1	2.1	0.0	3.5	0.4	1.3	0.0	1.4	0.0	1.5	0.0	1.7	0.0
	20	3.0	0.1	2.6	0.1	7.9	1.3	1.6	0.0	1.8	0.0	2.1	0.0	2.5	0.1
	50	4.2	0.1	4.2	0.1	15.5	2.9	2.1	0.0	2.2	0.0	3.2	0.2	3.7	0.1
	80	4.9	0.1	5.7	0.2	21.6	4.2	2.3	0.0	2.6	0.0	4.4	0.3	4.7	0.2
	100	5.3	0.1	6.2	0.2	24.9	5.0	2.4	0.0	2.8	0.1	4.9	0.4	5.1	0.2
IPA	25	1.5	0.0	3.4	0.1	1.4	0.0	1.1	0.0	1.2	0.0	1.2	0.0	2.7	0.0
	50	3.1	0.1	3.9	0.0	3.4	0.1	1.5	0.0	2.0	0.0	2.3	0.0	3.2	0.0
	75	4.1	0.1	4.7	0.1	5.0	0.1	1.8	0.0	2.7	0.0	3.9	0.0	5.6	0.2
	100	5.3	0.1	6.2	0.2	6.7	0.2	2.1	0.0	4.0	0.0	6.0	0.1	8.7	0.2
	125	6.2	0.1	7.5	0.2	8.1	0.2	2.4	0.0	4.9	0.0	7.5	0.2	11.2	0.3
Acet	0.5	1.1	0.0	1.1	0.0	1.1	0.0	1.0	0.0	1.2	0.1	1.1	0.1	1.1	0.0
	1	1.3	0.0	1.2	0.0	1.1	0.0	1.1	0.0	1.2	0.0	1.1	0.0	1.1	0.0
	2	1.6	0.0	1.4	0.1	1.2	0.0	1.1	0.0	1.3	0.0	1.2	0.0	1.2	0.0
	5	1.9	0.0	1.6	0.1	1.4	0.0	1.2	0.0	1.4	0.0	1.3	0.0	1.3	0.0
	8	2.2	0.0	1.8	0.1	1.5	0.0	1.1	0.0	1.4	0.0	1.3	0.0	1.3	0.0
	10	2.3	0.0	1.8	0.1	1.6	0.0	1.1	0.0	1.4	0.0	1.3	0.0	1.3	0.0
Tol	2.5	1.1	0.0	1.5	0.1	1.1	0.0	1.1	0.0	1.2	0.0	1.3	0.1	1.3	0.1
	5	1.4	0.0	1.6	0.1	1.4	0.0	1.2	0.0	1.4	0.0	1.7	0.1	1.5	0.0
	10	1.9	0.1	2.3	0.0	2.2	0.1	1.5	0.0	1.8	0.0	2.6	0.1	2.7	0.2
	25	2.8	0.1	3.5	0.1	3.2	0.1	1.8	0.0	2.3	0.0	4.6	0.1	6.5	0.1
	40	3.4	0.1	4.4	0.1	4.0	0.2	2.0	0.1	2.8	0.1	6.4	0.2	11.2	0.7
	50	3.8	0.2	4.9	0.1	4.4	0.2	2.1	0.0	3.1	0.0	7.5	0.4	14.6	1.3
Eth	5	1.1	0.0	1.0	0.0	1.1	0.0	1.1	0.0	1.2	0.0	1.2	0.1	1.5	0.5
	10	1.2	0.0	1.0	0.0	1.1	0.0	1.4	0.0	1.4	0.0	1.4	0.0	1.5	0.2
	20	1.3	0.0	1.0	0.0	1.1	0.0	1.7	0.0	1.6	0.0	1.8	0.0	1.7	0.0
	50	1.4	0.0	1.0	0.0	1.1	0.0	2.1	0.0	2.1	0.1	2.3	0.0	2.1	0.1
	80	1.5	0.0	1.0	0.1	1.2	0.0	2.3	0.0	2.3	0.0	2.7	0.0	2.4	0.1
	100	1.5	0.0	1.1	0.0	1.3	0.0	2.4	0.0	2.5	0.0	2.9	0.0	2.6	0.1
Prop	10	1.2	0.0	1.1	0.0	1.2	0.1	1.5	0.0	1.5	0.0	1.5	0.0	1.4	0.0
	20	1.3	0.0	1.1	0.0	1.1	0.0	1.8	0.0	1.9	0.1	2.0	0.1	1.9	0.1
	50	1.5	0.0	1.3	0.0	1.1	0.0	2.3	0.0	2.4	0.1	2.7	0.2	2.6	0.1
	80	1.6	0.0	1.4	0.0	1.1	0.0	2.6	0.1	2.8	0.1	3.2	0.2	3.1	0.1
	100	1.7	0.0	1.4	0.0	1.1	0.0	2.8	0.0	3.1	0.1	3.5	0.2	3.4	0.0
But	5	1.1	0.1	1.2	0.0	1.1	0.0	1.2	0.1	1.2	0.1	1.2	0.1	1.8	0.1
	10	1.4	0.1	1.2	0.0	1.1	0.0	1.6	0.0	1.7	0.1	1.8	0.1	2.0	0.2
	20	1.7	0.1	1.4	0.1	1.3	0.1	2.0	0.1	2.4	0.2	2.5	0.2	2.7	0.3
	50	2.1	0.1	1.7	0.1	1.4	0.1	2.6	0.1	3.3	0.2	3.5	0.3	3.8	0.5
	80	2.3	0.1	1.9	0.1	1.5	0.1	3.0	0.1	3.8	0.2	4.3	0.3	4.7	0.6
	100	2.4	0.1	2.0	0.1	1.5	0.1	3.2	0.1	4.2	0.2	4.7	0.4	5.2	0.6
CO	50	1.0		1.0		1.0		1.0		1.0		1.1		1.0	
	100	1.0		1.0		1.0		1.0		1.0		1.1		1.0	
	150	1.0		1.0		1.0		1.0		1.0		1.1		0.9	
	200	1.0		1.0		1.0		1.0		1.0		1.1		0.9	
	250	0.9		1.0		1.0		1.0		1.0		1.1		1.0	
	400	1.2		2.1		2.7		2.9		3.4		1.0		2.5	
	500	1.3		2.5		3.3		3.7		4.3		1.1		3.1	
NO_2	10	1.0		1.0		1.0		1.0		1.0		1.0		1.0	
	20	1.0		1.0		1.1		1.0		1.0		1.0		1.0	
	50	1.1		1.0		1.1		1.0		1.0		1.0		0.9	
	80	1.1		1.0		1.1		1.0		1.0		1.0		0.9	
	100	1.1		1.1		1.1		1.0		1.0		1.0		0.9	

Table 8-3 Admixed SnO_2 sensor responses to a range of gases at 400 ˚C. Only the percentage weight has been included with the three-letter coding for each zeolite (LTA = Na-A, MFI = H-ZSM-5 and FAU = H-Y) type. The standard deviation (SD) of three repeat tests (when SD <0.1 computed as zero) has been included. The red numbering indicates p-type behaviour. EtOH refers to ethanol, IPA to isopropyl alcohol, acet to acetone, tol to toluene, eth to ethane, prop to propane, but to butane.

Sensor Responses According to Sensor Type													
Gas Type	Conc. (ppm)	10% LTA	SD	30% LTA	SD	10% MFI	SD	30 % MFI	SD	10% FAU	SD	30% FAU	SD
EtOH	5	2.7	0.2	1.2	0.0	1.2	0.1	1.1	0.0	1.2	0.1	1.1	0.0
	10	3.1	0.0	1.6	0.1	1.6	0.1	1.5	0.1	1.8	0.1	1.5	0.1
	20	4.6	0.2	2.8	0.2	2.4	0.2	2.2	0.2	2.4	0.2	2.4	0.1
	50	9.0	0.4	4.4	0.3	3.9	0.4	3.4	0.3	3.5	0.3	3.8	0.2
	80	13.6	0.7	5.7	0.3	5.1	0.6	4.3	0.4	4.3	0.3	4.9	0.3
	100	15.3	0.7	6.5	0.4	5.8	0.7	4.8	0.5	4.7	0.4	5.6	0.4
IPA	25	28.6	7.3	2.1	0.0	1.8	0.2	1.5	0.1	1.4	0.1	2.2	0.2
	50	32.2	9.6	3.4	0.6	4.2	0.3	3.4	0.3	3.6	0.3	9.9	0.8
	75	39.8	11.3	6.1	0.4	8.1	0.7	9.9	1.4	11.2	0.2	15.4	0.8
	100	51.8	14.6	9.1	0.1	13.0	1.2	18.7	0.9	17.3	0.9	19.5	1.0
	125	68.4	18.7	11.9	0.3	17.7	1.5	25.0	1.2	21.4	1.4	22.2	1.1
Acet	1	2.3	1.0	1.0	0.0	1.0	0.0	1.0	0.0	1.0	0.0	1.0	0.0
	2	3.0	0.4	1.2	0.0	1.1	0.1	1.1	0.0	1.1	0.0	1.1	0.1
	5	4.1	0.0	1.5	0.0	1.4	0.1	1.4	0.1	1.4	0.1	1.5	0.1
	8	6.2	0.1	2.0	0.0	1.8	0.2	1.8	0.1	1.7	0.1	2.3	0.1
	10	7.7	0.1	2.3	0.0	2.0	0.2	2.1	0.1	2.0	0.1	3.2	0.2
Tol	2.5	1.3	0.1	1.0	0.0	1.2	0.2	1.1	0.1	1.2	0.1	1.2	0.1
	5	1.3	0.0	1.0	0.0	2.0	0.2	1.7	0.2	1.9	0.1	1.9	0.1
	10	1.3	0.0	1.0	0.0	4.2	0.3	4.8	0.6	4.2	0.2	3.7	0.2
	25	1.5	0.1	1.2	0.1	8.4	0.5	11.3	1.1	7.6	0.4	5.8	0.5
	40	1.5	0.1	1.4	0.1	11.2	0.7	16.0	1.3	9.7	0.7	7.3	0.8
	50	1.4	0.1	1.4	0.2	12.6	0.8	18.9	1.5	11.0	0.9	8.3	1.1
Eth	10	1.1	0.0	1.3	0.0	1.0	0.0	1.1	0.0	1.0	0.0	1.2	0.1
	20	1.2	0.0	1.3	0.0	1.1	0.0	1.1	0.0	1.0	0.0	1.3	0.1
	50	1.7	0.1	1.4	0.0	1.2	0.1	1.0	0.0	1.0	0.0	1.6	0.0
	80	3.3	0.1	1.4	0.0	1.3	0.1	1.0	0.1	1.0	0.1	2.1	0.0
	100	8.9	0.5	1.5	0.0	1.5	0.1	1.1	0.1	1.1	0.1	2.6	0.0
Prop	10	1.0	0.0	1.0	0.0	1.1	0.1	1.2	0.0	1.2	0.0	1.0	0.1
	20	1.0	0.0	1.2	0.0	1.1	0.1	1.6	0.0	1.4	0.0	1.1	0.0
	50	1.2	0.0	1.4	0.0	1.1	0.1	2.1	0.0	1.8	0.0	1.2	0.0
	80	1.4	0.0	1.5	0.0	1.1	0.0	2.5	0.0	2.1	0.0	1.3	0.0
	100	2.0	0.0	1.6	0.0	1.1	0.0	2.7	0.0	2.2	0.0	1.3	0.0
But	10	1.1	0.0	1.3	0.0	1.2	0.0	1.3	0.0	1.3	0.0	1.2	0.1
	20	1.1	0.0	1.2	0.0	1.4	0.1	1.7	0.1	1.6	0.1	1.1	0.0
	50	1.4	0.0	1.2	0.0	1.7	0.1	2.2	0.1	2.0	0.1	1.1	0.0
	80	2.1	0.1	1.2	0.0	1.9	0.2	2.5	0.1	2.3	0.2	1.1	0.0
	100	3.6	0.3	1.2	0.0	2.0	0.2	2.7	0.1	2.6	0.3	1.2	0.0

Table 8-4 Zeolite-overlaid SnO_2 sensor responses to a range of gases at 400 ˚C. 'L' refers to layer and the number to the depositions. The three-letter coding for each zeolite (LTA = Na-A, MFI = H-ZSM-5 and FAU = H-Y) has been used for labelling. The standard deviation (SD) of three repeat tests (when SD <0.1 it was computed as zero) has been included. The red numbering indicates p-type behaviour. IPA refers to isopropyl alcohol, acet to acetone, tol to toluene, eth to ethane, prop to propane, but to butane.

Sensor Response According to Sensor Type															
Gas Type	Conc. (ppm)	SnO_2 CTL	SD	1L LTA	SD	3L LTA	SD	1L FAU	SD	3L FAU	SD	1L MFI	SD	3L MFI	SD
IPA	25	1.7	0.1	4.0	0.4	1.4	0.0	1.2	0.1	1.2	0.0	1.3	0.1	2.9	0.4
	50	4.2	0.3	4.7	0.1	3.5	0.2	1.9	0.0	2.6	0.2	3.3	0.2	3.9	0.4
	75	5.9	0.5	6.3	0.4	5.3	0.4	2.6	0.0	3.8	0.3	5.2	0.4	8.7	0.8
	100	7.7	0.6	9.3	0.4	7.4	0.5	3.7	0.1	5.2	0.4	7.5	0.6	15.6	1.1
	125	9.1	0.7	12.0	0.4	9.4	0.6	4.8	0.2	6.4	0.4	9.7	0.8	21.6	1.1
Acet	0.5	1.2	0.0	1.2	0.1	1.2	0.0	1.1	0.0	1.1	0.0	1.1	0.0	1.1	0.1
	1	1.3	0.0	1.2	0.0	1.2	0.0	1.1	0.0	1.2	0.1	1.1	0.0	1.0	0.0
	2	1.7	0.1	1.4	0.0	1.4	0.0	1.2	0.0	1.3	0.1	1.3	0.1	1.2	0.1
	5	2.1	0.1	1.7	0.0	1.7	0.0	1.3	0.0	1.5	0.1	1.5	0.1	1.5	0.1
	8	2.5	0.1	1.9	0.0	1.8	0.1	1.3	0.0	1.6	0.1	1.7	0.1	1.6	0.1
	10	2.6	0.1	2.0	0.0	1.9	0.1	1.3	0.0	1.7	0.1	1.8	0.1	1.6	0.0
Tol	5	1.2	0.0	1.6	0.1	1.1	0.0	1.1	0.0	1.1	0.0	1.1	0.0	1.5	0.1
	10	1.7	0.0	1.6	0.1	1.4	0.0	1.4	0.0	1.5	0.0	2.0	0.1	1.9	0.1
	20	2.7	0.1	2.4	0.1	1.9	0.1	1.9	0.0	2.4	0.0	4.2	0.3	5.2	0.2
	50	4.3	0.2	3.7	0.2	2.5	0.1	2.8	0.1	3.9	0.1	8.4	0.4	11.7	0.4
	80	5.6	0.2	4.6	0.2	3.0	0.2	3.7	0.1	5.1	0.1	11.7	0.4	16.4	0.7
	100	6.4	0.2	5.2	0.2	3.3	0.2	4.2	0.1	5.8	0.0	13.4	0.4	19.1	0.9
Eh	5	1.2	0.0	1.0	0.0	1.0	0.0	1.1	0.0	1.1	0.0	1.1	0.0	1.0	0.0
	10	1.2	0.0	1.0	0.0	1.0	0.0	1.2	0.1	1.1	0.0	1.1	0.0	1.0	0.0
	20	1.2	0.1	1.0	0.0	1.0	0.0	1.4	0.1	1.1	0.0	1.1	0.1	1.0	0.0
	50	1.2	0.1	1.0	0.0	1.1	0.0	1.7	0.1	1.1	0.0	1.2	0.1	1.1	0.0
	80	1.2	0.1	1.2	0.0	1.2	0.0	2.0	0.1	1.2	0.1	1.3	0.1	1.1	0.0
	100	1.1	0.1	1.4	0.0	1.4	0.0	2.1	0.1	1.2	0.1	1.4	0.1	1.2	0.0
Prop	10	1.1	0.0	1.1	0.1	1.0	0.0	1.5	0.1	1.3	0.1	1.2	0.1	1.1	0.1
	20	1.2	0.0	1.1	0.0	1.1	0.0	1.9	0.2	1.4	0.1	1.5	0.2	1.1	0.1
	50	1.2	0.0	1.2	0.0	1.1	0.0	2.5	0.2	1.7	0.2	1.9	0.3	1.3	0.2
	80	1.2	0.0	1.3	0.0	1.2	0.1	2.9	0.2	1.9	0.2	2.3	0.4	1.4	0.2
	100	1.1	0.0	1.3	0.0	1.5	0.1	3.2	0.2	2.0	0.2	2.5	0.4	1.4	0.2
But	5	1.1	0.0	1.2	0.0	1.1	0.0	1.1	0.0	1.1	0.0	1.1	0.0	1.2	0.0
	10	1.2	0.0	1.2	0.0	1.1	0.0	1.6	0.1	1.4	0.1	1.4	0.2	1.2	0.1
	20	1.4	0.1	1.3	0.0	1.1	0.1	2.3	0.2	1.8	0.2	2.0	0.3	1.4	0.2
	50	1.5	0.1	1.5	0.0	1.1	0.1	3.2	0.2	2.3	0.2	2.8	0.4	1.9	0.2
	80	1.6	0.1	1.6	0.1	1.0	0.1	3.8	0.3	2.7	0.3	3.4	0.5	2.2	0.3
	100	1.6	0.1	1.6	0.0	1.0	0.0	4.1	0.3	2.9	0.3	3.7	0.6	2.3	0.3

Table 8-5 Admixed Cr_2O_3 sensor responses to a range of gases at 400 ˚C. CTL refers to Control. Abbreviations correspond to: Tol = toluene, Eth = ethanol, Meth = methanol, Acet = acetone, Ethane.

		Sensor Responses According to Sensor Type				
Gas Type	Conc. (ppm)	Cr_2O_3 CTL	Cr_2O_3 + 10% (wt.) H-ZSM-5	Cr_2O_3 20% (wt.) H-ZSM-5	Cr_2O_3 + 30% (wt.) H-ZSM-5	Cr_2O_3 + 40% (wt.) H-ZSM-5
Tol	5	1.1	1.6	1.2	1.3	1.3
	10	1.1	1.8	1.3	1.4	1.4
	25	1.2	2.0	1.4	1.6	1.5
	40	1.2	2.1	1.5	1.7	1.5
	50	1.2	2.2	1.6	1.8	1.6
Eth	10	1.2	1.8	1.1	1.3	1.1
	20	1.2	2.1	1.1	1.5	1.2
	50	1.3	2.6	1.2	1.7	1.2
	80	1.3	3.1	1.2	1.8	1.2
	100	1.4	3.3	1.2	1.9	1.2
Meth	10	1.1	1.6	1.0	1.3	1.1
	20	1.2	1.8	1.1	1.4	1.1
	50	1.3	2.0	1.1	1.5	1.1
	80	1.3	2.1	1.1	1.6	1.1
	100	1.3	2.2	1.1	1.7	1.1
Acet	1	1.2	1.7	1.2	1.3	1.1
	2	1.3	1.9	1.5	1.5	1.2
	5	1.3	2.4	1.6	1.6	1.2
	8	1.4	2.8	1.9	1.7	1.2
	10	1.4	3.0	2.2	1.8	1.2
Ethane	10	1.1	1.3	1.0	1.1	1.1
	20	1.1	1.3	1.1	1.1	1.1
	50	1.1	1.2	1.1	1.2	1.1
	80	1.0	1.2	1.1	1.1	1.1
	100	1.0	1.1	1.1	1.1	1.1

Table 8-6 Sensor responses of a Cr_2O_3 sensor and a Cr_2O_3 sensor modified by admixture with 10% (wt.) zeolite Na-A upon exposure to toluene at 350 ˚C.

		Sensor Type According to Sensor Type	
Gas Type	Conc. (ppm)	Cr_2O_3 CTL	Cr_2O_3 + 10% (wt.) Na-A
Toluene	5 ppm	1.1	1.1
	10 ppm	1.1	1.2
	25 ppm	1.3	1.5
	40 ppm	1.5	2.7
	50 ppm	1.6	4.2

Table 8-7 Sensor responses of Cr_2O_3 sensor overlaid with zeolite H-Y to a range of gases at 400 ˚C.

Gas Type	Conc. (ppm)	Cr_2O_3 CTL	Cr_2O_3 + H-Y layers	Gas Type	Conc. (ppm)	Cr_2O_3 CTL	Cr_2O_3 + H-Y layers
Toluene	5 ppm	1.1	1.4	Acetone	10 ppm	1.2	1.2
	10 ppm	1.1	1.5		20 ppm	1.3	1.3
	25 ppm	1.2	2.4		50 ppm	1.3	1.6
	40 ppm	1.2	4.8		80 ppm	1.4	2.0
	50 ppm	1.2	6.9		100 ppm	1.4	2.3
Ethanol	10 ppm	1.2	1.2	Ethane	10 ppm	1.1	1.1
	20 ppm	1.2	1.3		20 ppm	1.1	1.1
	50 ppm	1.3	1.6		50 ppm	1.1	1.1
	80 ppm	1.3	2.1		80 ppm	1.0	1.1
	100 ppm	1.4	2.5		100 ppm	1.0	1.1
Methanol	10 ppm	1.1	1.1				
	20 ppm	1.2	1.2				
	50 ppm	1.3	1.3				
	80 ppm	1.3	1.6				
	100 ppm	1.3	1.9				

Table 8-8 Summary of maximum resistive (R/R_0) and maximum conductive (R_0/R) responses attained with 'SnO_2 + 10% (wt.) H-ZSM-5' and 'SnO_2 +10%(wt.) Na-A' selected to carry out SVM classification tests upon exposure to nine test gases. Note that additional information was inputted for SVM analysis such as the value of the responses after 5 secs, 10 secs, 50 secs, 100 secs, 200 secs, 300 secs, 400 secs and 500 secs. Tests that led to high variability between tests were also left out of the input dataset for SVM analysis.

Class	Conc.	R.R.SnO_2.10ZSM5	C.R.SnO_2.10ZSM5	R.R.SnO_2.10Na-A	MCoSnO_2.10Na-A
Toluene	5	0.5	2.0	0.8	1.3
Toluene	10	0.2	4.0	0.8	1.3
Toluene	25	0.1	8.0	0.7	1.4
Toluene	40	0.1	11.0	0.7	1.3
Toluene	50	0.1	12.3	0.8	1.3
NO_2	0.05	1.1	0.9	1.0	1.0
NO_2	0.1	1.2	0.9	1.2	0.9
NO_2	0.2	1.3	0.8	1.6	0.6
NO_2	0.5	2.0	0.5	3.3	0.3
NO_2	0.8	8.1	0.1	7.3	0.1
Butane	10	0.9	1.1	1.1	0.9
Butane	20	0.7	1.4	1.1	0.9
Butane	50	0.6	1.7	1.4	0.7
Butane	80	0.5	2.0	2.0	0.5
Butane	100	0.5	2.1	3.3	0.3
Ethanol	10	0.6	1.6	0.3	3.1
Ethanol	20	0.4	2.4	0.2	4.7
Ethanol	50	0.3	4.0	0.1	9.3
Ethanol	80	0.2	5.3	0.1	14.1
Ethanol	100	0.2	6.0	0.1	16.0
Ethane	10	1.0	1.0	1.1	0.9
Ethane	20	1.0	1.0	1.2	0.8
Ethane	50	1.2	0.9	1.7	0.6
Ethane	80	1.3	0.8	3.3	0.3
Ethane	100	1.5	0.7	9.3	0.1
Propane	10	1.0	1.0	1.0	1.0
Propane	20	1.0	1.0	1.0	1.0
Propane	50	0.9	1.1	1.2	0.9
Propane	80	0.9	1.1	1.4	0.7
Propane	100	1.0	1.0	2.0	0.5
Ammonia	5	0.8	1.3	0.9	1.1
Ammonia	10	0.6	1.5	0.8	1.3
Ammonia	25	0.6	1.7	0.6	1.5
Ammonia	40	0.6	1.7	0.6	1.6
Ammonia	50	0.6	1.7	0.6	1.6
MB	37	0.0	32.1	0.0	46.5
MB	74	0.0	29.3	0.0	42.9
MB	184	0.0	29.8	0.0	50.6
MB	276	0.0	34.0	0.0	54.7
Acetone	0.5	1.0	1.0	0.4	2.7
Acetone	1	1.0	1.0	0.3	3.2
Acetone	2	0.8	1.3	0.2	4.2
Acetone	5	0.6	1.6	0.2	6.4
Acetone	8	0.6	1.8	0.1	8.0

Table 8-9 Summary of maximum resistive (R/R_0) and maximum conductive (R_0/R) responses attained with 'Cr_2O_3 + 40% (wt.) H-ZSM-5' and 'Cr_2O_3 + H-Y' selected to carry out SVM classification tests upon exposure to nine test gases. Note that additional information was inputted for SVM analysis such as the value of the responses after 5 secs, 10 secs, 50 secs, 100 secs, 200 secs, 300 secs, 400 secs and 500 secs. Tests that led to high variability between tests were also left out of the input dataset for SVM analysis.

Class	Conc.	R.R.Cr_2O_3.40.ZSM5	C.R.Cr_2O_3.40.ZSM5	R.R.Cr_2O_3.HY	C.R.Cr_2O_3.HY
Toluene	5	1.4	0.7	1.4	0.7
Toluene	10	1.4	0.7	1.5	0.7
Toluene	25	1.5	0.7	2.4	0.4
Toluene	40	1.5	0.7	4.8	0.2
Toluene	50	1.6	0.6	6.9	0.1
Ethanol	10	1.3	0.8	1.4	0.7
Ethanol	20	1.2	0.9	1.3	0.8
Ethanol	50	1.2	0.8	1.6	0.6
Ethanol	80	1.2	0.8	2.1	0.5
Ethanol	100	1.2	0.8	2.5	0.4
Ethane	10	1.2	0.8	1.2	0.8
Ethane	20	1.1	0.9	1.2	0.8
Ethane	50	1.1	0.9	1.2	0.8
Ethane	80	1.1	0.9	1.2	0.8
Ethane	100	1.1	0.9	1.2	0.8
Ammonia	5	1.2	0.8	1.3	0.8
Ammonia	10	1.2	0.8	1.2	0.8
Ammonia	25	1.2	0.8	1.2	0.8
Ammonia	40	1.2	0.8	1.3	0.8
Ammonia	50	1.2	0.8	1.3	0.8
MB	37	7.8	0.1	13.2	0.1
MB	55	2.8	0.4	10.2	0.1
MB	74	2.9	0.3	11.2	0.1
MB	92	3.8	0.3	12.5	0.1
MB	276	17.8	0.1	14.6	0.1
Acetone	10	1.2	0.8	1.4	0.7
Acetone	20	1.1	0.9	1.2	0.8
Acetone	50	1.1	0.9	1.5	0.7
Acetone	80	1.2	0.8	1.9	0.5
Acetone	100	1.2	0.8	2.2	0.4

9. *References*

1. Haddi Z, Amari A, Alami H, El Bari N, Llobet E, Bouchikhi B. A portable electronic nose system for the identification of cannabis-based drugs. Sensors Actuators, B Chem [Internet]. 2011;155(2):456–63.
2. Voss A, Witt K, Kaschowitz T, Poitz W, Ebert A, Roser P, et al. Detecting cannabis use on the human skin surface via an electronic nose system. Sensors (Basel). 2014;14(7):13256–72.
3. Hernández PT, Naik AJT, Newton EJ, Hailes SM V., Parkin IP. Assessing the potential of metal oxide semiconducting gas sensors for illicit drug detection markers. J Mater Chem A 2014;2(23):8952.
4. United Nations Office on Drugs and Crime - World Drug Report. New York; 2016.
5. United Nations Office on Drugs and Crime - World Drug Report. New York; 2013.
6. Parmeter JE, Murray DW, Hannum DW. Guide for the Selection of Drugs Detectors for Law enforcement applications. NIJ Guide 601-00. 2000;
7. Korotcenkov G, Cho BK. Thin film SnO_2-based gas sensors: Film thickness influence. Sensors Actuators B Chem. 2009 Oct;142(1):321–30.
8. Zolghadr S, Khojier K, Kimiagar S. Study of sensitivity and selectivity of α-Fe_2O_3 thin films for different toxic gases and alcohols. Mater Sci Semicond Process. 2016;54:6–13.
9. Jin H, Huang Y, Jian J. Plate-like Cr_2O_3 for highly selective sensing of nitric oxide. Sensors Actuators, B Chem. 2015;206:107–10.
10. Picasso G, Sun Kou MR, Vargasmachuca O, Rojas J, Zavala C, Lopez A, et al. Sensors based on porous Pd-doped hematite (α-Fe_2O_3) for LPG detection. Microporous Mesoporous Mater. 2014;185:79–85.
11. Pokhrel S, Simion CE, Quemener V, Bârsan N, Weimar U. Investigations of conduction mechanism in Cr_2O_3 gas sensing thick films by ac impedance spectroscopy and work function changes measurements. Sensors Actuators B Chem. 2008;133(1):78–83.
12. Becker T, Ahlers S, Bosch-v.Braunmühl C, Müller G, Kiesewetter O. Gas sensing properties of thin- and thick-film tin-oxide materials. Sensors Actuators, B Chem. 2001;77(1–2):55–61.
13. Choi J-K, Hwang I-S, Kim S-J, Park J-S, Park S-S, Jeong U, et al. Design of selective gas sensors using electrospun Pd-doped SnO_2 hollow nanofibers. Sensors Actuators B Chem. 2010;150(1):191–9.
14. Kou X, Wang C, Ding M, Feng C, Li X, Ma J, et al. Synthesis of Co-doped SnO_2 nanofibers and their enhanced gas-sensing properties. Sensors Actuators, B Chem. 2016;236:425–32.
15. Binions R, Afonja A, Dungey S, Lewis DW, Parkin IP, Williams DE. Discrimination Effects in Zeolite Modified Metal Oxide Semiconductor Gas Sensors. IEEE Sensors Journal 2011;11(5):1145–51.
16. Xu C, Tamaki J, Miura N, Yamazoe N. Grain size effects on gas sensitivity of porous SnO2-based elements. Sensors Actuators B Chem. 1991; 3(2):147–55.
17. Yamazoe N, Shimanoe K. Roles of Shape and Size of Component Crystals in Semiconductor Gas Sensors: II. Response to NO_2 and H_2. J Electrochem Soc. 2008;155(4):J93–8.
18. Moon WJ, Yu JH, Choi GM. Selective CO gas detection of SnO_2–Zn_2SnO_4 composite gas sensor. Sensors Actuators B Chem. 2001; 80(1):21–7.
19. Naik AJT, Gruar R, Tighe CJ, Parkin IP, Darr JA, Binions R. Environmental sensing semiconducting nanoceramics made using a continuous hydrothermal synthesis pilot plant. Sensors Actuators, B Chem. 2015;217:136–45.
20. Ilić B, Wettstein SG. A review of adsorbate and temperature-induced zeolite framework flexibility. Microporous Mesoporous Mater. 2016;239.
21. Vilaseca M, Coronas J, Cirera A, Cornet A, Morante JR, Santamaría J. Use of zeolite films to improve the selectivity of reactive gas sensors. Catal Today.

2003;82(1–4):179–85.
22. Vilaseca M, Coronas J, Cirera A, Cornet A, Morante JR, Santamaria J. Gas detection with SnO_2 sensors modified by zeolite films. Sensors Actuators B Chem. 2007;124(1):99–110.
23. Varsani P, Afonja A, Williams DE, Parkin IP, Binions R. Zeolite-modified WO_3 gas sensors - Enhanced detection of NO_2. Sensors Actuators, B Chem. 2011;160(1):475–82.
24. Sahner K, Hagen G, Schonauer D, Reis S, Moos R. Zeolites — Versatile materials for gas sensors. Solid State Ionics. 2008 Dec 31;179(40):2416–23.
25. Afonja A, Binions R, Dungey S, Parkin IP, Lewis DW, Williams DE. Zeolites as transformation elements in discriminating semiconductor metal oxide sensors. Procedia Eng. 2010;5(x):103–6.
26. Hagen G, Dubbe A, Rettig F, Jerger A, Birkhofer T, Müller R, et al. Selective impedance based gas sensors for hydrocarbons using ZSM-5 zeolite films with chromium(III)oxide interface. Sensors Actuators B Chem. 2006;119(2):441–8.
27. Pugh DP, Hailes SMV, Parkin IP. A gas-sensing array produced from screen-printed, zeolite-modified chromium titanate. Meas Sci Technol. 2015;26(8):85102.
28. Peveler WJ, Binions R, Hailes SM V, Parkin IP. Detection of explosive markers using zeolite modified gas sensors. J Mater Chem A. 2013;1(7):2613.
29. Afonja A. Use of Zeolites to Effect Discrimination in Metal Oxide Semiconductor Gas Sensors. Thesis. University College London; 2012.
30. Vilaseca M, Coronas J, Cirera A, Cornet A, Morante JR, Santamaria J. Development and application of micromachined Pd/SnO_2 gas sensors with zeolite coatings. Sensors Actuators B Chem. 2008;133(2):435–41.
31. Reiß S, Hagen G, Moos R. Zeolite-based Impedimetric Gas Sensor Device in Low-cost Technology for Hydrocarbon Gas Detection. Sensors. 2008;8(12):7904–16.
32. Hagen G, Dubbe A, Fischerauer G, Moos R. Thick-film impedance based hydrocarbon detection based on chromium(III) oxide/zeolite interfaces. Sensors Actuators B Chem. 2006;118(1–2):73–7.
33. Cerreta MM, Furton KG. An assessment of detection canine alerts using flowers that release methyl benzoate, the cocaine odorant, and an evaluation of their behavior in terms of the VOCs produced. Forensic Sci Int. 2015;251:107–14.
34. Furton KG, Hong Y-C, Hsu Y-L, Luo T, Rose S, Walton J. Identification of odor signature chemicals in cocaine using solid-phase microextraction-gas chromatography and detector-dog response to isolated compounds spiked on U.S. paper currency. J Chromatogr Sci. 2002;40(3):147–55.
35. Moos R, Sahner K, Fleischer M, Guth U, Barsan N, Weimar U. Solid state gas sensor research in Germany - A status report. Sensors. 2009;9(6):4323–65.
36. Capone S, Forleo A, Francioso L, Rella R, Siciliano P, Spadavecchia J, et al. Solid State Gas Sensors: State of the Art and Future Activities. ChemInform. 2004;35(29).
37. Wales DJ, Grand J, Ting VP, Burke RD, Edler KJ, Bowen CR, et al. Gas sensing using porous materials for automotive applications. Chem Soc Rev. 2015;44(13):4290–321.
38. Van den Bossche M, Rose NT, De Wekker SFJ. Potential of a low-cost gas sensor for atmospheric methane monitoring. Sensors Actuators B Chem. 2017;238(2):501–9.
39. Bart M, Williams DE, Ainslie B, McKendry I, Salmond J, Grange SK, et al. High Density Ozone Monitoring Using Gas Sensitive Semi-Conductor Sensors in the Lower Fraser Valley, British Columbia. Environ Sci Technol. 2014;48(7):3970–7.
40. Moos R, Müller R, Plog C, Knezevic A, Leye H, Irion E, et al. Selective ammonia exhaust gas sensor for automotive applications. Sensors Actuators B Chem. 2002;83(1–3):181–9.
41. Mirzaei A, Leonardi SG, Neri G. Detection of hazardous volatile organic compounds (VOCs) by metal oxide nanostructures-based gas sensors: A review. Ceram Int. 2016;42(14):15119–41.

42. Tiggemann L, Ballen S, Bocalon C, Graboski AM, Manzoli A, De Paula Herrmann PS, et al. Low-cost gas sensors with polyaniline film for aroma detection. J Food Eng. 2016;180:16–21.
43. Sberveglieri V, Carmona EN, Zappa D, De Leo R, Ponzoni A. Sweat for the Discrimination of Human's Habit using NWs Gas Sensors Technology. Mater Today Proc. 2016;3(2):603–7.
44. Timmer B, Olthuis W, Berg A van den. Ammonia sensors and their applications—a review. Sensors Actuators B Chem. 2005;107(2):666–77.
45. Castro M, Kumar B, Feller JF, Haddi Z, Amari a., Bouchikhi B. Novel e-nose for the discrimination of volatile organic biomarkers with an array of carbon nanotubes (CNT) conductive polymer nanocomposites (CPC) sensors. Sensors Actuators B Chem. 2011;159(1):213–9.
46. Salehi S, Nikan E, Khodadadi AA, Mortazavi Y. Highly sensitive carbon nanotubes-SnO_2 nanocomposite sensor for acetone detection in diabetes mellitus breath. Sensors Actuators, B Chem. 2014;205:261–7.
47. Jia Q, Ji H, Zhang Y, Chen Y, Sun X, Jin Z. Rapid and selective detection of acetone using hierarchical zno gas sensor for hazardous odor markers application. J Hazard Mater. 2014;276:262–70.
48. Vashist SK, Zheng D, Al-Rubeaan K, Luong JHT, Sheu FS. Advances in carbon nanotube based electrochemical sensors for bioanalytical applications. Biotechnol Adv. 2011;29(2):169–88.
49. Compagnone D, Faieta M, Pizzoni D, Di Natale C, Paolesse R, Van Caelenberg T, et al. Quartz crystal microbalance gas sensor arrays for the quality control of chocolate. Sensors Actuators, B Chem. 2015;207(PB):1114–20.
50. Fang G, Wang H, Yang Y, Liu G, Wang S. Development and application of a quartz crystal microbalance sensor based on molecularly imprinted sol-gel polymer for rapid detection of patulin in foods. Sensors Actuators, B Chem. 2016;237:239–46.
51. Sekhar PK, Brosha EL, Mukundan R, Linker KL, Brusseau C, Garzon FH. Trace detection and discrimination of explosives using electrochemical potentiometric gas sensors. J Hazard Mater. 2011;190(1–3):125–32.
52. Tomeček D, Premysl F, Vlček, Marešová E, VrnataT Detection of taggants in explosives on nanostructured metal/silver phthalocyanine chemiresistors: Influence of analyte photoactivation. Sensors Actuators, B Chem. 2017;239:147–56.
53. Sekhar PK, Wignes F. Trace detection of research department explosive (RDX) using electrochemical gas sensor. Sensors Actuators, B Chem. 2016;227:185–90.
54. Kim BY, Cho JS, Yoon JW, Na CW, Lee CS, Ahn JH, et al. Extremely sensitive ethanol sensor using Pt-doped SnO_2 hollow nanospheres prepared by Kirkendall diffusion. Sensors Actuators, B Chem. 2016;234:353–60.
55. Dhahri R, Leonardi SG, Hjiri M, Mir L El, Bonavita A, Donato N, et al. Enhanced performance of novel calcium/aluminum co-doped zinc oxide for CO_2 sensors. Sensors Actuators, B Chem. 2017;239:36–44.
56. Sahner K, Schönauer D, Kuchinke P, Moos R. Zeolite cover layer for selectivity enhancement of p-type semiconducting hydrocarbon sensors. Sensors Actuators B Chem. 2008;133(2):502–8.
57. Comini E, Faglia G, Sberveglieri V, editors. Solid State Gas Sensing. New York: Springer; 2009. 2 p.
58. Cavicchi RE. Pulsed desorption kinetics using micromachined microhotplate arrays. J Vac Sci Technol A Vacuum, Surfaces, Film. 1994;12(4):2549.
59. Xu L, Dai Z, Duan G, Guo L, Wang Y, Zhou H, et al. Micro/Nano Gas Sensors: A New Strategy Towards In-Situ Wafer-Level Fabrication of High-Performance Gas Sensing Chips. Sci Rep. 2015;5:10507.
60. Simon I, Bârsan N, Bauer M, Weimar U. Micromachined metal oxide gas sensors: Opportunities to improve sensor performance. Sensors Actuators, B Chem. 2001;73(1):1–26.

61. Monereo O, Casals O, Prades JD, Cirera A. A low-cost approach to low-power gas sensors based on self-heating effects In large arrays of nanostructures. Procedia Eng. 2015;120:787–90.
62. Evans GP, Buckley DJ, Adedigba A-L, Sankar G, Skipper NT, Parkin IP. Controlling the Cross-Sensitivity of Carbon Nanotube Based Gas Sensors to Water Using Zeolites. ACS Appl Mater Interfaces. 2016;acsami.6b10042.
63. Aswal DK, Gupta SK. Science and Technology of Chemiresistive Gas Sensors. Nova Publishers; 2007. 1-6.
64. Korotcenkov G. Handbook of Gas Sensor Materials. 1st ed. Springer-Verlag New York; 2013. 13-14 p.
65. Prasad RM, Gurlo A, Riedel R, Hübner M, Barsan N, Weimar U. Microporous ceramic coated SnO_2 sensors for hydrogen and carbon monoxide sensing in harsh reducing conditions. Sensors Actuators B Chem. 2010;149(1):105–9.
66. Hulanicki A, Glab S, Ingman F. Chemical sensors: definitions and classification. Pure Appl Chem. 1991;63(9):1247–50.
67. Liu X, Cheng S, Liu H, Hu S, Zhang D, Ning H. A Survey on Gas Sensing Technology. Sensors. 2012;12(7):9635–65.
68. Tierney WM, Kim H-OL. Electrochemical Gas Sensor with Extremely Fast Response Times. Anal Chem. 1993;65:3435–40.
69. Xiong L, Compton RG. Amperometric gas detection: A review. Int J Electrochem Sci. 2014;9(12):7152–81.
70. Yadava RDS, Verma VK. A diffusion limited sorption-desorption noise model for polymer coated SAW chemical sensors. Sensors Actuators, B Chem. 2014;195:590–602.
71. Patil SJ, Duragkar N, Rao VR. An ultra-sensitive piezoresistive polymer nano-composite microcantilever sensor electronic nose platform for explosive vapor detection. Sensors Actuators, B Chem. 2014;192:444–51.
72. Jones BTA, Walsh PT. Flammable Detection. 1988;(2):50–60.
73. Ayerden NP, Ghaderi M, Enoksson P, de Graaf G, Wolffenbuttel RF. A miniaturized optical gas-composition sensor with integrated sample chamber. Sensors Actuators, B Chem. 2015;236:917–25.
74. Tan Q, Tang L, Yang M, Xue C, Zhang W, Liu J, et al. Three-gas detection system with IR optical sensor based on NDIR technology. Opt Lasers Eng. 2015;74:103–8.
75. Fine GF, Cavanagh LM, Afonja A, Binions R. Metal oxide semi-conductor gas sensors in environmental monitoring. Sensors (Basel). 2010;10(6):5469–502.
76. Hübert T, Boon-Brett L, Black G, Banach U. Hydrogen sensors – A review. Sensors Actuators B Chem. 2011;157(2):329–52.
77. Guha PK, Ali SZ, Lee CCC, Udrea F, Milne WI, Iwaki T, et al. Novel design and characterisation of SOI CMOS micro-hotplates for high temperature gas sensors. Sensors Actuators, B Chem. 2007;127(1):260–6.
78. Brattain W, Bardeen J, Surface properties of germanium. The Bell system Tech Journal 1953;32(1) p.1-41.
79. Seiyama T, Fujiishi K, Nagatani M, Kato A. A New Detector for Gaseous Components Using Zinc Oxide Thin Films. J Soc Chem Ind Japan. 1963;66(5):652–5.
80. Ghosh S, Narjinary M, Sen A, Bandyopadhyay R, Roy S. Fast Detection of Low Concentration Carbon Monoxide using Calcium-loaded Tin Oxide Sensors. Sensors Actuators B Chem. 2014;203 p.490-496.
81. Jaaniso R, Kian Tan O, editors. Semiconductor Gas Sensors. 1st Edition. Woodhead Publishing; 2013.
82. Korotcenkov G, Cho BK. Engineering approaches to improvement of conductometric gas sensor parameters. Part 2: Decrease of dissipated (consumable) power and improvement stability and reliability. Sensors Actuators B Chem. 2014;198:316–41.
83. Meng G, Zhuge F, Nagashima K, Nakao A, Kanai M, He Y, et al. Nanoscale Thermal Management of Single SnO_2 Nanowire: pico-Joule Energy Consumed

Molecule Sensor. ACS Sensors. 2016;1:997-1003.
84. Sahm T, Gurlo A, Bârsan N, Weimar U. Basics of oxygen and SnO_2 interaction; work function change and conductivity measurements. Sensors Actuators B Chem. 2006;118(1–2):78–83.
85. Matsunaga N, Sakai G, Shimanoe K, Yamazoe N. Diffusion equation-based study of thin film semiconductor gas sensor-response transient. Sensors Actuators B Chem. 2002;83(1–3):216–21.
86. Korotcenkov G, Brinzari V, Boris Y, Ivanov M, Schwank J, Morante J. Influence of surface Pd doping on gas sensing characteristics of SnO_2 thin films deposited by spray pirolysis. Thin Solid Films 2003 J;436(1):119–26.
87. Korotcenkov G, Cho BK. Instability of metal oxide-based conductometric gas sensors and approaches to stability improvement (short survey). Sensors Actuators B Chem. 2011;156(2):527–38.
88. Carlo S Di, Falasconi M. Drift Correction Methods for Gas Chemical Sensors in Artificial Olfaction Systems: Techniques and Challenges. Adv Chem Sensors. 2012;305–26.
89. Amico AD, Natale C Di. A contribution on some basic definitions of sensors properties. IEEE sensors Journal 2001;1(3):183–90.
90. Bochenkov VE, Sergeev GB. Sensitivity, Selectivity, and Stability of Gas-Sensitive Metal-Oxide Nanostructures. Met Oxide Nanostructures Their Appl. 2010;3:31–52.
91. Afonja A. Use of zeolites to effect discrimination in metal oxide semiconductor gas sensors. University College London; 2012.
92. Baimpos T, Gora L, Nikolakis V, Kouzoudis D. Selective detection of hazardous VOCs using zeolite/Metglas composite sensors. Sensors Actuators A Phys. 2012;186:21–31.
93. Shackleford J. Introduction to Materials Science for Engineers. 8th ed. Pearson Higher Ed, 2015; 2015.
94. Batzill M, Diebold U. The surface and materials science of tin oxide. Prog Surf Sci. 2005;79(2–4):47–154.
95. Park WJ, Choi KJ, Kim MH, Koo BH, Lee J-L, Baik JM. Self-assembled and highly selective sensors based on air-bridge-structured nanowire junction arrays. ACS Appl Mater Interfaces. 2013;5(15):6802–7.
96. Li Z, Huang Y, Zhang S, Chen W, Kuang Z, Ao D, et al. A fast response & recovery H_2S gas sensor based on α-Fe_2O_3 nanoparticles with ppb level detection limit. J Hazard Mater. 2015;300:167–74.
97. Francioso L. Nanosensors for Chemical and Biological Applications. Nanosensors for Chemical and Biological Applications. Elsevier; 2014. 101-124 p.
98. Gurlo A, Riedel R. In situ and operando spectroscopy for assessing mechanisms of gas sensing. Angew Chemie - Int Ed. 2007;46(21):3826–48.
99. Gurlo A. Interplay between O2 and SnO2: Oxygen ionosorption and spectroscopic evidence for adsorbed oxygen. ChemPhysChem. 2006;7(10):2041–52.
100. Naisbitt SC, Pratt KFE, Williams DE, Parkin IP. A microstructural model of semiconducting gas sensor response: The effects of sintering temperature on the response of chromium titanate (CTO) to carbon monoxide. Sensors Actuators, B Chem. 2006;114(2):969–77.
101. Korotcenkov G. The role of morphology and crystallographic structure of metal oxides in response of conductometric-type gas sensors. Mater Sci Eng R Reports. 2008;61(1–6):1–39.
102. Shankar P, Bosco J, Rayappan B. Gas sensing mechanism of metal oxides : The role of ambient atmosphere , type of semiconductor and gases - A review ScienceJet. Sci Jet. 2015;4:126.
103. Moseley PT, Williams DE. A selective ammonia sensor. Sensors Actuators B Chem. 1990;1(1–6):113–5.
104. Williams DE. Semiconducting oxides as gas-sensitive resistors. Sensors Actuators B Chem. 1999;57(1–3):1–16.

105. Sahner K, Tuller HL. Novel deposition techniques for metal oxide: Prospects for gas sensing. J Electroceramics. 2010;24(3):177–99.
106. Yamazoe N, Shimanoe K. Proposal of contact potential promoted oxide semiconductor gas sensor. Sensors Actuators B Chem. 2013;187:162–7.
107. Kim H-J, Lee J-H. Highly sensitive and selective gas sensors using p-type oxide semiconductors: Overview. Sensors Actuators B Chem. 2014;192:607–27.
108. Martinelli G, Carotta MC. Sensitivity to reducing gas as a function of energy barrier in SnO_2 thick-film gas sensor. Sensors Actuators B Chem. 1992;7(1–3):717–20.
109. Akamatsu T, Itoh T, Izu N, Shin W. NO and NO2 sensing properties of WO_3 and Co_3O_4 based gas sensors. Sensors. 2013;13(9):12467–81.
110. Kim H-J, Lee J-H. Highly sensitive and selective gas sensors using p-type oxide semiconductors: Overview. Sensors Actuators B Chem. 2014;192:607–27.
111. Ruiz AM, Sakai G, Cornet A, Shimanoe K, Morante JR, Yamazoe N. Microstructure control of thermally stable TiO_2 obtained by hydrothermal process for gas sensors. Sensors Actuators, B Chem. 2004;103(1–2):312–7.
112. Yamazoe N, Kurokawa Y, Seiyama T. Effects of additives on semiconductor gas sensors. Sensors and Actuators. 1983;4:283–9.
113. Barsan N, Weimar U. Conduction model of metal oxide gas sensors. J Electroceramics. 2001;7(3):143–67.
114. Yamazoe N, Shimanoe K. Theoretical approach to the rate of response of semiconductor gas sensor. Sensors Actuators B Chem. 2010;150(1):132–40.
115. Traversa E. Ceramic sensors for humidity detection: the state-of-the-art and future developments. Sensors Actuators B Chem. 1995;23(2–3):135–56.
116. Wang C, Yin L, Zhang L, Xiang D, Gao R. Metal oxide gas sensors: Sensitivity and influencing factors. Sensors. 2010;10(3):2088–106.
117. Betty CA, Choudhury S. Charge carrier transport in nanocrystalline SnO_2 thin film sensor and temperature dependence of toxic gas sensitivity. Sensors Actuators B Chem. 2016;237:787–94.
118. Ahlers S, Müller G, Doll T. A rate equation approach to the gas sensitivity of thin film metal oxide materials. Sensors Actuators, B Chem. 2005;107(2):587–99.
119. Korotcenkov G. Metal oxides for solid-state gas sensors: What determines our choice? Mater Sci Eng B Solid-State Mater Adv Technol. 2007;139(1):1–23.
120. Tschöpe A. Grain size-dependent electrical conductivity of polycrystalline cerium oxide. II: Space charge model. Solid State Ionics. 2001;139(3–4):267–80.
121. Bârsan N. Conduction models in gas-sensing SnO_2 layers: grain-size effects and ambient atmosphere influence. Sensors Actuators B Chem. 1994;17(3):241–6.
122. Savu R, Ponce MA, Joanni E, Bueno PR, Castro M, Cilense M, et al. Grain size effect on the electrical response of SnO_2 thin and thick film gas sensors. Mater Res. 2009;12(1):83–7.
123. Gurlo A, Ivanovskaya M, Bârsan N, Schweizer-Berberich M, Weimar U, Göpel W, et al. Grain size control in nanocrystalline In_2O_3 semiconductor gas sensors. Sensors Actuators B Chem. 1997;44(1–3):327–33.
124. Williams DE, Pratt KFE. Microstructure effects on the response of gas-sensitive resistors based on semiconducting oxides. Sensors Actuators, B Chem. 2000;70(1–3):214–21.
125. Chabanis G, Parkin IP, Williams DE. A simple equivalent circuit model to represent microstructure effects on the response of semiconducting oxide-based gas sensors. Meas Sci Technol. 2003;14(1):76–86.
126. Shimizu Y, Maekawa T, Nakamura Y, Egashira M. Effects of gas diffusivity and reactivity on sensing properties of thick film SnO_2-based sensors 1. 1998;46:163–8.
127. Shimizu, Yasuhiro , Nakamura Y, Egashira M. Effects of diffusivity of hydrogen and oxygen through pores of thick film SnO_2-based sensors on their sensing properties. Sensors Actuators B Chem. 1993;13(14):128–31.
128. Ahlers S, Müller G, Doll T. Factors Influencing the Gas Sensitivity of Metal Oxide Materials. Encylcopedia of Sensors Vol. 10. 2006. 1-35 p.

129. Bakrania SD, Wooldridge MS. The effects of two thick film deposition methods on tin dioxide gas sensor performance. Sensors. 2009;9(9):6853–68.
130. Liljeholm L. Reactive Sputter Deposition of Funcinal Thin Films. Digit Compr Summ Uppsala Diss from Fac Sci Technol. 2012;1–52.
131. Vijayalakshmi K, Jereil SD. High performance electrochemical H_2O_2 sensor based on MWCNT thin films fabricated by novel electron beam evaporation. Ceram Int. 2016;42(14):15493–501.
132. Du X, George SM. Thickness dependence of sensor response for CO gas sensing by tin oxide films grown using atomic layer deposition. Sensors Actuators, B Chem. 2008;135(1):152–60.
133. Preiß EM, Rogge T, Krauß A, Seidel H. Tin oxide-based thin films prepared by pulsed laser deposition for gas sensing. Sensors Actuators B Chem. 2016;236:865–73.
134. Lee S, Lee G-G, Kim J, Kang S-JL. A novel process for fabrication of SnO_2-based thick film gas sensors. Sensors Actuators B Chem. 2007;123(1):331–5.
135. Lin HW, Chang CP, Hwu WH, Ger M Der. The rheological behaviors of screen-printing pastes. J Mater Process Technol. 2008;197(1–3):284–91.
136. Naik AJT. Hetero-junction and nanomaterial systems for metal oxide semiconductor based gas sensing. UCL; 2014.
137. Menil, Lucat, Debeda. Thick-film route to selective gas sensors. Sensors Actuators, B Chem. 1995;B25(1–3 pt 2):415–20.
138. Gebicki J. Application of electrochemical sensors and sensor matrixes for measurement of odorous chemical compounds. TrAC Trends Anal Chem. 2016;77:1–13.
139. Sahner K, Moos R, Matam M, Tunney JJ, Post M. Hydrocarbon sensing with thick and thin film p-type conducting perovskite materials. Sensors Actuators B Chem. 2005;108(1–2):102–12.
140. Tamaki J. Detection of dilute nitrogen dioxide and thickness effect of tungsten oxide thin film sensors. Sensors Actuators B Chem. 2003;95(1–3):111–5.
141. Liewhiran C, Phanichphant S. Influence of Thickness on Ethanol Sensing Characteristics of Doctor-bladed Thick Film from Flame-made ZnO Nanoparticles. Sensors. 2007;7(2):185–201.
142. Viricelle JP, Riviere B, Pijolat C. Optimization of SnO_2 screen-printing inks for gas sensor applications. J Eur Ceram Soc. 2005;25(12 SPEC. ISS.):2137–40.
143. Montmeat P, Lalauze R, Viricelle J-P, Tournier G, Pijolat C. Model of the thickness effect of SnO_2 thick film on the detection properties. Sensors Actuators B Chem . 2004;103(1–2):84–90.
144. Ivanov P, Llobet E, Vilanova X, Brezmes J, Hubalek J, Correig X. Development of high sensitivity ethanol gas sensors based on Pt-doped SnO_2 surfaces. Sensors Actuators B Chem. 2004;99(2–3):201–6.
145. Barbosa MS, Suman PH, Kim JJ, Tuller HL, Varela JA, Orlandi MO. Gas sensor properties of Ag- and Pd-decorated SnO micro-disks to NO_2, H_2 and CO: Catalyst enhanced sensor response and selectivity. Sensors Actuators, B Chem. 2017;239:253–61.
146. Yamazoe N. Toward innovations of gas sensor technology. Sensors Actuators B Chem. 2005;108(1–2):2–14.
147. Tyagi P, Sharma A, Tomar M, Gupta V. Metal oxide catalyst assisted SnO_2 thin film based SO_2 gas sensor. Sensors Actuators, B Chem. 2016;224:282–9.
148. Lee C-S, Choi J-H, Park Y-H. Development of metal-loaded mixed metal oxides gas sensors for the detection of lethal gases. J Ind Eng Chem. 2015;29:321–9.
149. Wang C, Liu J, Yang Q, Sun P, Gao Y, Liu F, et al. Ultrasensitive and low detection limit of acetone gas sensor based on W-doped NiO hierarchical nanostructure. Sensors Actuators, B Chem. 2015;220:59–67.
150. Niskanen AJ, Varpula A, Utriainen M, Natarajan G, Cameron DC, Novikov S, et al. Atomic layer deposition of tin dioxide sensing film in microhotplate gas sensors. Sensors Actuators, B Chem. 2010;148(1):227–32.
151. Mozalev A, Calavia R, Vázquez RM, Gràcia I, Cané C, Correig X, et al. MEMS-

microhotplate-based hydrogen gas sensor utilizing the nanostructured porous-anodic-alumina-supported WO_3 active layer. Int J Hydrogen Energy. 2013;38(19):8011–21.
152. Yoon J-H, Kim J-S. Study on the MEMS-type gas sensor for detecting a nitrogen oxide gas. Solid State Ionics. 2011;192(1):668–71.
153. Behera B, Chandra S. An innovative gas sensor incorporating ZnO-CuO nanoflakes in planar MEMS technology. Sensors Actuators, B Chem. 2016;229:414–24. 9
154. Pandya HJ, Chandra S, Vyas AL. Integration of ZnO nanostructures with MEMS for ethanol sensor. Sensors Actuators, B Chem. 2012;161(1):923–8.
155. Tan W, Ruan X, Yu Q, Yu Z, Huang X. Fabrication of a SnO_2-based acetone gas sensor enhanced by molecular imprinting. Sensors. 2015;15(1):352–64.
156. Jiang Z, Zhao R, Sun B, Nie G, Ji H, Lei J, et al. Highly sensitive acetone sensor based on Eu-doped SnO_2 electrospun nanofibers. Ceram Int. 2016;42(14):15881–8.
157. Qiang Z, Ma SY, Jiao HY, Wang TT, Jiang XH, Jin WX, et al. Highly sensitive and selective ethanol sensors using porous SnO_2 hollow spheres. Ceram Int. 2016;
158. Vergara A, Martinelli E, Llobet E, Giannini F, D'Amico A, Di Natale C. An alternative global feature extraction of temperature modulated micro-hotplate gas sensors array using an energy vector approach. Sensors Actuators, B Chem. 2007;124(2):352–9.
159. Yun J, Jin CY, Ahn J-H, Jeon S, Park I. A self-heated silicon nanowire array: selective surface modification with catalytic nanoparticles by nanoscale Joule heating and its gas sensing applications. Nanoscale. 2013;5(15):6851–6.
160. Ahn J-H, Yun J, Moon D-I, Choi Y-K, Park I. Self-heated silicon nanowires for high performance hydrogen gas detection. Nanotechnology. 2015;26(9):95501.
161. Yang F, Taggart DK, Penner RM. Joule heating a palladium nanowire sensor for accelerated response and recovery to hydrogen gas. Small. 2010;6(13):1422–9.
162. Prades JD, Jimenez-Diaz R, Hernandez-Ramirez F, Barth S, Cirera A, Romano-Rodriguez A, et al. Ultralow power consumption gas sensors based on self-heated individual nanowires. Appl Phys Lett. 2008;93(12):32–5.
163. Chen G, Paronyan TM, Pigos EM, Harutyunyan AR. Enhanced gas sensing in pristine carbon nanotubes under continuous ultraviolet light illumination. Sci Rep. 2012;2:343.
164. Gardner JW, Bartlett PN. A brief history of electronic noses*. Sensors Actuators B. 1994;19:18–9.
165. Gardner JW, Shurmer HV, Tan TT. Application of an electronic nose to the discrimination of coffees. Sensors Actuators B Chem. 1992;6(1–3):71–5.
166. Di Natale C, Macagnano A, Davide F, D'Amico A, Paolesse R, Boschi T, et al. An electronic nose for food analysis. Sensors Actuators B Chem. 1997;44(1):521–6.
167. El Barbri N, Llobet E, El Bari N, Correig X, Bouchikhi B. Electronic Nose Based on Metal Oxide Semiconductor Sensors as an Alternative Technique for the Spoilage Classification of Red Meat. Sensors. 2008;8(1):142–56.
168. Cerrato Oliveros MC, Pérez Pavón JL, García Pinto C, Fernández Laespada ME, Moreno Cordero B, Forina M. Electronic nose based on metal oxide semiconductor sensors as a fast alternative for the detection of adulteration of virgin olive oils. Anal Chim Acta. 2002;459(2):219–28.
169. Martinelli E, Polese D, Catini A, D'Amico A, Di Natale C. Self-adapted temperature modulation in metal-oxide semiconductor gas sensors. Sensors Actuators, B Chem. 2012;161(1):534–41.
170. Editor S, Urban G, Kohl C. Gas Sensing Fundamentals.
171. Tan P-N, Steinbach M, Kumar V. Classification : Basic Concepts , Decision Trees , and. Introd to Data Min. 2006;67(17):145–205.
172. Shevade SK, Keerthi SS, Bhattacharyya C, Murthy KRK. Improvements to the SMO algorithm for SVM regression. IEEE Trans Neural Networks. 2000;11(5):1188–93.
173. Han H, Jiang X. Overcome support vector machine diagnosis overfitting. Cancer

Inform. 2014;13(Suppl 1):145–58.
174. Platt JC. Sequential Minimal Optimization: A Fast Algorithm for Training Support Vector Machines. Adv kernel methods. 1998;185–208.
175. Nowotny T, Berna AZ, Binions R, Trowell S. Optimal feature selection for classifying a large set of chemicals using metal oxide sensors. Sensors Actuators B Chem. 2013;187:471–80.
176. Pardo M, Sberveglieri G. Classification of electronic nose data with support vector machines. Sensors Actuators, B Chem. 2005;107(2):730–7.
177. Ben-Hur A, Weston J. A user's guide to support vector machines. Methods Mol Biol. 2010;609:223–39.
178. Hamel L. Knowledge Discovery with Support Vector Machines. Canada: Wiley & Sons; 2009.
179. Wang L. Support Vector Machines: Theory and Applications. Netherlands: Springer; 2005.
180. Distante C, Ancona N, Siciliano P. Support vector machines for olfactory signals recognition. Sensors Actuators, B Chem. 2003;88(1):30–9.
181. Milgram J, Cheriet M, Sabourin R. "One Against One" or "One Against All": Which One is Better for Handwriting Recognition with SVMs? Tenth Int Work Front Handwrit Recognit. 2006;1–6.
182. Evgeniou T. 03 - Leave One Out Error, Stability, and Generalization of Voting Combinations of Classifiers.pdf. (1996):1–29.
183. Huang J, Lu J, Ling CX. Comparing naive Bayes, decision trees, and SVM with AUC and accuracy. Third IEEE Int Conf Data Min. 2003;11–4.
184. Caruana R, Niculescu-Mizil A. An empirical comparison of supervised learning algorithms. Proc 23rd Int Conf Mach Learn. 2006;C(1):161–8.
185. Lakshmi TM, Martin A, Begum RM, Venkatesan VP. An Analysis on Performance of Decision Tree Algorithms using Student's Qualitative Data. Int J Mod Educ Comput Sci. 2013;5(5):18–27.
186. L.Gupta D, K. Malviya a., Singh S. Performance Analysis of Classification Tree Learning Algorithms. Int J Comput Appl. 2012;55(6):39–44.
187. Mitchell TM. Decision Tree Learning. Machine Learning. 1997. p. 52–80.
188. Heilig A, Bârsan N, Weimar U, Schweizer-Berberich M, Gardner JW, Göpel W. Gas identification by modulating temperatures of SnO_2-based thick film sensors. Sensors Actuators B Chem. 1997 Sep [cited 2016 Mar 16];43(1–3):45–51.
189. Lee SH, Ho DM, Jacobson AJ, Lee TR. Transparent, Homogeneous Tin Oxide (SnO_2) Thin Films Containing SnO_2 Coated Gold Nanoparticles. Chem Mater. 2013;25(23):4697–702.
190. Dai ZR, Pan ZW, Wang ZL. Growth and structure evolution of novel tin oxide diskettes. J Am Chem Soc. 2002;124(29):8673–80.
191. Wang H, Rogach AL. Hierarchical SnO_2 Nanostructures: Recent Advances in Design, Synthesis, and Applications. Chem Mater. 2014;26(1):123–33.
192. Takenaka S, Takahashi R, Sato S, Sodesawa T, Matsumoto F, Yoshida S. Pore size control of mesoporous SnO_2 prepared by using stearic acid. Microporous Mesoporous Mater. 2003;59(2–3):123–31.
193. de Angelis L, Riva R. Selectivity and stability of a tin dioxide sensor for methane. Sensors Actuators B Chem. 1995;28(1):25–9.
194. Ponce MA, Aldao CM, Castro MS. Influence of particle size on the conductance of SnO2 thick films. J Eur Ceram Soc. 2003;23(12):2105–11.
195. Bruno L, Pijolat C, Lalauze R. Tin dioxide thin-film gas sensor prepared by chemical vapour deposition. Sensors Actuators B Chem. 1994;18(1):195–9.
196. Sakai G, Baik NS, Miura N, Yamazoe N. Gas sensing properties of tin oxide thin films fabricated from hydrothermally treated nanoparticles. Sensors Actuators B Chem. 2001;77(1–2):116–21.
197. Martinelli G, Carotta MC. Thick-film gas sensors. Sensors Actuators B Chem. 1995;23(2–3):157–61.
198. Mandayo GG, Castaño E, Gracia FJ, Cirera A, Cornet A, Morante JR. Strategies to enhance the carbon monoxide sensitivity of tin oxide thin films. Sensors

Actuators B Chem. 2003;95(1–3):90–6.
199. Lee SW, Tsai PP, Chen H. Comparison study of SnO_2 thin- and thick-film gas sensors. Sensors Actuators, B Chem. 2000;67(1):122–7.
200. Bârsan N, Ionescu R. The mechanism of the interaction between CO and an SnO_2 surface: the role of water vapour. Sensors Actuators B Chem. 1993;12(1):71–5.
201. Sekiyama M, Katada N, Niwa M. Molecular shape-selective detection by tin oxide film sensor modified with chemical vapor deposition of molecular-sieving silica overlayer using organic template. Sensors Actuators B Chem. 2007;124(2):398–406.
202. Hahn S., Bârsan N, Weimar U, Ejakov S., Visser J., Soltis R. CO sensing with SnO_2 thick film sensors: role of oxygen and water vapour. Thin Solid Films. 2003;436(1):17–24.
203. Pavelko RG, Vasiliev AA, Llobet E, Sevastyanov VG, Kuznetsov NT. Selectivity problem of SnO_2 based materials in the presence of water vapors. Sensors Actuators B Chem. 2012;170:51–9.
204. Hyodo T, Abe S, Shimizu Y, Egashira M. Gas-sensing properties of ordered mesoporous SnO_2 and effects of coatings thereof. Sensors Actuators, B Chem. 2003;93(1–3):590–600.
205. Hyodo T, Nishida N, Shimizu Y, Egashira M. Preparation and gas-sensing properties of thermally stable mesoporous SnO_2. Sensors Actuators, B Chem. 2002;83(1–3):209–15.
206. Zhu Y, Chen J, Li H, Zhu Y, Xu J. Synthesis of mesoporous SnO_2-SiO_2 composites and their application as quartz crystal microbalance humidity sensor. Sensors Actuators, B Chem. 2014;193:320–5.
207. Stashans A, Jácome S. Local structure, magnetic and electronic properties of N-doped α -Cr_2O_3 from the first-principles. Comput Mater Sci. 2014;81:353–7.
208. Kim T-H, Yoon J-W, Kang YC, Abdel-Hady F, Wazzan AA, Lee J-H. A strategy for ultrasensitive and selective detection of methylamine using p-type Cr_2O_3: Morphological design of sensing materials, control of charge carrier concentrations, and configurational tuning of Au catalysts. Sensors Actuators B Chem. 2017;240:1049–57.
209. Golbamaki N, Rasulev B, Cassano A, Marchese Robinson RL, Benfenati E, Leszczynski J, et al. Genotoxicity of metal oxide nanomaterials: review of recent data and discussion of possible mechanisms. Nanoscale. 2015;7(6):2154–98.
210. Balouria V, Kumar A, Singh A, Samanta S, Debnath AK, Mahajan A, et al. Temperature dependent H_2S and Cl_2 sensing selectivity of Cr_2O_3 thin films. Sensors Actuators, B Chem. 2011;157(2):466–72.
211. Ma H, Xu Y, Rong Z, Cheng X, Gao S, Zhang X, et al. Highly toluene sensing performance based on monodispersed Cr_2O_3 porous microspheres. Sensors Actuators, B Chem. 2012;174):325–31.
212. Suryawanshi DN, Patil DR, Patil LA. Fe_2O_3-activated Cr_2O_3 thick films as temperature dependent gas sensors. Sensors Actuators, B Chem. 2008;134(2):579–84.
213. Cao J, Xu Y, Sui L, Zhang X, Gao S, Cheng X, et al. Highly selective low-temperature triethylamine sensor based on Ag/Cr_2O_3 mesoporous microspheres. Sensors Actuators B Chem. 2015;220:910–8.
214. Sun H, Wang L, Chu D, Ma Z, Wang A. Facile fabrication of multishelled Cr_2O_3 hollow microspheres with enhanced gas sensitivity. Mater Lett. 2015;140(399):158–61.
215. Huang Y, Chen W, Zhang S, Kuang Z, Ao D, Alkurd NR, et al. A high performance hydrogen sulfide gas sensor based on porous α-Fe_2O_3 operates at room-temperature. Appl Surf Sci. 2015;351:1025–33.
216. Flak D, Braun A, Mun BS, Döbeli M, Graule T, Rekas M. Electronic Structure and Surface Properties of Non-Stoichiometric Fe_2O_3-δ (α and γ) and Its Application in Gas Sensing. Procedia Eng. 2012;47:257–60.
217. Rosso KM, Smith DMA, Dupuis M. An ab initio model of electron transport in

hematite (α-Fe_2O_3) basal planes. J Chem Phys. 2003;118(14):6455–66.
218. Sun G, Chen H, Li Y, Ma G, Zhang S, Jia T, et al. Synthesis and triethylamine sensing properties of mesoporous α-Fe_2O_3 microrods. Mater Lett. 2016;178:213–6.
219. Liang S, Li J, Wang F, Qin J, Lai X, Jiang X. Highly sensitive acetone gas sensor based on ultrafine α-Fe_2O_3 nanoparticles.pdf. Sensors Actuators B Chem. 2017;238(3):923–7.
220. Jin WX, Ma SY, Tie ZZ, Xu XL, Jiang XH, Li WQ, et al. Enhanced acetone sensing performance of monodisperse porous hamburger-like α-Fe_2O_3 microparticles. Mater Lett. 2015;160:484–7.
221. Hung CM, Hoa ND, Van Duy N, Van Toan N, Thanh Le DT, Van Hieu N. Synthesis and gas-sensing characteristics of α-Fe_2O_3 hollow balls. J Sci Adv Mater Devices. 2016;1(1):1–6.
222. Mirzaei A, Janghorban K, Hashemi B, Bonyani M, Leonardi SG, Neri G. Highly stable and selective ethanol sensor based on α-Fe_2O_3 nanoparticles prepared by Pechini sol-gel method. Ceram Int. 2015;42(5):6136–44.
223. Tan J, Huang X. Ultra-thin nanosheets-assembled hollowed-out hierarchical α-Fe_2O_3 nanorods: Synthesis via an interface reaction route and its superior gas sensing properties. Sensors Actuators B Chem. 2016;237:159–66.
224. Cuong ND, Khieu DQ, Hoa TT, Quang DT, Viet PH, Lam TD, et al. Facile synthesis of α-Fe_2O_3 nanoparticles for high-performance CO gas sensor. Mater Res Bull. 2015;68(2):302–7.
225. Dzade N, Roldan A, de Leeuw N. A Density Functional Theory Study of the Adsorption of Benzene on Hematite (α-Fe_2O_3) Surfaces. Minerals. 2014;4:89–115.
226. Sonker RK, Yadav BC. Low temperature study of nanostructured Fe_2O_3 thin films as NO_2 sensor. Mater Today Proc. 2016;3(6):2315–20.
227. Balouria V, Singh A, Ramgir NS, Debnath AK, Mahajan A, Bedi RK, et al. Enhanced H_2S response of Au modified Fe_2O_3 thin films. AIP Conf Proc. 2013;1512:782–3.
228. Gurlo A, Sahm M, Oprea A, Barsan N, Weimar U. A p- to n-transition on α-Fe_2O_3-based thick film sensors studied by conductance and work function change measurements. Sensors Actuators, B Chem. 2004;102(2):291–8.
229. Kubička D, Kikhtyanin O. Opportunities for zeolites in biomass upgrading-Lessons from the refining and petrochemical industry. Catal Today. 2015;243(C):10–22.
230. Roth WJ, Gil B, Marszalek B. Comprehensive system integrating 3D and 2D zeolite structures with recent new types of layered geometries. Catal Today. 2014;227:9–14.
231. Auerbach MS, Carrado AK, Dutta KP. Handbook of Zeolite Science and Technology. New York: Marcel Decker, Inc.; 2003.
232. Zheng Y, Li X, Dutta PK. Exploitation of unique properties of zeolites in the development of gas sensors. Sensors. 2012;12(4):5170–94.
233. Kulprathipanja S. Zeolites in Industrial Separation and Catalysis. John Wiley & Sons; 2010.
234. Al-Dughaither AS, De Lasa H. HZSM-5 zeolites with different SiO_2/Al_2O_3 ratios. Characterization and NH_3 desorption kinetics. Ind Eng Chem Res. 2014;53(40):15303–16.
235. Viswanadham N, Murali Dhar G, Prasada Rao TSR. Pore size analysis of ZSM-5 catalysts used in n-heptane aromatization reaction: An evidence for molecular traffic control (MTC) mechanism. J Mol Catal A Chem. 1997;125(2–3):87–90.
236. Desroches F. Research on Upper Level Drug Trafficking: A Review. J Drug Issues. 2007;37(4):827–44.
237. Breiger RL, Schoon E, Melamed D, Asal V, Rethemeyer RK. Comparative configurational analysis as a two-mode network problem: A study of terrorist group engagement in the drug trade. Soc Networks. 2014;36:23–39.
238. Akiba O. International trade in narcotic drugs. Futures. 1997;29(7):605–16.

239. Boivin R. Risks, prices, and positions: A social network analysis of illegal drug trafficking in the world-economy. Int J Drug Policy. 2014;25(2):235–43.
240. Ruggiero V, Khan K. British South Asian communities and drug supply networks in the UK: A qualitative study. Int J Drug Policy. 2006;17(6):473–83.
241. Crime Threats > Drugs. National Crime Agency - Drugs. 2016 [cited 2016 Sep 3]. Available from: http://www.nationalcrimeagency.gov.uk/crime-threats/drugs
242. Mcsweeney T, Turnbull PJ, Hough M. UK : Tackling Drug Markets and Distribution Networks , in the UK. Distribution. 2008. 30-31 p.
243. Crime and Policing Analysis Unit. Seizures of drugs in England. Home Off Stat Bull. 2015;(November):1–38.
244. Hackner A, Beer S, Müller G, Fischer T, Mathur S. Surface ionization detection of amphetamine-type illicit drugs. Sensors Actuators, B Chem. 2012;162(1):209–15.
245. Chan DY, Sega AG, Lee JY, Gao T, Cunin F, Renzo F Di, et al. Optical detection of C_2 hydrocarbons ethane, ethylene, and acetylene with a photonic crystal made from carbonized porous silicon. Inorganica Chim Acta. 2014;422:21–9.
246. Li C, Dong L, Zheng C, Tittel FK. Compact TDLAS based optical sensor for ppb-level ethane detection by use of a 3.34 μm room-temperature CW interband cascade laser. Sensors Actuators, B Chem. 2016;232:188–94.
247. Jayaraman VK, Maldonado Álvarez A, Olvera Amador M de la L. A simple and cost-effective zinc oxide thin film sensor for propane gas detection. Mater Lett. 2015;157:169–71.
248. Sironi L, Amadasi A, Zoja R. Recreational inhalation of butane and propane in adolescents: Two forensic cases of accidental death. Forensic Sci Int. 2016;266:e52–8.
249. Saberi MH, Mortazavi Y, Khodadadi AA. Dual selective Pt/SnO_2 sensor to CO and propane in exhaust gases of gasoline engines using Pt/$LaFeO_3$ filter. Sensors Actuators B Chem. 2015;206:617–23.
250. Pati S, Maity A, Banerji P, Majumder SB. Temperature dependent donor-acceptor transition of ZnO thin film gas sensor during butane detection. Sensors Actuators, B Chem. 2013;183:172–8.
251. Ning Z, Wubulihairen M, Yang F. PM, NO_x and butane emissions from on-road vehicle fleets in Hong Kong and their implications on emission control policy. Atmos Environ. 2012;61(2):265–74.
252. Ray I, Chakraborty S, Chowdhury A, Majumdar S, Prakash A, Pyare R, et al. Room temperature synthesis of γ-Fe_2O_3 by sonochemical route and its response towards butane. Sensors Actuators, B Chem. 2008;130(2):882–8.
253. Su PG, Chen IC. Laminating two-layer thick films structure tin oxide-based butane gas sensor operating at low temperature. Sensors Actuators, B Chem. 2004;99(2–3):304–9.
254. Pandey P, Srivastava JK, Mishra VN, Dwivedi R. Pd-gate MOS sensor for detection of methanol and propanol. J Nat Gas Chem. 2011;20(2):123–7.
255. Péres LO, Li RWC, Yamauchi EY, Lippi R, Gruber J. Conductive polymer gas sensor for quantitative detection of methanol in Brazilian sugar-cane spirit. Food Chem. 2012;130(4):1105–7.
256. Turner C, Španěl P, Smith D. A longitudinal study of ethanol and acetaldehyde in the exhaled breath of healthy volunteers using selected-ion flow-tube mass spectrometry. Rapid Commun Mass Spectrom. 2006;20(1):61–8.
257. Park S, Kim S, Sun G-J, Choi S, Lee S, Lee C. Ethanol sensing properties of networked In_2O_3 nanorods decorated with Cr_2O_3-nanoparticles. Ceram Int. 2015;41(8):9823–7.
258. Choi KS, Park S, Chang S-P. Enhanced ethanol sensing properties based on SnO_2 nanowires coated with Fe_2O_3 nanoparticles. Sensors Actuators B Chem. 2017;238:871–9.
259. Hsueh TJ, Hsu CL, Chang SJ, Chen IC. Laterally grown ZnO nanowire ethanol gas sensors. Sensors Actuators, B Chem. 2007;126(2):473–7.
260. Pawar NK, Kajale DD, Patil GE, Wagh VG, Gaikwad VB, Deore MK, et al.

Nanostructured Fe_2O_3 thick film as an ethanol sensor. Int J Smart Sens Intell Syst. 2012;5(2):441–57.
261. Rydosz A, Maciak E, Wincza K, Gruszczynski S. Microwave-based sensors with phthalocyanine films for acetone, ethanol and methanol detection. Sensors Actuators B Chem. 2016;237:876–86.
262. Leoncini R, Rentocchini F. Let it snow! Let it snow! Let it snow! Estimating cocaine production using a novel dataset based on reported seizures of laboratories in Colombia. Int J Drug Policy. 2012;23(6):449–57.
263. Stojanovska N, Fu S, Tahtouh M, Kelly T, Beavis A, Kirkbride KP. A review of impurity profiling and synthetic route of manufacture of methylamphetamine, 3,4-methylenedioxymethylamphetamine, amphetamine, dimethylamphetamine and p-methoxyamphetamine. Forensic Sci Int. 2013;224(1–3):8–26.
264. Nichols DE, Fantegrossi WE. Emerging Designer Drugs. The Effects of Drug Abuse on the Human Nervous System. Elsevier; 2014. 575-596 p.
265. Salehi A. A highly sensitive self heated SnO_2 carbon monoxide sensor. Sensors Actuators, B Chem. 2003;96(1–2):88–93.
266. Ding X, Zeng D, Zhang S, Xie C. C-doped WO_3 microtubes assembled by nanoparticles with ultrahigh sensitivity to toluene at low operating temperature. Sensors Actuators, B Chem. 2011;155(1):86–92.
267. Qi Q, Zhang T, Liu L, Zheng X. Synthesis and toluene sensing properties of SnO_2 nanofibers. Sensors Actuators, B Chem. 2009;137(2):471–5.
268. Ma H, Xu Y, Rong Z, Cheng X, Gao S, Zhang X, et al. Highly toluene sensing performance based on monodispersed Cr_2O_3 porous microspheres. Sensors Actuators, B Chem. 2012;174:325–31.
269. Li J, Wang L, Liu H, Zhao J, Li X, Wei H, et al. Synthesis and enhanced toluene gas sensing properties of 1-D α-MoO_3/$Fe_2(MoO_4)_3$ heterostructure. J Alloys Compd. 2017;694:939–45.
270. Dobrokhotov V, Oakes L, Sowell D, Larin A, Hall J, Kengne A, et al. Toward the nanospring-based artificial olfactory system for trace-detection of flammable and explosive vapors. Sensors Actuators, B Chem. 2012;168:138–48.
271. Wang C, Wang T, Wang B, Zhou X, Cheng X, Sun P, et al. Design of α-Fe_2O_3 nanorods functionalized tubular NiO nanostructure for discriminating toluene molecules. Sci Rep. 2016;6:26432.
272. Chi X, Liu C, Zhang J, Liu L, Li H, He Y, et al. Toluene-sensing properties of In_2O_3 nanotubes synthesized by electrospinning. J Semicond. 2014;35(6):64005.
273. Kumar V, Mishra VN, Dwivedi R, Das RR. Fabrication and Characterization of Integrated Thick Film Gas Sensor Array for Detection of LPG, Nitrous Oxide, Acetone and 2-Propanol. Adv Sci Eng Med. 2014;6(11):1210–7.
274. Wang J, Yang P, Wei X. High-Performance, Room-Temperature, and No-Humidity-Impact Ammonia Sensor Based on Heterogeneous Nickel Oxide and Zinc Oxide Nanocrystals. ACS Appl Mater Interfaces. 2015 doi/abs/10.1021/am508807a
275. Patil DR, Patil LA, Patil PP. Cr_2O_3-activated ZnO thick film resistors for ammonia gas sensing operable at room temperature. Sensors Actuators B Chem. 2007 Oct;126(2):368–74.
276. Mani GK, Rayappan JBB. A highly selective room temperature ammonia sensor using spray deposited zinc oxide thin film. Sensors Actuators B Chem. 2013;183:459–66.
277. Myriokefalitakis S, Daskalakis N, Fanourgakis GS, Voulgarakis A, Krol MC, Aan de Brugh JMJ, et al. Ozone and carbon monoxide budgets over the Eastern Mediterranean. Sci Total Environ. 2016;563–564:40–52. A
278. Janik MK, Wachsmann A, Chrz O. In fl uence of air pollution on exhaled carbon monoxide levels in smokers and non-smokers . A prospective cross-sectional study. Environ Research. 2016. http://dx.doi.org/10.1016/j.envres.2016.09.004
279. Yamazoe N, Shimizu Y. Humidity sensors: Principles and applications. Sensors and Actuators. 1986;10(3–4):379–98.
280. Tischner A, Maier T, Stepper C, Köck A. Ultrathin SnO_2 gas sensors fabricated by

spray pyrolysis for the detection of humidity and carbon monoxide. Sensors Actuators B Chem. 2008;134(2):796–802.
281. Blank TA, Eksperiandova LP, Belikov KN. Recent trends of ceramic humidity sensors development: A review. Sensors Actuators, B Chem. 2016;228:416–42.
282. Hübner M, Simion CE, Tomescu-Stănoiu A, Pokhrel S, Bârsan N, Weimar U. Influence of humidity on CO sensing with p-type CuO thick film gas sensors. Sensors Actuators B Chem. 2011;153(2):347–53.
283. Shimizu Y, Jono A, Hyodo T, Egashira M. Preparation of large mesoporous SnO_2 powder for gas sensor application. Sensors Actuators, B Chem. 2005;108(1–2 SPEC. ISS.):56–61.
284. Kim MY, Choi YN, Bae JM, Oh TS. Carbon dioxide sensitivity of La-doped thick film tin oxide gas sensor. Ceram Int. 2012;38:S657–60.
285. Srivastava JK, Pandey P, Mishra VN, Dwivedi R. Sensing mechanism of Pd-doped SnO_2 sensor for LPG detection. Solid State Sci. 2009;11(9):1602–5. A
286. Hübner M, Pavelko RG, Barsan N, Weimar U. Influence of oxygen backgrounds on hydrogen sensing with SnO_2 nanomaterials. Sensors Actuators, B Chem. 2011;154(2):264–9.
287. Lupan O, Chow L, Chai G, Heinrich H, Park S, Schulte A. Synthesis of one-dimensional SnO_2 nanorods via a hydrothermal technique. Phys E Low-Dimensional Syst Nanostructures. 2009;41(4):533–6.
288. Wetchakun K, Samerjai T, Tamaekong N, Liewhiran C, Siriwong C, Kruefu V, et al. Semiconducting metal oxides as sensors for environmentally hazardous gases. Sensors Actuators B Chem. 2011;160(1):580–91.
289. Mcaleer JF, Moseley PT, Norris JW, Williams DE, Ora OOX. Dioxide Gas Sensors. 1987;1323–46.
290. Garrido Pedrosa AM, Souza MJB, Melo DMA, Araujo AS. Cobalt and nickel supported on HY zeolite: Synthesis, characterization and catalytic properties. Mater Res Bull. 2006;41(6):1105–11.
291. Shoumkova A, Stoyanova V. SEM-EDX and XRD characterization of zeolite NaA, synthesized from rice husk and aluminium scrap by different procedures for preparation of the initial hydrogel. J Porous Mater. 2013;20(1):249–55.
292. Song C, Garcés JM, Sugi Y. Introduction to Shape-Selective Catalysis. 1999;1–16.
293. Ibrahim A, Lin YS. Pervaporation Separation of Organic Mixtures by MOF-5 Membranes. Ind Eng Chem Res. 2016;55(31):8652–8.
294. Bayne S, Carlin M. Forensic Applications of High Performance Liquid Chromatography. CRC Press; 2010. 36 p.
295. Yin K, Liao F, Zhu Y, Gao A, Wang T, Shao M. Enhanced gas-sensing response by gamma ray irradiation: Ag/Ag_2 SnO_3 nanoparticle-based sensor to ethanol, nitromethane and acetic acid. J Mater Chem C. 2014;2(47):10082–6.
296. Freeman B, Yampolskii Y, Ipinnau N. Materials Science of Membranes for Gas and Vapor Separation. John Wiley & Sons; 2006. 9
297. Mann DP, Paraskeva T, Pratt KFE, Parkin IP, Williams DE. Metal oxide semiconductor gas sensors utilizing a Cr-zeolite catalytic layer for improved selectivity. Meas Sci Technol. 2005;16(5):1193–200.
298. Yoon JW, Kim HJ, Jeong HM, Lee JH. Gas sensing characteristics of p-type Cr_2O_3 and Co_3O_4 nanofibers depending on inter-particle connectivity. Sensors Actuators, B Chem. 2014;202:263–71.
299. Kim JH, Jeong HM, Na CW, Yoon JW, Abdel-Hady F, Wazzan AA, et al. Highly selective and sensitive xylene sensors using Cr_2O_3-$ZnCr_2O_4$ hetero-nanostructures prepared by galvanic replacement. Sensors Actuators, B Chem. 2016;235:498–506. http://dx.doi.org/10.1016/j.snb.2016.05.104
300. Mann DP, Pratt KFE, Paraskeva T, Parkin IP, Williams DE. Transition Metal Exchanged Zeolite Layers for Selectivity Enhancement of Metal-Oxide Semiconductor Gas Sensors. IEEE Sens J. 2007;7(4):551–6.
301. Wang L, Wang S, Xu M, Hu X, Zhang H, Wang Y, et al. A Au-functionalized ZnO nanowire gas sensor for detection of benzene and toluene. Phys Chem Chem Phys. 2013;15(40):17179–86.

302. Sahner K, Schönauer D, Matam M, Post M, Moos R. Selectivity enhancement of p-type semiconducting hydrocarbon sensors-The use of sol-precipitated nano-powders. Sensors Actuators, B Chem. 2008;130(1):470–6.
303. Wu J, Tao K, Miao J, Norford LK. Improved Selectivity and Sensitivity of Gas Sensing Using a 3D Reduced Graphene Oxide Hydrogel with an Integrated Microheater. ACS Appl Mater Interfaces. 2015;7(49):27502–10.
304. Gales L, Mendes A, Costa C. Hysteresis in the cyclic adsorption of acetone, ethanol and ethyl acetate on activated carbon. Carbon N Y. 2000;38(7):1083–8.
305. BARSAN N, KOZIEJ D, WEIMAR U. Metal oxide-based gas sensor research: How to? Sensors Actuators B Chem. 2007;121(1):18–35.
306. Newbury DE. Mistakes encountered during automatic peak identification of minor and trace constituents in electron-excited energy dispersive X-ray microanalysis. Scanning. 2009;31(3):91–101.
307. Pina MP, Mallada R, Arruebo M, Urbiztondo M, Navascus N, De La Iglesia O, et al. Zeolite films and membranes. Emerging applications. Microporous Mesoporous Mater. 2011;144(1–3):19–27.
308. Baertsch CD, Funke HH, Falconer JL, Noble RD. Permeation of Aromatic Hydrocarbon Vapors through Silicalite–Zeolite Membranes. J Phys Chem. 1996;100(18):7676–9.
309. Ghosh S, Narjinary M, Sen A, Bandyopadhyay R, Roy S. Fast detection of low concentration carbon monoxide using calcium-loaded tin oxide sensors. Sensors Actuators, B Chem. 2014;203:490–6.
310. Bai G, Dai H, Liu Y, Ji K, Li X, Xie S. Preparation and catalytic performance of cylinder- and cake-like Cr_2O_3 for toluene combustion. Catal Commun. 2013;36(3):43–5.
311. Azambre B, Westermann A, Finqueneisel G, Can F, Comparot JD. Adsorption and desorption of a model hydrocarbon mixture over HY zeolite under dry and wet conditions. J Phys Chem C. 2015;119(1):315–31.
312. Kim KS, Baek WH, Kim JM, Yoon TS, Lee HH, Kang CJ, et al. A nanopore structured high performance toluene gas sensor made by nanoimprinting method. Sensors. 2010;10(1):765–74.
313. Yang HM, Ma SY, Yang GJ, Jin WX, Wang TT, Jiang XH, et al. High sensitive and low concentration detection of methanol by a gas sensor based on one-step synthesis α-Fe_2O_3 hollow spheres. Mater Lett. 2016;169:73–6.
314. Tan J, Chen J, Liu K, Huang X. Synthesis of porous α-Fe_2O_3 microrods via in situ decomposition of FeC_2O_4 precursor for ultra-fast responding and recovering ethanol gas sensor. Sensors Actuators, B Chem. 2016;230:46–53.
315. Navale ST, Bandgar DK, Nalage SR, Khuspe GD, Chougule M a., Kolekar YD, et al. Synthesis of Fe_2O_3 nanoparticles for nitrogen dioxide gas sensing applications. Ceram Int. 2013;39(6):6453–60.
316. Long NV, Yang Y, Yuasa M, Thi CM, Cao Y, Nann T, et al. Gas-sensing properties of p-type α-Fe_2O_3 polyhedral particles synthesized via a modified polyol method. RSC Adv. 2014;4(16):8250.
317. Gurlo A, Barsan N, Oprea A, Sahm M, Sahm T, Weimar U. An n- to p-type conductivity transition induced by oxygen adsorption on α-Fe_2O_3. Appl Phys Lett. 2004;85(12):2280.
318. Yi S, Tian S, Zeng D, Xu K, Peng X, Wang H, et al. A novel approach to fabricate metal oxide nanowire-like networks based coplanar gas sensors array for enhanced selectivity. Sensors Actuators, B Chem. 2014;204:351–9.
319. Yamashita T, Hayes P. Analysis of XPS spectra of Fe^{2+} and Fe^{3+} ions in oxide materials. Appl Surf Sci. 2008;254(8):2441–9.
320. Aronniemi M, Lahtinen J, Hautojärvi P. Characterization of iron oxide thin films. Surf Interface Anal. 2004;36(8):1004–6.
321. Fujii T, de Groot FMF, Sawatzky G a, Voogt FC, Hibma T, Okada K. In situ XPS analysis of various iron oxide films grown by NO_2-assisted molecular-beam epitaxy. Phys Rev B. 1999;59(4):3195–202.
322. Santilli C V., Bonnet JP, Dordor P, Onillon M, Hagenmuller P. Influence of

structural defects on the electrical properties of α-Fe_2O_3 ceramics. Ceram Int. 1990;16(1):25–32.
323. Arulsamy AD, Eleršič K, Modic M, Cvelbar U, Mozetič M. Reversible Carrier-Type Transitions in Gas-Sensing Oxides and Nanostructures. ChemPhysChem. 2010;11(17):3704–12.
324. Hackner A, Legner W, Müller G, Biavardi E, Dalcanale E, Zampolli S, et al. Surface ionization detection of amine containing drugs. Sensors Actuators B Chem. 2013;185:771–6.
325. Visser HAAH, Visser-Van Leeuwen M, Huizer H. Residual solvents in methylenedioxymethamphetamine tablets as a source of strategic information and as a tool for comparative analysis: The development and application of a static headspace gas chromatography/mass spectrometry method. Bull Narc. 2005;57(1–2):167–82.
326. Man G, Stoeber B, Walus K. An assessment of sensing technologies for the detection of clandestine methamphetamine drug laboratories. Forensic Sci Int. 2009;189(1–3):1–13.
327. CDC [Internet]. Occupational Safety and Health Guideline for Ammonia. 1992 [cited 2016 Nov 28]. Available from: https://www.cdc.gov/niosh/docs/81-123/pdfs/0028-rev.pdf
328. Leidinger M, Sauerwald T, Reimringer W, Ventura G, Schütze A. Selective detection of hazardous VOCs for indoor air quality applications using a virtual gas sensor array. J Sensors Sens Syst. 2014;3:253–63.
329. Korotcenkov G, Brinzari V, Cerneavschi A, Ivanov M, Golovanov V, Cornet A, et al. The influence of film structure on In_2O_3 gas response. Thin Solid Films. 2004;460(1–2):315–23.
330. Korotcenkov G, Brinzari V, Golovanov V, Cerneavschi A, Matolin V, Tadd A. Acceptor-like behavior of reducing gases on the surface of n-type In_2O_3. Appl Surf Sci. 2004;227(1–4):122–31.
331. Stella R, Barisci JN, Serra G, Wallace GG, De Rossi D. Characterisation of olive oil by an electronic nose based on conducting polymer sensors. Sensors Actuators B. 2000;63(1–2):1–9.
332. Abakar KAA, Yu C. Performance of SVM based on PUK kernel in comparison to SVM based on RBF kernel in prediction of yarn tenacity. Indian J Fibre Text Res. 2014;39(1):55–9.
333. Sangeetha R, Kalpana B. Performance Evaluation of Kernels in Multiclass Support Vector Machines. Int J Soft Comput Eng. 2011;1(5):138–45.
334. Goel A, Srivastava SK. Role of Kernel Parameters in Performance Evaluation of SVM. 2016 Second Int Conf Comput Intell Commun Technol. 2016;166–9.
335 Mann P. D, K. F. E. Pratt, Paraskeva T, Parkin I.P, Williams D.E, Transition metal exchanged zeolite layers for selectivity enhancement of metal-oxide semiconductor gas sensors. IEEE Sensors Journal, 2007;7(4):551-556.